The Birkhead Formation: Reservoir Characterisation of the Gidgealpa South Dome and Sequence Stratigraphy of the Eromanga Basin, Australia.

by

Elio Lanzilli

VOLUME 1 OF 2

2 3 JUL 1 .
LIBRARY

This thesis was submitted for the degree of Doctor of Philosophy at the Department of Applied Geology, University of South Australia.

March, 1999

TABLE OF CONTENTS

VOLUME 1

DECLARATION i

ACKNOWLEDGEMENTS ii

LIST OF FIGURES iii

LIST OF TABLES viii

LIST OF PLATES ix

LIST OF EQUATIONS x

LIST OF ABBREVIATIONS xi

SUMMARY xii

1 INTRODUCTION 1

1.1 AIM AND OBJECTIVES 1

2 HISTORY OF THE GIDGEALPA AND GIDGEALPA SOUTH DOME AREA 3

2.1 LOCATION 3
2.2 PRE-DISCOVERY 3
2.3 DISCOVERY AND PRODUCTION 5

3 LOCAL GEOLOGY 8

3.1 GIDGEALPA STRUCTURE 8
3.2 REGIONAL STRUCTURAL FRAMEWORK OF THE EROMANGA BASIN 8
3.3 STRATIGRAPHY OF THE EROMANGA BASIN 17
3.3.1 Introduction *17*
3.3.2 Warburton Basin *17*
3.3.3 Cooper Basin *19*
3.3.4 Eromanga Basin *20*
3.3.4.1 Introduction 20
3.3.4.2 Poolowanna Formation 22
3.3.4.3 Hutton Sandstone 22
3.3.4.4 Birkhead Formation 24
3.3.4.5 Namur Sandstone 28
3.3.4.6 Murta Formation 29
3.3.4.7 Cadna-owie Formation 29
3.3.4.8 Wallumbilla Formation 30
3.3.4.9 Toolebuc Formation to Mackunda Formation 31
3.3.4.10 Winton Formation 32
3.4 SOURCE POTENTIAL OF THE COOPER/EROMANGA BASINS 32
3.4.1 Introduction *32*
3.4.2 Hydrocarbon Geochemistry: Permian or Jurassic Source? *35*
3.4.3 Implications for Migration and Entrapment *39*
3.4.4 Source Rock Potential of the Birkhead Formation *45*
3.4.5 Geochemistry of Hydrocarbons in Jurassic Reservoirs *47*
3.4.6 Maturity Indicators for Jurassic Source Rocks *47*
3.4.7 The Gidgealpa South Dome *49*

4 CORE LOGGING, SEDIMENTOLOGY AND FACIES MODELS 55

4.1 SEDIMENTOLOGY OF THE BIRKHEAD FORMATION AND HUTTON SANDSTONE, GIDGEALPA SOUTH DOME 55
4.2 LITHOFACIES DESCRIPTION IN CORE 61
4.2.1 Gravel Lithofacies 61
4.2.1.1 Lithofacies Gm (massive to crudely bedded gravel) 61
4.2.1.2 Lithofacies Gt (trough-crossbedded gravel) 62
4.2.2 Sandy Lithofacies 63
4.2.2.1 Lithofacies St (Trough-crossbedded sand) 63
4.2.2.2 Lithofacies Sp (Planar cross-bedded sand) 64
4.2.2.3 Lithofacies Sm (Massive sand) 65
4.2.2.4 Lithofacies Sh (Horizontally-bedded sand) 65
4.2.2.5 Lithofacies Sr (Ripple cross-laminated sand) 66
4.2.2.6 Lithofacies Sd (Soft Sediment deformed sand/mud) 67
4.2.3 Fine Grained Lithofacies 67
4.2.3.1 Lithofacies Sb/Fb (Bioturbated Sand/Mud) 67
4.2.3.2 Lithofacies Fl (Laminated sand, silt and mud) 68
4.2.3.3 Lithofacies Fm (Mud/Silt Drape) 69
4.2.3.4 Lithofacies Fcs (Carbonaceous silt/mud) 70
4.2.3.5 Lithofacies Fos (Oxidised silt/mud) 70
4.2.3.6 Lithofacies C (Coal) 71
4.3 LITHOFACIES SUCCESSIONS ANALYSED USING EMBEDDED MARKOV CHAIN ANALYSIS 79
4.3.1 Method and Results using Embedded Markov chain Analysis 80
4.3.2 Embedded Markov Chain Analysis: Discussion 86
4.3.3 Notes on Embedded Markov Chain Analysis 89
4.4 LITHOFACIES SUCCESSIONS INTERPRETED IN WIRELINE LOGS 91
4.4.1 Calibration of Wireline Log Curves from Cored Intervals 91
4.4.1.1 Wireline Log Facies I 93
4.4.1.2 Wireline Log Facies II 93
4.4.1.3 Wireline Log Facies III 93
4.4.1.4 Wireline Log Facies IV 93
4.4.1.5 Wireline Log Facies V 94
4.4.1.6 Wireline Log Facies VI 94
4.5 DEPOSITIONAL MODEL OF THE HUTTON SANDSTONE AND BIRKHEAD FORMATION 94
4.5.1 Existing Model of the Birkhead Formation 95
4.5.2 Revised Model of the Birkhead Formation 95
4.6 DELTAS 96
4.6.1 Introduction 96
4.6.2 Classification of Deltas 98
4.6.3 River Dominated Deltas: Background 101
4.6.4 The Gidgealpa south dome: a river dominated delta system 102
4.6.4.1 Sedimentology of The Gidgealpa south dome 102
4.6.4.2 Hutton Sandstone 104
4.6.4.3 Birkhead Formation 105
4.6.4.3.1 Channel 105
4.6.4.3.2 Interchannel / Distributary Margins 107
4.6.4.3.3 Channel Mouth Bar 109
4.6.4.3.4 Lacustrine 111
4.6.4.3.5 Facies Associations 111
4.6.5 The Mississippi Delta: An Example 122
4.7 DIPMETER INTERPRETATION AND PALAEOCURRENTS 126
4.7.1 Introduction: Use of the Dipmeter to determine Palaeocurrents 126
4.7.2 Methodology 127
4.7.3 Structural Dip 128
4.7.4 Regional Dipmeter Interpretation 129
4.7.5 Dipmeter Interpretation at the Gidgealpa south dome 133
4.7.5.1 Dipmeter processing 133
4.8 NEODYMIUM MODEL AGE INTERPRETATION 140

4.8.1 Eromanga Basin *140*
4.8.2 Gidgealpa south dome *142*
4.9 SIDERITE FORMATION 146
4.9.1 Siderite Formation within the Birkhead Formation. *150*
4.9.2 Siderites in the Birkhead Formation, Gidgealpa south dome *152*
4.9.3 Siderite Formation and wireline logs *155*
4.9.4 Implications of HC migration and entrapment at the Gidgealpa south dome *157*

5 SEQUENCE STRATIGRAPHY 160

5.1 INTRODUCTION 160
5.2 SEQUENCE STRATIGRAPHY: EROMANGA BASIN 161
5.2.1 Why use sequence stratigraphy? *161*
5.2.2 Methodology *164*
5.2.3 Cause and effects of Base level Change *166*
5.2.4 Lowstand systems tract *169*
5.2.5 Transgressive systems tract *179*
5.2.6 Highstand Systems Tract *184*
5.3 SEQUENCE STRATIGRAPHIC CLASSIFICATION OF THE BIRKHEAD FORMATION 188
5.3.1 Datum Determination *191*
5.4 UNIT DETERMINATION OF THE BIRKHEAD FORMATION 192
5.4.1 Unit L1 - Lowstand Systems Tract *194*
5.4.2 Unit L2 - Transgressive Systems Tract *196*
5.4.3 Unit L3 - Highstand Systems Tract *197*
5.5 SEQUENCE STRATIGRAPHY OF THE BIRKHEAD FORMATION, GIDGEALPA SOUTH DOME 198
5.5.1 Sequence Stratigraphy of the Delta sequence *210*
5.6 SUMMARY OF THE SEQUENCE STRATIGRAPHY AT THE GIDGEALPA SOUTH DOME 216

6 PETROLOGY 226

6.1 METHODS 226
6.2 COMPOSITION AND TEXTURE OF FACIES AT THE GIDGEALPA SOUTH DOME 230
6.2.1 Quartz *232*
6.2.2 Feldspars *237*
6.2.3 Lithics *244*
6.2.4 Mica *248*
6.2.5 Heavy Minerals *250*
6.2.6 Matrix *251*
6.2.7 Clays *253*
6.2.8 Cements *260*
6.2.8.1 Quartz 260
6.2.8.2 Carbonate 264
6.3 DIAGENETIC SEQUENCE 270
6.4 FACTORS AFFECTING POROSITY AND PERMEABILITY 274
6.5 DISCUSSION 281
6.5.1 Provenance Change *282*
6.5.2 Diagenesis *287*
6.5.3 Porosity and Permeability *290*

7 CORE ANALYSIS 293

7.1 CAPILLARY PRESSURE 293
7.1.1 Background *293*
7.1.2 Results and Discussion *300*
7.2 DETERMINATION OF PERMEABILITY AND POROSITY FROM CORE PLUGS 309
7.2.1 Sample Preparation *309*
7.2.2 Definition and Determination of Porosity *310*
7.2.3 Definition and Determination of Permeability *312*
7.2.4 Relationship between permeability and porosity *316*
7.3 PROBE PERMEAMETRY 319
7.3.1 Theory and Calibration of the Probe Permeameter *320*

7.3.2 Probe Permeability Method and Results 329
7.3.2.1 Probe Permeability Profiles 329
7.3.2.2 Averaging Permeability 333
7.3.2.3 Permeability Histograms 333
7.3.2.4 Semi-variograms 337

8 RESERVOIR CHARACTERISTICS OF THE GIDGEALPA SOUTH DOME 340

8.1 GROSS SAND TRENDS 340
8.2 LOG EVALUATION 343
8.2.1 Introduction 343
8.2.2 Log Interpretation: Background, Theory and Method 351
8.2.2.1 Porosity 351
8.2.2.2 Water Saturation 354
8.2.2.3 Permeability 357
8.2.2.4 Log Interpretation Results 359
8.2.3 Reservoir Mapping 364
8.2.4 Reservoir Engineering Characteristics 367
8.2.5 Drill Stem Test Review 371
8.2.6 Production History 372
8.2.6.1 Introduction 372
8.2.6.2 Reservoir Pressure Analysis 375
8.2.6.3 Well Production Summary 376
8.2.7 Drive Mechanism 380
8.2.8 Reserves Estimation 384
8.2.9 Reservoir Characteristics: Summary 389

9 WATERFLOODING 396

9.1 INTRODUCTION 396
9.2 WATERFLOODING OPERATIONS AT THE GIDGEALPA SOUTH DOME 398

10 CONCLUSIONS 404

11 RECOMMENDATIONS AND FURTHER RESEARCH 412

12 REFERENCES CITED 414

VOLUME 2

APPENDICES

Declaration

I declare that this thesis does not incorporate without acknowledgment any material previously submitted for a degree or diploma in any university.

Signed _____ date _____

Where previous work has been incorporated, due reference has been made within the appropriate text or figure. Direct quotes from text are in italics. Words added to enhance meaning within quotes are in bracketed non-italics. Words missed out within quotes, because they are superfluous, are indicated by hyphenation between italicised words.

Acknowledgments

In relation to this thesis, my thanks to:

My parents Luigi and Josie Lanzilli and family who aided, supported and assisted me throughout my candidature. Melissa Stevens who stuck by me through the good and bad times.

Jim Jago, my principle supervisor who helped me to stay on the straight and narrow path and who's knowledge was invaluable. My other supervisor and colleague, Peter Boult who supplied wisdom, expertise and countless discussions on a whole variety of related and unrelated topics. Maris Zwigulis (Senior Geologist) from SANTOS, without whose support this work would not have been possible.

All the support staff at the University of South Australia including Dawn Leonard, Peter Cotton, David Carver, Bernie Farrow, Max Frater, Bob Wiltshire and John Cann. My fellow students; Paul Theologou, Simon Clinch, Chris Bentley, Peter Haines and Justin Gum. Also from the University of Adelaide and NCPGG; Dave McKirdy, Bernd Michaelsen, John Foden, Nick Lemon and Andy Mitchell

SANTOS staff including Neil Gibbins, Dave Hudson, Mandy Marlow, Seiw Luii and all other staff who aided me in my endeavours as well as Brian Logan from the MESA core library.

Figures

All figures drafted and produced or figures that display the 'after **Author**' caption were produced or modified by the author of this thesis. Where figures are obtained from other sources due reference has been made.

Figure 1 Location map of the Gidgealpa field.

Figure 2 Gidgealpa south dome top Toolachee Formation and Hutton Sandstone structure with reservoir pool overlay (figure after McIntyre et. al, 1989, overlay after Boult, 1996).

Figure 3 Regional structural trends in the south western Cooper / Eromanga Basin (from Theologou, 1995).

Figure 4 Pattern of spreading around Australia showing the ages of the developing arc complex on the eastern side of Australia (after Veevers et. al, 1991).

Figure 5 Summary of tectonic models for the evolution of the Cooper / Eromanga Basins (from Boucher, 1991).

Figure 6 Continental composition of Australia during the Early Cambrian (after Roberts et. al, 1990).

Figure 7 Model of the compressional tectonics along a convergent margin that caused the formation of the Cooper and Galilee Basins in the Early / Middle Triassic (from Moore et. al, 1986).

Figure 8 NE-SW and N-S structural trends of the Eromanga Basin during the Early / Middle Triassic (after Wecker, 1989).

Figure 9 Palaeogeographic change of the Australian continent through the Jurassic to Cretaceous (from Alexander and Sansome, 1996).

Figure 10 Stratigraphic column of the Cooper / Eromanga Basins at the Gidgealpa south dome (from McIntyre et. al, 1989).

Figure 11 West to east cross section of the Eromanga and Surat Basins (from Boult, 1996).

Figure 12 Idealised stratigraphic profile of the Birkhead Formation (from Paton, 1986).

Figure 13 Stratigraphic section showing the life span of two known Jurassic biomarkers and the source of oil in various reservoirs in the sequence (after Alexander et. al, 1988 and Kantsler et. al, 1983).

Figure 14 Logarithmic cross-plot of hopanes and norhopanes from source rocks and oils within the Cooper and Eromanga Basins (from Boult et. al, 1997).

Figure 15 Partial GC-FID traces and mass fragmentograms of aromatic fractions from typical Jurassic and Permian samples (from Alexander et. al, 1998).

Figure 16 Log graph of source parameters to distinguish Permian from Jurassic oils in the western Eromanga Basin (from Alexander et. al, 1996).

Figure 17 Recharge and natural discharge areas and directions of regional groundwater flow through aquifers in the Great Artesian Basin (from Habermehl, 1980).

Figure 18 E-W cross section of the Great Artesian Basin aquifer system (from Bowering, 1982).

Figure 19 Produced oil from various formations of the Eromanga Basin (from Alexander, 1996).

Figure 20 Permian source-migration model (from Heath et. al, 1989).

Figure 21 Hydrocarbon accumulations in the Chookoo-Naccowlah South area, Eromanga Basin (from Vincent et. al, 1985).

Figure 22 Vitrinite reflectance profile for the top Birkhead Formation (from Wecker, 1984).

Figure 23 Hydrogen index versus T_{max} plots of Birkhead Formation source rocks in the South Australian sector of the Eromanga Basin (from Michaelsen and McKirky, 1996).

Figure 24 Schematic cross sections of the Eromanga Basin displaying isoreflectance profiles (from Kantsler et. al, 1983).

Figure 25 Subsidence/maturation history in Cuttapirrie 1, north-western Patchawarra Trough, Eromanga Basin (from Kantsler et. al, 1983).

Figure 26 Maceral proportions in coals and shales from the Birkhead Formation, Gidgealpa south dome (from Ryan, 1996).

Figure 27 Top Hutton Sandstone depth map, showing isoreflectance contours and the possible present-day drainage area from Tindilpie to the Gidgealpa south dome areas (from Boult et. al, 1998).

Figure 28 GC-MS-MS chromatograms of DST 3 oil (Birkhead Formation) and DST 4 (Hutton Sandstone) from Gidgealpa 17, Gidgealpa south dome (from Boult et. al, 1997).
Figure 29 Distribution of C_{27}, C_{28}, C_{29} regular steranes indicating source input (from Ryan, 1996).
Figure 30 Gidgealpa 17 core description summary (from Boult, 1996).
Figure 31 Generalised sequence through the top Hutton Sandstone and Birkhead Formation.
Figure 32 Gravel lithofacies – Gm and Gt: from the top Hutton Sandstone and Birkhead Formation Gidgealpa south dome cores.
Figure 33 Sandy Lithofacies – St and Sp: from the top Hutton Sandstone and Birkhead Formation Gidgealpa south dome cores.
Figure 34 Sandy Lithofacies – Sm: from the top Hutton Sandstone and Birkhead Formation Gidgealpa south dome cores.
Figure 35 Sandy Lithofacies - Sh and Sr: from the top Hutton Sandstone and Birkhead Formation Gidgealpa south dome cores.
Figure 36 Sandy Lithofacies – Sd: from the top Hutton Sandstone and Birkhead Formation Gidgealpa south dome cores.
Figure 37 Fine Grained Lithofacies – Sb/Fb, Fl and Fm: from the top Hutton Sandstone and Birkhead Formation Gidgealpa south dome cores.
Figure 38 Fine Grained Lithofacies – Fcs, Fos and C: from the top Hutton Sandstone and Birkhead Formation Gidgealpa south dome cores.
Figure 39 Tally Matrix for embedded Markov chain analysis.
Figure 40 Transitions probability matrix for embedded Markov chain analysis.
Figure 41 Independent trials probability matrix for embedded Markov chain analysis.
Figure 42 Difference matrix for embedded Markov chain analysis.
Figure 43 Facies relationship diagrams produced from (A) the difference matrix and (B) binomial probability determination.
Figure 44 Idealised sequences through the Birkhead Formation based on embedded Markov chain analysis.
Figure 45 Factors that affect the morphology and stratigraphy of a delta system (from Galloway, 1975).
Figure 46 Subdivided zones of a generalised delta plain (from Wright, 1985).
Figure 47 Classification of deltas based on sediment input, wave energy flux and tidal energy (from Galloway, 1975).
Figure 48 Classification of deltas based on sediment input, wave energy flux and tidal energy and including grainsize (after Galloway, 1994).
Figure 49 Sand geometries produced from different types of deltas (Coleman and Wright, 1975).
Figure 50 Bifurcating channel and middle-ground bar patterns associated with a friction-dominated, river-dominated delta (from Wright, 1977).
Figure 51 Channel morphology in a bifurcating river-dominated delta system (from Coleman and Wright, 1975).
Figure 52 Comparison of River dominated delta facies in Tantanna 3, Gidgealpa 29 and the Mississippi Delta.
Figure 53 Example of an interdistributary bay sequence from a river dominated delta in the Dunvegan Formation, Alberta (from Bhattacharya and Walker, 1992).
Figure 54 Example of an interdistributary channel sequence from a river dominated delta in the Dunvegan Formation, Alberta (from Bhattacharya and Walker, 1992).
Figure 55 Comparison of fluvial to wave dominated deltas in the Upper Cretaceous Dunvegan Formation, Alberta (from Bhattacharya and Walker, 1992).
Figure 56 Evolution of a delta morphology through time from the Tertiary clastic cycle of the Gulf Coast Basin (from Galloway, 1975).
Figure 57 Sedimentary framework of Mississippi delta (from Le Blanc, 1975).
Figure 58 Holocene chronologic sequence of delta lobe development for the Mississippi Delta (from Wright, 1985).
Figure 59 Deformational structures formed in the Mississippi Delta (from Wright, 1985).
Figure 60 Evolution of the Mississippi delta facies (from Le Blanc, 1975).
Figure 61 Gidgealpa 53 original and corrected rose diagrams after removal of structural dip.
Figure 62 Regional palaeo-current directions in the south western Eromanga Basin top Hutton Sandstone and basal Birkhead Formation.

Figure 63 Palaeo-current data of the Hutton Sandstone and Birkhead Formation in ATP 269(1) (from Watts, 1987).
Figure 64 Gidgealpa south dome map showing locations of interpreted, uninterpreted and missing dipmeter data.
Figure 65 Dipmeter data of the top Hutton and base Birkhead at the Gidgealpa south dome.
Figure 66 Dipmeter data of the top Birkhead Formation at the Gidgealpa south dome.
Figure 67 Histograms of Neodymium model ages in ATP 269(1) (from Whitford et. al, 1994).
Figure 68 Variations in and Neodymium model age trends across the Eromanga basin in the Mid to Late Jurassic.
Figure 69 Neodymium model age plot of time versus depth.
Figure 70 Correlation of wells with core across the Gidgealpa south dome showing the location of Neodymium model ages and thin sections.
Figure 71 Siderite phase diagram (after Krauskopf, 1967).
Figure 72 Siderite occurrences found in the Birkhead Formation, Gidgealpa south dome.
Figure 73 Formation of siderite nodules within a marsh environment (from Moore et. al, 1992).
Figure 74 Wireline log responses from siderite cemented zones.
Figure 75 Palynological zone chrono-position of Birkhead Formation Eromanga Basin (from Boult, 1996).
Figure 76 Map showing regional sequence stratigraphic sections within the Eromanga Basin.
Figure 77 Relationship of parameters affecting base level change within the Eromanga Basin (after Galloway, 1989).
Figure 78 Effects of base level fall on fluvial incision (from Allen, 1994).
Figure 79 3D block diagram of the Tindilpie to Gidgealpa south dome cross section showing fluvial incision by meandering rivers at the base of the Birkhead Formation.
Figure 80 Identification of different types of lowstand sediments applied to the top Hutton Sandstone (after Allen, 1994).
Figure 81 Interpreted sequence stratigraphic cross-section of B-B'.
Figure 82 Initial change from reworked Hutton Sandstone sediments to volcanic-arc derived sediments during early Birkhead time in the eastern Eromanga Basin (after Boult, 1996).
Figure 83 Climatic conditions and annual rainfall over the earth during the late Jurassic (from Frakes et. al, 1992).
Figure 84 The effects of varying the ratio of relative base level rise and sediment influx (from Allen, 1994).
Figure 85 Effects of increasing rate of relative base level rise on a fluvial profile (from Allen, 1996).
Figure 86 Sequence stratigraphic and associated chronostratigraphic model of the Eromanga Basin during late Hutton Sandstone and early Birkhead Formation time.
Figure 87 Variations in the allocation of sequence boundaries by Galloway and Exxon for the Cardium Formation, Alberta, Canada (from Walker, 1990).
Figure 88 Comparison of unit allocations of the Birkhead Formation.
Figure 89 Summary of common, idealised wireline log signatures (from Walker 1992).
Figure 90 Seismic section hung on the DN horizon (top Cadna-owie) showing truncation of a seismic reflector from erosion within the top Hutton Sandstone (after Boult, 1996).
Figure 91 Stratigraphic cross section through Gidgealpa 29, 20, 36, 17, 50.
Figure 92 Stratigraphic cross section through Gidgealpa 22, 23, 21, 48, 45.
Figure 93 Stratigraphic cross section through Gidgealpa 23, 22, 29, 40, 46.
Figure 94 Stratigraphic cross section through Gidgealpa 55, 42, 21, 48, 50.
Figure 95 Highstand systems tract signature of Gidgealpa 20showing 3 prograding parasequence sets.
Figure 96 Sequence stratigraphic components of a deltaic sequence (after Allen and Mercier, 1988).
Figure 97 Sequence stratigraphic components of the Gidgealpa 29 deltaic sequence.
Figure 98 Variations in sand stacking patterns depending on the subsidence and sediment influx ratio (from Allen, 1994).
Figure 99 Detailed sequence stratigraphic correlation of Gidgealpa 30, 26, 29 and 32 using core data.

Figure 100 Chronological sequence from the Gidgealpa south dome Birkhead Formation showing the position of the stacked delta lobes.
Figure 101 Block diagrams of successive stages of delta development at the Gidgealpa south dome.
Figure 102 Classification used for the naming of sandstones based on Folk (1974).
Figure 103 Classification used for the naming of sandstones from Lemon (1992).
Figure 104 Summary of diagenetic events in the Hutton Sandstone and Birkhead Formation at the Gidgealpa south dome.
Figure 105 Graphs showing the effects of kaolin on point counted and core plug porosities (from Schulz-Rojahn and Phillips, 1989).
Figure 106 Porosity and permeability relationships of artificially mixed and wet packed sand of different grain sizes and sorting (from Sneider, 1992).
Figure 107 Folk's classification assigning facies and depositional environment.
Figure 108 Determination of climate and tectonic activity at the time of deposition of the Hutton Sandstone and Birkhead Formation from the analysis of feldspars (after Folk, 1980).
Figure 109 Example of mercury injection curve from Jennings (1987).
Figure 110 Idealised graphs of samples with different pore throat distributions (from Vavra et. al, 1993).
Figure 111 Example of how the PTS value is calculated from a capillary pressure curve (from Jennings, 1987).
Figure 112 Graph showing injection and withdrawal curves (from Vavra et. al, 1993).
Figure 113 Summary of mercury injection data from the Gidgealpa south dome, grouped by facies.
Figure 114 Comparison of capillary pressure and pore throat distribution graphs of samples from the Gidgealpa south dome.
Figure 115 Drainage and imbibition curves of selected samples from the Gidgealpa south dome.
Figure 116 Height above free water level and wetting phase saturation of samples from . the Gidgealpa south dome.
Figure 117 Schematic flow diagram of the Jones Permeameter.
Figure 118 Summary of permeability-porosity crossplots of samples from the Gidgealpa south dome.
Figure 119 Schematic diagram representing the components of the EPS probe permeameter.
Figure 120 Normal distribution of probe perm frequencies showing low end spike (from Boult et. al, 1995).
Figure 121 Schematic diagram showing the apparatus used for calibration of the mass flowmeter.
Figure 122 Resultant graph produced from the calibration of the mass flowmeter.
Figure 123 Crossplot of permeability from the probe versus the Hassler-Sleeve apparatus.
Figure 124 Comparison of Gidgealpa 29 core, core plug permeability and probe permeability data.
Figure 125 Frequency distribution of log(probe permeability) values of the Birkhead Formation and top Hutton Sandstone.
Figure 126 Histograms of probe permeability data for each facies within the Birkhead Formation at the Gidgealpa south dome.
Figure 127 Comparison of semi-variogram plots from various depositional environments within the Hutton Sandstone and Birkhead Formation.
Figure 128 Isopach map of the thickness between the maximum flooding surface and the transgressive surface, indicating topography on the transgressive surface.
Figure 129 Gross sand map of all sand packages present within the lower Birkhead Formation.
Figure 130 Birkhead Formation, Sand A thickness isopach.
Figure 131 Birkhead Formation, Sand B thickness isopach.
Figure 132 Birkhead Formation, Sand C thickness isopach.
Figure 133 Birkhead Formation, Sand D thickness isopach.
Figure 134 Birkhead Formation, Sand E thickness isopach.
Figure 135 Fence diagram illustrating delta sand distribution within the Gidgealpa south dome Birkhead Formation.
Figure 136 Steps used in GEOLOG to determine petrophysical properties of the lower Birkhead Formation and top Hutton Sandstone.

Figure 137 Pickett Plot used to determine *a* and R_W (from Cleneay, 1992).
Figure 138 Crossplot of probe permeability and the density log over the Birkhead Formation cored interval.
Figure 139 Log interpretation summary and results of Gidgealpa 26 top Hutton Sandstone and Birkhead Formation.
Figure 140 Log interpretation summary and results of Gidgealpa 29 top Hutton Sandstone and Birkhead Formation.
Figure 141 Relative permeability curve of the Birkhead Formation Reservoir sands (from Wu, 1995).
Figure 142 Comparison of porosity and hydrocarbon pore volume maps for sands A to D within the basal Birkhead Formation, Gidgealpa south dome section.
Figure 143 Total porosity map of the basal Birkhead Formation section of the Gidgealpa south dome.
Figure 144 Total hydrocarbon pore volume map of the Basal Birkhead section of the Gidgealpa south dome.
Figure 145 Total hydrocarbon pore volume map of the top Hutton Sandstone section of the Gidgealpa south dome.
Figure 146 Pressure history graph of the Gidgealpa south dome Birkhead Formation.
Figure 147 Production history in barrels of oil per day, Gidgealpa south dome Birkhead Formation.
Figure 148 Comparisons of the production rate and reservoir pressure for the Birkhead Formation reservoir at the Gidgealpa south dome.
Figure 149 Graph of cumulative oil production versus reservoir pressure for the Birkhead Formation reservoir at the Gidgealpa south dome.
Figure 150 Pay thickness maps of the Birkhead Formation, A and B Sands.
Figure 151 Pay thickness maps of the Birkhead Formation, C and D Sands.
Figure 152 Birkhead Formation reservoir structural cross-section of Gidgealpa 27, 30, 20, 32, 25 and 53.
Figure 153 Birkhead Formation reservoir structural cross-section of Gidgealpa 27, 22, 43, 26, 48 and 19.
Figure 154 Birkhead Formation reservoir structural cross-section of Gidgealpa 16, 49, 21, 50, 24 and 46.
Figure 155 Theoretical production rates of a solution gas drive reservoir that has a waterflood scheme implemented (after Helander, 1988).
Figure 156 Production history of the Birkhead Formation reservoir in the Gidgealpa 26 well.
Figure 157 Gidgealpa south dome total production history with projected production from waterflood and CO_2 schemes.

Tables

Table 1 Information summary of wells drilled on the Gidgealpa south dome.
Table 2 Summary of lithofacies identified from the Hutton Sandstone and Birkhead Formation.
Table 3 Binomial probability table from embedded Markov Chain Analysis.
Table 4 Neodymium model age dates of samples at the Gidgealpa south dome.
Table 5 XRD characteristics of various siderite species.
Table 6 Summary of data obtained from transmitted light, SEM,XRD and lithofacies analysis.
Table 7 Quartz species present within the Hutton Sandstone and Birkhead Formation.
Table 8 Feldspar species present within the Hutton Sandstone and Birkhead Formation.
Table 9 Summary of XRD results.
Table 10 Summary of mercury injection data.
Table 11 Factors effecting withdrawal efficiency.
Table 12 Parameters used for the determination of height above free water level.
Table 13 Summary of porosity and permeability values from core plugs.
Table 14 Average values of core plug permeability and porosity for each lithofacies.
Table 15 Comparison of probe and core plug permeabilities in Gidgealpa 29 (6038'-6042').
Table 16 Permeability statistics of lithofacies within the Hutton sandstone and Birkhead Formation.
Table 17 Summary of Permeability Class characteristics.
Table 18 Summary of log evaluation data for the Birkhead Formation reservoir.
Table 19 Summary of physical properties of the Birkhead Formation reservoir.
Table 20 Summary of DST results from the Birkhead Formation.
Table 21 Summary of OOIP from volumetric calculations.
Table 22 Summary of injector or producer allocation of wells for waterflooding of the Birkhead Formation reservoir.

Plates

Plate 1 Sandstone diapir in prodelta sequence from Gidgealpa 29, formed due to sediment loading at the Gidgealpa south dome.

Plate 2 Transmitted light photomicrographs showing straight and undulose extinction of plutonic (common) quartz in the Hutton Sandstone and Birkhead Formation.

Plate 3 Transmitted light photomicrographs of volcanic quartz from the Birkhead Formation showing its characteristic hexagonal shape, large embayments and solid inclusions.

Plate 4 Transmitted light Photomicrographs of reworked sedimentary quartz from the Birkhead formation showing a number of rounded quartz overgrowths on a single grain.

Plate 5 Transmitted light photomicrographs of microcline and orthoclase feldspars from the Hutton Sandstone.

Plate 6 Transmitted light photomicrographs of plagioclase and sanidine feldspars from the Birkhead formation.

Plate 7 Transmitted light photomicrographs of anorthoclase and the presence of authigenic feldspar growing on plagioclase from the Birkhead formation.

Plate 8 Transmitted light photomicrographs of micas and oversized porosity from labile grain dissolution within the Hutton Sandstone and Birkhead Formation.

Plate 9 Transmitted light photomicrographs of metamorphic and sedimentary rock fragments from the Birkhead Formation.

Plate 10 Transmitted light photomicrographs of volcanic rock fragments from the Birkhead Formation.

Plate 11 Transmitted light photomicrographs of primary and secondary matrix from the Hutton Sandstone and Birkhead formation.

Plate 12 Scanning electron micrographs illustrating the presence of illite and smectite in the Birkhead Formation.

Plate 13 Scanning electron micrographs indicating the various morphologies of kaolin within the Birkhead Formation.

Plate 14 Cathodoluminescence photos of kaolin from the Birkhead Formation and Hutton Sandstone.

Plate 15 Scanning electron micrographs of the various sized kaolin from the Hutton Sandstone and Birkhead Formation.

Plate 16 Cathodoluminescence photos of quartz overgrowths and carbonate cements from the Hutton Sandstone and Birkhead Formation.

Plate 17 Scanning electron micrographs showing the presence of quartz overgrowths from the Hutton Sandstone and Birkhead Formation.

Plate 18 Transmitted light photomicrographs showing the various types of carbonate present within the Birkhead Formation.

Plate 19 Transmitted light photomicrographs showing carbonate growing into a vacant pore space.

Plate 20 Scanning electron micrographs showing carbonates filling pore space and occupying large areas of the rock sample within the Birkhead Formation.

Equations

Equation 1 Independent trials probability determination for embedded Markov chain analysis.
Equation 2 Binomial probabilities calculation for embedded Markov chain analysis.
Equation 3 Calculation of number of possible combinations in binomial probability for embedded Markov chain analysis.
Equation 4 Calculation of capillary pressure.
Equation 5 Calculation of the pore throat sorting value.
Equation 6 Calculation of withdrawal efficiency.
Equation 7 Conversion of mercury-air data to the brine-hydrocarbon system.
Equation 8 Height above free water level calculation.
Equation 9 Calculation of seal capacity.
Equation 10 Calculation of effective porosity.
Equation 11 Calculation of grain volume.
Equation 12 Calculation of pore volume.
Equation 13 Calculation of porosity.
Equation 14 Determination of permeability.
Equation 15 Calculation of permeability using the Jones permeameter.
Equation 16 Calculation of permeability from the probe permeameter.
Equation 17 Calculation of semi-variance.
Equation 18 Calculation of total porosity using the density log.
Equation 19 Calculation of total porosity using the sonic log.
Equation 20 Calculation of effective porosity from logs.
Equation 21 Calculation of formation factor from resistivity.
Equation 22 Basic Archie equation.
Equation 23 Calculation of the cementation exponent.
Equation 24 Modified Archie equation incorporating saturation and cementation exponents.
Equation 25 Archie equation incorporated with excess conductivity due to shale content.
Equation 26 Indonesia equation developed by Poupon and Leveaux.
Equation 27 Determination of **a** and $\mathbf{R_w}$ from the Pickett plot equation.
Equation 28 Calculation of hydrocarbon pore volume.
Equation 29 Calculation of original oil in place.
Equation 30 Determination of bulk reservoir volume.

Abbreviations

TOC	total organic carbon
MPI	Methylphenanthrene Index
GC	gas chromatography
Py-GC	pyrolysis-gas chromatography
GC-MS	gas chromatography-mass spectrometry
DST	drill stem test
Pr / Ph	Pristane / Phytane ratio
MFS	maximum flooding surface
CL	cathodoluminescence
SEM	scanning electron microscopy
XRD	X-ray diffraction
bopd	barrels of oil per day
bwpd	barrels of water per day
bbls	barrels
EOR	enhanced oil recovery
OOIP	original oil in place
Ma	million annum

Summary

The Gidgealpa south dome structure in the Eromanga Basin, central Australia is a producing oil and gas field with hydrocarbons sourced from number of sub-surface horizons within the Permian Cooper Basin and Mesozoic Eromanga Basin. Within the Jurassic Birkhead Formation this field has currently reached the end of its primary production and is now moving into the secondary production phase.

Regionally, the Birkhead Formation acts as a seal and the underlying Hutton Sandstone is a major producing reservoir within the Eromanga Basin. The change from reservoir to seal is sharp to transitional across the basin and is accompanied by a change in depositional environment from braided fluvial to fluvial-deltaic and deltaic-lacustrine facies. From Neodymium model age dating and dipmeter interpretation, the decrease in depositional energy is associated with the presence of a significant provenance change from quartzose, craton-derived sediment to lithic rich, volcanic-arc derived sediment.

In sequence stratigraphic terms, the transition from a braided fluvial to a fluvial deltaic depositional environment is separated by a regional sequence boundary within the Hutton Sandstone. Overlying the erosional break are lowstand systems tract sediments, with the beginning of the Birkhead Formation marked by a transgressive surface and decrease in depositional energy. Within the Birkhead Formation the base level continued to rise until the entire Eromanga Basin had been flooded, producing a maximum flooding surface.

The Birkhead Formation at the Gidgealpa south dome has been interpreted as a fluvial-deltaic to deltaic lacustrine depositional environment from facies analysis and embedded Markov chain analysis. These facies include channel fill, abandoned channel, interdistributary bay, crevasse splay, delta mouth bar and lacustrine environments. At the Gidgealpa south dome the progradation

and subsequent retrogradation of a delta sequence into a lacustrine environment has been envisaged as the facies model. The Hutton Sandstone basically consists of channel and abandoned channel fill facies of a braided fluvial sequence.

The delta complex of the Birkhead Formation consists of a number of isolated and partly isolated sand bodies that represent separate delta lobes. The isolated nature of the sand packages has caused reservoir compartmentalisation. Petrological analysis indicates that sediments of reservoir quality are isolated to the high energy, distributary channels. Sediment composition also has a dramatic effect on quality with the volcanic arc derived sediments having very poor to no reservoir quality. The loss in reservoir quality in the volcanic arc derived sediments is due to the abundance of lithics and authigenic cements identified from SEM and XRD analysis that formed from the alteration of labile grains reducing porosity and permeability. Permeability analysis from probe permeability and core plug data indicates that channel fill, over-bank and floodplain facies have good, intermediate and poor reservoir characteristics respectively. Results from core analysis also follow this trend.

The reservoir facies identified from petrology and core analysis was further characterised buy using mercury injection and petrophysics. The analysis allowed for the identification of flow units within the Birkhead Formation reservoir. Reserves estimation and a secondary oil recovery strategy have been determined from the reservoir characteristics.

1 Introduction

This study is concerned with the reservoir characterisation at the Gidgealpa south dome and the sequence stratigraphy of the Eromanga Basin Hutton Sandstone / Birkhead Formation transition. The determination of these parameters require a multidisiplinary approach where the integrated study of sedimentology, chronostratigraphy, sequence stratigraphy, petrology and core analysis are used and interwoven to form a coherent geological model on a local and regional scale. In this light, I have applied the varying disciplines of geological analysis and subsequently gained a greater understanding of the Birkhead Formation at the local reservoir scale and basin wide regional scale. Through reading this thesis I hope that you will also gain the insight that I achieved of the geology of the Birkhead Formation within the Eromanga Basin.

1.1 Aim and Objectives

Initially, SANTOS Limited required the development of a depositional model for the Birkhead Formation at the Gidgealpa south dome to establish sand correlations and define the impact on oil pool distribution. Determination of this information was necessary to extract the maximum amount of hydrocarbons from the geologically complex reservoir that had a rapidly declining production rate. To achieve this successfully the geology on the local scale needed to be related to the regional scale. Relating the Birkhead Formation to the underlying Hutton Sandstone was also an important aspect of the study since this transition will effect hydrocarbon distribution.

From the outset the objectives of this thesis were clear although the exact content to achieve these goals varied as the study progressed. The limitation of information or expansion of ideas while working on the data helped to shape this report. The following objectives are listed in the order that they

occur within this thesis which is the same order that they were approached while undertaking the research, although in most cases these objectives were conducted with significant overlap.

1) Define the sedimentary environment at the Gidgealpa south dome by determining facies and lithofacies present, using embedded Markov chain analysis, dipmeter interpretation and Neodymium model age dating.

2) Define the Birkhead Formation and Hutton Sandstone in terms of a sequence stratigraphic framework regionally and then locally at the Gidgealpa south dome.

3) Conduct a petrographic study on the sediments at the Gidgealpa south dome including SEM, XRD and CL

4) Conduct core analysis on samples from the Hutton Sandstone and Birkhead Formation at the Gidgealpa south dome including Mercury Injection and porosity / permeability characterisation.

5) Combine the above information to determine reservoir characteristics of the Gidgealpa south dome Birkhead Formation reservoir and include log evaluation using petrophysics and the correlation of sand bodies to determine gross sand distribution.

6) Analyse and produce a waterflood strategy based on reservoir characteristics and production history.

2 History of the Gidgealpa and Gidgealpa South Dome Area

The history of the Gidgealpa oil and gas field is well documented in Greer, (1965) and McIntyre et. al (1989), which give an account of exploration and production within the area. This section is a summary of these two papers with further information obtained from well completion reports.

2.1 Location

Gidgealpa is located within the Petroleum Exploration Licenses 5 and 6 (PEL 5&6) of the Eromanga Basin and is close to the southern edge of the Cooper Basin, in the north-east of South Australia. The field is approximately 24 km north-west of the Moomba Gas Plant, 805 km from Adelaide and approximately 1130 km from the other capital cities in eastern Australia (figure 1).

2.2 Pre-Discovery

The first geological information from Gidgealpa and the surrounding area was in the form of an aero-magnetic survey flown in 1961. This did not reveal any sub-surface structure at Gidgealpa but did show a pronounced 'nose', or magnetic anomaly. In early 1963 a refractive seismic survey was shot and revealed two prominent anticlinal features, a north and south dome separated by a saddle with a thick sequence of sediments on the flanks of the anticline. Due to thinning and truncation on the structures, the first well to be drilled on the Gidgealpa structure was on the flank to obtain maximum stratigraphic information. Gidgealpa 1 drilled in 1963, encountered a thick Mesozoic and

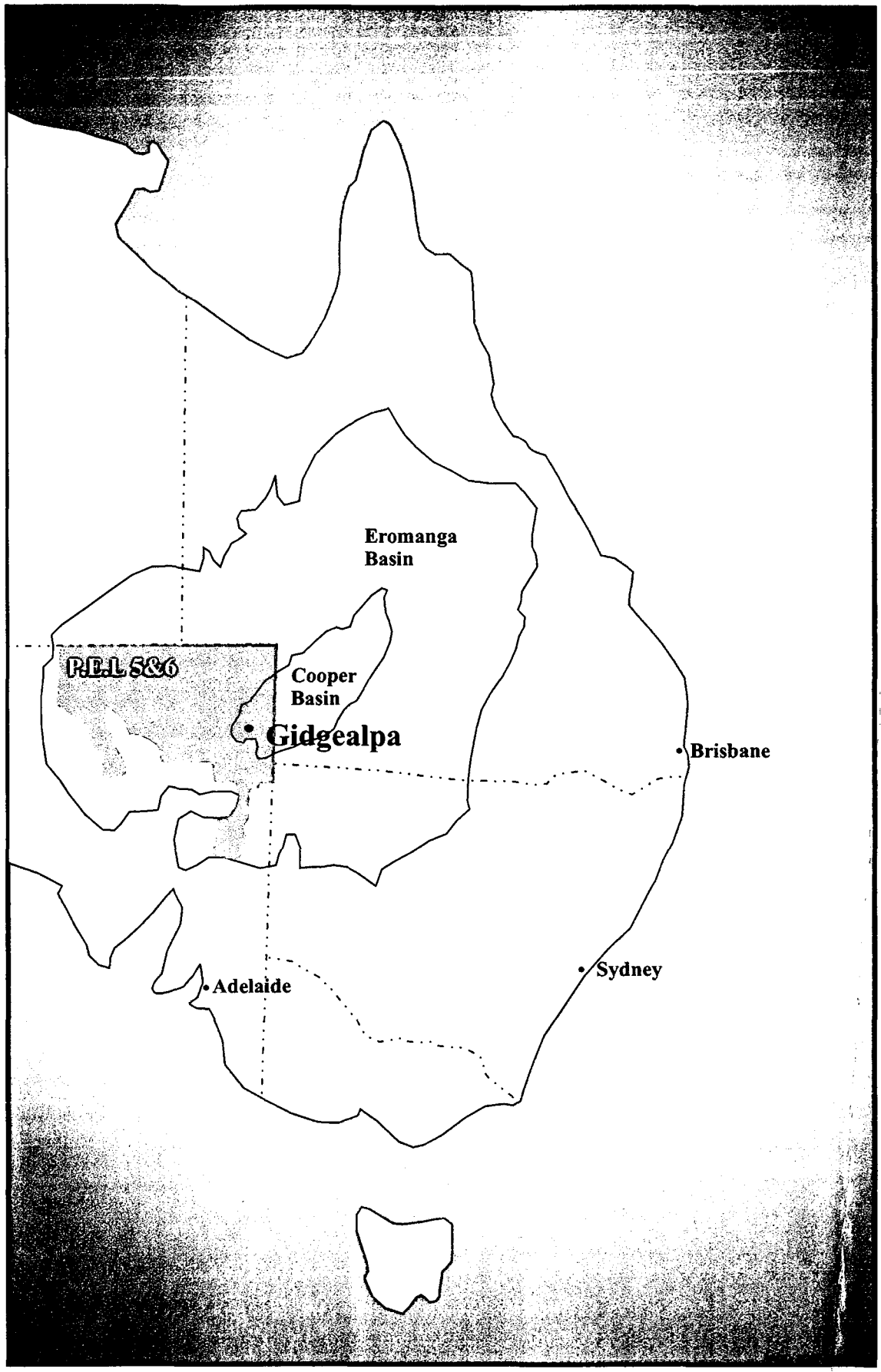

Figure 1 Location map of the Gidgealpa south dome area. The field is located in PELs 5&6 within the Eromanga Basin.

Permo-Triassic sequence underlain by Cambrian carbonates, shale and tuffaceous sediments.

2.3 Discovery and Production

The first hydrocarbons discovered at Gidgealpa was Permian gas within the Toolachee Formation on December 31, 1963 by Delhi Australian Petroleum Ltd and Santos Ltd. The well, Gidgealpa 2, was drilled in the north dome, up dip from Gidgealpa 1. Jurassic oil was discovered in 1984 when Gidgealpa 17 was drilled on the south dome. The time between the discoveries of the Permian and Jurassic hydrocarbons was due to the belief that the aquifer system within the Jurassic had flushed hydrocarbons from structures; for this reason the main exploration effort concentrated on the Permian sequence (Bowering, 1982).

After the discovery of the reservoirs in both the Gidgealpa north and south domes (figure **2**) a series of appraisal wells were drilled to evaluate the size of the accumulations and to explore for more reservoirs within the intervals of interest. A summary of well operations on the Gidgealpa south dome can be seen in table **1**. All wells including those in the north dome are summarised in appendix **1**.

Gidgealpa south dome Hydrocarbon Accumulations

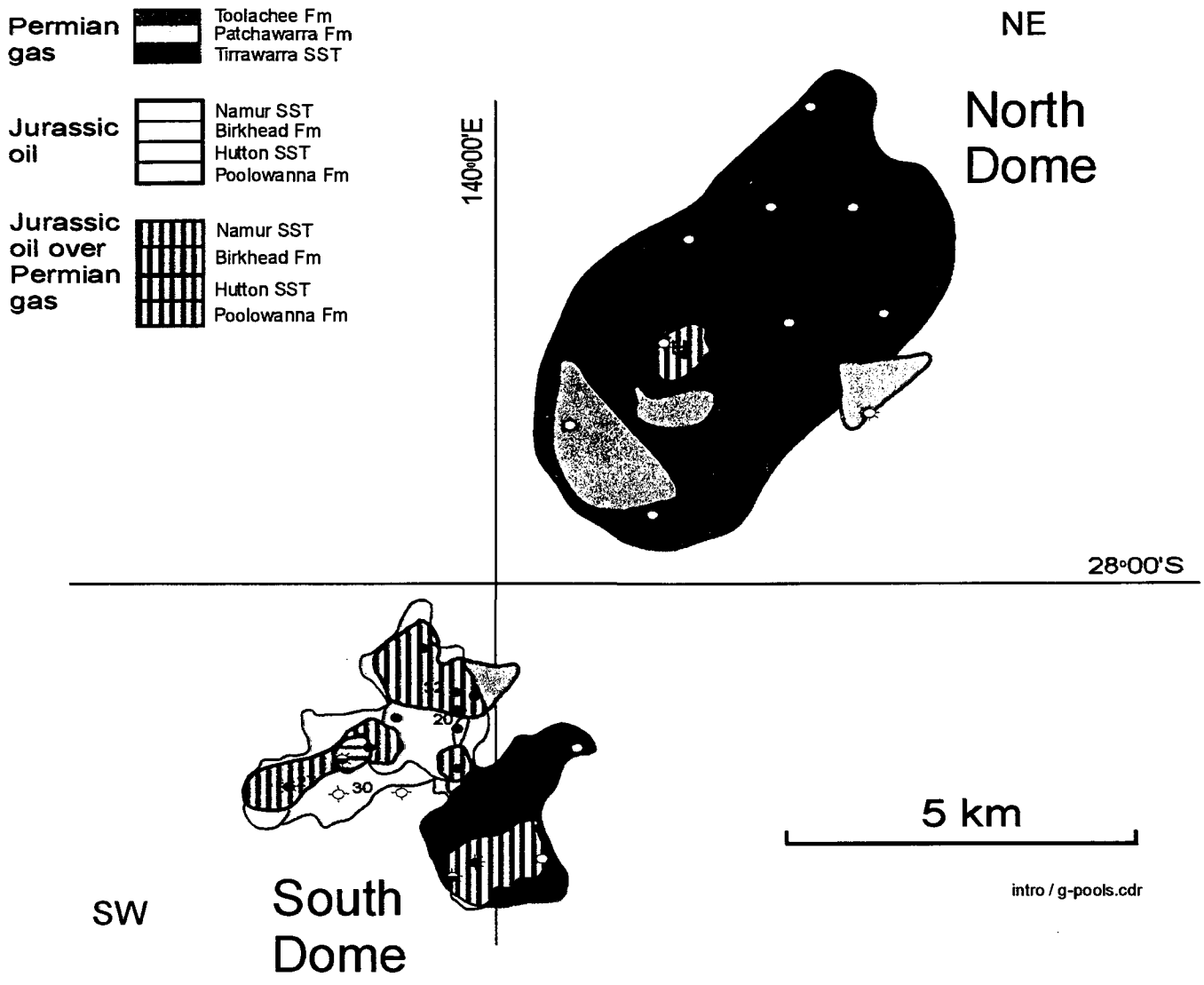

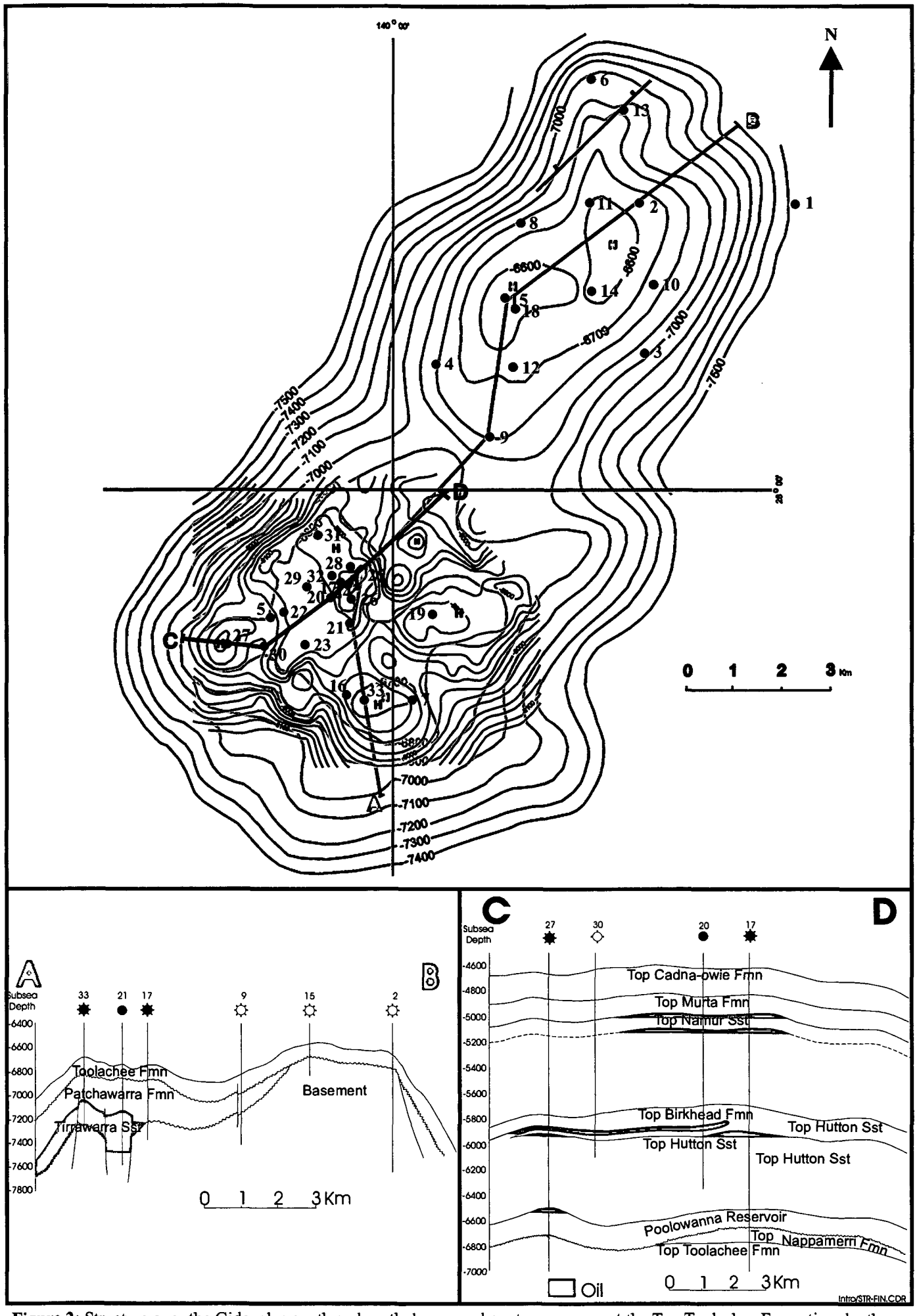

Figure 2: Structure over the Gidgealpa south and north domes, red contours represent the Top Toolachee Formation depth, black contours represent Top Hutton Sandstone depth. Structure cross sections AB and CD are indicated on the structure map (After McIntyre et al., 1989). **Overlay:** map of the Gidgealpa field showing hydrocarbon pools at different stratigraphic levels (from Boult, 1996 , after McIntyre et. al, 1989).

Well Num.	YEAR Drilled	Appraisal/ Explorat'n or Development		PURPOSE	RESULTS
5	1964	*		Appraisal of the Permian section.	Cased as a gas well in the Permian from 7090 to 7193 feet
7	1964	*		Appraisal of Permian sands.	Gas flowed from the top and middle Permian. Well cased for dual completion in the Permian.
16	1979	*	*	Appraisal within the Permian section on the south dome	Well completed in a gas pool within Toolachee Formation , separate to the North Dome pools. Patchawarra had minor HC saturation
17	1984	*	*	Appraisal within the Permian and Jurassic section on the south dome	32' Gas pay in Patchawarra, 3 cores cut and 34' Oil Pay in Hutton, 59' oil pay in Mooga Fmn/Namur Sst.
18	1984	*		Appraisal well for the Hutton Sandstone and secondary Namur Sandstone	Mud and water recovered from the Murta Member. 15 feet pay in Hutton Sandstone, well cased and suspended as a Hutton oil well
19	1884	*		Appraisal well for oil accumulations discovered in Gidgealpa 17 in the Namur Sandstone and Hutton Sandstone	No HCs found in Jurassic. Well drilled into Permian-gas found in the Toolachee and Patchawarra, well cased as a gas well in Toolachee
20	1984	*		Appraisal well for oil accumulations discovered in Gidgealpa 17 in the Namur Sandstone and Hutton Sandstone	Well completed with a dual dual string, triple completion in the Namur (top and mid) and Hutton Sandstones.
21	1984	*		Drilled to appraise Namur and Hutton Sandstones and the Patchawarra Formation	Oil in Namur, Birkhead, Hutton, gas in Basal Hutton, Toolachee and Patchawarra Formations. Cased as Namur/Hutton oil well
22	1984	*		Appraise Hutton Sandstone and Basal Hutton. Secondary objective: appraise HC shows in the Murta Member	HCs found in the Birkhead Formation. All other formations were water wet.
23	1985	*		Appraisal well for oil accumulations discovered in Gidgealpa 17 in the Namur Sandstone and Hutton Sandstone	No pay found, the well was plugged and abandoned.
24	1985	*	*	Well designed to evaluate and develop Namur and Hutton Sandstone	Cased as a dual oil well in the Namur and Hutton Sandstones.
25	1985		*	Well drilled to develop Namur and Hutton Sandstone reservoirs	Well completed as a dual, single string well in the Namur and Hutton Sandstones
26	1986		*	Develop the Namur and appraise the mud Namur, Birkhead and Hutton reservoirs	Core cut in the Birkhead. Well cased and suspended as a Hutton oil producer.
27	1987		*	Well designed to test oil potential of Jurassic (Namur and Hutton) and gas potential in Permian (Tool., Patch, Tirra)	Oil found in the Birkhead Formation. Well cased and completed as a Poolowanna oil producer.
28	1987		*	Well drilled to develop the Namur and Hutton Sandstones and test the limits of the Basal Birkhead Reservoir.	Well suspended pending completion as a Namur/Hutton oil well.
29	1987		*	Development well for the Birkhead oil reservoir	Well cased and suspended as a Birkhead oil producer/injector (for proposed water flood scheme). 60' core over Birkhead interval
30	1987		*	Designed to evaluate the Birkhead oil reservoir and assist in the development of a proposed water flood scheme.	60' core cut from the Birkhead. No HCs found, well subsequently suspended pending completion as a Birkhead injection well.
31	1988	*		Well drilled to evaluate the extent of the oil pool in the Birkhead. Well also drilled as a potential injection site for water flooding.	Well cased and completed as a Hutton oil producer. 60' core cut from the Birkhead
32	1988	*		Evaluate sand channel in the upper Hutton Sandstone. Secondary objectives - appraisal of the Namur and Basal Birkhead.	60' core cut from the Birkhead/Hutton. No oil found in the Namur Sandstone. Well cased and suspended as a Hutton oil producer.
33	1988	*		Appraisal well for the Namur, Birkhead, Hutton Basal Hutton, Tirrawarra, Patchawarra and Toolachee.	180' of net gas pay in the Permian and 30' net oil pay in the Poolowanna Formation. Stratigraphic control obtained.
34	1989	*	*	Appraisal of the Poolowanna Formation and development of the Tirrawarra Sandstone.	60' core in the Poolowanna. Oil pay in the Birkhead, Gas pay in the Toolachee, Patchawarra ,Tirrawarra. Future Permian gas producer
35	1989	*		Appraisal of Tirrawarra, Patchawarra and Toolachee. Secondary targets - Namur, Birkhead and Hutton.	Well cased and suspended as a Permian Gas well.
36	1989	*	*	Jurassic development, Toolachee gas appraisal, Patchawarra gas development and Cambrian exploration	Jurassic oil absent, Toolachee depleted, Patchawarra flowed condensate in a new pool. Cased as future Patchawarra gas Producer
37	1990		*	Well drilled as a Jurassic oil Development well.	Pay mapped in the Namur and Hutton. Well cased an completed as a Namur oil Producer.
40	1990	*	*	To appraise Hutton oil and Permian gas.	Oil shows in Birkhead. 14' oil pay in Hutton. Gas pay in Toolachee, Patchawarra. Cased and suspended for prod. In Hutt, Tool and Patch.
41	1990	*		Provide drainage point in Tirrawarra. Appraisal of Namur, Hutton, Birkhead, Poolowanna Toolachee and Patchawarra.	Gas found in Tirrawarra and Patchawarra. Well completed as a Tirrawarra oil and gas producer.
42	1991	*		Appraisal of Tirrawarra and Hutton. Namur, Birkhead, Poolowanna, Toolachee and Patchawarra secondary.	90' core from the Tirrawarra. Net oil pay in Namur, Hutton and Tirrawarra. Net gas in Toolachee and Patchawarra.
43	1991		*	Appaisal of Namur, Birkhead and Tirrawarra oil. Gas appraisal in the Toolachee, Patchawarra and Poolowanna	Permian section water saturated. Net pay within the Hutton and Namur. Well suspended as a future Hutton/Namur producer?
44	1991	*	*	Well drilled for Hutton development and Tirrawarra appraisal.	Large core in Permian. Net oil pay in Hutton and Toolachee. Gas pay within Toolachee. Well cased and suspended for later completion.
45	1991	*	*	Evaluate Hutton and Namur for unaccessed oil. Appraisal of the Poolowanna.	Net oil pay in Hutton and Namur. Well cased and completed as a Namur/Hutton oil well.
46	1991	*	*	Hutton oil development. Appraisal in the Namur, Birkhead, Poolowanna, Toolachee and Patchawarra.	Oil pay in Poolowanna, Birkhead, Hutton and Patchawarra. Gas pay in Toolachee and Patchawarra. Well suspended to be a permian producer.
48	1991	*	*	Development of the Hutton and Namur. Appraisal of the Poolowanna.	Net oil pay in the Hutton and Birkhead. Well cased and completed in the Hutton.
49	1991	*	*	Development of the Hutton. Appraisal of the Tirrawarra.	Net oil pay in Hutt, Pool, Tirra. Gas pay in Nappa, Tool, Patch, Tirra. Cased and suspended as a Jurassic/Permian producer.
50	1991		*	Development of Hutton. Secondary development of Namur and Birkhead.	Net oil pay in Birkhead. Cased and suspended as a future Birkhead oil Producer.
51	1991	*		Appraisal of the Patchawarra. Secondary objectives - Namur, Hutton, Poolowanna, Toolachee and Tirrawarra.	Net gas pay in Patchawarra and Toolachee. Well cased and suspended as a future Patchawarra gas producer.
52	1991	*		Appraisal of Toolachee, Patchawarra.	Net oil pay in Hutton/Birkhead. Net gas pay in Toolachee. Well completed as a Hutton oil producer.
53	1993			Appraisal of crest Hutton and Namur seen on 3D seis. Birkhead, Poolowanna, Toolachee and Patchawarra - 2ndary targets.	Only trace shows found. Well plugged and abandoned.
54st	1993	*	*	Development of Namur, and Hutton. Secondary target - Birkhead. Appraisal of Tirrawarra, Toolachee and Patchawarra.	Cores cut in the Tirrawarra. No pay found. Well plugged and abandoned?
55	1993		*	Development of Hutton Sandstone with secondary targets in the Birkhead Formation and Poolowanna Formation.	Fluorescence shows in the Namur, Birkead, Hutton, Toolachee. Oil pay in Poolowanna. Well plugged back and deviated as Gidgealpa 55A
56	1994		*	Namur was the primary target with the Birkhead Formation and Hutton Sandstone secondary objectives	9' net pay in the Namur sandstone. Birkhead section was uneconomic and the Hutton was water wet. Well completed as a Namur producer

Table 1: Summary of well development at the Gidgealpa south dome.

3 Local Geology

3.1 Gidgealpa Structure

The Gidgealpa field consists of an asymmetric anticline of moderate relief within the upper Permian and Mesozoic sections, the anticline forms two structural closures within a northern and southern area, termed the north dome and south dome respectively (McIntyre et. al, 1989). These two domes are separated by a shallow saddle which formed from basement associated faulting (figure **2**). The associated basement faulting is part of a number of fault blocks which have moved in the Early Permian and throughout Cooper Basin and Eromanga Basin time. In doing so the movement has affected deposition in the Permian and Jurassic sections. The Gidgealpa field is located on the south western part of the north-east / south-west trending, north-east plunging crest of the Gidgealpa-Merrimelia-Innaminka ("GMI") Ridge; figure **3** shows regional structural trends as well as the other fields associated with the GMI Ridge.

3.2 Regional Structural Framework of the Eromanga Basin

From 515 Ma to 95 Ma convergent plate-margin tectonics have been in operation in eastern Australia and the eastward migration of arc complexes resulted in superposition of gently subsiding cratonic down warps on previously active back-arc basins (Veevers, 1984). The formation of the Eromanga Basin occurred between the Late Permian / Early Triassic and is one of two major down warps (Moore, 1986, Roberts et. al, 1990) which occurred in eastern Australia, the first down warp occurring before the accumulation of sediments in the Cooper Basin. The formation of the basin is directly related to Late Paleozoic tectonic events with Mesozoic sediments draping over older structures (Moore, 1986). Most tectonic events which

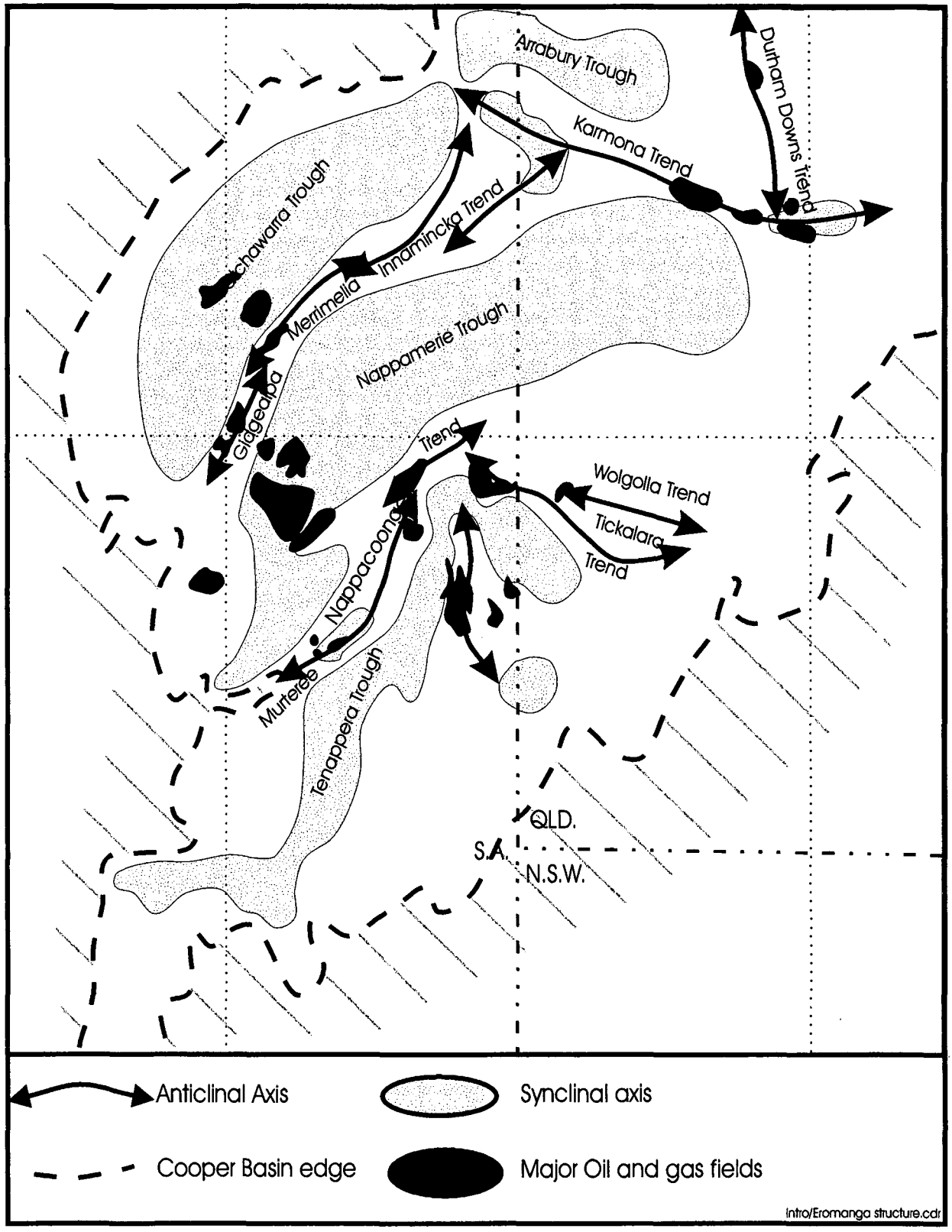

Figure 3: Regional structural elements of the south western Cooper/Eromanga Basin area with major oil and gas fields (from Theologou, 1995, modified after Thornton, 1979).

occurred in the eastern part of Australia throughout its history of formation were related to Australia wide tectonic events (figures **4** and **5**).

Around Early Cambrian time (approx. 545 Ma) the eastern part of Australia was controlled by divergent plate tectonics along the Tasman Line (Figure **6**) which separated the stable Precambrian, western part of Australia from the eastern Phanerozoic terrain (Veevers, 1984). This rifting was part of the Pangea super continent breakup producing smaller continents such as Laurasia and Gondwanaland (Baillie et. al, 1994). The precursor to the Cooper / Eromanga Basin is the Cambrian-Ordovician Warburton Basin (figure **5**). This basin formed at the time of divergence along the eastern margin with the presence of volcanics seen right along the Tasman Line (Roberts et. al, 1990), and was thought to be caused from a relief of stress by the conversion of intra-plate shear to plate divergence (Veevers, 1984).

In the Late Cambrian, during Templetonian time (approx. 515 Ma) there was a change in the tectonic regime along the eastern margin of Australia from divergence to periodic convergence lasting up to the Late Cretaceous Cenomanian time (95 Ma) (Veevers, 1984, Baillie et. al, 1994). The first convergent period lasted 15 Ma with the accretion of parts of the eastern margin and associated intrusion of granitoids. When convergence commenced once again in the early Ordovician the island arc had moved a significant distance eastward. The Late Devonian saw another period of deformation with the whole region forming part of a foreland and epicratonic basin with the bulk of the sediment fill consisting of quartzose clastics from the Precambrian craton to the west of the Tasman Line (Veevers, 1984).

The movement of Australia from low to high latitudes in the mid Carboniferous caused the whole of the Australian continent to become glaciated. The massive ice sheet covering the continent at that time started to melt in the latest Carboniferous / early Permian and was followed by regional

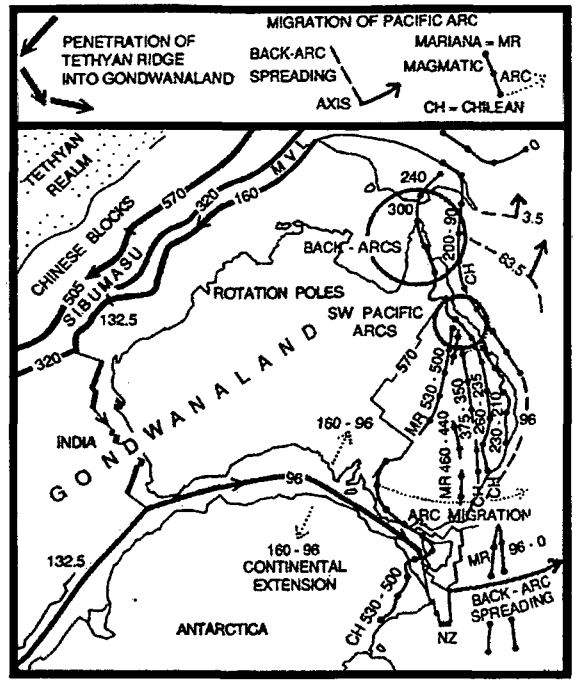

Figure 4: The pattern of spreading around Australia (after Veevers et. al, 1991). "The pattern of spreading around Australia was determined by two long standing (Phanerozoic) factors that operated in a counter-clockwise direction; (1) penetration from the NW by the Tethyan divergent ridge; and (2) rotation from the NE of the Pacific convergent arc and back-arc. The larger dotted circle indicates the rotation poles of the back-arc spreading in the Tasman Sea (dotted arrow indicates spreading direction) and the smaller dotted circle the node of the precursor Palaeozoic and Early Mesozoic arcs (dotted arrow indicates arc migration). Terranes along the Tethyan margin are Chinese Blocks, China-Burma-Malaya_Sumartra (SIBUMASU) blocks and the Mt Victoria Land (MVL) block."

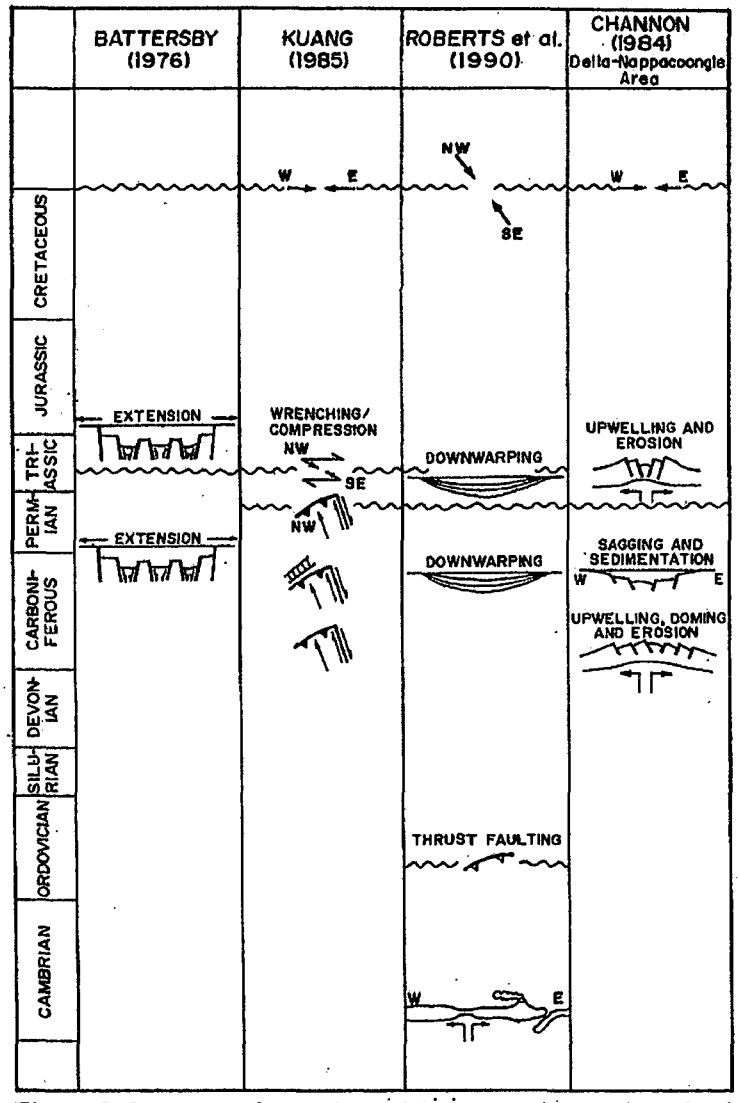

Figure 5: Summary of tectonic models from various authors for the evolution of the Cooper/Eromanga Basins (Boucher, 1991).

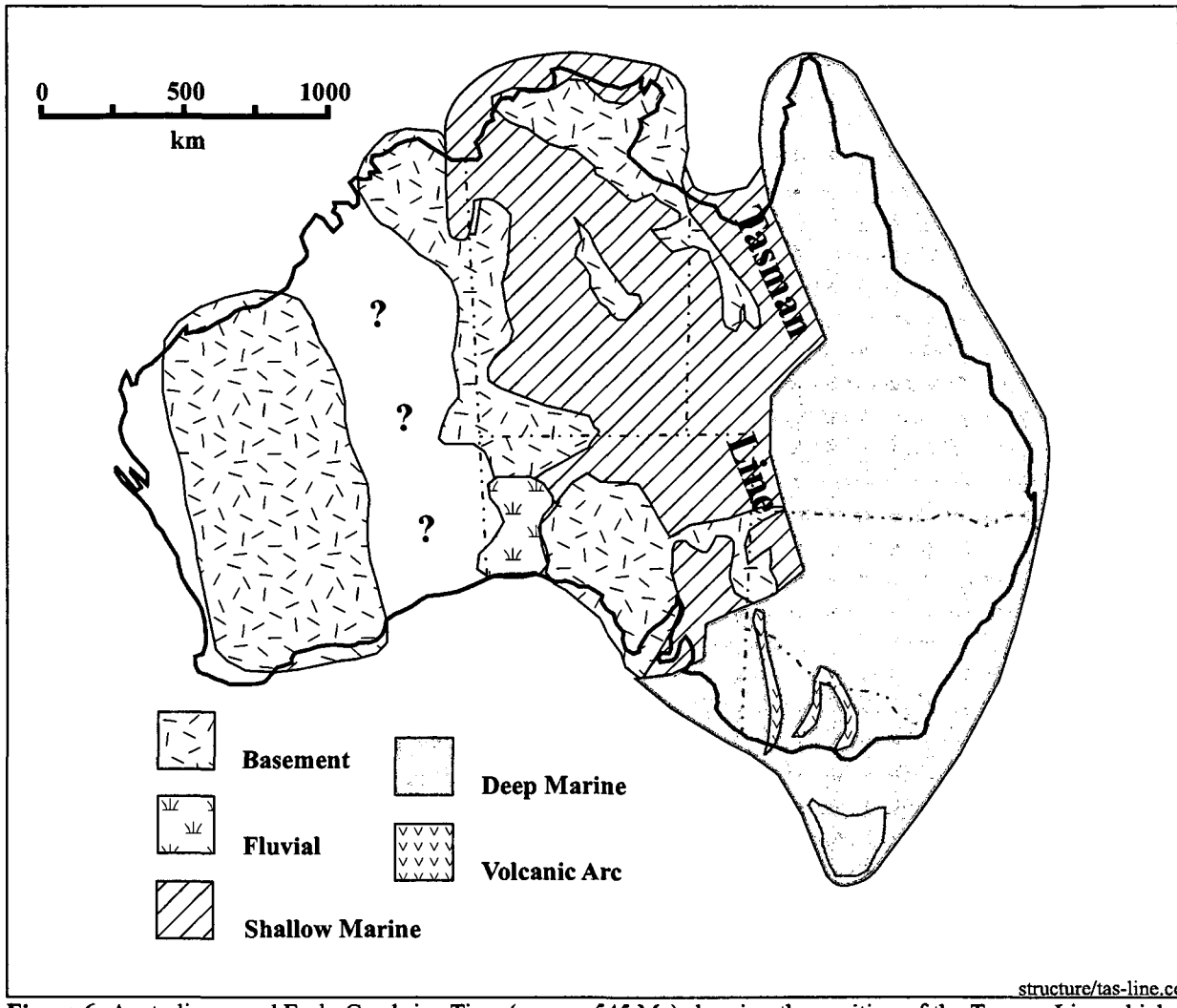

Figure 6: Australia around Early Cambrian Time (approx 545 Ma) showing the position of the Tasman Line which marked the eastern edge of the continent. This figure also illustrates the extent of basement rock, volcanics and sediments. At this time the eastern part of Australia was dominated by divergent plate tectonics (after Roberts et. al, 1990).

uplift that caused major erosion and subsequent deposition of sediments (Veevers, 1984, Elliott, 1993, Baillie et. al, 1994). Deposition of fluvial-glacial sediments that occurred in the interior basins of central and Southern Australia, formed in the mid Carboniferous. The mid Carboniferous also marks the time of collision between Gondwanaland and Laurasia.

After the initial jump eastwards of the magmatic arc in the Late Carboniferous, it virtually stayed in the same place up to the Early / Middle Triassic. Associated with this jump was the formation of the foreland Bowen-Sydney Basin (Veevers, 1984). Further to the west crustal down warping caused sediments to accumulate in the epicratonic Cooper and Galilee Basins that underlie the central part of the Eromanga Basin. The cause of the down warp was believed to be due to a north-west / south-east and then east-west compression as shown in figure 7 from oblique slip on the plate boundaries (Moore et. al, 1986). These events plus similar stresses throughout the basins history has produced north-east / south-west and north-south oriented structures (figure **8**) (Apak et. al, 1995).

The Permian saw the persistence of the Australian continent at high latitudes up to the Triassic (Veevers, 1984, Baillie et. al, 1994). At the end of this period another structural event occurred with the uplift of the foreland and epicratonic basins that was related to the further break up of Pangea. This break up marks the boundary between the Cooper / Bowen and Eromanga / Surat successions. Structures within the Eromanga and Surat Basins were formed from re-activation of the older structures. The re-activation caused the formation of subtle drape within the basins, which then subsequently compacted with sediment loading (Moore et. al, 1986). Regional tilting during this period saw the slight displacement of the Eromanga depocentre from the Cooper Basin depocentre to the north-east (Wecker, 1989).

In the Early to Middle Jurassic, the eastern section of Australia started to sag (Elliott, 1993) and magmatic-arc activity became prevalent again. By the end

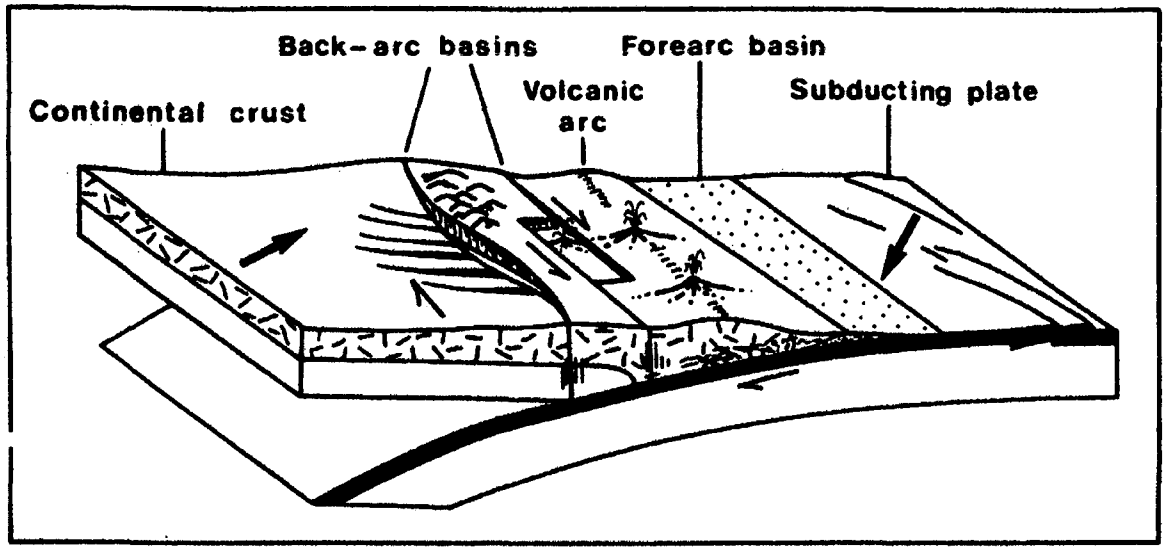

Figure 7: Model of the compressional tectonics along a convergent margin that caused the formation of the Cooper and Galilee Basins in the Early/Middle Triassic (from Moore et. al, 1986).

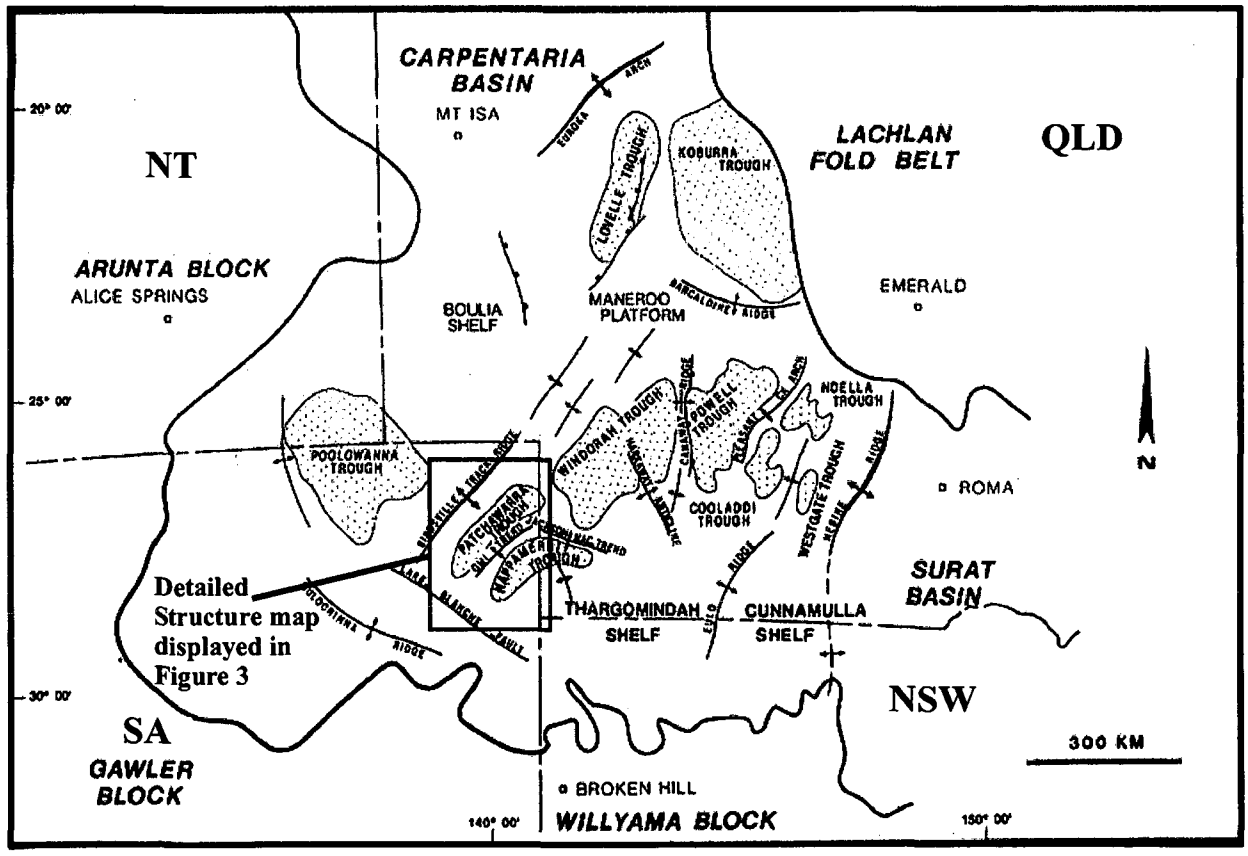

Figure 8: NE-SW and N-S structural trends of the Eromanga Basin from northeast-southwest and east-west compression during the Early/Middle Triassic (after Wecker, 1989).

of the Middle Jurassic (160 Ma) volcanic sediment from the activity was shed over the Surat Basin and Eromanga Basin (Veevers, 1984). Further pulses of volcanic sediment in between craton derived clastics occurred as a result of fluctuating volcanic arc activity (Moore et. al, 1986). Convergence at this time also terminated around the Cretaceous Cenomanian (95 Ma) relating to the break up of Gondwanaland and the eastern margin of Australia becoming divergent (Moore et. al, 1986, Veevers, 1991, Baillie, 1994). The last significant phase of structural development in eastern Australia occurred some time between the Late Cretaceous and Tertiary (Elliott, 1993). Figure **9** shows a summary of the important structural features and events as well as latitudinal variations of the Australian continent during the Late Jurassic to Late Cretaceous.

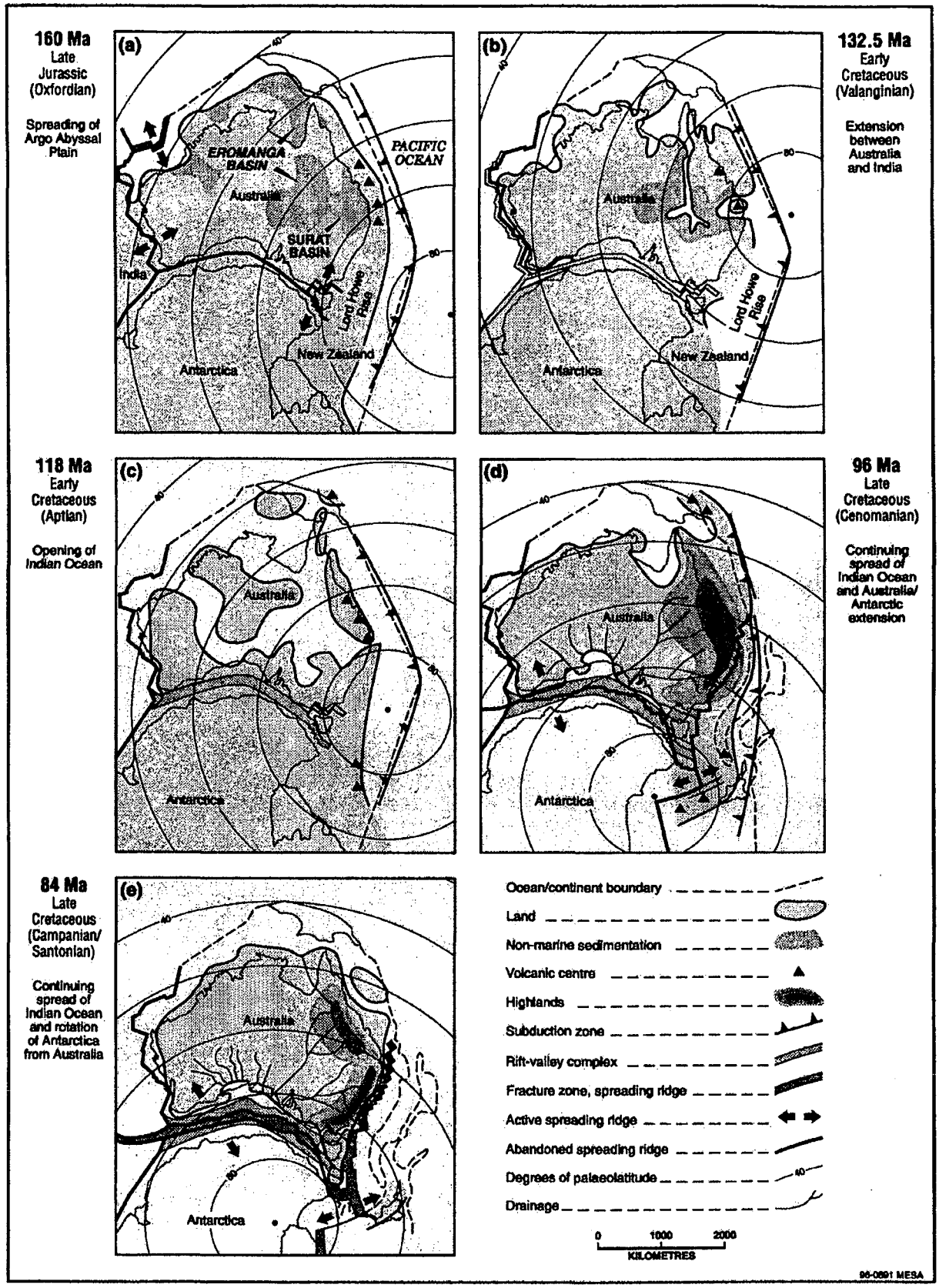

Figure 9: Palaeogeographic change of the Australian continent through the Jurassic to Cretaceous (From Alexander and Sansome, 1996, After Veevers et. al, 1991 and Baillie et. al, 1994).

3.3 Stratigraphy of the Eromanga Basin

3.3.1 Introduction

The main focus of this study is on the Hutton Sandstone and Birkhead Formation within the Eromanga Basin; for this reason the stratigraphy of the basins underlying the Eromanga Basin intersected at the Gidgealpa south dome (figure **10**) will be discussed only briefly here. The underlying basins consist of the Cambrian to Ordovician Warburton Basin and the Carboniferous to Triassic Cooper Basin.

3.3.2 Warburton Basin

The Warburton Basin formed as a result of stress relief from the conversion of intra-plate shear to plate divergence that caused the formation of the continental breakup along the Tasman Line (figure **6**, page 12). The Basin sediments sit on igneous rocks of Precambrian age. Above the basement are Early Precambrian volcanics such as tuffs interbedded with dolomite and sandstones (Gatehouse, 1986). Sediments of Middle to Late Cambrian age within the basin have been interpreted as carbonates and shales. Some of the shales have been found to be highly tuffaceous (McIntyre et. al, 1989). At the end of the Cambrian the volcanics ceased with the deposition of sandstones, siltstones and black pyritic shales in the Ordovician. Also of an uncertain age are a set of calcareous, red sandy shales with micaceous mudstones (Gatehouse, 1986).

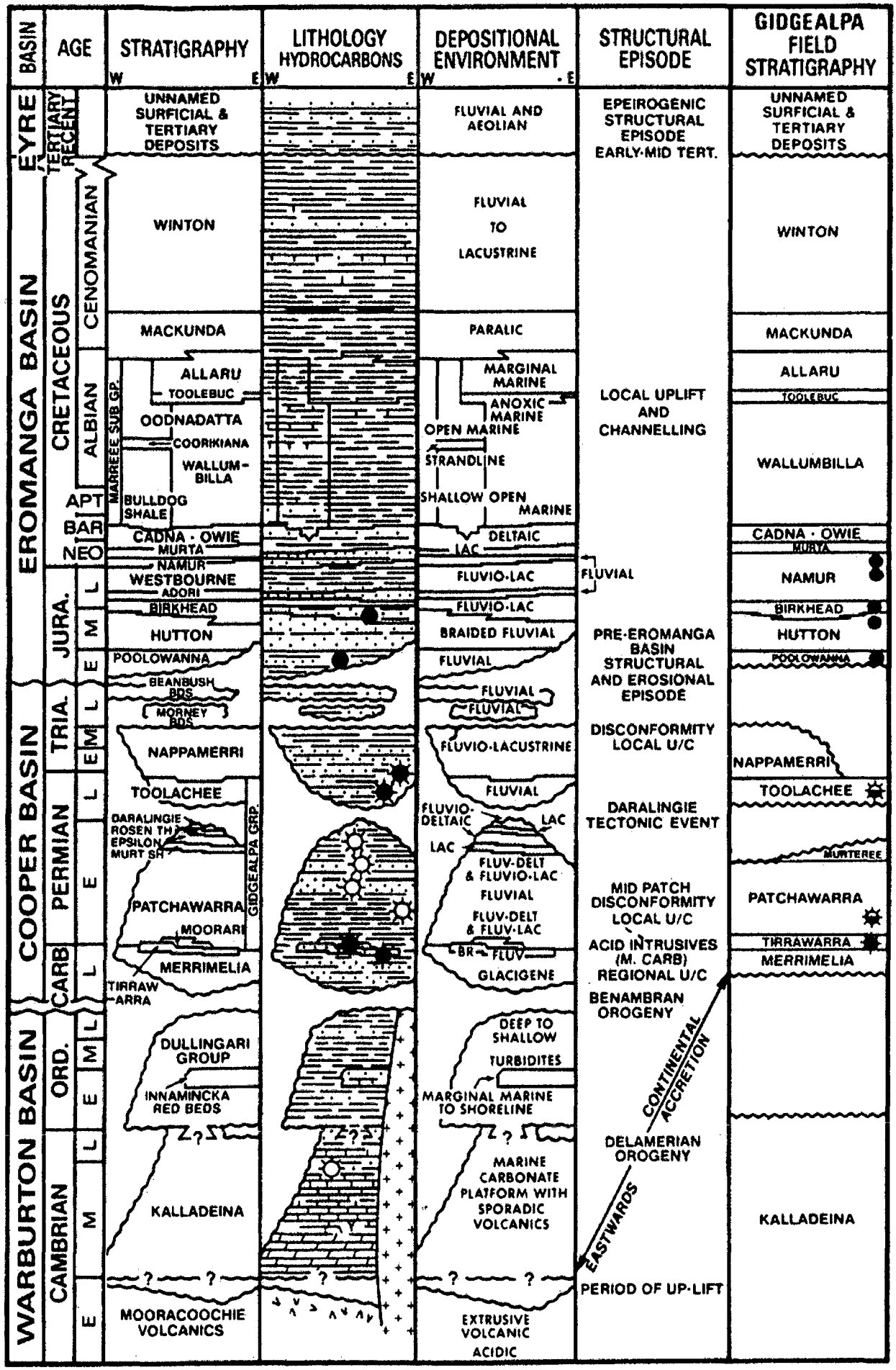

Figure 10: Stratigraphic section of the Warburton, Cooper and Eromanga Basins for the Gidgealpa area (From McIntyre et. al, 1989).

3.3.3 Cooper Basin

The Cooper Basin is Late Carboniferous to Early Triassic in age and overlies the Warburton Basin and Carboniferous igneous rocks (Gatehouse, 1986). The basin is mildly compressional with north-east, north-west, north-south and east-west structural elements. The main structural trends in the Cooper Basin are the north-east / south-west Gidgealpa-Merrimelia-Innamincka Ridge, the Nappacoongee-Murteree Trend and north-west trending lineaments. These features are considered to be the main structural elements that had a strong control on basin development (Apak et. al, 1995). The large structural trends are thought to have formed during the pre-Permian compressional regime and are reactivated thrust faults within the Cooper Basin (Apak et. al, 1995, Alexander and Sansome, 1996). Troughs exist between the structural highs that have accumulated over 2000 m of sediment (Wiltshire, 1989, Alexander and Sansome, 1996).

Sediments within the basin consist of stacked non-marine depositional sequences starting with the glacial and periglacial coarse clastics of the Gidgealpa Group Merrimelia Formation deposited unconformably on the Warburton Basin (Wiltshire, 1989). Above the Merrimelia Formation is the Tirrawarra Sandstone representing a braided fluvial to proglacial outwash environment that is covered by peat swamp and floodplain facies of the Patchawarra Formation (Alexander and Sansome, 1996). Towards the top of the Gidgealpa Group are a number of formations starting with the lacustrine Murteree and Roseneath Shales, which are interleaved with the Epsilon and Daralingie Formations, the interleaving was caused by base level changes and changing depositional gradients. (Apak et. al, 1995). During the Early Permian an unconformity formed on top of the Daralingie Formation due to uplift, folding and faulting. Above this unconformity the stacked fluvial channels of the Toolachee formation cap the top of the Gidgealpa Group

sediments. Conformably overlying the Toolachee Formation are the Nappamerri Group sediments consisting of fluvial successions and a red-bed sequence (Apak et. al, 1995, Alexander and Sansome, 1996).

3.3.4 Eromanga Basin

3.3.4.1 Introduction

The Eromanga Basin has been described as an intracratonic down warp or sag basin (Moore et. al, 1986) with its formation caused by crustal or epeirogenic down warping that followed a phase of extensional tectonism in the Early to Middle Triassic. According to Wecker (1989) this tectonism was the cause of the development of the Eromanga Basin. The basin is of Early Jurassic to Late Cretaceous age with sediments being deposited relatively continuously over a wide area. (Alexander and Sansome, 1996). Depositional environments as well as the provenance of sediments was influenced by a volcanic arc off the present coast of Queensland and on the southern margin by the separation of Australia and Antarctica (Veevers, 1984, Alexander and Sansome, 1996) (figure **4**, page 11). Sediments originating from the southern margin of the basin consisted of braided and windblown fluviatile sandstones (Wiltshire, 1989) with minor shales. While from the eastern margin they consisted of sandstones, siltstones, and coals of a meandering fluvial to floodplain / lacustrine nature (Moore et. al, 1986, Wiltshire 1989, Alexander and Sansome, 1996). These two types of sediments alternate within the basin and are defined by different formations (figure **11**). The gentle down warping style of the basin allows for easy identification of sequence stratigraphic units and allows for a greater understanding of the depositional systems.

The two main depocentres within the Eromanga Basin are the Poolowanna, Nappamerri and Patchawarra Troughs (figure **11**), these palaeo-lows are a result of structural lineaments reflected in the basin from the Permian and Triassic with further compaction of the older sediments emphasising the

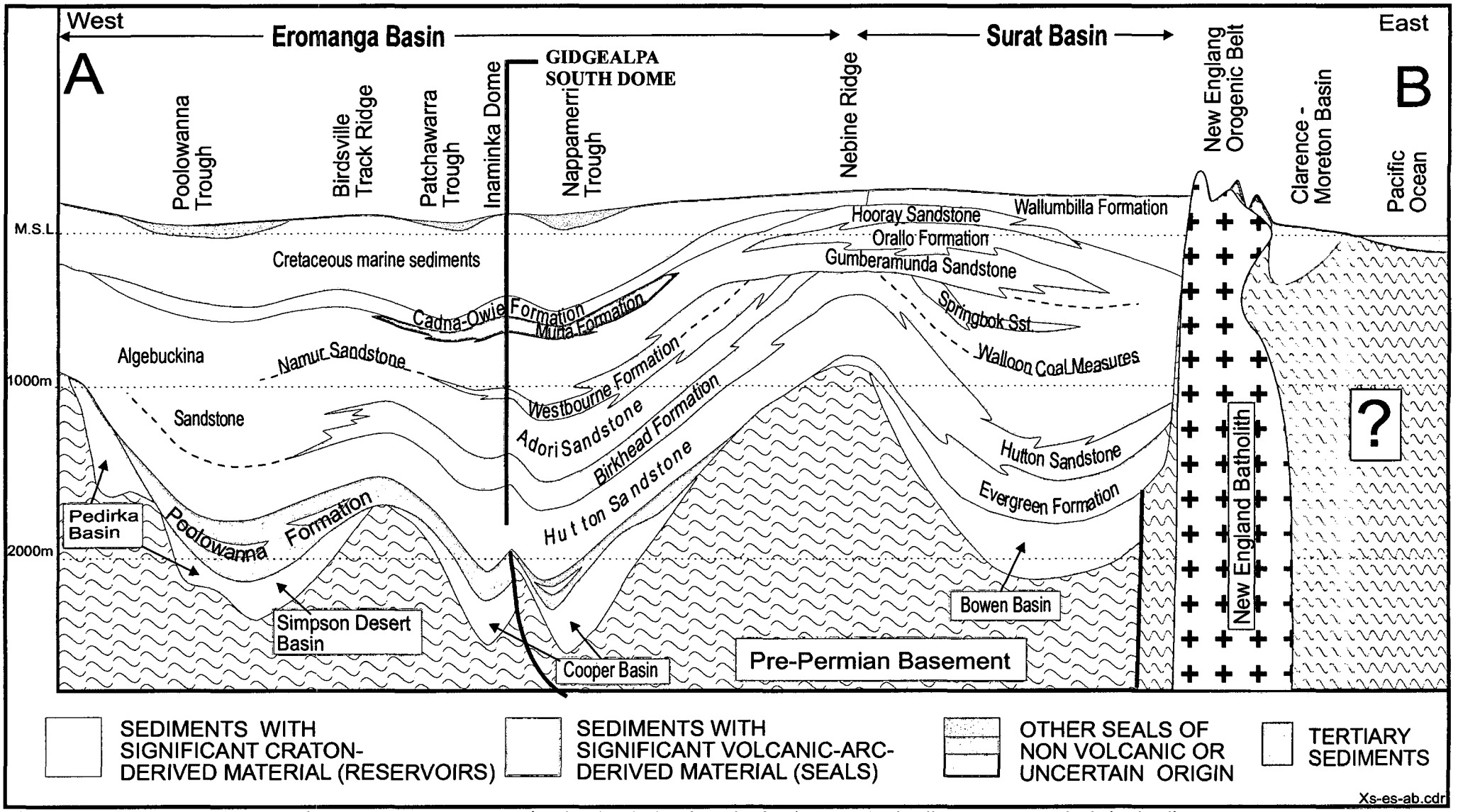

Figure 11: West to east cross section of the Eromanga and Surat Basins showing the interleaved volcanic-arc-derived sediments and cratonic-derived sediments (Modified from Boult, 1996, originally drafted by Theologou).

earlier structural grain (Wecker 1989). Sedimentation in the Eromanga Basin terminated in the Late Cretaceous with erosion and uplift and then the deposition of the Eyre Basin sediments.

3.3.4.2 Poolowanna Formation

The first deposition of sediments within the Eromanga Basin consisted of a series of low to moderate energy streams with lakes and swamps. Based on the lithological association and the presence of fining upwards cycles the depositional environment is interpreted to be meandering fluvial (Bowering 1982, Moore, 1986). These sediments are unconformable with the underlying Simpson Basin, Cooper Basin, Pedirka Basin and Warburton Basin or lie on basement rocks (Alexander and Sansome, 1996). The formation was first deposited in the Simpson Desert region and either pinches out, or passes laterally into the Hutton Sandstone to the east of the Birdsville Track Ridge (Moore, 1986). To the east, facies of a similar nature are developed sporadically at the base of the Eromanga Basin sequence and are considered to be of a similar nature to the sediments to the west of the ridge. The distribution of the facies was controlled by palaeotopography on the Late Triassic unconformity surface. The sediments are referred to as the 'basal Hutton' in Queensland (John and Almond 1987, John 1990, Alexander and Sansome, 1996). Poolowanna Formation sediments consist of interbedded sandstones, siltstones, shales and coals. Sandstones are commonly fine grained, labile to quartzose with occasional beds of granule and pebble conglomerates (Moore, 1986, John and Almond, 1987, Alexander and Sansome, 1996) Shales and siltstones are mid to dark grey and usually evenly laminated (Moore, 1986).

3.3.4.3 Hutton Sandstone

Sediments of the Hutton Sandstone were deposited during the Lower to Middle Jurassic. The lower boundary intertongues with the Poolowanna facies

or unconformably lies on the Cooper Basin and Warburton Basin sediments or on metamorphic or granitic basement (John and Almond, 1987, Alexander and Sansome, 1996). The Hutton Sandstone has been interpreted to be a sequence of stacked fluvial channels deposited in a high energy braided fluvial environment (Gravestock et. al, 1983, John and Almond, 1987, Salomon et. al, 1990). However more recently Wiltshire (1989) noted that the palaeoslope for the deposition of the low sinuosity sediments was not adequate to maintain this type of deposition and suggested that there was no substantial drainage exit at the time of deposition. Wiltshire (1989) hypothesised that the sediments initially entered the basin via braided fluvial streams and then were re-distributed by aeolian processes.

Paleoflow of the braided-fluvial streams carried sediments to the north-east and neodymium age dating indicate model ages between 1400 and 1900 Ma (Lanzilli and Boult 1996), which suggest that the Gawler Craton, and surrounding areas, (having a similar Sm/Nd model age) are the main sources of sediment. Moore et. al (1986) has suggested sediments have also originated from cratonic areas in the Northern Territory.

The formation has been divided into two units by Gravestock (1983) who interpreted the lower unit 'Unit 2' to be deposited relatively continuously and the upper Unit 'Unit 3', to have been deposited episodically with duricrusts formed during the depositional breaks. These two units may be conformably related, or Unit 3 may be thin or absent in areas of complex structure. Unit 2, Hutton Sandstone sediments consist of very fine to very coarse, slightly feldspathic, mineralogically mature quartzarenites, with monocrystalline quartz being the most abundant framework grain (Gravestock, 1983, John and Almond, 1987, Wecker 1989). Polycrystalline quartz is also present, originating from the erosion of schists and gneisses. Volcanics, carbonates and shales are absent from the sediments, microcrystalline feldspar is a minor constituent, heavy minerals such as zircons and garnets are in trace amounts (Gravestock, 1983). Unit 3 is distinguished from unit two by the presence of

siliceous and carbonate cements, otherwise the two units are mineralogically the same. Planar cross-bedding and horizontal bedding are common, in-channel sand and gravel bars, crevasse splays and abandonment fills within the Hutton Sandstone have also been described (Gravestock, 1983).

3.3.4.4 Birkhead Formation

The Birkhead Formation was deposited in the Middle to Late Jurassic (Paton, 1986) as interbedded dark grey / brown siltstones and mudstones with generally fine grained, grey to buff coloured sandstones and lenticular coal seams (Alexander and Sansome, 1996). The sediments also represent a marked facies change from low sinuosity braided fluvial to high sinuosity meandering fluvial environments (McIntyre et. al, 1989). In contrast to the Hutton Sandstone, this formation is lower energy and consequently consists of mainly floodplain deposits with fluvial channel and point bar deposits, minor levee bank, crevasse splay and coal swamp deposits (Boult, 1993). Siltstones and mudstones vary from laminated to massive to slumped and may also contain root casts and dewatering structures. Generally fine-grained sandstones consist of ripple cross or horizontal laminations or are massive. Larger grained sandstones are commonly trough to planar cross-bedded and contain coal fragments and clay casts. Pebble lags and intraclast breccias are also present (Alexander and Sansome, 1996).

It has been established that the Birkhead Formation was deposited from an easterly flowing fluvial system by Veevers (1984), Paton (1986), Watts (1987), Wecker (1989) and Salomon et. al (1990). Burger (1986) considers the change in energy to be related to rising sea level, this rise increased the accommodation space and lowered the depositional energy within the basin to meandering fluvial. However Watts (1987), Veevers (1984) and Paton (1986) believe that the change in energy was in fact caused by a blockage or restriction of the drainage system resulting in a base level rise of the lacustrine

lake that was isolated from the sea. The restriction of the system appears to be the result of the influx of volcanogenic sediment. It has been determined that the source of the volcanogenic sediment in the Birkhead Formation was an active volcanic arc off the coast of Queensland. Sediments were shed from this arc during intense arc activity and transported by fluvio-deltaic systems (Watts, 1987, Salomon et. al, 1990).

It is also possible that this arc activity was related to global tectonics which effects the changing sea level and thus may appear that the basin at this time is affected by sea level changes (Watts, 1987). Yet another theory is suggested by Wiltshire (1989) who believes that climate change may have been cause.

The boundary between the Hutton Sandstone and the Birkhead Formation has commonly been picked as the 'top of porosity' within the Hutton Sandstone using wireline logs (Paton, 1986, Watts, 1987, McIntyre et. al, 1989). The boundary has also been chosen by the appearance of lithic or mixed type sandstones (Watts, 1987). These changes in sediment types can easily be seen in hand specimen and by petrological studies. The boundary varies in different areas from transitional (eg Bodalla (Boult, 1993)) to sharp or erosional (eg Kenmore (Watts, 1987) (Paton, 1986, Salomon et. al, 1990)).

Generally the Birkhead Formation can be distinguished from the Hutton Sandstone by a change in sediment type. 'True' Birkhead Formation type sediments consist of labile, lithic sediments from a volcanic source while Hutton Sandstone sediments are comprised of quartzarenites from a cratonic source (Boult, 1993). Sediments shed from the volcanic arc off the eastern coast of Australia are very fine to medium grained lithic arenites. They consist of up to 50% quartz and also have relatively high percentages of potassium and plagioclase feldspar and lithic fragments consisting of labile minerals. Normally the lithic fragments are highly altered to kaolinite and chlorite or are replaced by carbonate cements such as siderite or dolomite. Glassy fragments have also been seen but usually are rare due to alteration. The composition of

the sandstones suggest that the volcanic arc that existed during the time of Birkhead Formation deposition to the east is a tectonically mobile belt containing volcanics (acid to intermediate), regional metamorphics and meta-sedimentary rocks. Tourmaline, pyroxene, mica, zircon and feldspars are present in trace amounts (Watts, 1987, Alexander and Sansome, 1996).

Paton (1986) divided the Birkhead Formation into 3 units consisting of sediments deposited in a meandering fluvial environment (Unit 1 (basal Birkhead Formation)), coal swamp to lacustrine environment (Unit 2 (mid Birkhead Formation)) and a meandering to braided fluvial environment (Unit 3 (top Birkhead Formation))(figure **12**). Unit 1 sediments were deposited in a floodplain to delta plain environment. With an increase in water depth a widespread lake formed (unit 2) depositing coals and shales within a marginal lake and lacustrine environment. Although the Birkhead Formation lake was almost wholly fluvial there is evidence that conditions may have been brackish near the Euroka Arc where the Eromanga Basin connects to the Carpentaria Basin from the identification of rare spinose acritarchs (Burger, 1986). At the conclusion of Unit 2 deposition, Unit 3, high energy fluvial sediments filled Lake Birkhead.

The Birkhead Formation has been thought to extend to the edge of the Birdsville Track Ridge (Paton, 1986, Salomon et. al, 1990); however, recent evidence has seen the formation extend further west from the ridge (Alexander and Sansome, 1996). The western edge of the sediments intertongue with the Algebuckina Sandstone. The Birkhead Formation varies in thickness from 120 metres in the Cooper Basin region (Paton, 1986, Salomon et. al, 1990) to over 150 metres in the Patchawarra and Nappamerri Troughs (Alexander and Sansome, 1996) and is approximately 140 metres thick at the Gidgealpa south

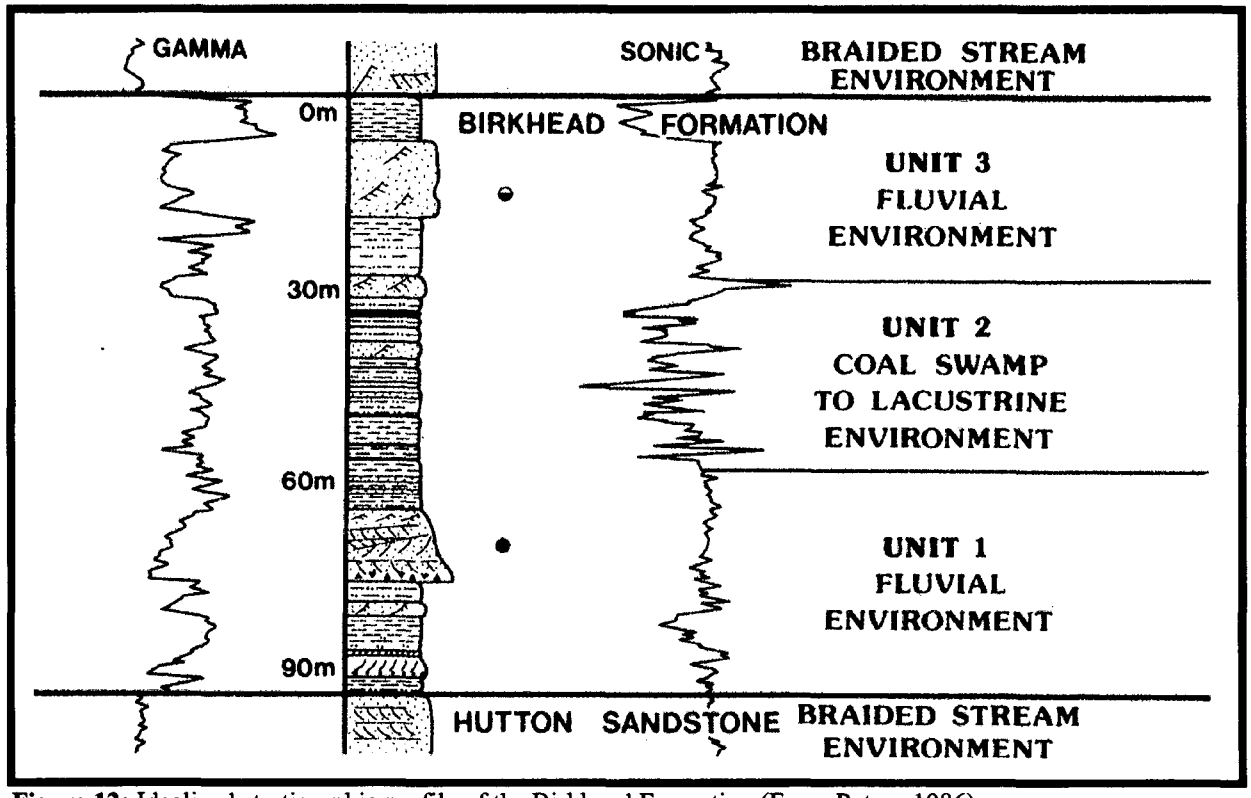

Figure 12: Idealized stratigraphic profile of the Birkhead Formation (From Paton, 1986).

dome. The upper boundary of the Birkhead Formation is conformable with the Namur Sandstone to the east or Adori Sandstone to the west of the Eromanga Basin (Alexander and Sansome, 1996).

3.3.4.5 *Namur Sandstone*

The Namur Sandstone is Late Jurassic to Early Cretaceous in age and forms the base of a set of formations that from the literature vary in nomenclature. In Queensland the formation is part of the Hooray Sandstone while in South Australia, until recently, it formed part of the Mooga Formation where it has been elevated to formation status (Gravestock et. al, 1995). The formation sediments were deposited in a low sinuosity fluvial environment forming high-angle tabular and ripple cross-bedding (Theologou, 1995). Sediments consist of conglomerates, fine to coarse grained sandstones with minor siltstones and mudstone interbeds (Bowering, 1982). Dipmeter interpretation studies show a northerly palaeocurrent trend suggesting a similar source of sediments as the Hutton Sandstone (Alexander and Sansome, 1996).

The Namur Sandstone is situated on top of the Birkhead Formation in the Gidgealpa south dome area. To the west of the area the Adori Sandstone occurs on the top of the Birkhead Formation and is laterally equivalent to the Namur Sandstone. The Adori Sandstone then grades onto a high sinuosity fluvial to lacustrine Westbourne Formation which has similar characteristics to the Birkhead Formation both compositionally and environmentally (Wecker, 1989). The Westbourne Formation was deposited to the west at the same time as Namur Sandstone. To the west, the termination of lacustrine conditions was caused by the deposition of the Namur Sandstone sediments that filled in the lakes and surrounding areas (Bowering, 1982). My own personal observation of wireline logs at the Gidgealpa south dome would appear to indicate that the contact between the Birkhead Formation and the Namur Sandstone is erosive which is supported by Boult (1996).

3.3.4.6 *Murta Formation*

The Murta Formation was formally known as the Murta Member forming the top part of the Mooga Formation until recently when Gravestock et. al (1995) upgraded the member to formation status. The formation was deposited under mainly shallow lacustrine conditions in the Neocomian (early Cretaceous) over the Cooper Basin area (Moore et. al, 1986, Wecker, 1989). Sediments mainly consist of alternating grey shales and siltstones (Bowering, 1982) with laterally extensive rippled and reservoir quality sandstones. Sands are thought to represent sub-lacustrine fans which are subsequently disturbed and re-deposited as ripple laminated sandstones by wave and storm activity (Moore et. al, 1986); bouma sequences, slump and water escape structures as well as bioturbation also occur (Alexander and Sansome, 1996). Sediments are deposited in fresh (Moore et. al, 1986) to brackish water (Alexander and Sansome, 1996).

The boundary of the formation intertongues with the Algebuckina Sandstone to the west; the lower boundary intertongues with the Namur and McKinlay Member further to the east and grades into the Cadna-owie Formation above (Alexander and Sansome, 1996).

3.3.4.7 *Cadna-owie Formation*

During the deposition of the Cadna-owie Formation global sea level changes affected deposition within the Eromanga Basin (Burger, 1986). The Cadna-owie Formation was deposited during a period of rising sea level in the Early Cretaceous (Neocomian to Aptian) with sediments extending over the entire Artesian Basin (Wecker, 1989). The sequence is relatively uniform consisting of a coarsening up package of sediments, probably caused by a progradational event after the initial deepening at the base. Sediments of thinly interbedded

grey siltstones and very fine sandstones graded up to fine-grained calcareous sandstones of fluvial to deltaic / lower-shoreface origin at the top of the formation. Sandstones consist of quartz to feldspathic, sub-labile to lithic labile grains depending on the area. The deposition of these two types of sediments was probably caused by sediment being sourced from the south and east respectively (Bowering, 1982, John and Almond, 1987, Wecker, 1989, Alexander and Sansome, 1996).

In the eastern Eromanga Basin the shoreface sandstone is called the Wyandra Sandstone Member, with sediment composition being predominantly quartzose to feldspathic-labile (John and Almond, 1987). The sandstone along with the Wallumbilla Formation above the Cadna-owie Formation provides a widely correlatible seismic marker known as the 'C horizon'(Bowering, 1982). The top of the Wyandra Sandstone is conformably but sharply overlain by the Wallumbilla Formation mudstones (John and Almond, 1987, Alexander and Sansome, 1996).

3.3.4.8 Wallumbilla Formation

The Wallumbilla Formation was deposited during the Aptian at a time when the Eromanga Basin was transferring from a period of low regional subsidence, due to tectonic stability, to a period of rapid subsidence. Sediments consist of thick marine, dark grey mudstones and shales (Bowering, 1982, Moore and Pitt, 1984, Alexander and Sansome, 1996).

This formation is also known as the Bulldog Shale in other parts of the basin. Near the top of the formation is a regressive marine sand called the Coorikiana Sandstone that was deposited as a widespread sheet in the southern and western parts of the Eromanga Basin (Bowering, 1982, Moore and Pitt, 1984). The sandstone is mainly fine grained and glauconitic with minor siltstones.

The upper boundary between the Wallumbilla Formation and the Toolebuc Formation is conformable (Alexander, and Sansome, 1996).

3.3.4.9 *Toolebuc Formation to Mackunda Formation*

The Toolebuc Formation, Allaru Sandstone and Mackunda Formation are a conformable sequence deposited in a marine environment. Sandstones deposited during this time consist of abundant feldspars and lithic fragments envisaged to be sourced from the active arc complex to the east, similar to the source during Birkhead Formation time (Veevers, 1984). During the latest middle to late Albian of the Cretaceous the Toolebuc Formation was deposited. The formation has a strong positive gamma-ray anomaly that makes an excellent wireline log marker. The marker is due to the decay of uranium isotopes associated with organic carbon and phosphatic skeletal fish remains (John, 1990, Moore and Pitt, 1984, Alexander and Sansome, 1996).

The Toolebuc Formation is widespread over the Eromanga Basin with the deeper areas typically consisting of soft dark, gray to black marls, siltstones and mudstones (Bowering, 1982, Moore and Pitt, 1984). The depositional environment of sediments was probably in a shallow restricted epeiric sea with periods of sub-aerial exposure. The dark nature of the sediments is due to oxygen depletion with oil shales forming from algal or fungal fauna (Moore and Pitt, 1984, Alexander, and Sansome, 1996). The Toolebuc Formation was deposited during the maximum stage of the transgression (Alexander and Sansome, 1996) and with the subsequent decrease in water depth the upper boundary of the formation terminates conformably with the Allaru Mudstone. The Allaru Mudstone is a continuation of sediment deposition in a shallow marine environment. It consists of calcareous siltstones and minor sandstone beds deposited in the Early Cretaceous (Late Albian) (Alexander and Sansome, 1996). The Mackunda Formation is the continuation of the

regressive cycle with deposition of fossiliferous sandy siltstones and shales within a marginal marine environment (Moore and Pitt, 1984, Wecker, 1989).

3.3.4.10 Winton Formation

The Winton Formation is conformable with the Mackunda Formation and was deposited in the Late Cretaceous (Albian to Cenomanian). The formation consists of grey / blue fine to coarse-grained sandstones, siltstones and carbonaceous shales with minor coal interbeds (Moore and Pitt, 1984, Alexander and Sansome, 1996). Sediments deposited at this time were sourced from the east by a final pulse of volcanic activity filling the basin with volcano-lithics, feldspars and various other minerals (Alexander and Sansome, 1996, Veevers, 1984).

The depositional environment indicated a change from marine to terrestrial low energy meandering fluvial caused by an increase in depositional energy associated with basin margin activity (Moore and Pitt, 1984, Wecker, 1989). Rapid subsidence within the Eromanga Basin continued until the early Late Cretaceous when sedimentation terminated with uplift and erosion signalling the top of the basin. (Wecker, 1989).

3.4 Source Potential of the Cooper/Eromanga Basins

3.4.1 Introduction

Early exploration within the Eromanga Basin was conducted due to the evidence of dissolved natural gas within the Great Artesian Basin. This exploration however, was generally unsuccessful with the consensus that the basin was unproductive due to the flushing of migrating and reservoired hydrocarbons and from the discovery of common water filled anticlinal structures (Bowering 1982, Kantsler et. al, 1983). This was the case until 1976

when gas was found in commercial quantities at Namur 1 (Bowering, 1982). Since this discovery vast quantities of both oil and gas have been found within the Eromanga Basin and the question has been, 'where has the Eromanga oil been sourced from within the Eromanga Basin?'

Hydrocarbons from both the Permian and the Jurassic sequences are believed to be mainly sourced from terrigenous continental coals and shallow lacustrine source rocks (Kantsler et. al, 1983, Smyth et. al, 1984, Heath et. al, 1989). These fair to good source rocks generally consist of type II/III and type III kerogens. Permian sediments are generally rich in gas prone inertinite and also contain vitrinite (Kantsler et. al, 1983, Wecker, 1989) while Jurassic rocks contain inertinite and are abundant in vitrinite. The organic matter in various areas of the Eromanga Basin has been known to contain abundant oil prone exinite and suberinite; bacterially degraded vitrinite can occur with other macerals making source rocks more oil prone (Kantsler et. al, 1983, Vincent et. al, 1985, Salomon et. al, 1990).

Oil within the Eromanga Basin is sourced from various coaly formations in the Permian and / or the Poolowanna, Birkhead or Murta Formations of the Jurassic to Early Cretaceous (figure **13**). The Mesozoic formations have the best source potential due to evolutionary changes of flora in the Jurassic increasing source potential (Vincent et. al, 1985) with total organic carbon (TOC) ranging from 0.5 to 2.0% (Michaelsen and McKirdy, 1996). Overall the Birkhead Formation has the best potential for hydrocarbon generation with TOC ranging up to 4.5% (Vincent et. al, 1985). The Triassic has little evidence of source rocks and the Cretaceous section has occasional, fair to good source rocks but pyrolysis yields suggest that it is commonly organically lean (Kantsler et. al, 1983).

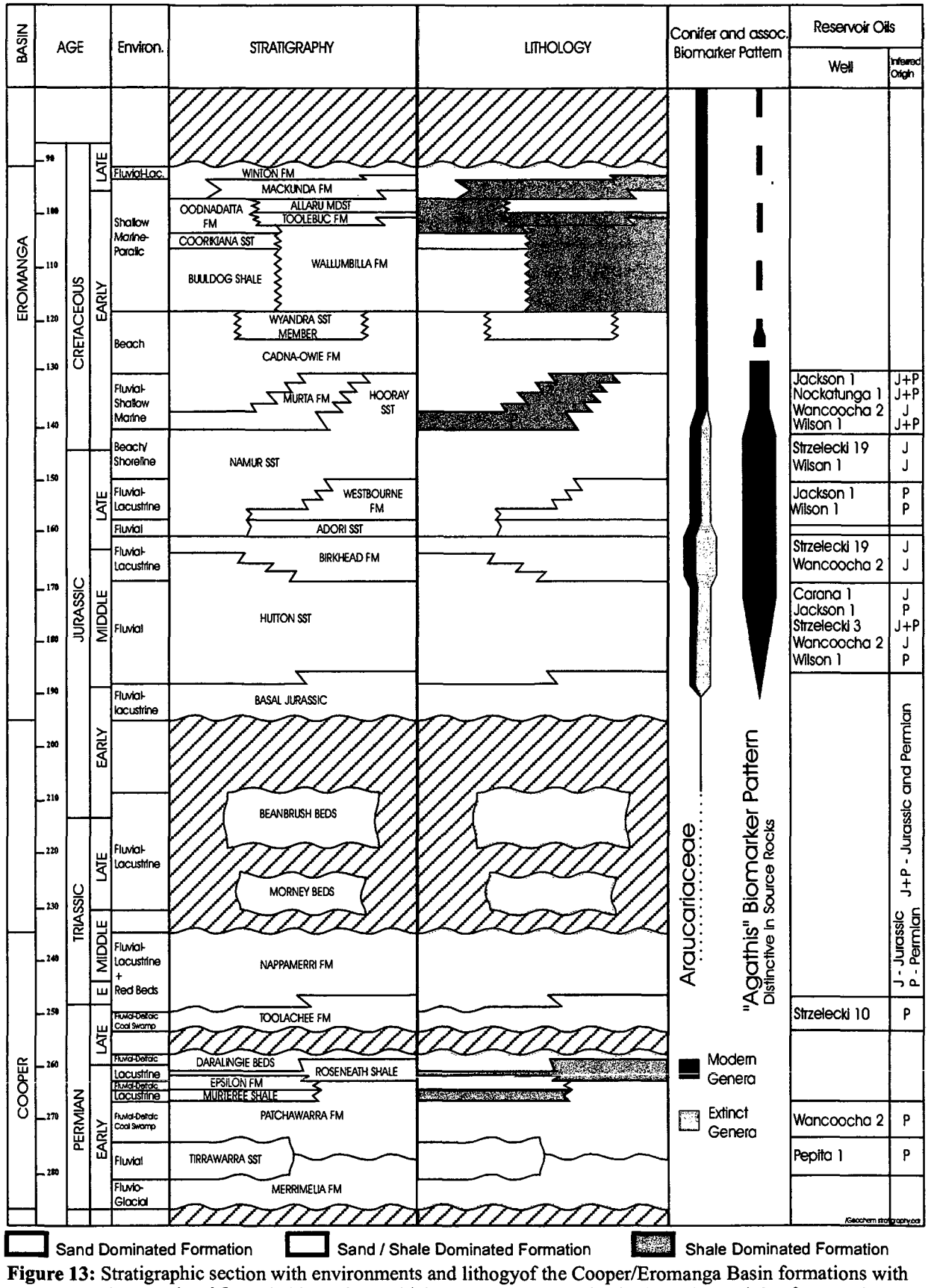

Figure 13: Stratigraphic section with environments and lithogyof the Cooper/Eromanga Basin formations with the associated Jurassic biomarkers which are used to determine hydrocarbon origins from various reservoirs within the sequence (After Alexander et. al, 1988 and Kantsler et. al, 1983).

3.4.2 Hydrocarbon Geochemistry: Permian or Jurassic Source?

The origins of oil within the Eromanga Basin have been an area of much debate in the past due to the implications of either a Permian or Jurassic source. Knowledge of the origin of hydrocarbons has obvious advantages for exploration for future discoveries within the basin. While the age of source rocks has not been fully constrained it is generally accepted that most of the hydrocarbons are sourced from continental terrestrial matter (Kantsler et. al, 1983, Smyth et. al, 1984, Vincent et. al, 1985). More recently Ryan (1996) showed that when hopanes and norhopanes of oils, shales and coals are plotted on a graph the coals and oils plot on a straight line while the shale from the Birkhead Formation plots as an outlier (figure **14**). This apparent relationship and the fact that the coal sourced Patchawarra oil from the Permian also plots on the same trend suggest that hydrocarbons originate from coals rather than shales within the Eromanga Basin. Aromatic hydrocarbons have been used as a maturity indicator for the time of expulsion of oil from source rocks. Oils have been associated with source rocks by the use of calculated vitrinite reflectance (R_c) using the methylphenanthrene index (MPI). Jurassic oils generally have a R_c = 0.64-1.04% compared to the Cooper Basin which have R_c = 0.95 - 1.10 (Alexander et. al, 1988).

In recent years geochemical evidence, through the presence or absence of organic biomarker compounds, has been used to deduce either a Permian or Jurassic source origin for hydrocarbons within the Eromanga Basin (Alexander et. al, 1988, Heath et. al, 1989, Michaelsen and McKirdy, 1996). These biomarkers consist of aromatic compounds originating from the Araucariaceae conifer family which are absent in the Permian but became prominent in the Early to Middle Jurassic (figure **13**, page 34). Thus determination of whether oils have been sourced from the Jurassic or Permian is dependent upon the

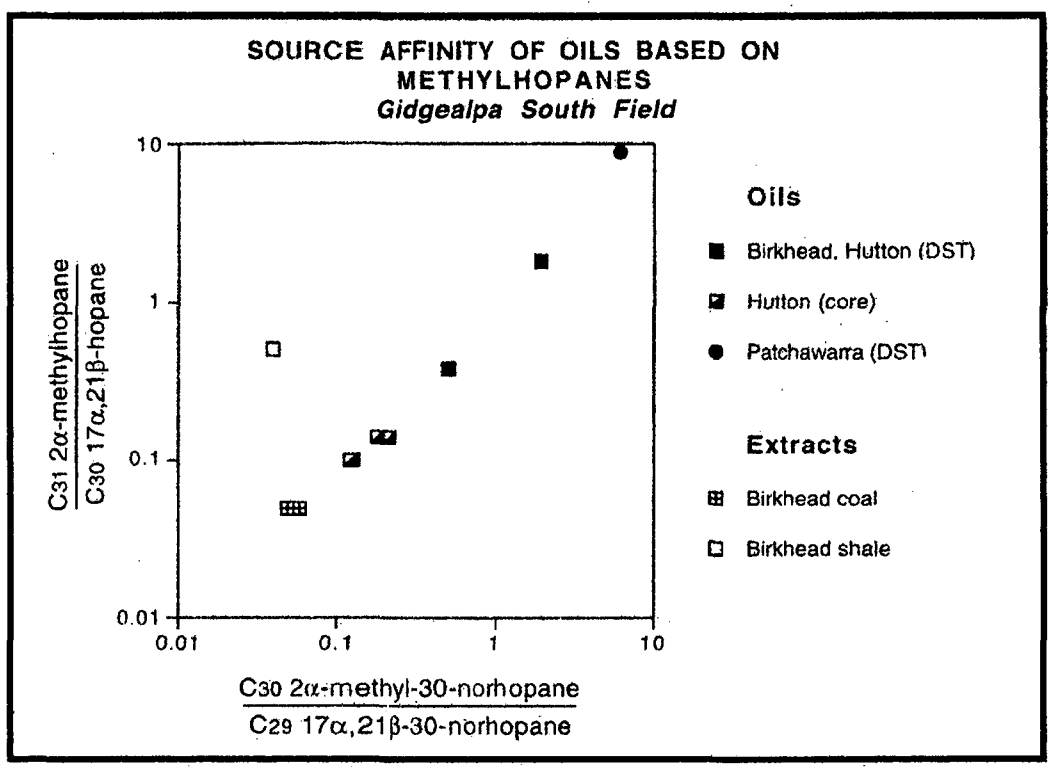

Figure 14: Logarithmic cross-plots of hopanes and norhopanes showing the the relationship between coals and oils in the Eromanga Basin (From Boult et. al, 1997).

presence of the Araucariacean plants in the Jurassic and their absence in the Permian (Alexander and Kagi, 1988).

Oils sourced from the Araucariacean plants are rich in 1-methylphenanthrene relative to 9-methylphenanthrene and the 1,2,5-trimethyl-naphthalene / 1,3,6-trimethylnaphthalene and 1-methylphenanthrene / 9-methylphenanthrene ratios are also higher in the Jurassic than in the Permian (Alexander et. al, 1988, Michaelsen and McKirdy, 1996). The individual biomarkers alone do not prove that they are derived from the Jurassic conifers but collectively they provide strong evidence that they are sourced from the Jurassic (Alexander et. al, 1988, Alexander and Kagi, 1988). Figure **15** plots the relative abundance of compounds from partial chromatogram traces showing the comparison of a Jurassic and Permian oil with similar maturities from their dimethylnaphthalene content. The figure shows a marked difference in the trimethylnapthalene and alkylphenanthrene contents due to their differences in original source material. While the Araucariacean biomarkers are abundant in the Jurassic, variations in quantities can occur due to differences in deposition, diagenesis and maturation of the source materials (Alexander and Kagi, 1988).

The Araucariaceae biomarkers have been successfully used in the western part of the Eromanga Basin to determine source for the oil within the Jurassic. Figure **16** shows the distinctive separation of the different aged oils when biomarker abundances are plotted (Alexander et. al, 1996). Studies of terpane fragmentograms from oils have revealed a compound that has not previously been identified and seems only to occur within Permian oils. Further investigations have indicated that this biomarker is present in approximately 50% of Permian reservoirs, suggesting that it may be a source specific molecule (Alexander et. al, 1996). The discovery of a Permian specific biomarker has important implications for the determining of oil source. If a reliable marker can be found then oils from either the Cooper or Eromanga Basins can be confidently determined based on the presence or absence of both the Jurassic or Permian Biomarkers. However until this elusive biomarker is

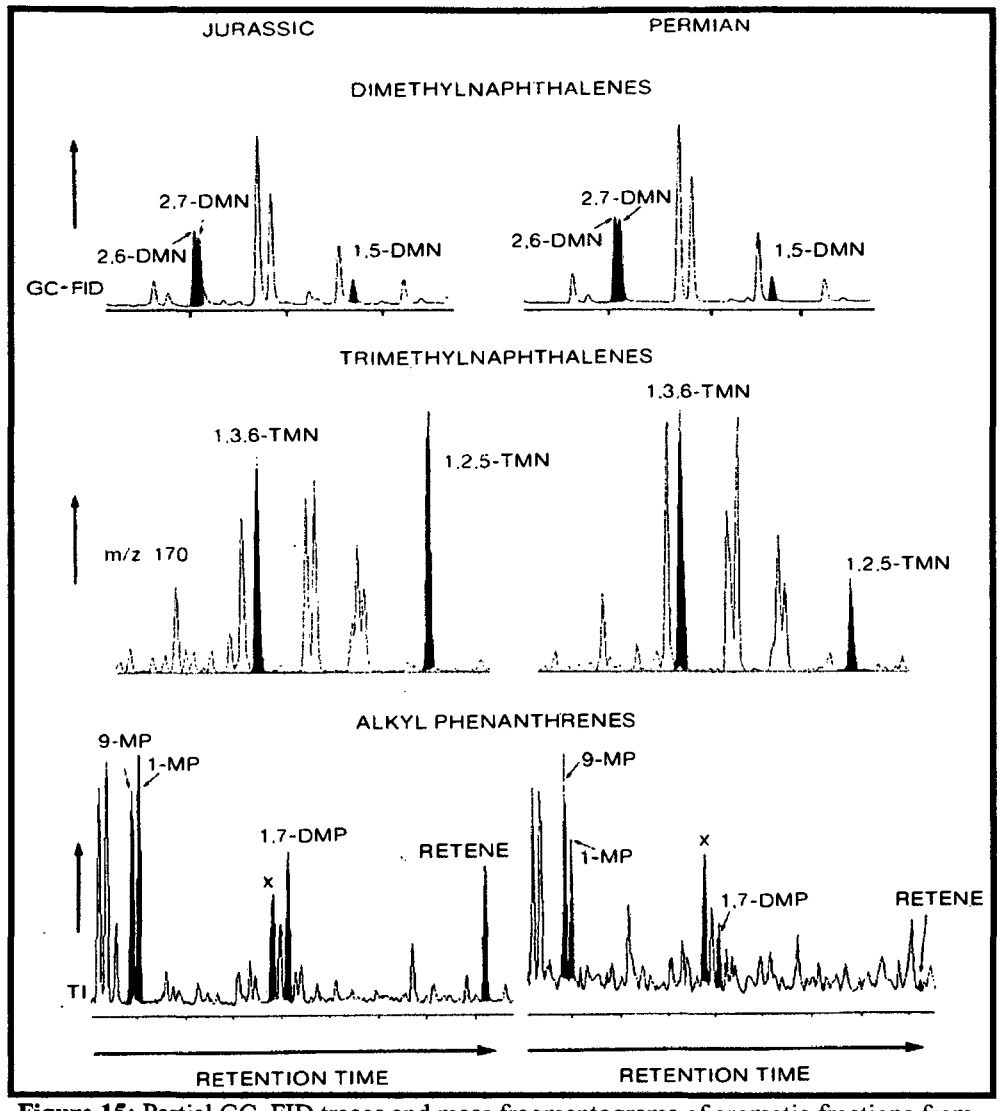

Figure 15: Partial GC_FID traces and mass fragmentograms of aromatic fractions from typical Jurassic and Permian samples (From Alexander et. al, 1988).

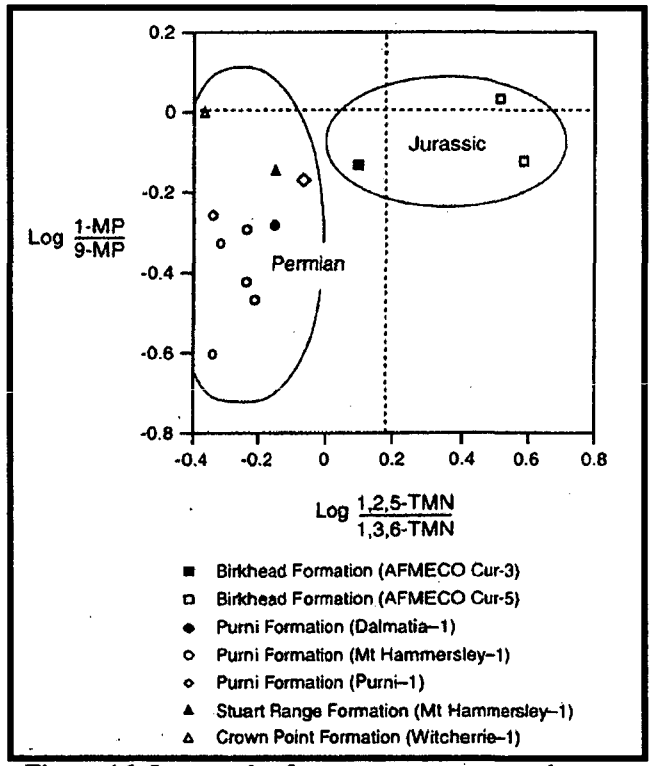

Figure 16: Log graph of source parameters used to distinguish Permian from Jurassic oils (From Alexander et. al, 1996).

found critics will be unconvinced of the origins of oil from within the Eromanga Basin.

With the identification of the terpane fragmentograms; this new geochemical tool seems to clearly indicate that it is possible to determine the origins of oils within the Jurassic section on the basis of the presence or absence of the Araucariaceae biomarkers. The absence of the biomarkers would suggest that oils are from Permian source rocks while their presence would suggest that the origin was from Jurassic source rocks. Alexander et. al (1988) analysed a number of oils from the Jurassic and found that a number of fields either had the biomarkers present or absent. Using this fact they associated the oils with sources either from the Jurassic or Permian respectively. The analysis of other samples were found to be relatively low in the Jurassic markers suggesting a mixed Jurassic / Permian source for the oil (figure **13**, page 34) (Alexander et. al, 1988, Alexander and Kagi, 1988). Thus the effectiveness of the correlation and ultimate determination of source is dependent on the amount of Araucariacean plant matter present within the source rocks and corresponding oils (Alexander et. al, 1988, Michaelsen and McKirdy, 1996).

3.4.3 Implications for Migration and Entrapment

Heath et. al (1989) points out the fact that the present day aquifer system within the Eromanga Basin is more than enough to adequately dissolve gas from migrating hydrocarbons, causing oils to have a low gas content. The stripped gas is then carried within the aquifer system and escapes from the sub-surface around the Lake Eyre area. Figures **17** and **18** show the extent and flow direction of the aquifer system with charging occurring from the Great Dividing Range. From the source, water then flows through high energy deposited sediments that have corresponding high permeabilities such as the Hutton Sandstone and Namur Sandstone with the lacustrine and lower energy formations such as Birkhead and Westbourne Formations, acting as aquifer

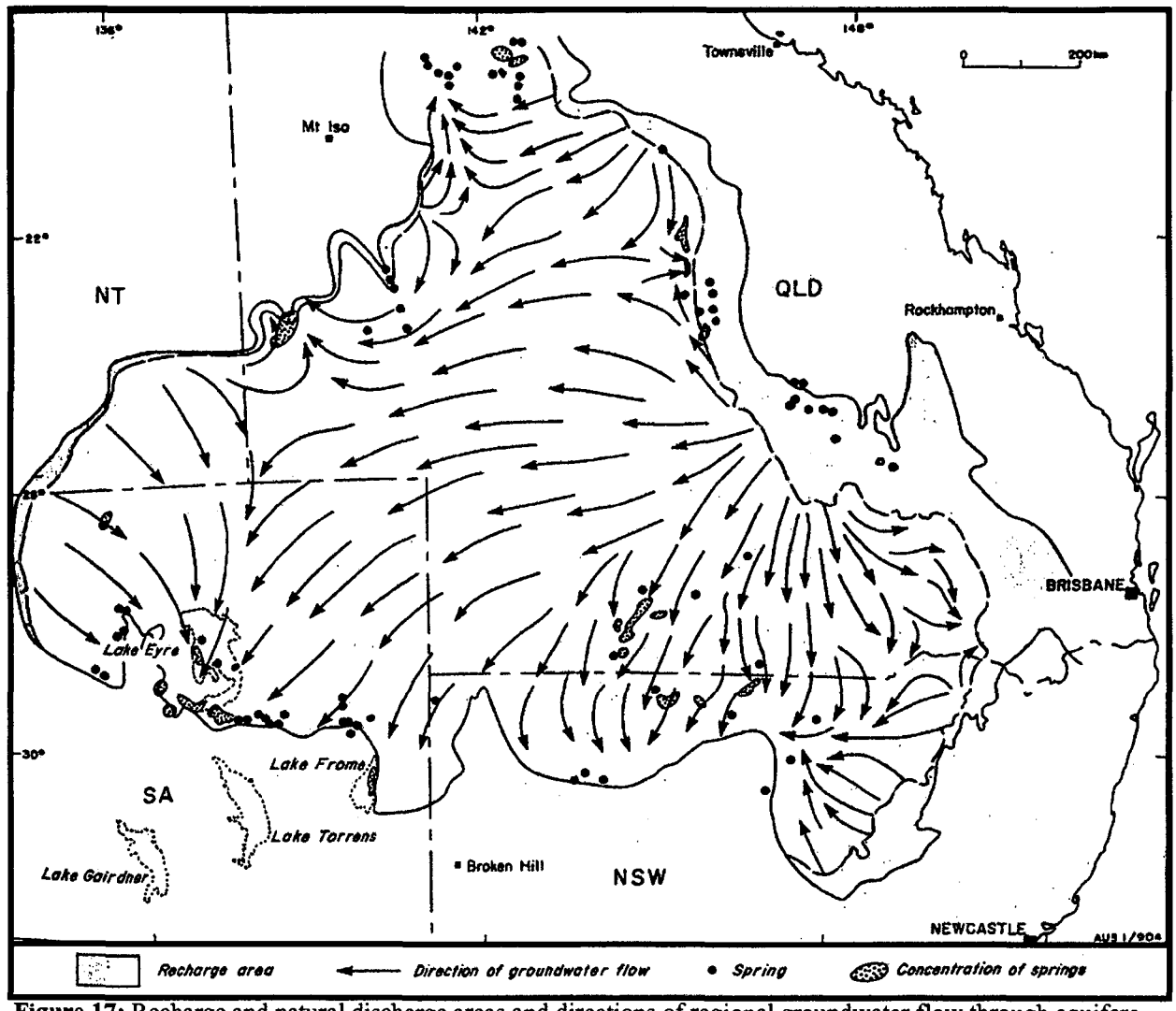

Figure 17: Recharge and natural discharge areas and directions of regional groundwater flow through aquifers in the Great Artesian Basin (From Habermehl, 1980).

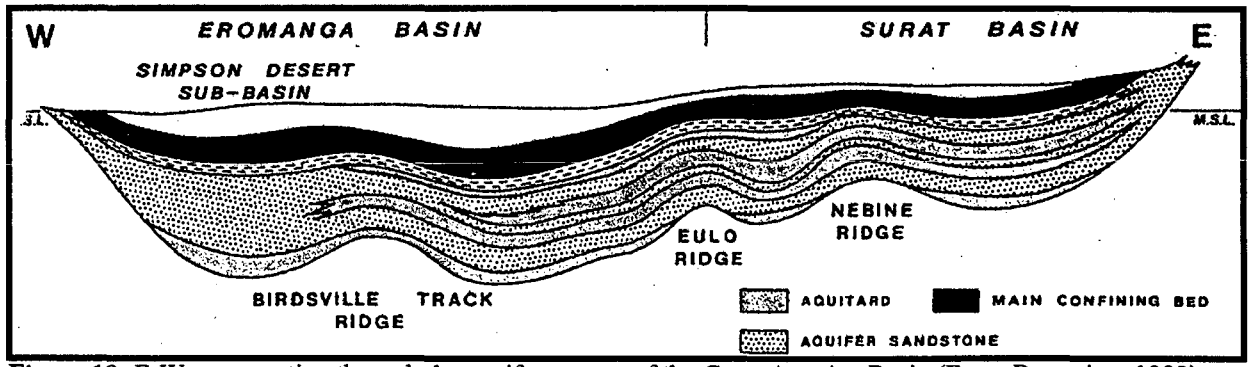

Figure 18: E-W cross section through the aquifer system of the Great Artesian Basin (From Bowering, 1982).

barriers (Habermehl, 1980, Bowering, 1982, Kantsler et. al, 1983). According to Bowering (1982) the generation of hydrocarbons from Jurassic and lower Cretaceous sediments took place during the Late Cretaceous to Early Tertiary, or before the development of the aquifer system. Thus early-formed structures are considered to have a higher potential to hold oil. However, other evidence suggests that the aquifer system was also stronger then at present and may have caused partial flushing of reservoirs. Currently, energy associated with the flowing water within the aquifer system is considered to not be sufficient to cause loss of hydrocarbons from accumulations (Kantsler et. al, 1983). Hydrocarbons within the Jurassic and Cretaceous section, in the vicinity of the Cooper Basin region, are generally trapped in vertically stacked reservoirs of fault bounded anticlinal structures. These structures are generally located on structural highs adjacent to the Nappamerri, Windorah and Patchawarra Troughs (Kantsler et. al, 1983, Wecker, 1989, Lowe-Young et. al, 1997). Reservoirs occur within the Poolowanna Formation, Hutton Sandstone, Birkhead Formation, Namur Sandstone, McKinklay Member and Murta Formation (figure **19**), with the most productive formation being the Hutton Sandstone (Kantsler et. al, 1983).

It has been reported by Wecker (1989), Salomon et. al (1990) and Lowe-Young et. al (1997) that most discoveries are related to the Cooper Basin, Triassic 'zero edge' or erosional sections of the Triassic highs. The authors suggest that this relationship is due to the Triassic section acting as a sealing unit and thus acts as a barrier to the migration of hydrocarbons into the overlying Eromanga Basin from the Permian. Heath et. al (1989) also agree with this Permian sourcing scenario where Cooper Basin oil migrates vertically into the Eromanga Basin sequence. Heath et. al (1989) go on to state that the Permian oils are significantly altered physically and chemically in their characteristics by water washing and fractionation (figure **20**). The water washing strips the light end hydrocarbons of the oil making the gas to oil ratio higher, while fractionation and distillation processes are caused by decreasing temperature and pressure producing higher API and lower pour

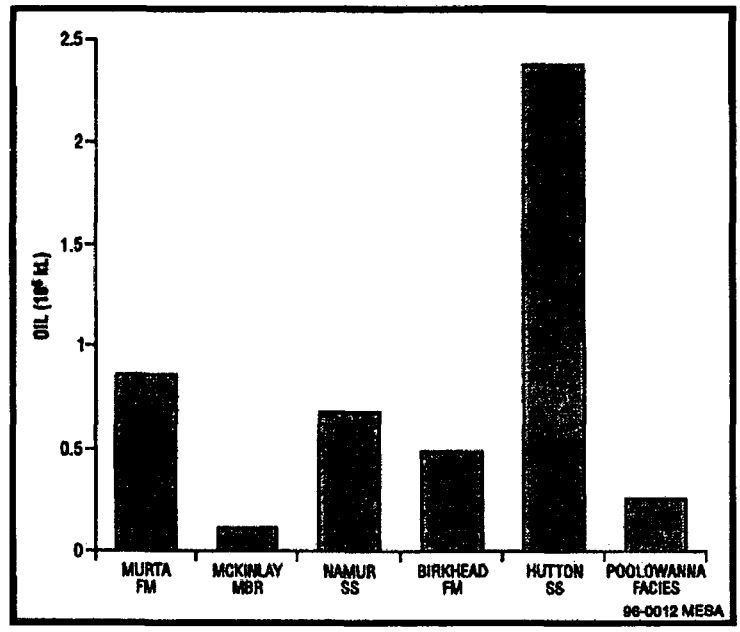

Figure 19: Produced oil from various formations of the Eromanga Basin (From Alexander, 1996).

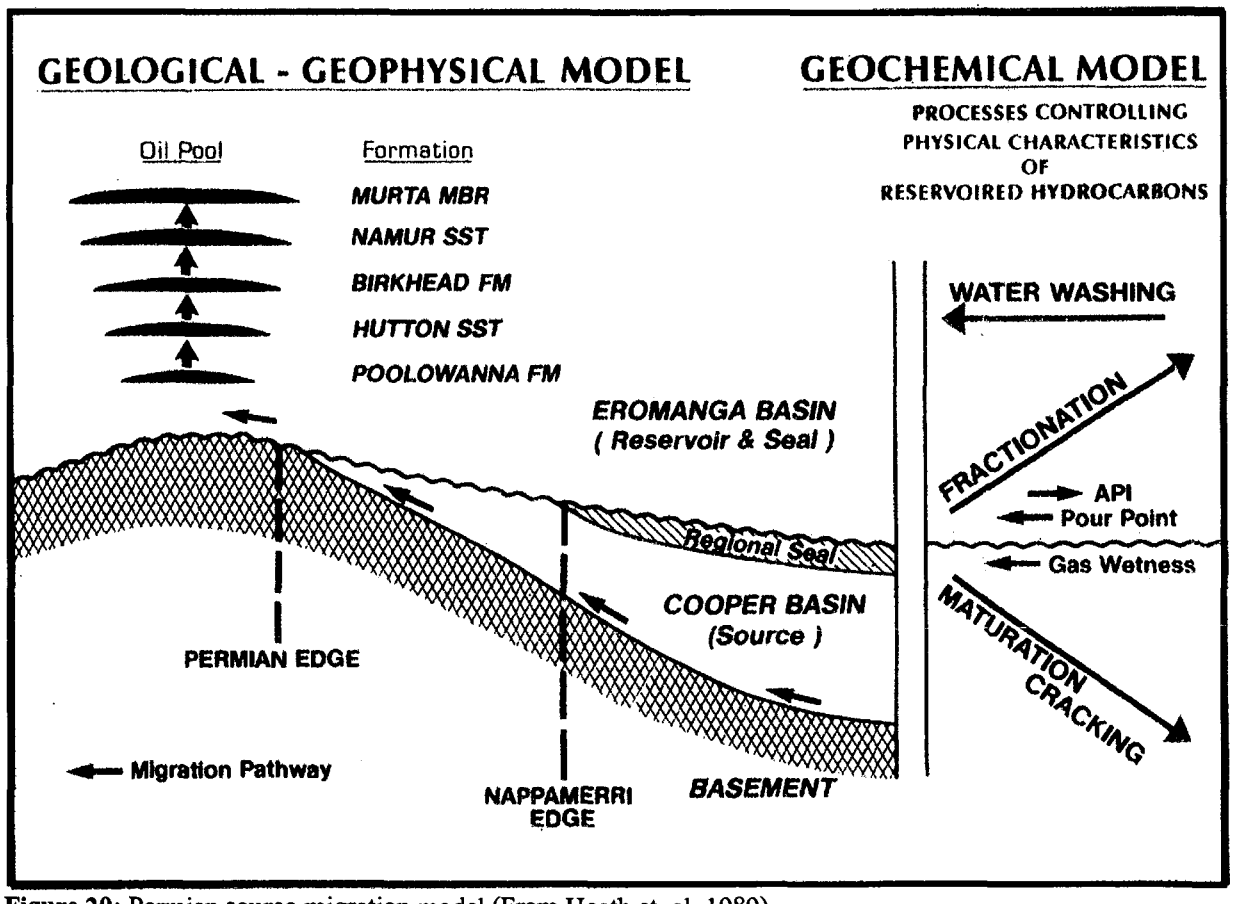

Figure 20: Permian source-migration model (From Heath et. al, 1989) .

point oils. If the Triassic is considered to be the main barrier to oil migration it follows that large accumulations of oil would be present where the Triassic is present, however this does not appear to be the case (Salomon et. al, 1990).

Wecker (1989) discounts a Jurassic source for Jurassic oil since the sequence is considered to be only marginally mature for gas generation; however, more recently it has been found that vitrinite within the Jurassic has been suppressed by the presence of the Araucariacean plant matter (B. Michaelsen, pers. comm.).

So it is possible that where source rock maturity appears to only be gas bearing, they are in fact able to produce oil at peak generation due to vitrinite suppression. Reservoirs may also have been minimally charged from locally, thermally mature rocks within the Jurassic (Kantsler et. al, 1983). A possible model for oil sourced from Jurassic shales and coals within higher maturity troughs is by migration laterally and / or vertically into adjacent reservoirs (Heath et. al, 1989).

In deeper areas such as the Nappamerri Trough, hydrocarbon generation started in the Early Tertiary. Secondary migration pathways focused oil along the Naccowlah-Jackson trend from this source kitchen into nearby highs (Nelson, 1985, Vincent et. al, 1985). Figure **21** shows density separation of hydrocarbons (known as the Gussow principle) from deeper within the trough where less dense gas has displaced oil to a higher stratigraphic level.

Most exploration activity and discoveries within the Jurassic have been concentrated along the zero edge of the Cooper Basin using the Permian model of hydrocarbon generation. More recently, commercially viable hydrocarbons have been discovered at Inland, along the Windorah Trough, 70 km away from the Cooper Basin zero edge. (Lowe-Young et. al, 1997). If a Permian source is considered for this reservoir then hydrocarbons would have to migrate 70km to reside at Inland. It is more likely that the hydrocarbons have been sourced

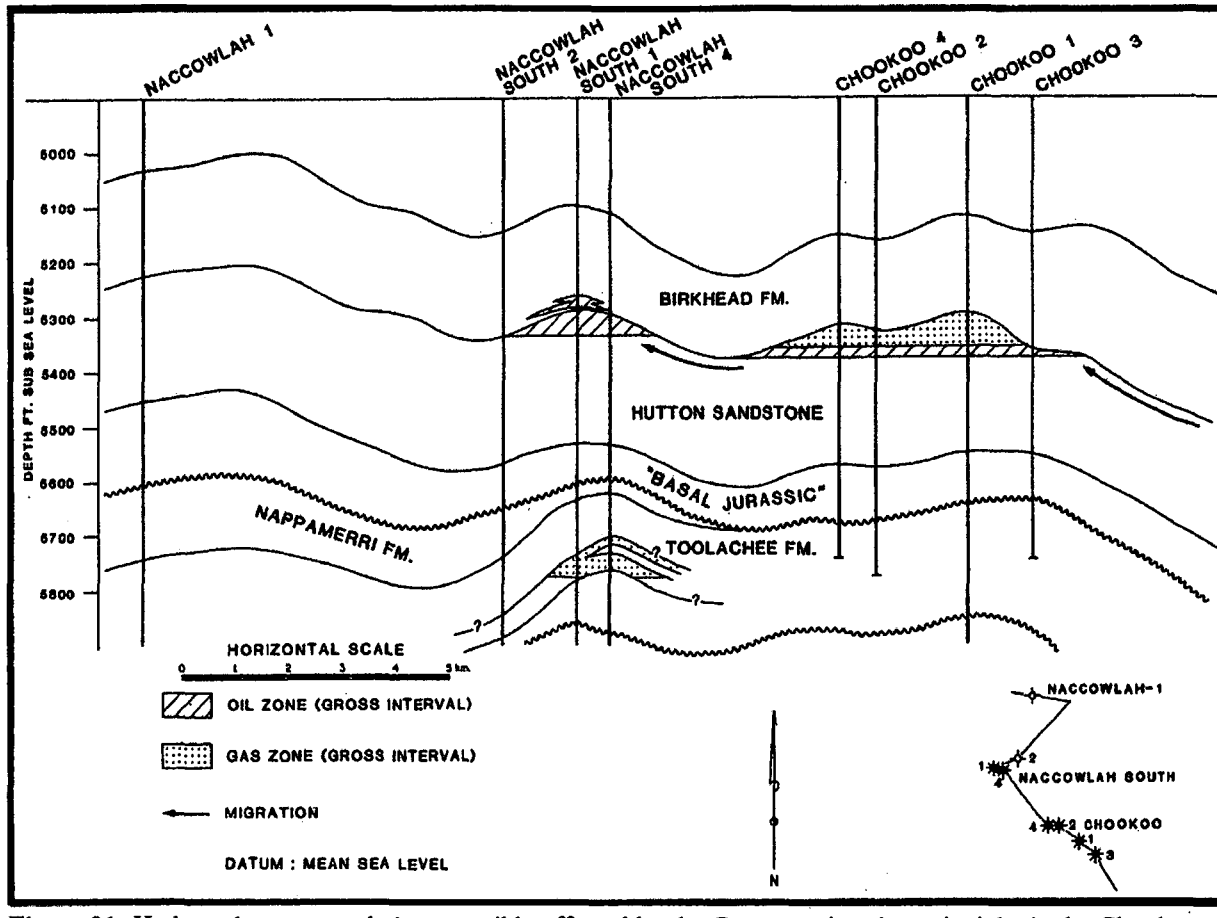

Figure 21: Hydrocarbon accumulations possibly affected by the Gussow migration principle in the Chookoo-Naccowlah South Area (From Vincent et. al, 1985).

from the Windorah Trough which juxtaposes the Inland field, however much more work is required to confirm or deny this fact.

3.4.4 Source Rock Potential of the Birkhead Formation

Source rocks in the Birkhead Formation have been rated as fair to very good for hydrocarbon generation (Smyth et. al, 1984) with initial generation occurring within the Birkhead at approximately R_o=0.55%. In the lower part of the Eromanga Basin the Birkhead Formation is the thickest and most extensive source unit. Figure **22** is a top Birkhead Formation vitrinite reflectance map and shows that most of the formation is initially mature (V_r=0.5-0.6%). The Windorah and Nappamerri Troughs have the best source potential with R_o=0.7-0.9%, making these areas the principal zone of oil generation. Areas within the troughs have gone as high as R_o=1.3 which indicates that peak oil generation has already occurred (Smyth et. al, 1984, Vincent et. al, 1985, Wecker et. al, 1989).

Pyrolysis gas chromatography (Py-GC) and gas chromatography (GC) analysis of organic matter within the Birkhead Formation indicates a terrestrial source and under the appropriate conditions of maturation waxy oils can be produced (Smyth et. al, 1984). Kerogen type varies in different areas from type II to II/III to III with type III kerogens tending to dilute organic matter in some areas (figure **23**) (Michaelsen and McKirdy, 1996). Macerals within organic matter consists of vitrinite that is high in telocollinite. Micrinite is also present within coals along with suberinite which suggests hydrocarbon generation is likely, exinite such as sporinite and liptodetrinite are also present (Kantsler et. al, 1983, Smyth et. al, 1984).

In the western part of the Eromanga Basin, Birkhead Formation source rocks are highly varied from fair to excellent (Michaelsen and McKirdy, 1996). The Birkhead Formation equivalent facies of the Algebuckina Sandstone within the

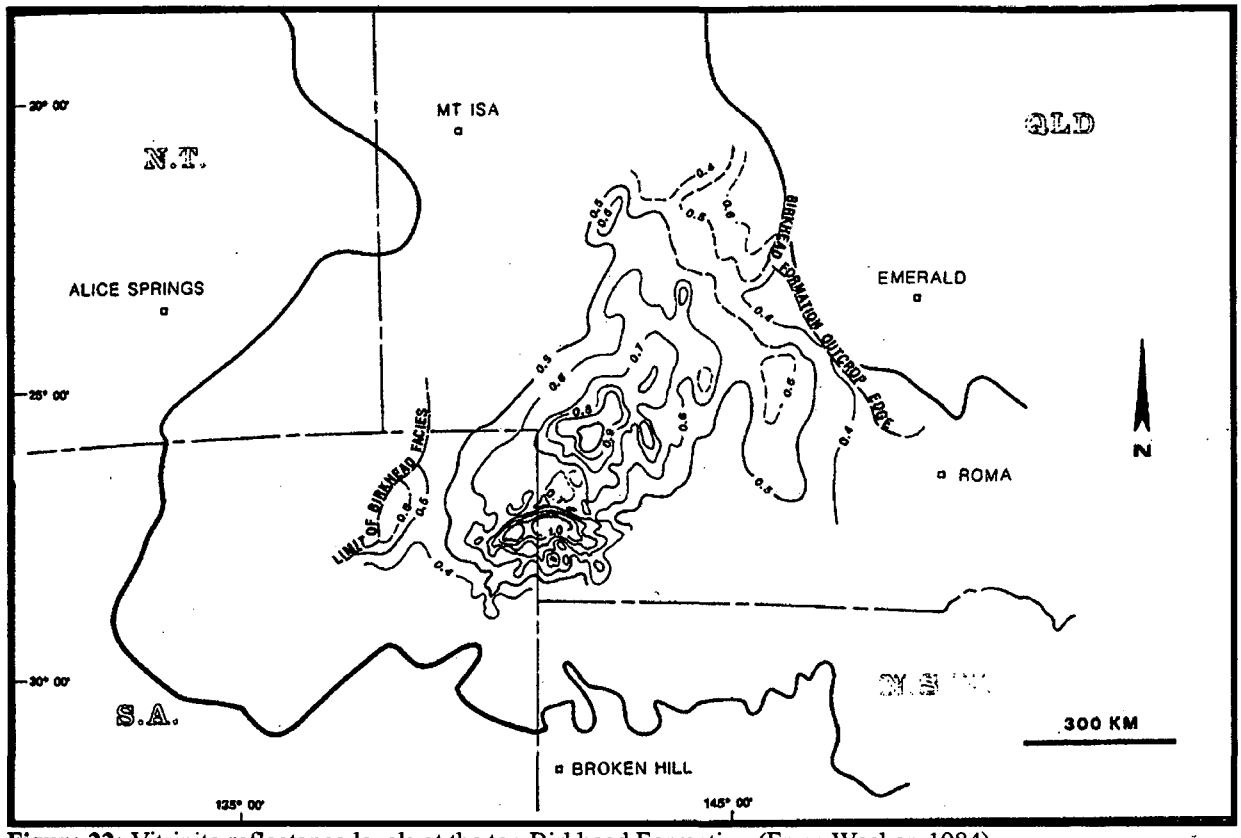

Figure 22: Vitrinite reflectance levels at the top Birkhead Formation (From Wecker, 1984).

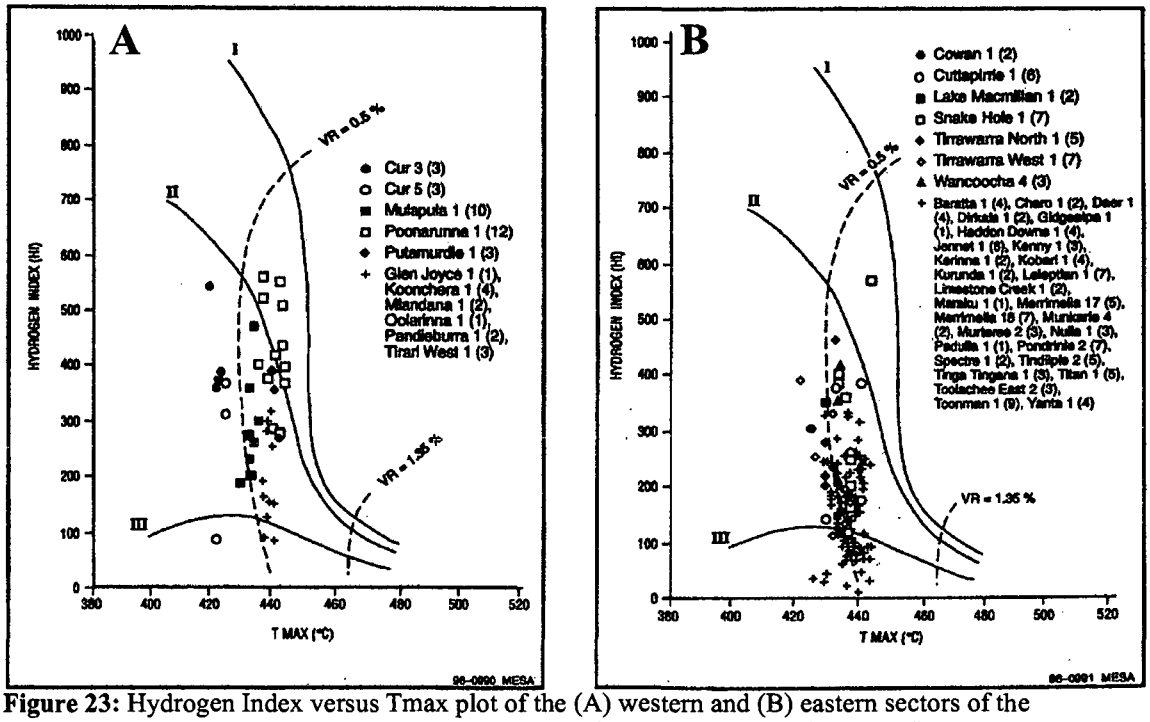

Figure 23: Hydrogen Index versus Tmax plot of the (A) western and (B) eastern sectors of the Eromanga Basin, South Australia (From Michaelsen and McKirdy, 1996).

Poolowanna Trough have coals with excellent source rock potential with type II to type II/III kerogen present (figure **23**). The kerogen is also of terrestrial origin but has been reworked by bacteria causing source rocks to generate more hydrocarbons and oil at lower R_o values (Alexander et. al, 1996, Michaelsen and McKirdy, 1996).

3.4.5 Geochemistry of Hydrocarbons in Jurassic Reservoirs

Jurassic, Eromanga oils are generally paraffinic to naphthenic, characteristically light (40°-51° API), have a very low gas content and tend to be variable in wax content with a pour point ranging from 20°-40° (Kantsler et. al, 1983, Wecker 1989, Heath et. al, 1989). The gasoline range fraction of the Eromanga oils are low in aromatic compounds when compared with Permian oils, possibly due to water washing of the hydrocarbons (Heath et. al, 1989). Higher in the Eromanga Basin, the Murta oils tend to be geochemically distinct from the oils found deeper in the section. They tend to be more waxy and are thought to be sourced from mature source rocks with a marine component in the Upper Jurassic / Lower Cretaceous (Kantsler et. al, 1983).

3.4.6 Maturity Indicators for Jurassic Source Rocks

Aromatic hydrocarbons from oils have indicated that the central Cooper Basin area of the Jurassic is low to moderate in maturity while in the Permian oils are mainly moderate (Alexander et. al, 1988). Some high maturity oils are present and probably originated from the post mature central Nappamerri Trough (Kantsler et. al, 1983). Iso-reflectance maps of the southern Cooper Basin area (figure **24**, section A-B) shows that the Nappamerri Trough is well placed to have sourced a large quantity of hydrocarbons discovered within the Eromanga Basin. Source rocks of the Middle to Lower Jurassic passed into the oil generation window in the Late Cretaceous and Tertiary or post Cadna-owie deposition with the upper section nearing oil generation (Kantsler et. al, 1989).

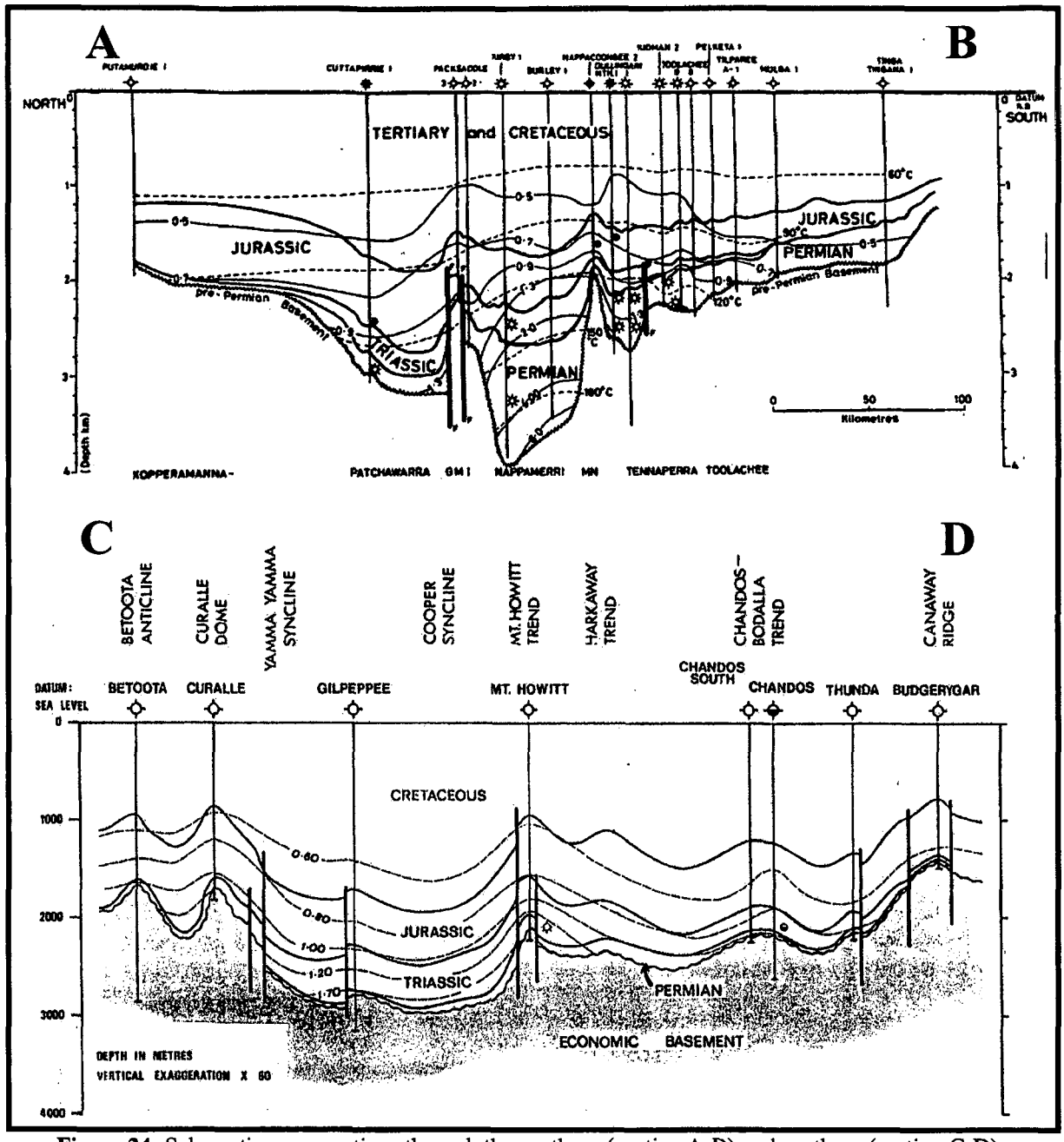

Figure 24: Schematic cross sections through the southern (section A-B) and northern (section C-D) Cooper/Eromanga Basin with profile of isoreflectance surfaces (From Kantsler et. Al, 1983).

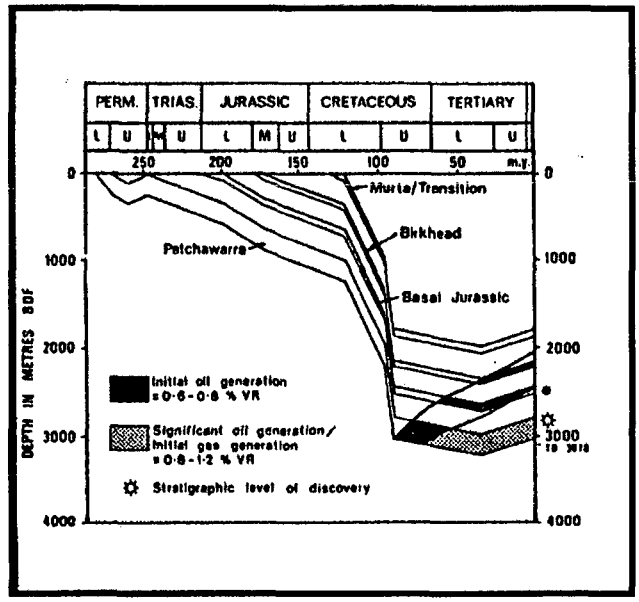

Figure 25: Subsidence/maturation history Cuttapirrie-1, northwestern Patchawarra Trough. (From Kantsler et. al, 1983).

At present, only the flanks are in the peak oil window, however a section through the Northern Cooper Basin area (figure **24**, section C-D) shows that most of the Jurassic has only just entered peak oil generation. From maturation data the time of highest hydrocarbon generation within the basin is likely to have post dated the deposition of the Winton Formation (Late Cretaceous) (figure **25** (previous page)) (Kantsler et. al, 1983).

3.4.7 The Gidgealpa South Dome

Coals and shales within the Birkhead Formation at the Gidgealpa south dome consist of Type II and type II/III kerogens (Michaelsen and McKirdy, 1996) with gas chromatography-mass spectrometry (GC-MS) of regular steranes showing that macerals are derived from higher plants or terrestrial matter. Maceral assemblages of dispersed organic matter are sporadic in occurrence with variations from well to well. Vitrinite, exinite, liptinite, cutinite and resinite are all present with abundant suberinite occurring in coals (figure **26**) (Mudge 1980, Paton 1986, Ryan 1996). These macerals can generate liquid hydrocarbons at relatively low maturity, at the south dome maturity values range from 0.48% - 0.6% R_o. Thus the area has the potential to produce its own oil (Mudge, 1980). As discussed previously Rock eval pyrolysis data suggests that coal has a higher potential to produce hydrocarbons than shales (figure **14**, page 36) (Ryan, 1996).

The origin of oil reservoired within the lower Birkhead Formation and top Hutton Sandstone has long been thought to be sourced from the Permian. As was discussed in section **3.4.2**, there is evidence that oil may also be sourced from the Eromanga Basin sequence. The maturity and source affinity of the oils at the Gidgealpa south dome was established by using sterane and terpane biomarkers (Ryan, 1996). These biomarkers identified two different types of oils at the Birkhead Formation / Hutton Sandstone interface. The first oil from DST 3, which was obtained from above the reservoir in Gidgealpa 17, was

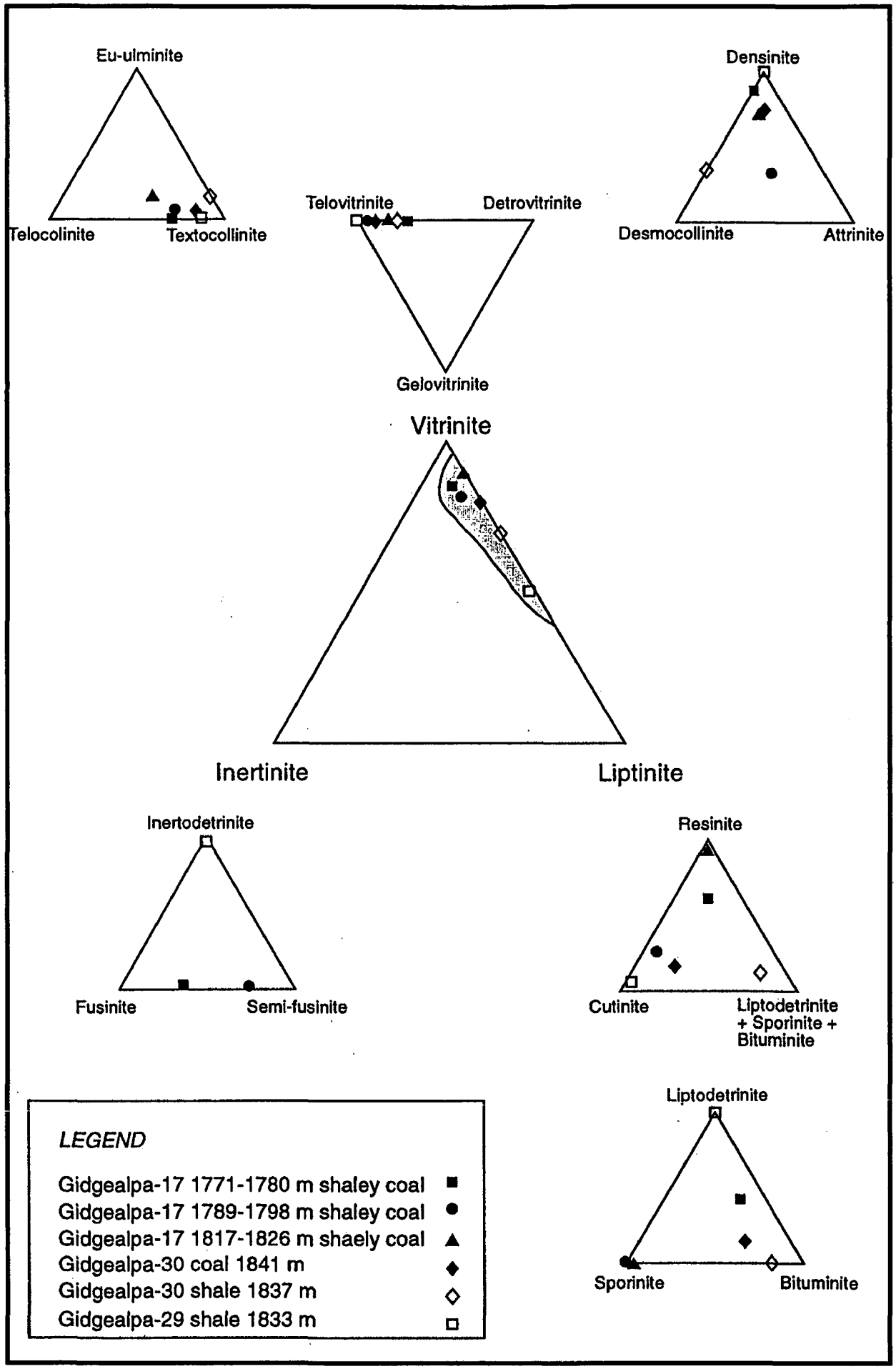

Figure 26: Maceral proportions in coals and shales from the Birkhead Formation, Gidgealpa south dome (From Ryan, 1996).

sourced from coals and is thought to be related to the palaeo-oil column. The relationship between these oils is likely since the DST 3 oil occurs within the sealing section to the present day oil column. Thus, at some time during the past, the Birkhead Formation seal was breached and the oil that was formally trapped below the seal leaked. While the oil migrated through the seal small amounts of oil became trapped within the sandier sections of the upper Birkhead Formation. The second oil, obtained from Gidgealpa 17, DST 4, the within the Hutton Sandstone contains immature 17β,21β-hopane and C_{31} 22R homohopane and is related to the live oil column (Ryan, 1996). The presence of the two oils has been attributed to a dual charge history at the Gidgealpa south dome area from thermal modelling. The first charge is interpreted to have accumulated approximately 90 Ma ago from the Nappamerri Trough and migrated up structural dip while the second charge is currently migrating from Patchawarra Trough.

The presence of a live and palaeo-oil column has been attributed to the changing nature of the seal at the south dome . Boult et. al (1997) determined that the barrier to oil migration was in fact the volcano-lithic arenite sands undergoing diagenesis and not shales which are thought to only have a relatively short lateral extent due to their thin nature. Thus leaking of the initial oil accumulation was due to the organic matter within the sealing sands of the Birkhead Formation maturing and producing hydrocarbons. The production of the hydrocarbons changed the nature of the seal from a water wet to a mixed water / oil or oil wet seal by lowering the capillary entry pressure. The leaky nature of the seal means that the second charge is probably only recently accumulated at the south dome and with time would probably also eventually leak off.

From the MPI it has been determined that the live oil (second charge) was expelled from coaly source rocks at a maturity of approximately 0.65% R_o. Taking into account structural and stratigraphic dips, Boult et. al (1997) established a possible origin for the oil reservoired at the Gidgealpa south

dome. Figure **27** shows that the possible origin of the oil is from the Tindilpie area where R_o=0.64%, the oil has migrated stratigraphically southwards due to the shallow dip as indicated by the lightly shaded area. Once the oil encounters a steep dip (dark shaded area) it can migrate up structure where, in this case it has been trapped by the Gidgealpa south dome structure. What was also noted from sterane and terpane biomarkers was the presence of 17β,21β-hopanes (figure **28**) within the oil, these biomarkers only occur in source rocks with maturities of less than 0.5% R_o and have been suggested to have leached into migrating oil while coming into contact with immature shales and coals. The fact that these biomarkers are present suggests that migration and entrapment of this oil is occurring at present since the ββ hopanes are not stable in hotter areas such as at the Gidgealpa south dome (Ryan, 1996, Boult. et. al, 1997).

Sampled oils within the Birkhead Formation and Hutton Sandstone have elevated levels of Araucariaceae biomarkers present and are thus likely to be sourced from the Jurassic since comparisons of the oils with the Permian sourced oil in the Patchawarra Formation show a significant reduction in concentrations of the biomarkers (Boult et. al, 1997). Further evidence from MPI and R_c show a similar maturity for the Birkhead Formation and the oil within the reservoir, whereas the Permian oils have higher values. Reduced concentrations of methylnapthalenes in both the live and residual oils indicate water washing while Pr / Ph ratios suggests an oxic coal swamp environment of source rocks which are similar to Birkhead Formation source rock samples (figure **29**).

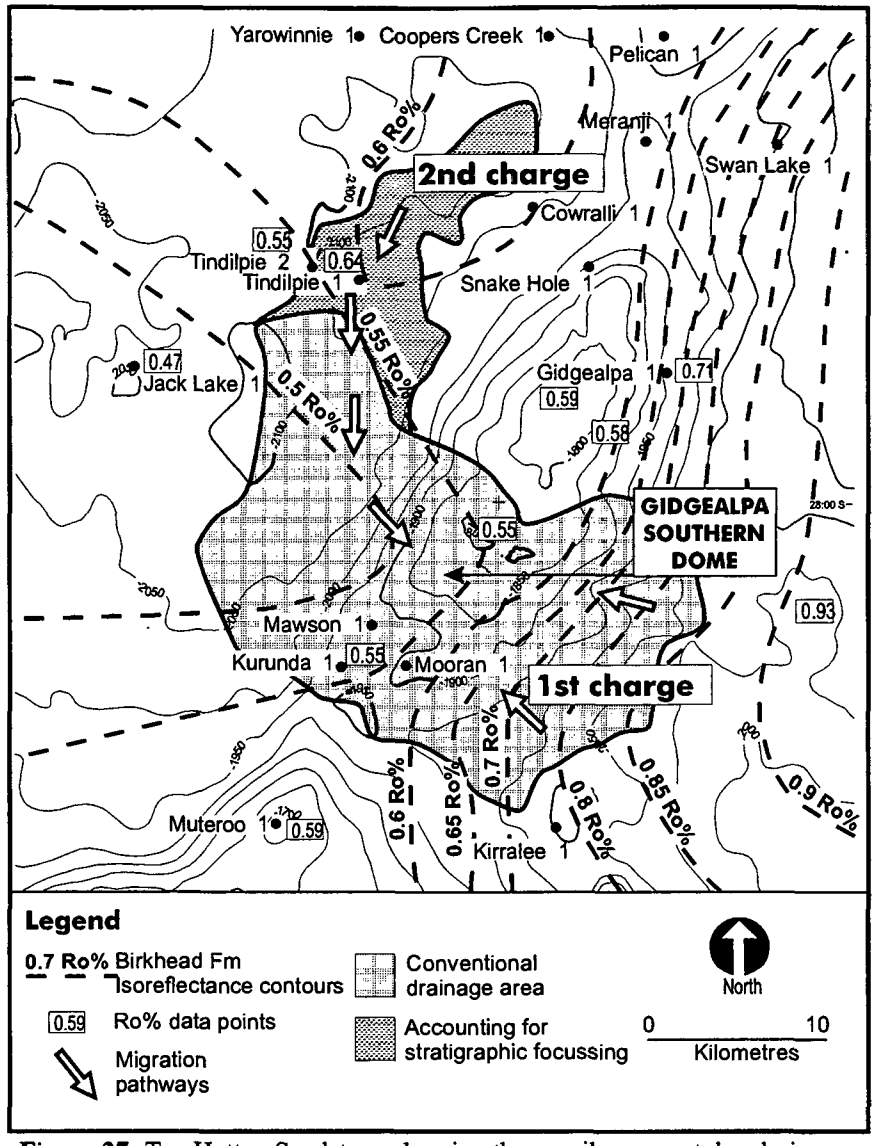

Figure 27: Top Hutton Sandstone showing the possibe present day drainage areas and virtinite isoreflectance contours from the Tindilpie to Gidgealpa south dome areas (From Boult et. al, 1998).

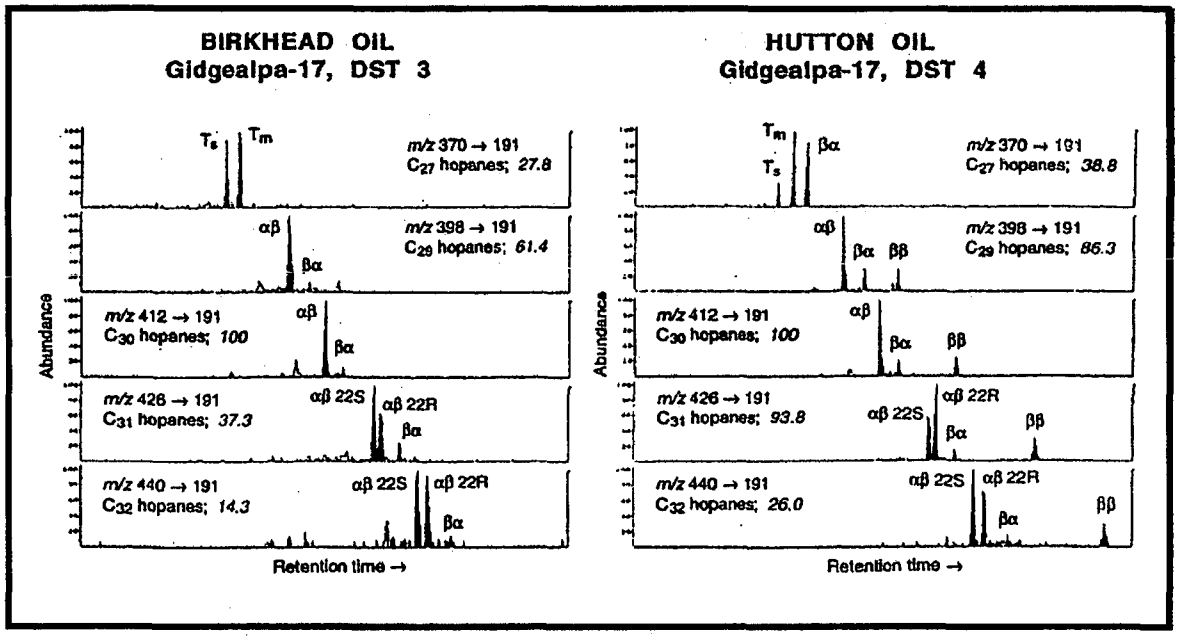

Figure 28: GC-MS-MS chromatograms for DST 3 (Birkhead Formation) and DST 4 (Hutton Sandstone) oil from Gidgealpa 17. Note that the Hutton oil contains the beta-beta peak while it is absent in the Birkhead oil (from Boult et. Al, 1997).

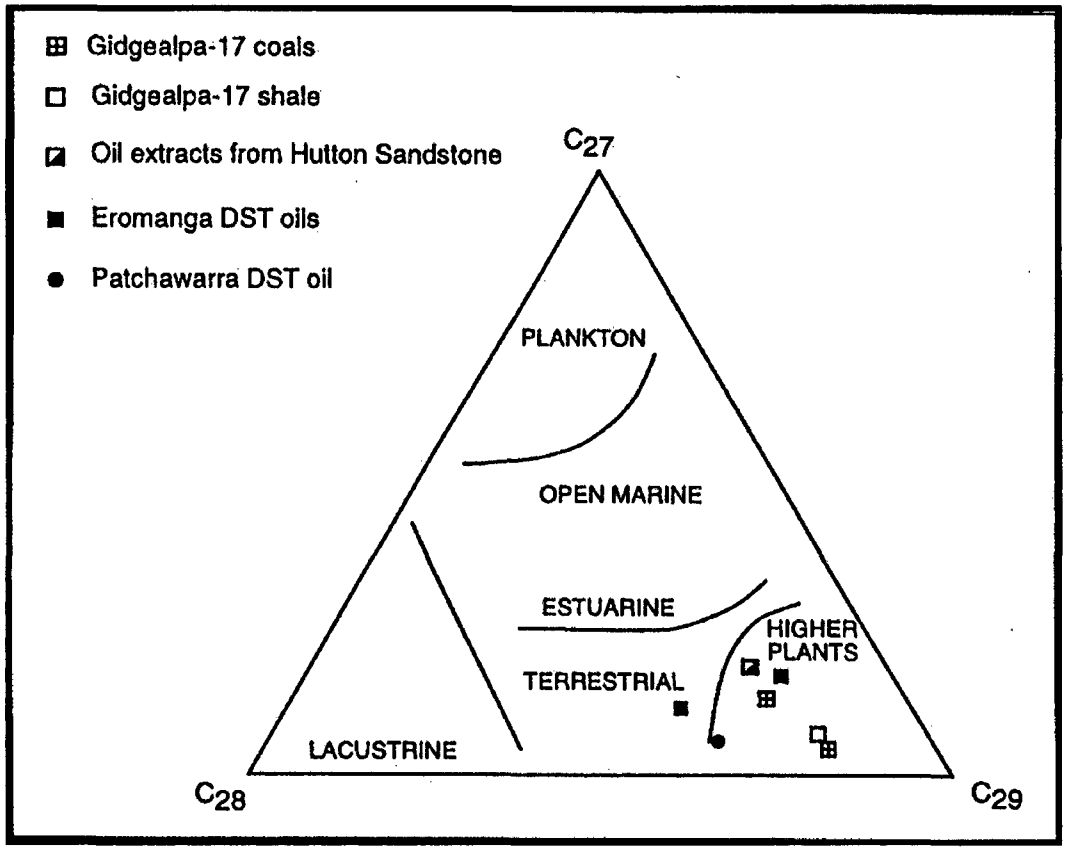

Figure 29: Distribution of regular steranes indicating source input (From Ryan, 1996).

4 Core Logging, Sedimentology and Facies Models

In order to fully understand and characterise a reservoir, detailed core logging is a necessity rather than just a consideration. Core logging gives the geologist insight into depositional environments and allows a degree of anticipation of sediments away from the well bore (or core) thus providing a more accurate determination of reservoir facies and their distribution . Core logging and the determination of facies allows for possible correlation with wireline logs and thus provides another identification tool in wells where core is unavailable.

At the Gidgealpa south dome 6 cores with a total length of 360 feet have been cut. Three traverse the basal section of the Birkhead Formation (Gidgealpa 26, 30 and 31), two cover the basal part of the Birkhead Formation and the top Hutton Sandstone transition (Gidgealpa 29 and 32) and one core is entirely within the top Hutton Sandstone (Gidgealpa 17). All of the cores with the exception of Gidgealpa 17 (summarised in figure **30**), were logged in detail at a scale of 1:12 to fully characterise the facies. Core log descriptions can be found in appendix **2**.

4.1 Sedimentology of the Birkhead Formation and Hutton Sandstone, Gidgealpa south dome

Walker (1984) stated that:

"Subdivision of a rock body into constituent facies (or units of similar aspect) is essentially a classification procedure, and the degree of subdivision must first and foremost be governed by the objectives of the study."

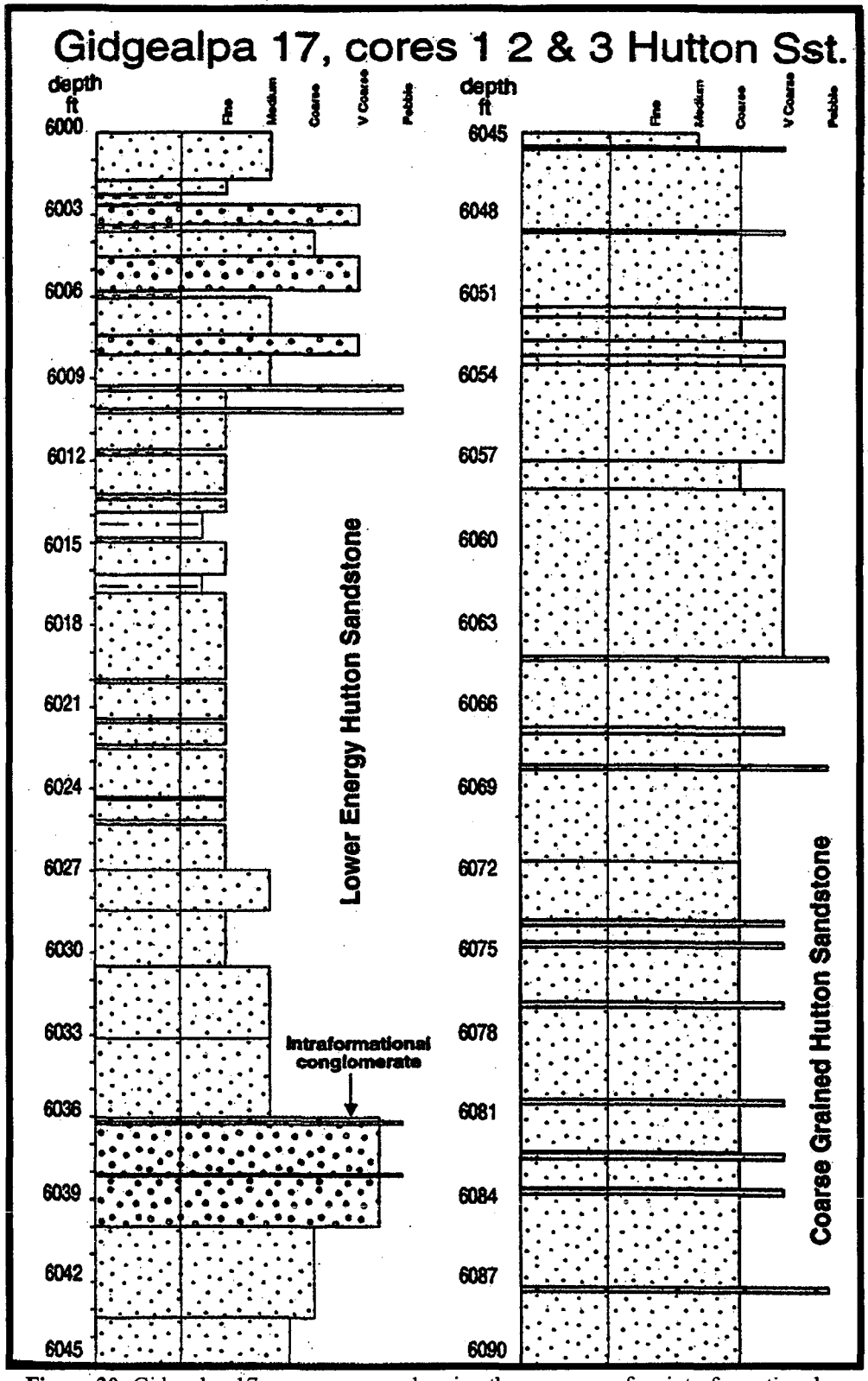

Figure 30: Gidgealpa 17 core summary showing the presence of an intraformational conglomerate separating higher and lower energy deposited facies (From Boult, 1996).

From cores at the Gidgealpa south dome, I have used a highly detailed classification procedure. The detailed description of sediments is necessary for 3 reasons:

1) to accurately define the sedimentary environments
2) to determine the interaction of different facies with each other, and
3) to determine heterogeneities within flow units for conducting reservoir description.

Determination of sedimentary environment and the interaction of facies go hand in hand. Facies which are deposited in a braided fluvial environment will interact differently than if they are deposited in a meandering fluvial environment. To understand the relationships between facies they must be finely subdivided, otherwise the interaction of these facies will not be seen at the broader scale. For example if we consider a meandering fluvial environment and broadly divide the sequence into channel or floodplain sediments then fine grained silt beds which may be present between channel sandstones will be overlooked. The same applies to floodplain sediments; if the sequence is not analysed in detail then the internal structure of sheet sands of crevasse splays can be missed. Thus the first two reasons to subdivide at a fine scale will ultimately have an effect on the third. For reservoir characterisation the finer grained silts which may be present between channel sands may act as barriers to fluid flow, while sands within floodplain sequences may also contain internal barriers or a variation in the type of sands present. In both cases the internal identification of facies in sands will effect reserve estimation and ultimate recovery.

Although the fine scale determination of facies is important, the rock sequence in question must be examined at a broader scale to get an 'overall' idea of the facies present. Starting at a broader scale I was able to determine the changing depositional environments of the sediments and also estimate how many different facies types would be needed to accurately characterise the

sediments. After detailed inspection of the cores I was able to produce a generalised sequence through the top Hutton Sandstone and the Birkhead Formation showing the change in depositional environments (figure **31**). The top Hutton Sandstone and the basal Birkhead Formation sequence was determined by the use of core while the upper Birkhead Formation was inferred from the wireline log signatures since no core was present. From the analysis of the Gidgealpa wells 11 lithofacies were defined and are summarised in table **2**.

For this study the naming of the lithofacies units has been adopted from Miall (1977 and 1992). The first letter in the name describes grain size characteristics, ie.

G: Gravel, including pebbles
S: Sand, fine to coarse grained
F: Fine sediments, silts and muds

while the suffix is related to the sedimentary structure within the lithofacies, ie.

p: planar crossbeds
t: tabular crossbeds
m: massive

and so on. Thus as an example; a sand that is fine to medium grained and has planar cross-beds would be identified as being lithofacies Sp while a laminated siltstone would be identified as lithofacies Fl.

The detailed descriptions from the cores along with an interpretation of the depositional setting of each of the lithofacies in table **2** are displayed below in sections **4.2** to **4.2.3**. Due to the limited amount of data that can be derived from the one-dimensional core, interpretation from various authors has been relied upon to determine the likely size and distribution of some of the lithofacies.

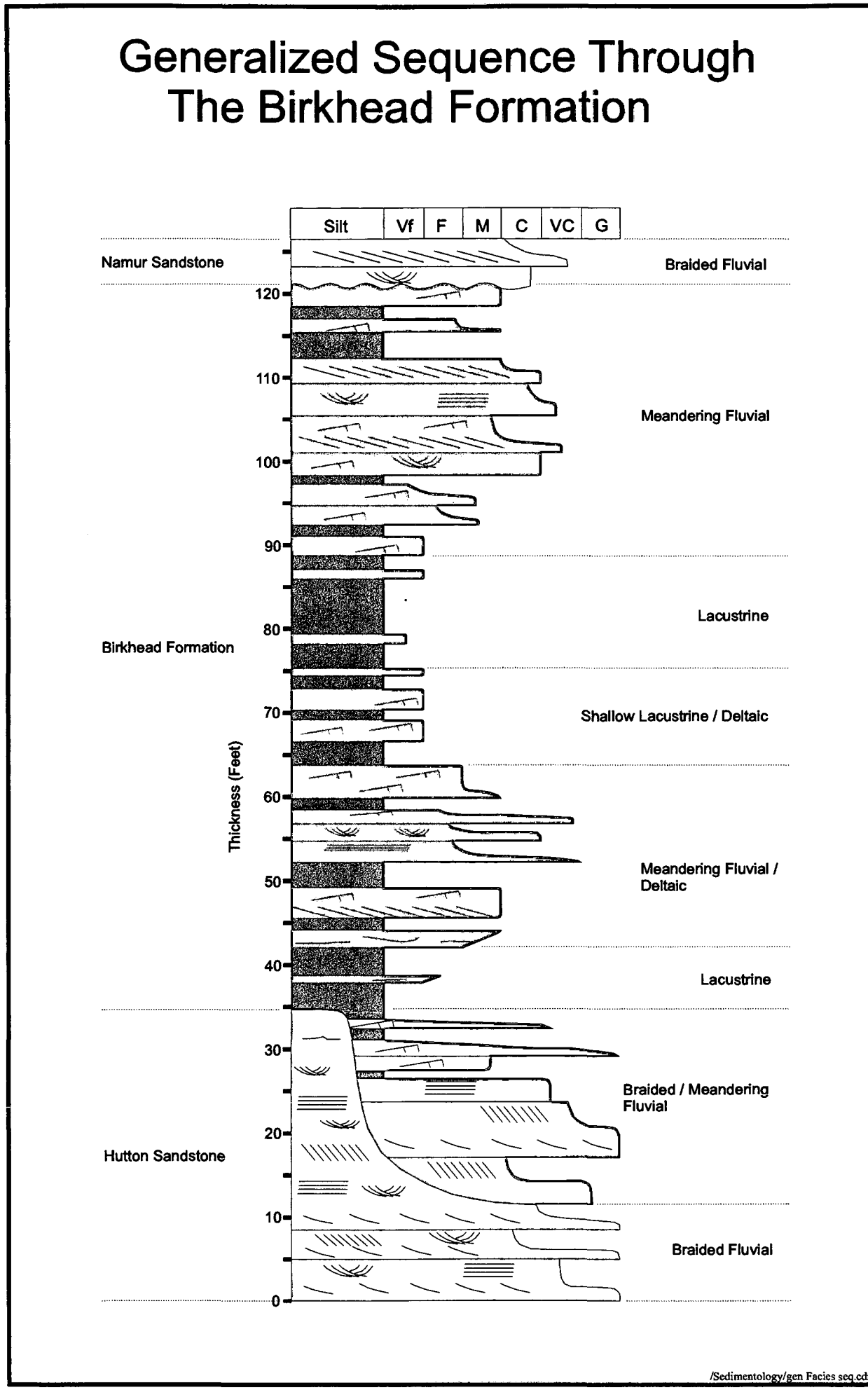

Figure 31: Generalized sequence through the Birkhead Formation and top Hutton sandstone.

Lithofacies Identifier	Sediment Type	Sedimentary structures	Interpretation
Gm	gravel, massive or crudly bedded, minor sand, silt or clay lenses	ripple marks, crossbeds in sand units, gravel imbrication	longitudinal bars, channel lag deposits
Gt	gravel, stratified	broad, shallow trough crossbeds, imbrication	minor channel fills
St	sand, fine to very coarse, may be pebbly	solitary (theta) or grouped (pi) crossbeds	dunes (lower flow regime)
Sp	sand, fine to very coarse, may be pebbly	solitary (alpha) or grouped (omikron) planar crossbeds	linguoid bars, sand waves (upper and lower flow regime)
Sm	sand, fine to coarse	massive	caused by plant bioturb, or dewatering of the sand
Sh	sand, very fine to very coarse, may be pebbly	horizonal lamination, parting or streaming lineation	planar bed flow (lower and upper regime
Sr	sand, very fine to coarse	ripple marks of all types, including climbing ripples	ripples, (lower flow regime)
Sd	sand, medium to very fine grained, silt/mud interbedded	contorted, microfractured bedding	abandoned channel fill, floodplain deposits, delta front facies
Sb/Fb	sand, medium to very fine grained, silt/mud interbedded	bedding destroyed by bioturbation, trace fossils	slow or periodic deposition
Fl	sand (very fine), silt, laminated mud, interbedded	ripple marks, undulatory bedding, plant rootlets	deposits of waning floods, overbank deposits, subaqueous levees
Fm	mud,silt	rootlets, desiccation cracks	drape deposits formed in pools of standing water
Fcs	very fine sand, mud, silt	massive to faintly laminated, organic matter(small roots present	poorly drained swamp
Fos	very fine sand, mud, silt	massive to faintly laminated (oxidised)(larger roots present)	well drained swamp
C	coal	massive/plant material	highly vegetated swamp

Table 2: Hutton Sandstone / Birkhead Formation lithofacies summary (based on Miall classification).

Figures illustrating the lithofacies in the following sections can be found in figures **32** to **38** (pages 72 to 78).

4.2 Lithofacies Descriptions in Core

4.2.1 Gravel Lithofacies

4.2.1.1 Lithofacies Gm (massive to crudely bedded gravel)

Core Description: (figure 32)

This crudely horizontal stratified to massive pebble or cobble gravel occurs as either clast or matrix supported gravels of varying thickness. Occasional thin crossbedded or ripple bedded sands may also occur with the gravels as well as sub-planar bedding. The base of this lithofacies is erosional and channel lag deposits are also included. Granule to pebble (2mm - 8mm) grains are typically sub-rounded to sub-angular and consist mainly of quartz (especially in the Hutton Sandstone). Large, pebble to gravel sized, angular to rounded mud clasts are also present (mainly within the Birkhead Formation) and range in size from 0.5 - 2.5 cm. Coaly fragments range from 1 cm up to 5 cm in length and 2 cm in width.

Interpretation:

Lithofacies Gm is deposited in high, upper flow energy regimes as a traction load in the form of longitudinal migrating bar deposits and channel lags (Williams, 1982). The longitudinal bar deposits are mainly found in pebbly braided rivers and form by a build up of gravel over an obstruction or channel lag deposit. The low relief of longitudinal bars can be explained by the low depositional dips observed in drill core (Miall 1977). This lithofacies can form superimposed sediment sets up to 4 metres thick

with a lateral extent of hundreds of metres; however at Gidgealpa the thickness is restricted to approximately 12 cm with a possible lateral extent of tens of metres. Longitudinal bars are very common in braided fluvial deposits and is unlikely to be seen in a meandering system. This lithofacies can also form as channel lags during flood stage when water velocity is high in the deepest parts of both Hutton Sandstone, braided fluvial and Birkhead Formation, meandering channels. The thickness of these sediments is usually in the order of tens of centimetres and has a lateral extent that is restricted to the deep parts of the fluvial channel. Large coaly fragments commonly seen associated with these sediments within the Birkhead Formation consist of woody material which has become water logged and has subsequently sunk to the base of the channels.

4.2.1.2 Lithofacies Gt (trough-crossbedded gravel)

Core Description: (**figure** 32)

This stratified gravel consists of trough to planar cross bedded units of no more than 5 cm in thickness. The cross beds are generally low angle with the occurrence of either cross bed type appearing to be deposited in a random order. Grains tend to be aligned in places with grain size varying from coarse sand (0.5mm) to small to medium sized pebbles (0.8cm to 1.5cm), larger sand grains tend to be rounded to sub-angular. Cross beds of coarse sand can occur between gravel and pebble crossbeds.

Interpretation:

Sediments occur in broad, shallow, minor channels, normally 20cm to 3m deep and 1 to 12m wide (Miall,

1977); the channels intersect and cut each other laterally and vertically by cross channels. The erosional nature of this lithofacies means that a lag may be present filling the base of the troughs. Foreset dip is dependent on trough size, with the largest dip in the smaller troughs. Trough-cross bedded gravel forms during intermediate to flood stage where water velocity is high enough to move gravel and cobble sized grains (Doeglas, 1962). This lithofacies appears only to occur in the Hutton Sandstone and is rare.

4.2.2 Sandy Lithofacies

4.2.2.1 Lithofacies St (Trough-crossbedded sand)

Core Description: **(figure** 33)

Trough cross bedded sandstones occur as either groups of mutually exclusive cross-cutting poorly to well defined troughs or individual scours which can be erosional at the base of the lithofacies. Sand within the lithofacies is generally moderately to moderately well sorted and grain sizes range from medium to coarse. Sediment grading is common with a fining up pattern occurring within individual beds, pebbles are occasionally deposited at the base of beds. Set thicknesses range from 5 to 30 cm with smaller sets more common in the Birkhead Formation.

Interpretation:

This lithofacies forms dunes in the lower flow regime, within the main channel (Miall 1992, Williams 1982). Trough cross bedded sands may also be deposited as lateral compound bars and in abandonment fills and proximal crevasse splay sands (Williams 1982).

4.2.2.2 Lithofacies Sp (Planar cross-bedded sand)

Core Description: (**figure** 33)

This lithofacies includes both high and low angle planar crossbeds, the sediments range from very well sorted to poorly sorted and grain size ranges from fine to very coarse. Sediment grading may also occur as in lithofacies St. In cross-section the planar crossbeds consist of sharp, flat or slightly scoured bases and tops.. Sets can occur singly or in co-sets where thickness and width can range in size from 5 to 40 cm sets.

Interpretation:

This lithofacies is deposited in the lower flow regime and develops on flat surfaces, truncating the St lithofacies on linguoid bars or advancing sand sheets and sand waves in the upper and lower flow regime (Cant and Walker 1976, Brierley, 1991, Miall 1992). Lithofacies Sp is also formed by the migration of transverse bars (Rust, 1971). Planar crossbed fore-sets represent avalanche slopes and can be seen by grain size variations (particularly in the Hutton Sandstone). Reactivation surfaces may also be present (Williams and Rust, 1969, Miall, 1977). In three dimensions the cross strata are slightly sinuous in a lateral direction with individual troughs extending downstream as much as 6 m but have also been seen to extend up to 18 m (Cant and Walker, 1976).

4.2.2.3 Lithofacies Sm (Massive sand)

Core Description: (**figure** 34)

Thickness varies from centimetres to tens of centimetres, with grain sizes ranging from fine to medium. In the Birkhead Formation massive sandstones are generally well sorted and can contain root casts and rare pebbles and/or mud clasts. Hutton Sandstone Sm lithofacies is generally moderately well sorted and has common pebble sized grains.

Interpretation:

This lithofacies, especially in the Birkhead Formation, is thought to have been formed by the destruction of the original bed forms by mechanisms such as root or animal bioturbation or by diagenetic overprinting (Williams, 1982). Massive sandstones may also be formed by channel bank collapse or where sediments are rapidly dumped by deposition of sediment pulses or by fluid escape (most likely within the Hutton Sandstone). This lithofacies is seen in channels, crevasse splay and mouth bar sandstones. Careful study of the rock must be carried out as some sediments which appear to be massive are actually low angled to horizontally bedded.

4.2.2.4 Lithofacies Sh (Horizontally-bedded sand)

Core Description: (**figure** 35)

Grainsize characteristics range from very fine (Birkhead Formation) and well sorted to coarse (Hutton Sandstone) and moderately sorted, with the occasional pebble or intraformational debris. This lithofacies occurs with parting or streaming lineations. Individual bed boundaries of the lithofacies within the Birkhead Formation are generally rich

in micaceous or carbonaceous material. Overall bed thickness of this lithofacies ranges from 2 to 25 cm.

Interpretation: The type of horizontal bedding produced seems to be dependent on depositional environment with sediments being deposited in either the upper or lower flow regime. Sediments occur as cut off channel fills, spill offs on the lee side of gravel bars, bar veneers and occasionally as small dunes and sandy transverse bars (Smith, 1974).

4.2.2.5 Lithofacies Sr (Ripple cross-laminated sand)

Core Description: **(figure** 35) Lithofacies Sr is by far the most abundant within the Birkhead Formation; in the Hutton Sandstone however, it is very rare and occurs within Hutton / Birkhead transitional sediments. This lithofacies ranges in thickness from 2 cm to 1 m with grain sizes ranging from very fine to fine. Internal structures formed by ripple migration include solitary ripple trains, small scale trough and planar cross bedding and climbing ripples.

Interpretation: This sediment is deposited under lower flow regime conditions in isolated active channels depending on flow velocity and the rate of sediment supply . Variations in ripple type depends on flow velocity and the rate of sediment supply (Allen, 1970). This lithofacies is found in the upper part of compound bars of meandering fluvial channels, in crevasse lobes, in flood plain sequences and is abundant in delta mouth bar and delta front sediments as well as subaerial and subaqueous levees.

4.2.2.6 Lithofacies Sd (Soft Sediment deformed sand/mud)

Core Description: (**figure** 36)

This lithofacies is a silty to fine to very fine grained sandstone which can undergo a number of sedimentary processes. Original bedding which appears to have originally sharp and continuous has been disturbed and contorted; in other parts where sediments are more consolidated microfractures have formed. Structures also formed include ball and pillow structures and fluid escape structures. Root casts and coaly stringers may be present and limited bioturbation may occur.

Interpretation:

Structures produced by soft sediment deformation include sediment loading, roots and dewatering. When a package of sediment of higher density is deposited on a previous set of sediments liquefaction and lateral intrastratal flow may occur. Distortions can also occur by turbulent sandstone flows during rapid deposition. These sediments are found as crevasse splays that contain coaly stringers and delta front and channel fills (Watts, 1987). Channel fill sediments are observed as usually have high angle bed dips.

4.2.3 Fine Grained Lithofacies

4.2.3.1 Lithofacies Sb/Fb (Bioturbated Sand/Mud)

Core Description: (**figure** 37)

Most of the Birkhead sediments are bioturbated when compared with the Hutton Sandstone. Bioturbation occurs in sandstones, siltstones and interbedded

sandstone / siltstones. Trace fossils vary in type and abundance depending on the surrounding environment and types of sediment with *Endichnia* being the main type (Collinson and Thompson, 1989). In many cases original sedimentary structures have been severely distorted or destroyed.

Interpretation: Bioturbation within the Birkhead Formation occurs in most depositional environments such as floodplain and accreted over bank deposits where deposition is slow or periodic. The sediments are submerged in oxygenated waters allowing burrowing animals to establish themselves in the sediment surface.

4.2.3.2 Lithofacies Fl (Laminated sand, silt and mud)

Core Description: **(figure** 37) This lithofacies consists of sets of siltstone laminations with occasional very fine sandstone lenses occurring between laminations. The laminations themselves may also display low amplitude ripples. Sandstone lenses tend to contain internal structures such as small scale ripple marks and cross laminations. Siltstone laminations may show undulating to wavy bedding and occasional burrows from bioturbation may be present. Bed thickness for lithofacies Fl within the Birkhead Formation ranges from centimetres to tens of centimetres.

Interpretation: Miall (1977) has determined that this lithofacies has variable lateral extent and is possibly dependent on the available area of deposition. Laminated siltstones

deposited in cut off channels and on the lee side of channel bars will be of limited lateral extent due to local topography of the channel whereas Fl lithofacies deposited on the floodplain after crevasse splay incursion will have a greater aerial extent. This lithofacies may also be associated with the lower part of upward-coarsening sequences (Williams 1982).

4.2.3.3 Lithofacies Fm (Mud/Silt Drape)

Core Description: **(figure** 37)

This lithofacies consists of dark grey massive to laminated silts and muds, the lithofacies can also appear light brown where siderite cementation has occurred. Carbonaceous streaks may also be present but are rare. While laminations of very fine sand are usually horizontal they can occur as wave oscillations or at high angles with associated contorted bedding. Bed thickness ranges from approximately 1 - 12 cm.

Interpretation:

This lithofacies is deposited from suspension and occurs as drape over underlying sediments. Sediments are found in similar environments as lithofacies Fl, in low-lying areas which is commonly water-logged (Smith, 1974). Where high angle laminations and contorted bedding occur, these sediments have been deposited as abandonment channel fill, probably on point bar sands and subsequent loading has caused slumping to occur (Watts 1987).

4.2.3.4 Lithofacies Fcs (Carbonaceous silt/mud)

Core Description: (**figure** 38)

This lithofacies is light to dark brown and can contain interbeds of lithofacies C. Primary structures are rare due to intense root bioturbation, roots are generally no more than 1 cm in length. Laminations, when present are parallel. The sediments also have a high organic content with coalified small roots, twigs and leaves, bands of high organic content also occur (usually no more than 5 cm in thickness). Siderite nodules are common.

Interpretation:

This lithofacies is interpreted as poorly drained swamp deposits (Ethridge et. al, 1981). Within the Birkhead Formation, the high content of carbonaceous material is probably due to anoxic conditions preserving the organic matter in the sediments. When organic matter is abundant coal may form. Favourable reducing conditions allow siderite nodules to form soon after burial. This lithofacies is associated with crevasse splay and floodplain sediments as well as well drained swamp deposits (lithofacies Fos).

4.2.3.5 Lithofacies Fos (Oxidised silt/mud)

Core Description: (**figure** 38)

These mostly massive claystones are olive grey to brown / olive green in colour and have a high silt content and low organic content. Internal structure has been destroyed by large roots and possibly invertebrate bioturbation. The thickness of this lithofacies can range up to 1 metre.

Interpretation: Lithofacies Fos are well drained swamp deposits. Oxidisation has caused the characteristic colouring and lack of organic matter during short periods of sub-aerial exposure (Ethridge et. al, 1981 and the lack of exposure time means that soils were never developed. Like lithofacies Fcs, this lithofacies is usually found deposited on the floodplain near crevasse splay and poorly drained swamp deposits.

4.2.3.6 Lithofacies C (Coal)

Core Description: **(figure** 38) Lithofacies C consists of brown to black, lignitic compacted organic material such as plant debris and layers of dark brown dirt / mud interbeds. Bed thickness is generally in the order of tens of centimetres.

Interpretation: These coals are probably autochthonous, forming from local vegetation such as shrubs and reeds in a swamp / marsh environment, thus coal lithofacies are associated with poorly drained swamp deposits. Locally, the thinness of the coal suggests a limited aerial extent.

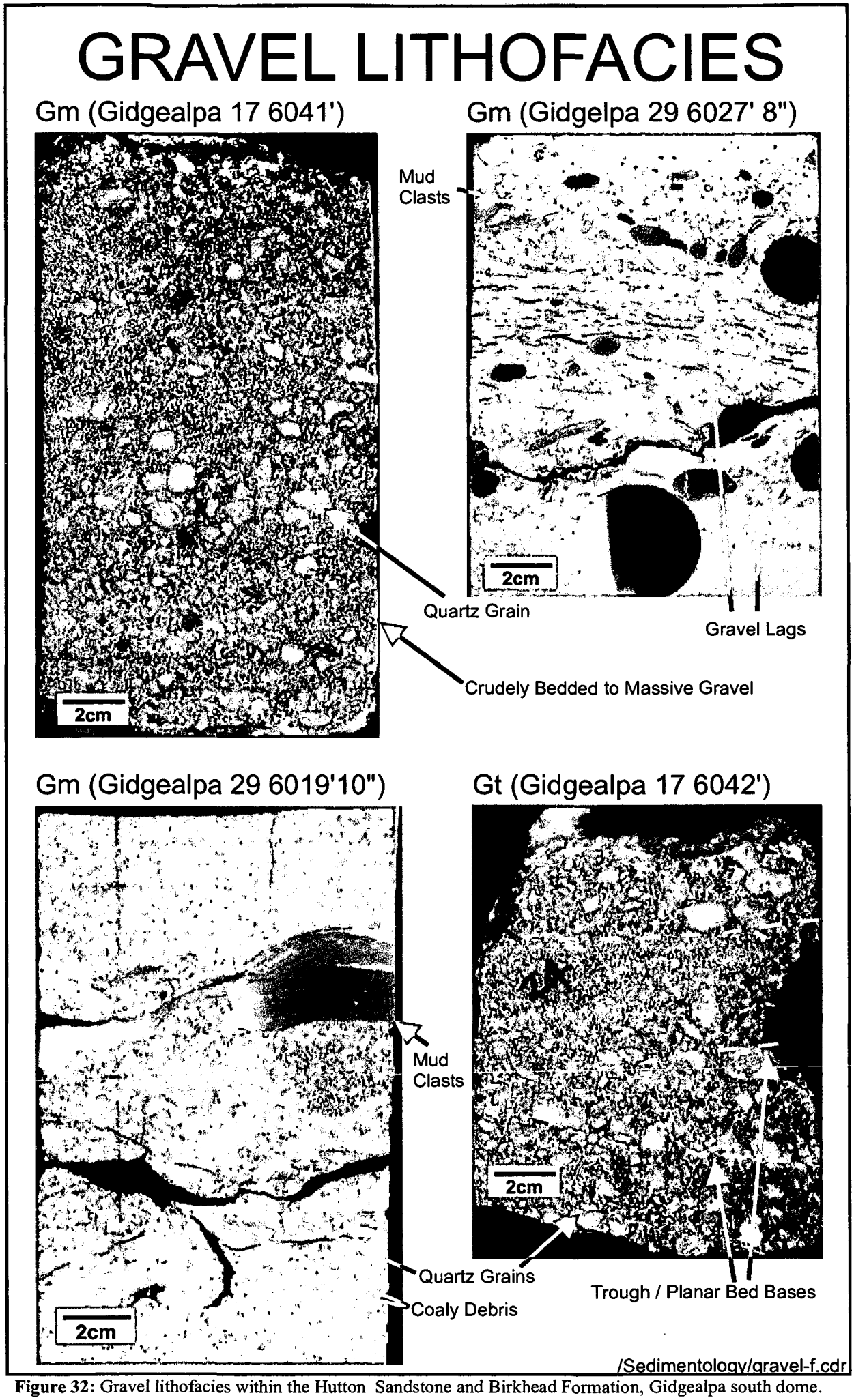

Figure 32: Gravel lithofacies within the Hutton Sandstone and Birkhead Formation, Gidgealpa south dome.

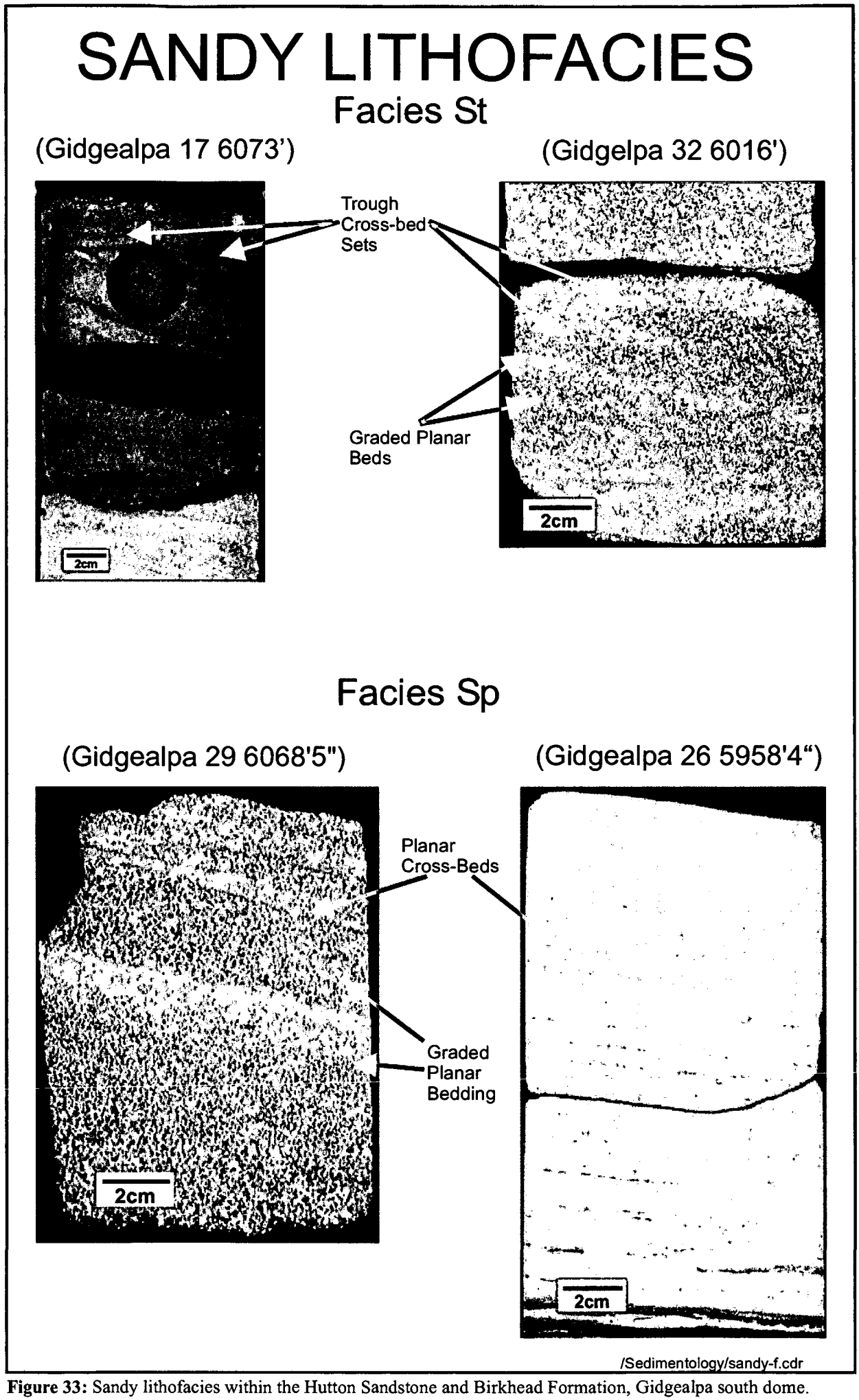

Figure 33: Sandy lithofacies within the Hutton Sandstone and Birkhead Formation, Gidgealpa south dome.

SANDY LITHOFACIES

Facies Sm

(Gidgealpa 29 6040'7"')

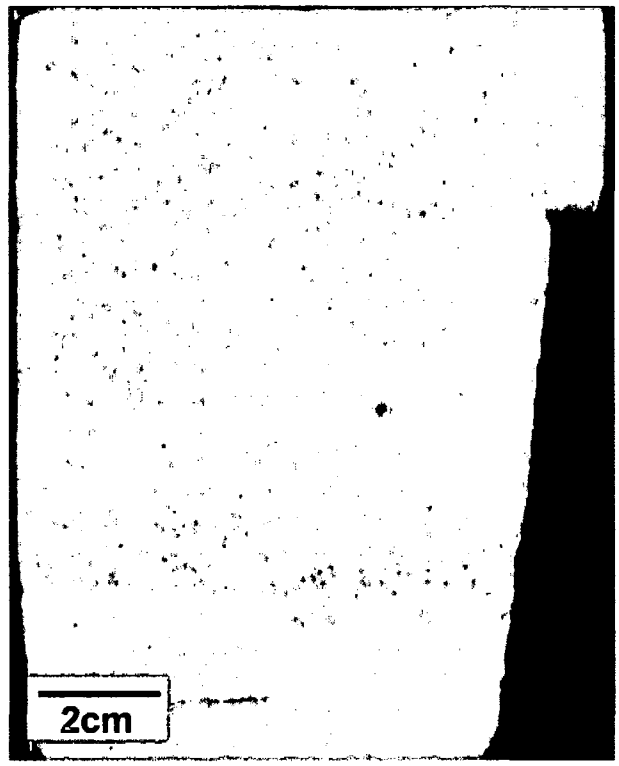

(Gidgelpa 31 5978')

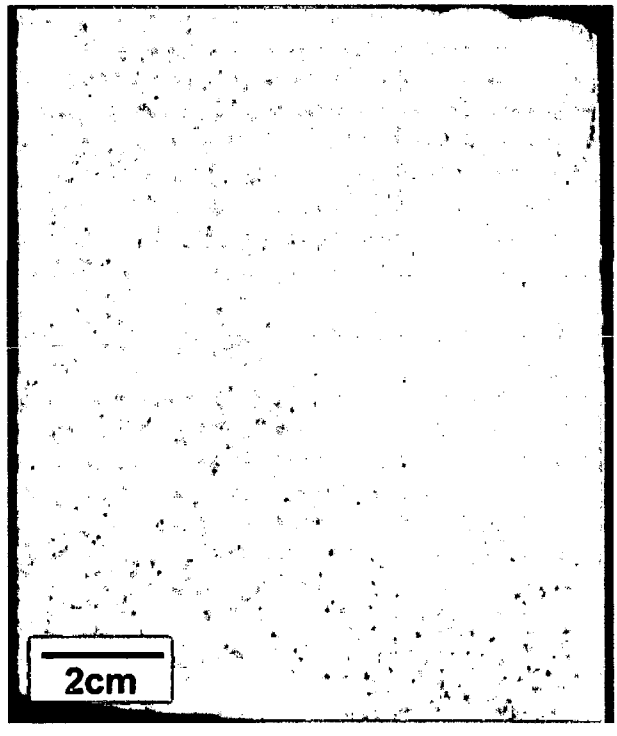

/Sedimentology/Sandy-f3.cdr

Figure 34: Examples of lithofacies Sm within the Hutton Sandstone and Birkhead Formation, Gidgealpa south dome.

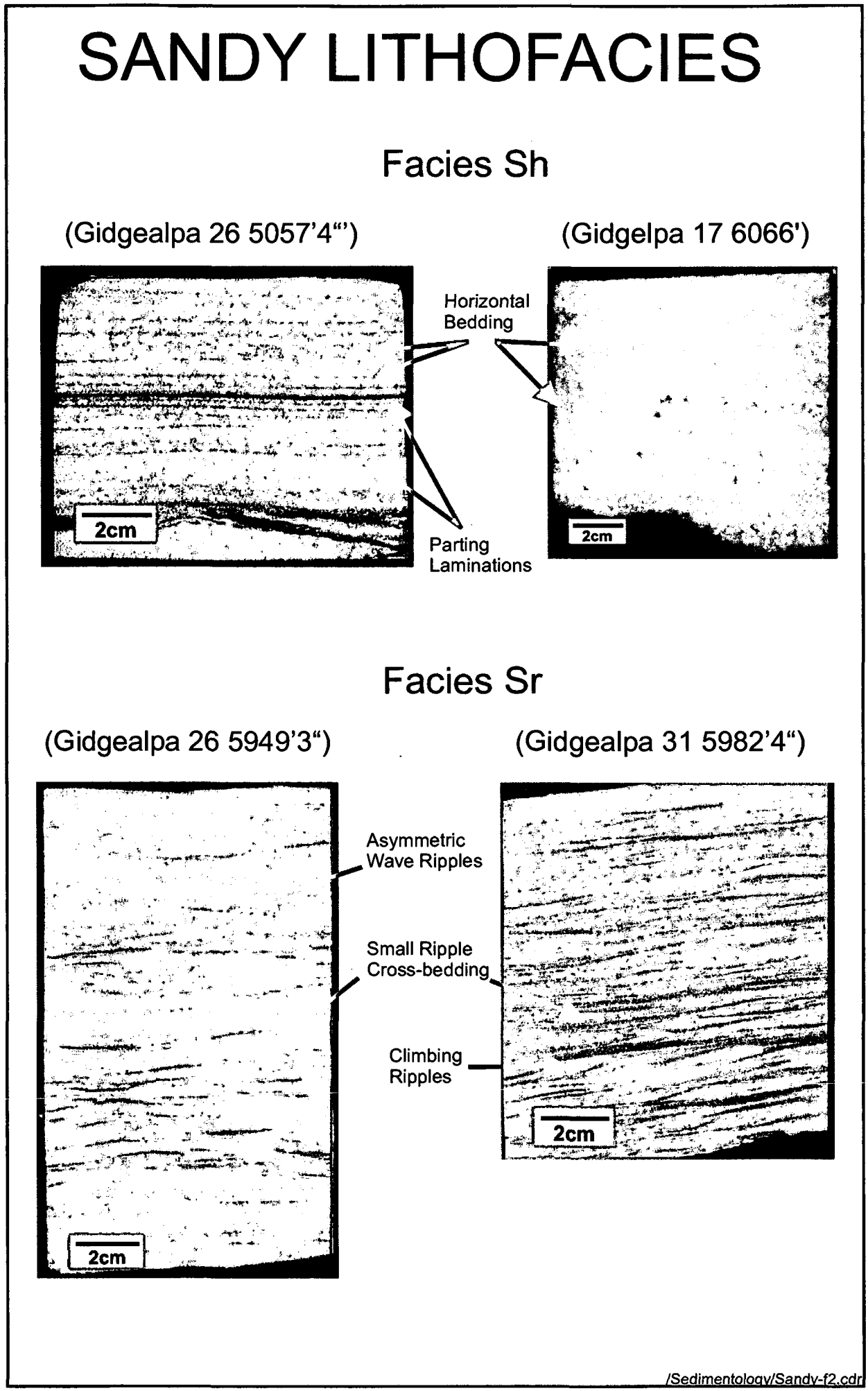

Figure 35: Examples of lithofacies Sh and Sr within the Hutton Sandstone and Birkhead Formation, Gidgealpa south dome.

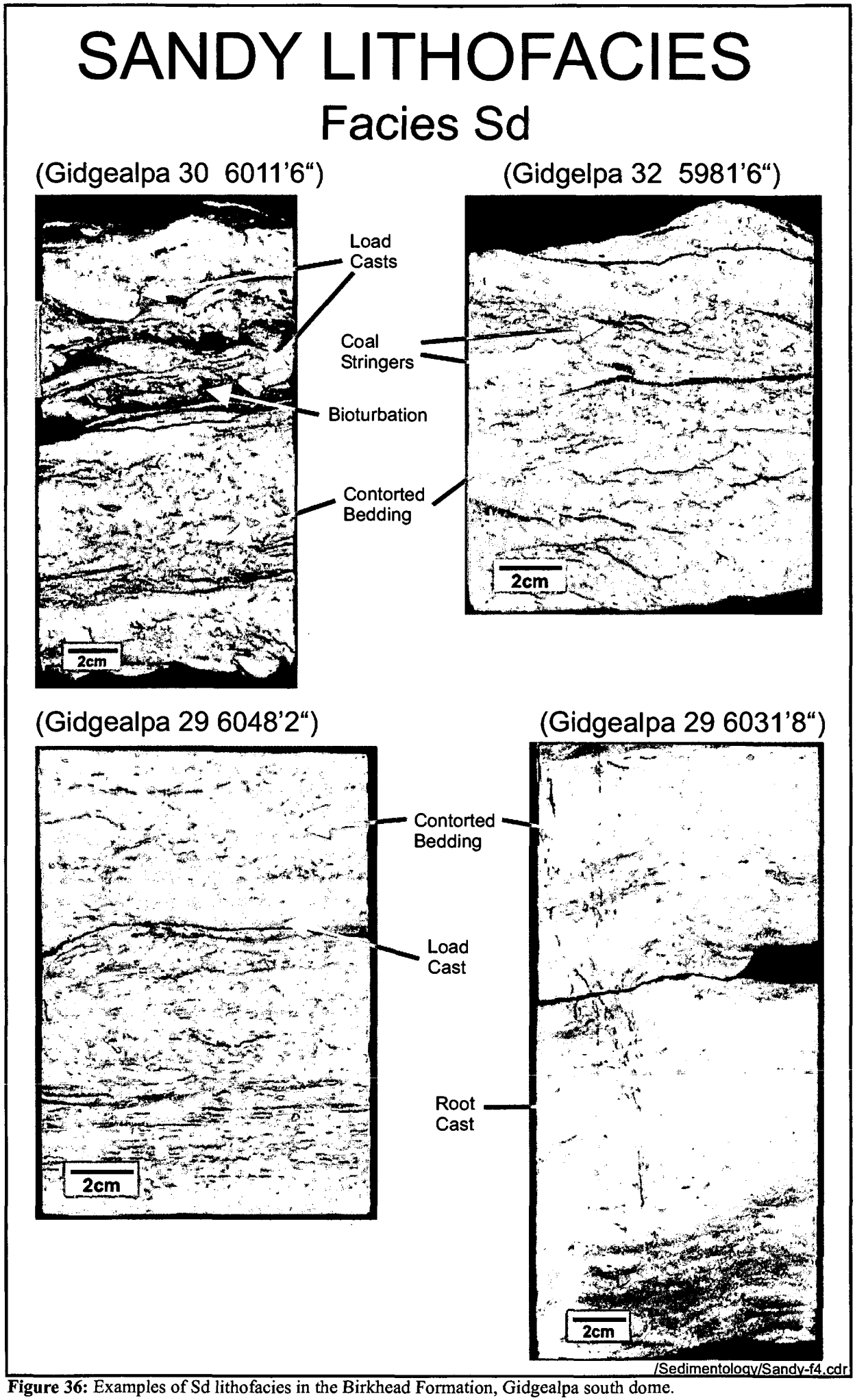

Figure 36: Examples of Sd lithofacies in the Birkhead Formation, Gidgealpa south dome.

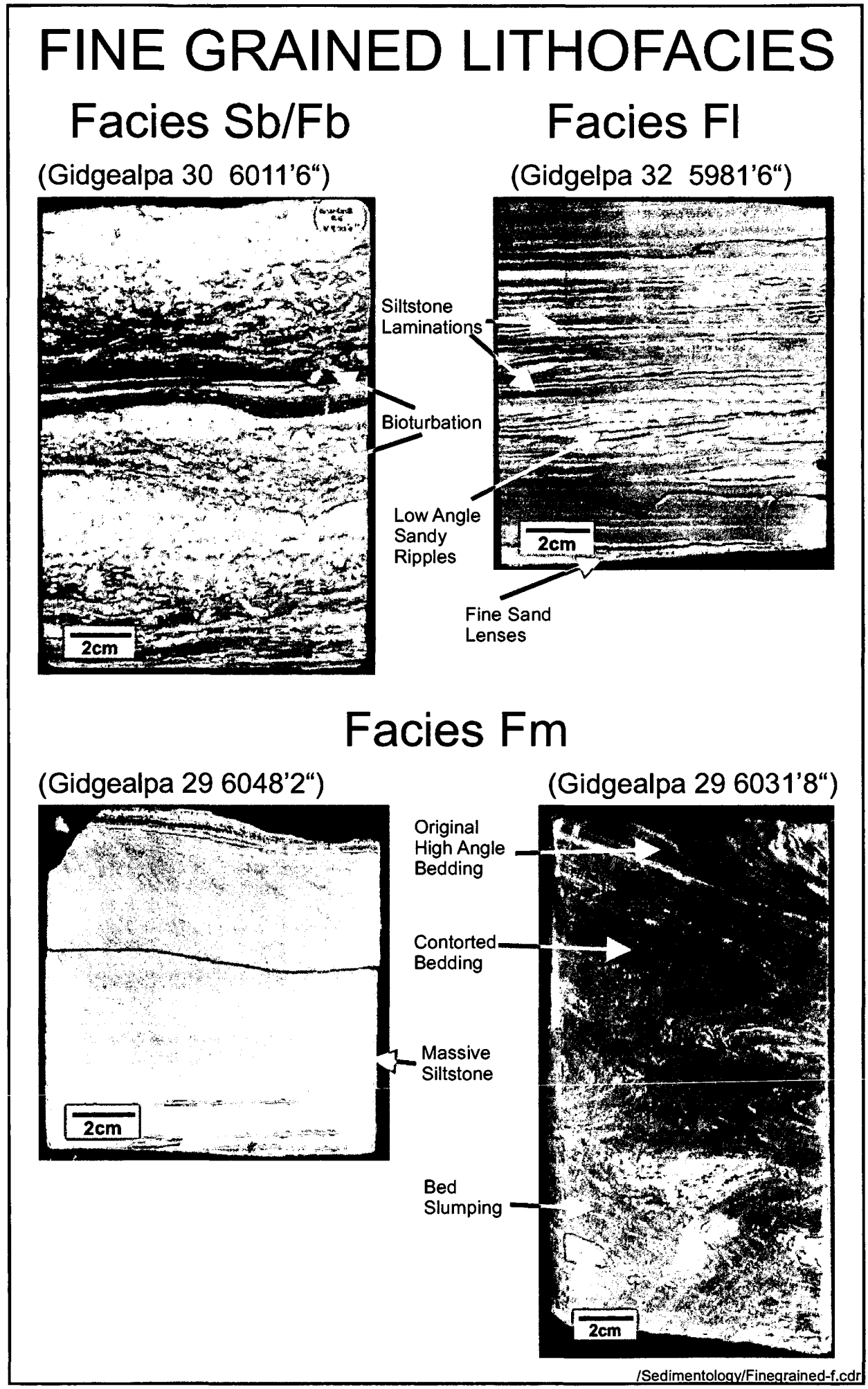

Figure 37: Examples of lithofacies Sb/Fb, Fl and Fm within the Birkhead Formation, Gidgealpa south dome.

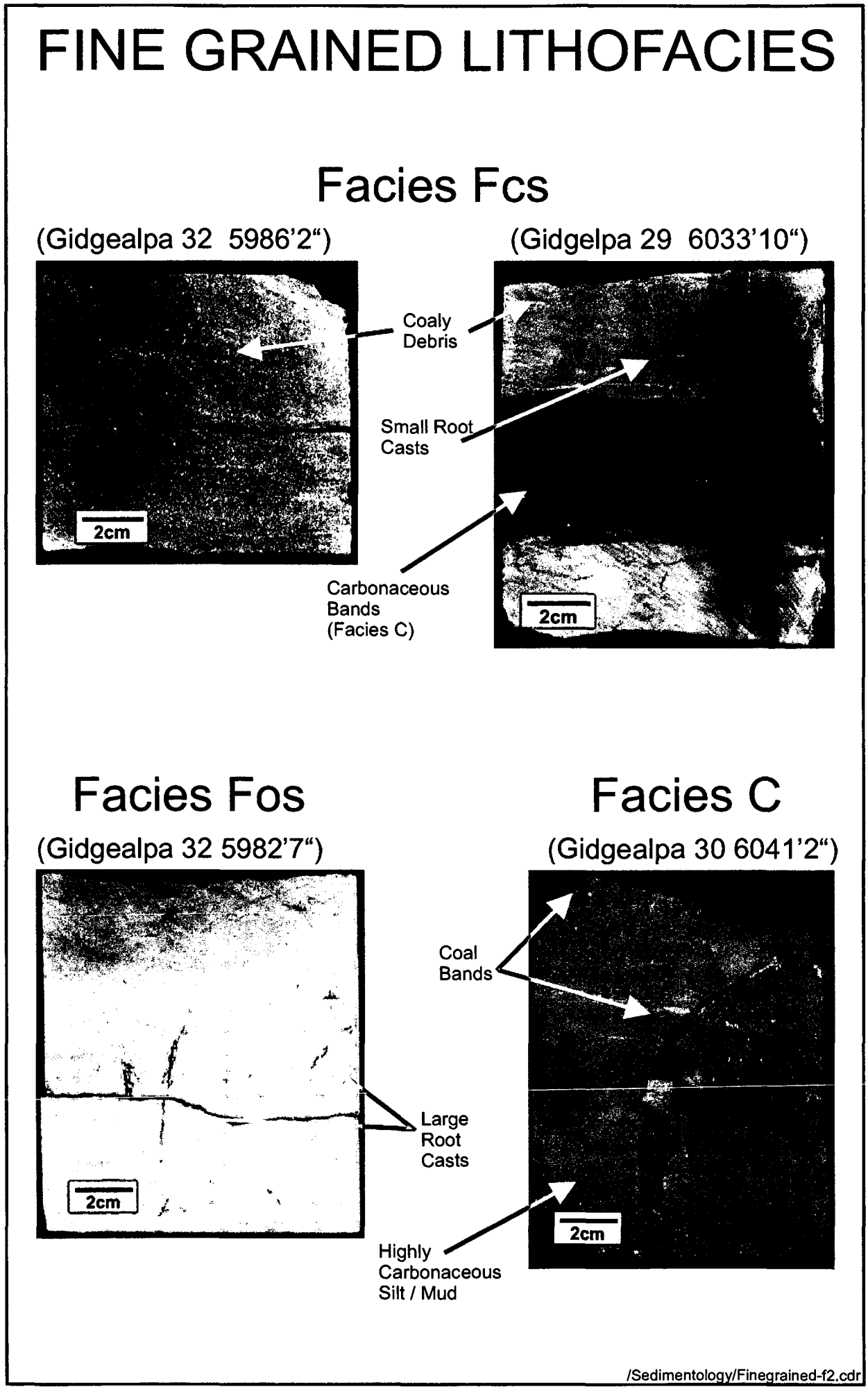

Figure 38: Examples of lithofacies Fcs, Fos and C within the Birkhead Formation, Gidgealpa south dome.

4.3 Lithofacies Successions Analysed using Embedded Markov Chain Analysis

Attempts to determine a general sequence over the Gidgealpa south dome using core and wireline logs is difficult due to the complex and variable nature of the sequences in the wells. One important consideration is whether the lithofacies within the sequences observed from core are indeed part of a facies association (ie facies are restricted to a range of interrelationships) or occur as random events. Interrelationships of facies within a fluvial, fining-upward sequence can be statistically analysed by using Embedded Markov chain analysis which has been extensively used by authors such as Miall (1973), Carr (1982) and Powers and Easterling (1982) plus many others. The use of the analysis allows for considerable detail to be drawn from the results in terms of the evolution through time or the sedimentological conditions at a given time in a depositional regime (Miall, 1973). Furthermore, the Embedded Markov process is a stochastic process where an event, at some time, is dependent upon, or will be influenced by the state of the system before the deposition of that event. The presence of a Markov process within a system or sequence also implies a degree of ordering of the events present (Carr, 1982).

To determine if any relationships existed between the lithofacies within the Birkhead Formation sequence Embedded Markov chain analysis was applied to the core data over the Gidgealpa south dome. The analysis is a relatively simple process which involves the use of a number of matrices and can be carried out using the spreadsheet program EXEL. The method I have used below is set out in a series of steps and follows the process used by Miall (1973) and Lindholm (1987). Along with the step-by-step procedure of the method, the results from the Gidgealpa south dome follow.

4.3.1 Method and Results using Embedded Markov chain Analysis

1) The Tally Matrix

The Markov chain depends on the determination of single steps, such as the relationship of a bed of a particular lithofacies and the bed of a different lithofacies which is deposited immediately above it. Thus, from the cored intervals (appendix **2**), which have been assigned lithofacies types for the beds present, a tally matrix (also know as a transition count matrix) is produced by summing the number of times a bed of a particular lithofacies is succeeded by a bed of a different lithofacies within a stratigraphic sequence. For example, figure **39** shows that the massive gravel lithofacies (Gm) has succeeded a scour surface (SS) 7 times. Also included in the analysis are scour surfaces (lithofacies SS), which although not being a lithofacies, are important events in the Markovian sedimentary cycle.

	SS	Gm	Gt	St	Sp	Sm	Sh	Sr	Sd	Sb/Fb	Fl	Fm	Fcs	Fos	C	Total
SS		7		3	2	6										18
Gm						2		5								7
Gt																0
St							1				2	3				6
Sp	1			1			3	3				1				9
Sm	1			1	2		1	3	4		2	2		1		17
Sh					2			1			1		1			5
Sr	6	1			4	4	1		3	15	79	17	1			131
Sd	1					7		2			8	2	4	2	1	27
Sb/Fb				1				26			10	1		1		39
Fl	5				1	2		51	12	19		4	1			95
Fm	3							20	4	3	5			1		36
Fcs	1							1	4		1			1	1	9
Fos								1	2		1	1	2			7
C								1			1					2
Total	18	8	0	6	11	21	6	114	29	37	110	31	9	6	2	408

Figure **39** Tally matrix of data obtained from core.

The tally matrix indicates the total number of transitions in each row as shown on the right hand column while the total of each column is tallied at the bottom of each column of the matrix. A row and column total is also shown in the bottom right hand corner of the matrix.

At this point it would be possible to produce a flow diagram (known as a facies relationship diagram) showing the interaction of the facies with each other. However, from the data obtained in the matrix the facies relationship diagram would be too complex to be of much value. Thus the data in the tally matrix must be processed to determine which transitions are 'significant' and which are not.

2) Transition Probabilities Matrix

A second matrix is constructed by converting the observed numbers from the tally matrix into transition probabilities (figure **40**). This matrix is produced by dividing the number of transitions in each well by the row total where the number resides. For example, in the first row lithofacies SS is overlain by lithofacies Gm 7 times, lithofacies St 3 times, lithofacies Sp 2 times and lithofacies Sm 6 times. Thus results on calculation of the transition probabilities (p_{ij} where i is the row number and j is the column number) are 0.339 (7/18), 0.167 (3/18), 0.111 (2/18) and 0.333 (6/18) respectively (see the first row of figure **40**).

	SS	Gm	Gt	St	Sp	Sm	Sh	Sr	Sd	Sb/Fb	Fl	Fm	Fcs	Fos	C
SS		0.389		0.167	0.111	0.333									
Gm						0.286		0.714							
Gt															
St							0.167				0.333	0.500			
Sp	0.111			0.111			0.333	0.333				0.111			
Sm	0.059			0.059	0.118		0.059	0.176	0.235		0.118	0.118		0.059	
Sh					0.400			0.200			0.200		0.200		
Sr	0.046	0.008			0.031	0.031	0.008		0.023	0.115	0.603	0.130	0.008		
Sd	0.037					0.259		0.074			0.296	0.074	0.148	0.074	0.037
Sb/Fb				0.026				0.667			0.256	0.026		0.026	
Fl	0.053				0.011	0.021		0.537	0.126	0.200		0.042	0.011		
Fm	0.083							0.556	0.111	0.083	0.139			0.028	
Fcs	0.111							0.111	0.444		0.111			0.111	0.111
Fos								0.143	0.286		0.143	0.143	0.286		
C								0.500			0.500				

Figure **40**: Transition probabilities matrix

3) Independent Trials Probability Matrix

The next step in the process is to produce an independent trials probability matrix. This matrix is produced on the assumption that all the facies

transitions at the Gidgealpa south dome occur as random events. The matrix elements are calculated by use of the equation:

$$R_{ij} = SC_j/(T - SC_i) \qquad \text{Equation } \mathbf{1}$$

where R_{ij} = random probability of transition from lithofacies i to j
SC_j = the random number of occurrences of lithofacies j (column total for facies j)
T = total number of transitions for all lithofacies
SC_i = the number of occurrences of lithofacies I (column total for lithofacies i)

To demonstrate the use of the equation consider the transition of lithofacies SS to lithofacies Gm. In this case where i = lithofacies SS and j = lithofacies Gm and from figure **39** (page 80) the column total (SC_i) for the lithofacies SS is 18 while the column total for SC_j for lithofacies Gm is 8 and the total for all transitions is 408. So using these values, the random possibility of transition (R_{ij}) from lithofacies SS to Gm is 8/(408-18) = 0.0205. This value is then entered as the first entry of the new matrix (figure **41**)

	SS	Gm	Gt	St	Sp	Sm	Sh	Sr	Sd	Sb/Fb	Fl	Fm	Fcs	Fos	C
SS		0.021	0.000	0.015	0.028	0.054	0.015	0.292	0.074	0.095	0.282	0.079	0.023	0.015	0.005
Gm	0.045		0.000	0.015	0.028	0.053	0.015	0.285	0.073	0.093	0.275	0.078	0.023	0.015	0.005
Gt	0.044	0.020		0.015	0.027	0.051	0.015	0.279	0.071	0.091	0.270	0.076	0.022	0.015	0.005
St	0.045	0.020	0.000		0.027	0.052	0.015	0.284	0.072	0.092	0.274	0.077	0.022	0.015	0.005
Sp	0.045	0.020	0.000	0.015		0.053	0.015	0.287	0.073	0.093	0.277	0.078	0.023	0.015	0.005
Sm	0.047	0.021	0.000	0.016	0.028		0.016	0.295	0.075	0.096	0.284	0.080	0.023	0.016	0.005
Sh	0.045	0.020	0.000	0.015	0.027	0.052		0.284	0.072	0.092	0.274	0.077	0.022	0.015	0.005
Sr	0.061	0.027	0.000	0.020	0.037	0.071	0.020		0.099	0.126	0.374	0.105	0.031	0.020	0.007
Sd	0.047	0.021	0.000	0.016	0.029	0.055	0.016	0.301		0.098	0.290	0.082	0.024	0.016	0.005
Sb/Fb	0.049	0.022	0.000	0.016	0.030	0.057	0.016	0.307	0.078		0.296	0.084	0.024	0.016	0.005
Fl	0.060	0.027	0.000	0.020	0.037	0.070	0.020	0.383	0.097	0.124		0.104	0.030	0.020	0.007
Fm	0.048	0.021	0.000	0.016	0.029	0.056	0.016	0.302	0.077	0.098	0.292		0.024	0.016	0.005
Fcs	0.045	0.020	0.000	0.015	0.028	0.053	0.015	0.286	0.073	0.093	0.276	0.078		0.015	0.005
Fos	0.045	0.020	0.000	0.015	0.027	0.052	0.015	0.284	0.072	0.092	0.274	0.077	0.022		0.005
C	0.044	0.020	0.000	0.015	0.027	0.052	0.015	0.281	0.071	0.091	0.271	0.076	0.022	0.015	

Figure **41**: Independent trials probability matrix.

4) Difference Matrix

Once the random probability matrix has been produced it is subtracted from the transition probabilities matrix to produce a difference matrix (figure **42**).

	SS	Gm	Gt	St	Sp	Sm	Sh	Sr	Sd	Sb/Fb	Fl	Fm	Fcs	Fos	C
SS		0.273	0.000	0.151	0.033	0.279	-0.015	-0.292	-0.074	-0.095	-0.282	-0.079	-0.023	-0.015	-0.005
Gm	-0.045		0.000	-0.015	-0.028	0.233	-0.015	0.429	-0.073	-0.093	-0.275	-0.078	-0.023	-0.015	-0.005
Gt	-0.044	-0.020		-0.015	-0.027	-0.051	-0.015	-0.279	-0.071	-0.091	-0.270	-0.076	-0.022	-0.015	-0.005
St	-0.045	-0.020	0.000		-0.027	-0.052	0.152	-0.284	-0.072	-0.092	0.000	0.423	-0.022	-0.015	-0.005
Sp	0.068	-0.020	0.000	0.026		-0.053	0.318	0.045	-0.073	-0.093	-0.277	0.033	-0.023	-0.015	-0.005
Sm	0.012	-0.021	0.000	0.043	0.089		0.043	-0.118	0.160	-0.096	-0.167	0.038	-0.023	0.043	-0.005
Sh	-0.045	-0.020	0.000	-0.015	0.373	-0.052		-0.084	-0.072	-0.092	-0.074	-0.077	0.178	-0.015	-0.005
Sr	-0.015	-0.020	0.000	-0.020	-0.007	-0.041	-0.013		-0.076	-0.011	0.229	0.024	-0.023	-0.020	-0.007
Sd	-0.010	-0.021	0.000	-0.016	-0.029	0.204	-0.016	-0.227		-0.098	0.006	-0.008	0.124	0.058	0.032
Sb/Fb	-0.049	-0.022	0.000	0.009	-0.030	-0.057	-0.016	0.359	-0.078		-0.040	-0.058	-0.024	0.009	-0.005
Fl	-0.008	-0.027	0.000	-0.020	-0.026	-0.049	-0.020	0.154	0.029	0.123		-0.062	-0.020	-0.020	-0.007
Fm	0.036	-0.021	0.000	-0.016	-0.029	-0.056	-0.016	0.253	0.034	-0.015	-0.153		-0.024	0.012	-0.005
Fcs	0.086	-0.020	0.000	-0.015	-0.028	-0.053	-0.015	-0.175	0.372	-0.093	-0.165	-0.078		0.108	0.108
Fos	-0.045	-0.020	0.000	-0.015	-0.027	-0.052	-0.015	-0.141	0.214	-0.092	-0.131	0.066	0.283		-0.005
C	-0.044	-0.020	0.000	-0.015	-0.027	-0.052	-0.015	0.219	-0.071	-0.091	0.229	-0.076	-0.022	-0.015	

Figure 42: Difference matrix

From the difference matrix the values are between +1.0 to -1.0 for each transition possibility with the positive values (shown in red) indicating transitions which occur more frequently than if the facies were deposited in a random order while negative values indicate transitions which occur less than randomly.

5) Facies Relationship Diagram

From the difference matrix a facies relationship diagram can be produced using the 'high' positive values which are greater than 0.1 (figure **43**a). In figure **43**a the high positive values are drawn as solid arrows while the lower positive values of less than 0.1 are drawn in using dashed arrows, the arrow direction indicates transition direction.

6) Binomial Probability

The positive values obtained from the difference matrix does not prove that when the random value is subtracted from the observed probability the answer is statistically significant. For example if we consider the transition from lithofacies SS to Gm the difference is 0.368 or the transition from lithofacies Gm to Sm is 0.233, it is hard to determine if these values are significant by just

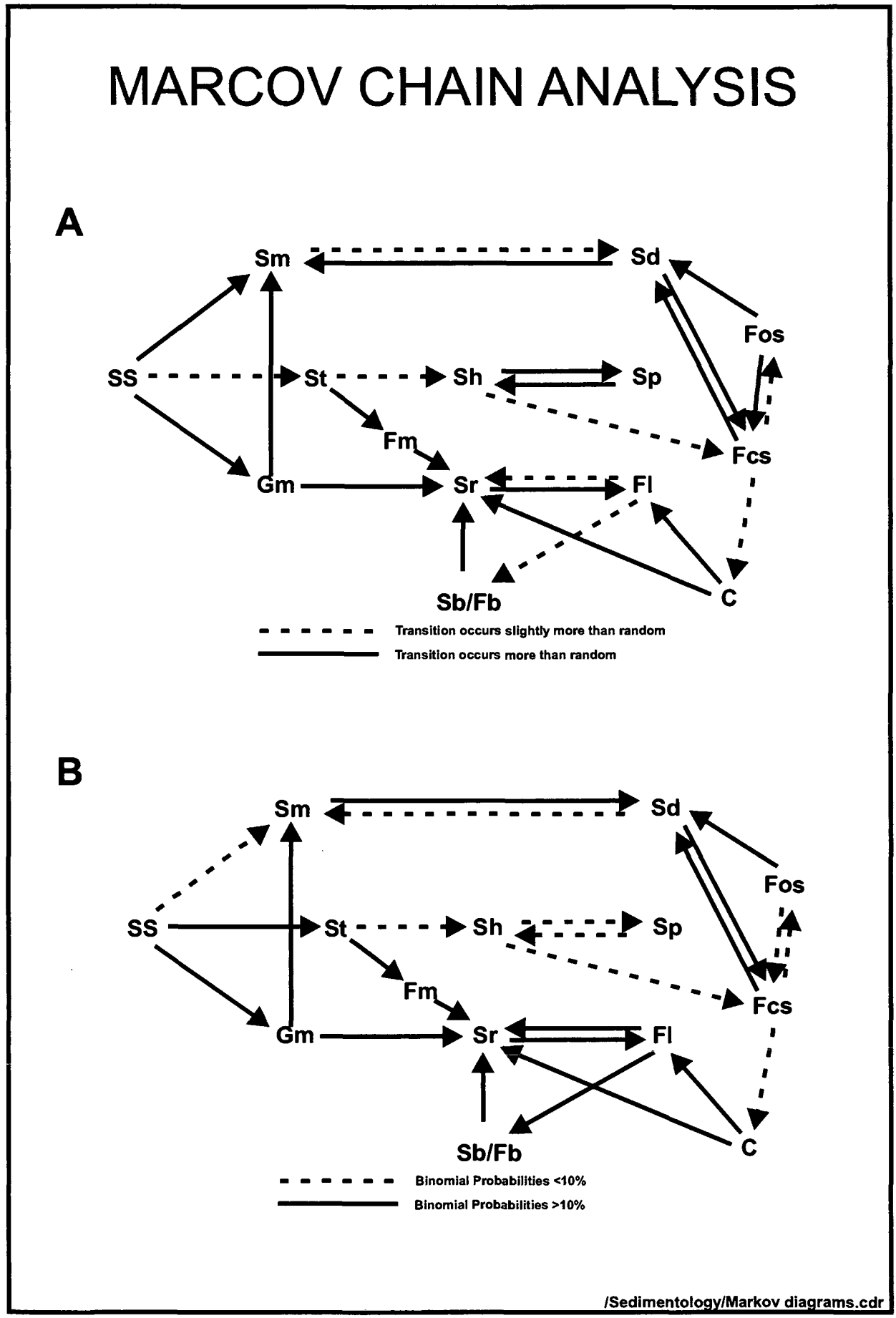

Figure 43: Lithofacies relationship diagrams produced from (A) the difference matrix and (B) Binomial probability determination.

using subjective conjecture. This problem can be easily and rapidly overcome by the use of binomial probability. The binomial probability of at least N_{obs} successes in N trials is given by

$$\sum_{n=nobs}^{n=N} C(N,n)\, p^n q^{N-0} \qquad \text{Equation 2}$$

where $C(N,n)$ = the number of possible combinations of N objects taken n at a time and is given by

$$C(N,n) = \frac{N!}{(N-n)!n!} \qquad \text{Equation 3}$$

where p = the probability of success on a single trial in the independent trials probability matrix (figure **41**, page 82) and $q = 1 - p$

As an example of applying the binomial probability consider the transition of lithofacies SS to lithofacies Gm. From the difference matrix (figure **42**, page 83) the probability difference is +0.368, where p = the probability of success in a single trial = 0.021 (from figure **41**, page 82) and q = the probability of failure in a single trial: 1 - 0.021 = 0.979. Also, observing from the tally matrix (figure **39**, page 80), 7 successes (from lithofacies SS to Gm) were observed out of 18 transitions from lithofacies SS to another lithofacies; therefore $n_{obs} = 7$ and $N = 18$. Thus using equation **2** above the probability of at least n_{obs} successes in N trials is 0.0066. This means that 7 successes in 18 trials would occur less than 1% of the time if the transitions occurred randomly and if a significance level of 10% is chosen. Therefore, the observed transition of lithofacies SS to lithofacies Gm is not significant.

I have applied binomial probability calculations to all transitions (table **3**) shown in the lithofacies relationship diagram (figure **43**a) and produced a revised diagram (figure **43**b, page 84) where the solid arrows represent

transitions that are significant while the dashed arrows represent transitions which are not significant at an arbitrary significance level of 10%.

Lithofacies transition	P	M	N	Probability	10% significance
SS===>Gm	0.389	8	7	0.0066	Yes
SS===>St	0.167	6	3	0.0538	Yes
SS===>Sm	0.333	21	6	0.1702	No
Gm===>Sm	0.286	21	2	0.0285	Yes
Gm===>Sr	0.714	114	5	0.0000	Yes
St===>Sh	0.167	6	1	0.4019	No
St===>Fm	0.5	31	3	0.0000	Yes
Sp===>Sh	0.333	6	3	0.2191	No
Sm===>Sd	0.235	29	4	0.0894	Yes
Sh===>Sp	0.4	11	2	0.0887	Yes
Sh===>Fcs	0.2	9	1	0.3020	No
Sr===>Fl	0.603	110	79	0.0035	Yes
Sd===>Sm	0.259	21	7	0.1368	No
Sd===>Fcs	0.148	9	4	0.0271	Yes
Sb/Fb===>Sr	0.667	114	26	0.0000	Yes
Fl===>Sr	0.537	114	51	0.0120	Yes
Fl===>Sb/Fb	0.2	37	19	0.0000	Yes
Fm===>Sr	0.556	114	20	0.0000	Yes
Fcs===>Sd	0.444	29	4	0.0004	Yes
Fcs===>C	0.111	2	1	0.1974	No
Fcs===>Fos	0.111	6	1	0.3698	No
Fos===>Sd	0.286	29	2	0.0037	Yes
Fos===>Fcs	0.286	9	2	0.2786	No
C===>Sr	0.5	114	1	0.0000	Yes
C===>Fl	0.5	110	1	0.0000	Yes

Table 3: Binomial Probability calculations table where P = transition probability for a random sequence, N = the number of transitions from the lower facies and M = the number of transitions from the lower to the upper lithofacies.

4.3.2 Embedded Markov Chain Analysis: Discussion

Although the Birkhead Formation varies in its depositional environment depending on the depth of interest, cores only cover the basal section of the formation at the Gidgealpa south dome. Within these cores sediments are deposited as floodplain to meandering fluvial / upper delta plain facies which grade into lower delta plain to delta front facies. These depositional environment trends are reflected in the results of the embedded Markov chain analysis.

From the facies relationship diagrams (figure **43**a & b, page 84) produced from embedded Markov chain analysis four 'most likely' sedimentary sequences were produced and labelled as sequences 1 to 4 in figure **44**. The sequences

consist of a general fining up sequence starting from a scour surface generally overlain by a medium to coarse sands or lag deposits, all sequences then finish as siltstones and fine grained sandstones. After initial sedimentation, the sequences can be divided into two groups on the basis of sediment deposition. From here on in the sequences have been labelled as 'Birkhead Formation Group 1 sequences' and 'Birkhead Formation Group 2 sequences'.

Birkhead Formation Group 1 Sequences (BFG-1)

Sediments within sequence 1 and sequence 2 (figure **44**) are characterised by the classical point bar, fining upward cycle of deposition in channels. Sediments start as medium to coarse grained sands or gravel lags and grade into finer grained sediments such as fine to medium grained massive sandstones (Sm), deformed sandstones (Sd) and horizontal bedded sandstones (Sh). Sediments then grade into floodplain sediments consisting of deformed sandstones (Sd), well drained swamp deposits (Fos), poorly drained swamp deposits (Fcs) and are topped by coal horizons (C).

Birkhead Formation Group 2 Sequences (BFG-2)

Sediments within sequence 3 and sequence 4 (figure **44**) are characterised by the deposition of channel trough cross-bedded sandstones (St) or gravel lags which are overlain by ripple cross-laminated sands (Sr) massive mudstone / siltstones (Fm) or heavily bioturbated silts and sands (Sb/Fb). These sediments represent a significant reduction in grain size due to channel cut-off and abandonment.

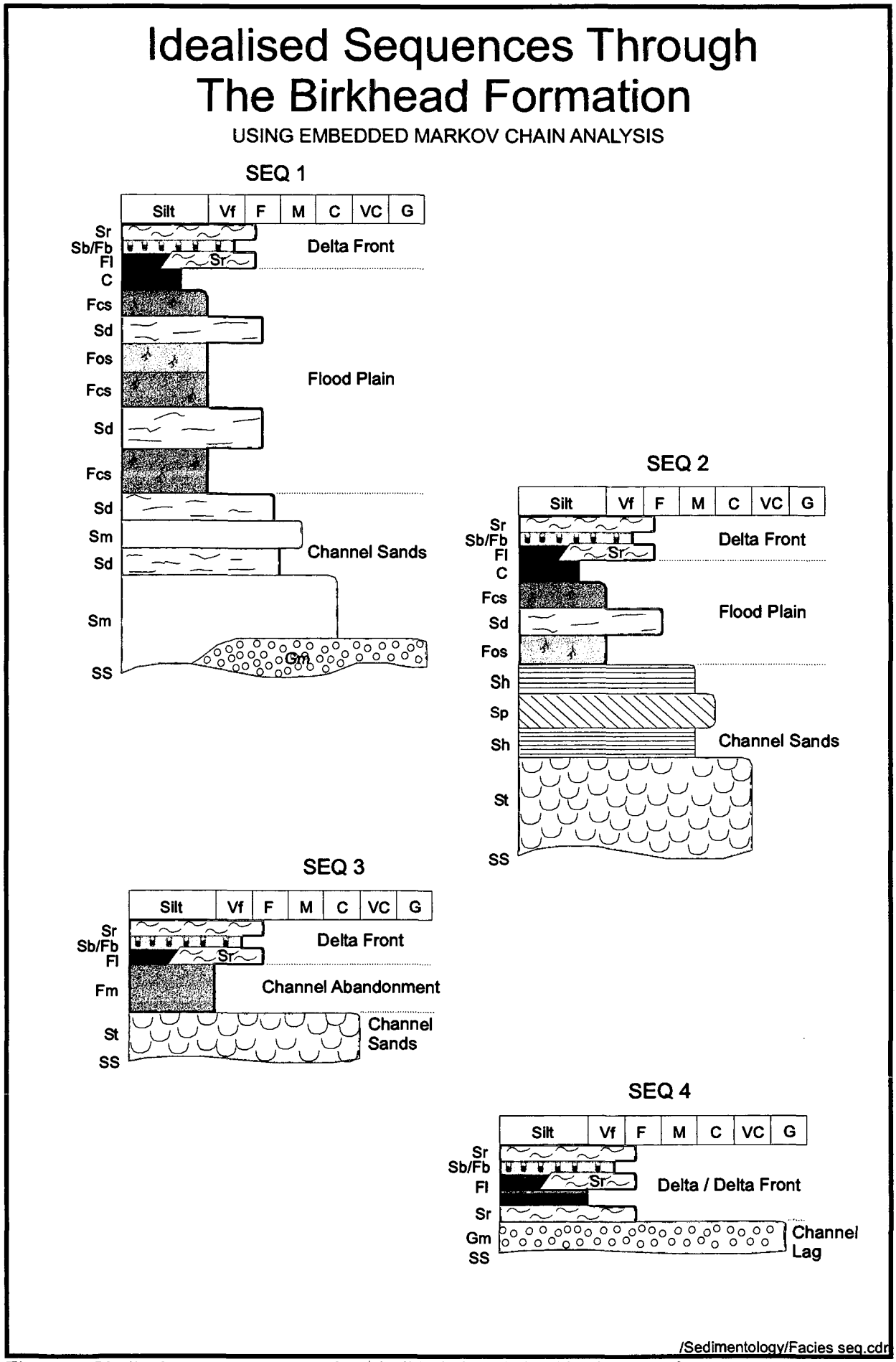

Figure 44: Idealized sequences produced from the lithofacies relationship diagrams of embedded Markov chain analysis.

4.3.3 Notes on Embedded Markov Chain Analysis

Lindholm (1987) noted some potential problems associated with the use of Embedded Markov chain analysis, they are listed on the following page:

1) The type of contact between facies is often not considered,
2) Data input into the analysis is often oversimplified to facilitate statistical analysis,
3) Minor facies are subordinated or eliminated due to their statistical insignificance but may however be geologically important and;
4) The embedded Markov chain analysis itself is statistically incorrect.

While all these factors should be considered, they may also be overcome or are not important in the analysis. Lindholm (1987) considered the problem of the contacts between facies and suggested the use of a contact matrix. However I think a much simpler approach would be to determine contacts by looking at the cores for an overall indication. I have deduced that there are 2 significant types of contacts between different lithofacies in the Gidgealpa south dome. The contacts are sharp and may be straight, undulatory or graded contacts that are characterised by a general trend of one facies into another. Only these 2 types of contacts need to be considered in this case since they will effect the outcome of reservoir characterisation and the properties of flow units. From lithofacies analysis one possible method of formation of lithofacies Sm is by sediments being dumped by deposition of sediment pulses or by fluid escape. If this is the case then we would expect lithofacies Sm to be associated with lithofacies Sd which indeed it is, so whenever lithofacies Sd is overlain by lithofacies Sm it is highly likely that the contact between the two is graded. Swamp lithofacies (Foc and Fcs) also show graded properties due to their similar environments of deposition. Most other contacts between facies are generally sharp.

Input data for the embedded Markov chain analysis has not been simplified or modified from the lithofacies descriptions and thus is not seen as a potential problem when carrying out the analysis. The elimination or subordination of minor facies is seen as a problem at the Gidgealpa south dome since minor facies may effect the properties of flow units. However, the low proportion of these beds from visual inspection of the core means that they may not have a large bearing on the results when conducting reservoir characterisation.

And finally, the embedded Markov chain analysis has been considered to be statistically incorrect by authors such as Carr (1982) and Walker (1984). They believe that a matrix of random probabilities, where the matrix has structurally empty cells along its main diagonals (seen as shaded cells in figures **39** (page 80) to **42** (page 83)), due to the in-ability to distinguish between the same facies is unrealistic since, as Carr (1982) stated;

"zeros cannot result from a simple independent random process."

To overcome this problem an alternative type of Markov chain analysis is discussed in Miall (1973). He terms the analysis 'method 2' analysis as compared to the normal method of analysis which he terms 'method 1'. Doveton (1994) uses the method 2 analysis where instead of inputting the number of lithofacies transitions into a matrix, a fixed interval is chosen and the lithofacies that are encountered at the end of each interval length are input into the matrix. So for example if lithofacies A is noted at position 1 then at position 1+i (where i is some fixed length) the lithofacies is B, then the change from lithofacies A to lithofacies B is added to the matrix. This method overcomes the problem of structurally empty cells since the event of a certain lithofacies occurring at a fixed length away from the same lithofacies is possible.

This method also creates its own potential problems since the unit length chosen will effect the results. If a too-shorter length is chosen then the amount

of occurrences where a lithofacies is followed by itself (from the same beds) will be excessive. Alternatively if a too-larger interval is chosen then beds of a smaller thickness may be missed. In either case the matrix will not be representative of the facies present within the core. Because of this fact I have used the 'method 1' analysis due to the high variation of bed thicknesses within the Birkhead Formation.

4.4 Lithofacies Successions Interpreted in Wireline Logs

Core within the basal section of the Birkhead Formation is limited to 5 wells at the Gidgealpa south dome. As a consequence, to try to determine sedimentary sequences and the overall depositional environment of the area wells with core data must be calibrated with the wireline logs over the corresponding intervals. The calibration data obtained can then be applied to the other wells within the field where wireline logs are present and core data is absent.

4.4.1 Calibration of Wireline Log Curves from Cored Intervals

Wireline log tool resolution is poor compared to the geology seen on core logs, with tools usually measuring an averaged log response over intervals of 6 inches to 1 foot (15-30cm). Thus the use of wireline logs can only resolve an area of the rock within the borehole rather than individual beds and sedimentary characteristics. Therefore, as has been conducted on the cores to determine lithofacies, the wireline logs can be analysed to determine 'wireline log facies'. The wireline log facies are described in terms of various types of depositional environments that are discussed in the following section (Section **4.5**) and also contain various associated lithofacies (fron section **4.2**).

To determine the relationship between the rocks (by using the cores) and the wireline logs the detailed core log description that I produced (see appendix **2**) was correlated with the corresponding wireline logs over the intervals. The

correlations are displayed in appendix **10**. In these correlations the gamma ray log has been used as a detector of the amount of radioactive material that is contained within the rocks which is usually associated with the siltstone and claystone. Therefore the wireline log curves can be used to determine the 'shalyness' of the rocks.

To help with the classification of the wireline log facies, API unit cutoff values were also applied to the gamma ray curve. The API unit cutoffs were placed at 70 and 90. Gamma ray signatures that occur between 0 to 70 API units represent clean sandstones, log responses between 70 and 90 API units represent shaly sandstones and/or interbedded sandstones and siltstones and log responces of 90 API units or higher represent siltstones and/or claystones.

Along with using API unit cutoff values, association of a particular section of the wireline log to the sections above and below it can aid in allocation where some question may exist as to the interpretation. This allocation, or likely relationship between wireline log facies can be developed using the results obtained from the embedded Markov chain analysis (see section **4.3**, page 79).

Figure **70** (page 158) is a summary of the wireline log and core log correlations for the 5 cores. In the figure, the 70 and 90 API unit cutoffs are drawn and separate the large spaced shaded and close spaced shaded areas that represent the clean sandstones and the siltstones and/or claystones respectively. The area in between the two cutoff values, which has not been shaded, represents the shaly sandstones and/or interbeded sandstones and siltstones. Also added to Figure **70** are the depositional environments from core descriptions. From this data 6 wireline log facies have been identified and are discussed below.

4.4.1.1 Wireline Log Facies I

This wireline log facies consists of the gamma ray curve with API unit values greater than 70 and represents clean sandstones deposited as channel fill sediments. The log generally displays a sharp base with a gradual increase in the API unit values or short intervals where the curve displays a sharp top and bottom.

4.4.1.2 Wireline Log Facies II

Core description data indicate that this wireline log facies corresponds to sheet sands and crevasse splays. The gamma ray curve in this case is smooth and has API unit values between 70 and 90 and generally displays decreasing values upwards from 90 to 70 API units. The top of this wireline log facies is generally sharp indicating rapid termination of deposition.

4.4.1.3 Wireline Log Facies III

This wireline log facies corresponds to levee and channel overbank sediments and generally has API unit values between 70 and 90 but may also have values slightly higher than 90. There may be some difficulty distinguishing this facies to wireline log facies II that has similar characteristics. However, this facies tends to be more serrated and can be distinguished by its close association with wireline log facies I.

4.4.1.4 Wireline Log Facies IV

Wireline log facies IV consists of highly variable and smooth gamma ray signatures with API unit values between 70 and 90 although values may occur that are slighty lower than 70. This facies represents sediments that were

deposited as distributary mouth bar to delta front sediments. The facies is also heavily associated with wireline log facies VI.

4.4.1.5 Wireline Log Facies V

This wireline log facies corresponds to sediments depostied in a swamp setting. The gamma ray curve typically displays API unit values that are greater than 90. The log displays a variable and serrated character and this facies is associated with wireline log facies IV or VI. This wireline log facies generally has higher API unit values than wireline log facies VI.

4.4.1.6 Wireline Log Facies VI

Wireline log facies VI represents lacustrine facies that are usually associated with wireline log facies IV and V. It usually displays gamma ray API unit values between 90 to 110 and has a relatively variable but smooth log character.

4.5 Depositional Model of the Hutton Sandstone and Birkhead Formation

The previous interpretation of the depositional environment of the Birkhead Formation at the Gidgealpa south dome is different to the interpretation that has been conducted by this author. When interpretating the depositional environment; well, core, pressure and 3D seismic data are invaluble as well as any other data that may aid in interpretation such as dipmeter (see section **4.7.5**) and neodymium model age dating (see section **4.8.2**). In other studies, detailed 3D seismic can be utilised to delineate sand body geometries and was considered for use here, however in the case of the Gidgealpa south dome, resolution of the data is below that of the sand body thickness (Boult, P.J.,

pers. comm.) and thus was not used. Thus there is more of a reliance on the other available data. In this section I will briefly discuss the previous interpretation and then, in more detail, go on to discuss my interpretation using the data available. I will then relate the current interpretation to a modern day analogue for comparison.

4.5.1 Existing Model of the Birkhead Formation

Previous in house interpretations have determined the Birkhead Formation at the Gidgealpa south dome to be deposited within an alluvial floodplain where a high proportion of the sediments are floodplain deposits (McIntyre et. al, 1989) and the sands are of a fluvial origin with the recognition of channel fill/splay and levee deposits (SANTOS, 1996). The interpretation appears to be limited to the use of the wireline logs and pressure data which did not allow for the consideration of other factors that will effect the application of a depositional environment such as palaeoflow direction and facies relationships.

More specifically, the previous interpretation indicated the presence of three sands that are isolated by floodplain shales. The lowest sand package was interpreted as a north-south channel on the western side of the field, the second sand was located centrally over the field and was interpreted as an east-west channel while the final sand was interpreted as a thin channel in a north-south orientation positioned on the eastern section of the field (SANTOS, 1996).

4.5.2 Revised Model of the Birkhead Formation

From wireline data and core logs (appendix **2**), I have interpreted the lower Birkhead Formation at the Gidgealpa south dome to consist of a river dominated delta system. While the available data over the area has allowed the identification of the depositional environment, the highly variable nature of

a delta plain environment means that a model must be applied to predict environments away from the well bore where geological data is unavailable.

The following sections lay out a logical path for the recognition of the depositional environments of the Birkhead Formation at the Gidgealpa south dome. These sections cover an introduction and classification of deltas, and specifically a discussion of river dominated deltas. The link between this data and the Birkhead Formation is then applied and related showing the characteristic paramaters of the depositional system. Finally, a comparison of the depositional system is compared with a modern day analogue where active processes and sequences can be directly compared.

4.6 Deltas

4.6.1 Introduction

From Bates (1984) a delta is defined as:

"the nearly flat alluvial tract of land at the mouth of a river, commonly forming a triangular or fan shaped plain... in plan view. [Deltas are] *crossed by many distributaries, and results from the accumulation of sediment supplied by the river."*

From modern examples, the main parameters affecting the formation of deltas are the interplay of river discharge, discharge variability, wave and tidal energy (Wright and Coleman, 1973, Galloway, 1975, Orton and Reading, 1993). Figure **45** illustrates both the major and minor factors affecting the morphology and stratigraphy of a delta system.

While the shape of deltas can vary to a large extent, their overall morphologies are similar. On a large scale, Wright (1985) has subdivided the delta plain into basic "*physiographic zones*" shown in figure **46**. Generally, deltas consist of a

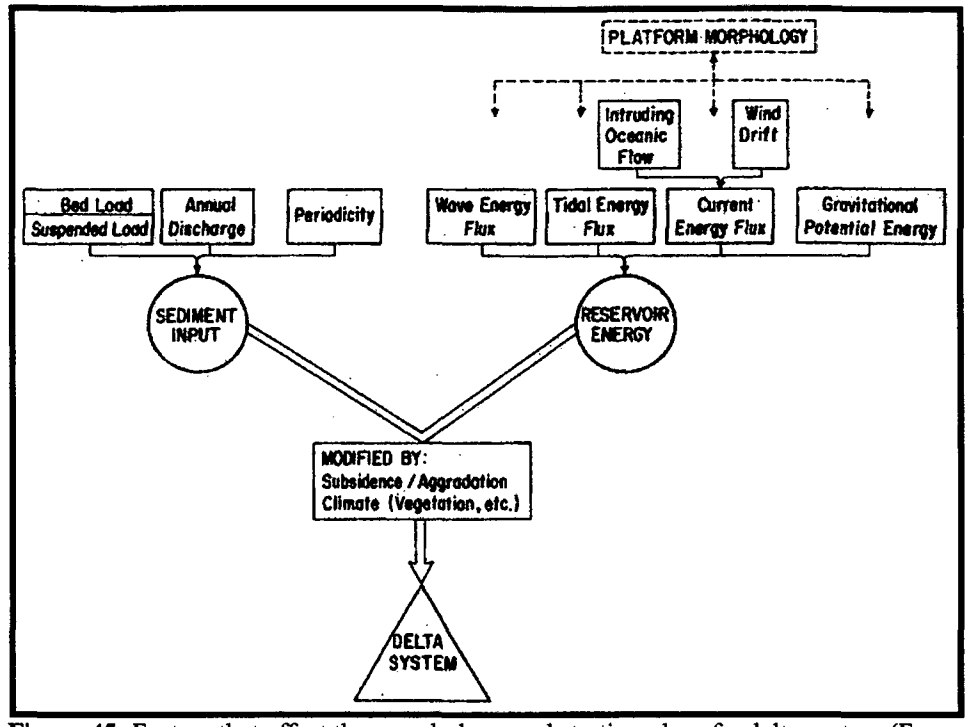

Figure 45: Factors that effect the morphology and stratigraphy of a delta system (From Galloway, 1975).

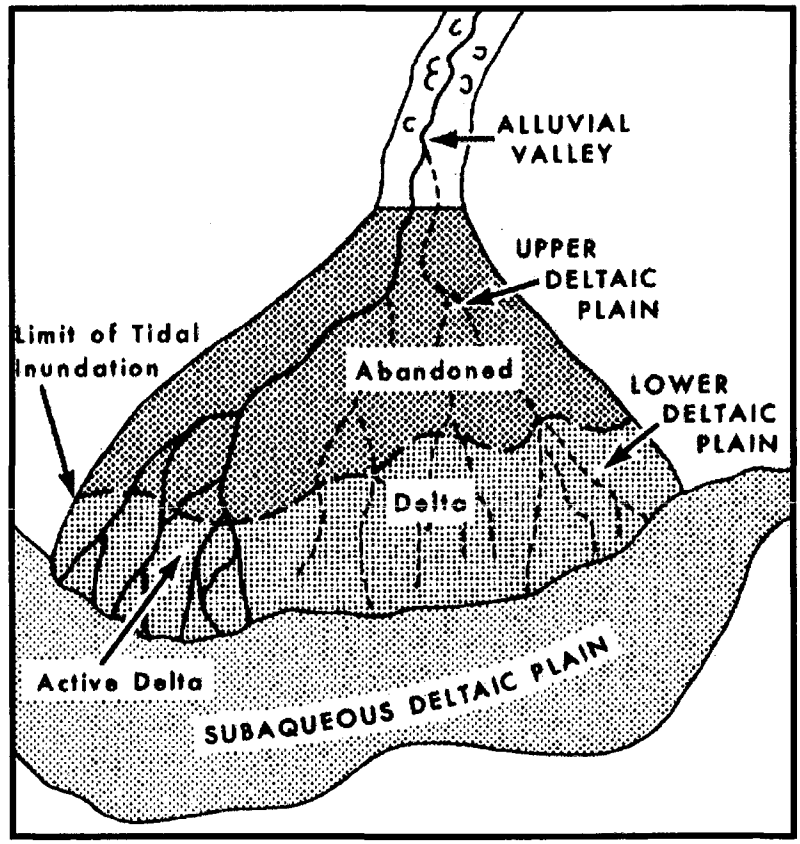

Figure 46: Components of a Delta system (From Wright, 1985).

subaqueous and subaerial zone that can vary in size considerably. The subaqueous delta is characterised by increasingly fine sediments away from the delta mouth with the most seaward part, the prodelta, containing the finest sediments. The subaerial delta experiences a greater number of processes and thus displays a more complex distribution of sedimentary environments. This part of the delta is subdivided into an upper and lower delta plain with the upper delta plain being the older portion of the subaerial delta plain.
Figure **46** shows that a delta can also be divided into active and abandoned zones. The active part of the delta will continue to prograde into the water column while the abandoned area may prograde, remain stable or retrograde depending on the marine processes present. The abandoned plain is a result of the river changing its lower course thus causing a shift in the locus of river mouth sedimentation (Wright, 1985).

4.6.2 Classification of Deltas

Confined fluvial flow, wave flux and tidal currents are the only elements which appear to be capable of reworking or transporting large amounts of sand in or out of a delta system. For this reason the processes have been used to characterise deltas. Figure **47** shows the three end members depending on whether wave, tidal or fluvial energy dominates. The relative strengths and interaction of these processes will ultimately determine the morphology of a delta system (Galloway, 1975). Orton and Reading (1993) further classified deltas by taking sediment grain size into account, since grain size is an essential measurable quantity. They go on to state that this parameter has a considerable effect on the environments, physical processes and morphology of deltas. Figure **48** is a classification of modern deltas using the tripartate subdivision in two dimensions and grainsize variations in the third dimension.

Sand distribution from varying combinations of the processes mentioned above have been classified into six categories which are shown in figure **49**.

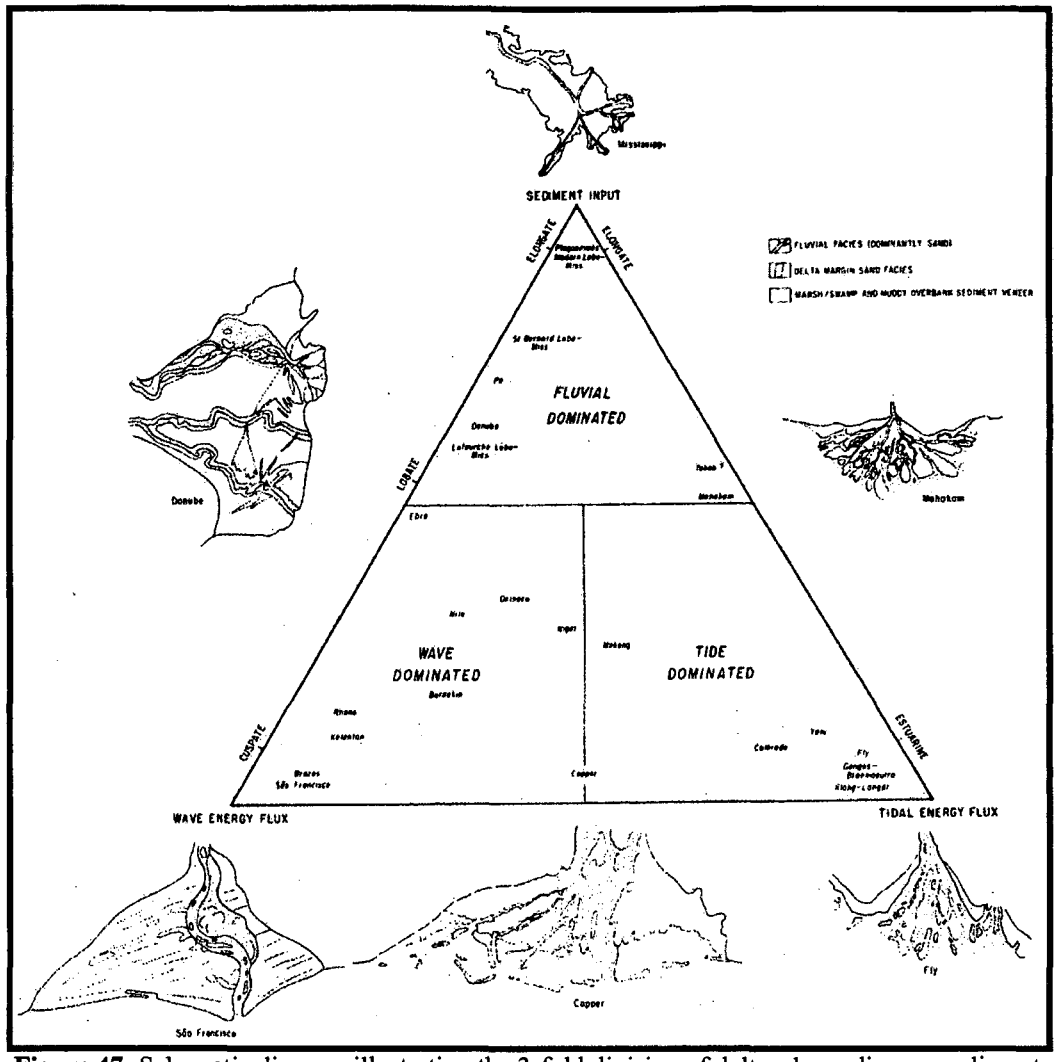

Figure 47: Schematic diagram illustrating the 3-fold division of deltas depending on sediment input, wave energy flux and tidal energy (From Galloway, 1975).

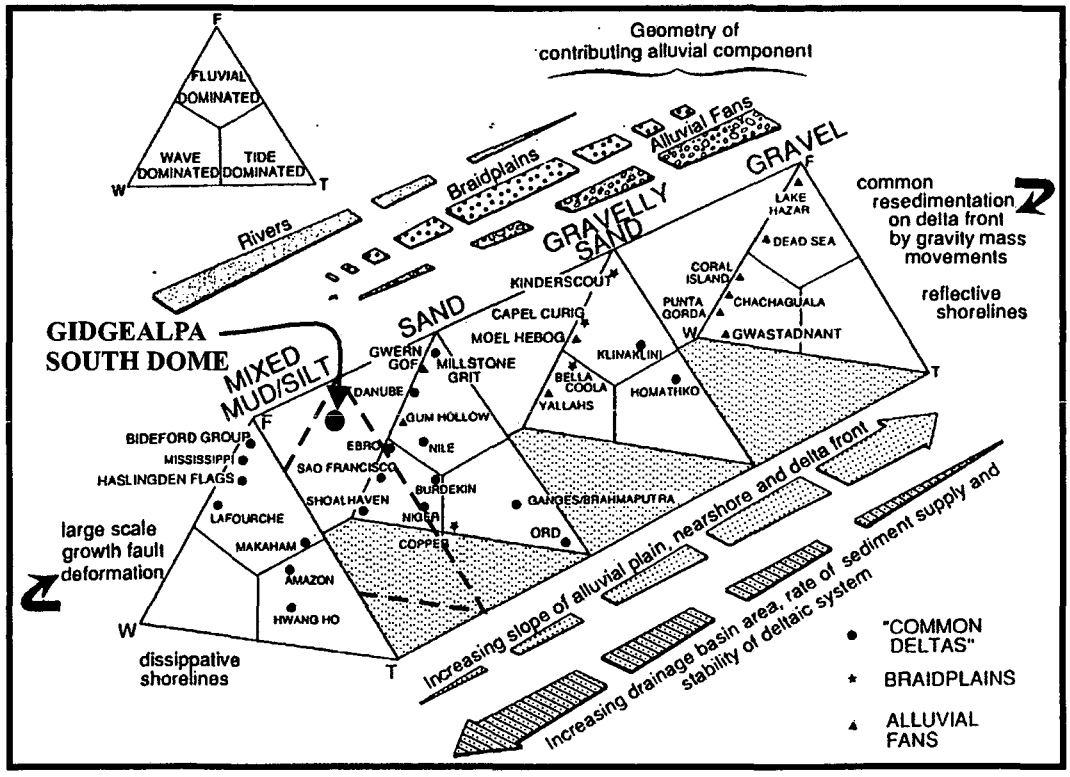

Figure 48: Generalised classification prismof deltas including grainsize parameters from mud dominated to gravel dominated deltas (From Galloway, 1994 after Orton and Reading (in press)).

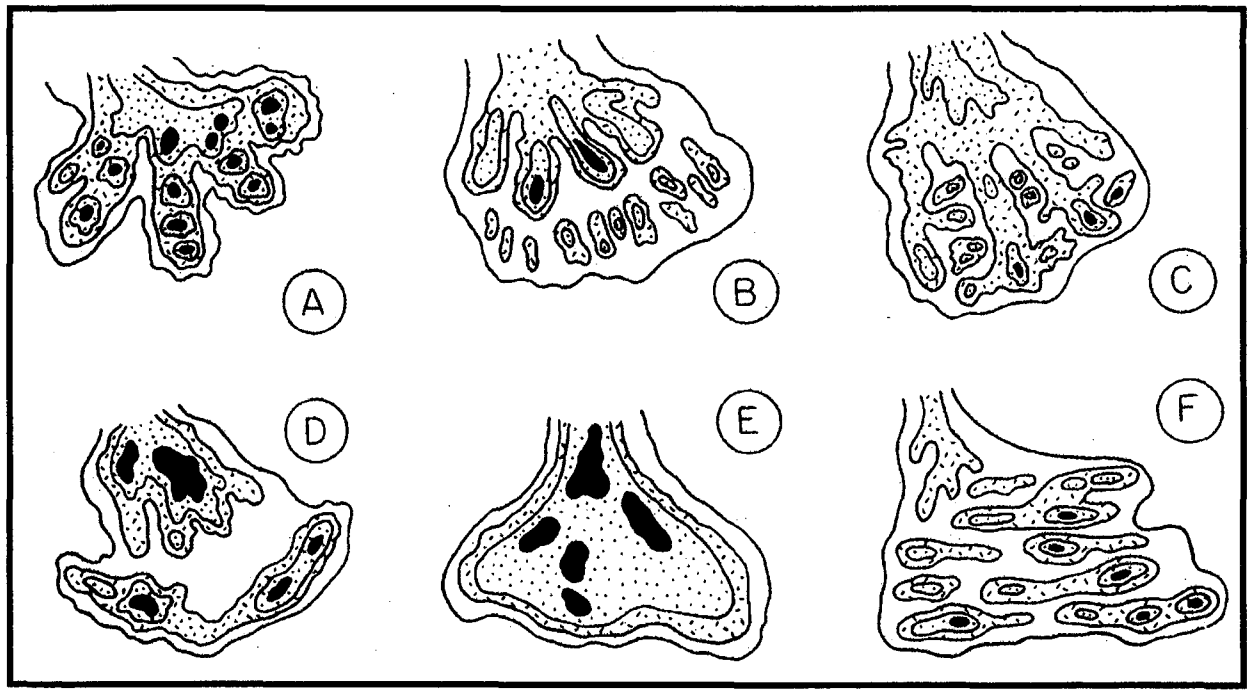

Figure 49: Delta models from Colman and Wright (1975). A) River dominated delta with low wave, tide energy and low littoral drift, B) River dominated delta with low wave energy, high tide range and low littoral drift, C) intermediate wave energy, high tide and low littoral drift, D) Intermediate wave energy and low tide range, E) High wave energy and low littoral drift, F) high wave energy and strong littoral drift (From Miall, 1992).

So if we take the modern day Mississippi Delta as an example; the fluvial input is dominated by silts and muds, is fluvial dominated, has a low tidal range and is affected by low wave energy and therefore plots on the top corner of the triangle at the mixed silts and muds end of figure **48**. From these characteristics we can classify the delta as having a 'type A' sand distribution (from figure **49**).

4.6.3 River Dominated Deltas: Background

River dominated deltas form when the tidal range and wave power at a river mouth are negligible compared to river outflow. They typically occur in micro tidal lakes, estuaries, enclosed or semi-enclosed seas and shallow areas which attenuate wave energy (Wright, 1977). These deltas are characterised by highly irregular and protruding shorelines with interdistributary sediments dominating most areas, the absence of wave built features and low lateral continuity of sands (Wright and Coleman, 1973, Wright, 1985). If subsidence is minimal the shallow platform on which these deltas commonly deposit, tend to rapidly form thin sheets (Wright, 1985).

A river dominated delta will usually form in a lake if there is a negligible density contrast between the lake and the entering river water (Bates, 1953, Wright, 1977). In this case the river water will rapidly decelerate and mix when coming into contact with the standing body of water and therefore deposit large amounts of sediment. Bed friction is greatly increased by shallow depths immediately basin-ward of a river mouth causing rapid deceleration and the formation of triangular 'middle ground' bars by lateral expansion and subsequent channel bifurcation (Wright, 1977, 1985). Borichansky and Mikhailov (1966) who carried out a series of laboratory experiments first noticed these features. The experiments showed a shoaling seaward trend of a river mouth from the deposition of sediments and the formation of a positive feedback loop, which increased the friction induced

deceleration and spreading of effluent as well as the shoaling rate. To regain stability divergent bifurcating channels were produced on the margins of the effluent to minimise the frictional effects of the out flowing waters. Figure **50** shows the levee bounded channels fringing a triangular shaped middle ground where turbulent and frictional forces are relatively low. On a larger scale, deltas of this nature tend to contain multiple channel bifurcations with multiple associated middle-ground shoals (figure **51**)(Coleman and Wright, 1975, Wright, 1977).

4.6.4 The Gidgealpa south dome: a river dominated delta system

In this study I have interpreted the area as an upper to lower, fluvio-deltaic sequence grading to open lacustrine higher up-section. More specifically I have interpreted the deltaic sequence to be of a river dominated origin, based on core and wireline data. Due to the wealth of geological information and its river dominated character, I have also used the Mississippi Delta as a modern analogue to describe sedimentary facies, their associations and distributions.

4.6.4.1 Sedimentology of The Gidgealpa south dome

A significant proportion of identification of the depositional system within the Birkhead Formation has come from the interpretation of facies and the assembly of these facies to form facies associations. The facies present are described here and is followed by a discussion of the facies association present at the Birkhead Formation, Gidgealpa south dome.

Also described in some detail are the facies present within the Hutton Sandstone. The description of the top of this Formation is necessary when determining the relationship between it and the overlying Birkhead Formation.

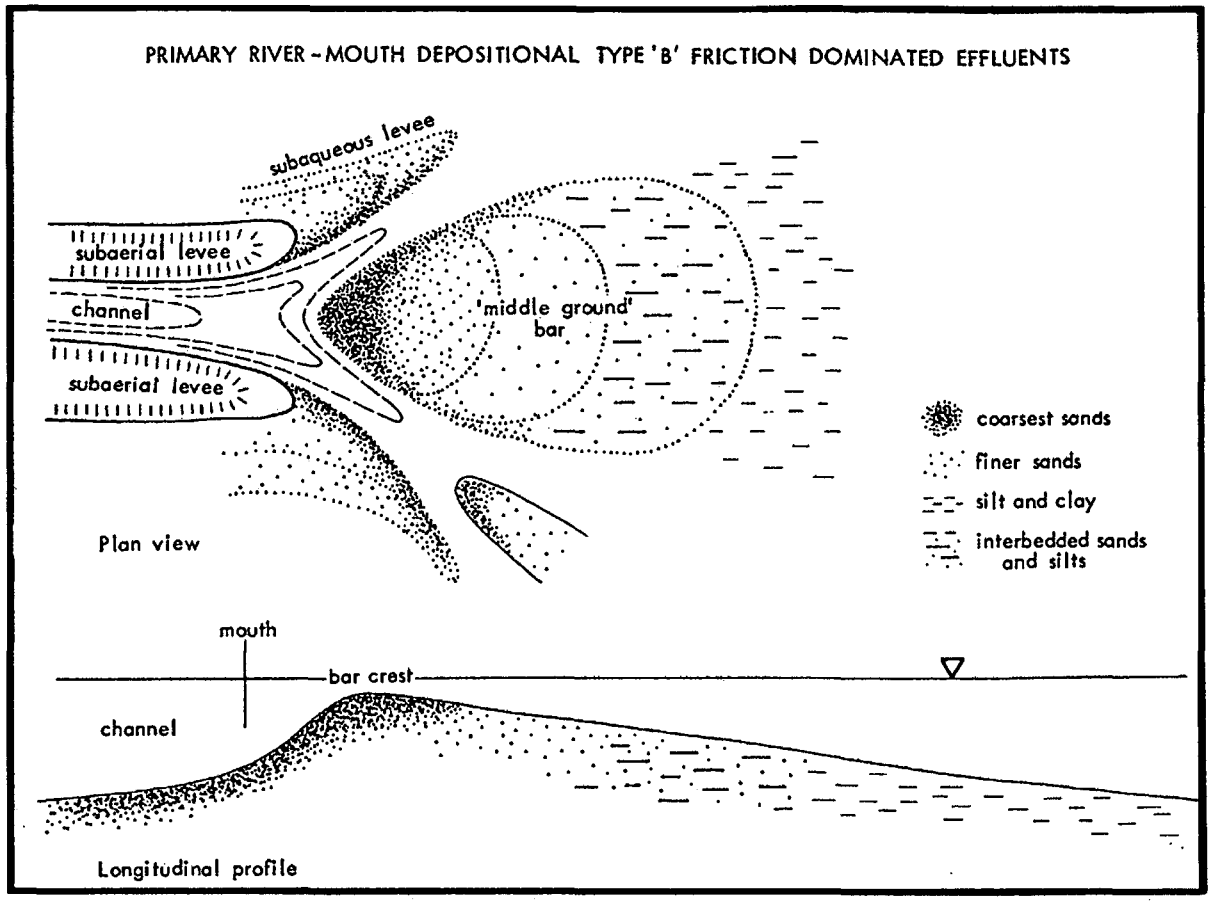

Figure 50: Bifurcating channel and middle-ground bar patterns associated with a friction-dominated, river-dominated delta (From Wright, 1977).

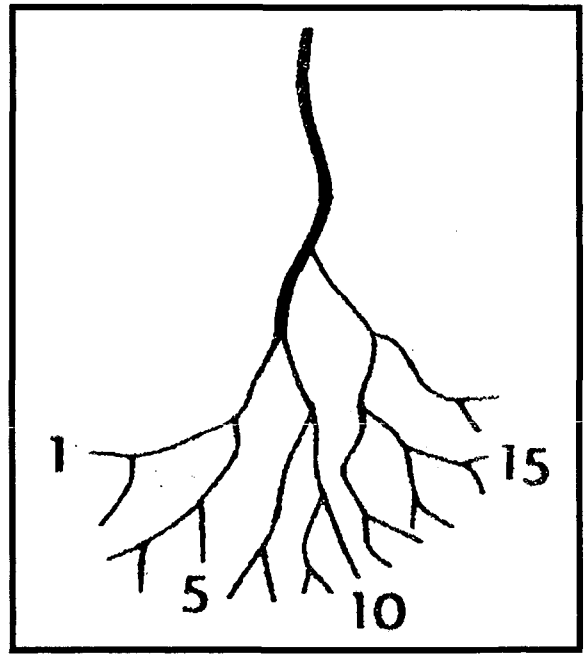

Figure 51: Channel morphology in a bifurcating river-dominated delta, numbers represent the number of bifurcating channels present (From Coleman and Wright, 1975).

4.6.4.2 Hutton Sandstone

The relatively uniform low GR log character with occasional thin high GR bands indicate that the sediments within the Hutton Sandstone were deposited as braided fluvial channels (Burger, 1986, Paton, 1986, Watts, 1987, McIntyre et. al, 1989). On inspection of cores the characteristics are re-enforced, at the top of the Hutton Sandstone the sediments were deposited as either channel fill or abandoned channel fill facies (see following page).

Active Channel Fill

These sediments are by far the most abundant within the Hutton Sandstone due to the multiple bed stacking nature of the braided streams. The sediments consist of craton derived quartz arenites with grain size ranging from medium to coarse and are well to very well sorted with the occasional coal fragments and stringers, mud clasts, granule beds and rare pebbles associated with lags or graded bedding. Sedimentary structures within the channels include graded planar cross beds (both high and low angle), massive beds, gravel lags and horizontal bedding. Common lithofacies associated with channel fill sediments are Gm, Gt, Gp, St, Sh, Sm and Sp. The multiple stacking of channels filled with clean quartz arenites means that this environment has good to excellent, consistent reservoir quality. An example of channel fill sediments can be seen in Gidgealpa 32, 6015'8" to 6022' (appendix **3**).

Abandoned Channel Fill

Sediments deposited in abandoned channels consist of interbedded black to dark grey, laminated to massive, carbonaceous siltstones and very fine to occasional medium grained massive to rippled quartzose sandstones. Siltstone beds are often contorted due to sediment loading by rapidly deposited

sandstones; bioturbation is also a characteristic but is uncommon; Gidgealpa 32, 6009' to 6010' (appendix **3**) is a typical example of this type sediment. Common lithofacies present are Sr, Sm, Fl, and Fm with interbedding caused by sand pulses entering the abandoned channels during flood periods and the accumulation of silts during sediment bypass of the areas. The ratio of silts to sand towards the top of the Hutton Sandstone becomes very high within the abandoned channels with sands only occurring very rarely (Gidgealpa 29, 6064'6" to 6065' (appendix **3**)). As Boult (1996) points out, these sediments may represent inter-tonguing of low energy Birkhead Formation sediments back-filling channels after periods of heavy flooding

4.6.4.3 Birkhead Formation

Wireline log character and core logging indicates that the basal part of Birkhead Formation at the Gidgealpa south dome starts as a shallow lacustrine sequence which grades up into fluvial-deltaics and then reverts back to lacustrine conditions.

4.6.4.3.1 Channel

The type of sediments present within a distributary channel is highly dependent on the dynamic environment and dominant river-mouth processes (Wright, 1985). The mixed load character of the sediments that entered the Gidgealpa south dome area caused abandoned channels to fill with silts and clays above a scour base. Nearer to the shallow river mouth the frictional effects of the sediment laden water caused distributary channels to be filled by cross bedded sands.

Active Channel Fill (Distributary Channel)

Sediments consist of craton derived quartz arenites and / or lithic labile volcanic arc derived sediments that are commonly fine to medium grained but may also be coarse grained or contain pebbles. Sands are moderately to well sorted. The distributary channels show a general fining upward character and an increase in interbeds of abandoned channel fill with the increasing age of the channel which also caps active channel fill sequences (Gidgealpa 29, 6019'6" to 6012' (appendix **3**)). Channels usually, but not always, consist of a scour base and gravel lag that may consist of siderite mud clasts; pebble to gravel sized quartz grains or large coal fragments. The gravel lag may occur with either a sharp or gradational contact with the sediments that are subsequently deposited above (Gidgealpa 32, 5977'8" to 5979'8" and Gidgealpa 29, 6020' (appendix **3**)). Above possible channel lags are a number of sedimentary structures within the sands including trough, planar and ripple crossbeds and massive sandstones. Common associated lithofacies are Gm, Sr, Sp, St, Sm (Gidgealpa 29, 6029' to 6025' and 6023'4" to 6022'(appendix **3**)). Sediments consisting of quartz arenites have good reservoir quality while lithic rich arenites are usually poor.

Abandoned Channel Fill

Abandoned channel fill sediments can usually be identified by a channel lag overlain by fine grained sediments such as laminated siltstones or dark grey to black carbonaceous shales. Shales deposited are commonly contorted due to the high angle of depositional dip that was caused by sediment slumping (as in figure **37**, page 77). Common associated lithofacies are Fl, Fm, Sr and Fcs. Abandoned channel fill sediments are probably laterally restricted and are non-reservoir rocks. An example is shown in Gidgealpa 30, 6028'1" to 6029'3" (appendix **3**).

4.6.4.3.2 Interchannel / Distributary Margins

Sedimentary environments above the delta front are highly variable over short distances. Beyond distributary channels and their bounding subaqueous and subaerial levees, the over-bank deposits are generally wedge shaped, consisting of interbedded sands and silts (Wright, 1985).

Shallow Lagoon/Lake Margin

Sediments consist of very well sorted, very fine, light grey sands and grey to brown silts which grade into very fine sandstone lenses with wavy siltstone laminations, clay drapes and current ripple laminations are common with root bioturbation also occurring. Rare pebbles or drop stones may be present from vegetation rafts. The sediments are usually associated with distal crevasse splays and swamps. Non-reservoir lithofacies Sr, Sd and Fl are common. An example is shown in Gidgealpa 29, 6034'3" to 6035'9" (appendix **3**).

Crevasse Splay

Crevasse splay sediments commonly consist of moderately to well sorted, cream to buff brown, fine to medium grained sandstones, dark grey to dark brown siltstones and claystones. The sediments show a coarsening or cleaning up sequence with rare trough cross beds, climbing ripples and low angle wavy cross bedding. Gidgealpa 32, (5980'6" to 5982'2" and 5986'6" to 5988'3" (appendix **3**)) shows load casts, soft sediment deformation, scour and fill structures and the presence of large coal fragments that indicate periods of rapid deposition. Occasional root casts and bioturbation are present. Common lithofacies associated with crevasse splay sediments are St, Sd, Sr, and Fl. Sediments are of a generally poor to non-reservoir quality but may improve at the top of coarsening-up sequences.

Levee

Levee deposits (Gidgealpa 29, 6024'10" to 6025'3"(appendix **3**)) consist of fine grained, moderately to well sorted sandstones with ripple cross laminations and laminations of siltstones which may be coaly, bioturbated or have small scours in places. Levee sediments consist mainly of lithofacies Sr and Fl and are non-reservoir.

Well Drained Swamp

Well drained swamp deposits are olive to olive-grey in colour and consist mainly of clay, silts and rarely contain very fine sand lenses. Organic content is low due to oxidation in an aerobic environment and sediments are predominantly homogeneous due to heavy animal and root bioturbation. Large root casts are common throughout indicating subaerial exposure which is re-enforced by the possible early stage formation of a pedogenic surface (Gidgealpa 32, 5990'1" to 5990'3"(appendix **3**)). Where sands are present they are very fine grained and beds appear to be distorted. These sediments are non-reservoir and consist mainly of lithofacies Fcs. Well drained swamp deposits can be seen in Gidgealpa 32, 5990'3" to 5992'(appendix **3**) and are associated with poorly drained swamp deposits.

Poorly Drained Swamp

Sediments consist of dark grey to dark brown carbonaceous siltstone and mudstone which commonly grade into coal. Rare fine grained sandstone lenses may also occur. The coal in the lower Birkhead Formation tends to be thin since the climate at the time was temperate causing plant matter be in limited supply. Thus conditions for the formation of coal could not be sustained for long periods of time (Frakes et. al, 1992). Along with thin beds, the coal tends to have a short lateral extent that often inter-fingers with fine grained clastic and carbonaceous deposits (Coleman and Wright, 1975).

The high organic content and dark colour of the sediments is due to deposition in anaerobic conditions with the presence of small roots indicating that water level was close to or above surface of the sediments. Most sedimentary structures have been distorted or destroyed by heavy root bioturbation, sandstone lenses generally show ripple cross laminations and climbing ripples. Lithofacies Fos and minor Sr are present within these sediments. An example is shown in Gidgealpa 29, 6032'7" to 6034'3" (appendix **3**). These sediments are of non-reservoir quality.

4.6.4.3.3 Channel Mouth Bar

The channel mouth bar sediments over the Gidgealpa south dome have generally formed in open lacustrine areas where flooding of former fluvio-deltaic sediments has occurred in the upper section of the basal Birkhead Formation. These sediments appear to be initiated as distal bar sediments which generally coarsen up in sequence indicating shoreline regression or progradation of the delta.

Bar Top

Bar top sediments are generally medium grained, buff brown crossbedded sandstones with sets ranging in thickness from 10 to 40 cm. Bedload currents probably rapidly deposited sandstones. These sediments are mainly restricted to the upper parts of the basal Birkhead Formation where the raising of base level has pushed channel mouth bar sediments over former fluvial sediments. Common associated lithofacies are St and Sh. Reservoir quality is generally poor due to the lithic content of the sediments. An example is shown in Gidgealpa 26, 5953' to 5953'7" (appendix **3**).

Bar Front

Bar front sediments consist of massive to tabular low angled planar to horizontal bedded and ripple laminated fine to very fine grained, well sorted sandstones. Associated with the sandstones are occasional clay drapes. These sediments generally coarsen up to bar top facies as seen in Gidgealpa 26, 5958'7" to 5955'2" (appendix **3**). Associated lithofacies are Sp, Sh and Sm with sediments being generally non-reservoir.

Subaqueous Levee

Subaqueous levee sediments are generally associated with bar top and bar front sediments. They consist of interbedded to interlaminated wavy, current and climbing ripple cross laminated fine grained sands with horizontal to wavy laminated siltstones. Occasional bioturbation and the presence of root casts indicate the positions of these sediments in relatively shallow water. Subaqueous levee sediments are indicated in Gidgealpa 26, 5949'2" to 5949'10" (appendix **3**) and commonly consist of Sr and Fl lithofacies. These sediments are non-reservoir.

Distal Bar

Distal bar sediments generally indicate the start of a coarsening up delta sequence commencing on top of lacustrine sediments. Distal bar sediments consist of interbedded, very fine to fine grained ripple laminated sandstones and massive to laminated siltstones which occasionally have sandstone lenses and are commonly bioturbated in the top part of the beds. Sandstones range in thickness from 2 to 20 cm and have common climbing and wavy bedded structures. The common formation of the siltstone beds and their subsequent bioturbation indicate periods of non-deposition, possibly caused by periodic deposition of sands from turbidity currents, storm deposits or wave reworking. Examples of these sediments can be seen in Gidgealpa 26, 5969' to 5977'4"

(appendix **3**) and in Gidgealpa 32, 5964'2" to 5975" (appendix **3**) with common Sr, Sb/Fb, Fm and Fl lithofacies. Distal bar sediments are generally of non-reservoir quality.

4.6.4.3.4 Lacustrine

Lacustrine conditions occur after the inundation of the Gidgealpa south dome from a relative rise in lake base level. This forced the lake edge and subsequent sediment deposition further to the east, up dip, starving the area of any significant clastic input.

Open Lacustrine

Open lacustrine sediments are mainly dark grey to black massive to horizontal laminated, highly carbonaceous, siltstone/claystones. Occasional sand lenses occur but are commonly thin (less than 1 cm) and were most likely deposited during storm activity where sands were reworked from shallower parts of the lake. The fine grained nature of the sediments and the absence of any post-depositional structures such as bioturbation or dewatering structures implies sediment deposition from suspension. Open lacustrine sediments are of non-reservoir quality and consist of lithofacies Fl and Fm as shown in Gidgealpa 29, 6012' 6" to 6009' (appendix **3**).

4.6.4.3.5 Facies Associations

From wireline logs and associated cores, the Gidgealpa south dome area can be divided into an upper and lower delta plain environment. Within these two zones the lower Birkhead Formation can be can be further divided into three major facies associations. Delta plain sediments reflect a varied depositional setting including distributary channels, abandoned distributary fill, subaerial and subaqueous levee deposits, crevasse splays, marshes, swamps, lakes and

bays (Williams, 1982). I have found that these sedimentary environments were active at the time of Birkhead Formation deposition at the Gidgealpa south dome. Donaldson (1967) stated that a delta plain may contain:

1) An upper delta plain with meandering distributary channels containing point bar, massive to trough cross-bedded sandstones and gravel lags which may be abundant in plant and wood fragments.

2) A lower delta plain containing linear distributary channels. Here stream currents are unidirectional with active channels filling with the coarsest river sediments. Large scale cross bedding is present while abandoned channels contain shales or siltstones containing plant fragments.

3) Natural levees result from over-bank flow of sediments during flooding. Here, thin beds of fine grained current rippled sandstones and siltstones are interbedded and may be disrupted by roots.

4) Swamps containing dark carbonaceous shales and coals depositing in well or poorly drained areas along with occasional crevasse splay deposits.

5) Lakes that consist of laminated shales and may contain iron concretions.

Association 1 consists of prodelta facies, distributary mouth bars, distributary channels and subaqueous levees. Characteristic gamma ray wireline log signatures of the lower delta plain consist of decreasing API values representing a coarsening up sequence by prograding prodelta and delta front facies followed by a section with relatively low API values representing bar top and distributary channel facies. An increasing gamma ray signature on top of distributary channel sediments represents a fining up sequence of interdistributary bay facies up to open lacustrine due to a deepening water depth. Figure **52** shows the gamma ray signature of the delta facies in Gidgealpa 29. Interpreted sedimentary structures and sedimentary

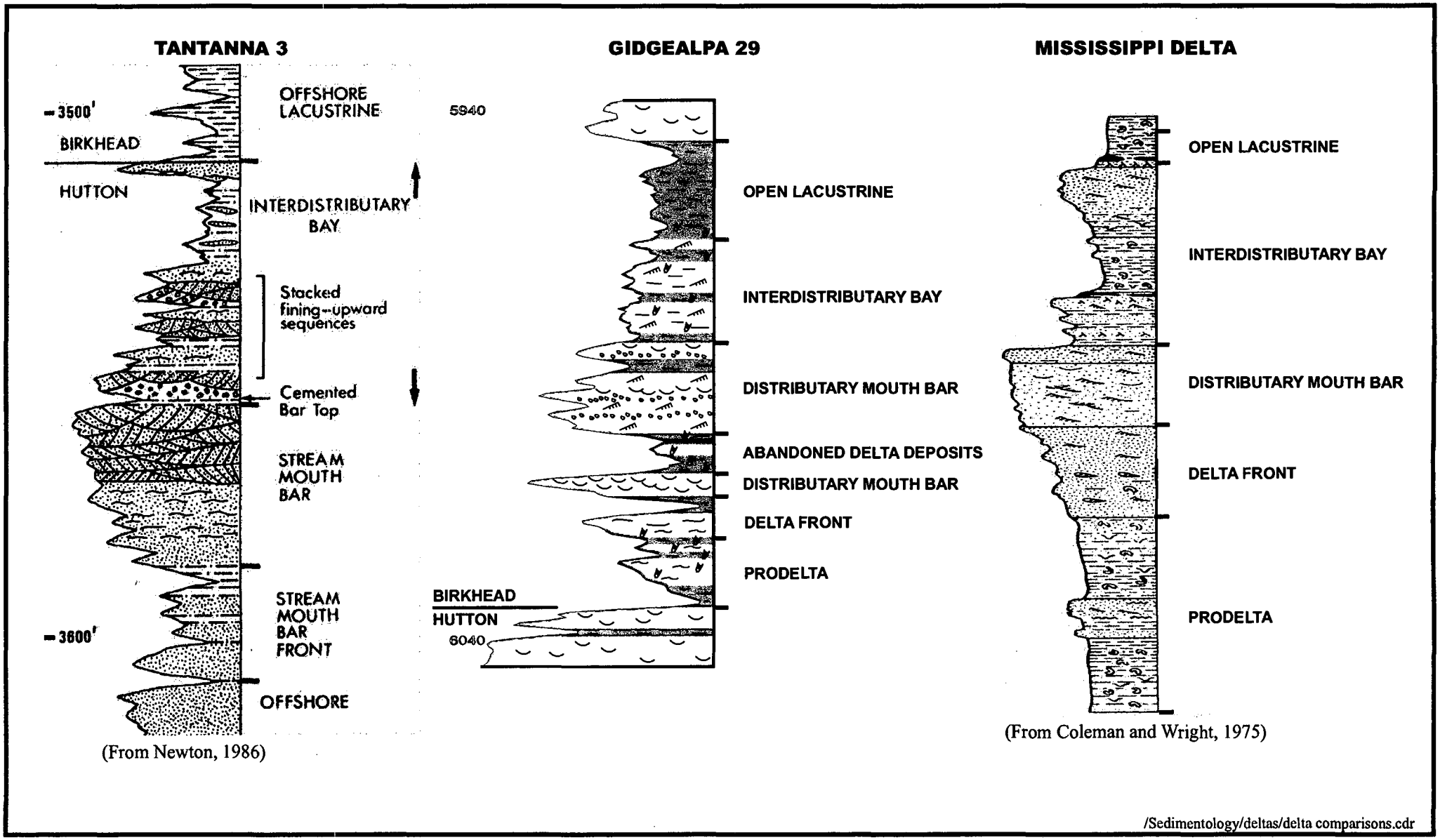

Figure 52: Association 1 of Gidgealpa south dome, Birkhead Formation sediments compared with the fluvial dominated sequences from Tantanna (Eromanga Basin) and the Mississippi Delta.

environments have been determined from core and are compared to two sections from the Tantanna field deltaic sequence in the Queensland section of the Eromanga Basin (Newton, 1986) and the Mississippi Delta (Coleman and Wright, 1975). Figure **52** illustrates the similarities in log signature and sedimentary structures of the deltaic sequences which vary from prodelta and delta front facies to distributary mouth bars to interdistributary bays and lacustrine facies from bottom to top. In the figure note the similar thickness of the sand packages of both Tantanna 3 and Gidgealpa 29. This fluvial character is particularly noticeable in the early stages of delta development or the prodelta stage. The lower delta plain environment is situated on the western side of the Gidgealpa south dome area and incorporates Gidgealpa 20, 22, 27, 29, and 31 (refer to figure **100** on page 217 for well locations).

Association 2 contains upper delta plain sediments to the east of the Gidgealpa south dome area which differ from those in the west This association consists primarily of fine grained silts and clays with a significantly lower sand content indicative of interdistributary bay sediments. Characteristic gamma ray signatures of these wells with generally high API values are serrated in appearance representing swamps and shallow lagoons with the occasional thin (0.5 to 1 m) coarsening upward or sharp based fining upward sequences, which occur as a downward decrease in gamma ray API values. The higher API values represent finer grained sediments that contain an abundance of silts and clays since these sediments have higher quantities of radioactive potassium. The upward decrease in the gamma ray values represent crevasse splay or crevasse channels respectively. Similar sequences to those seen in figure **53**, which shows an example of interdistributary bay facies, are seen in Gidgealpa 46, 40, 28, 17, 25 and 37.

Association 3 is also present within the upper delta plain and consists of distributary channels and interdistributary lacustrine and swamp sediments. The channels have sharp contacts with the underlying low energy facies and generally show a fining upward sequence represented by low API gamma ray

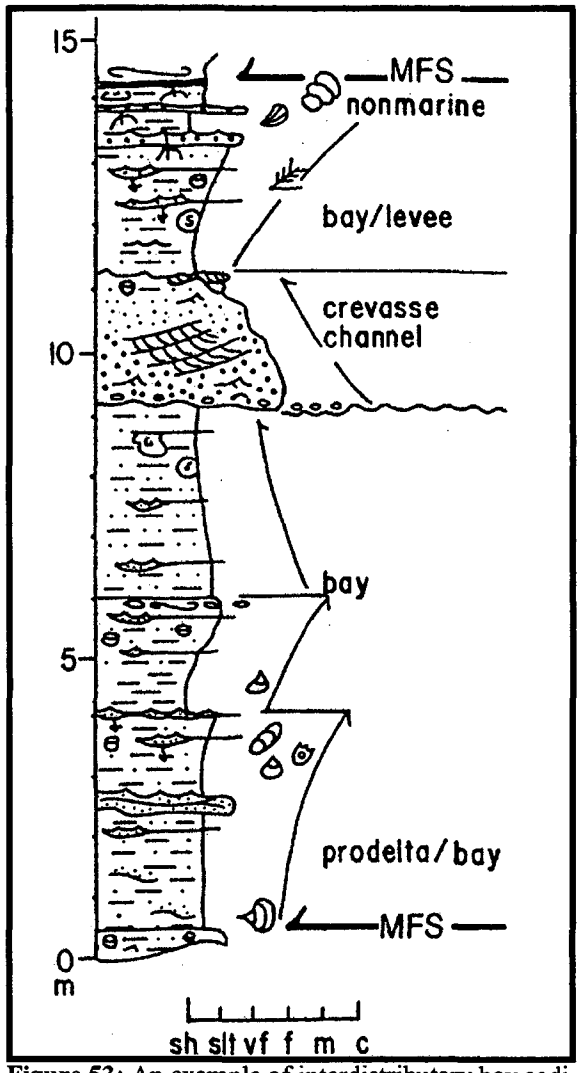

Figure 53: An example of interdistributary bay sediments from the Cretaceous Dunvegan Formation in Alberta, Canada is similar to Association 2 of the Gidgealpa south dome. The Birkhead Formation sediments are dominated by overbank fine grained sands, silts and muds (From Bhattacharya and Walker, 1992)(symbol legend located in figure 55).

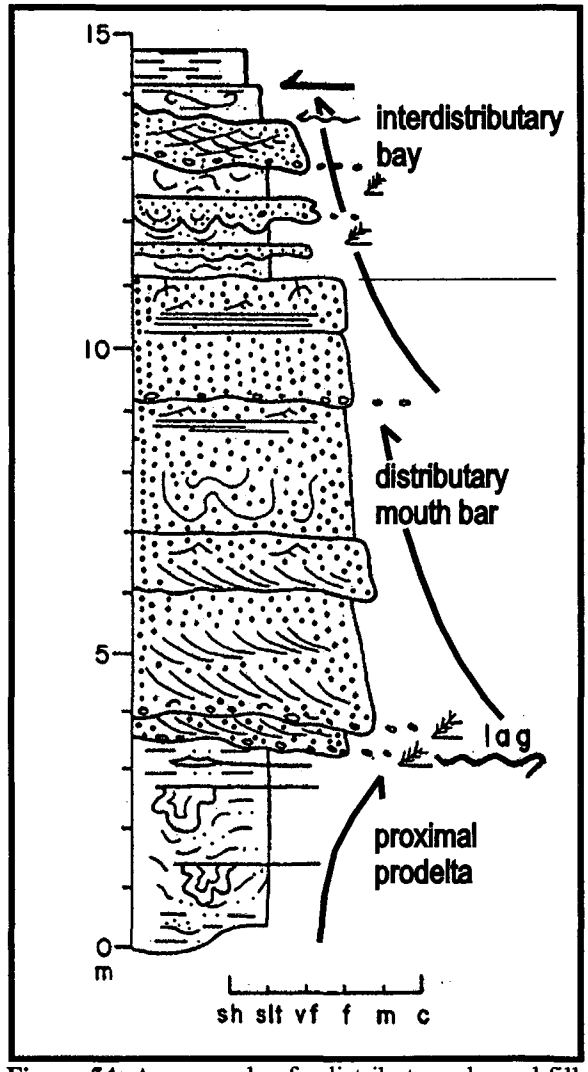

Figure 54: An example of a distributary channel fill sequence from the Cretaceous Dunvegan Formation in Alberta, Canada is similar to Association 3 of the Gidgealpa south dome. The Birkhead Formation sediments show the coarse grained channel sands and upper delta plain sediments (From Bhattacharya and Walker, 1992)(symbol legend located on figure 55).

values which generally increase upward. The high value gamma ray spikes present within channel sequences in some wells are passive channel fill silts and clays that probably represent breaks in sediment entering the area from the east. Abrupt terminations of sand in active channel sediments may also occur and represent channel abandonment and filling by silts and clays that have a higher API values. These distributary channel facies only occur in Gidgealpa 36, 24, 26 and 50 due to channel bank stability (to see characteristic gamma ray long signatures refer to figures **91** - **94** on pages 202 to 205). Figure **54** (previous page) is a succession from a river dominated delta in the Dunvegan Formation, Alberta showing an example of this type of facies association.

A river dominated setting for the delta complex at the Gidgealpa south dome has been determined using the criteria above (section **4.6.3**). If we take Gidgealpa 29 as an example (figure **52** on page 113), it can be seen that from the cores and wireline data, the processes present are primarily fluvial with no evidence of wave or tidal influences. Figure **55** shows the fluvial prodelta sediments of the river dominated delta consisting of inter-bedded sands and fine grained silts with load casts, ripple bedding and the presence of coals. Comparison with wave influenced or wave dominated deltas shows the different morphologies with prodelta facies being dominated by marine processes producing predominantly clean sands indicative of shoreface facies and the absence of fine grained sediments and coals.

Wright (1985) stated that after the deposition of a delta sequence, the moulding or shaping processes of the sediments continue due to delta front sediments prograding over the older prodelta causing deformation and flowage of sediments. At the Gidgealpa south dome, evidence of sediment deformation by loading on the prodelta is shown by the presence of deformational structures. One such structure that I have observed from cores can be seen in plate **1** which is the end product of fast migrating sediments that squeezed and deformed fluidised sands, forming miniature diapirs. The formation of the

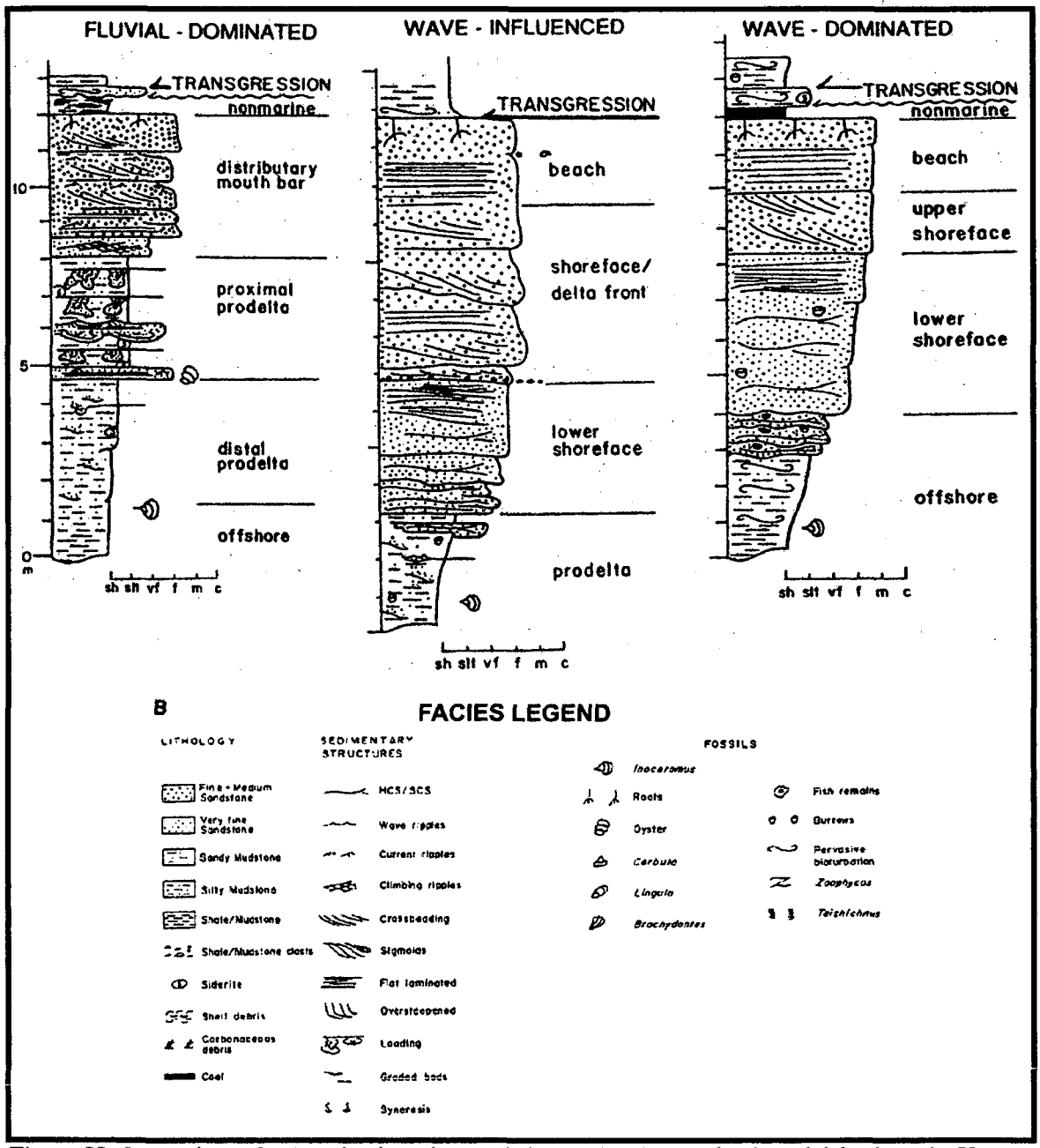

Figure 55: Comparison of a river dominated, wave influenced and wave dominated delta from the Upper Cretaceous Dunvegan Formation, Alberta (From Bhattacharya and Walker, 1992).

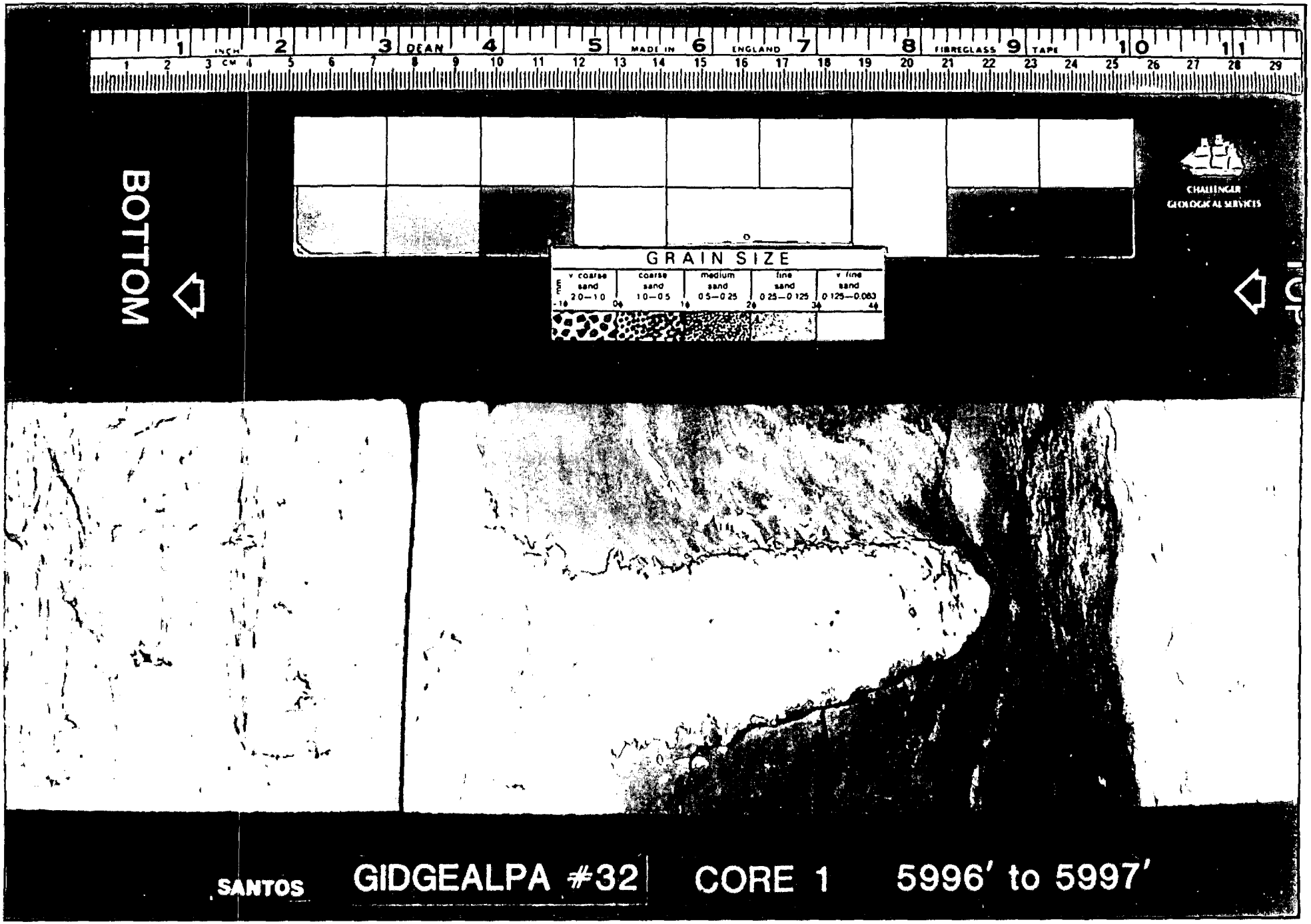

Plate 1: A miniature sandstone diapir formed by deformation of fluidized sands due to rapid deposition of deltaic sediments.

fluidised sands is also a product of rapid deposition. This process is also seen in the Mississippi Delta and is discussed in section **4.6.5** below.

The concept of a river dominated delta at the Gidgealpa south dome is strengthened by the fact that a favourable geological setting would have existed at the time of deposition of the sediments which is similar to the geology described in section **4.6.3** on page 101. The presence of an intracratonic lake (Burger, 1986) that was isolated from the sea for a period of time means that the body of water would have lacked tides. Any waves that may have been produced by storm activity would have been attenuated by the shallowly inclined ramp dipping to the west (see figure **81** on page 174) of the Gidgealpa area. The minimal density contrast between the lake and fluvial waters would have also favoured the formation of bifurcated channels within the delta mouth bar.

Observations I have made from cores indicate that the Gidgealpa south dome river effluent entering the area consists of sandy mixed load sediments and is slightly coarser grained than sediments at the Mississippi Delta. However the presence of a large percentage of fine grained sediment in both cases caused the delta complexes to have similar morphologies. Thus grain size from the feeder system has a considerable effect on the physical processes, environments and shape of the delta (Orton and Reading, 1993). According to Orton and Reading (1993), sandy mixed load deltas have gradients of less that 1m/km and distributaries tend to maintain the same pathway due to consolidation of channels and levees by clay and silts. Channel branches will also tend to prograde as isolated point sources and channels will shift by avulsion. These characteristics are seen at the Gidgealpa south dome. Isopach maps (see section **8.1**) show the shoestring nature of distributary channels in the upper delta plain and their fixed location compared with the lower delta plain where avulsion occurs. More detail of the delta sand architecture will be discussed in section **5.5.**

While the Gidgealpa south dome consists of a river dominated delta, the morphology of the sands deposited in the area vary through early to late development. The differences in shape of the delta system is a result of variations in the rate of sediment input into the area. In the early stages of development the delta progrades rapidly forming an elongate shape, then as the sediment influx decreases the slower rate of sand influx will allow for minor modification of the still prograding delta by wave activity forming a lobate configuration. A further decrease in the sediment input rate and transgression of the sediments allowed for greater modification of the delta lobe by wave activity thus allowing the formation of a wave dominated sand package which is aligned parallel with the shoreline. Galloway (1975) has interpreted this type of delta evolution for the Tertiary clastic cycle of the northern Gulf of Mexico Basin (figure **56**).

Thus from wireline log correlations and sand contour mapping (see section **8.1**) the delta system has three predominant configurations. These configurations from oldest to youngest are:

1) a fluvially dominated elongate bird foot structure
2) a fluvially dominated lobate structure and
3) a wave influenced fluvially dominated structure

The variations in shape of the delta with time can also be explained by the observations of Elliott (1974). He noted that the initial flood into an interdistributary bay area is not limited by the formation of levees, thus sands entering the area during floods will have a sheet-like configuration. As time progresses however, alluvial ridges will develop and restrict the accumulation of sediments to certain areas making the distribution of channel sands more complex. This concept can be used on a larger scale with the initial sediments being unrestricted, then as levees form the sands become more restricted and complex.

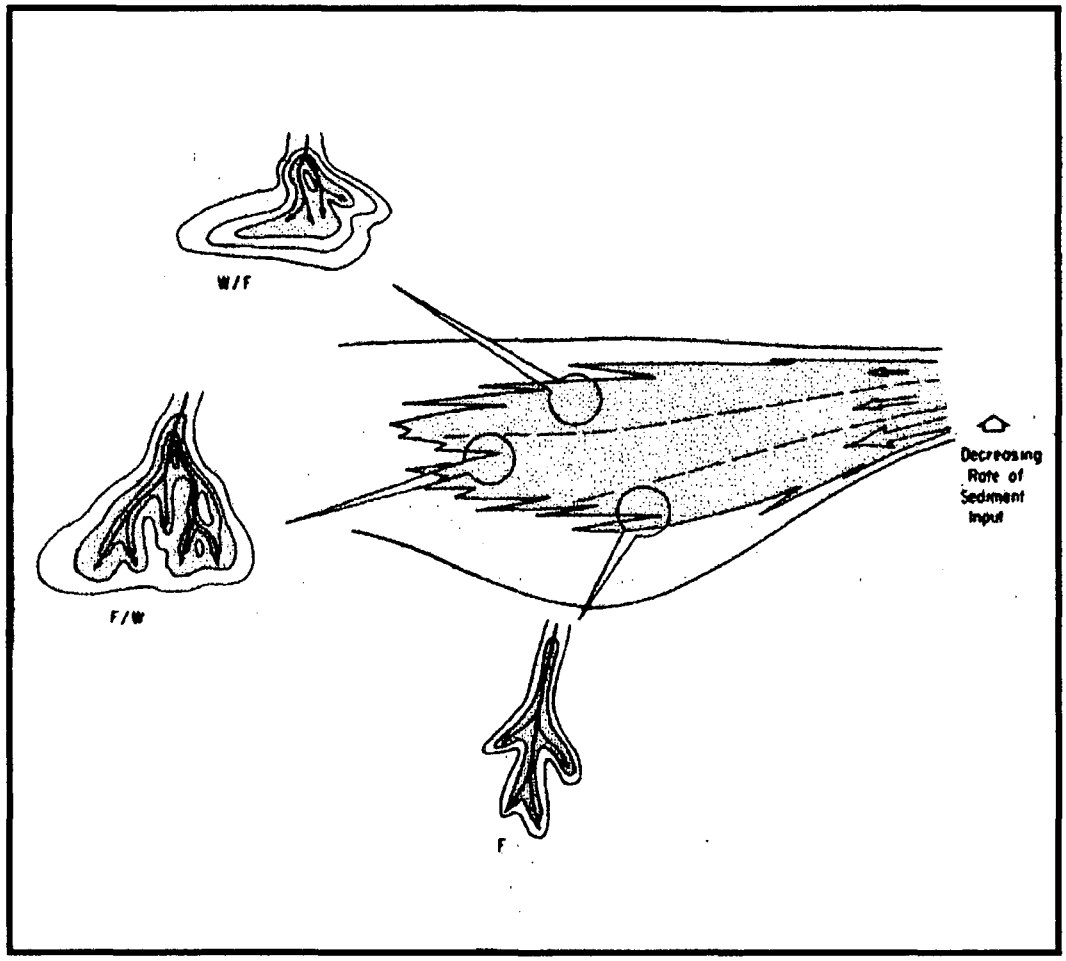

Figure 56: Evolution of a delta from the Tertiary clastic cycle of the Gulf Coast Basin. In this case the delta has evolved from a river dominated bird foot delta to an intermediate lobate shaped river dominated delta to a fluvially influenced wave dominated delta. In this example the fluvial effects on the delta are waning with time (From Galloway, 1975).

The processes, which occurred to produce the delta system at the Gidgealpa south dome, can be studied in a modern day analogue. The river dominated nature of the Mississippi Delta has been heavily studied and although it enters into a marine setting and has a larger vertical and lateral thickness than the Gidgealpa south dome Birkhead Formation its morphology and facies distribution is very similar. For this reason I have summarised the important features in the following section.

4.6.5 The Mississippi Delta: An Example

The Mississippi delta is a present day example of a river dominated delta. The delta is characterised by a highly indented marsh coast line with low relief and protruding digitate distributaries surrounded by bays, marshes, swamps and lakes (figure **57**). Wave dominant features are rare or subdued, if present, and channel sands have a bar finger like geometry (Wright and Coleman, 1973, Coleman and Wright, 1975). The Mississippi Delta also has a series of lobes that have built out in different directions seven times over 4000 years (figure **58**). The lobe switch occurs when the channel system becomes overextended and inefficient (Wright, 1985). Although this delta extends into more dense, saline water the shallowness and small volume of many of the interdistributary troughs causes saline water to be flushed from the areas by a hydraulic head allowing crevasse inflow to occur under homopycnal conditions (Bates, 1953).

The formation of a Mississippi subdelta has been well described by Wright (1977, 1985). A delta lobe rapidly forms from a crevasse breaking through a levee of a major distributary channel into a shallow interdistributary bay. Initially a broad, radial bar is formed due to the shallow depth of the bay causing increased bed friction and rapid effluent expansion and deceleration. A short time later subaqueous levees will develop on top of the former bar and inhibit further expansion of the effluent. As the bar continues to grow upwards, at the end, channelisation will occur creating bifurcating channels

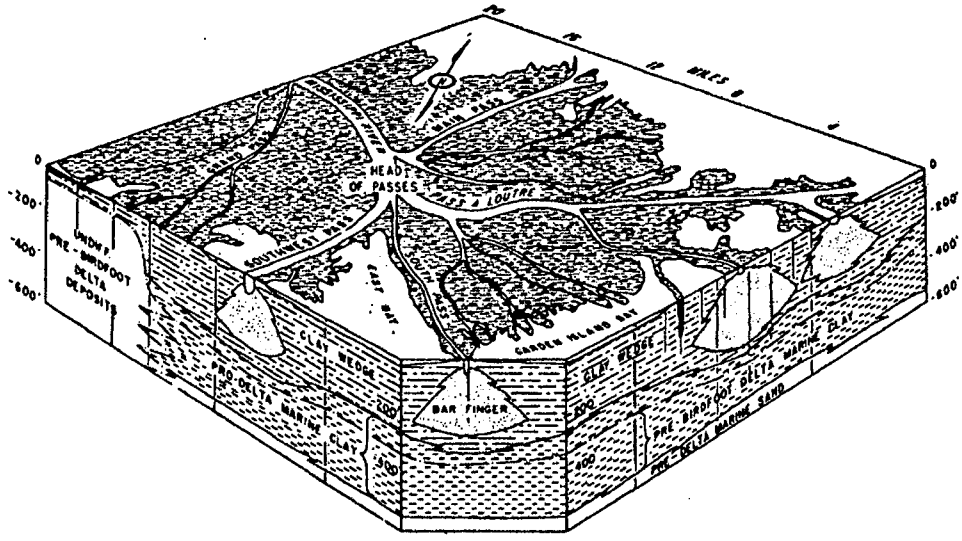

Figure 57: Sedimentary framework of the modern Mississippi Delta (From Le Blanc, 1975 after Fisk et. al, 1954).

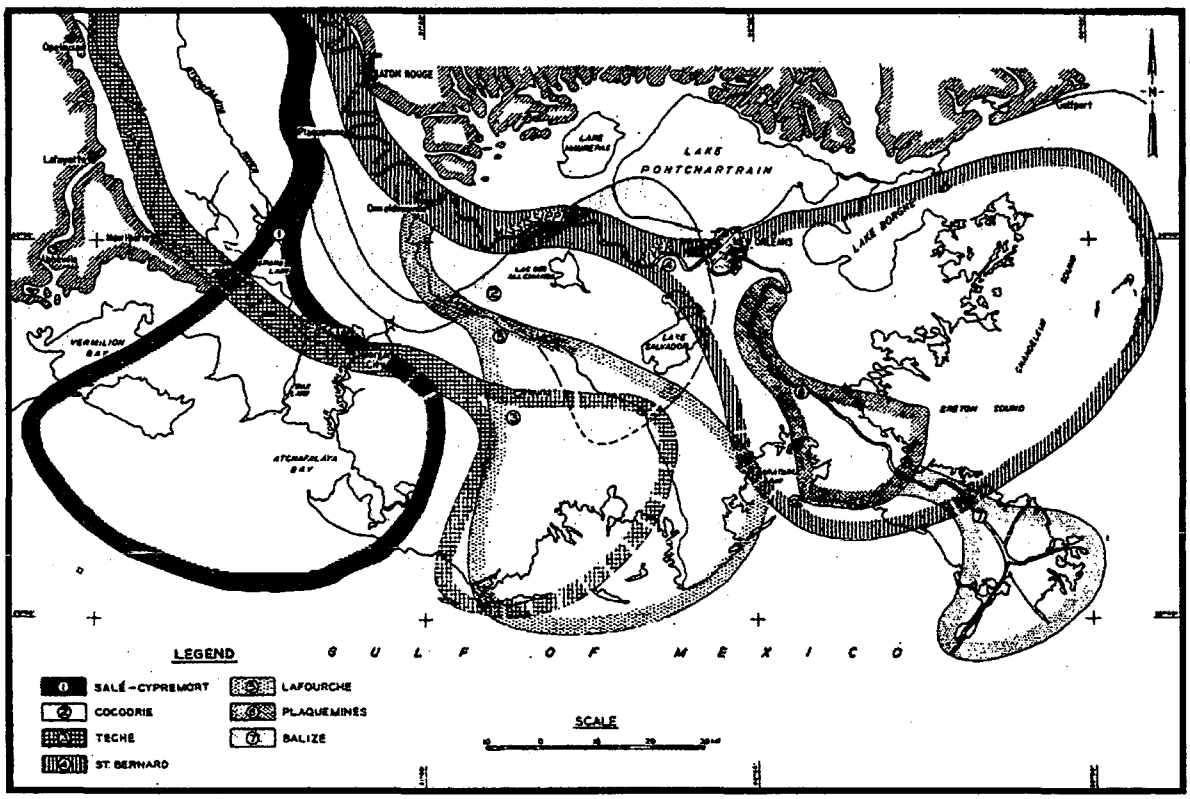

Figure 58: Holocene chronologic sequence of delta lobe development for the Mississippi Delta (From Wright, 1985).

and the formation of a triangular shoal as in figure **50** (page 103). At the outlet coarser bed-load material accumulates at the bar crest and along the inner flanks of the channels creating subaqueous levees while the finer grained material accumulates further from the outlet, over the middle and distal parts of the shoal.

The primary sediments consist of silt and clay with only a small portion of coarser material present while most of the sediment is deposited more distally than the sands that are deposited at the bar front (Bates, 1953). The dominantly suspended load sediments will also allow distributary banks to be well established and difficult to erode forming relatively persistent linear channels occurring in a fixed position for a long period of time. In this situation levees generally become well vegetated and channel width to depth ratios are low (Orton and Reading, 1993).
The rapid deposition of denser distributary channel and bar sediments on older low density prodelta deposits causes differential loading and subsequent deformation. Deformational structures can consist of peripheral slumping, mudflow gullying, clay diapirism, mass wasting by degassing of fine sediments and shelf edge faulting (figure **59**) (Coleman and Wright, 1975, Wright, 1985). Figure **60** describes the evolution of the Mississippi delta showing progradation of channels over delta bar deposits, bifurcation of channels and distributary abandonment.

In summary, the depositional environment of the Gidgealpa south dome area consists of a mixed load, river dominated delta and therefore plots in the fluvial dominated region of the tripartate plot in figure **48** (page 99), on the mid point between the mixed mud / silt plain and the sand plain. These characteristics mean that the delta will have a birdfoot or digitate sand distribution or a type 'A' morphology (from figure **49**, page 100).

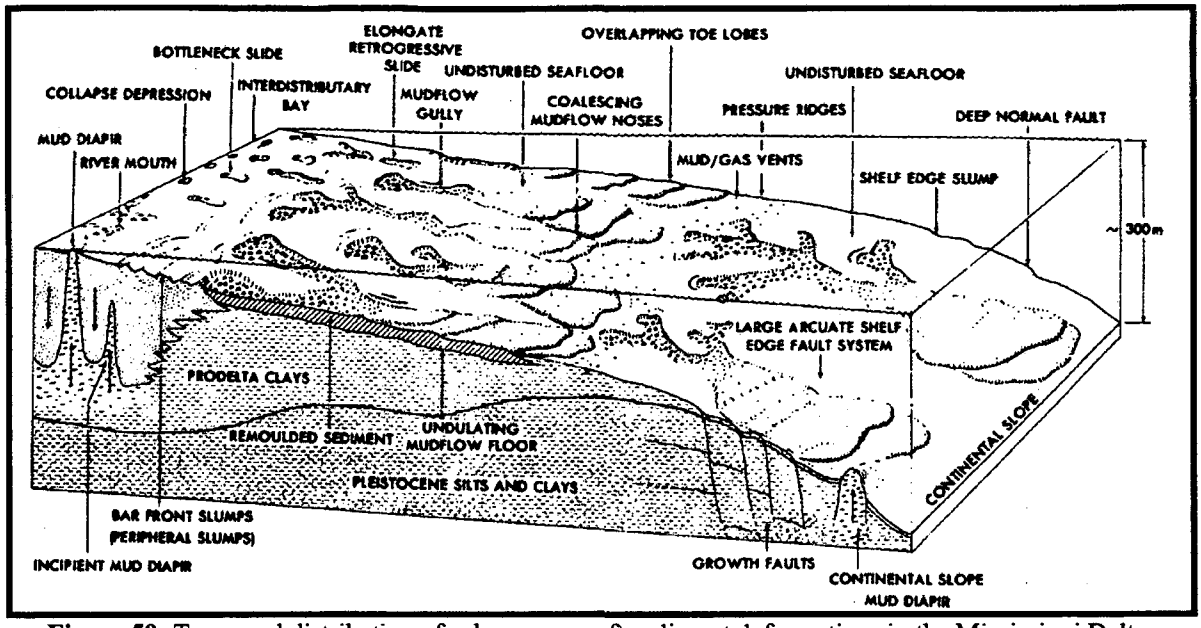

Figure 59: Types and distribution of subaqueous soft sediment deformations in the Mississippi Delta (FromWright, 1985).

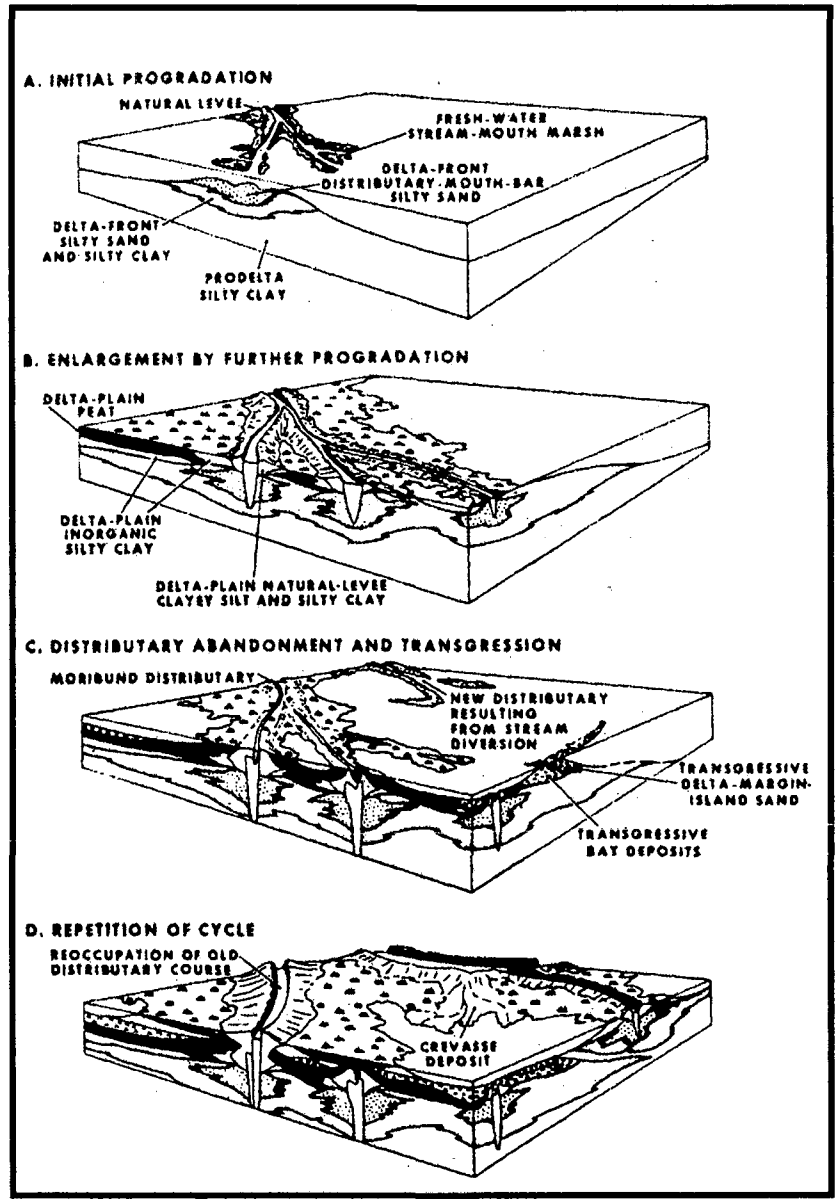

Figure 60: Development of the Mississippi deltaic facies (From Le Blanc after Frazier, 1967).

4.7 Dipmeter Interpretation and Palaeocurrents

4.7.1 Introduction: Use of the Dipmeter to determine Palaeocurrents

I have found interpretation of dipmeter data within the basal Birkhead Formation and the top Hutton Sandstone sections to be a wealth of information. The data has also been invaluable for the interpretation of palaeo-flow direction both locally at the Gidgealpa south dome and regionally within the Eromanga Basin. Dipmeter interpretation has also assisted in the correlation and distribution of reservoir sands at the reservoir scale. The value of dipmeter data becomes apparent when applied to fluvial reservoirs that have a complex sand distribution and geometry. It seems that this data has been under utilised within the Eromanga Basin in the past, a fact that is reflected in the limited amount of literature available on the use of dipmeter data in general. Due to the lack of general literature in the area of dipmeter use and application, I will attempt to cover a broad range of subjects to give a complete coverage and overall use and effectiveness of this data; applying it regionally and then focusing in on the Gidgealpa south Dome.

The Dipmeter tool is an effective instrument when it is used with other data such as wireline and core logs, lithofacies and stratigraphic interpretation. The dipmeter tool can be used to determine structural dip as it was in the early years of its use. The tool helped to identify major geological features, which have the potential to trap hydrocarbons. The determination and subsequent removal of this dip when determining palaeo-flow then allows for the determination of direction and magnitude of sedimentary dip (Selley 1989). Its use as an internal indicator of lithological structures was adapted as the tool and techniques became more refined with time, to a point where tools can now 'image' borehole walls.

Data is collected from the tool by measuring the differences in resistivity of different sedimentary beds as its pads pass over bed boundaries exposed within the bore hole. The raw data is then displayed as a continuous trace. Formation dip measurements are collected by the use of the conventional 'High Resolution Dipmeter' (HDT) and work on the principle that a bedding plane is crossed by at least 3 of the 4 tool pads. The HDT tool has been improved with the development of the Dual Dipmeter tool (SHDT) which can measure down to resistivities covering an area of 1 - 2 cm. The main improvement is the modification of the pads and measuring electrodes. The SHDT has a smaller surface area allowing for better connection to the well bore walls along with 2 electrodes instead of one to allow for a higher credibility of the data and better correlation between the 4 pads.

4.7.2 Methodology

Dipmeter data was acquired, both regionally and from the Gidgealpa south dome, from a variety of wells run by either the HDT or SHDT tools. Most of this data was processed using the CLUSTER or MEAN SQUARE DIP programs by Schlumberger, that use the "interval correlation method" of interpretation. The interval correlation method is a measurement of the 'commonalities' of two curves produced by the dipmeter tools. To determine bedding dips down the bore hole one curve is compared to the other curve of interest and a correlation function, or 'correlogram', is obtained for the two curves. The best fit of the two curves is when the correlogram is at its maximum. The procedure is repeated for other lengths of curves and the displacement of similar sections is used to calculate the dip.

For the interval correlation method to be effective the operator must specify a 'correlation interval', 'step distance' and 'search angle'. The correlation interval is a certain length of each curve to be compared at each round of

correlations while the step distance is the depth increment that a curve is moved between two successive rounds of correlation. The search angle is the maximum angle at which the program will scan for correlations down the curve before turning to another pair.

Some regional wells have also been processed using the GEODIP program by Schlumberger, this program uses the "feature correlation" method. Briefly, this method breaks down the resistivity curve into a depth ordered sequence of ranked elements or events; it then uses a hierarchical approach to match the individual features from different curves. This method has the advantage of being able to measure dips down to a finer scale than the interval correlation method since each event corresponds to a geological event. This fact makes the GEODIP program useful for fine structured sedimentary sections, as compared to the interval correlation programs which are limited to the lengths of the correlation interval and step distance.

Presentation of the processed dipmeter data is important for interpretation of the dip and palaeocurrent trends. The tadpole plot is a common method of displaying the processed data and shows all necessary data including hole drift, gamma ray and caliper logs, tadpole plot, dip frequency diagrams (rose plots) and the raw resistivity data from each pad.

4.7.3 Structural Dip

Using shale or floodplain sediment sections from GR logs; structural dip has been determined from the corresponding dipmeter plots to be no greater than 3°. Structural dip can be calculated on the assumption that floodplain sediments are laid down horizontally due to passive deposition of fine grained sediments. Any subsequent tilting of the horizontal beds will produce a dip value that can be seen on the dipmeter data. Boult (1996) also calculated structural dip from seismic lines and estimated the maximum dip to be 2.6°,

which is in excellent agreement with the interpreted dipmeter data. Structural dip can be characterised by the tadpoles, which have consistent dip angle and azimuth within fine grained or shale sections.

Structural dip in most wells was not corrected for since sedimentary dip angles are much greater than 3°. The higher angles of sedimentary structures mask the dip from structural tilting and thus do not significantly affect sedimentary dip interpretation. Figure **61** shows the effect of structural dips on the rose diagram of Gidgealpa 53. The original rose plot in the figure indicates a northerly mean azimuth value. However, the tadpole plot indicates that a large percentage of the interval consists of floodplain sediments and dips are due to structural tilting rather than sedimentary dip.

To determine true sedimentary dip at Gidgealpa 53 the values that correspond to the floodplain sediments were removed from the calculation of the rose diagram. Figure **61** indicates that 17 dip values were removed from the original rose diagram which originally contained 37 values and the resultant rose diagram with the structural dip removed is displayed from the remaining 20 dip values. From the rose diagram with the structural dip removed, the dip direction of sediments is to the west rather than to the north.

4.7.4 Regional Dipmeter Interpretation

Regional dipmeter data is very important for the interpretation of palaeo-current directions over a vast area. Knowledge of palaeo-flow direction can give the geologist a better insight into regional sand trends. Dipmeter trends can also give insight into the quality of sands depending on their distance from the source. In the case of the Eromanga Basin, at or near the Hutton / Birkhead interface, palaeo-flow direction, as a whole, can help determine the provenance of sediments. Sediments which are derived from the cratonic area to the south-west are likely to consist of clean, reservoir quality, quartz

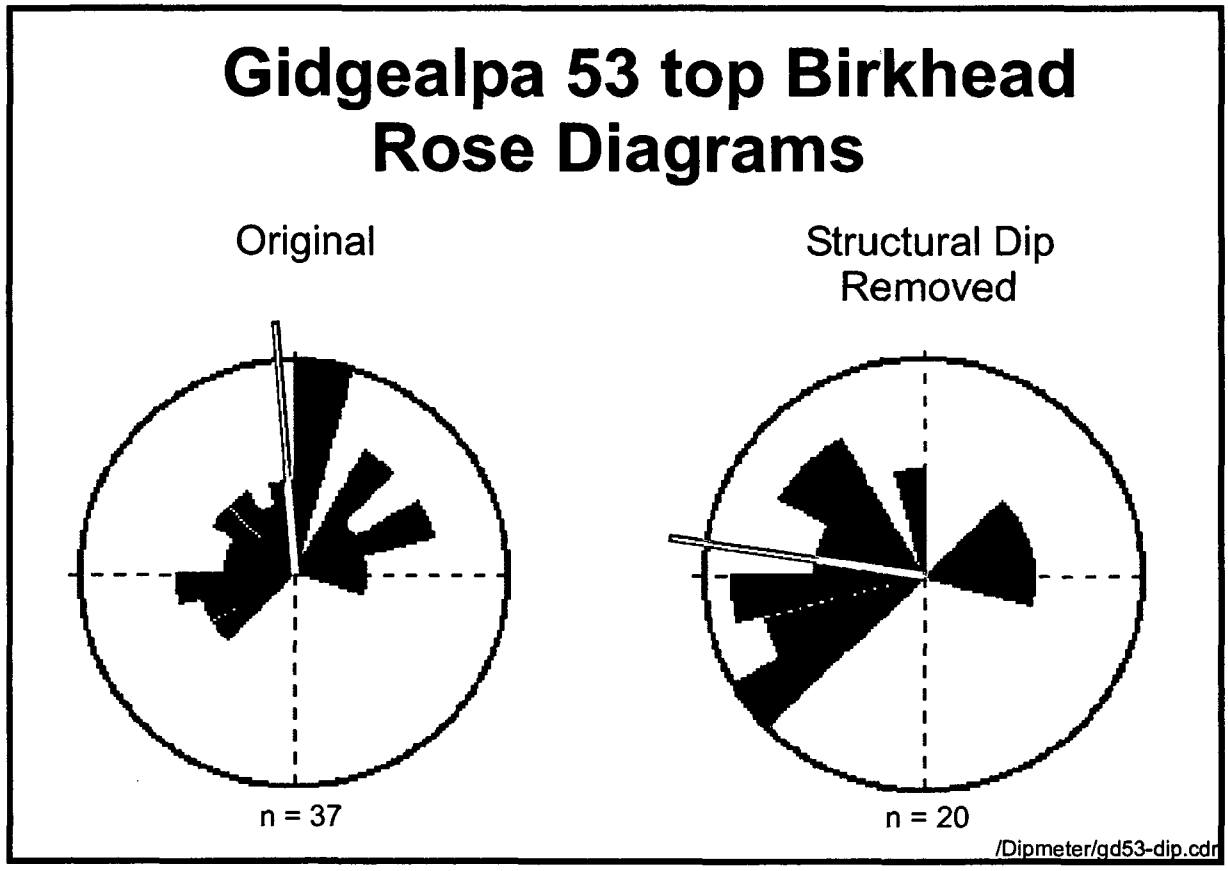

Figure 61: Original and structurally corrected rose diagrams for the top Birkhead Formation, Gidgealpa 53 (see figure 66). Note the different number of dip values: the affects of structural dip in the original rose diagram is removed by omitting values that have a dip of less than 2 degrees.

arenites, while sediments derived from the volcanic arc to the north-east of the basin consist of labile lithic arenites and make poor reservoir rocks. Although this is true in the most part variations will occur where palaeo-flow direction does not necessarily allow for the determination of sand type. In the case of the Gidgealpa south dome it has been seen (Boult, 1996) that the boundary of the change in dipmeter orientation does not occur at the same position as the provenance change. Petrology and Sm-Nd dating I have conducted confirm these observations (see section **4.8** and section **6**).

To determine the regional dipmeter pattern over the South Australian portion of the Eromanga Basin I obtained all processed dipmeter plots from SANTOS that covered the Hutton Sandstone and / or Birkhead Formation. These plots have been previously interpreted using the interval correlation method with a correlation interval of 4 feet, step distance of 2 feet and a search angle of 35°. From the interpreted log data the top Hutton Sandstone and the basal Birkhead Formation interval were determined. The dip azimuth directions were then read from the tadpole plots and entered into a program to produce a rose diagram for each interval. Each rose diagram was then positioned on a map at the appropriate stratigraphic level to determine palaeocurrent direction (figure **62**). The red arrows in the bottom right corner of each map in figure **62** show the inferred palaeocurrent directions for the central part of the maps while the red bars on each rose diagram indicates the mean direction of stream flow. The black bars present in the rose diagrams are dip azimuth values for each tadpole value with the direction of dip representing sedimentary dip in a 360° strike plain. The further the bars extend from the centre of the diagrams the higher the number of sedimentary structures that are dipping in that particular direction.

The rose plots indicate the change in the type of environment of the Hutton Sandstone and the Birkhead Formation. The low sinuosity braided fluvial Hutton Sandstone generally has a spread of approximately 90° from the mean value (red bar) while the high sinuosity meandering fluvial Birkhead

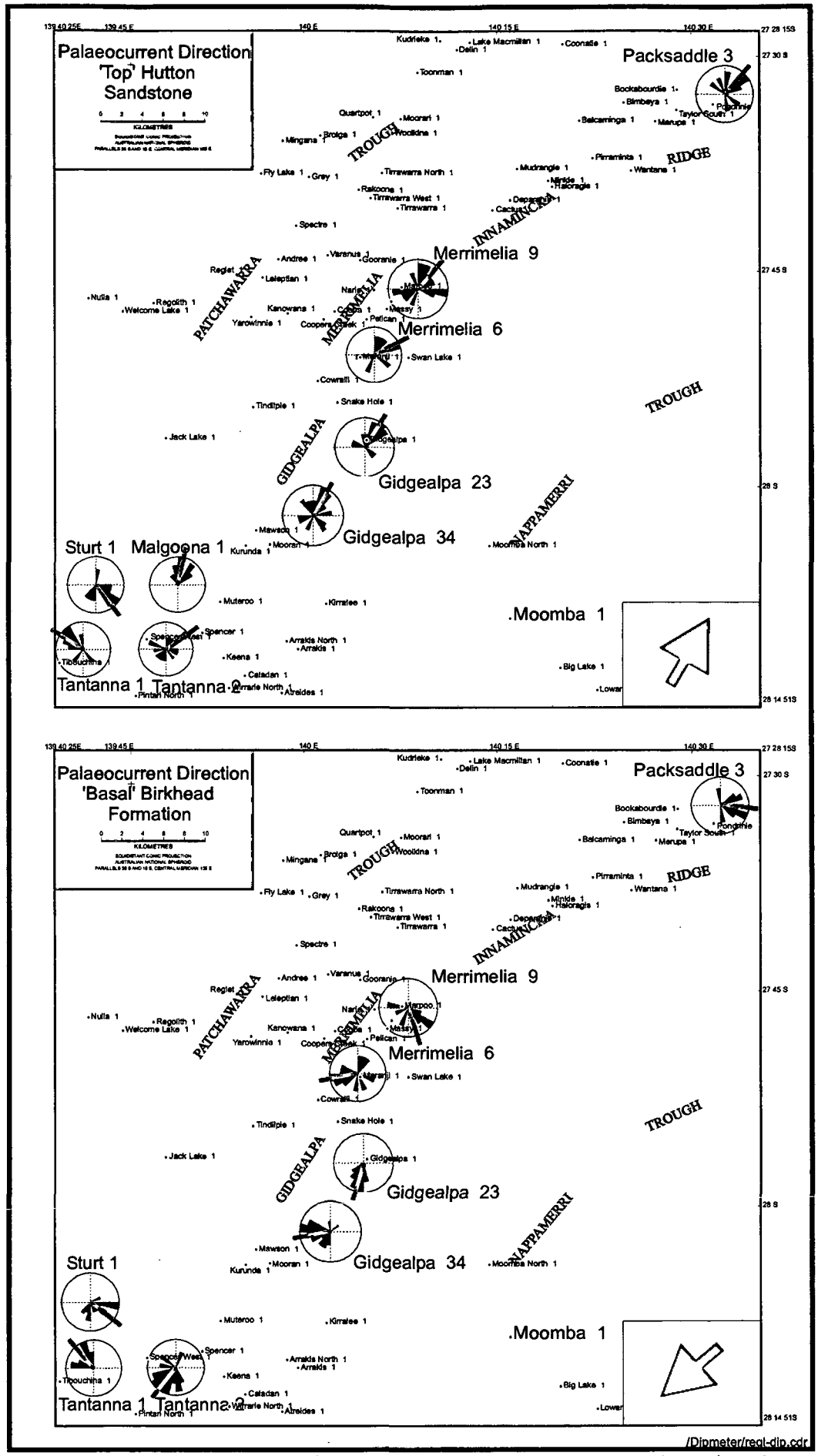

Figure 62: Regional paleo-current directions in the southwestern Cooper Basin portion of the of the Eromanga Basin for the top Hutton Sandstone and basal Birkhead Formation determined from various wells using rose diagrams. Red bars displayed on the rose diagrams represent mean dip for each well and the red arrows in the bottom right corner of each map displays the average regional dip direction.

Formation has a mean value spread of approximately 180° from the mean. The change in palaeo-current direction between the top Hutton Sandstone and basal Birkhead Formation is apparent in figure **62** with the top Hutton Sandstone dipping to the north-east and the basal Birkhead Formation dipping to the south-west. This dip pattern is consistent with that seen at ATP 269P(1) in Queensland (Watts, 1987) (figure **63**). Which demonstrates the change in dips of the top Hutton Sandstone and basal Birkhead Formation from north-east to south-west respectively.

4.7.5 Dipmeter Interpretation at the Gidgealpa south dome

4.7.5.1 Dipmeter processing

Well completion reports of wells at the Gidgealpa south dome reveal that the SHDT dipmeter tool was run in ten wells; of the ten wells four had been interpreted and one was missing (figure **64**). So to have a better understanding of sand trends and palaeo-flow direction I processed the remaining six sets of data at SANTOS using the Schlumberger GEOFRAME program. The raw data was loaded into the computer from reels. The interval of interest was selected and then converted to a readable format in Geoframe; processing was then carried out using the Schlumberger MSD program. The processed data was then plotted as a hard copy at a 1:240 scale. While the earlier processed data used a correlation interval of 4 feet and a step distance of 2 feet, I decided to reduce the parameters to 1 foot and 6 inches respectively so smaller depositional dip features could be resolved from the data.

The resolution of the dipmeter data is determined by the step distance. Thus sedimentary structures within the step distance range will be resolved. In this case structures that are 2 feet or 6 inches in size will be resolved where step distances of 2 feet and 6 inches have been used respectively. Dipmeter interpretation using a step distance of 2 feet will resolve bed sets without

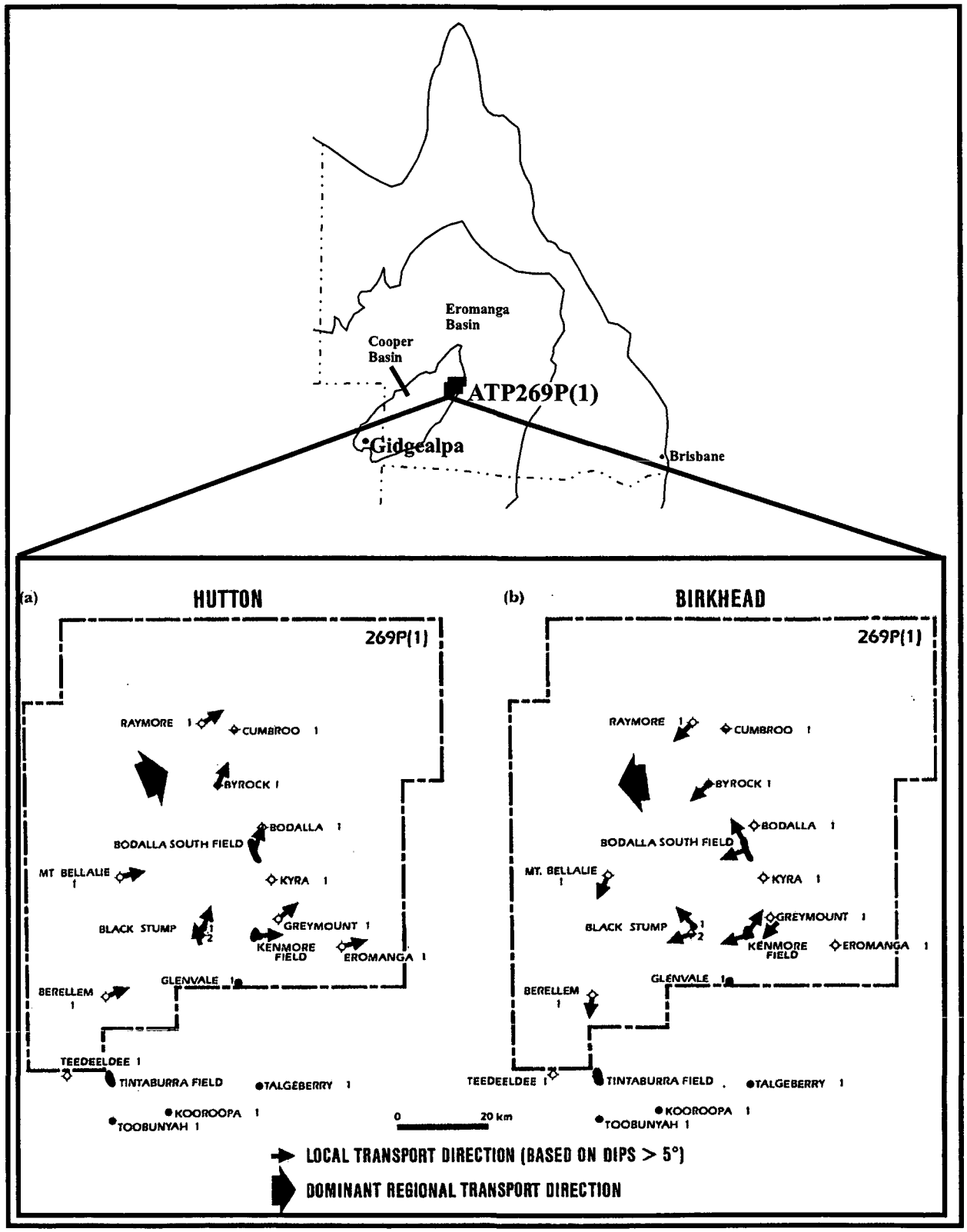

Figure 63: Palaeo-current data modified from Watts (1987) in ATP 269(1) for the top Hutton Sandstone and basal Birkhead Formation.

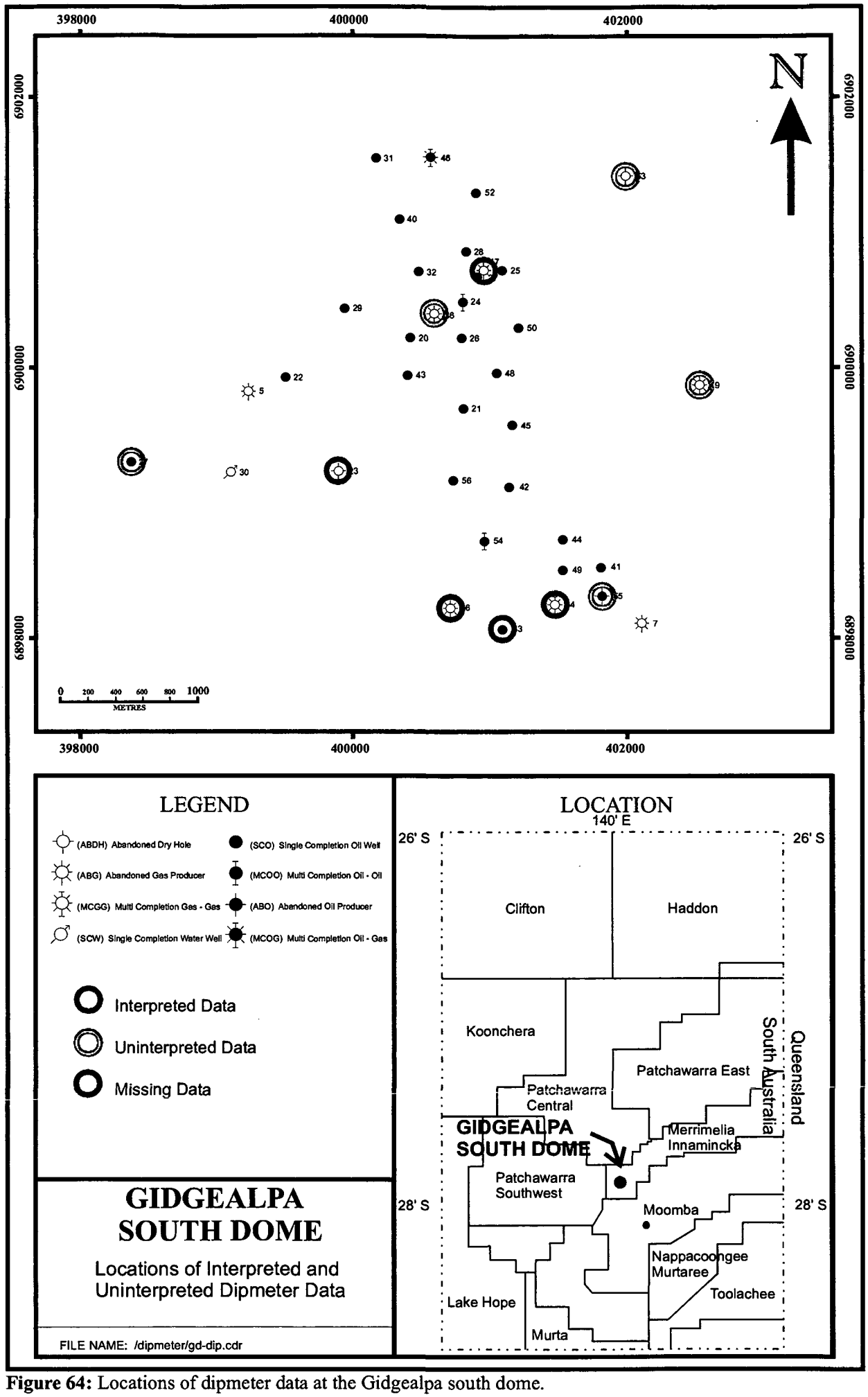

Figure 64: Locations of dipmeter data at the Gidgealpa south dome.

resolving the internal sedimentary structuring and will better determine palaeocurrent direction. On the other hand a step distance of 6 inches is similar to the size of sedimentary structures formed within the Gidgealpa south dome (see section **4.2**) and may allow for the identification of the sedimentary structures by viewing the tadpole signatures on the dipmeter logs.

The processed data for each well over the area was divided into two intervals. These intervals were then subsequently labelled 'top Hutton' and 'base Birkhead'. The top Hutton data is taken from the Hutton Sandstone / Birkhead Formation boundary down to approximately -60 feet (60 feet below the formation boundary), the base Birkhead consists of the data from the formation boundary to the mid Birkhead Formation marker (maximum flooding surface). These two intervals correspond to the intervals used to determine the regional dipmeter trends (section **4.7.4**). For each interval the rose diagrams were placed on a base map of the Gidgealpa south dome area for comparison of the mean palaeocurrent directions (figures **65** and **66**).

Figure **65** shows the palaeocurrent trends from a number of wells at the Gidgealpa south dome for the top Hutton Sandstone interval. The mean azimuth values for each rose indicates a north to north-east orientation indicating that the sediment source was from the south to south-west direction. The one exception to this trend is Gidgealpa 27 that indicates a mean azimuth orientation of 178° (south). However, closer inspection of the rose diagram reveals that the spread of the sedimentary dips are throughout the 360° range and that the number of dips for a particular orientation are similar. Thus the mean azimuth value for the Gidgealpa 27 well is unrepresentative of the multiple and widespread dips of the top Hutton Sandstone interval at the well and should not be included when attempting to determine the overall palaeocurrent direction for the interval.

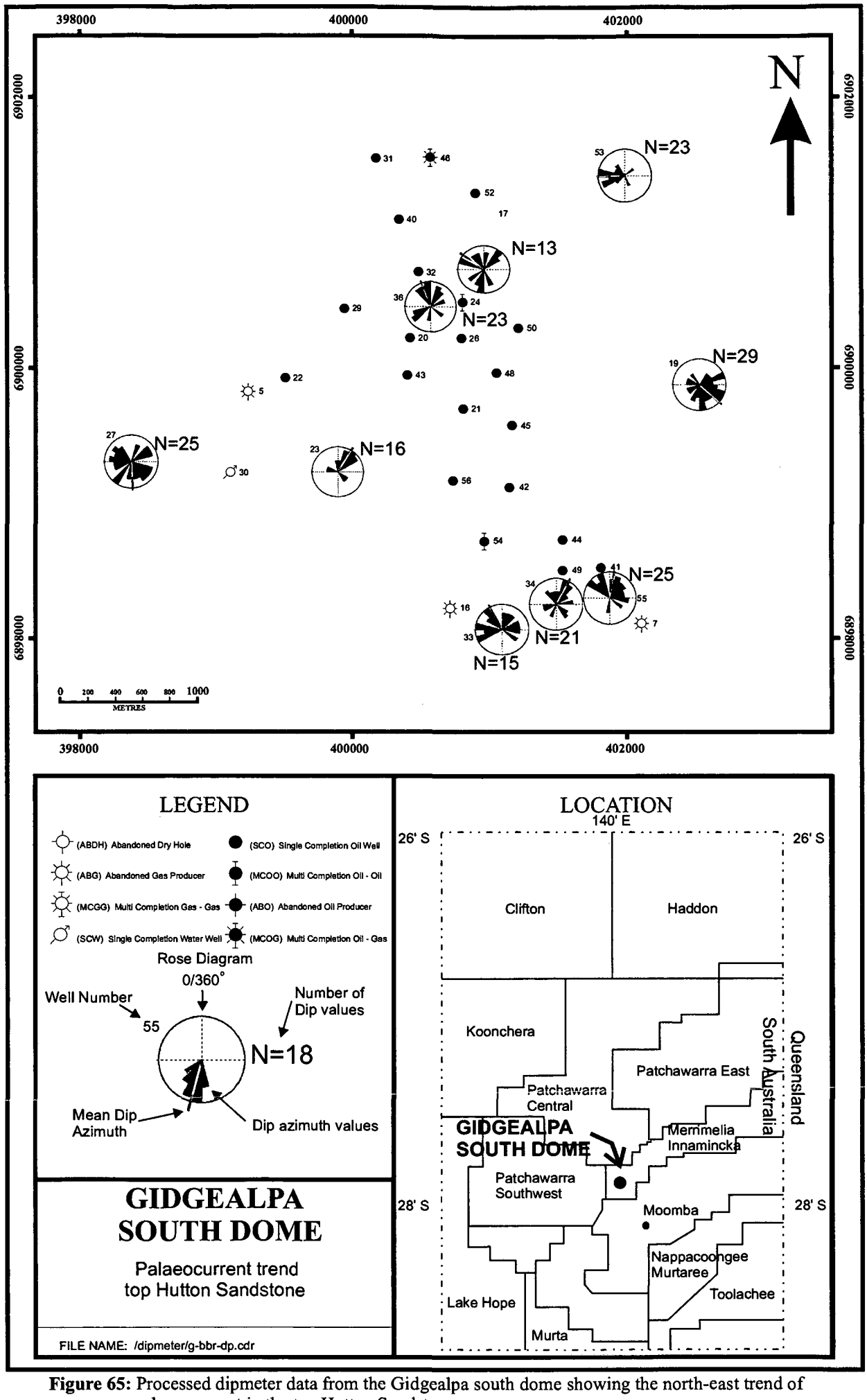

Figure 65: Processed dipmeter data from the Gidgealpa south dome showing the north-east trend of palaeo-current in the top Hutton Sandstone.

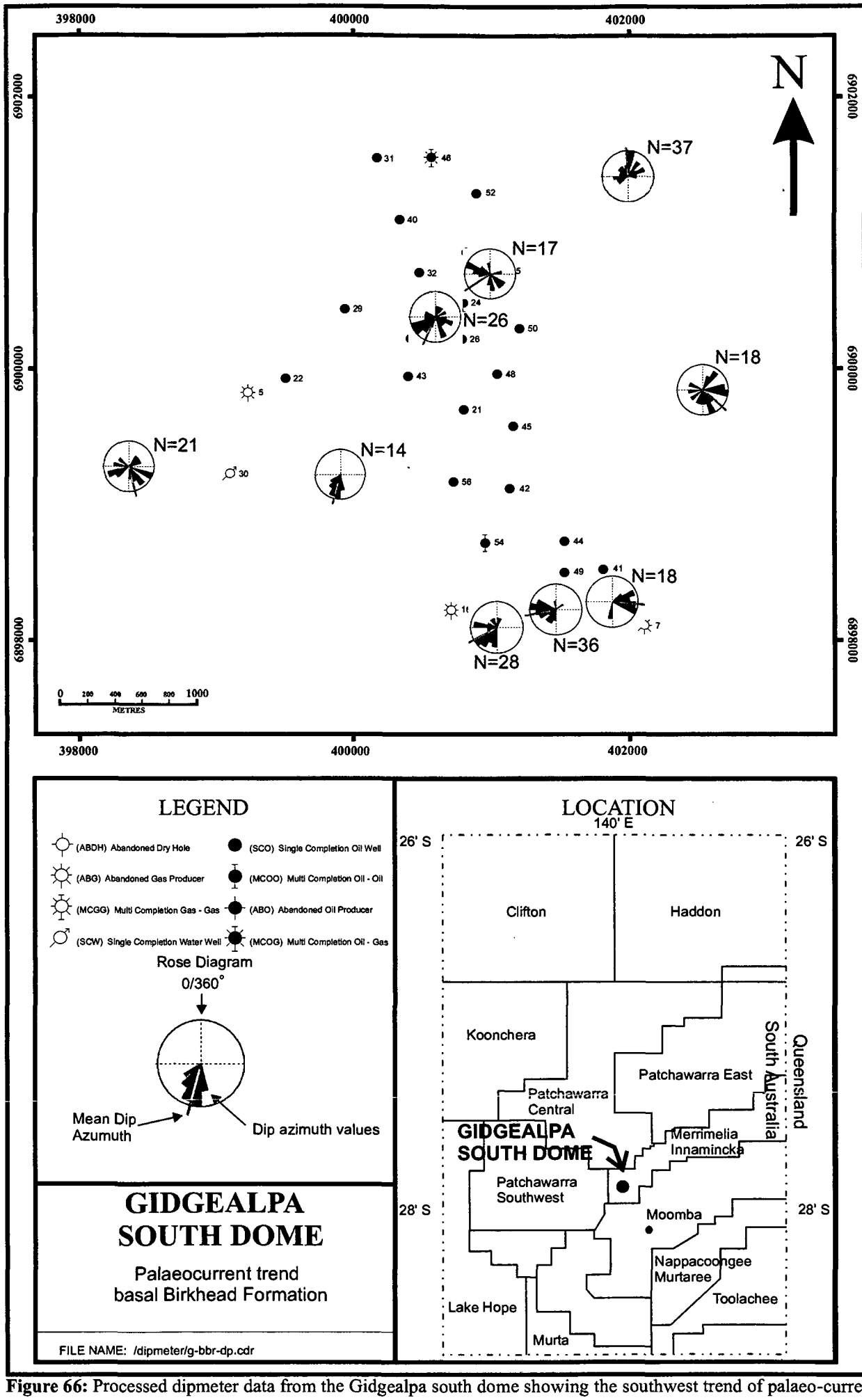

Figure 66: Processed dipmeter data from the Gidgealpa south dome showing the southwest trend of palaeo-current.

The dips of the top Hutton Sandstone can vary sharply from zero to 35 degrees and direction is typically within a 90° arc which reflects the direction of elongation of the sand bodies. Angles of upto 180° may also occur.

Figure **66** is a map showing palaeocurrent trends for the base Birkhead Formation. The mean azimuth values for this interval indicate an overall south-west orientation for streams. The exception to this trend is Gidgealpa 53 which is dipping to the north. On inspection of the tadpole plot of the well, it is apparent that the interpreted dip is due to structural and not sedimentary dip. The correction of this data was previously explained in section **4.7.3**.

The rose diagrams (figure **66**) within the basal section of the Birkhead Formation display sediments deposited within distributary channels and distributary mouth bars. The distributary channel dips tend to be relatively low and may reflect pre-depositional sedimentary structures such as channel cutting. Dip direction reflects sand elongation with relatively little scatter, a good example of dip direction of a distributary channel can be seen at Gidgealpa 23 and 34. These wells also indicate a dip direction component at 90° to the main dips and are likely to represent sand bar growth during the channel fill processes. Gidgealpa 27 shows a larger scatter of dip directions and probably reflects the variable processes that occur within a distributary mouth bar environment.

A comparison of the top Hutton and base Birkhead dipmeter data shows consistancy with the regional data of the Eromanga Basin (figure **62**, page 130), with the palaeocurrent direction switching from north-east in the top Hutton Sandstone interval to south-west in the base Birkhead Formation interval.

4.8 Neodymium Model Age Interpretation

The Sm-Nd isotope system can be used as a geochronological tool for the derivation of sediment provenance due to their geochemical coherence. The stability of the rare earth elements is due to the fact that they do not undergo any significant fractionation with respect to each other during crustal processes. The similar chemical properties of the isotopes mean that the Sm-Nd model ages should be able to date the first extraction of material from the mantle to form crustal rocks (McCulloch and Wasserburg, 1978, Fletcher et. al, 1983). McCulloch and Wasserburg (1978), using a number of different examples, go on to show how neodymium model age dating can be used to assign provenance to sediments. Age variations can also occur from crustal or sediment mixing; an example would be two sediments with different provenances, the neodymium model age of the sediments would be an 'average' value of the two.

4.8.1 Eromanga Basin

In the Bodalla field area of the Eromanga Basin (ATP 269), Whitford et. al (1994) used neodymium model age interpretation to show the age variation of the sediments above and below the provenance change near the Hutton / Birkhead interface. They determined that the volcanic arc derived, lithic labile sediments of the Birkhead Formation originated from rocks that ranged in age from 800 - 1000 Ma and were derived from sources either to the north or east. While the cratonic derived quartzose sediments of the Hutton Sandstone originated from rocks that ranged in age from 1100 and 1600 Ma and are sourced from the south (figure **67**). Boult (1996) carried out similar analyses at Moorari and Gidgealpa. He found that age variations at Moorari were 1000 Ma and 1400 - 1760 Ma while at Gidgealpa ages varied from 950 Ma to 1400 - 1900 Ma. These results are in excellent agreement with a source area located to the south and south-west of the Eromanga Basin corresponding to the

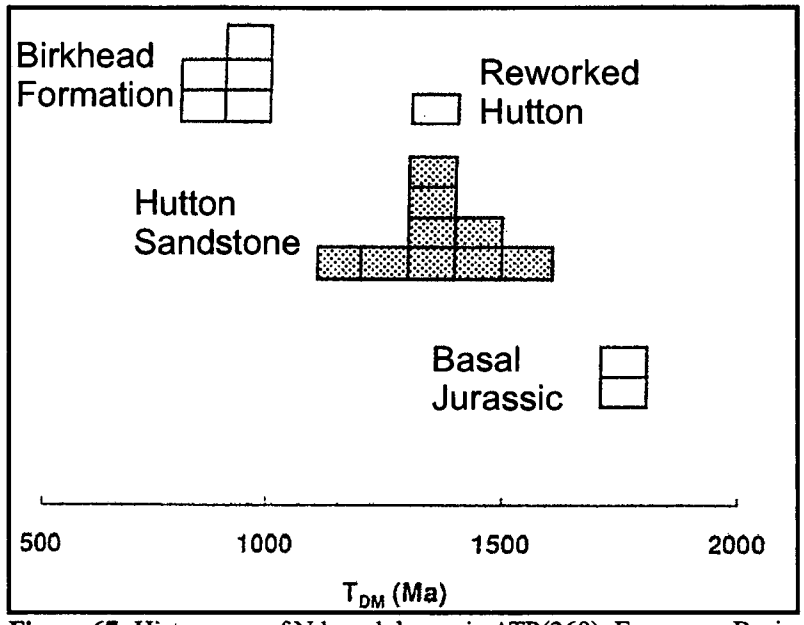

Figure 67: Histograms of Nd model ages in ATP(269), Eromanga Basin (After Whitford et. al, 1994).

Gawler Craton. This cratonic area has rocks ranging in age from 1400 to 2000 Ma.

Apatite fission track ages that have been determined in the Birkhead Formation sediments at Mulapula 1 (western Eromanga Basin) (Gibson et. al, 1995), indicate an eruption age of 135 +/- 21 Ma which confirms the sourcing of sediments from a volcanic arc off the coast of Queensland. The data also confirms that the Birkhead Formation was deposited during the formation and subsequent erosion of the volcanic arc (see figure **4**, page11) (Gibson et. al, 1995). Details on apatite fission age determination can be found in Tingate (1994). It has also been noted that neodymium model ages of the Birkhead Formation are older than fission track ages due to the magma assimilating older crust and the mixing of the sediments with crustal material that had formed before the formation of the volcanic arc.

The effects of sediment mixing on neodymium model age dating is apparent from the results at Moorari, Gidgealpa and Bodalla. Gidgealpa and Moorari are more proximal to the cratonic source area which is supplying the quartzose sediments and has model ages between 1400 to 1900 Ma while wells further to the east have younger model ages of between 1100 to 1600 Ma (figure **68**). The younger model ages at Bodalla is due to its more distal position from the source. The longer travel path allows sediments to mix with younger sediments of differing provenance lowering its overall neodymium model age. Conversely volcanic arc derived sediment samples show variations in model age between the two areas. Wells in the Bodalla area are more proximal to the source area and therefore have younger ages than at Gidgealpa or Moorari due to less mixing with cratonic derived sediments.

4.8.2 Gidgealpa south dome

While Neodymium model age dating can be used in regional studies it can also be used on a local scale within a field. Whitford et. al (1994) used model age

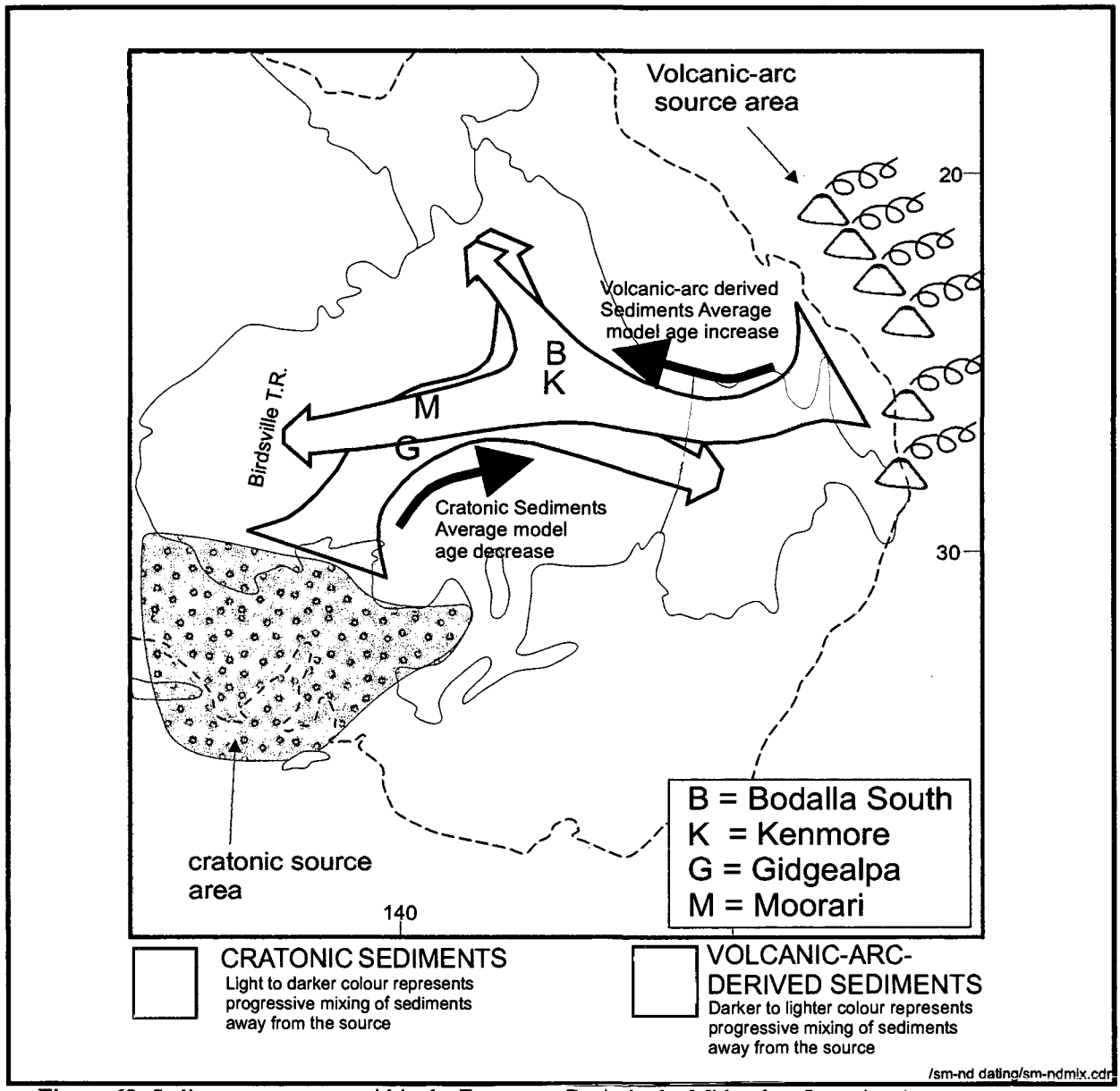

Figure 68: Sediment movement within the Eromanga Basin in the Mid to late Jurassic. Arrows represent changing Nd-model ages as the sediments from the different sources mix.

dating to correlate sands within the Harriet field, Barrow Sub-basin, Northwest Shelf. At the Gidgealpa south dome I have collected a number of samples to further characterise the Hutton Sandstone / Birkhead Formation transition.

I selected a total of 7 sandstone samples in the area from a number of wells with the results of the Neodymium model age dating shown in table **4**.

Well	Gidgealpa 29	Gidgealpa 29	Gidgealpa 29	Gidgealpa 29	Gidgealpa 32	Gidgealpa 30	Gidgealpa 31
Depth	6059'4"	6042'4"	6027'10"	6015'4"	5978'3"	6037'6"	5978'3"
Sample Type	CD sandstone	CD sandstone	VAD sandstone	CD/VAD sandstone	VAD sandstone	CD sandstone	VAD sandstone
Nd ppm	30.53	15.57	15.8	14.64	15.31	9.31	18.48
Sm ppm	6.17	2.92	3.19	3.13	3.18	1.93	3.8
143/144 Nd	0.512328	0.512134	0.512453	0.512427	0.512524	0.512342	0.512507
Sm/Nd	0.2021	0.1875	0.2019	0.2138	0.2077	0.2073	0.2056
147Sm/144Nd	0.1222	0.1134	0.1221	0.1293	0.1256	0.1254	0.1244
Epsilon Nd	-6.04715	-9.8315	-3.60878	-4.11596	-2.22379	-5.77405	-2.55541
143/144(T)	0.5122	0.512015	0.512325	0.512292	0.512392	0.512211	0.512377
Init. Epsilon Nd	-4.53	-8.13	-2.09	-2.74	-0.77	-4.32	-1.08
Model age (Ga)	1.24	1.40	1.05	1.17	0.98	1.26	0.99

Table 4: Sm/Nd isotope results and calculated model ages over the Hutton Sandstone / Birkhead Formation transition at the Gidgealpa south dome. All analyses performed at the University of Adelaide. Model age calculations based on 143Nd/144Nd of present day depleted mantle = 0.513108 and 147Sm/144Nd = 0.2157. Present day CHUR = 0.512638, with 147Sm/144Nd = 0.1967. Initial ratios and epsilon values calculated at 0.16 Ma. Analytical techniques are described in Foden et. al (1995).

The model age dates were then compared to results from Boult (1996). Figure **69** shows all the data plotted from the Gidgealpa south dome on a depth versus model age graph. Similar trends can be seen between the data from Boult (1996) and the findings from this study. Model ages of the cratonic quartz arenites below the provenance change range in age between 1240 and 1900 Ma while above, the volcanic-arc derived lithic sandstones show similar ages between 950 and 1100 Ma.

The Neodymium model ages at the Gidgealpa south dome have also highlighted the diachronous nature of the provenance change and re-enforced the idea that avulsion processes have occurred within a delta lobe system.

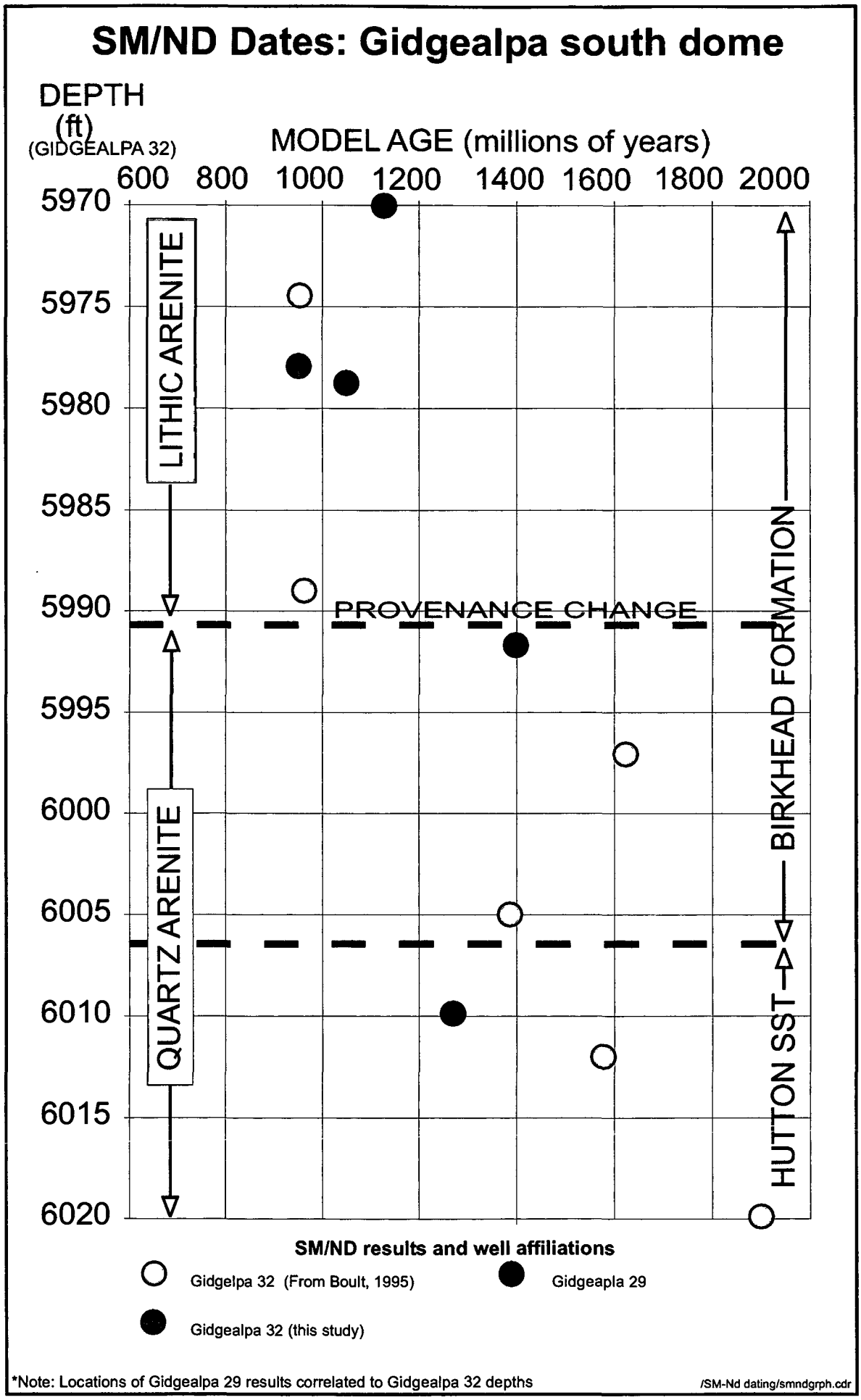

Figure 69: Neodynium model ages of various samples taken from the Gidgealpa south dome. Note the decrease in model ages above the provenance change representing a change from cratonic to volcanic arc derived sediments.

Figure **70** shows the changing depth of the provenance change from left to right or south to north which was determined using the model age dates (indicated as the red arrows and was complemented by petrology data (indicated as black arrows, see section **6**). The increasing depth of this change (increasing distance below the mid Birkhead Formation maximum flooding surface) is attributed to the fact that the sediments from these wells were deposited as a set of delta lobes. So if we take Gidgealpa 29 from figure **70** for example, the channel sand just below the provenance change, which is represented by the dashed line, is the first delta lobe to be deposited. After abandonment of the lobe another formed, but this time was deposited in the Gidgealpa 30 area. At some stage during the deposition of this lobe the provenance changed. This change is reflected by younger model ages of the remaining sediments in the area. The abandonment of the lobe and subsequent deposition of the lobes in the Gidgealpa 29 (second lobe in this area), 32 and 31 areas from then on were of a volcanic arc derived nature. For further details on the deposition sequence of delta sediments see section **5.5**.

4.9 Siderite Formation

Siderite within the Birkhead Formation is common, occurring as cemented zones and nodules formed both in situ and from erosion, transport and deposition. The highly specific parameters that are needed for its genesis mean that the depositional environment, or conditions at the time of formation, can be accurately determined where the siderites have formed. Also, due to its abundance within the formation, siderite may have an effect on the reservoir quality of sandstones at the Gidgealpa south dome. For these reasons it is important to consider the genesis of siderites and the effects (if any) it has on the Birkhead Formation reservoir. For the formation of siderite, conditions must be anaerobic (low Eh) and sulphide iron partial pressure must be high ($pS^{=}$) (figure **71**). Berner (1971) showed that this set of conditions is not likely to occur in marine environments since the anaerobic decomposition of organic matter includes the reduction of sulfate ions to hydrogen sulphide (H_2S).

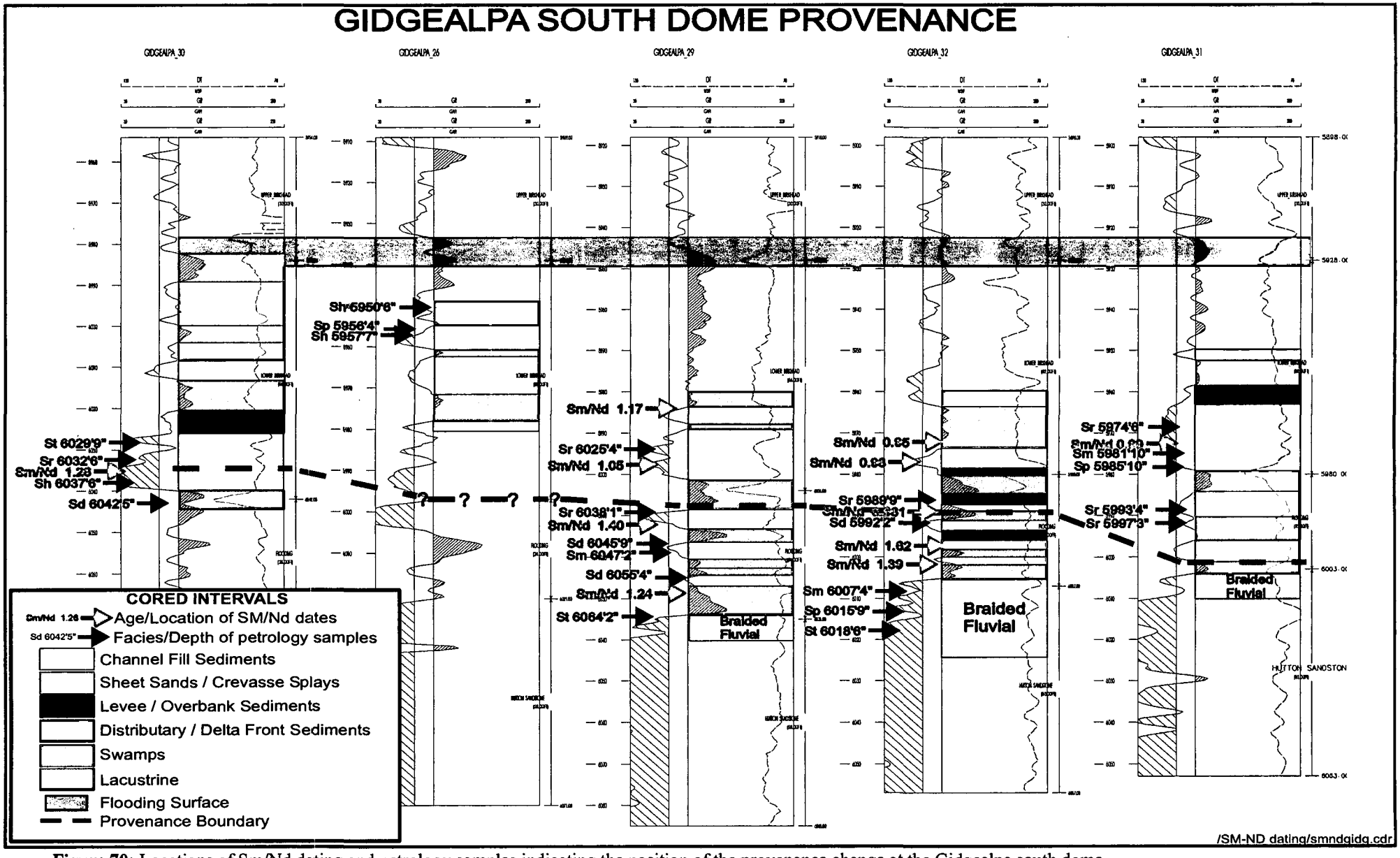

Figure 70: Locations of Sm/Nd dating and petrology samples indicating the position of the provenance change at the Gidgealpa south dome.

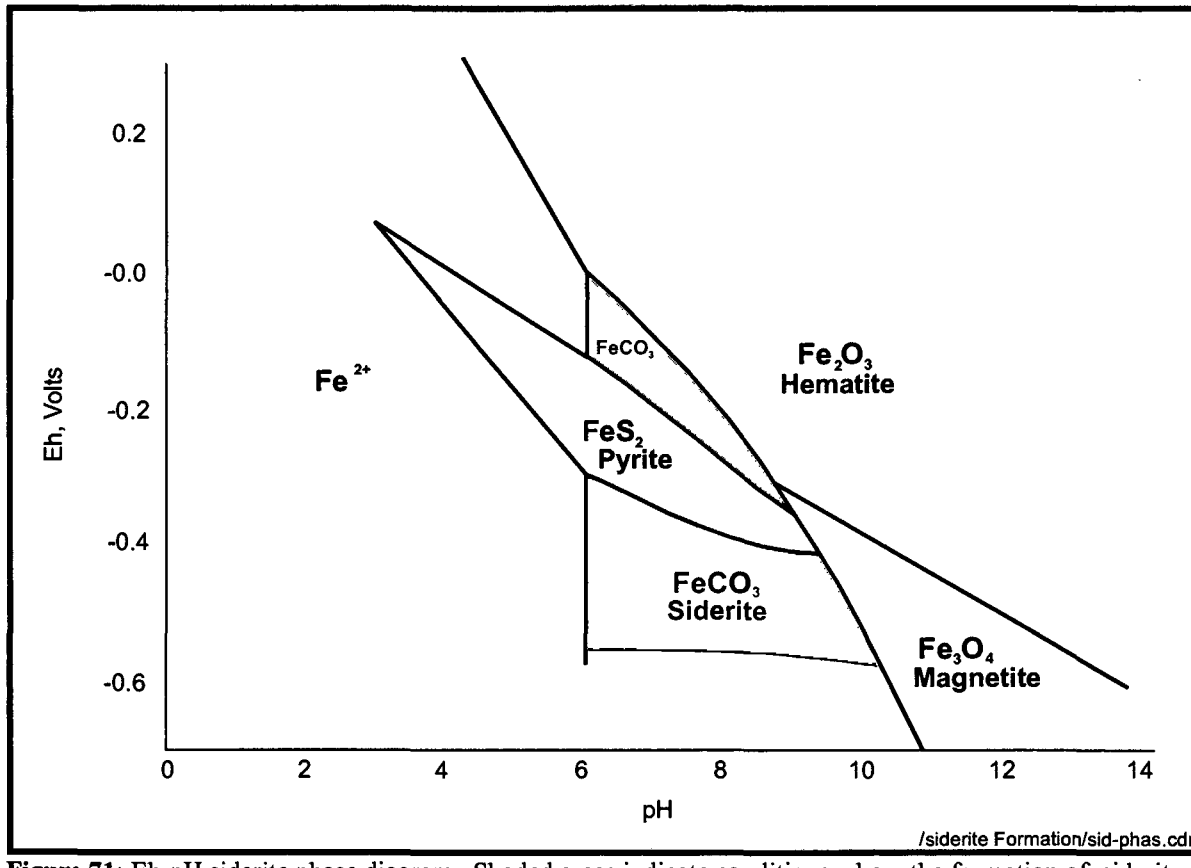

Figure 71: Eh-pH siderite phase diagram. Shaded areas indicate conditions where the formation of siderite is stable (After Krauskopf, 1967).

However in non-marine sediments siderite is often a common constituent and is commonly associated with coal beds and fresh water clays where dissolved sulphate is low and organic matter is high. Since siderite is a carbonate it is soluble in acidic conditions and thus will not form in swamps and bogs where mineral content is low. Siderite is also unable to form in water which is rich in calcium since:

$$FeCO_{3(siderite)} + Ca_{aq}^{2+} \leftarrow \rightarrow CaCO_{3(calcite)} + Fe_{aq}^{2+}$$

where $K = 0.05 = a_{Fe2+} / a_{Ca2+}$

Thus, water conditions must be at least 5% higher in ferrous iron than calcium for siderite to be stable. Studies carried out by Postma (1982) confirm the theoretical findings of Berner (1971). From studies carried out at the Skjerna delta in Denmark, siderite was found in freshwater sediments with pore water containing little or no dissolved sulfide and high concentrations of ferrous iron. The origin of the iron was determined to be from the river system and was either carried down in suspension or by bottom sediment transport. Further study by Postma (1982) found that in siderite rich sediments the pore waters were supersaturated by siderite which allowed for the extremely small crystal size of the iron carbonate. Subsequently, these small crystals easily form overgrowths.

Postma (1982) also suggested that siderite may be found in brackish or marine environments as well as fresh water environments and is thus not a reliable indicator of palaeo-environment. One such example is the Upper Cretaceous Gammon Shale of the northern Great Plains covering the boarders of US states: Montana, Wyoming, North Dakota and South Dakota (Gautier, 1982). Here, marine sediments containing siderite concretions formed in association with methanogenesis. The formation of the siderite is dependent on the rate that sediments and associated organic matter pass through the zones of aerobic oxidation and sulfate reduction. When the rate is high then the organic matter is available for methane generation. However when the sediment

accumulation is slow, siderite precipitation and methane generation are inhibited by the persistence of dissolved sulfates and iron sulphides instead of siderite (Gautier, 1982).

The association of methanogenesis and siderite precipitation has also occurred in the sediments of the Terrebonne Marsh in the Mississippi River Delta Plain (Moore et. al,1992). Here, siderite concretions were found less than 7 metres below the surface and in brackish conditions, they are rich in ^{13}C and are most likely the result of methanogenesis.

While Postma (1982) suggested that siderite is not a reliable indicator for palaeo-environment, Baker et. al (1995) determined that the stable isotopic composition of early diagenetic siderite might be used to determine either a marine or non-marine depositional environment. They concluded that the siderites in the Triassic Rewan Group in the southern Bowen Basin have high negative values of $\partial^{18}O$ and $\partial^{13}C$ which is characteristic of a non-marine depositional environment. Also considered was the amount of magnesium and calcium found within the siderites from substitution of iron. If they are marine then they would have expected the siderites to contain higher quantities of these elements.

4.9.1 Siderite Formation within the Birkhead Formation.

Theologou (1995) conducted a detailed XRD study of siderites within the Murta Formation. He found that the siderites contained 8 different species, with some samples that appeared to contain siderite in hand specimen actually consisting of calcium carbonate rather than iron carbonate. The minerals identified from his analysis can be seen in table **5**. Most of the minerals identified have also been seen from analysis I conducted on a number of samples in the Birkhead formation. The XRD data is displayed in table **9** (section **6.2.7**). In the table the siderite species have not been displayed

separately since further, more detailed, analysis of the samples is required to confirm the findings. While Theologou (1995) tested siderite horizons I conducted XRD analysis on samples other than the siderite horizons to observe what effects the siderite cement have on the reservoir quality sandstones. As a result the abundance of carbonates are likely to be significantly lower than the concentrations seen in the samples from Theologou (1995).

Carbonate Species	Major Cations	XRD Peak (Å)
Magnesium Siderite	(Mg, Fe, (Zn))	2.78
Siderite	(Fe)	2.80
Manganoan Siderite	(Fe, Mn, Zn)	2.82
Dolomite	(Ca, Mg)	2.89
Ankerite/Ferroan Dolomite	(Ca, Mg, Fe)	2.90
Calcium Kutnohorite	(Ca, Mn, Mg)	2.98
Calcite	(Ca, Mn, Mg & Ca)	3.02 & 3.04

Table 5: Summary of carbonate species present within the Murta Formation (From Theologou, 1995).

In the southern part of the Eromanga Basin, Queensland, Green et. al (1989) described the presence of siderite and sideroplesite (high Mg siderite). It was determined from isotope analysis that fine grained, dark brown pleochroic siderite was precipitated relatively soon after burial from connate waters and then later re-crystallisation occurred. This re-crystallisation caused the replacement of iron with magnesium altering the siderite to the magnesium rich siderite, or sideroplesite. Timing of the two siderites was also determined from thin section analysis with the sideroplesite forming later due to elevated levels of magnesium. The magnesium was probably expelled from the alteration of smectite to illite in mudrocks in the overlying Birkhead Formation and then forming the authigenic minerals in the Hutton Sandstone.

Gravestock et. al (1983) considered that the formation of siderite within the Hutton Sandstone and Birkhead Formation was from the replacement of calcite cements formed early in the diagenetic history of the sediments at times of non-deposition. However, this seems unlikely since I have found (section **6**), as Theologou (1995) and Green et. al (1989) had also discovered, that early

formed iron carbonates are normally pure siderites which are subsequently replaced by elements such as magnesium and calcium as diagenesis progresses. If the iron carbonates have in fact formed later in the diagenetic history then it would be expected that the siderites are highly contaminated by elements such as calcite and magnesium.

4.9.2 Siderites in the Birkhead Formation, Gidgealpa south dome

Siderite within the Birkhead Formation at the Gidgealpa south dome is common with occurrences in most wells ranging from cemented zones and horizons to nodules and channel lag gravel clasts (figure **72**). From cores the areas cemented by siderite are easily identified by its characteristic light brown, to brown / red colour. I have found from the cored intervals that all of the siderite cemented horizons range in size from 1 - 15cm and occur within siltstone beds. Figure **72**a shows the light brown colour of the cemented horizon as compared with other siltstone beds which are dark brown in colour. In figure **72**a note the post-siderite bioturbation which has not been cemented, this suggests that sideritisation occurred soon after deposition of the siltstone and then bioturbation occurred at a later stage. Boult (1996) interpreted the early siderite as a "*soft mineral phase proto-siderite*" which had gel like properties allowing bioturbation to easily occur after siderite formation. This feature of early siderite formation and then subsequent bioturbartion is commonly seen throughout the cores, especially in Gidgealpa 26, 5972' - 5977" (appendix **3**) and Gidgealpa 32, 5964' - 5976' (appendix **3**). Siderite cementation commonly effects sedimentary laminations within the siltstones, with the degree of homogenisation being dependent on the amount of cementation. This feature was also noted by Theologou (1995).

Siderite can form as nodules (figure **72**b) in silty sands. These nodules probably precipitated after burial, not long after deposition since siltstone laminations show a high degree of compaction around the siderite cemented

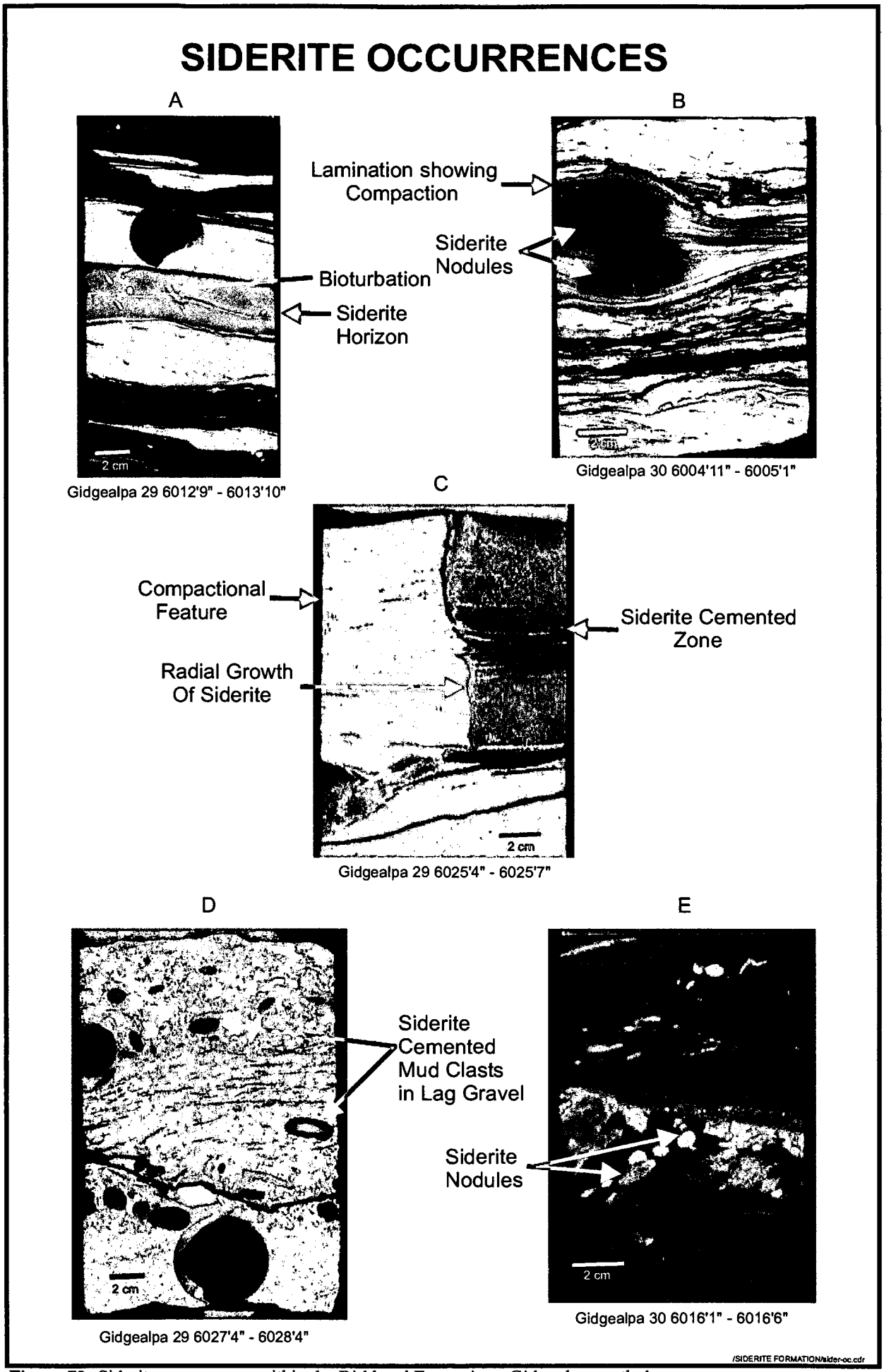

Figure 72: Siderite occurrences within the Birkhead Formation, Gidgealpa south dome.

zones. The continuation of the siltstone laminations through the nodules and the diffuse nature of the cement boundaries is testimony to their formation in-situ. Figure **72**c shows a rare example of a siderite cemented zone within a sandstone. This occurrence has been interpreted by Boult (1996) as a proto-siderite or gel in the early stages of the siderite formation as in the cemented siltstone horizons (figure **72**a) The zonation occurred due to preferential dissolution in places by moving pore fluids through restricted areas of the sandstones. It is likely however, that the formation of this siderite zone is possibly due to the up-welling of iron rich pore fluids. The high concentrations of siderite in these zones causes the precipitation and subsequent growth of sideritic zones.

The apparent progressive 'growth' of the siderite in a radial direction (horizontally) has been noted from a cross section of the core and is probably from lateral flow of the fluids within the permeable sandstone. If this is in fact the case, then the cementation will only be of a limited extent within the sandstone. This type of cementation has also occurred relatively early since differential compaction can be seen. The cementation would probably have occurred during early burial of the sediments; after the proto-siderite gel had formed.

Figure **72**d shows siderite cemented mud clasts as a channel lag. The fact that the clasts are predominantly mud suggests that they have only been carried a short distance from their source. The mud clasts are likely to have originated from recently deposited floodplain sediments of the Birkhead Formation that are subsequently eroded and transported downstream. Their well rounded nature may also be an indication that the siderite was not 'set' and was still in a gel or preset state allowing for easy erosion or deformation.

The final occurrence of siderite is as nodules within massive mudstone / siltstones (figure **72**e). Moore et. al (1992) determined that Fe^{2+} rich siderites can form as nodules by displacement re-crystallisation within marsh type

environments if anoxic conditions developed rapidly. They go on to state that meteoric water sources are the initial contributors of bicarbonate to the ephemeral oxic and suboxic zones (figure **73**), and when subsidence or flooding occurs the sediments move directly into the methanic zone (from Berner 1971) and Fe^{2+} is incorporated into siderite.

While siderite formation is common within the Birkhead Formation, ironstones are rare and tend to be restricted to, or are close to the Hutton Sandstone / Birkhead Formation boundary (Gidgealpa 32, 6007' - 6007' 4" (appendix **3**)). The ironstones were probably formed when sediments were buried and partially consolidated (Berner 1971, Krauskopf 1967). Krauskopf (1967) showed that for these ironstones to form there must either be a large supply of ferrous iron or a reducing environment must be maintained for a long period of time to precipitate large quantities of siderite. Further concentration of iron may occur by the presence of oxygen since:

$$2H_2O + 2FeCO_3 + \tfrac{1}{2}O_2 \leftarrow \rightarrow Fe_2O_3 + 2H_2CO_3$$

I believe the presence of ironstone at the formation boundaries is due to the close proximity of the organic matter in shales and siltstones which are associated with the transgressive surface (see section **5.2.5**). The organic matter can produce a reducing environment while the large supply of ferrous iron can originate from pore waters which circulate within the top of the Hutton Sandstone. Similar ironstones have been seen in regional wells within the Eromanga Basin (see appendix **5**)and occur in a similar position within the Birkhead Formation as in Gidgealpa 32.

4.9.3 Siderite Formation and wireline logs

Siderite horizons can be identified from the sonic, resistivity, neutron porosity, density and photo electric effect (PEF) logs and appear as spikes on visual

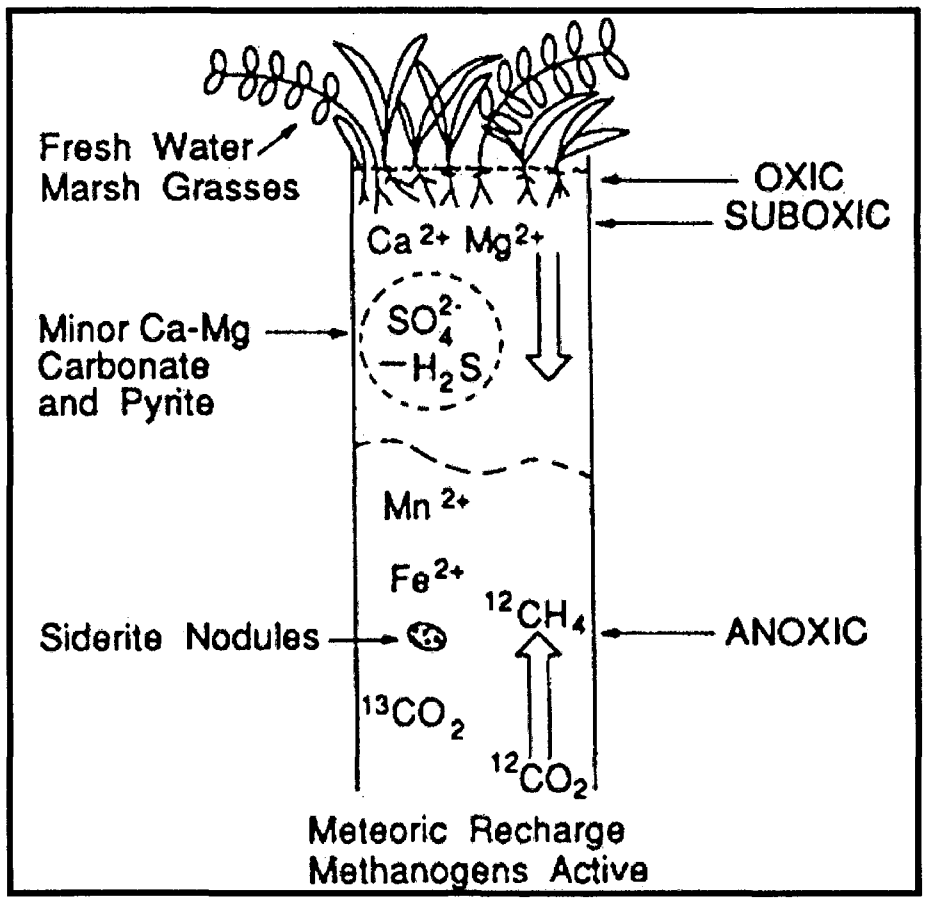

Figure 73: Formation of in-situ siderite nodules in a marsh setting (From Moore et. al, 1992).

plots (figure 74). However, for the siderite to register on the wireline logs the cemented zone must be at least 15cm in thickness due to the resolution of the tools. From the core it is evident that siderite zones that are thinner than 15cm are not detected by the tools (as in figure 72a (page 143)); thus only thick siderite beds, are detected.

Wireline log traces show that the siderite horizons occur throughout the Birkhead Formation and tend to be related to shaly areas. Characteristic responses are also seen in sandstones but tend to be restricted to near the top or base on the sands. Ironstone horizons in the Birkhead Formation show a similar characteristic response to the siderite horizons on wireline log data.

4.9.4 Implications of HC migration and entrapment at the Gidgealpa south dome

From observations discussed previously it is clear that siderites are not acting as major barriers to hydrocarbon movement. Observations from the well cores indicate that siderite cemented horizons, having permeabilities of less than 1md, are restricted to siltstone beds which themselves have low permeabilities. Since the siderite cemented siltstones are generally thin and are never greater than 15 cm in thickness the extent of these horizons will also be limited. Indeed attempts to correlate siderites across the area was unsuccessful when using wireline logs. Although Theologou (1995) correlated cemented horizons over the Murta Formation he also states that the horizons are not laterally extensive and found no evidence to suggest that the horizons were acting as hydrocarbon barriers. Even if the siderites were extensive over the area their thin nature would mean that breaching by fracturing or uncemented areas would be common.

Other siderite occurrences within the Birkhead Formation do not act as complete barriers to hydrocarbon flow due to their limited aerial extent but

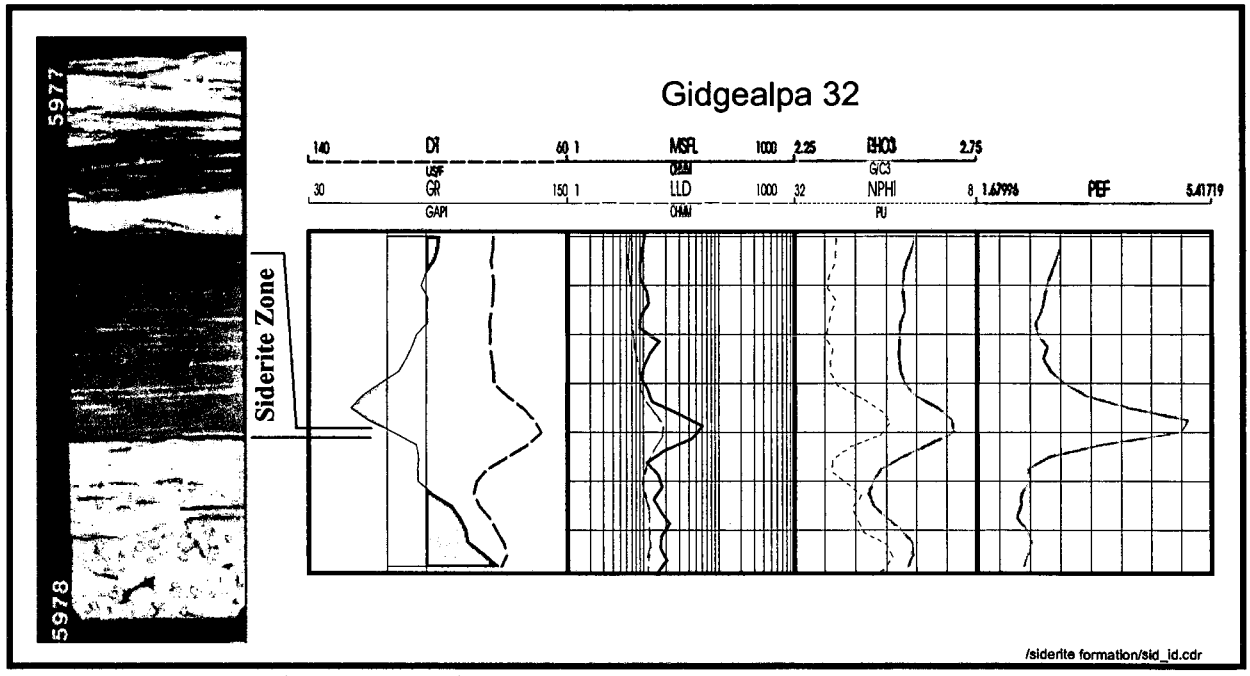

Figure 74: Characteristic log response from siderite cemented zones at the Gidgealpa south dome. Of note are the spikes that are produced over the siderite zone on all of the logs.

may act as baffles. The siderite baffles may trap small quantities of hydrocarbons and may subsequently effect hydrocarbon reserves estimation. The abundance of siderite may also affect reserves estimation of the Birkhead Formation reservoir if the total volume of the siderites are considered as a whole.

5 Sequence Stratigraphy

5.1 Introduction

Sequence stratigraphy was first developed in the late 1960s to 70s by Exxon Production Research Company using seismic data (Posamentier and Weimer, 1993) Born out of the research were stratigraphic techniques and principles which resulted in an alternative way to subdivide, correlate and map sedimentary rocks. The application of the data uses seismic reflections corresponding to chronostratigraphic surfaces (surfaces of the same age) rather than lithostratigraphic surfaces which relate similar packages of sediments. Sediments bounded above and below by chronostratigraphic surfaces have been termed depositional sequences and systems tracts; these surfaces separate younger rocks above from older rocks below (Vail, 1988, Posamentier and Weimer, 1993).

Early application of sequence stratigraphy relied on the use of eustatic sea level changes for fluctuations of the base level in a depositional system (Schumm, 1993). Since these early times it has been realised that other factors such as sediment supply, climate change and local tectonics will effect, or even control changes in base level (Galloway, 1989, Posamentier and Weimer, 1993, Schumm, 1993, Allen, 1994). But before I continue, I believe it is important to define what "base level" is with respect to sequence stratigraphy; after all, changes in relative base level are the ultimate control of the sedimentary processes within a depositional system or basin. Schumm (1993) analysed the concept of base level in detail and concluded that:

"one need only turn to the definition of the words base and level. Base is the lowest part, and level is a horizontal line or plane positioned along a horizontal axis. Therefore, in the sense that the term was

created, base level is effectively sea level, although we know that rivers erode slightly below it."

While base level is defined as sea level it should also be noted that within areas such as the intracratonic Eromanga basin where the main drainage system end point was lacustrine during the Jurassic and Early Cretaceous, base level is defined as the water level of the lake that was present at the time. From most of the literature it would appear that this internal lake system was not affected by, or connected to global eustatic sea level change.

5.2 Sequence Stratigraphy: Eromanga Basin

5.2.1 Why use sequence stratigraphy?

Posamentier and Weimer (1993) have identified two scales for applying sequence stratigraphy for petroleum geology. They are wildcat exploration scale and mature basin exploration and field development scale. The first scale of sequence stratigraphic application is referred to as low-resolution sequence stratigraphy and applies to areas where data is sparse and interpretation relies heavily on seismic data. Generally the lack of well control forces interpretation to be more model driven and thus higher risk. On the other hand mature basin exploration and field development scale sequence stratigraphy is considered to be high resolution and is applied to areas where there is good data coverage such as close well spacing, extensive core and biostratigraphic control and closely spaced two-dimensional and three-dimensional seismic data.

From my own observations, it would appear that the Eromanga Basin is close to the mature basin stage of exploration and within the South Australian portion, the basin has been heavily explored in certain areas having relatively good well spacing and control. Substantial regional two-dimensional seismic

data and three-dimensional data over producing fields also covers the area. However, the sub-surface depth of the Hutton Sandstone and Birkhead Formation causes seismic to be of low resolution and only useful in identifying formation boundaries rather than detailed sequence stratigraphic horizons. The good well coverage in the area allows for a relatively detailed sequence stratigraphic analysis by well-to-well correlation and is greatly complemented by the presence of core data typically located over the Hutton Sandstone/Birkhead Formation interface or basal section of the Birkhead Formation. The Birkhead Formation lies within the PJ5 palynological zone (figure **75**), making biostratigraphic data of limited use.

To my knowledge, sequence stratigraphy has not been extensively applied to the regional Eromanga Basin of the mid to late Jurassic (Hutton Sandstone / Birkhead Formation time) This may be due to the fact that exploration has been successful without the need for in-depth studies of the relationship and distribution of sediments - a point which is reflected from the almost 50% success rate of exploration drilling in 1996/97. Other possibilities may be the inability to associate systems tracts to related sediment packages due to basin complexities; the identification and allocation of a regional marker within the Birkhead Formation or, as Allen et. al (1996) points out, the reluctance for geologists to apply the concepts to intracratonic, internal drainage basins containing non-marine sequences where eustatic sea level curves cannot be applied. Whatever the reason, sequence stratigraphic application to the Eromanga Basin will, as Posamentier and Weimer (1993) noted, give a better understanding of the interactions and properties of sediments in areas such as fluvial and coastal plain environments and improve field development. Application is especially useful in stratigraphic traps such as the basal Birkhead Formation at the Gidgealpa south dome.

Difficulties occur when sediments within the Birkhead Formation are attempted to be correlated in a lithostratigraphic sense since depositional settings over time and area change within the Eromanga Basin. This fact was

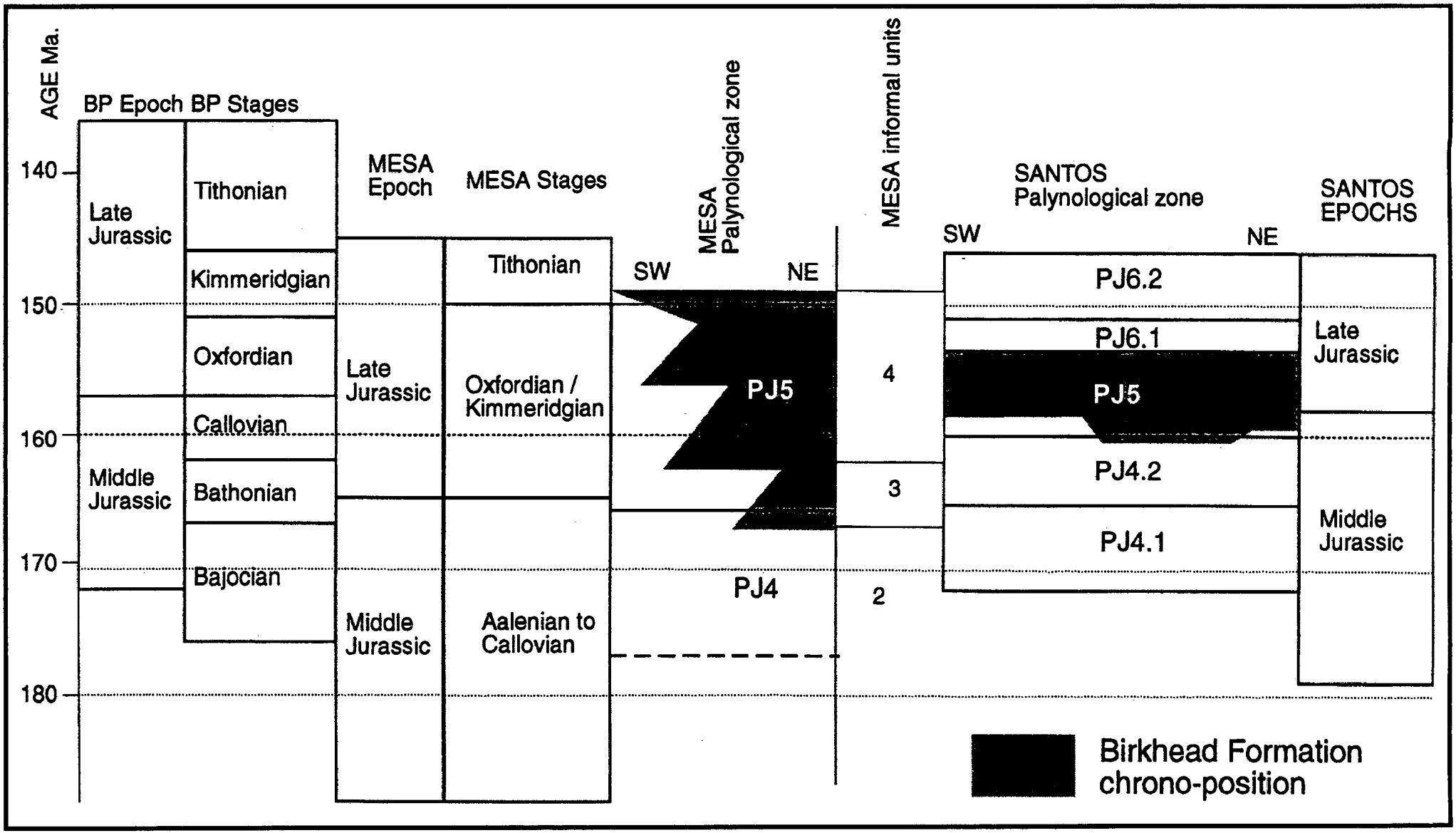

Figure 75: Birkhead Formation chrono-position showing BP, MESA and SANTOS time scales (From Boult, 1996).

recognised by Solomon and Ormsby (1984) and Boult (1996). Problems, of which Herbert (1995) stated, can be overcome since sequence stratigraphy:

"emphasizes the correlation of key surfaces, rather than lithologies,"

Key surfaces such as the maximum flooding surface or sequence boundaries of the Birkhead Formation can be used to correlate successions.

5.2.2 Methodology

An example where the successful use of extensive wireline data for sequence stratigraphic interpretation has been used by Reynolds (1994) where he applied the data to the Viking Formation in south central Alberta, Canada. Due to the relatively large database of wells I have also conducted my stratigraphic interpretation using mainly wireline data and incorporated core and seismic data where applicable within the Eromanga Basin. All other data, which I have deemed useful in determining base level change, such as tectonics and changing sediment provenance, has also been incorporated to give the best sequence stratigraphic interpretation whilst lowering the risk of systems tract allocations within the Eromanga Basin.

To correlate the Birkhead Formation I used the gamma ray and sonic logs at a scale of 1"=50' and used the maximum flooding surface (MFS) (inter-Birkhead Formation marker) as the datum. The wells were then tied together to produce a number of cross-sections at a scale of 1"=300'. In the South Australian section of the Eromanga Basin a grid pattern was used while to the east in Queensland three cross-sections were produced, one strike section running north-east to south-west and two dip sections running north-south (figure 76).

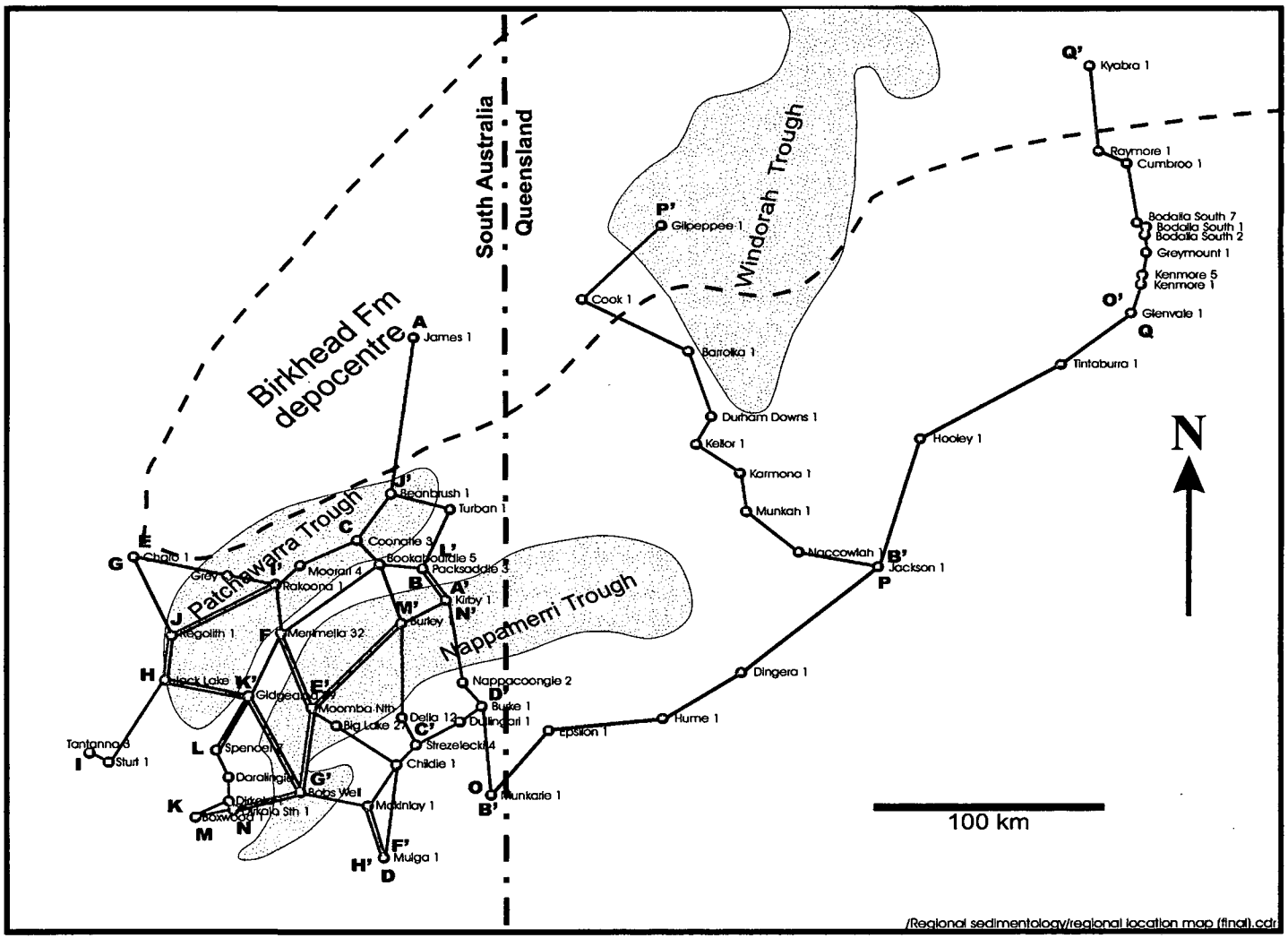

Figure 76: Regional map of the southwestern portion of the Eromanga Basin showing the location of regional sections produced in this sequence stratigraphic study (See appendix 4 for corresponding sections).

Once cross-sections had been produced, the Birkhead Formation was then divided into sequence stratigraphic units of lowstand, transgressive and highstand systems tracts. The lowstand systems tract is bounded by the sequence boundary within the top section of the Hutton Sandstone to the base of the Birkhead Formation which also corresponds to the transgressive surface. The transgressive systems tract is bounded from the transgressive surface to the MFS and the highstand systems tract occurs between the MFS and the base of the Adori Sandstone / Namur Sandstone. For a detailed description of sequence stratigraphic allocations see section **5.4**. Even with the lithological variations apparent from the cross-sections across the Eromanga Basin the wells are relatively easy to correlate using the sequence stratigraphic units.

For this study I created a number of sequence stratigraphic sections over the Eromanga Basin which are shown in appendix **4** and their locations displayed on figure **76**. These sections were produced using regional core data that I interpreted (appendix **5**) and sequence stratigraphic concepts that are discussed below in section **5.4**. Sections A-A', B-B', C-C' and J-J' are dip sections showing fluvial incision in the south-east and the development of lowstand systems tract sediments towards the depocentre (north and north-west). Towards the depocentre a marked increase in the thickness of the Birkhead Formation is also noted. Strike sections (D-D', G-G' and H-H') show the variation in thickness of the Birkhead Formation and the presence of incised valleys on a fluvial landscape in some wells (Childie 1, Jack Lake 1 and Charo 1) running perpendicular to the sections.

5.2.3 Cause and effects of Base level Change

Systems tracts can be identified by their bounding surfaces and internal geometry. The allocation of a systems tract to a depositional sequence is dependent on cycles of relative base level change (Emery and Myers 1996); for this reason it is important to determine the cause of the changes. Authors including Vail (1988), Galloway, (1989), Schumm (1993) and Posamentier

and Weimer (1993) recognise that there are four parameters affecting relative base level change on a coastal margin depositional system. They are listed on the following page and their interrelationships are demonstrated in figure **77**:

1) tectonic subsidence
2) volume of sediments
3) change of climate
4) eustatic change of sea level

From my own observations, base level change within the Eromanga Basin is most likely controlled by the interrelationship of tectonics and the volume of sediments entering the depositional system. From Veevers (1984), Watts (1987), Whitford et. al (1994), Gibson et. al (1995), Boult et. al (1996, 1998), and work I have conducted (sections **4.7** and **4.8**), it is well established that during the Middle to Late Jurassic there was a provenance change from craton derived (Hutton Sandstone) to volcanic-arc derived (Birkhead Formation) sediments and associated evidence of tectonic activity occurring at this time.

Tectonic tilting probably caused the demise of the south-western sourced Hutton Sandstone by regional tilting of the Eromanga Basin as well as uplift on the eastern edge associated with the formation of the volcanic arc complex off the coast of Queensland (Veevers, 1984).

The activity continued throughout the early Birkhead Formation with the former Hutton Sandstone sediment source area, near the south-western edge of the basin, showing evidence of the tectonic movement by thickness variations in the correlated strike sections (section G-G' and H-H', appendix **4**) and the formation of incised channels in the down thrown areas. While thickness variations of the Birkhead Formation are evident from the cross-sections it is also possible that the differences in the formation thickness could be a result of fluvial incision by the Namur Sandstone deposited above the Birkhead Formation. The following section is a summary of the events which caused

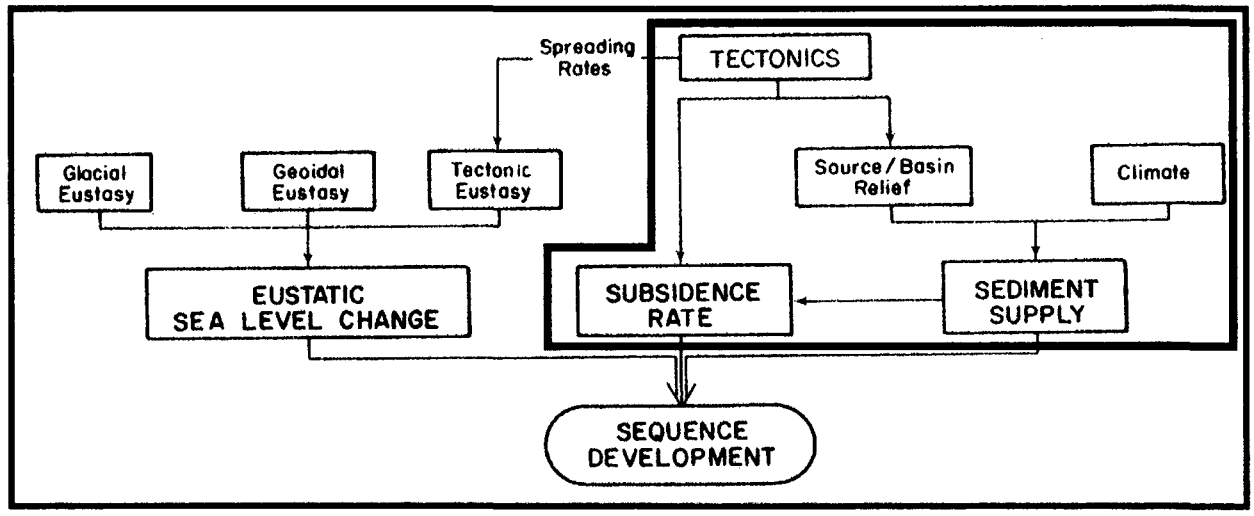

Figure 77: Variables that influence depositional history and sequence stratigraphy of prograding basin margins. Boxed area represents parameters active in the Eromanga Basin, affecting sequence stratigraphy. (After Galloway, 1989).

the formation of the various systems tracts during the Jurassic within the Eromanga Basin.

5.2.4 Lowstand systems tract

Regional tilting uplifted the eastern side (central Australia region) of the Eromanga Basin causing a relative fall in base level of the north-west side (Queensland) of the Eromanga Basin by the over-steepening of the theoretical equilibrium fluvial profile, (ie producing negative accommodation space)(Allen et. al, 1996)) from east to west. The effects of the base level fall on the newly exposed lake floor and fluvial section is dependent on the slope of the exposed section and therefore determines the behaviour of the fluvial river system. If the slope is greater than that of the fluvial profile then fluvial incision will occur (Allen, 1994) as it does in this case. This is demonstrated in figure **78** which shows fluvial erosion due to a base level fall and steepening profile. Thus, to counteract the increased gradient from the east the fluvial system 'cut' into the landscape forming a series of incised valleys. Incision occurred at Munkarie 1, Childie 1, Jack Lake 1, Tantanna 1, Greymount 1, Kenmore 1 and Spencer 7 and can be seen in sections D-D', G-G', I-I' and Q-Q' (appendix **4**).

While the palaeoslope increased in an east- west direction, in the south-west the Hutton Sandstone source and drainage system within the lowstand systems tract experienced a decrease in depositional energy. The fluvial system in the South Australian portion of the Eromanga Basin consisted mainly of incised meandering channels flowing to the north reflecting this decrease in depositional energy of sediments into the system. Figure **79** shows the lower energy, aggrading, incised valley-fill facies at Tindilpie representing lowstand systems tract sediments caused by a slowly rising base level where shoreline regression was maintained (Allen and Posamentier 1993). The slow rate of rise of the lake allowed the lowstand systems tract sediments to completely in-fill the incisions. Incision occurred although palaeoslope dip had decreased in

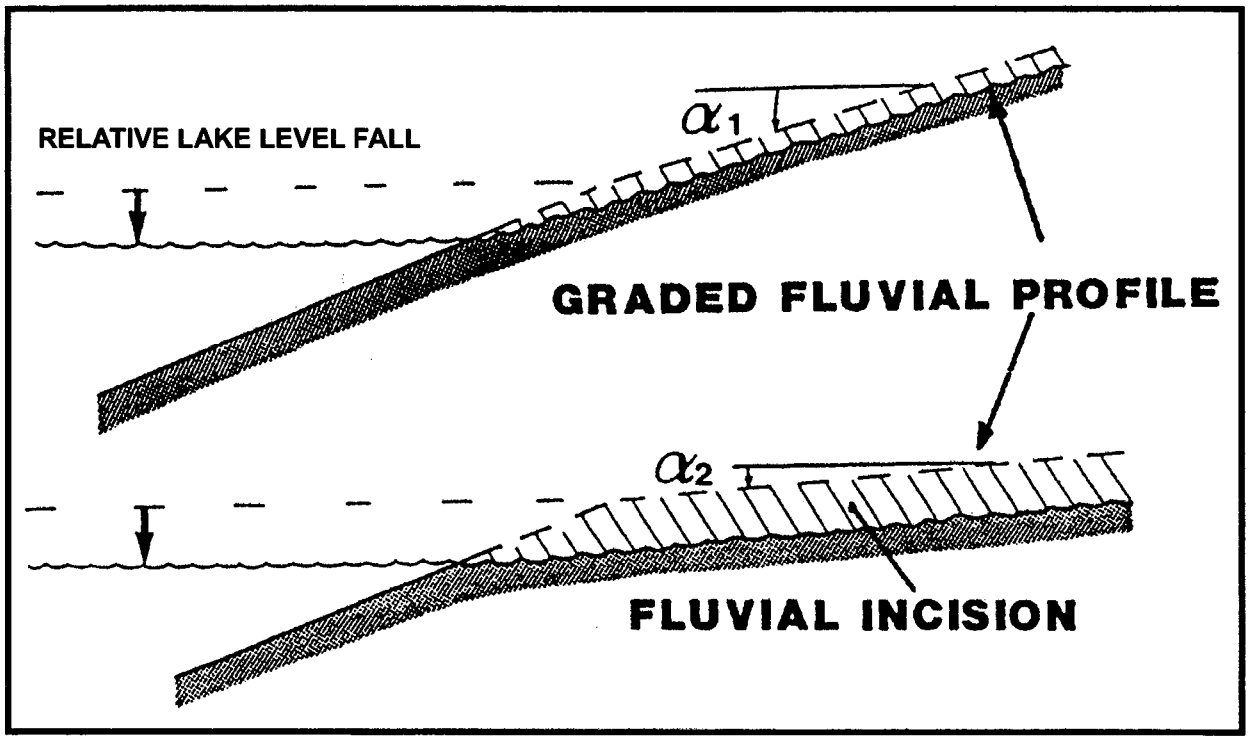

Figure 78: The effects of a base level fall on fluvial incision. The depth of incision increases when the slope of the exposed lake floor is greater than the slope of the fluvial equilibrium profile (α_1 and α_2). In the bottom section the slope of the exposed lake floor is much greater than the slope of the equilibrium fluvial profile and will therefore have a greater depth of fluvial incision (From Allen, 1994).

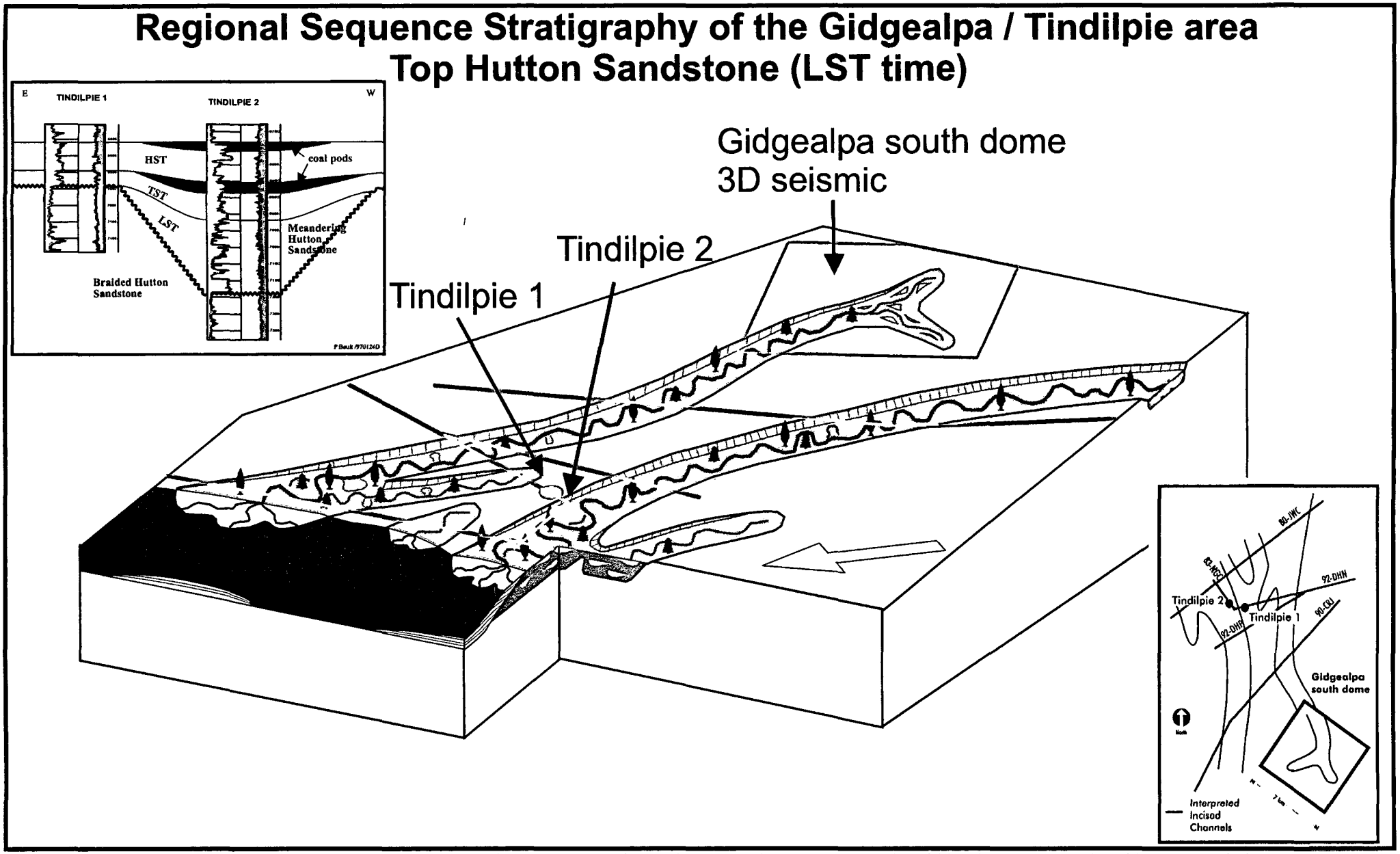

Figure 79: Schematic 3D reconstruction of the palaeo-geography during the deposition of the lowstand systems tract of the Birkhead Formation in the Gidgealpa/Tindilpie area. Top left inset is a cross section of Tindilpie 1 and 2 showing the amount of relief of the fluvial incision (over 300 feet). Bottom right inset is a map in plan view of the Gidgealpa/Tindilpie area showing 2-D and 3D seismic locations as well as indicating the positions of the fluvial channels.

the area at this time since base level fall was greater than the slope change. Thus a relative fall in base level had still occurred in a south to north direction. The type of lowstand sediments deposited, whether incised valley fill or lowstand systems wedge sediments can be identified by the facies stratal pattern. Distal valley fill sediments are characterised by blocky shale and sand packages that are characteristic of meandering fluvial channels where avulsion has occurred. However, lowstand wedge sediments are usually stacked coarsening up sequences and are probably a result of delta lobe switching within the shallow lake. Characteristic signatures can be seen in figure **80**.

Proximal lowstand systems tract sediments can also be identified within the Eromanga Basin sequence and are illustrated in the interpreted sequence stratigraphic section of figure **81**. Note in the figure the more blocky nature of the lowstand systems tract sediments in the more proximal wells as compared to the more distal wells closer to the lake margin. Figure **81** illustrates the ramp nature of the stratigraphic section when compared to the ramp setting model from Emery and Myers (1996).

Fluvial incision also occurred in the eastern Eromanga Basin. In Queensland the regional tilting and subsequent relative fall in base level caused sediments to be increasingly sourced from the east as well as from the southern margin of the basin where sediment supply waned. Initially, sediments from the east probably consisted of local reworked Hutton Sandstone, which itself had only just terminated deposition. The fact that the Hutton Sandstone consists of coarse grained quartzose sandstones allowed it to be easily eroded due to its unconsolidated properties. The erosion also formed incised valleys similar to those produced in the west. As time progressed and increasing volumes of sediment were eroded from the volcanic arc to the east, lithic labile sediments then expanded into the Eromanga Basin and deposited on top of the reworked and previously deposited Hutton Sandstone (figure **82**).

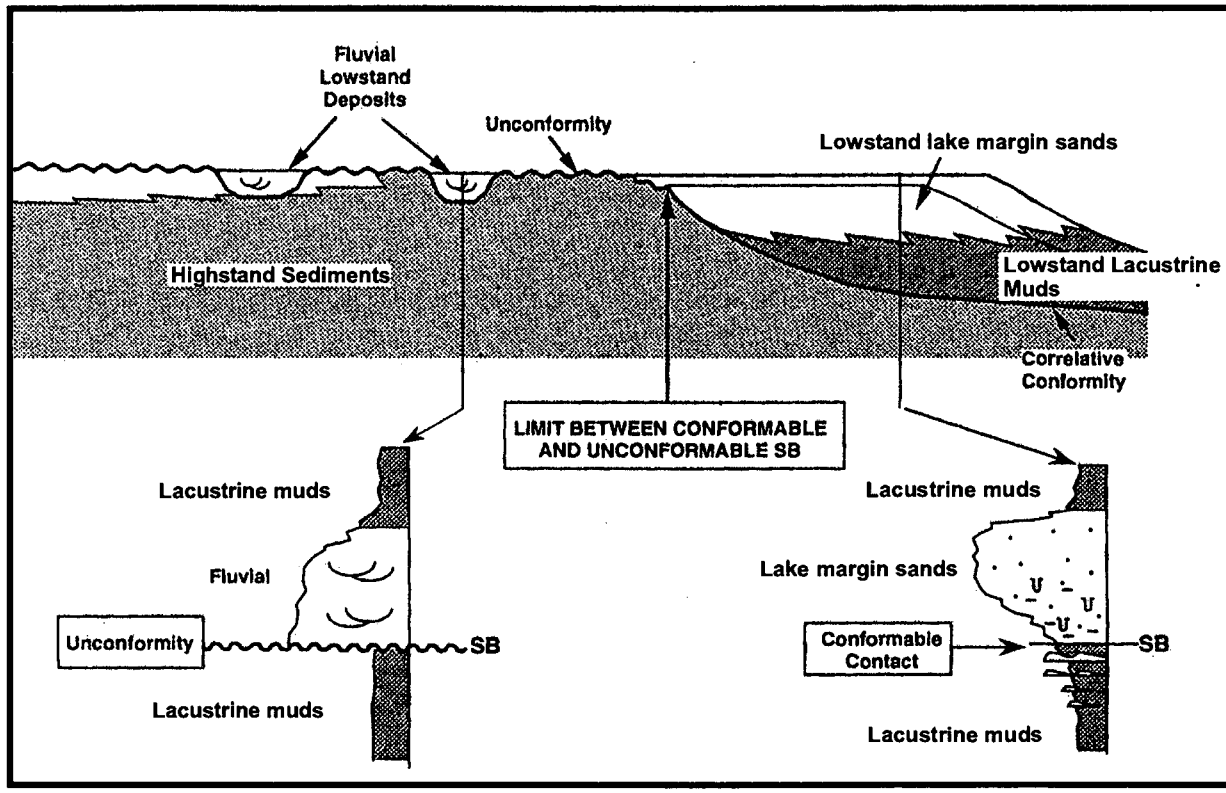

Figure 80: This figure can be applied to the Eromanga Basin and indicates the facies and stratal patterns in lowastand deposits. On the fluvial profile fluvial sands with a blocky signature occur on the sequence boundary while closer to the lake prograding sands produces a coarsening up sequence (After Allen, 1994).

Regional Sequence Stratigraphy of the South Western Eromanga basin

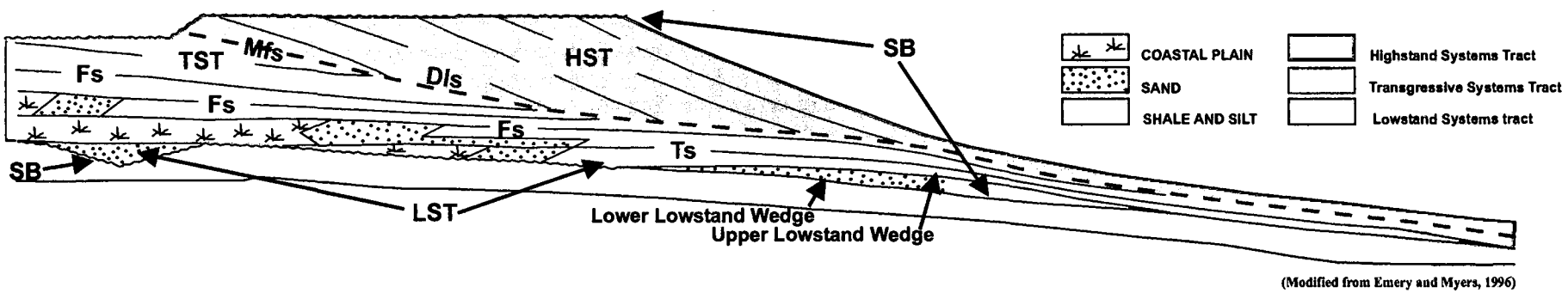

(Modified from Emery and Myers, 1996)

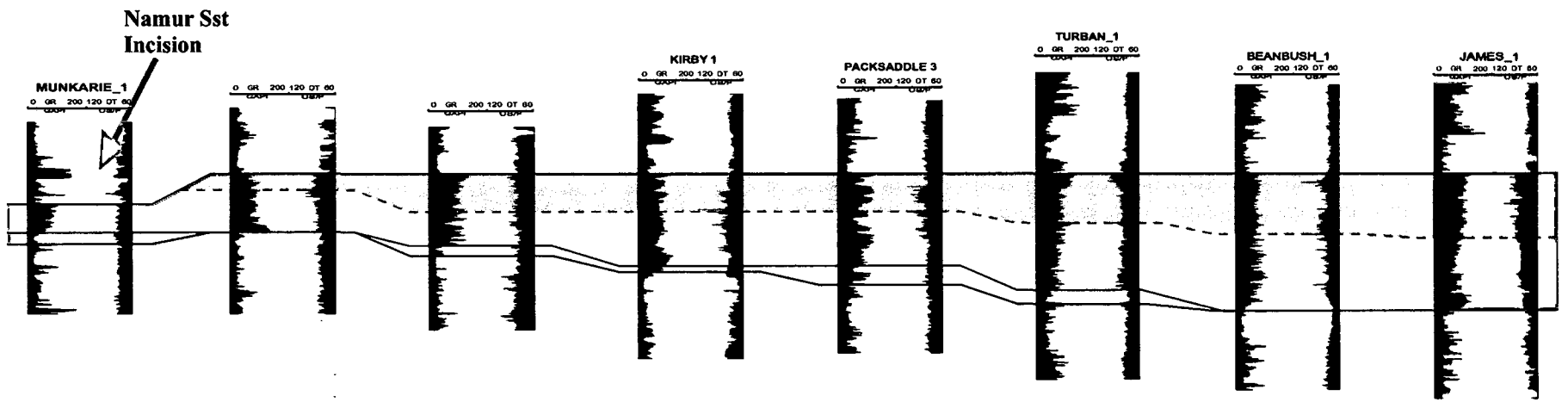

/Regional sedimentology/ seq strat section(final).cdr

Figure 81: Comparison of a ramp style margin setting and interpreted sequence stratigraphic cross section (section B-B' from Figure 76 and appendix 4).

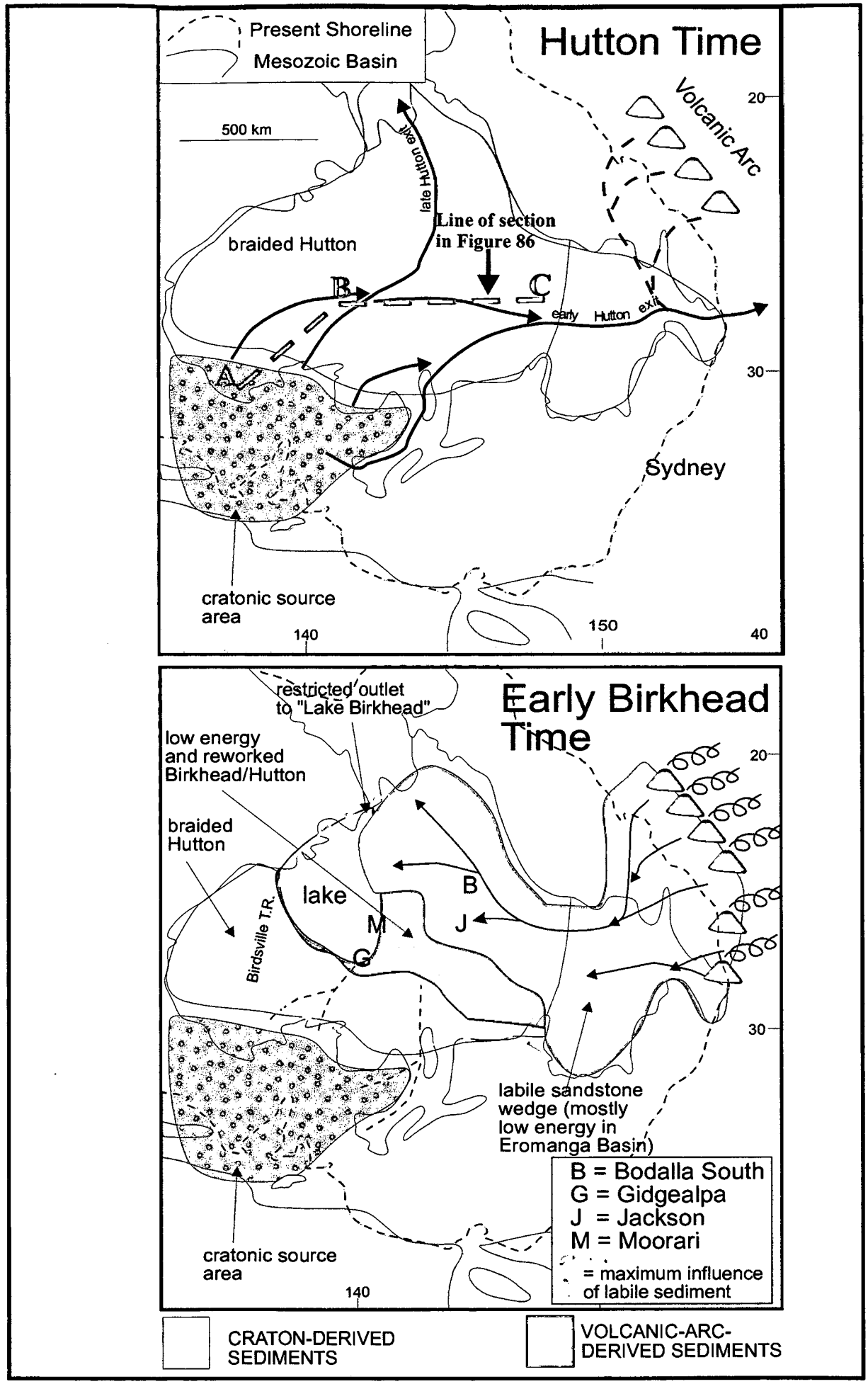

Figure 82: Top figure indicates palaeo-drainage direction and source area below the sequence boundary during Hutton time. With tilting of the Eromanga Basin and uplift of the volcanic arc to the east the cratonic sediments from the southwest waned and sediments from the volcanic arc deposited as lowstand sytems tract sediments (After Boult, 1996).

Assessment of palynological data by the Department of Mines and Energy and SANTOS Ltd has demonstrated that the lower part of the Birkhead Formation is older in the north-east of the basin, along the axis of the depocentre (figure **75**, page 163). Newton (1986) also recognised this when he stated that the top of the Hutton Sandstone at Tintaburra (figure **76**, page 165) is time equivalent with the mid Birkhead Formation wells to the north-west. The age difference from north-east to south-west reflects the sediment fill pattern within the Eromanga Basin of the volcanic arc derived sediments (figure **82**). The sediments entered the basin from the east and were then carried by rivers and streams down dip, which at the time was to the north and north-west, ending up in the depocentre. The increased influx of sediments in this area probably caused the basin depocentre outlet along the Euroka Arch (see figure **8**, page 14) to become blocked as well as displace the water from the area which was once lacustrine.

While the main influx of sediments was volcanic arc derived sediments from the east, sediments from the south-west cratonic area may have contributed to the base level rise but only in a minor sense. The water displacement and blocking of the drainage outlet to the north thus initiated base level rise and subsequent formation of the transgressive systems tract sediments. This base level rise, I believe, is what probably caused the change in depositional patterns from lowstand systems tract to a transgressive systems tract sequence within the basin.

The progressive advancement of the volcanic arc derived sediments in the lowstand systems tract is demonstrated in cross-sections P-P' and Q-Q' (appendix **4**) which shows a general thickening of the sequence down dip, from south to north. This characteristic is not seen in the cross-sections from the western Eromanga Basin since the volcanic arc derived sediments and tectonic tilting did not have the same effects as in the east. Thus the lowstand systems tract sediments to the west are relatively thin and are deposited as

more typical sediment wedges (figure **81**, page 174). The thickening of the lowstand systems tract sediments down dip in the north-east of the Eromanga Basin is indicating the effects of the tectonic tilting and changing sediment provenance by changing the dip section in the Hutton Sandstone to a more characteristic strike section within the basin.

The differences in sediment depositional styles of the fluvial incision and lowstand systems tract sequence within the Eromanga Basin represent different controls on relative base level movement (Allen 1994). In the west the tectonic tilting is only minor and base level change is due more to a drop in lake level rather than tectonic tilting which predominated in the east. In other words the higher tectonic activity to the north-east has effected the local drop of the entire Lake Birkhead more than the effects of tectonism in the south-west portion of the Eromanga Basin.

The fact that fluvial incision in the south-west section of the basin increases as rivers approach the shoreline due to the falling lake level and not tectonic tilting (Allen 1994) is illustrated in figure **79** (page 171), showing that incision at Tindilpie is approximately 300 feet where as at Gidgealpa incision is only approximately 70 feet. In the east of the basin, where the tectonism is more apparent, erosion of the previously deposited Hutton Sandstone is more evident upstream from the over steepening fluvial profile (Allen 1994). These sediments were then re-deposited towards the depocentre.

The influence of climate change is a minor cause of base level change when compared to tectonic tilting and provenance change since during the transition between the Hutton Sandstone and Birkhead Formation the world climate changed from a warm mode, and in particular it was humid at its conclusion in the early Jurassic, to a cool mode in the Mid to Late Jurassic (Frakes et. al, 1992). While there was a change in climate, the area over the eastern part of Australia is still interpreted to have been wet as well as temperate due to its position in high latitudes at this time (figure **83**). Hence it would appear that

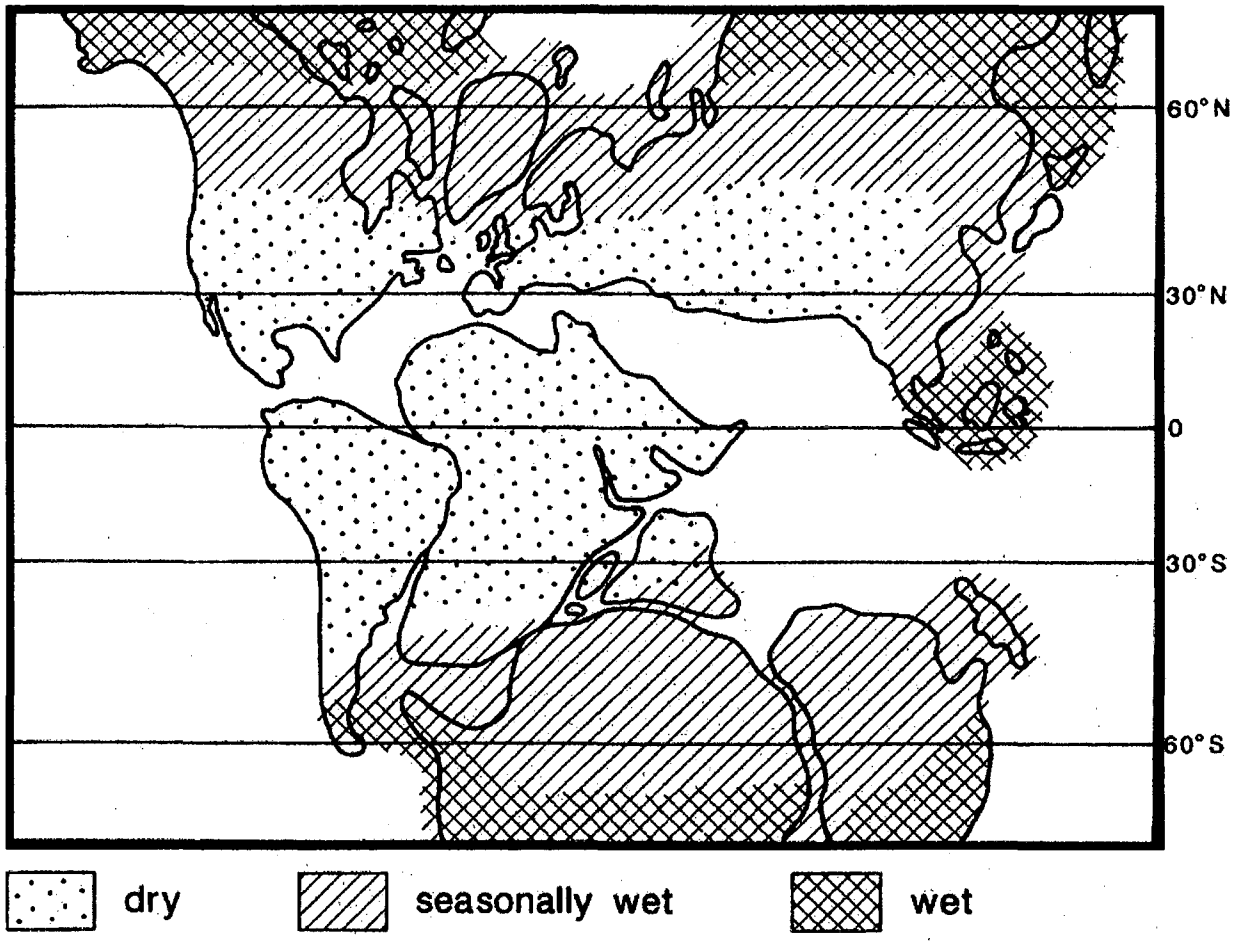

Figure 83: Palaeo-climatic belts during the Late Jurassic (From Hallam, 1985 and Frakes et. al, 1992).

annual rainfall did not dramatically change over the period (Frakes et. al, 1992). Because the internal drainage system of the Eromanga Basin flowed into an intra-cratonic lake system to the north, eustatic change in sea level did not effect the lake base level since the waterway was not connected to the sea (Allen et. al, 1996).

5.2.5 Transgressive systems tract

As previously mentioned the rise in base level within the lower Birkhead Formation was caused by volcanic arc derived sediments filling the depocentre and blocking the drainage outlet of lake Birkhead. Allen (1994) and Allen et. al (1996) have stated that:

"the fluvial response to a rise in relative sea level [base level in this case] *will depend on the rate of sediment influx and the rate of the relative sea level rise"*,

in other words if the rate of supply of sediment is greater than the rate of base level rise then there will be a regression. Figure **84** shows the effect of varying the ratio of rate of base level rise and the influx of sediments on a fluvial coastal plain. So it wasn't until the rate of rise of Lake Birkhead was greater than sediment influx into the basin that sediments were deposited as a transgressive sequence. The rise in base level and subsequent transgression was probably due to a combination of waning of the volcanic arc derived sediments from the east and continued tectonism and uplift on the Euroka Arch. The subsidence rate decreased reducing the slope of the fluvial profile and at the same time fluvial sediment flux also waned causing fluvial sediments to aggrade and eventually retrograde since sediment supply was unable to keep up with base level rise.

The transgressive systems tract consists of retrogradational, back-stepping parasequences which have an overall deepening upward signature and are a

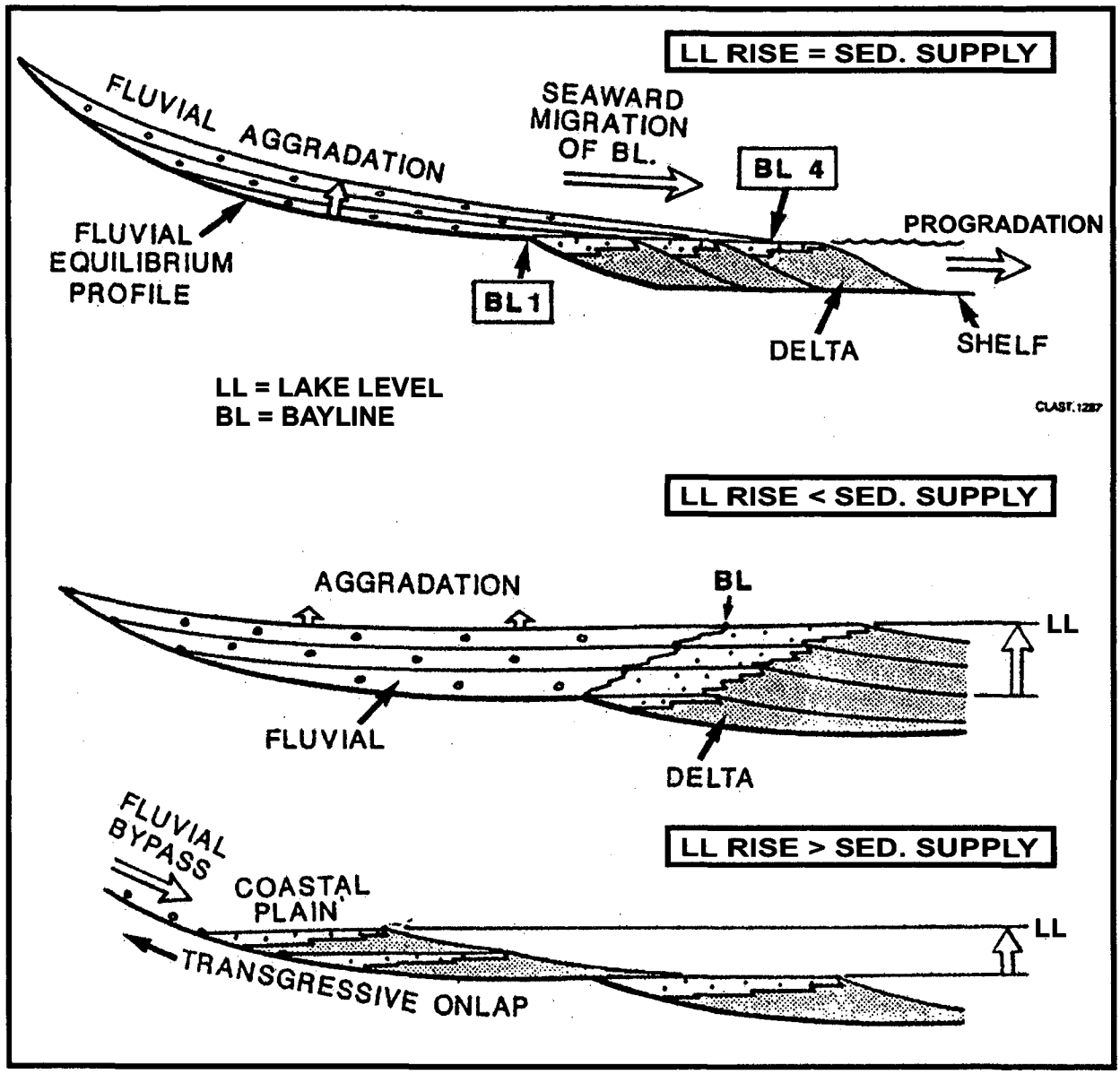

Figure 84: Effect of varying rates of relative baselevel rise and sediment influx on fluvial and coastal sedimentation patterns. Top section: sediment influx and baselevel rise are constant. Middle section: sediment supply is greater than relative baselevel rise. Bottom section: sediment supply is less than relative baselevel rise (from Allen, 1994).

result of relative base level rise outweighing sediment supply (Vail, 1988, Allen 1994, Emery and Myers 1996). A transgressive surface marks the base of the transgressive systems tract which covers the lowstand systems tract incised valley fill sediments and Hutton Sandstone sediments on the interfluves. The surface can be recognised by in situ reworking and winnowing of sediments or the production of hardgrounds (Emery and Myers 1996). The transgressive surface within the basal part of the Birkhead Formation is characterised by the presence of these iron hard-grounds seen in Gidgealpa 32, 6007' (appendix **3**), Tantanna 3, Dirkala 1, Spencer 7 and Strezelecki 4 (appendix **5**). However, in situ sediment reworking is absent since the usual wave and tide action associated with coastal areas are absent in this case where the depocentre is lacustrine. The transgressive surface pinches out at a point landward, from this point the surface corresponds to the unconformable sequence boundary (Vail, 1988).

As the volcanic arc derived sediment flux continued to wane, the rate of relative base level rise escalated causing an increase in fluvial accommodation space and thus an increase in fluvial aggradation. Fine grained sediments such as silts and clays then filled the rapidly forming accommodation space instead of bypassing the fluvial profile (Allen et. al, 1996). Figure **85** shows the effects of differing rates of relative base level rise. The formation of the various stacking patterns from figures **85**a to d are similar to what is seen in the transgressive systems tract of the Birkhead Formation. Looking at it from a sedimentological point of view, the increasing rate of base level rise causes the sand to silt ratio to decrease due to the increasing accommodation space which causes an overall fining up of the sediments from figure **85**a - d.

Well data in the Eromanga Basin show characteristic signatures of transgressive systems tract sediments in the basal section of the Birkhead Formation. This tract is characterised by the presence of coals, over bank deposits and lagoonal to lacustrine deposits as well as associated deltaic

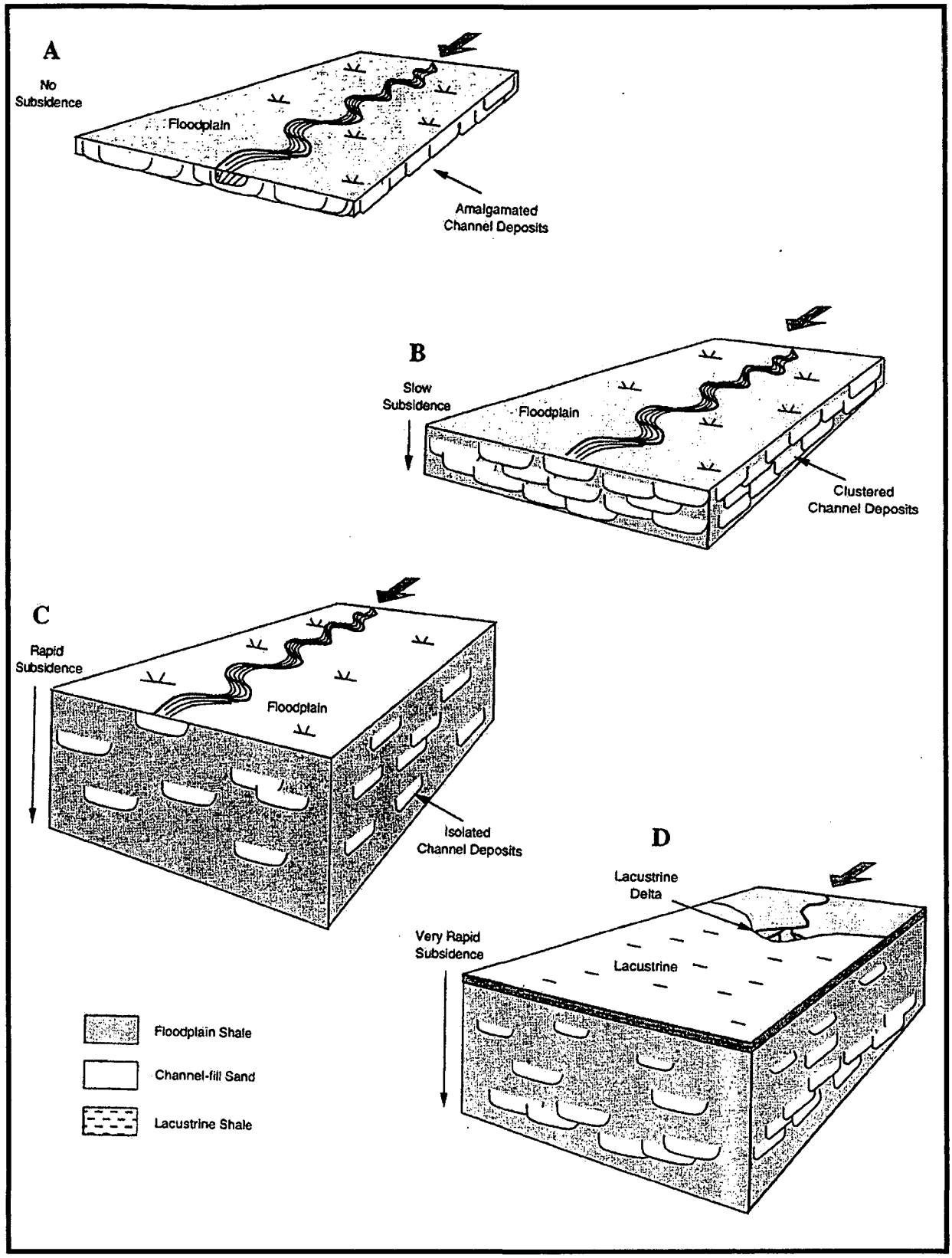

Figure 85: The effects of increasing rate of fluvial accommodation on fluvial stacking patterns. In these examples sediment rate is assumed to be constant with fluvial accommodation being controlled by tectonic subsidence. From the figures it is evident that the higher the rate of accommodation increase the more isolated the channels become within flood plain sediments. In case (D) where the increase in accommodation is much higher than sediment supply a lacustrine system is formed (From Allen et. al, 1996).

sediments (seen in Kirby 1, Coonatie 3, Strezeleki 4, McKinlay 1, Gidgealpa 29).

At some point in a transgressive systems tract sequence the relative rate of base level rise reaches its maximum and according to Allen et. al (1996):

"represents a change from non-filling to filling available accommodation."

At this point a maximum flooding surface (MFS) marks the uppermost limit of transgression and the maximum land-ward extent of lacustrine conditions (Allen, 1994, Emery and Myers 1996). Within the Eromanga Basin the MFS can be easily identified by a high gamma ray spike, or a more easily identified sonic spike. The sonic spike reflects the presence of organic-rich, low-density, condensed section caused by sediment starvation within and close to the depocentre. Allen et. al (1996) believe that the MFS on a fluvial plain may be represented by a coaly interval if the climate is suitable and indeed I have found is to be the case in the Eromanga Basin. Because of the regional extent of this surface it has been used as the datum to correlate well logs within the basin in appendix **4**. The sonic spike has been seen to cover almost the entire study area including the depocentre and towards the southern basin edge (edge of the study area). Wells that occur near the southern edge of the study area include Boxwood 1 and Munkarie 1 (figure **76**, page 165 and appendix **4**).

The formation of the MFS was probably caused by a combination of the termination of sediment supply from the volcanic arc to the east and the depocentre restriction stopping the drainage of the lake waters. Tectonics was also playing a part at this time with the south-western part of the basin being slightly uplifted once again shedding sediments towards the depocentre and mixing with the volcanic arc derived sediments in the upper part of the transgressive systems tract at Gidgealpa.

5.2.6 Highstand Systems Tract

Sediments from the south-west became increasingly eroded and transported towards the depocentre in the closing stages of the transgressive systems tract and was probably associated with uplift of the cratonic area to the south and south-west. Therefore, during the transgressive systems tract the depositional dip was essentially from east to west but then changed back to a south to north orientation after the MFS occurred. Therefore the depositional dip had returned to the position it was in during the deposition of the top of the Hutton Sandstone and lowstand systems tract sediments of the basal Birkhead Formation. This change in palaeoslope can be seen in appendix **4** where the south to north orientated section P-P' and Q-Q' show a relatively uniform thickness of the transgressive systems tract and thickening of the highstand systems tract to the north.

Tectonism and subsequent tilting during the mid Birkhead Formation probably also allowed Lake Birkhead to once again drain out to sea through the Euroka Arch. This caused the relative base level rise to decrease to a stage where sediments were filling the accommodation as fast as it could be created resulting in fluvial aggradation. When the relative rate of sediment input increased to a level above the rate of creation of accommodation, the sediments then prograded into the depocentre and became more sandy.

In the initial stages of the highstand, prograding deltas and / or the lake shoreline will advance across the drowned sequence formed by the maximum flooding event depositing deltaic sands and related sediments on top of deeper water silts and condensed sediments (Emery and Myers 1996). In the study area this is seen in wells Turban 1, Packsaddle 3, Coonatie 3, Bookabourdie 5, Mckinlay 1, Grey 1. Early highstand deposits tend to consist of poorly connected, vertically isolated sand bodies which become more amalgamated in the later stages as sediments continue to prograde and increasingly bypass the fluvial profile forming tabular channel sand bodies due to the decreasing

amount of accommodation space (Emery and Myers 1996). According to Emery and Myers (1996)

" the fluvial depositional record of the highstand will be effected significantly by the rate of sediment supply to the system",

thus the late Birkhead Formation sediments were probably being affected by the sediments eroding from the cratonic south-west margin of the basin.

Wireline logs from the south-west to north-east show that the highstand sediments continued to prograde into the depocentre and as a result became more restricted towards the Euroka Arch. The top of the highstand systems tract is bounded by a sequence boundary which formed due to the lowstand systems tract sediments of the Namur and Adori Sandstones eroding into the top of the Birkhead Formation during a period when negative accommodation was occurring.

The regional sequence stratigraphy of the Birkhead Formation can be summarised in figure **86** with the line of section indicated on figure **82** (page 175). The sequence stratigraphic model starts by showing erosion into the Hutton Sandstone during Birkhead Formation time. In the south-west the degree of fluvial incision is relatively varied over the area while to the east, due to the tectonic uplift in the area, more erosion occurs closer to the basin margins. At this time the chronostratigraphic section indicates that there is non-deposition and that sediment bypass is occurring and is being transported and deposited further towards the depocentre, or north, away from the section. At the same time or slightly after the uplift, volcanic arc derived sediments were shed into the basin from the east and started to fill the incised valleys that were previously formed. The incisions slightly further to the west were partially filled by reworked cratonic sediments before being filled by the lithics. At the same time to the south-west sediments continued to be shed

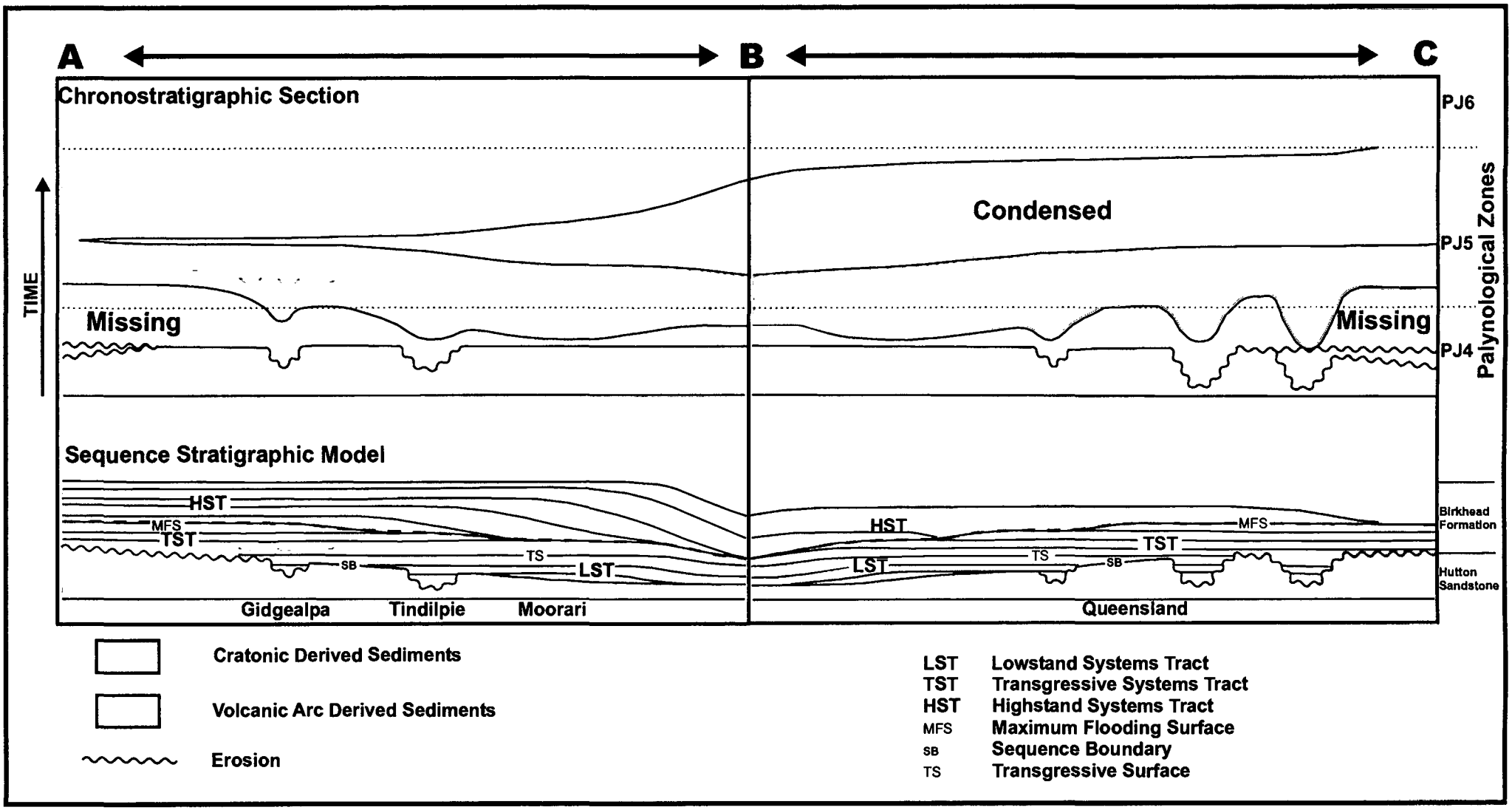

Figure 86: Sequence stratigraphic and chronostratigraphic summary of the Birkhead Formation, Eromanga Basin. (Line of section indicated in figure 82).

from the cratonic area in much lower quantities filling the incisions from the south of the basin.

Some time later, sediments within the lowstand systems tract, from both the south-west and east, had filled the fluvial incisions and began to aggrade sediments on the fluvial profile. The termination of the lowstand systems tract occurred at the point where lake base level rose at a greater rate than sediment influx. The rise in the base level was likely to have been caused by lithics from the volcanic arc blocking the lake outlet. To the south-west cratonic sediments occur above and below the transgressive surface. The cratonic sediment above the surface consisted of reworked quartzose sediments being transported locally from the east due to the easterly decreasing depositional dip. While further to the east, the section was being dominated by lithics due to its proximity to the volcanic source.

The transgressive systems tract saw the strengthening of lithic sediment influx from the east and waning of cratonic material from the south-west causing inter-tonguing of the two sediments. The larger supply of the lithics as compared to the cratonic sediments saw the volcanic arc derived sediments extend right over to the south-west corner of the basin. The chronostratigraphic section shows the initial inter-tonguing of the sediments and then the spread of the lithics over to the south-west with time. The widespread deposition of the volcanic arc derived sediment from east to west was preceded by lithics that were transported and deposited within meandering fluvial channels in the south Australian section of the Eromanga Basin (figure **86**).

As the volcanic arc derived sediment supply into the basin decreased and base level continued to rise, the point of maximum flooding was reached. After this point tectonic tilting again caused the cratonic sediments to the south-west to become dominant and shed sediments into the basin. The sequence stratigraphic model illustrates the prograding cratonic sediments from the left

of the figure (from the south-west) and progressively fills the basin towards the east. The direction of the sediment source caused the formation of a condensed section towards the north-east of the basin due to the much larger period of time where non-deposition occurred. The condensed section is in the chronostratigraphic section of figure **86**.

This influx of sediments, deposited as a highstand systems tract, was initially slow and with a continuation of base level rise the production of accommodation space resulted. Sediment supply from the south-east continued to increase and eventually outweighed base level rise until negative accommodation formed. The point at which the negative accommodation space occurs (ie the start of the Namur Sandstone or Adori Sandstone) marks the start of fluvial incision and the top of the Birkhead Formation.

5.3 Sequence stratigraphic classification of the Birkhead Formation

The identification of systems tracts and depositional sequences in wells, core and seismic is heavily dependent on the identification of *'key surfaces'* (Allen et. al, 1996). These key surfaces are the maximum flooding surface, related to changes in the rate of sediment fill of the available accommodation space and sequence boundaries which are surfaces created as a result of negative accommodation.

The use of sequence boundaries to define depositional sequences is based on the 'Exxon' model and is used extensively by many authors such as Allen and Mercier (1988), Vail (1988), Allen (1994), Allen et. al (1996) and Reynolds (1994). Alternatively Galloway (1989) defined a depositional sequence as:

" a sequence-stratigraphic unit bounded by surfaces of erosion or non-deposition and their correlative conformities", [and then later states that] *"stratigraphic manifestations of marine-flooding surfaces include both unconformities and condensed sections"*.

In essence Galloway (1989) stated that a depositional sequence can be bounded by successive maximum flooding surfaces which are a result of periods of non-deposition. These surfaces are used since they are generally easier to identify than sequence boundaries on wireline logs (Allen 1994). However, although the identification is easier they do not represent a stratigraphic unconformity since sedimentation is continuous as an associated condensed surface even though sedimentation is very slow (Allen 1994). Figure **87** is an example that shows the variation in assigning a sequence to the Cardium Formation in Alberta, Canada, as defined by the Galloway and Exxon models. In contrast to a maximum flooding surface used by Galloway, the sequence boundary of the 'Exxon' school represents a gap in deposition and thus has a missing section during this time. What is also important is the fact that a sequence boundary is only dependent on a base level fall whereas the maximum flooding surface is the result of both sediment supply and relative base level (Allen et. al, 1996).

These facts, I believe, point to the prefered use of the Exxon model that uses the sequence boundary as the end points of a depositional sequence and in terms of the Birkhead Formation signify major events of tectonic tilting within the Eromanga Basin. A sequence boundary is present at the base of the formation where fluvial incision has occurred and at the top of the formation where high energy facies lie on top of lower energy meandering fluvial and lacustrine facies. The use of these sequence boundaries seems a logical choice since sediments within the Birkhead Formation are affected by the interplay of sediments from the south-west and east, whereas the Hutton Sandstone below and the Namur Sandstone / Adori Sandstone above are dominantly characterised by sediments from the cratonic area along the south-west edge of the basin.

Solomon and Ormsby (1984) and many other authors use the top Cadna-owie Formation as the datum when correlating wells within the Birkhead

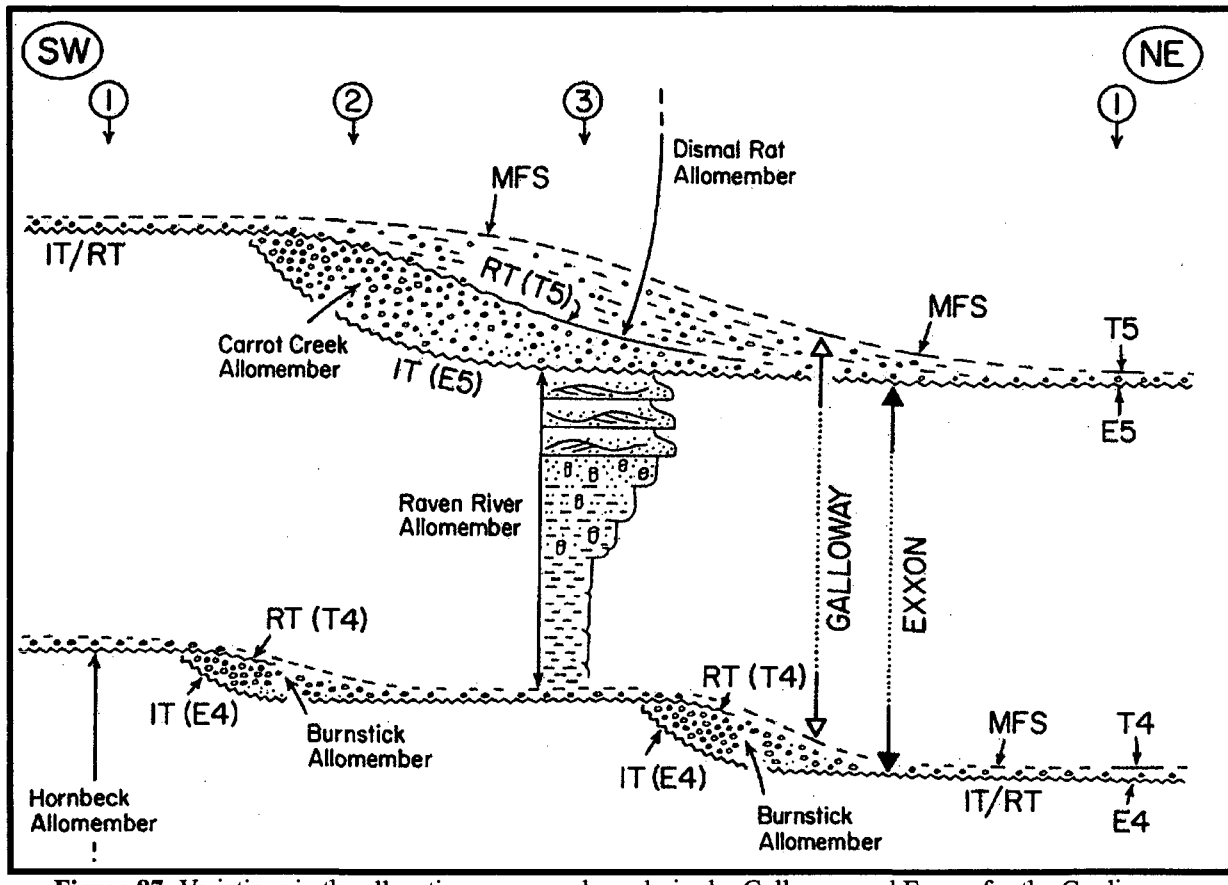

Figure 87: Variations in the allocation sequence boundaries by Galloway and Exxon for the Cardium Formation, Alberta, Canada (From Walker, 1990).

Formation. While this is feasible, the correlation of formations outside the Cadna-owie may not be as accurate as when an internal formation datum is used. This may especially be the case in areas such as the Gidgealpa-Merimmelia-Innaminka Ridge where syndepositional movements of the basement faulted blocks have occurred. Even outside this area where regional tilting is controlling formation changes, the basin tilt at the time of the Birkhead Formation may be different to that of the Cadna-owie Formation causing inaccurate correlations of wells.

5.3.1 Datum Determination

The need for a wireline based datum when determining the sequence stratigraphy of the Birkhead Formation is due to the lack of regional seismic data with sufficient resolution. If seismic data were readily available at a resolution to resolve internal stratigraphy then the units, or reflectors bounding the units, would be sufficient to determine which systems tract sediments relate to, purely by their shape and spatial relationship with other reflectors. Within the Birkhead Formation I have determined that the maximum flooding surface is an ideal datum in which to correlate wells. The ideal nature of this surface as a datum is due to the fact that it is easily identified since:

- it is present throughout the study area and occurs as a characteristic sonic spike,
- it is parallel to a number of other inter-Birkhead marker horizons also consisting of sonic spikes, but are of a lesser lateral extent and
- it is a chronostratigraphic surface occurring over most of the basin separating sediments below and above in time.

The magnitude of the sonic spike produced by non-deposition at the time of the MFS varies from well to well depending on its composition. The surface represents a condensed sequence consisting of abundant organic matter but at

some locations composition varies in terms of the amount of associated fine grained sediments. This variation can be seen throughout the Eromanga Basin. Organic rich shales show a sonic spike with a high corresponding gamma ray signature reflecting the clay content of the rock (James 1, Beanbush 1, Turban 1, Packsaddle 3, Nappacoongee 2 (appendix **4**)), in other areas the sonic spike is associated with a low gamma ray count indicating that the MFS consists of a coal (Strezelecki 4, Bobs Well 1, Regolith 1, Merrimelia 32 (appendix **4**)). The presence of coals will also tend to have a larger sonic spike (longer travel time) than the organic rich shales due to the lower density of the coal.

The application of the maximum flooding surface has also been used by Salomon et. al (1990) on a local scale for correlating wells at Bodalla. In this case the authors named or identified the horizon as the 'Longley Marker.'

5.4 Unit determination of the Birkhead Formation

The Birkhead Formation has been characterised and divided into units by authors such as Gravestock et. al (1983), Solomon and Ormsby (1984), Paton (1986) and Boult (1996) and has been summarised in figure **88**. The previous identification of units by Paton (1986) and Boult (1996) rely on similarities of lithofacies and presents difficulties to the authors such as varying wireline log signatures from well to well due to the diachronous nature of the sediments over Eromanga Basin. However, Solomon and Ormsby (1984) realised the diachronous nature of the Birkhead Formation and divided it into 3 'layer cake' units.

On inspection of over 100 wells and numerous cross sections, I have used a chronostratigraphic correlation rather than lithostratigraphic since classification is much simpler by the use of key surfaces rather than the correlation of similar lithological packages. I have defined 3 units within the Birkhead Formation which I have termed L1, L2 and L3 to avoid confusion with Paton (1986), Boult (1996) and Gravestock et. al (1983) (figure **88**). To

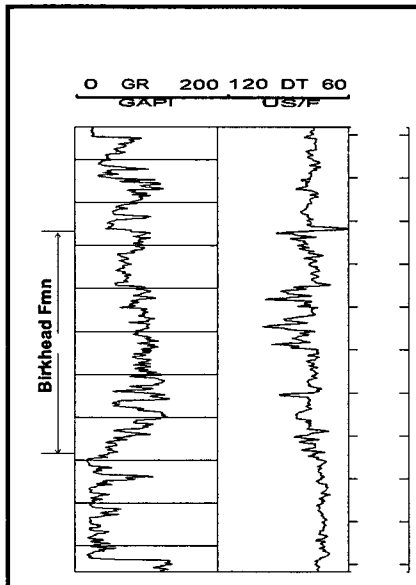

Gravestock et al. 1983	Paton 1986	Boult 1996	This Study
Unit 5 (G5)			
Unit 4 (G4)	Unit 3 (P3)	Unit 3 (B3)	Unit 3 (L3)
	Unit 2 (P2)		Unit 2 (L2)
	Unit 1 (P1)	Unit 2 (B2)	
Unit 3 (G3)		Unit 1 (B1)	Unit 1 (L1)
Unit 2 (G2)			

Figure 88: Comparison of unit allocations by different authors for the Birkhead Formation.

further discriminate between the authors unit allocations and my interpretation I have labelled the units from Paton (1986) as P1, P2 and P3, corresponding to the units 1 to 3. For Boult (1996) I have defined his units I, II and III as B1, B2 and B3 respectively. Similarly for Gravestock et. al (1983) I have allocated G1 to G5 for Units 1 - 5 respectively.

The units I have defined correspond to sequence stratigraphic lowstand, transgressive and highstand systems tracts. Allocating units to systems tracts means that they can be easily identified by their bounding surfaces, they are not restricted to one or several types of lithologies and no assumptions are required when determining the thickness of the units. Wireline character descriptions used are summarised in figure **89** and a brief description of the regional wireline variation is given in the following section. Wells mentioned in the following sections can be found in appendix **4**.

5.4.1 Unit L1 - Lowstand Systems Tract

This unit is defined by lowstand systems tract sediments, it is highly variable in thickness and is absent in some wells. Thickness variations are a result of erosion at the base of the unit which corresponds to a sequence boundary that occurred during the deposition of the Hutton Sandstone. The top of Unit L1 is defined by a transgressive surface which normally occurs as a gamma ray shale peak.

Within the South Australian sector of the Eromanga Basin Unit L1 wireline log signatures occur as incised valley fill and are slightly higher than the underlying Hutton Sandstone and more serrated in character. Close to the source (south-western margin) log signatures consist of cylindrical to bell shaped curves; where the latter signatures occur, the gamma ray signature represents only sandy sediment (Nappacoongee 2, Munkarie 1, Childie 1).

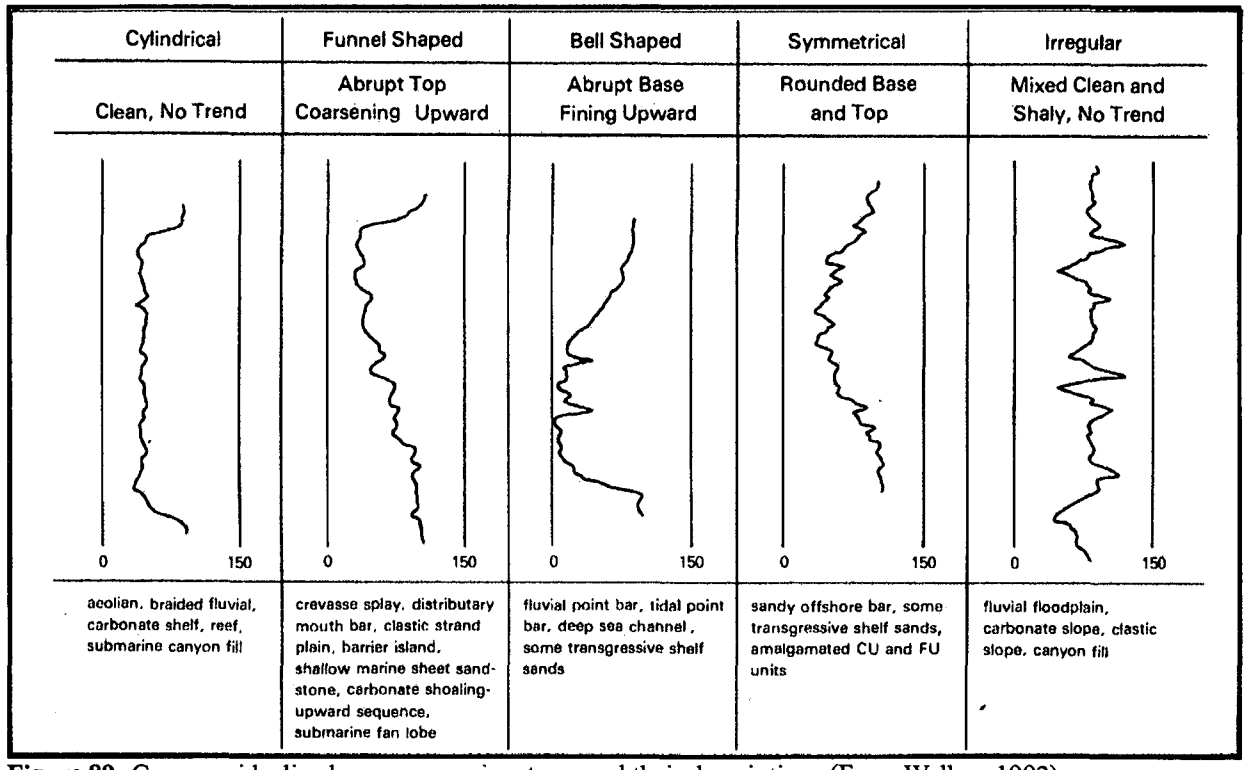

Figure 89: Common idealized gamma ray signatures and their descriptions (From Walker, 1992).

To the north, closer to the depocentre, sediments are deposited as incised valley fill and within lowstand fans. Due to tectonic tilting at the time the log signatures of the more distal incised valley fill sediments consist of alternating silty or shaly overbank deposits with clean channel sands of cylindrical sand and shale packages (Tindilpie 2, Merrimelia 32). Lowstand fan deposits generally consist of a series of coarsening up sequences seen as funnel shaped log signatures representing delta lobe switching (Packsaddle 3, Moorari 4).

Within Queensland cylindrical log signatures predominate due to the tectonic influence to the east depositing sediments in a high energy fluvial environment. Gamma ray logs are more serrated and some wells have a higher API reading due to the influx of the volcanic arc derived sediments rich in feldspars (Kenmore 5, Bodalla South 7, Glenvale 1). Towards the depocentre (Raymore 1, Kyabra 1) log signatures tend to be more serrated and slightly bell shaped reflecting a lower environment of deposition. Unit L1 is equivalent to Unit G3 of Gravestock et. al (1983).

5.4.2 Unit L2 - Transgressive Systems Tract

Unit L2 is present throughout the study area. It is bounded below by the transgressive surface overlying Hutton Sandstone sediments (Unit L1) and above by the MFS. The unit is thin or partly eroded (Munkarie 1) from the top by the upper Birkhead Formation sequence boundary on the basin margins and thickens towards the depocentre.

The log signature of this unit initially consists of a cylindrical gamma ray curve which is then commonly overlain by a bell shaped gamma ray log (Gidgealpa 29, Kirby 1, Burke 1). The initial cylindrical signature of unit L2 is due to the first flooding event during initial base level rise forcing a transgression of the lake margin, forcing sediments to be deposited in more

proximal areas of the basin. After a short time the sediments prograde back towards the depocentre causing a subsequent regression (bell shaped curve) and the deposition of delta fill and distributary channel sands along with shallow lacustrine silts and overbank deposits. The increase of the general sonic response is due to the deposition of the shallow lacustrine and delta fill sediments and associated coals which have a larger organic content due to slower deposition rates. After the deposition of the deltaic sediments the wireline log character shows a general increase in API reflecting the transgression of the lake and deposition of progressively siltier sediments in a lacustrine environment.

Within the depocentre the wireline character is irregular and highly serrated with a relatively high and uniform API value (James 1, Beanbush 1, Turban 1) due to the distal nature of these wells to the sediments entering the at the lake edge. The serrated nature of the gamma ray curve is due to thin sheet sands from deltas entering the lake or from storms which redistribute sands.

5.4.3 Unit L3 - Highstand Systems Tract

This unit is highly variable in thickness due to the erosive nature of the SB which defines the top of the Unit and Birkhead Formation, particularly close to the basin margin where unit L3 is sometimes completely absent (Dirkala South 1, Munkarie 1). This unit is by far the most variable in its log character with various wells showing a symmetrical (Moomba North 1, Turban 1), bell shaped (Nappacoongee 2, Strezelecki 4, McKinlay 1), funnel shaped (Mulga 1, Childie 1), irregular (James 1, Beanbush 1) or a combination of log characters (Packsaddle 3, Kirby 1). These log signatures represent an increase in depositional energy from unit L2 and reflect the various environments of a meandering fluvial depositional environment, including oxbow lakes, channel sands, swamps and associated coals and over bank deposits. While log

signatures are highly variable, unit L3 tends to become more sandy with increasing proximity to the source.

The top of unit L3 is easily distinguishable by the change in character of the gamma ray curve. The top of the unit is sharp with the overlying Namur Sandstone / Adori Sandstone showing a clean sand signature (consistent low API values) indicative of braided or high energy meandering fluvial deposits. The boundary between Unit L3 and the sediments above is also characterised by an abrupt increase in the sonic curve due to the presence of cemented clean sandstones and the absence of coals.

As mentioned previously my division of the Birkhead Formation is not related by lithostratigraphy but by sequence stratigraphy. Thus there is an overlap of units L1, L2 and L3 with that of P1, P2 and P3 of Paton (1986). Unit L2 generally corresponds with unit P1 and part of unit P2, L3 may also contain some of unit P2 and all of P3. The variation of lithologies from well to well means that unit P3 may be absent from those wells.

5.5 Sequence Stratigraphy of the Birkhead Formation, Gidgealpa south dome

The top Hutton Sandstone and Birkhead Formation at the Gidgealpa south dome represents a complete stratigraphic sequence. The formation of systems tracts in the area is similar to the regional interpretation of the Eromanga Basin. Recapping; the Hutton Sandstone probably represents deposition in a highstand systems tract where sediment accommodation is low depositing predominantly sandstones within a braided fluvial environment. With tectonic activity and regional tilting, negative accommodation and thus fluvial incision occurred into the top of the Hutton Sandstone throughout the south and south-eastern parts of the Eromanga Basin. This incision also occurred at the Gidgealpa south dome, probably due to continued uplift in the area, and was noticed from 3D seismic over the area by Boult (1996). Thickness variations

over the south dome are therefore attributed to incision by rivers and the subsequent formation of palaeo-valleys. Figure **90** is a 3D seismic section showing erosion and the formation of a palaeo-valley, indicated by arrows showing seismic truncation. The thickness map in figure **90** represents the magnitude of incision into the Hutton Sandstone. And was calculated between the top Birkhead Formation maximum pick and the top Hutton Sandstone maximum pick.

At the peak of the lowstand systems tract (termination of incision), the south dome sediments began to fill the valleys. The end of incision is marked by the presence of an intraformational conglomerate that was probably sourced locally from the interfluves (see figure **30**, page 56) forming a palaeoslope wash. The sediments above the erosional surface consists predominantly of fine to medium grained quartzose sandstone that increase in shale or siltstone interbeds up-section. This is in contrast with the sandstones below the erosional surface which consist of medium to coarse, poorly sorted quartzose sandstones. Sediments above the erosional surface in the lowstand systems tract are interpreted to have been deposited in a high energy braided to anastomosing fluvial environment. As fluvial accommodation increased towards the end of the systems tract sediment bypass decreased causing a concomitant increase in the number of fine grained interbeds.

While the erosional surface at the Gidgealpa south dome can be seen on seismic and in the Gidgealpa 17 core, it is very difficult to detect on well logs since the sediments above and below the erosional surface show a similar gamma ray and sonic signature. However on closer inspection, the seismic can greatly aid in the detection of the erosional surface on wireline logs. In most wells this surface shows up as a decrease in the sonic value (decrease in the travel time) within the rock and a corresponding low gamma ray reading. This signature was first noticed from core in Gidgealpa 17 where the intraformational conglomerate corresponds relatively closely to the top Hutton Sandstone maximum pick seismic reflector and has also been noted in other

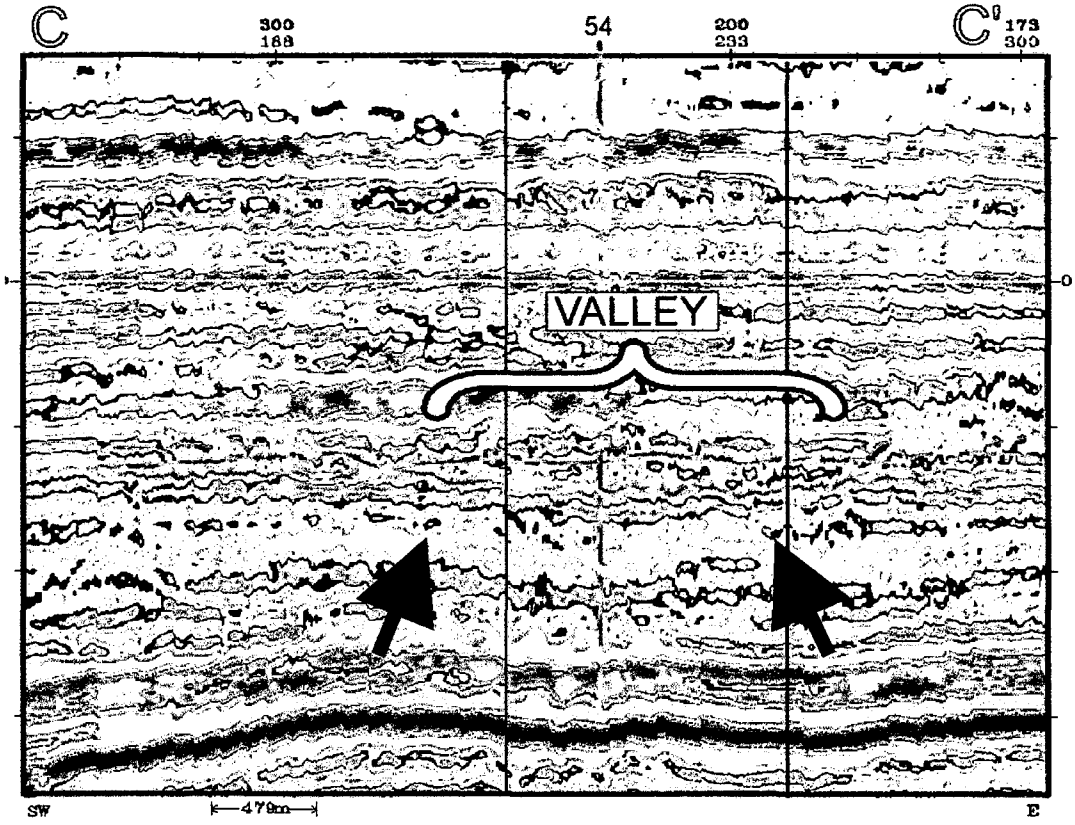

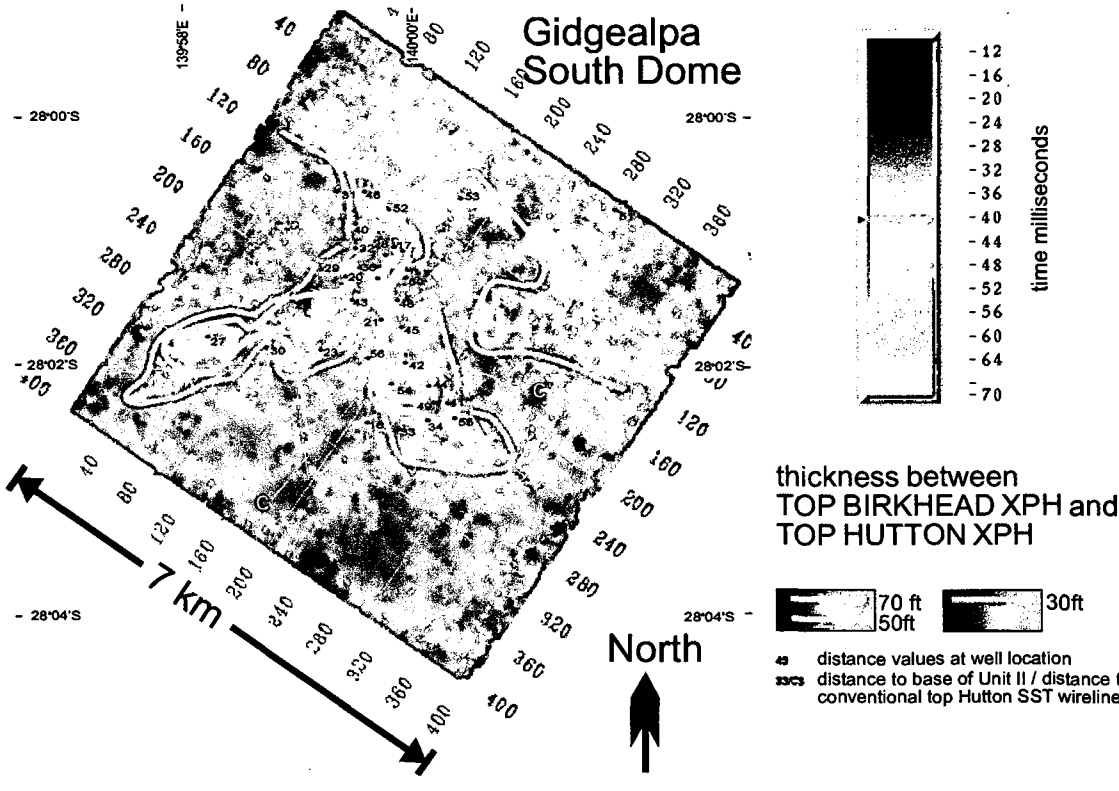

Figure 90: Top: Seismic section C-C' showing reflector truncation indicated by the arrows. The truncation is caused by the erosion of channels at the Gidgealpa south dome. Bottom: Plan view of Gidgealpa south dome showing the extent of channel erosion (After Boult, 1996).

wells in the area. This characteristic sonic spike can be seen in Gidgealpa 29, 20, 36, and 50 and in various other wells in the Gidgealpa south dome area.

Figures **91 - 94** show the sequence stratigraphy over the Gidgealpa south dome with the corrugated lines representing sequence boundaries (or erosion) and the straight lines representing conformable surfaces separating systems tracts. Thus the yellow section is the Lowstand systems tract which was identified by using seismic data and the characteristic electric log data. This section is overlain by the transgressive surface separating it from the transgressive systems tract which is shaded grey. The transgressive systems tract is bounded above by the maximum flooding surface, separating it from the orange shaded highstand systems tract that is subsequently capped by the sequence boundary separating the Birkhead Formation from the Namur Sandstone. In all four figures the maximum flooding surface is used as the datum.

With continued base level rise over the Gidgealpa south dome there was some point in time where the rate of creation of accommodation space out-stripped sediment input and thus the area was flooded. The flooding caused the formation of the transgressive surface which marked the end of the lowstand systems tract and beginning of the transgressive systems tract. Identification of the surface can be seen in cores from Gidgealpa 29 (6063') (appendix **2** and **3**), where lacustrine sediments lie directly on top of braided fluvial sands. The transgressive surface can also be identified by the presence of a hard-ground which is present in Gidgealpa 32 (appendix **1** (6007')). The flooding of the area caused the formation of lacustrine conditions with most sediments consisting of siltstones and fine to very fine sandstone lenses. The onset of lacustrine conditions is indicated as the high gamma ray signature in most wells, directly above the transgressive surface in figures **91 - 94**. Dipmeter data (section **4.7**) indicates that this break in deposition of coarse clastics also represents a change in sediment sourcing from southerly derived, cratonic, coarse grained, quartzose sandstones to easterly derived fine to very fine

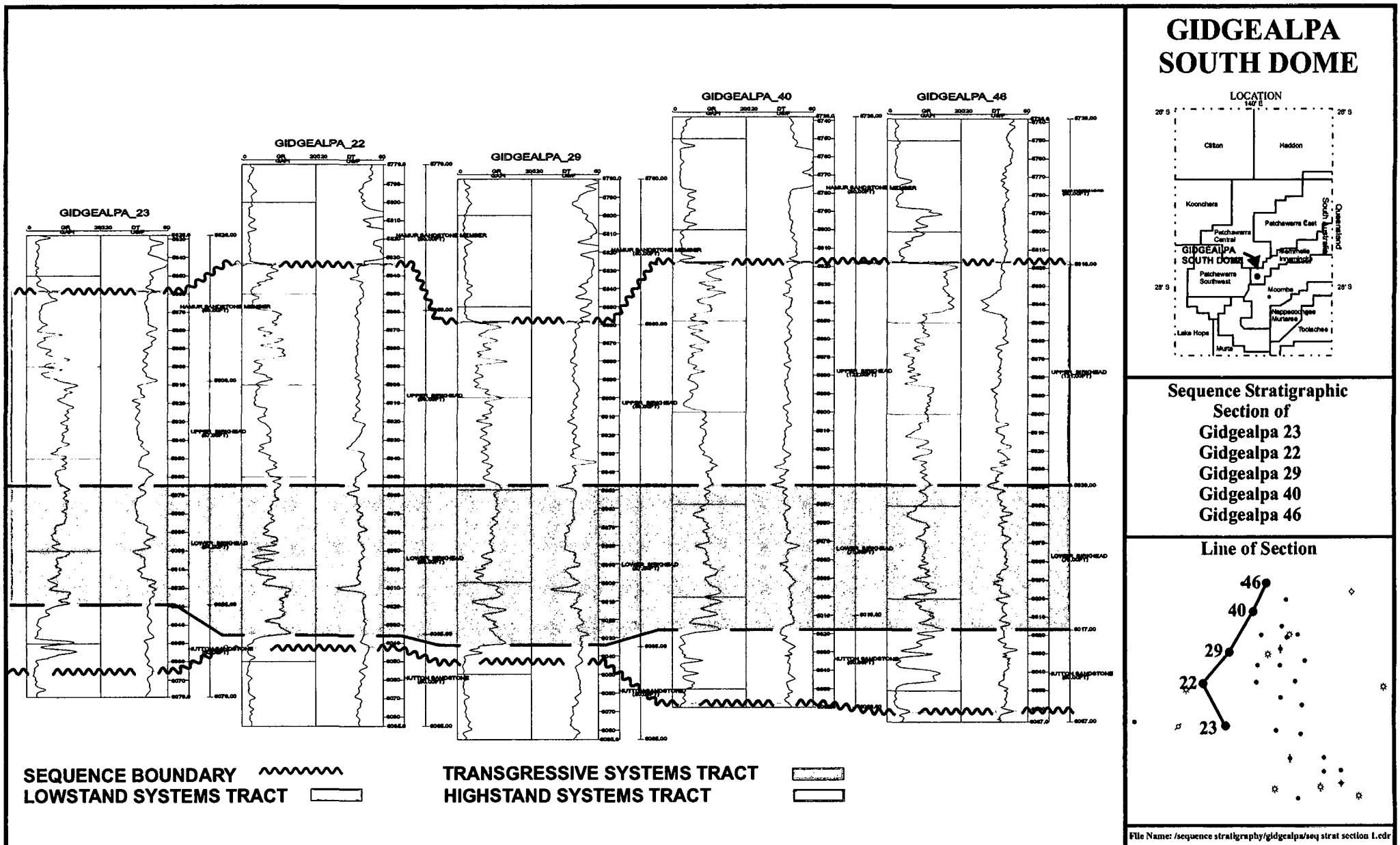

Figure 91: Section over the Gidgealpa south dome indicating sequence stratigraphic units. Section correlated using the MFS as the datum.

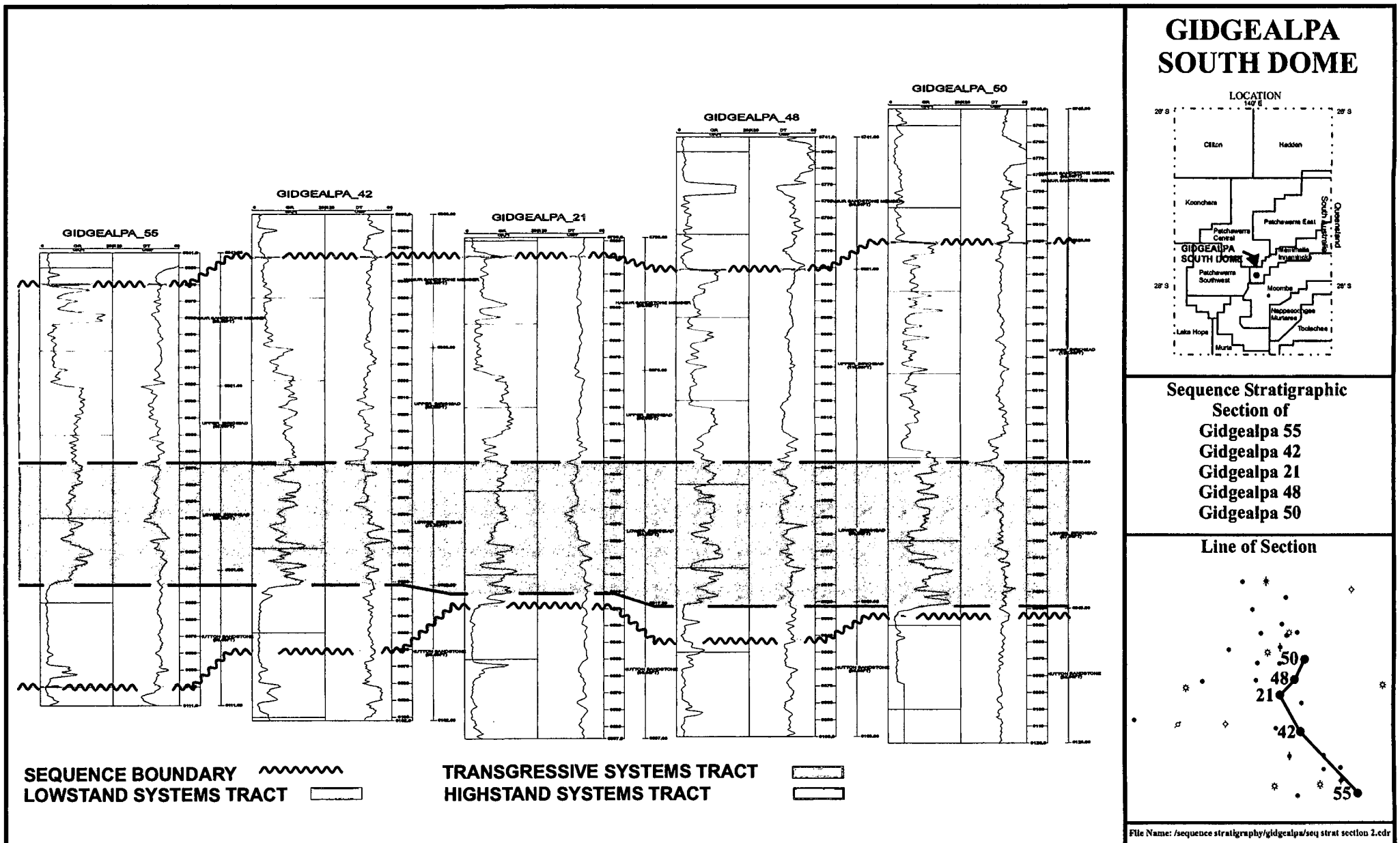

Figure 92: Section over the Gidgealpa south dome indicating sequence stratigraphic units. Section correlated using the MFS as the datum.

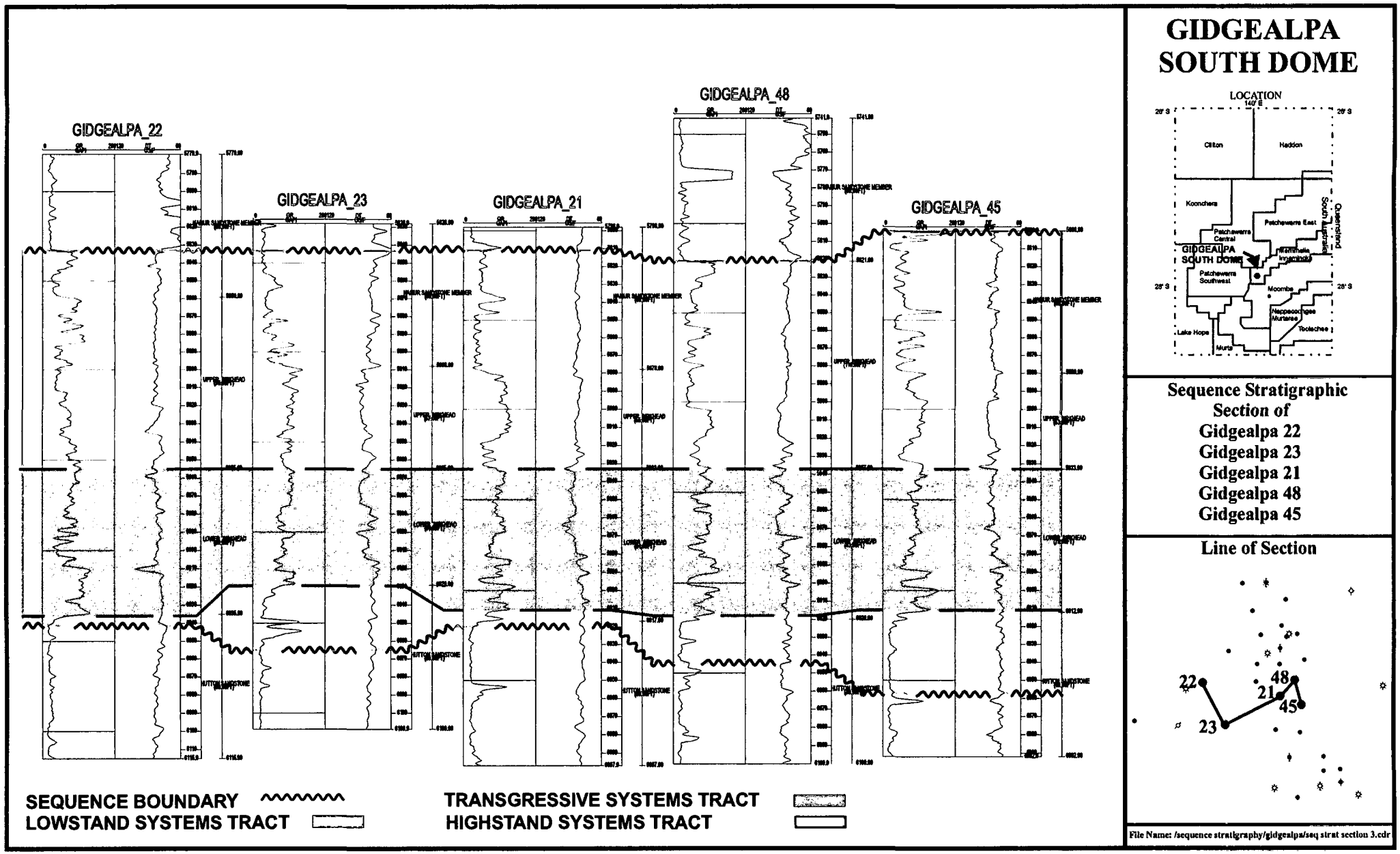

Figure 93: Section over the Gidgealpa south dome indicating sequence stratigraphic units. Section correlated using the MFS as the datum.

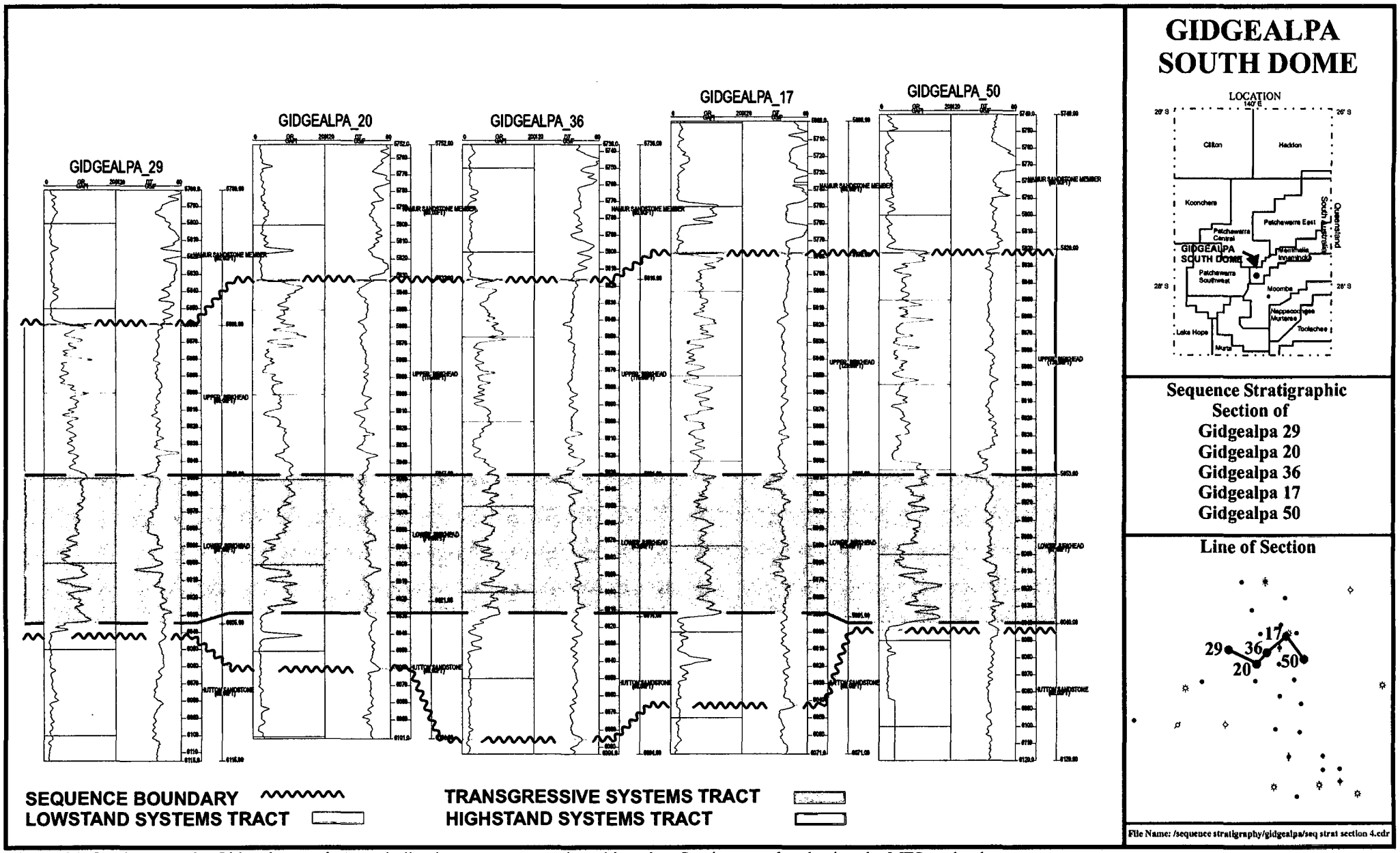

Figure 94: Section over the Gidgealpa south dome indicating sequence stratigraphic units. Section correlated using the MFS as the datum.

grained quartzose and eventually lithic labile volcanic sandstones due to tectonic activity within the Eromanga Basin at that time.

The transgressive systems tract at Gidgealpa basically consists of a coarsening or shoaling up sequence followed by a fining upwards sequence which represents two cycles of deltaic deposition. Before I proceed any further in the description of this systems tract I think it is important to define what a 'parasequence' is since studies of modern coastal depositional environments indicate packages of sediment seem to be deposited in regressive - transgressive cycles (Allen, 1994). The identification of a parasequence is important since these packages form the stratigraphic basis for the subdivision, correlation and mapping of individual sandstone reservoirs in deltaic sandstones (Allen, 1996). Van Wagoner et. al (1990) defined a parasequence as:

> *"relatively conformable successions of genetically related beds or bedsets bounded by marine flooding surfaces and their correlative surfaces."*

It is generally thought that most parasequences can form over several thousand to tens of thousands of years with the regressive phase of deposition occurring in as little as a few thousand years. In this time a deltaic shoreline can migrate tens or hundreds of kilometres (Allen 1994). The Gidgealpa south dome is no exception with the delta forming a deposit only approximately 30 feet (10 metres thick). This is further evidence that the delta prograded onto a relatively low angle ramp where water depth was shallow since delta deposits will only fill the accommodation space available (Allen 1994). A number of parasequences exist within the deltaic cycle at the Gidgealpa south dome and are described in detail in the following section (section **5.5.1**).

It follows that the transgressive systems tract at the Gidgealpa south dome was probably deposited in a relatively short period of time with common soft

sediment deformation, testament to the rapid progradation of the deltaic sediments. With the relatively slow rise in the base level, sediments were able to fill the water column up to the surface where a coastal plain developed. After this point any sediments that accumulate were a result of a rise in relative base level. If the relative rise was slow then sediments would tend to aggrade, or where base level is at a relative standstill sediments will avulse over the coastal plain (Allen 1994). Gidgealpa 29 is a an example where this occurs. At some point, in the case of the deltaic sediments at the Gidgealpa south dome, the rising base level outweighed sediment input and caused a transgression that subsequently drowned the lake margin area.

The drowning of the lake margin is a result of a decrease in sediment supply from the east while base level continued to rise. The increasing water depth and lack of sediments caused the water column to attain its maximum depth, where the subsequent maximum flooding surface formed. It was not until tectonics, which again caused movement within the Eromanga Basin, became active and sediments were again sourced from the south that the water depth at the Gidgealpa south dome began to decrease. The beginning of this decrease in water depth or end of the maximum flooding surface marks the beginning of the highstand systems tract.

Not a great deal is known about the highstand systems tract sediments at the Gidgealpa south dome (or in any other part of the Eromanga Basin for that matter) since study of the section has been scarce due to its low hydrocarbon trap potential. Although shows have been found in these sediments the high sand to shale ratio means that the formation of hydrocarbon traps are rare or absent. The low economic value of this systems tract also means that core is very rare and thus interpretation is based on wireline log evaluation.

The highstand systems tract ideally consists of a steadily decreasing gamma ray signature in wells representing an increase in grain size and shallowing of water depth over the area. The shallowing up sequence is due to an increasing

rate of sedimentation by progradation due to a decrease in the rate of base level rise. Therefore at this time the Gidgealpa south dome area experienced a relative base level fall. Towards the top of the highstand systems tract sediments become more sand prone due to the progradation of the sediments (Emery and Myers 1996). Ideal examples of this characteristic coarsening up sequence can be seen in Gidgealpa 29, Gidgealpa 22 (figure **91**, page 202), and Gidgealpa 20 (figure **93**, page 204). What can also be seen in these wells is the serrated, coarsening up parasequences of the highstand systems tract gamma ray curve. If we take Gidgealpa 20 in figure **95** as an example, from the gamma ray logs three prograding, coarsening up, parasequences can be seen.

The high overall percentage of sand to silts in the area is due to the closeness of the Gidgealpa south dome to the source at the southern end of the basin. The high variation in gamma ray signatures between wells, I believe is due to the high lateral variation characteristic of fluvial sediments which deposited the sediments during the highstand systems tract.

At some stage during the highstand systems tract the ratio of base level rise to sediment flux became so low that negative accommodation space developed. This scenario is what marks the top of the Highstand Systems tract at the Gidgealpa south dome and is represented by a sequence boundary. The sequence boundary can be easily identified on most wells (see figures **91 - 94**) and is marked by a sharp change in the gamma ray response, from median API values with a serrated character to a constant, low API, cylindrical signature. The sonic tool also shows a sharp change in character from a relativly smooth reading of approximately 100 μs/f (microseconds per foot) to an average value of 90 μs/f with a much higher variation in values over short distances. The log response above the sequence boundary is characteristic of braided fluvial sediments of the Namur Sandstone deposited as part of a lowstand systems tract. The higher sonic speeds of the Namur Sandstone as compared to the Hutton Sandstone is due to extensive calcite precipitation.

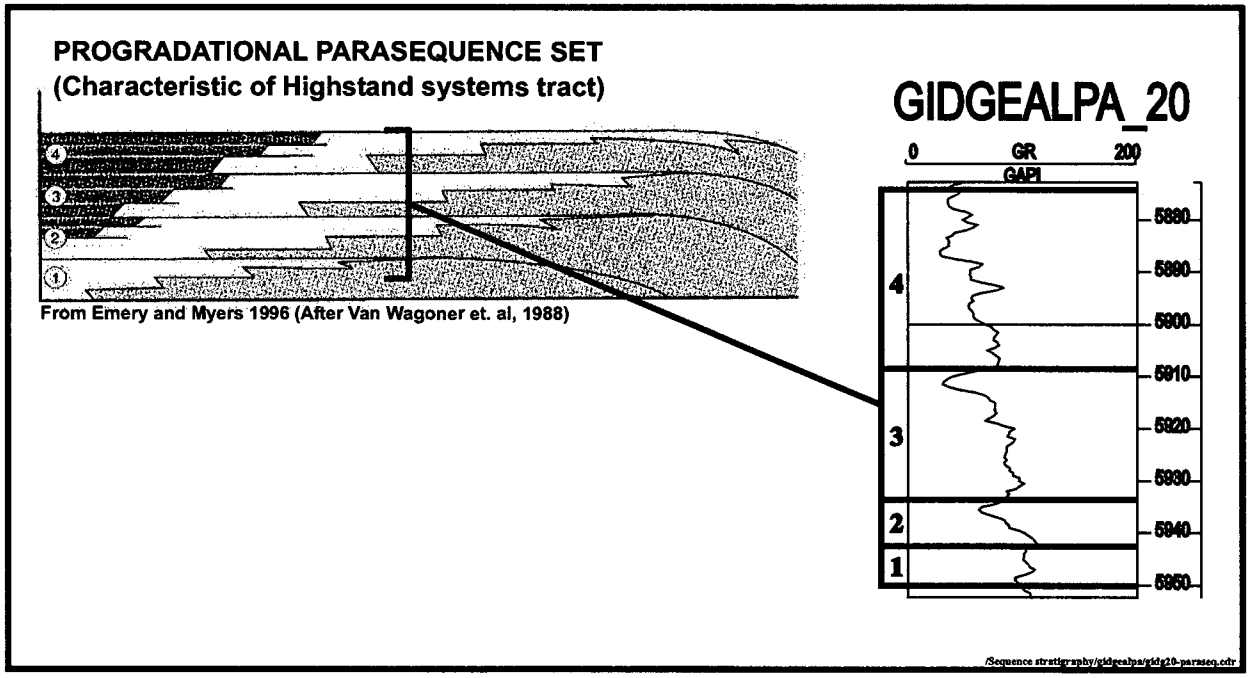

Figure 95: Characteristic coarsening up parasequences in Gidgealpa 20 highstand systems tract sediments caused by the prograding of sediments.

5.5.1 Sequence Stratigraphy of the Delta sequence

In section **5.5** it was briefly mentioned that the transgressive systems tract sediments at the Gidgealpa south dome consists of two delta cycles. Within these depositional cycles there are a number of parasequences or prograding packages of sediments that cause complexities in the reservoir geometry since the sands have a limited extent and discontinuous nature. To determine reservoir structure it is necessary to accurately correlate reservoirs over the field to evaluate hydrocarbon reserves and production strategies (Allen and Mercier, 1988). Literature on detailed sequence stratigraphy of deltas is rare; indeed I have only found several references pertaining to this topic. For this reason the following analysis has been adopted and referenced from the previous work of Allen and Mercier, (1988) and Allen (1994) unless otherwise stated.

In section **4** sedimentological analysis was carried out on the Gidgealpa south dome. In this section the sedimentology will be complemented by a stratigraphic analysis to delineate the Gidgealpa south dome Birkhead Formation reservoir. The Gidgealpa south dome Birkhead reservoir, on discovery, was interpreted as a fluvial channel complex with splay and levee facies recognisable. However, using sedimentological, wireline, dipmeter and neodymium model ages I have re-interpreted the area to be fluvial-deltaic. From this data a model of a river dominated delta was applied to delineate sand trends.

Before I continue with a stratigraphic interpretation of the Gidgealpa south dome, I will describe the sequence stratigraphic components of a delta system. These components (or discontinuity boundaries that mark the ends of the packages) are the key to successful sequence stratigraphic analysis of a delta complex when correlating different wells and cores with each other over a

field. A complete deltaic cycle is identified by three major discontinuity surfaces, these surfaces are displayed on figure **96** and consist of the 'delta progradation surface', the 'delta emergence surface' and the 'delta flooding surface'. These surfaces can also be identified at the Gidgealpa south dome from Gidgealpa 29 log and core data in figure **97**.

Delta Progradation Surface

This surface marks the lowest discontinuity of a delta cycle and start of a regressive deltaic sequence (figure **96**). This is the surface on which the delta progrades and in the case of the Gidgealpa south dome, corresponds to the regional transgressive surface.

Delta Emergence Surface

The emergence surface consists of an organic and rooted floodplain shale or coal which indicates the delta sequence has reached lake level and is thus sub-aerially exposed (figure **96**). This surface is produced at the end of a shallowing upward deposit and is usually easily identified on logs by its high GR value. For sediments to be deposited on top of this surface the deltaic sequence must either subside or the lake must rise to allow the influx of more sediments. In the case where river input is balanced by subsidence, fluvial deposits can accumulate on top of the emergence surface, indicating the transition from a prograding to aggradating delta. An example of aggradation above the emergence surface can be seen in Gidgealpa 29 (figure **97**); in this case aggradation is represented by interbedded sands and silts which culminates at the flooding surface.

Delta Flooding Surface

This surface represents drowning of the delta sequence and the end of the delta cycle (figure **96**). It will form if the rate of sediment supply is unable to fill the accommodation space produced by a rising base level or increased subsidence rate. In the case of Gidgealpa, the delta flooding surface is non-erosional since wave energy was low to nil and lagoon / bay muds were

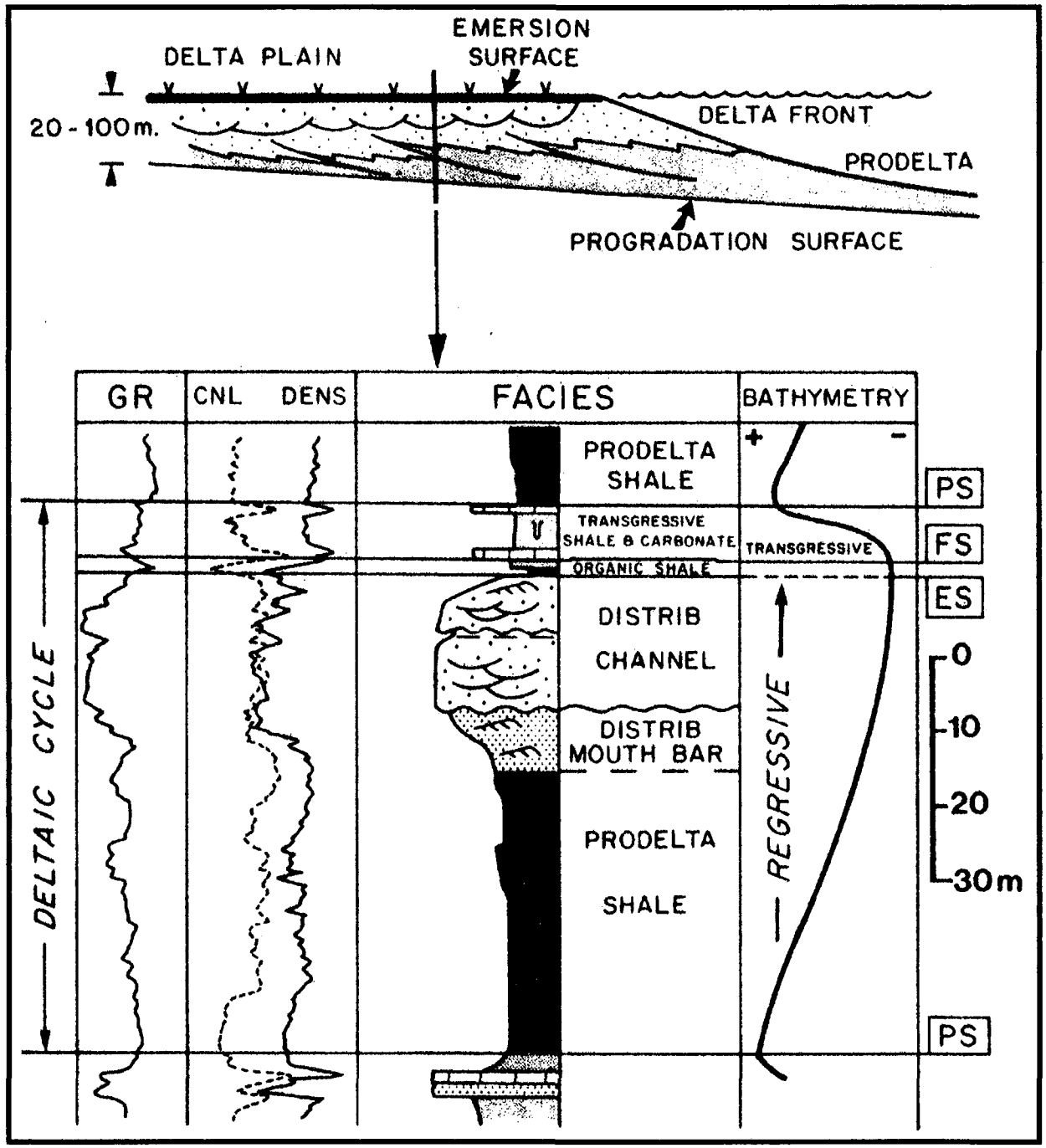

Figure 96: A complete deltaic cycle showing the progradation surface (PS) emersion surface (ES) and flooding surface (FS) (From Allen and Mercier, 1988).

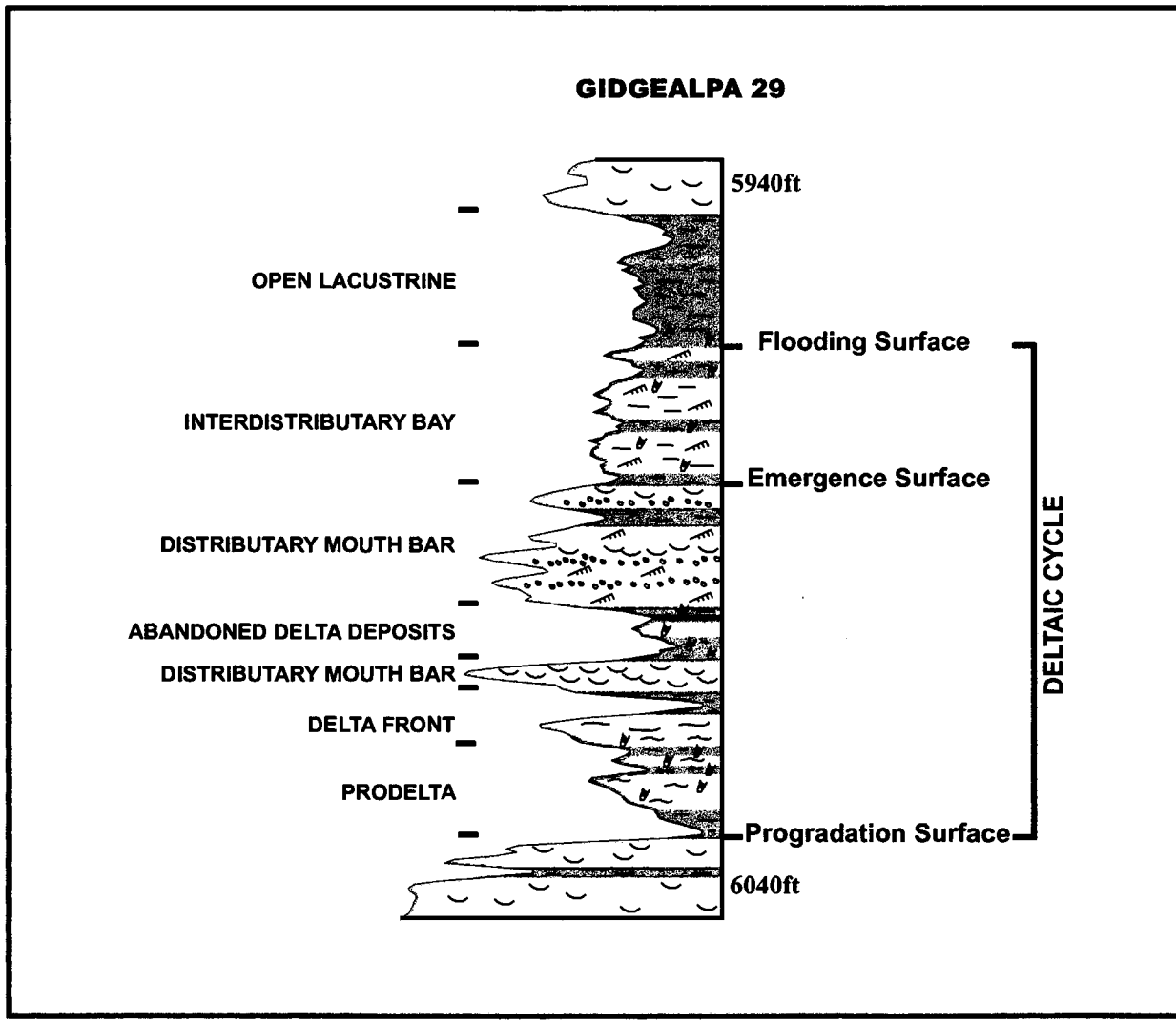

Figure 97: Gamma ray signature and core interpretation of the Gidgealpa 29 deltaic sequenceshowing the progradation, emergence and flooding surfaces.

overlain by lacustrine shales. Above this surface a transgressive lacustrine sequence was deposited (figure **97**). This surface is only representative of a local event at Gidgealpa and should not be confused with the maximum flooding surface which is the regional surface throughout the Birkhead Formation.

These surfaces are useful in the correlation of sediments and facies on a field scale. While the surfaces are not true time lines, on the scale of one to two kilometres they can be considered as local chronostratigraphic markers. However at the Gidgealpa south dome lack of core data and the subsequent difficulty of picking the surfaces from electric log data means that I have correlated on the regional MFS and used the deltaic surfaces as a secondary tool to check correlations hung on the MFS. The use of this surface has allowed for excellent correlation results when a fluvial dominated delta model is applied.

The isolated nature of the sandstones at the Gidgealpa south dome is attributed to the relatively rapid subsidence rate compared to sediment influx. The rapid subsidence in the area meant that sediments did not bypass the area but instead were deposited forming an overall low percentage of sands to silts. Therefore, instead of the sediments prograding they will aggrade due to the rapid production of the accommodation space. Thus, the larger the difference between sediment flux and the increase in accommodation, the lower the net to gross sand ratio and channel interconnections within a stratigraphic interval. Figure **98** illustrates the variations in the subsidence to sediment influx ratio and the associated sand to silt ratio or degree of sand channel amalgamation. Figure **98**B and C represents the conditions at the Gidgealpa south dome, forming the isolated sand packages or delta lobes.

Due to the low sand to silt ratio at the Gidgealpa south dome it is highly likely that the sand packages within the deltaic sequence are partially or totally isolated. To map these sand packages all of the wells over the field were used

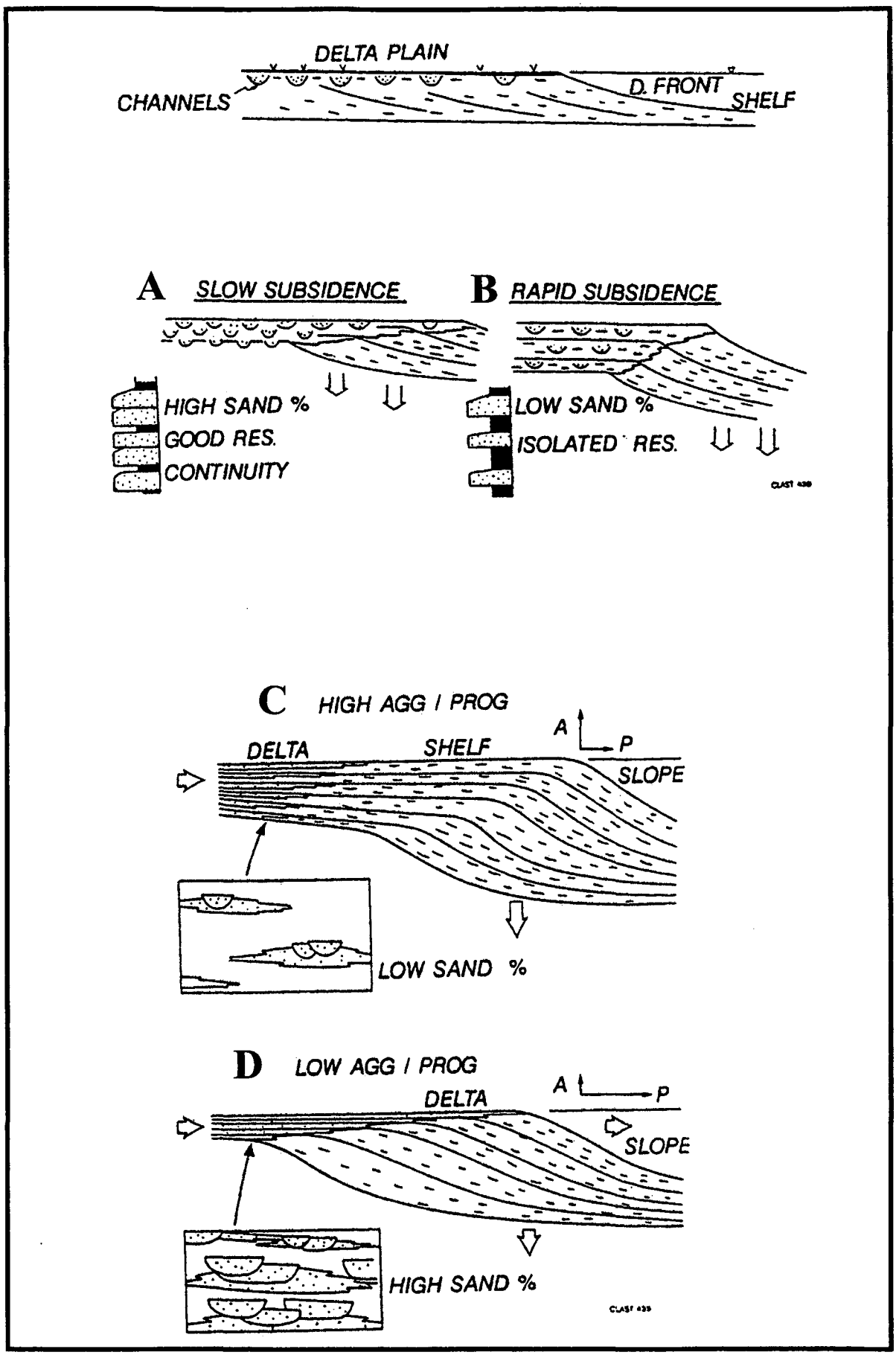

Figure 98: Effects of varing accommodation rates on coastal and shelf sediment patterns and sand/shale ratio (From Allen, 1994).

to produce wireline log correlations. Figure **99** is one such example where the deltaic sands can be correlated between the wells. The figure is orientated roughly perpendicular to the direction of sand progradation and indicates the overall coarsening and then fining upwards cycle of the transgressive systems tract and the various isolated sand packages that make up the Gidgealpa south dome delta complex. Core data has also been used in the figure to aid in the stratigraphic correlation of the sands.

The stratigraphic sections indicate that the two deltaic cycles at the Gidgealpa south dome consist of 5 prograding - aggrading sand packages. The sand packages have been interpreted to be deposited as a result of prograding to aggrading sediments occurring as pulses and delta lobe switching. Figure **100** illustrates the relative position and chronological order of delta development at the Gidgealpa south dome. Production data has been used to confirm the connective properties of the sand packages and is discussed in section **8.2.6.2**

5.6 Summary of the Sequence stratigraphy at the Gidgealpa south dome

As mentioned earlier the morphology of the delta system changes during its development. The following section is a summary of the sequence stratigraphy of the basal Birkhead sands at the Gidgealpa south dome. Figure **101** accompanies the summary by showing delta development at various stages of its history.

The relatively large accommodation space at the Gidgealpa south dome early in the delta development allowed the clean planar and trough crossbedded fluvial sediments to prograde rapidly and be deposited in a relatively unrestricted manner. Initially, the lack of restrictive barriers such as levees meant that an elongate bird-foot delta formed, with the deltaic sands depositing as sheets (figure **101**A). The high progradation rate is due to the fluvially dominated nature of the delta. During this time, the formation of smaller, sub-delta lobes or crevasse splays also occurred, depositing sands into

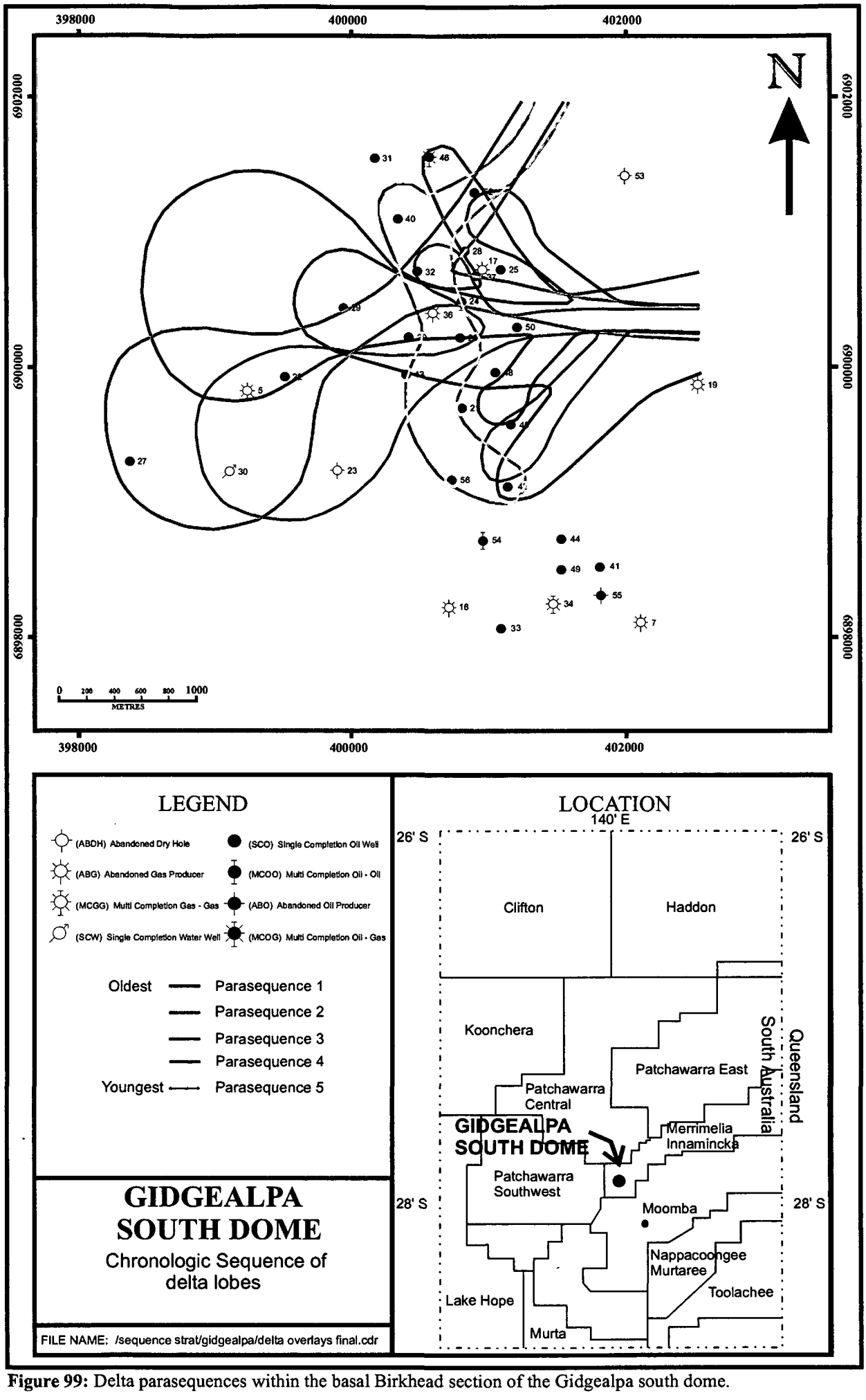

Figure 99: Delta parasequences within the basal Birkhead section of the Gidgealpa south dome.

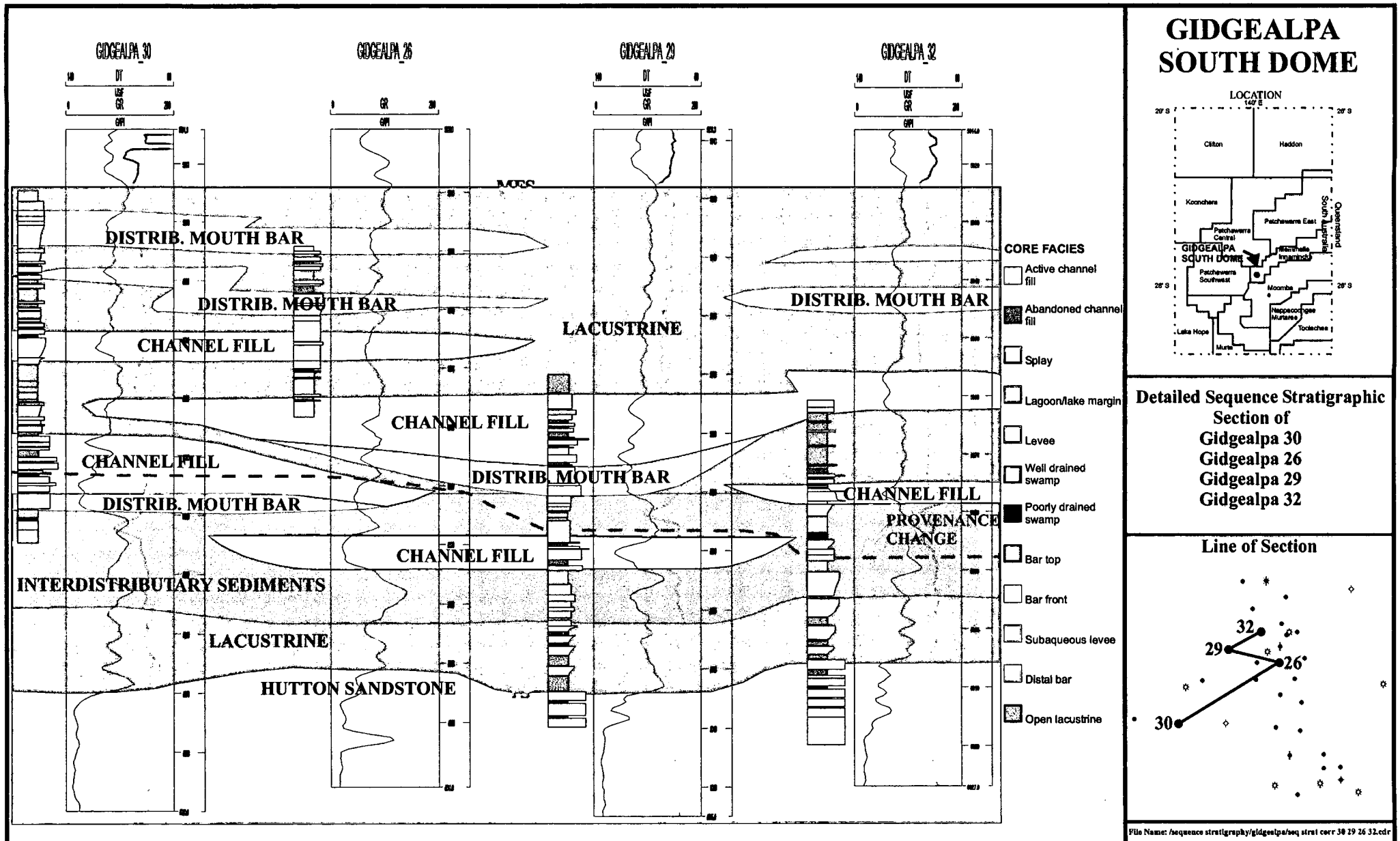

Figure 100: Sequence stratigraphic cross section through the Gidgealpa south dome showing the overall coarsening the fining up sequence in the transgressive systems tract. Note also the isolated nature of the channel sands.

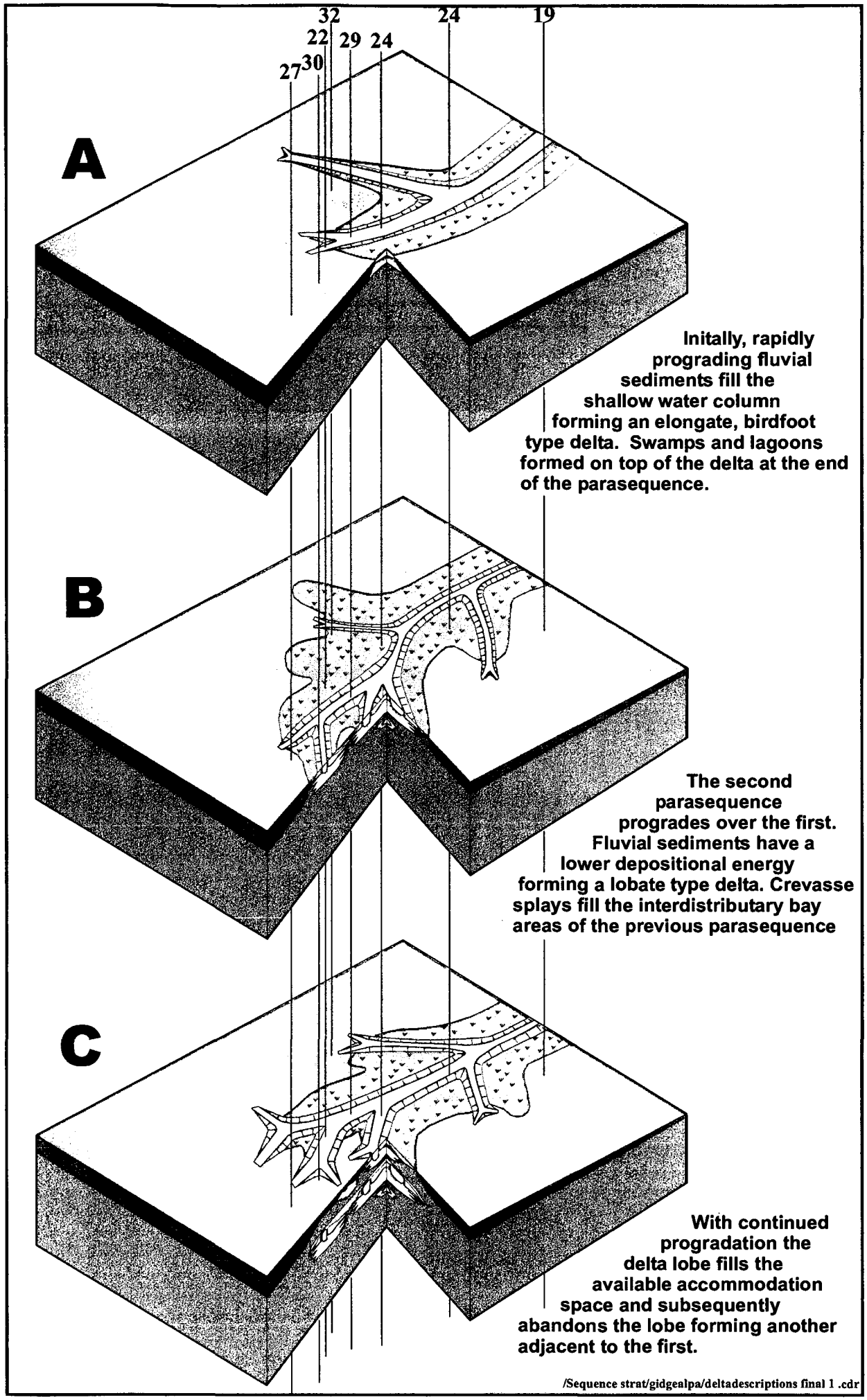

Figure 101A: Various stages of delta development at the Gidgealpa south dome.

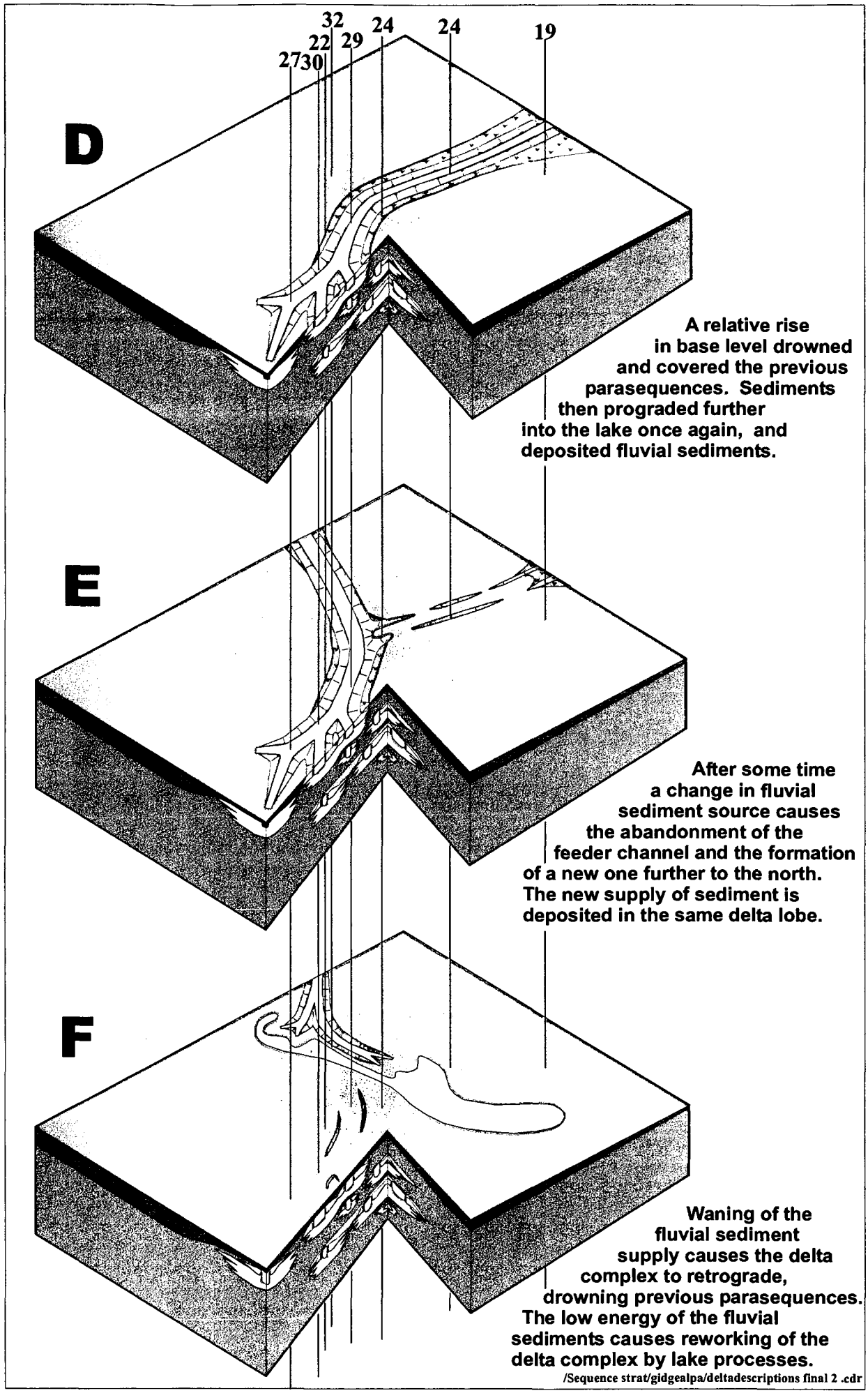

Figure 101B: Various stages of delta development at the Gidgealpa south dome (Cont.).

Lake Birkhead. The deposition of this deltaic sheet sand is the first parasequence to be deposited within the area. The relatively sharp base and top of this sand package seen in wells such as Gidgealpa 21, 48 and 50 (see figure **94**, page 205) is testimony to the rapid deposition. The prograding nature of the crevasse splay delta sub-lobe to the north of the main channel is illustrated in Gidgealpa 46 (see figure **93**, page 204) by a coarsening up sequence.

With continued deposition the sands prograded over the Gidgealpa south dome and subaerial levees developed on the edges of the distributary channel due to clay consolidating the channel banks. This consolidation also allowed the distributary channel to become restricted and maintain a fixed position with time (Orton and Reading, 1993). The continued compaction and dewatering of the underlying shales and silts may have also helped in maintaining the distributary channels position. The formation of levees and subsequent build up of the distributary channel means that the interdistributary areas were able to form shallow lakes.

At the time when the levees were forming, the distributary channel avulsed, bypassing the Gidgealpa 29 area and instead formed a second parasequence, depositing sands in the Gidgealpa 30 area (figure **101**B). The lateral shift of the delta lobe was due to the build up of sediments and the distributary system shifting to follow a steeper hydraulic gradient (Allen and Mercier, 1988). While this bypassing occurred to the west, further to the east the distributary system maintained the same position. Gamma ray logs of Gidgealpa 26 and 50 show the maintained presence of sand while in comparison to Gidgealpa 29 which shows a period of fine grained sediment deposition.

The lack of sediments in the now-abandoned Gidgealpa 29 area caused the deltaic sands to become flooded. With this increase in water depth lagoons, marshes and swamps formed (see appendix **2** and **3**, Gidgealpa 29 (6030'-6038') and Gidgealpa 32 (5979'8"-5986'6)). The formation of these low

energy deposits is due to a lack of water activity such as tides or waves which would have otherwise eroded these sediments and formed transgressive barriers or beaches (Allen and Mercier 1988, Allen 1994). The relatively slow subsidence rate related to the build up of the fine grained sediments also allowed the formation of the swamps and marshes. Similar depositional conditions were seen by Wright (1985) in the Mississippi Delta with the formation of both well drained and poorly drained swamps as in the Gidgealpa south dome, however slightly higher wave energy means that some sediments were reworked and resorted forming sandy lenticular laminations and cut and fill structures.

With the stabilisation of the distributary channel banks the morphology of the delta system changed. Within this parasequence the delta mouth bar became more lobate in character due to sediments exiting the river mouth from a relatively narrow opening (Coleman and Wright 1975). The river effluent was then directed through a series of bifurcating channels that distributed the sediments over the delta mouth bar.

The end of the second parasequence was again caused by the distributary channel avulsing since the area around Gidgealpa 30 had built up to a height where the channel could not maintain an adequate gradient for sediments to be transported and deposited. The sediments entering the Gidgealpa south dome were mixed load and sandy and the channel breach would have been narrow with the sediments prograding almost from a point source (Orton and Reading 1993). Thus a switch of sedimentary environments occurred with the Gidgealpa 30 area consisting of waning mouth bar deposits, eventually depositing open lacustrine sediments from delta lobe abandonment (figure **101**C). Alternatively, the Gidgealpa 29 area deposited distributary mouth bar sands on top of former low energy deposits.

Allen and Mercier (1988) stated that after some time the path of river sedimentation may shift back to the previous site of delta deposition and form

another delta lobe on top of the transgressive lacustrine deposits which cover the previously abandoned lobe. This is indeed what happened at the Gidgealpa south dome with the deposition of a third lobe that included Gidgealpa 20, 22 and 29. The delta lobe switch from the second to third parasequence and occurred with only a slight rise in base level since the position relative to the lake edge and the size of the successive lobes are similar.

Time passed with the deposition of the third parasequence and again sediment deposition in the distributary mouth bar waned marking the position of the delta emergence surface. However, as previously had occurred, the decrease in sediment input at this stage was not due to delta lobe switching but a decrease in the sediment flux entering the Gidgealpa south dome area and the subsequent abandonment of the distributary channel. This fact is reflected in the gamma ray log data of the wells (for example Gidgealpa 26, 29, and 50) which previously showed distributary channel deposits were then depositing low energy interdistributary bay type sediments. The bypass of sediments not only occurred where the distributary channel had formally been active, gamma ray logs from other wells also showed the absence of distributary channels over the entire area.

While the fluvial sediments were absent, the Gidgealpa south dome area consisted of a shallow lacustrine open bay with the deposition of mainly laminated siltstones which were subsequently bioturbated. The siltstones are interbedded with sandstone lenses formed either from deposition from a distal source to the east or sediment reworking which would have occasionally occurred from agitation of the lake waters due to storm or wind activity (see appendix 1 Gidgealpa 26. (5969' - 5977')).

Higher energy fluvial sediment bypass probably occurred as a result of the sediments being deposited laterally, some distance away from the Gidgealpa south dome along the lake edge. One possibility is that sediments were

deposited in the Gidgealpa north dome since gamma ray logs of wells from the area show a similar signature to wells in the south dome.

Again, after some time, sediment influx into the Gidgealpa south dome occurred with the deposition of the fourth parasequence (figure **101**D). This sediment package in the transgressive systems tract is totally isolated from the other parasequences since a sheet of lacustrine sediments totally blankets the former deltaic sediments. Sediments first re-entering the Gidgealpa south dome were probably as a result of re-activation of an abandoned channel to the east causing distributary channel sediments to be deposited in a similar position to the former channel. However, the present distributary channel prograded further west than the previous channel since the distributary mouth bar sediments had filled the water column up to, or close to lake level. Therefore, the then-current distributary mouth bar sediments were subsequently deposited in the Gidgealpa 27 area.

At some stage during the deposition of this parasequence the source direction of fluvial sediments changed from the east to a more north-east origin. This change can be noted from dipmeter data as well as the slight displacement in depths of distributary channels seen from wireline logs (figure **101**E). The change was probably a result of channel breaching of the main fluvial system further north than the previous and the subsequent decrease in sediment input from the east.

With an increasing rate of base level rise towards the end of deltaic deposition, a decrease in sediment supply relative to base level rise caused the deltaic sediments to retrograde. The associated fluvial system was pushed further to the east, making the Gidgealpa south dome area more distal. The final sand package of the transgressive systems tract that was deposited in the area was a result of lake processes dominating over the fluvial-deltaic processes producing an elongate sand body which was orientated parallel to the lakes edge (figure **101**F). The termination of the second deltaic cycle marks both the

emergence surface and flooding surface since base level continued to rise after the deltaic sequence had attained lake level. The base level continued to rise and subsequently obtained a sufficient height to drown the deltaic sediments. This rise caused the fluvial system from the east to become more distal and flooded and the maximum flooding surface or point of maximum transgression was obtained marking the change from the transgressive systems tract to the highstand systems tract.

6 Petrology

The stratigraphic nature of the Gidgealpa south dome, Birkhead reservoir, means that delineation of the reservoir can be difficult. Coupled with this are the effects of diagenetic overprinting and reservoir rock composition that complicates interpretation even further since these parameters ultimately effect permeability and porosity within a reservoir. This section attempts to characterise the physical reservoir characteristics of diagenesis and sandstone composition and with a greater understanding will aid in the identification of reservoir and non-reservoir sandstones.

6.1 Methods

I selected a number of samples from the 5 Gidgealpa cores (see figure **70** page 158) classing the samples with respect to their lithofacies affiliation (table **6**). Three samples were selected from each of the major reservoir lithofacies (lithofacies Sh, Sm, Sp and St) for inspection. Seven samples were selected from lithofacies Sr since it is the most abundant, reservoir facies within the cored intervals. Lithofacies Sr also shows a wide variation in character. Four samples were also selected from lithofacies Sd due to its highly variable nature and may have limited reservoir qualities for certain samples.

I described the selected samples in hand specimen before thin sections were produced (descriptions of both hand specimens and thin sections can be seen in appendix **6**). The samples were then sent to Pontifex and Associates Pty. Ltd. where they were impregnated with blue-dyed araldite to enhance the detection of porosity under the microscope. The slides were then polished for later use with the cathodoluminescence microscope . After receiving the thin sections, I examined each in turn determining the mineralogy from 300 point counts and then classifying the rock using Folk (1980) classification of clastics

Well Depth (Ft)	Gidgealpa 30 6042.42	Gidgealpa 29 6055.50	Gidgealpa 29 6045.75	Gidgealpa 32 5992.17	Gidgealpa 32 5989.75	Gidgealpa 31 5997.25	Gidgealpa 31 5993.33	Gidgealpa 31 5974.58	Gidgealpa 29 6038.08	Gidgealpa 29 6025.33	Gidgealpa 30 6032.50	Gidgealpa 31 5981.83
Facies **Lithology** **SEM** **CL** **Mercury Inject.**	Sd Muddy Sub-Litharenite no no no	Sd Muddy Sub-Litharenite no no no	Sd Slightly Muddy Litharenite no no no	Sd Slightly Muddy Litharenite yes yes yes	Sr Slightly Muddy Litharenite no no no	Sr Slightly Muddy Litharenite no yes no	Sr Volcanic Litharenite no no no	Sr Volcanic Litharenite yes no yes	Sr Sub-Litharenite no yes no	Sr Volcanic Litharenite no no yes	Sr Sub-Litharenite no no no	Sm Volcanic Litharenite yes yes yes
Grainsize **Sorting** **Structures**	v.Fine mod - poor bedding, cont-orted / deform	Fine - v.Fine mod partly laminated	Fine mod partly laminated	Fine - v.Fine mod whispy, horiz. bedding	v.Fine poor ripple laminated	v.Fine poor ripple laminated	Fine mod ripple laminated	v.Fine mod ripple laminated	Fine - Med poor ripple laminated	Fine mod ripple laminated	Fine mod ripple laminated	Fine - Med poor massive
Framework Gr												
Quartz	46.5	39.5	54	58.5	26	27.5	30	23.5	58.5	40.5	41	28
Feldspars	1.5	0.5	3	0.5	3	6	3	2.5	0.5	1.5	tr	3
Mica	1	4.50	2.5	1.5	1.5	1	1	0.5	tr	0.5	0.5	tr
Lithics	7.5	7	10.5	6	36.5	37	16	24.5	5	21	16	21
Accessory	tr	tr	tr	1	tr	tr	tr	tr	tr	tr	tr	tr
Matrix	2.5	45.50	19	17.5	13.5	10.5	2	3	tr	1	0.5	1
Organic matter	1	2.5	2	1	10	0.5	2	2	1	1.5	1	2
Authigenic min. and cements												
Silica	0.5	-	tr	0.5	tr	0.5	1	2	18.5	2.5	8.5	0.5
Kaolin	3	0.5	2	2	2.5	11.5	9	7	4	12.5	30.5	4
Carbonate	3.5	tr	3.5	5.5	7	4	33.5	3.5	3	7	2	40.5
Porosity												
Intergranular	-	-	tr	tr	-	-	-	-	6	3	-	-
Dissolution	tr	-	3.5	6	-	tr	2	2	3.5	9	tr	tr
Microporosity	-	tr	tr	tr	-	tr	tr	tr	tr	tr	tr	tr

Table 6: Summary of thin section descriptions of samples from the basal Birkhead Formation and top Hutton Sandstone.

Well Depth (Ft)	Gidgealpa 29 6047.33	Gidgealpa 32 6007.33	Gidgealpa 30 6037.50	Gidgealpa 26 5957.58	Gidgealpa 26 5950.50	Gidgealpa 29 6064.17	Gidgealpa 30 6029.75	Gidgealpa 32 6018.50	Gidgealpa 31 5985.83	Gidgealpa 26 5956.33	Gidgealpa 32 6015.75
Facies Lithology SEM CL Mercury Inject.	Sm Sub- Litharenite no no yes	Sm Quartz Arenite yes yes yes	Sh Quartz Arenite yes yes no	Sh Sub- Litharenite no yes yes	Sh Litharenite yes yes no	St Quartz Arenite no yes yes	St Quartz Arenite yes yes yes	St Quartz Arenite yes yes yes	Sp Litharenite yes no no	Sp Sub- Litharenite no yes yes	Sp Quartz Arenite yes yes yes
Grainsize Sorting Structures	Fine - Med poor massive	Fine - Coarse poor massive	Med - Coarse mod horizontal bedded	Fine mod horizontal bedded	Fine mod - well horizontal bedded	Med - Coarse mod - well trough cross-beds	Med - Coarse well trough cross-beds	Med - Coarse mod - poor trough cross-beds	Fine mod planar cross-beds	Fine mod - well planar cross-beds	Med - Coarse mod planar cross-beds
Framework Gr Quartz Feldspars Mica Lithics Accessory	 60 2.5 1.5 10 tr	 56.5 0.5 1 1.5 tr	 58 0.5 0.5 4.5 tr	 52 1 1 16 tr	 59.5 1 1 22.5 tr	 63 1 0.5 1 tr	 69 tr tr - tr	 69 1 tr 1 tr	 32 2.5 0.5 43.5 tr	 60 0.5 tr 12 tr	 56 1 0.5 2 tr
Matrix Organic matter	6 -	- 1	1.5 2	4.5 0.5	1.5 1	- -	- -	- -	4.5 1.5	2 2	- tr
Authigenic min. and cements Silica Kaolin Carbonate	 8 3.5 1	 17 4 10	 7 10.5 4.5	 7.5 7.5 5.5	 2 6 4.5	 12.5 3.5 5	 10.5 2.5 1.5	 13 1.5 2	 1 12.5 1	 7.5 3 6.5	 15 6 0.5
Porosity Intergranular Dissolution Microporosity	 4 4.5 tr	 4.5 4 tr	 1 3 tr	 - 2.5 tr	 - 1 tr	 10.5 3 tr	 12.5 4.5 tr	 9.5 3 tr	 - 0.5 tr	 1 5 tr	 14.5 4.5 tr

Table 6 (Cont): Summary of thin section descriptions of samples from the basal Birkhead Formation and top Hutton Sandstone.

and noting lithology, composition of matrix, framework and cements, textural relationships and porosity.

While identifying the relevant characteristics of each sample difficulties were encountered when I was attempting to identify some cements and clays. Thus I performed X-Ray Diffraction (XRD) analysis on all of the samples to facilitate descriptions. For XRD analysis samples were dry-ground using a mortar and pestle and sieved using a -200# mesh sieve, the powdered sample was then mounted on a side mount slide and lightly packed to produce a smooth exposed surface. A continuous scan was then run from 5 - 90 degrees 2θ with a step size of 0.02 degrees. For the XRD analysis a Phillips PW1050 diffractometer with a copper K alpha radiation at 30Kv and 20mA was used in conjunction with the 'Sietronics 112 X-ray Diffractometer Automation System'. I then processed the results using Sie 112 to remove the background radiation and to perform peak selection. The processed data was then input into the UPDSM program to peak match minerals by comparing to JCPDS files.

To complement and re-enforce observations that I obtained from thin section analysis a selection of samples from each facies group (table **6**) was chosen for scanning electron microscope (SEM) studies to identify pore space geometry and identify clay / framework grain relationships. Broken segments of the samples were mounted and fixed to aluminium pin-type stubs using araldite and then coated with carbon and gold prior to viewing in a CamScan 44FE Scanning Electron Microscope at 20Kv. For each mineral photographed the CamScan 44FE energy dispersive spectrometer (EDS) was used to determine elemental composition.

To further characterise the diagenetic history of the sandstones at the Gidgealpa south dome a number of polished thin sections (table **6**) were analysed by cathodoluminescence (CL). Polished thin sections were cleaned with ethanol before mounting in a vacuum chamber to minimise pumpdown

times for CL beam operational levels. The slides were then inspected using a Technosyn cold cathode luminoscope, Model 8200 MkII with the gun voltage at 20Kv and gun current of 100μA to excite silica (quartz luminescence). Photos were taken using a Leitz Orthomat E automatic microscope camera with high-speed Kodak Ektachrome film (1600 ASA)

6.2 Composition and Texture of Facies at the Gidgealpa South Dome

All samples were point counted and named using the Folk classification (Folk 1974) by calculating relative percentages of feldspar, quartz and rock fragments (figure **102**). The samples were further classified using a classification scheme by Lemon (1992), incorporating matrix content (figure **103**). Allocated names for samples are located in appendix **6** and summarised in table **6**.

The summary of rock types at the Gidgealpa south dome indicate that the dominant mineral is quartz and samples consist of quartz arenites, sublitharenites and litharenites with the latter two types varying in matrix content. They generally have a low feldspar content indicating the textural maturity of the sandstones and increases in feldspar occur with increasing levels of lithic fragments or a change in provenance. From figure **102** it can also be noted that the varying compositions of sandstones is a function of their position within the stratigraphic section. Variations in the percentage of lithics occur in the Hutton Sandstone and Birkhead Formation, pre-provenance and post-provenance change. The exception to this trend is the sample (Gidgealpa 30 (6029'9') located in the very top section of the triangle in figure **102** (indicated by the red dot) which has had heavy dissolution and removal of lithic and feldspar grains essentially leaving only framework quartz.

Sandstones range in grain size from very fine to medium-coarse with the latter sizes occurring within the Hutton Sandstone and cleaner quartz arenites. The

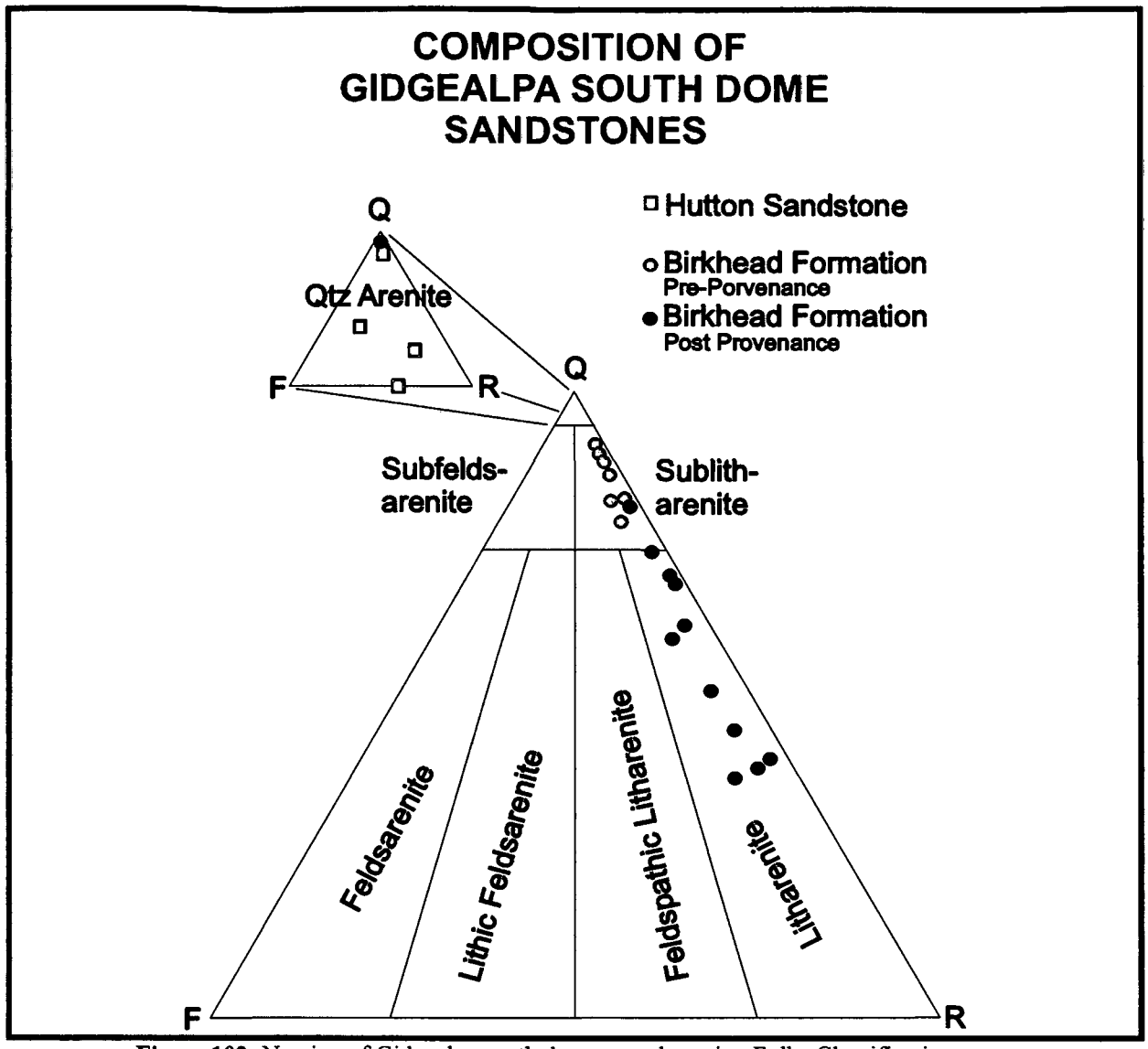

Figure 102: Naming of Gidgealpa south dome samples using Folks Classification.

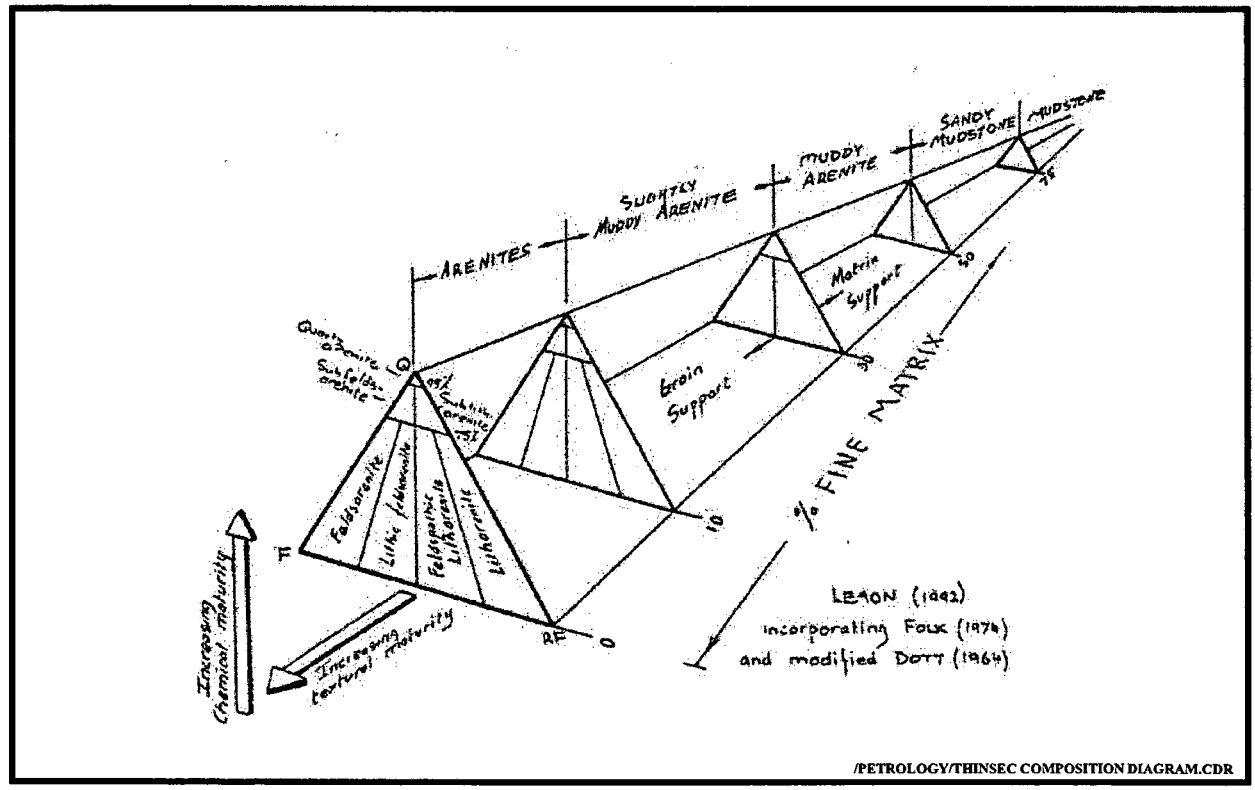

Figure 103: Further classification of samples accounting for matrix content. Samples range from arenites to sandy mudstones (From Lemon, 1993).

coarser sandstones also tend to be better sorted (moderately to well sorted) while the finer grained sandstones are generally poorly sorted. Detrital framework grains are rounded to well rounded within the Hutton Sandstone. Within the Birkhead Formation there is evidence of well rounded quartz as well as grains with multiple overgrowths occurring with more angular to sub-angular quartz within the same sample, suggesting reworking from the Hutton Sandstone. Observations of the Birkhead Formation indicate that the sediments are semi-mature while the Hutton Sandstone is mature. Grain contacts vary within samples with cleaner sandstones containing sutured and concavo-convex contacts and the more lithic rich sandstones consisting of tangential contacts. Grains may also float within the more ductile lithic grains where percentages are high enough.

6.2.1 Quartz

Quartz is the major mineral in all Hutton Sandstone samples and in most samples from the Birkhead Formation. Quartz percentages are generally the highest in quartz arenites, and sub-litharenites with values varying between 50% to 70% with an average value of approximately 60% (table **6**, page 227). Within the finer grained muddy sub-litharenites, muddy litharenites and litharenites, quartz content is greatly reduced with values ranging from as low as 26% up to 58.5% with average values of approximately 35%. The decrease in quartz content is sometimes, but not always, associated with an increase in lithics. The low quartz content may also occur due to elevated percentages of matrix (Gidgealpa 29, 6055'6"). However this matrix value may be excessively high due to the difficulty in identifying sedimentary lithic grains in the presence of matrix due to their similar optical properties.

In all samples, the dominant quartz type is plutonic quartz which is not surprising since this type of quartz originates from granite batholiths and / or granite-gneisses (table **7**). However, this type of quartz may also be sourced

Well	Depth (ft)	Igneous (plutonic)	Vein	Volcanic	Shistose Metamorphic	Recrystallized Metamorphic	Stretched Metamorphic
Gidgealpa 26	5950'6"	**Common**	-	Occasional	-	Occasional	Occasional
Gidgealpa 26	5956'4"	**Common**	-	Occasional	-	Rare	Rare
Gidgealpa 26	5957'7"	**Common**	Rare	-	-	Rare	Occasional
Gidgealpa 29	6025'4"	**Common**	-	Occasional	-	Occasional	Rare
Gidgealpa 29	6038'1"	**Common**	Rare	-	-	Rare	Rare
Gidgealpa 29	6045'9"	**Common**	-	-	-	Rare	-
Gidgealpa 29	6047'2"	**Common**	Rare	-	-	-	-
Gidgealpa 29	6055'4"	**Common**	-	-	-	-	Rare
Gidgealpa 29	6064'2"	**Common**	Rare	-	-	-	Occasional
Gidgealpa 30	6029'9"	**Common**	Rare	-	Rare	Occasional	Occasional
Gidgealpa 30	6032'6"	**Common**	Rare	Rare	Rare	Rare	Rare
Gidgealpa 30	6037'6"	**Common**	Rare	-	Rare	Rare	Rare
Gidgealpa 30	6042'5"	**Common**	-	-	-	Occasional	-
Gidgealpa 31	5974'6"	**Common**	-	Occasional	Rare		Rare
Gidgealpa 31	5981'10"	**Common**	-	Occasional	-	-	Occasional
Gidgealpa 31	5985'10"	**Common**	-	Occasional	-	Rare	Rare
Gidgealpa 31	5993'4"	**Common**	-	Occasional		Rare	Rare
Gidgealpa 31	5997'3	**Common**	-	Occasional	-	-	Rare
Gidgealpa 32	5989'9"	**Common**	-	Occasional	-	-	**Common**
Gidgealpa 32	5992'2"	**Common**	-	-	-	Rare	Rare
Gidgealpa 32	6007'4"	**Common**	-	-	Rare	Rare	Rare
Gidgealpa 32	6015'9"	**Common**	Occasional	-	Rare	Rare	Rare
Gidgealpa 32	6018'6"	**Common**	Occasional	-	-	Rare	Rare

Table 7: Types of quartz present within the Gidgealpa south dome samples. Where volcanic quartz grains are present (shaded column) a volcanic origin of the sediments is implied.

from metamorphic or vein quartz and thus is also referred to as 'common quartz' (Folk, 1980). Common quartz consists mostly of monocrystalline grains with straight to slightly undulose extinction (plate **2**, A1 and A2) and may contain arranged vacuoles due to healed fractures as well as mineral inclusions such as rutile, micas, feldspars and tourmaline. Some grains may be strongly undulose if they have been stressed after crystallisation or originate from gneisses. Composite grains present (plate **2**, B1 and B2) are also classed as plutonic quartz.

Volcanic quartz, although rare and sometimes difficult to identify, is an excellent indicator of a volcanic or active arc provenance. Samples from table **7** containing volcanic quartz (shaded column) show this related provenance. At the Gidgealpa south dome this type of quartz only appears within the Birkhead Formation above the provenance change. Volcanic quartz originates from rocks such as rhyolites, latites and dacites and is readily identified by shape, either as fragmental bipyramidal crystals lacking prism faces or hexagonal prisms with geometrically straight edges and rounded corners (Folk, 1980). The quartz commonly has characteristic large rounded embayments which is due to corrosion before extrusion (Lewis, 1984). Volcanic grains almost always have straight extinction and appear water-clear and may also contain fragments of volcanic glass or aphanitic volcanic ground-mass, negative hexagonal crystals may also form (Folk, 1980). Plate **3** is an excellent example of volcanic quartz, note the hexagonal crystal shape, large rounded embayments and inclusions including glass and volcanic ground mass.

Other types of quartz present with the sandstones include metamorphic vein and reworked sedimentary. All of these types are generally rare within both the Hutton Sandstone and Birkhead Formation samples and occur occasionally at most with the exception of Gidgealpa 32 (5989'9") which has common stretched metamorphic grains within the sandstone. Rare reworked sedimentary quartz has been found in Gidgealpa 32 (6015'9") and Gidgealpa

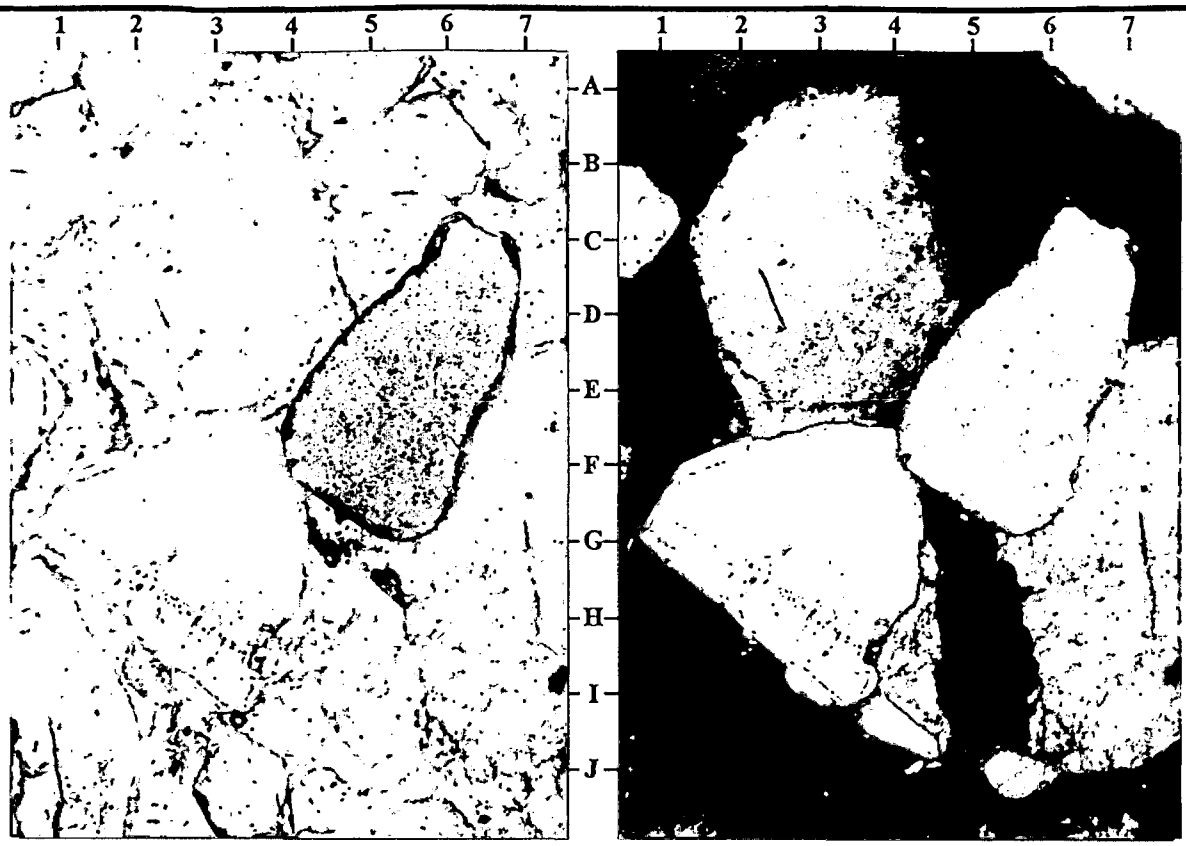

A1 Gidgealpa 32 6018'6" Field of view: 2mm

A2 Gidgealpa 32 6018'6" Field of view: 2mm

Quartz arenite under plain polarized light (ppl) (A1) and crossed nicolls (A2) showing abundant common quartz with straight extinction. Note also on the photographs the presence of well rounded tourmaline (E5).

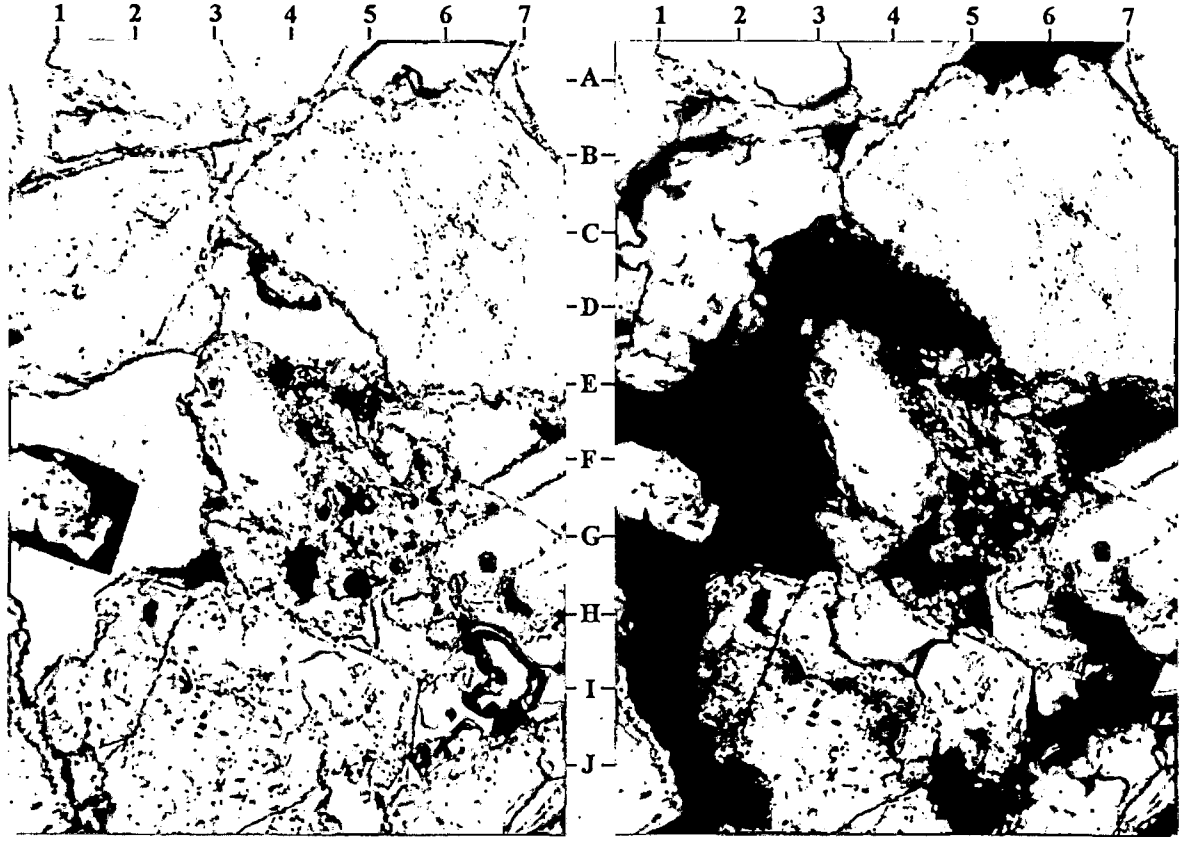

B1 Gidgealpa 32 6018'6" Field of view: 2mm

B2 Gidgealpa 32 6018'6" Field of view: 2mm

Quartz arenite under plain polarized light (ppl) (B1) and crossed nicolls (B2) showing the formation of slightly undulose extinction (I2) and composite grains from stress forces on the rock (C2).

PLATE 2

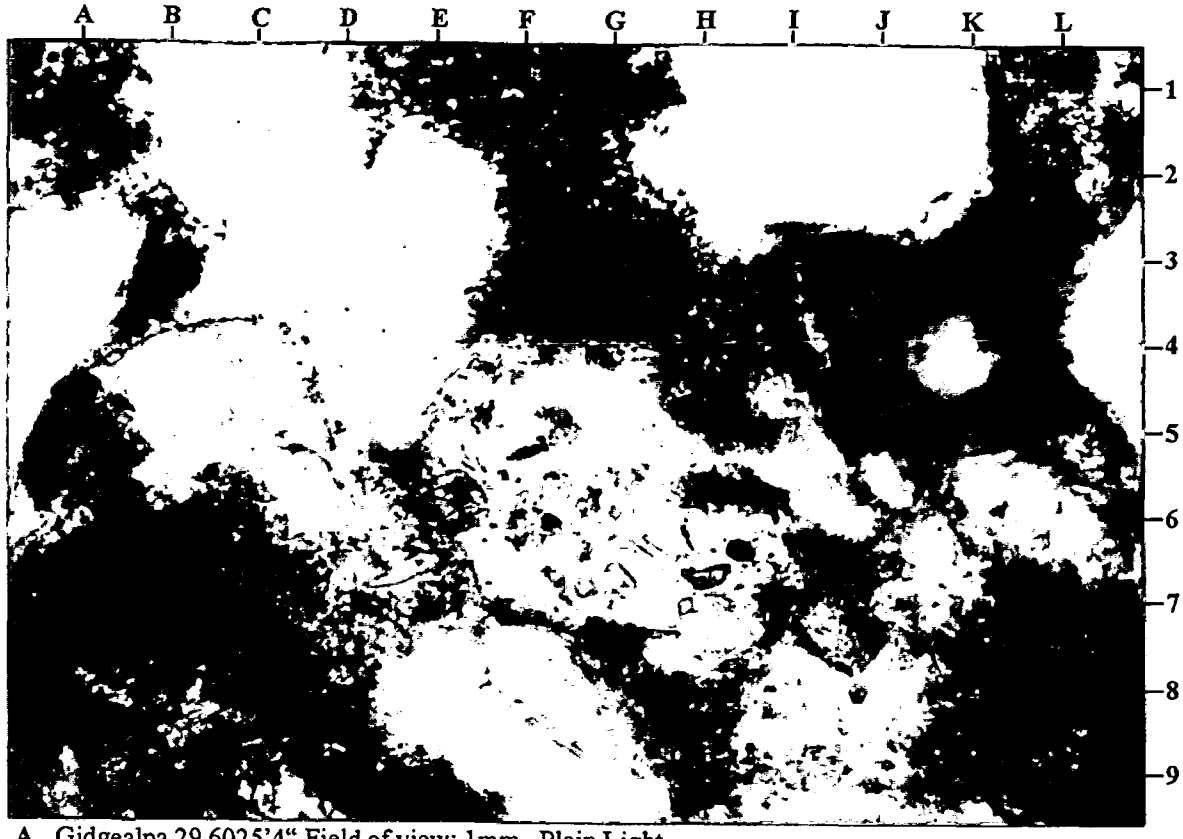

A Gidgealpa 29 6025'4" Field of view: 1mm. Plain Light

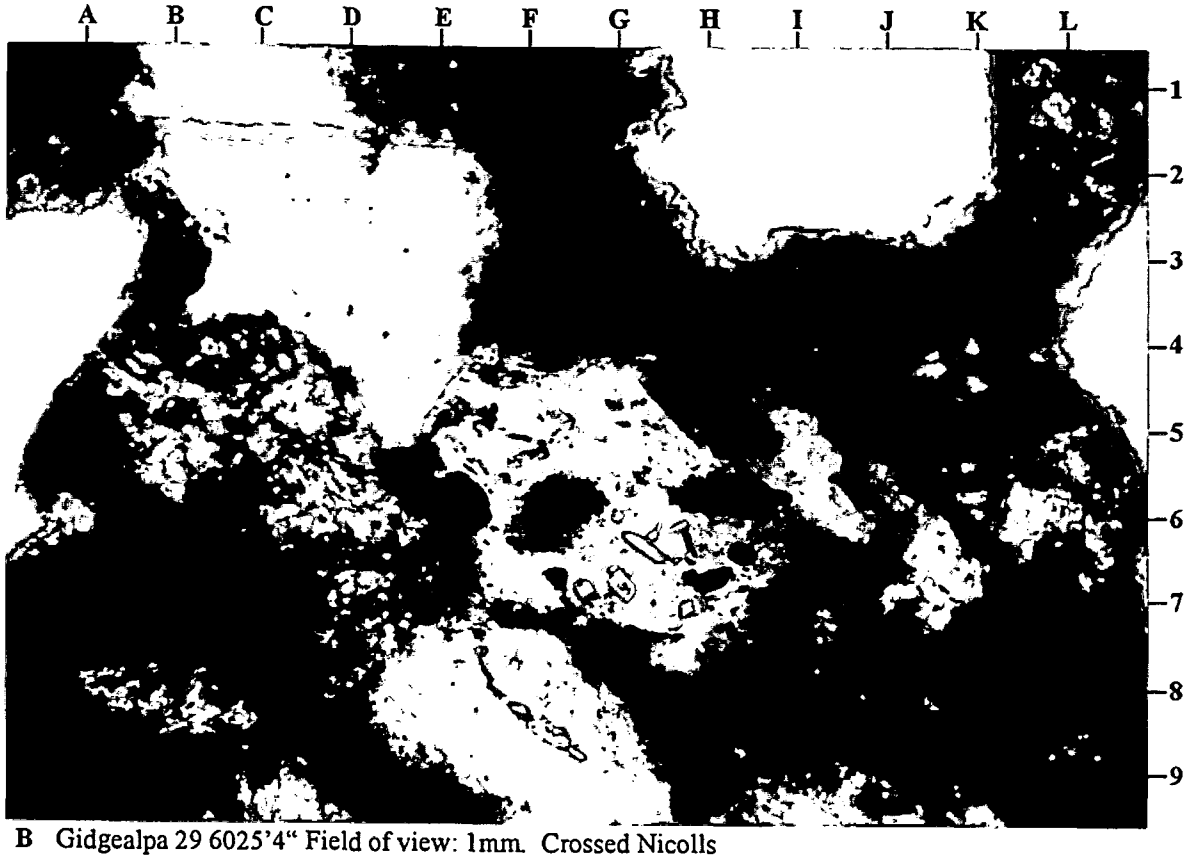

B Gidgealpa 29 6025'4" Field of view: 1mm. Crossed Nicolls

Volcaniclitharenite under ppl (A) and crossed nicolls (B) showing volcanic quartz (G5). Note the hexagonal shape of the grain, the large embayments, rounded corners and solid inclusions.

PLATE 3

30 (6037'6"). The examples in plate **4** (A1,A2 and B1,B2) show two stages of reworked overgrowths, the first is likely to be from the top of the Hutton Sandstone where overgrowths have formed and then the sediments have been reworked for the second stage in the Birkhead Formation before the provenance change.

6.2.2 Feldspars

Feldspars within the Hutton Sandstone and Birkhead Formation make up only a minor proportion of the total rock content. Within the Hutton Sandstone the amount of feldspar present is up to 1% (table **6**, page 227). Early quartzose sandstones before the provenance change of the Birkhead Formation also have percentages around 1%. The amount of feldspars after the provenance change increases with the sub and volcanic-litharenites containing between 1% and 6% (table **6**, page 227). The increase in detrital feldspar content after the provenance change is attributed to the volcanic nature of the sediments from the east. The change in content above and below the provenance change also marks a change from alkali (or potassium rich) feldspars to more sodium rich feldspars. Table **8** shows the types of feldspars present with the post-provenance change sediments containing feldspars of a volcanic origin (shaded columns).

Alkali feldspars (K feldspars) present within the quartzose sandstones of the top Hutton Sandstone and the basal Birkhead Formation (before and after the provenance change) consist of orthoclase and microcline. These two types of K feldspar are typical in sediments originating from granites and granite-gneisses. Their resistance to weathering compared to the other feldspars causes them to be commonly present within sediments. The identification of microcline is easily distinguished by its characteristic cross-hatched or tartan twinning (plate **5**, A1 and A2). In the case of orthoclase, the lack of twinning

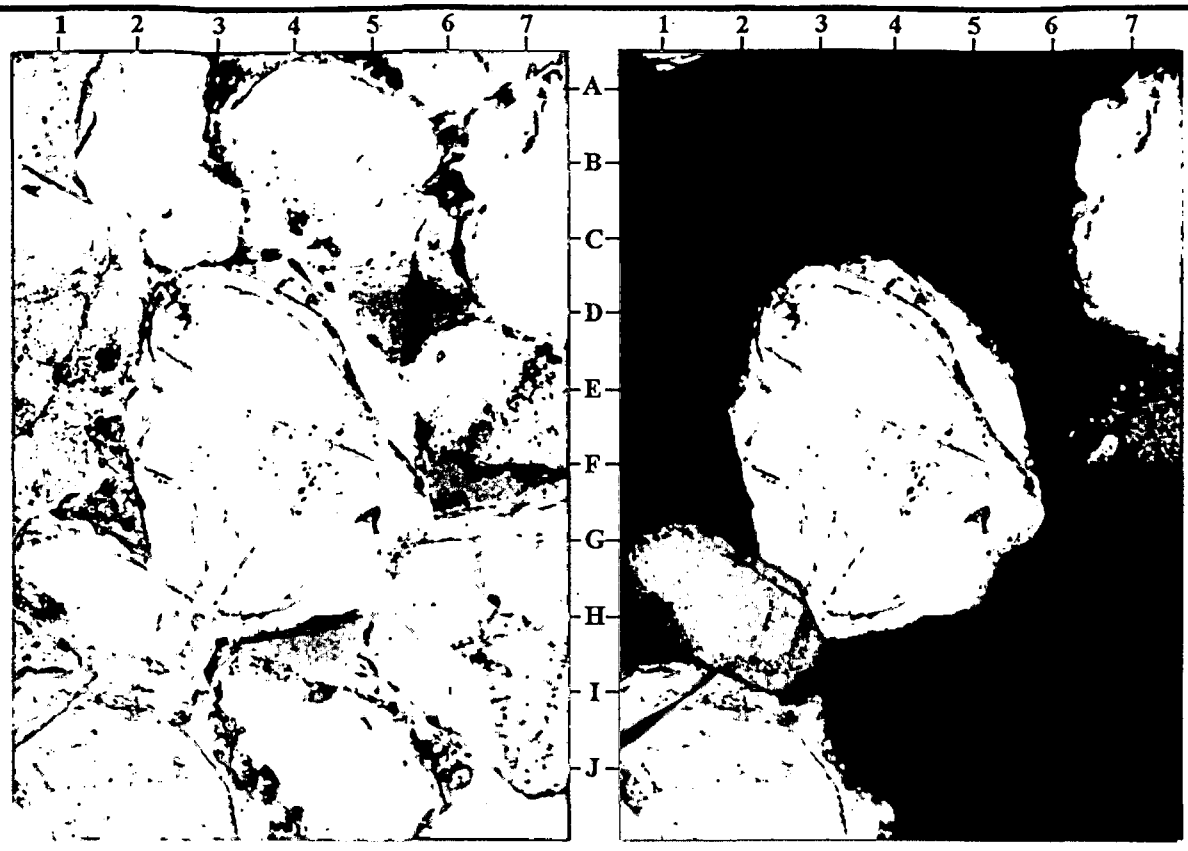

A1 Gidgealpa 32 6015'9" Field of view: 2mm

A2 Gidgealpa 32 6015'9" Field of view: 2mm

Quartz arenite under ppl (A1) and crossed nicolls (A2) showing the two stages of quartz overgrowths on a quartz grain (F4) from sediment reworking.

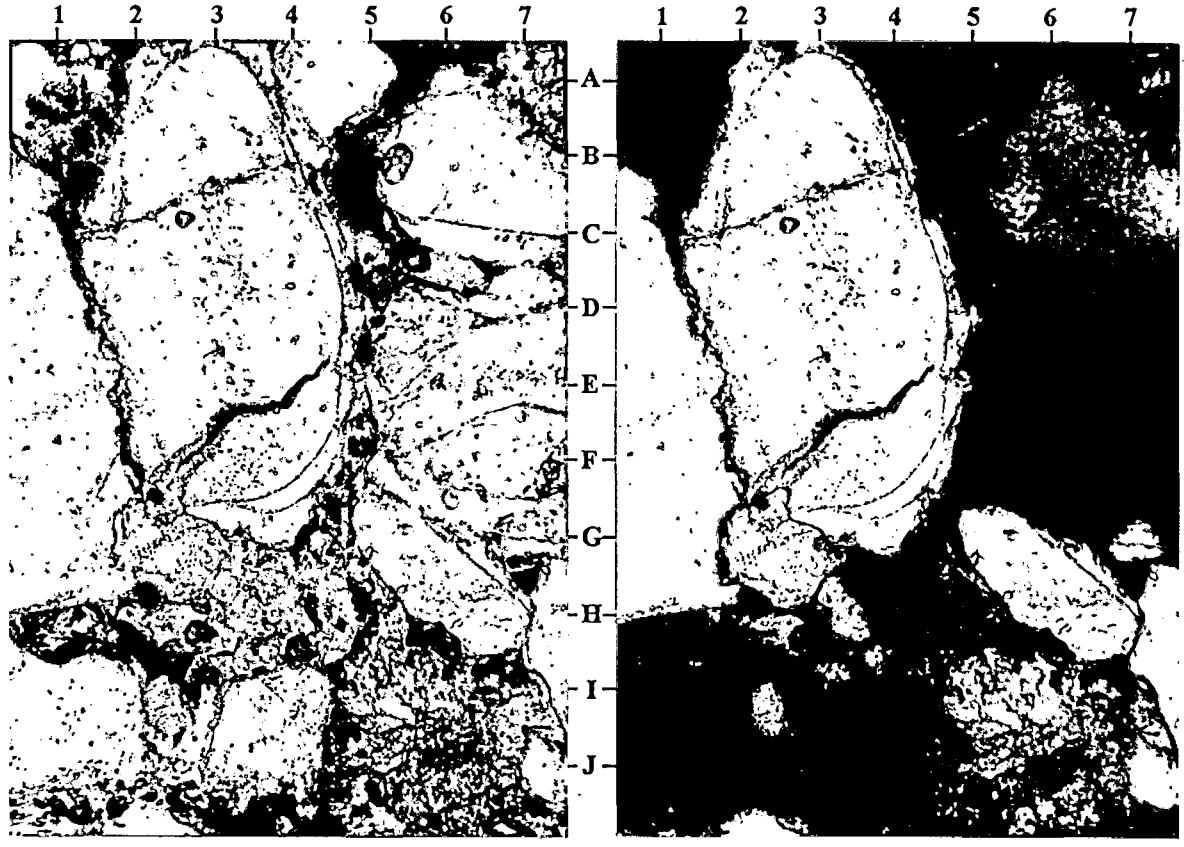

B1 Gidgealpa 30 6037'6" Field of view: 2mm

B2 Gidgealpa 30 6037'6" Field of view: 2mm

Quartz arenite under ppl (B1) and crossed nicolls (B2) showing the two stages of quartz overgrowths (D3) from sediment reworking. Sediment reworking of the grain and has caused fracturing.

PLATE 4

Well	Depth (ft)	Orthoclase	Microcline	Plagioclase	Sanadine	Anorthoclase
Gidgealpa 26	5950'6"	Yes	Yes	Yes	-	-
Gidgealpa 26	5956'4"	Yes	Yes	-	-	-
Gidgealpa 26	5957'7"	Yes	-	Yes	-	-
Gidgealpa 29	6025'4"	Yes	-	Yes	Yes	-
Gidgealpa 29	6038'1"	Yes	Yes	-	-	-
Gidgealpa 29	6045'9"	Yes	-	-	-	-
Gidgealpa 29	6047'2"	Yes	Yes	-	-	-
Gidgealpa 29	6055'4"	-	Yes	-	-	-
Gidgealpa 29	6064'2"	Yes	-	-	-	-
Gidgealpa 30	6029'9"	Yes	Yes	-	-	-
Gidgealpa 30	6032'6"	Yes	Yes	-	-	-
Gidgealpa 30	6037'6"	Yes	-	-	-	-
Gidgealpa 30	6042'5"	Yes	-	-	-	-
Gidgealpa 31	5974'6"	Yes	-	Yes	-	-
Gidgealpa 31	5981'10"	Yes	-	Yes	Yes	Yes
Gidgealpa 31	5985'10"	Yes	Yes	Yes	-	-
Gidgealpa 31	5993'4"	Yes	Yes	Yes	Yes	-
Gidgealpa 31	5997'3	Yes	-	Yes	Yes	-
Gidgealpa 32	5989'9"	Yes	Yes	Yes	-	-
Gidgealpa 32	5992'2"	Yes	-	-	-	-
Gidgealpa 32	6007'4"	-	Yes	-	-	-
Gidgealpa 32	6015'9"	Yes	-	-	-	-
Gidgealpa 32	6018'6"	Yes	Yes	-	-	-

Table 8: Types of feldspars present within the Gidgealpa south dome samples. Where feldspars are present in the shaded columns a volcanic origin of the sediments is implied.

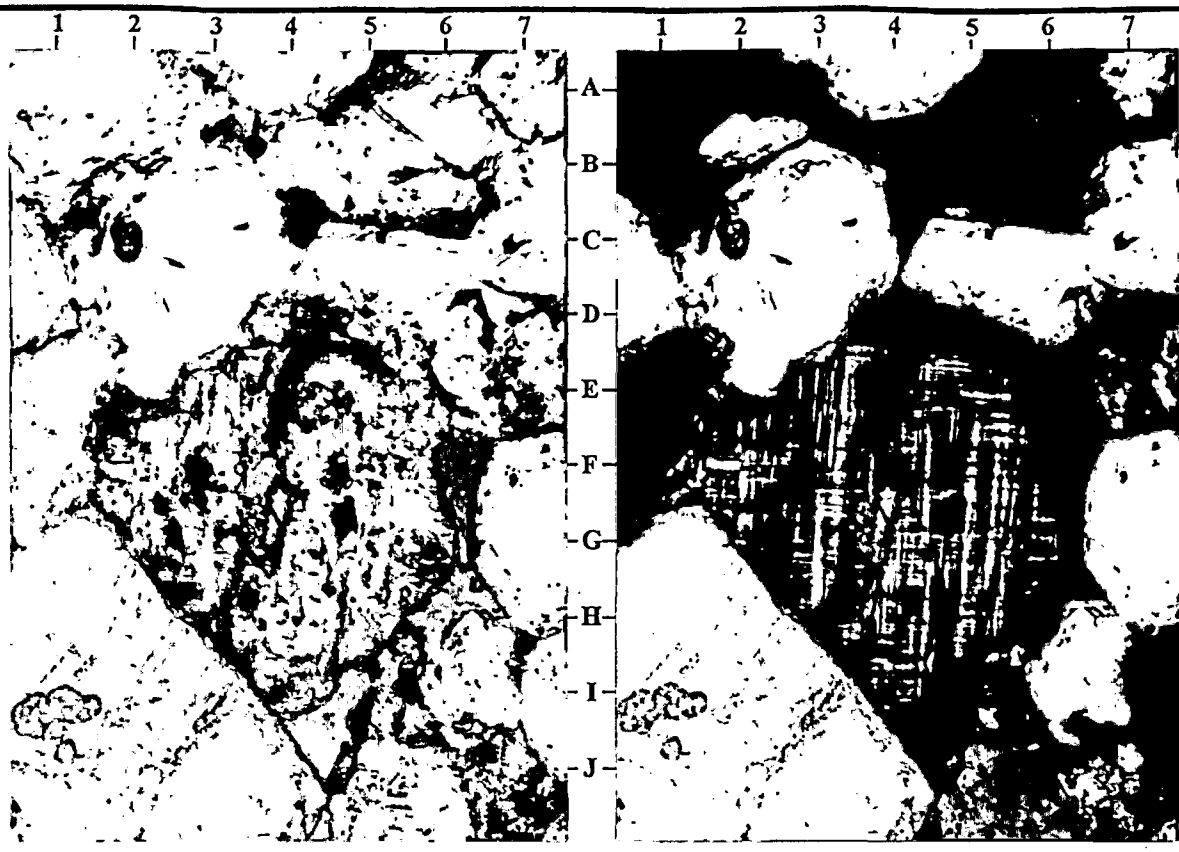

A1 Gidgealpa 32 6007'4" Field of view: 2mm

A2 Gidgealpa 32 6007'4" Field of view: 2mm

Quartz arenite in ppl (A1) and crossed nicolls (A2) showing the presence of a weathered and rounded microcline (G4) with its characteristic tartan twinning that can easily be seen under crossed nicolls.

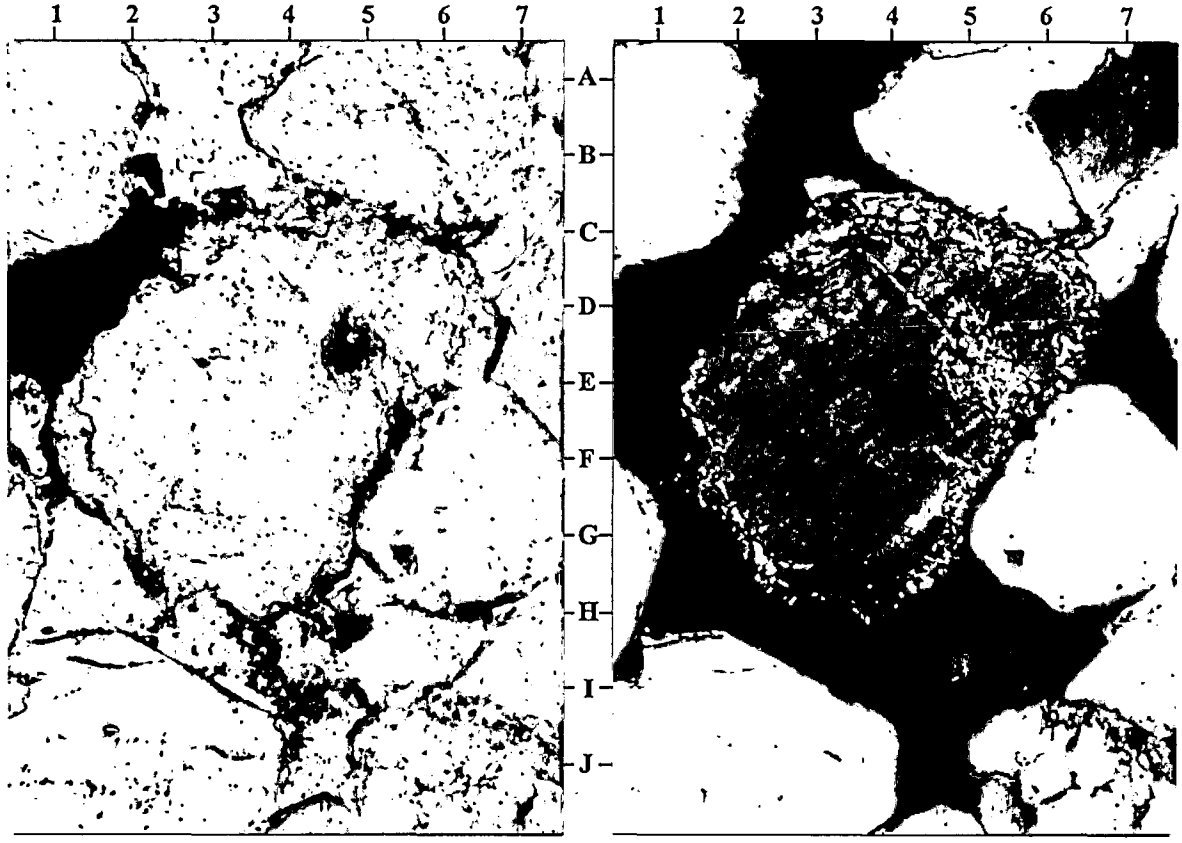

B1 Gidgealpa 32 6018'6" Field of view: 2mm

B2 Gidgealpa 32 6018'6" Field of view: 2mm

Quartz arenite in ppl (B1) and crossed nicolls (B2) showing the partial alteration of orthoclase (E3) to sericite (C4).

PLATE 5

or other distinguishing features causes the mineral to be difficult to identify when compared with quartz which has similar optical properties.

I used a number of methods to overcome the difficulties of identification of orthoclase. The feldspar was identified by looking for characteristic cleavage which may show alteration or dissolution along the plains. The feldspar is also commonly cloudy due to the presence of alteration products (Lewis, 1984), the feldspar also has a lower birefringence than quartz, and feldspar shows characteristic alteration to sericite (plate **5**, B1 and B2). The use of CL was also a great aid since the feldspars have low CL thresholds at low accelerating voltages and are easily identified by their brilliant blue colour (Miller, 1988).

Post provenance change, volcanic-arc derived sediments at the Gidgealpa south dome are marked by a change in feldspar composition from dominantly orthoclase and microcline to plagioclase, sanidine and anorthoclase. While these feldspars alone are not conclusive evidence of a particular source, combined they strongly suggest a volcanic origin. The elevated levels of plagioclase as compared to microcline and orthoclase is an indication of a volcanic source (MacKenzie and Guilford, 1982). The presence of this type of feldspar is easily noted by its multiple twinning character (plate **6**, A1 and A2). The other feldspars indicative of a volcanic source are the high temperature forming sanidine which has a characteristic simple twinning and strong cleavage (plate **6**, B1 and B2). The sodium rich K feldspar, anorthoclase is present and has tartan twinning caused by albite and pericline twin lamellae (Folk, 1980). While the texture is similar to microcline it differs in the fact that it has a different optical orientation and has very close grid twinning (MacKenzie and Guilford, 1982) (plate **7**, A1 and A2).

The softer nature of feldspars when compared to quartz as well as the presence of cleavage means that they are more prone to abrasion which subsequently reduces the grain size more rapidly than quartz (Folk, 1980). Adding to this is their lower stability due to alteration and dissolution along cleavage plains,

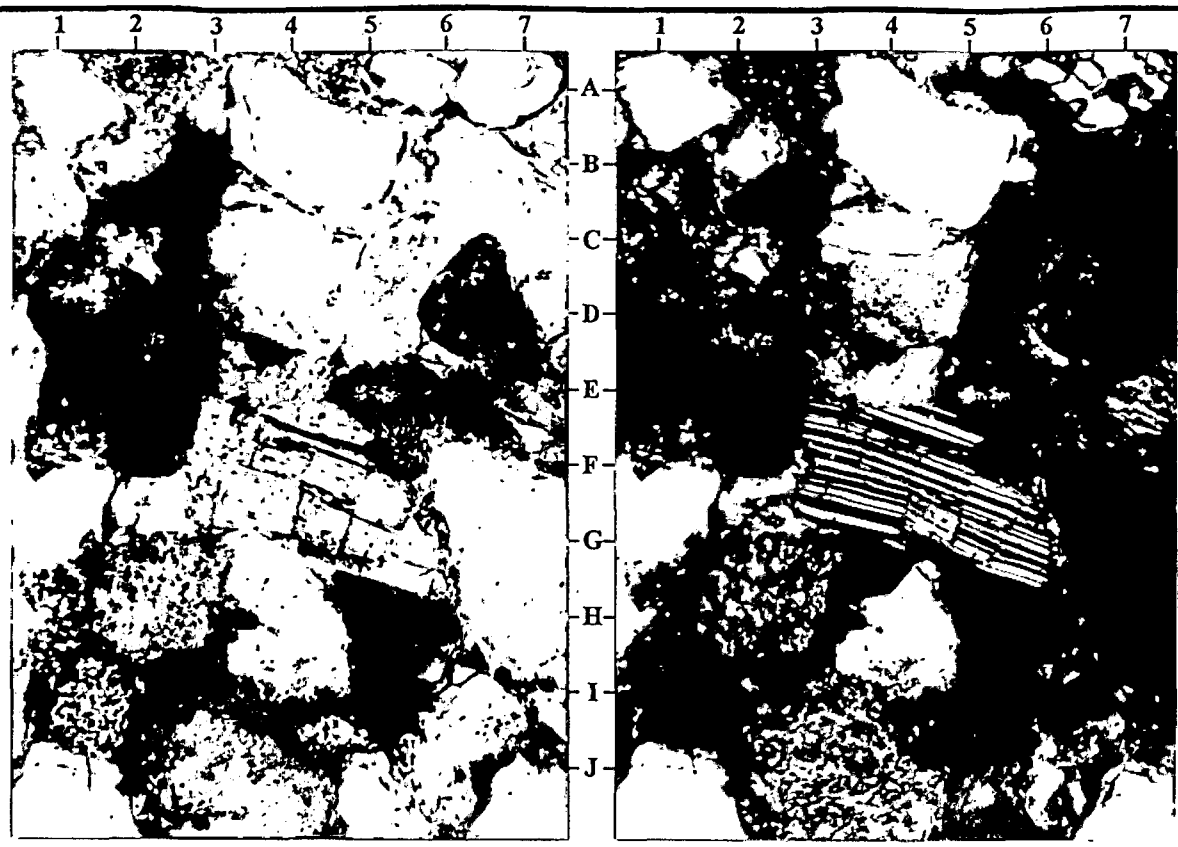

A1 Gidgealpa 29 6025'4" Field of view: 2mm

A2 Gidgealpa 29 6025'4" Field of view: 2mm

Volcanic litharenite under ppl (A1) and crossed nicolls (A2) showing a plagioclase feldspar (F4) which has undergone dissolution along its cleavage plains seen under ppl and its characteristic multiple twinning under crossed nicolls.

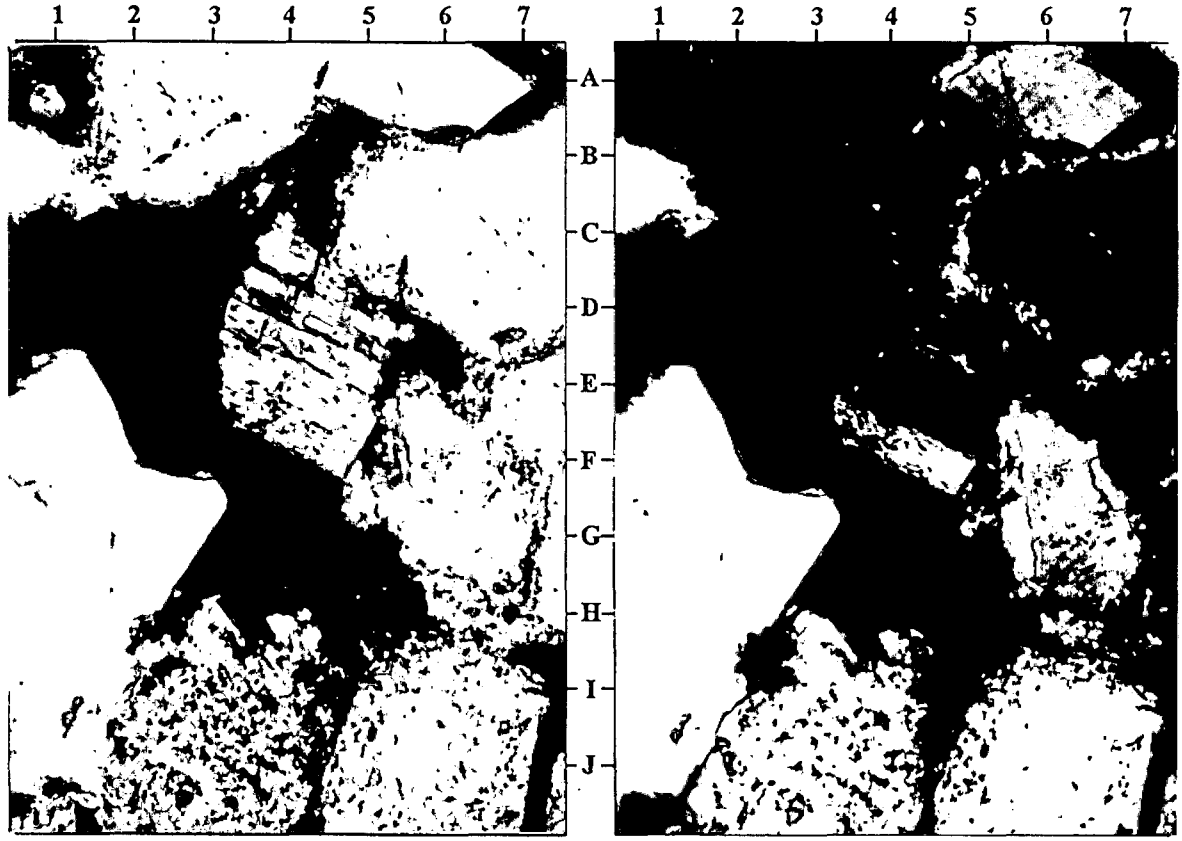

B1 Gidgealpa 29 6025'4" Field of view: 1mm

B2 Gidgealpa 29 6025'4" Field of view: 1mm

Volcanic litharenite under ppl (B1) and crossed nicolls (B2) showing the presence of a sanidine grain (E4). Note the strong cleavage which has preferential dissolution under ppl and the simple twinning under crossed nicolls.

PLATE 6

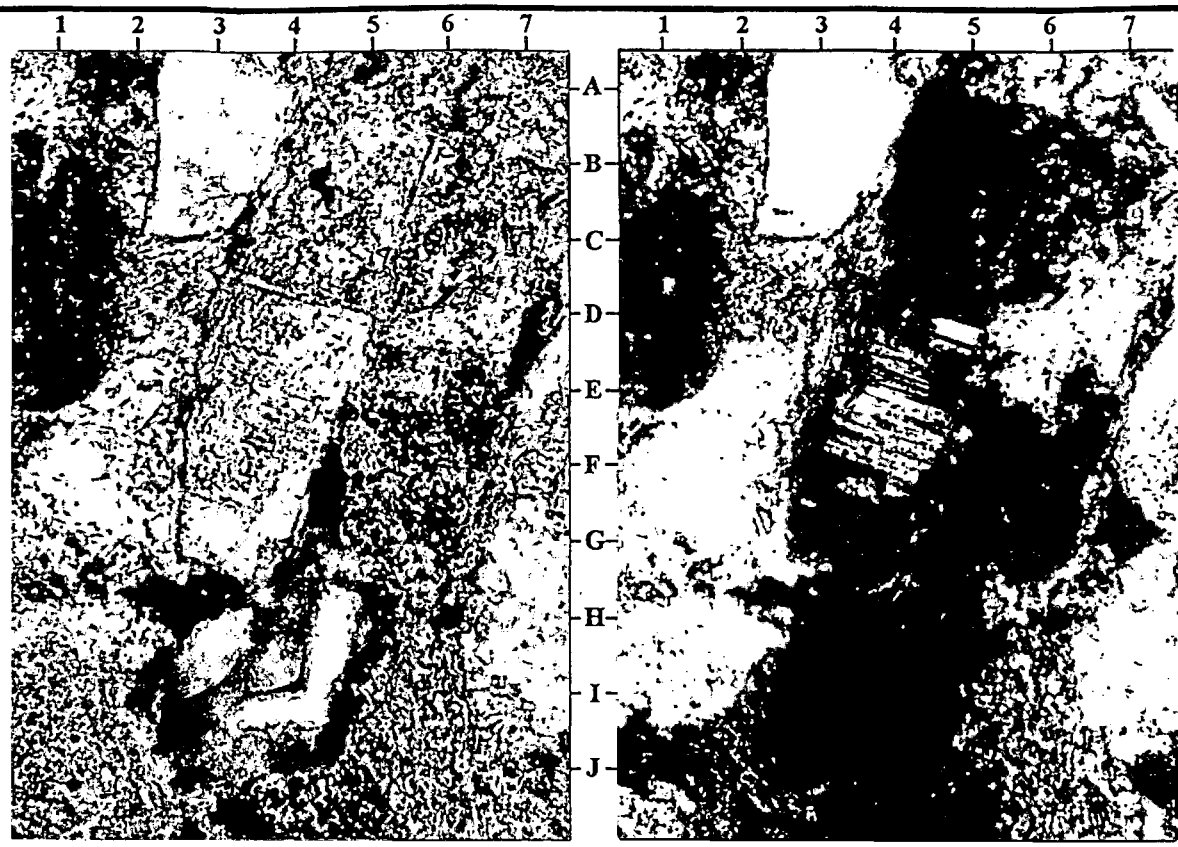

A1 Gidgealpa 31 5981'10" Field of view: 1mm **A2** Gidgealpa 31 5981'10" Field of view: 1mm

Volcanic litharenite under ppl (A1) and crossed nicolls (A2) showing the characteristic albite and pericline twin lamellae of an anorthoclase (F4) under crossed nicolls. Close by the feldspar (I3) is a ferromagnesian rich rock fragment that has altered to clays.

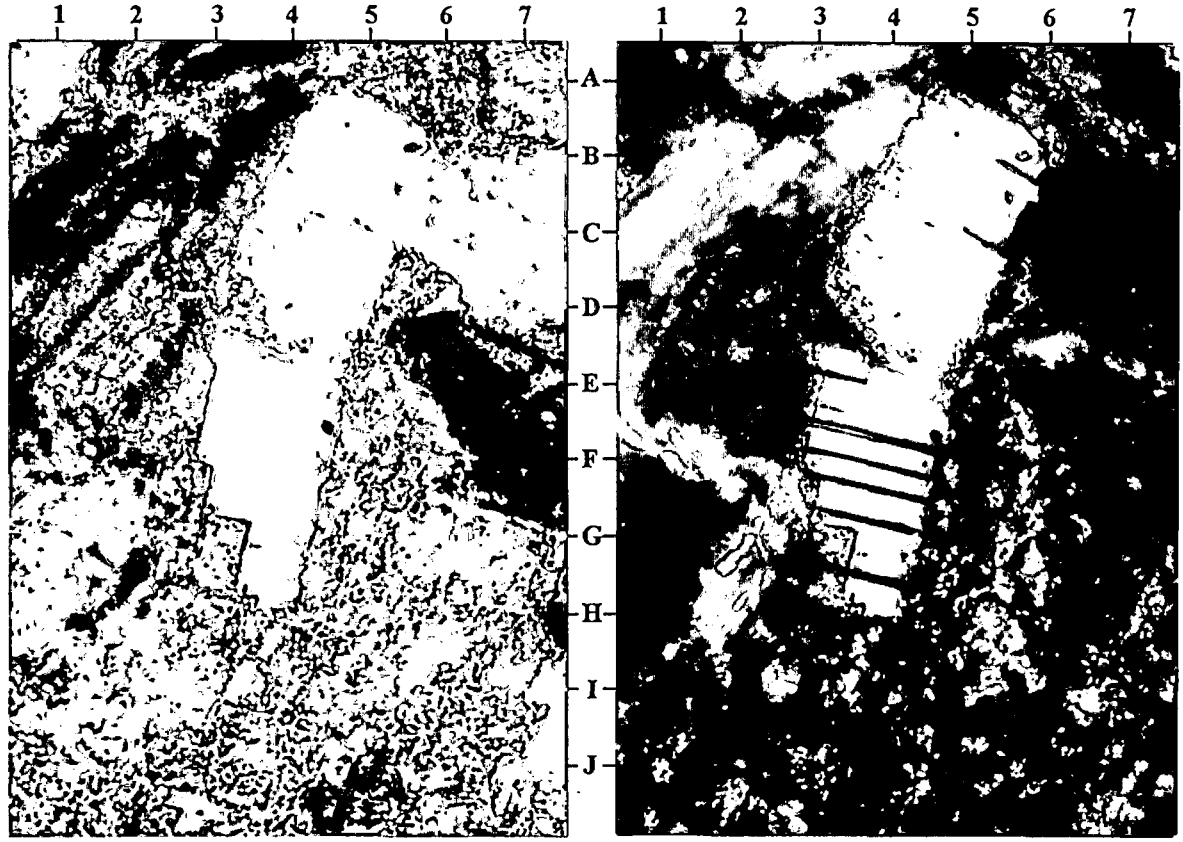

B1 Gidgealpa 32 5989'9" Field of view: 0.5mm **B2** Gidgealpa 32 5989'9" Field of view: 0.5mm

Slightly muddy litharenite under ppl (B1) and crossed nicolls (B2) showing the growth of diagenetic feldspar under cross nicolls (E3) by the replacement of nearby clays.

PLATE 7

particularly from certain weathering conditions (Folk, 1980). The feldspars at the Gidgealpa south dome for both the top Hutton Sandstone and the Birkhead Formation reflect the textural maturity of the sediments. Feldspars within quartzose sandstones, or below the provenance change are generally smaller than quartz, are all rounded to well rounded and appear to be weathered or slightly to well altered. Feldspar character within the Birkhead Formation lithic labile sandstones is slightly different with both quartz and feldspar exhibiting a similar grain size and angular nature indicating a lower textural maturity of the sediments. Alteration varies within these sediments with feldspars mainly altering to sericite. The formation of sericite is the end product from the alteration of illite by diagenesis (Lewis, 1982) which originated from the breakdown of the feldspars . The dissolution of feldspars vary from fresh to highly dissolved.

Rare authigenic feldspar has formed within the sediments of the Gidgealpa south dome and appear to only be present in the finer, more clay-rich sandstones such as the slightly muddy sublitharenite of Gidgealpa 32 (5989'9") (table **6**, page 227). Plate **7** (B1 and B2) shows an overgrowth growing from a plagioclase feldspar by replacement of the surrounding clays. For this replacement to occur potassic solutions are required, supplied either by connate or hydrothermal solutions (Folk, 1980).

6.2.3 Lithics

The percentage of lithics or rock fragments in the sediments at the Gidgealpa south dome varies greatly from absent to 43.5%. Looking more closely at the data, lithics within the Hutton Sandstone vary from 1% to 2%, in the Birkhead Formation (pre-provenance change) lithics range from 4.5% to 10.5 and the Birkhead Formation (post-provenance change) has lithics in the range of 12% to 43.5%. An exception is present for the post-provenance change and occurs in Gidgealpa 30 (6029'9") which has an abnormally low lithic content. The

absence of the lithics appears to be due to mass dissolution of lithics and feldspars and possibly carbonates that have occurred at this depth. The dissolution of the labile grains have produced oversized porosity, a characteristic which is not seen in other samples from the Birkhead Formation. Plate **8** (B1 and B2) and plate **16** (A1 and A2, see page 261) indicate the production of the porosity from the partial dissolution of kaolin and the dissolution of the original framework grains. Where these grains have been dissolved grain ghosts may be present.

The increase in lithic content from the top Hutton Sandstone to pre-provenance change Birkhead Formation and then a further increase to the post-provenance change Birkhead Formation is a reflection of the different sediments entering the area. The Hutton Sandstone contains rock fragments that are primarily of a metamorphic and sedimentary origin. The metamorphic rock fragments consist of slate, phyllite, schist or meta-quartzite that can be distinguished from shales by their coarser grain size and better orientation (plate **9**, A1,A2 and B1,B2). The origin of these rock fragments is from the southern cratonic area on the edge of the Eromanga Basin from the erosion of metamorphic rocks.

The sedimentary rock fragments present within the top Hutton Sandstone make up a minor portion of the total lithic content. The grains consist of reworked fragments of siltstone or shale which originated from the reworking of the Hutton Sandstone. Similar sedimentary rock fragments are found in the Birkhead Formation but are more abundant due to the decrease in depositional energy, thus causing the grains to be more resistive to mechanical breakdown (plate **9**, B1 and B2). Rarely, sedimentary rock fragments may also consist of silts and very fine grained sandstone that are elongated in shape and range up to 5mm in length. The grains have a chaotic boundary which is probably a result of grain deformation by compaction due to their very soft nature.

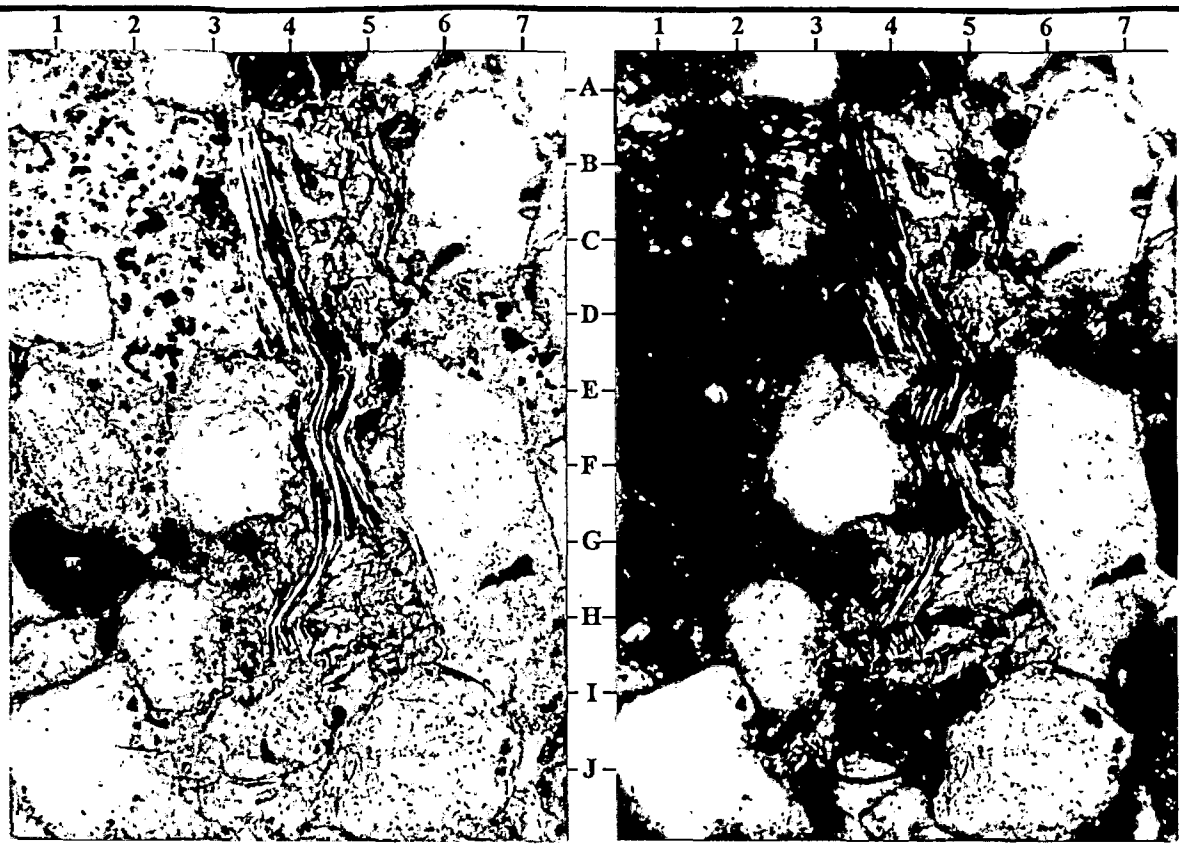

A1 Gidgealpa 30 6037'6" Field of view: 2mm **A2** Gidgealpa 31 6037'6" Field of view: 2mm

Quartz arenite under ppl (A1) and crossed nicolls (A2) showing the alteration of muscovite to iron rich minerals (D4). A2 also shows the common occurrence of carbonate growing within the mica cleavage and splitting the grain with continued growth (H5). Compaction has also caused the mica to bend and kink.

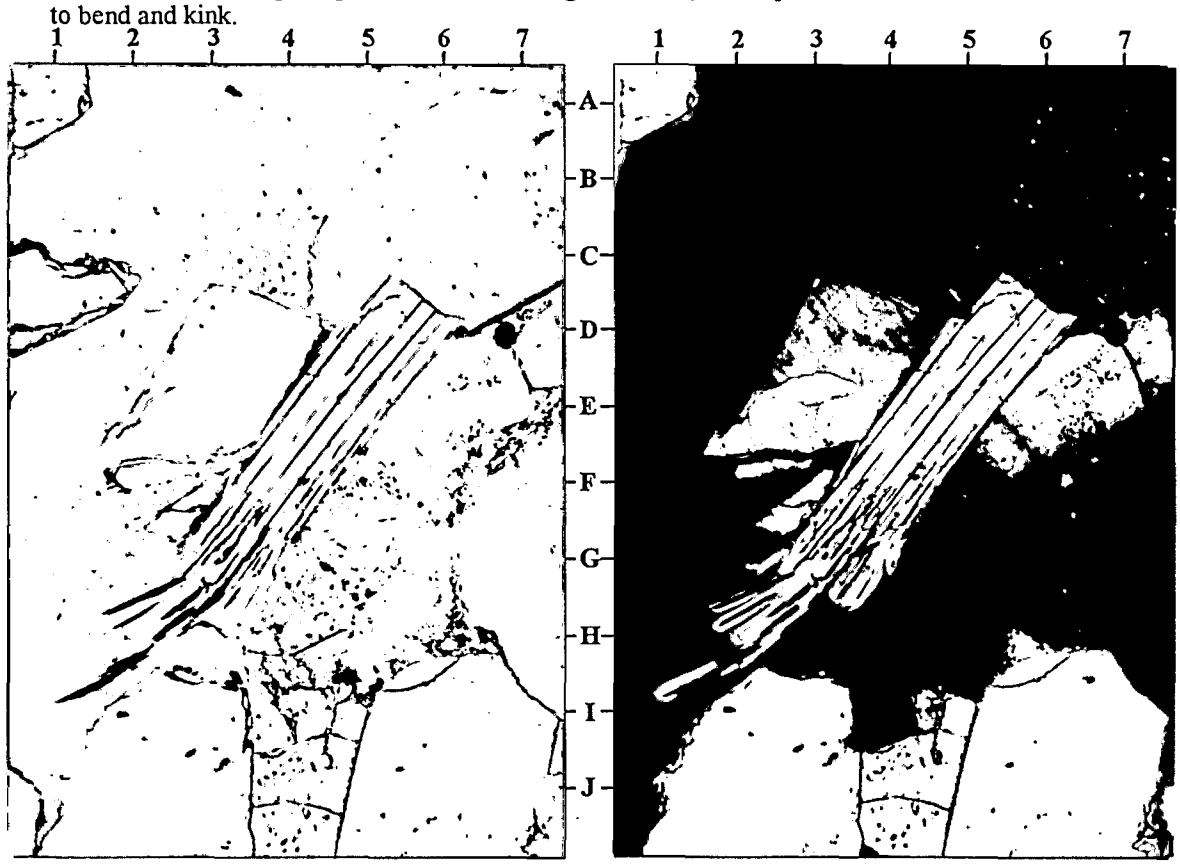

B1 Gidgealpa 30 6029'9" Field of view: 2mm **B2** Gidgealpa 30 6029'9" Field of view: 2mm

Quartz arenite under ppl (B1) and crossed nicolls (B2) showing muscovite with slight fanning at the grain end (G3). Also noticeable is the rare authigenic mica crystals growing from the grain (H2).

PLATE 8

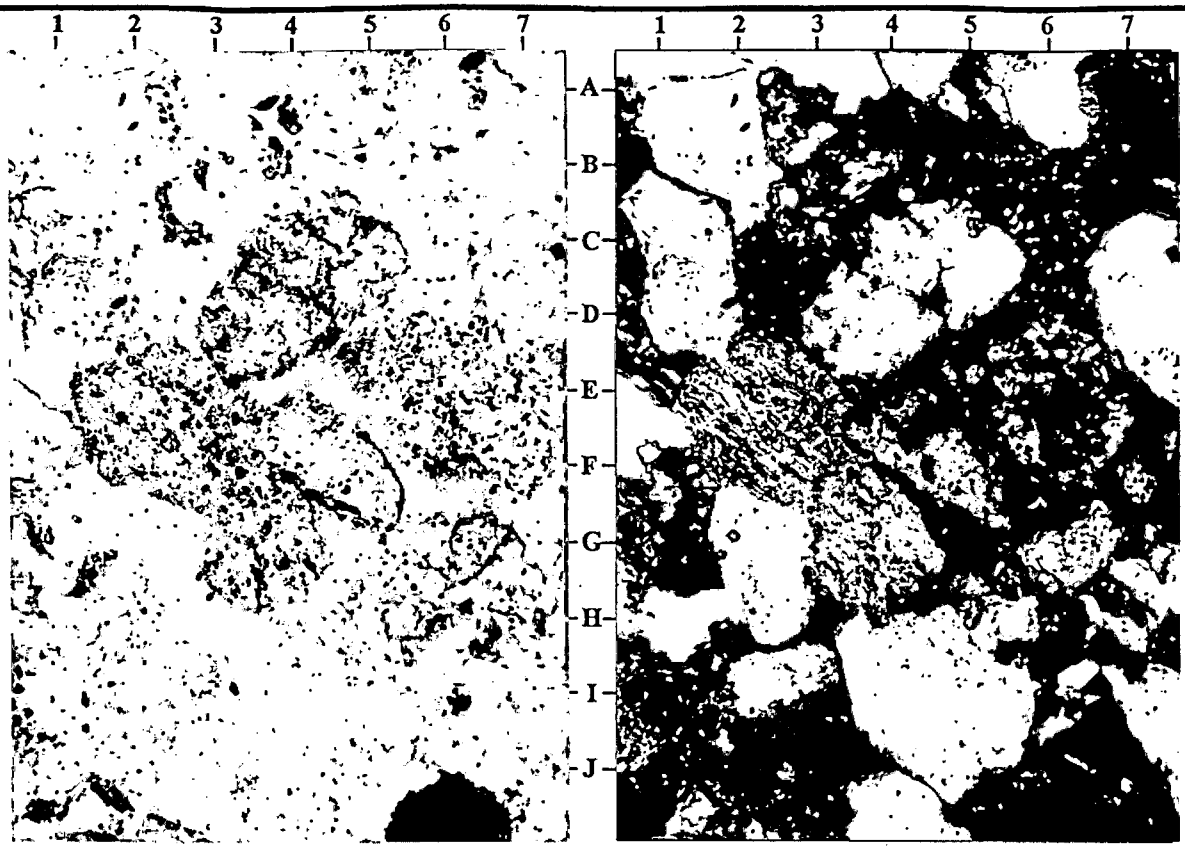

A1 Gidgealpa 30 6032'6" Field of view: 2mm

A2 Gidgealpa 30 6032'6" Field of view: 2mm

Sub-litharenite under ppl (A1) and crossed nicolls (A2)showing abundant rock fragments and authigenic kaolin (C6) as well as carbonate cement which can be seen under crossed nicolls (H7). In this photo a large metamorphic rock fragment is present (F3).

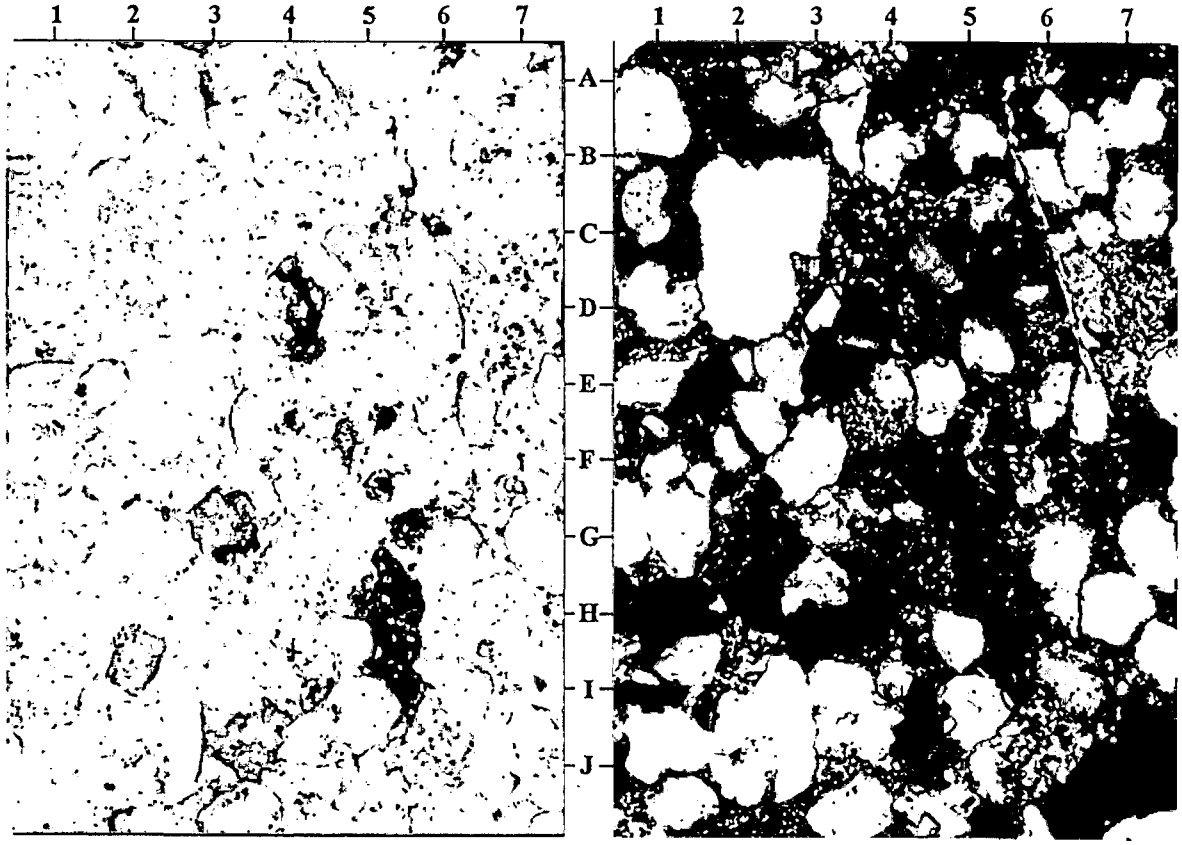

B1 Gidgealpa 30 6032'6" Field of view: 4mm

B2 Gidgealpa 30 6032'6" Field of view: 4mm

Sub-litharenite under ppl (B1) and crossed nicolls (B2) showing abundant metamorphic and sedimentary rock fragments. Note in the case of B2 the optical difficulty in distinguishing the rock fragments to the matrix (H5).

PLATE 9

The further increase in the lithic content of sediments above the provenance change is due to the influx of volcanic rock fragments into the area for the first time. Volcanic rock fragments are diagnostic of the sediment provenance; however, the ease at which the grains break down means that they are altered or dissolved relatively quickly. Volcanic rock fragments at the Gidgealpa south dome vary from slightly to completely altered or dissolved. Altered grains consist of ferromagnesian minerals or kaolin. The presence of kaolin within the lithic grains can be easily detected by the use of CL.

The lithic grains represent parts of the ground mass of lava flows, hypabyssal intrusives or volcanic ejectments (Folk, 1980). In thin section the volcanic rock fragments have a trachytic texture with feldspar laths occurring in a sub-parallel alignment. The grains commonly have ferromagnesian minerals within the ground mass which are too small to resolve (plate **10** A1,A2 and B1,B2).

6.2.4 Mica

The amount of mica within the samples taken from the Gidgealpa south dome varies between trace amounts to 4.5%. The highest content of 4.5% from Gidgealpa 29 (6055'6") however is unusual since most samples have a mica content of below 2.5% (table **6**, page 227). Although mica has a hardness between 2-3 and good cleavage, it is a very durable mineral since it is difficult to round or fracture (Folk, 1980). This resistance to breakdown is due to the elasticity of mica and its flaky shape that allows it to 'dodge' around grains during transport. The durability of the mica is reflected by the relatively constant percentages in all samples at the Gidgealpa south dome.

The predominant mica present within the pre-provenance change sediments is muscovite, probably sourced mostly from granites, pegmatites and metamorphics of the Gawler Craton region to the south. Biotite also originates

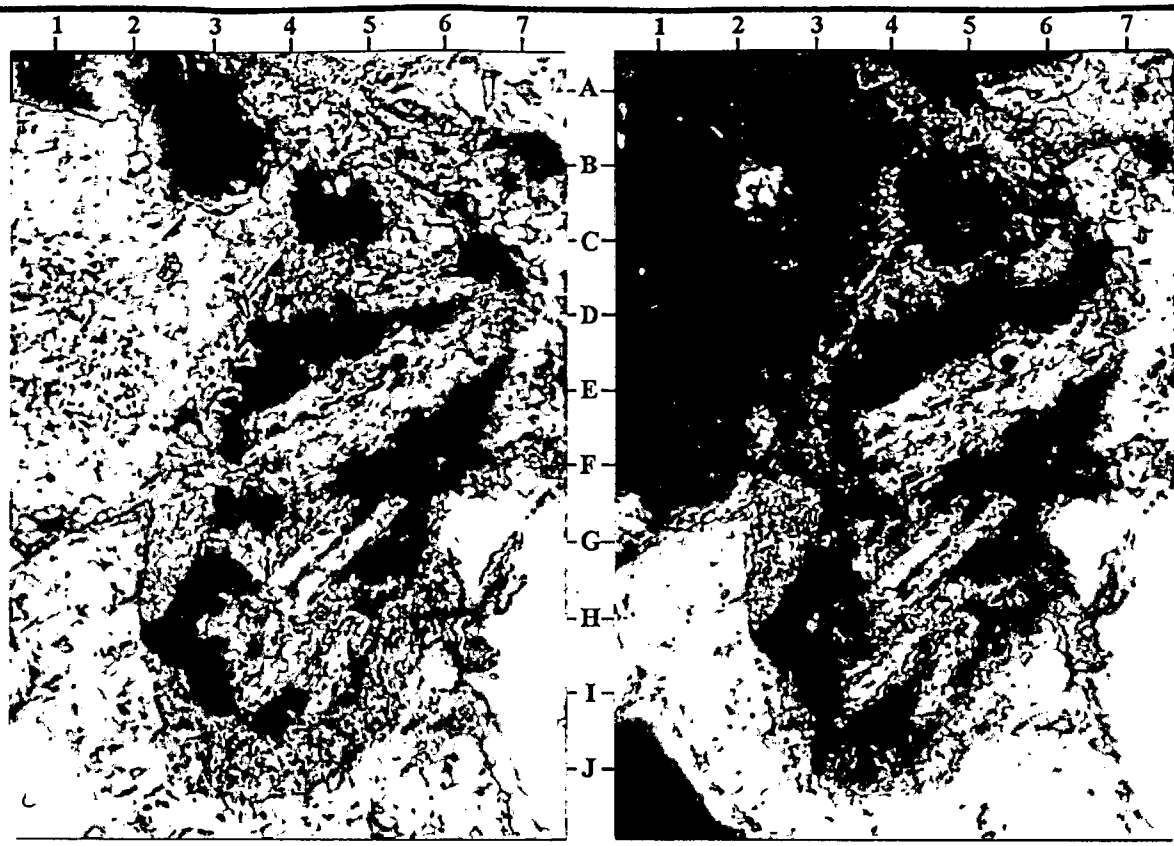

A1 Gidgealpa 31 5981'10" Field of view: 0.5mm

A2 Gidgealpa 31 5981'10" Field of view: 0.5mm

Volcanic litharenite under ppl (A1) and crossed nicolls (B2) showing the trachytic texture of a volcanic rock fragement (F4). Note the feldspar laths (G5) orientated sub-parallel and the dark ground mass from the dissolution of ferromagnesian minerals into clays.

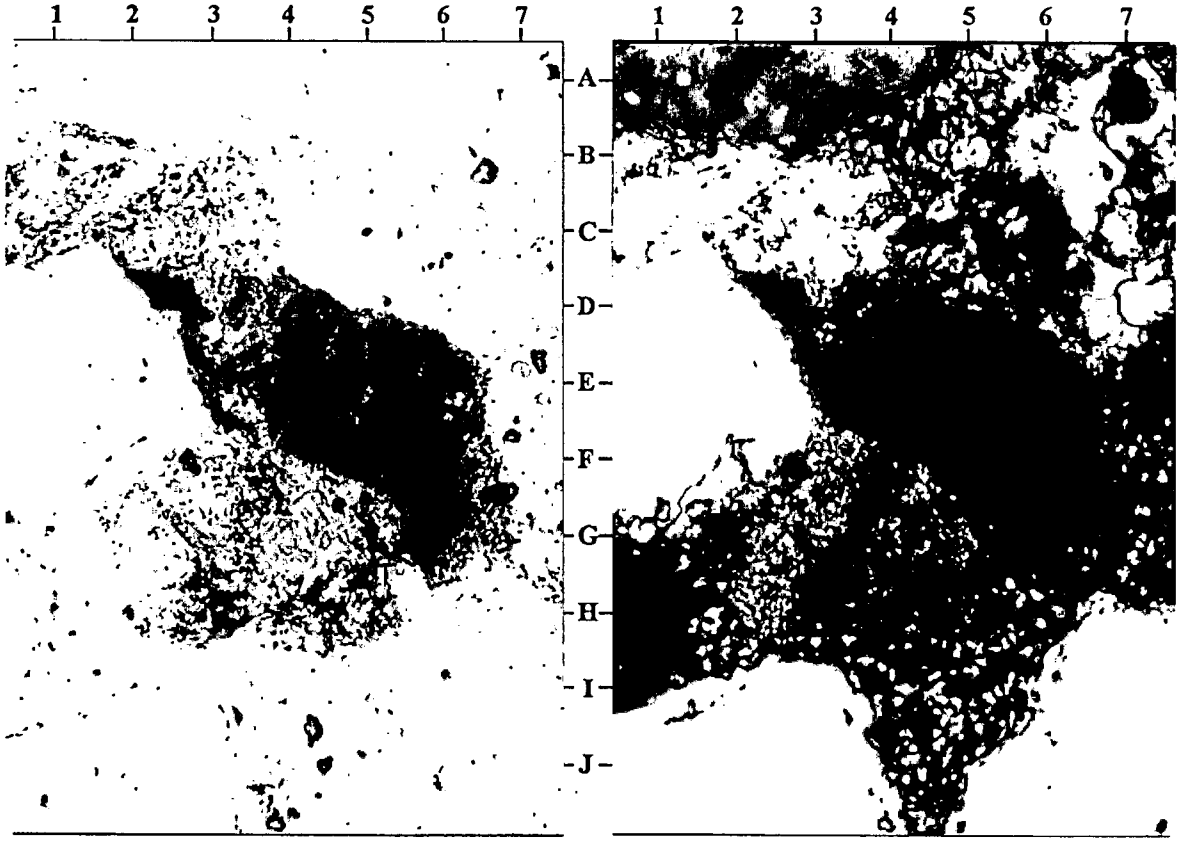

B1 Gidgealpa 30 6032'6" Field of view: 1mm

B2 Gidgealpa 30 6032'6" Field of view: 1mm

Sub-litharenite under ppl (B1) and crossed nicolls (B2) showing the presence of altered volcanic rock fragments (E4 and H3).

PLATE 10

from the same source but is absent within the sediments due to its instability and consequent breakdown within the relatively mature sediments. The post provenance sediments contain predominantly muscovite but some rare, highly dissolved biotite is present within two samples (Gidgealpa 30 (6037'6") and Gidgealpa 31 (5981'10"). This biotite is interpreted to originate from the eastern sourced volcanic sediments. It is almost the only primary mica that is present within the volcanics. The muscovite present in this case is probably from the sediments that were deposited before the provenance change and subsequently reworked and mixed with the volcanic sediments before deposition.

Mica commonly occurs as lath shaped flakes with a very large length to width ratio orientated sub-parallel to bedding. Almost all mica present shows grain bending and / or 'bow tie' structures (fanning at the end of the grains) indicating compaction within samples (plate **8** A1, A2 and B1, B2).

The state of mica varies with preferential dissolution at grain ends and along cleavage plains ranging from nil to minor within the same samples, while in others all grains are fresh. Alteration may occasionally occur with the breakdown along cleavage and the formation of chlorite and iron rich minerals (plate **8** A1, A2). Very rare authigenic mica occurs as needles nucleating and growing from the fanned end of grains (plate **8** B1, B2). Commonly, carbonate will also precipitate at grain ends or along cleavage plains and progressively split grains as the calcite crystals grow (plate **8** A1, A2).

6.2.5 Heavy Minerals

These minerals usually only occur in trace amounts within the samples. Easily identified heavy minerals include zircons, which are well rounded and have a high birefringence under cross nicolls, and tourmaline (plate **2**, page 235, A1 and A2) which appears a green / brown colour under plain light. Tourmaline

is very rarely seen and when present is well rounded. Zircons and opaque minerals are slightly more abundant but are still rare except in certain beds where heavy mineral banding has occurred. These minerals also appear to be rounded-to well rounded. Opaque minerals probably consist of ferrous minerals such as magnetite or haematite, however for this study the exact identification of composition was not investigated, nor thought necessary.

6.2.6 Matrix

Matrix content varies greatly for the sediments at the Gidgealpa south dome with values ranging from absent to 45.5% (table **6**, page 227). The amount present seems to be partially dependent on depositional environment and grain size. Low energy deposited lithofacies Sd generally has the highest matrix content overall while matrix content in the high energy St lithofacies is absent. Sediments with fine to very fine grain sizes have the highest matrix content while medium to coarse grained sediments have the lowest. Generally the matrix is amorphous and appears dirty from the presence of fine grained clays and silts. On closer inspection some crystallisation of kaolin has occurred with isolated booklets appearing scattered within the matrix. Some areas appear to be carbonate rich or associated with micritic siderite. The same matrix may also occur as a sericitic to illitic hash in places.

The matrix appears to have been formed by two different mechanisms. The first type is 'primary matrix' (Lewis, 1984) where the fine grained silts and clays were deposited pene-contemporaneously with the framework grains by mechanical means. The early deposition is identified by the absence of overgrowths on quartz grains due to the matrix surrounding the grains and inhibiting growth . The presence of primary matrix appears to be related to depositional environment since it is only present in the lower energy facies. An example is shown in plate **11** (A1 and A2); note the presence of the micritic siderite and sericitic / illitic hash associated with the matrix and the

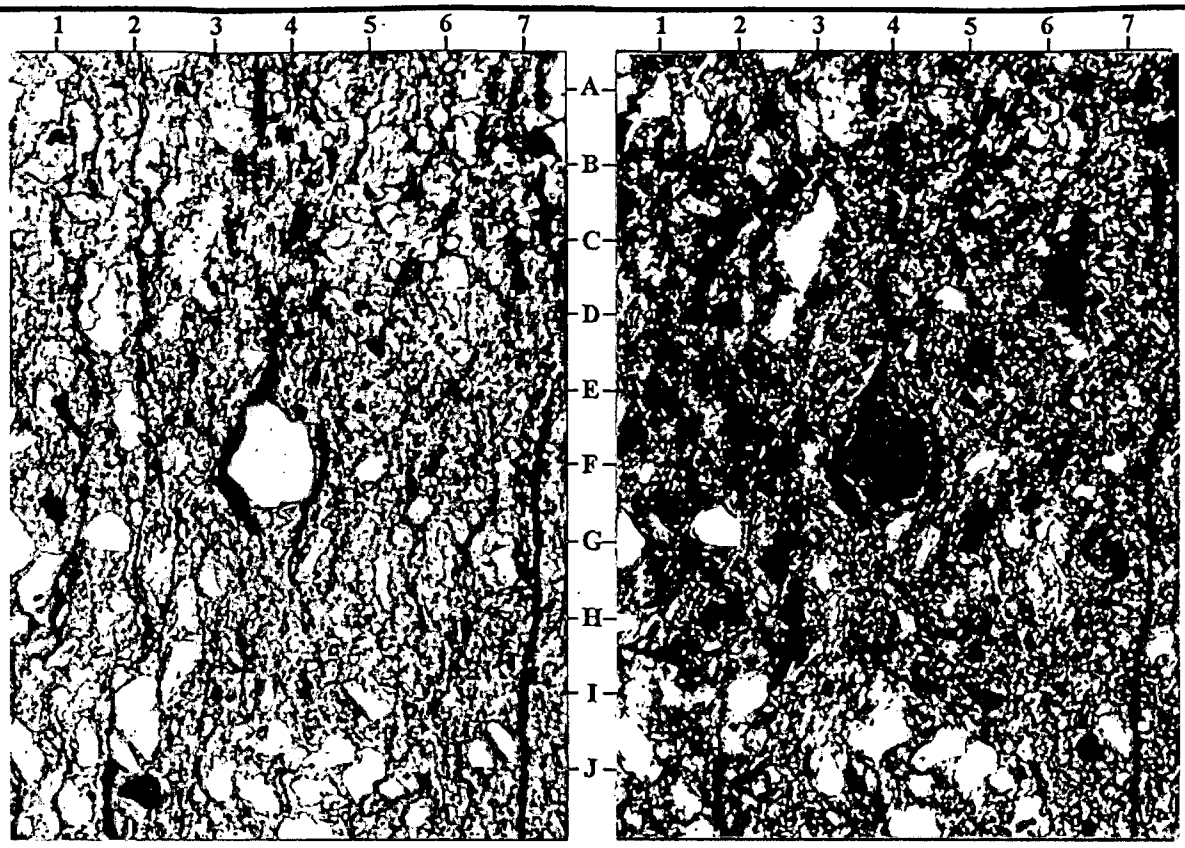

A1 Gidgealpa 29 6055'4" Field of view: 2mm **A2** Gidgealpa 29 6055'4" Field of view: 2mm

Muddy sub-litharenite under ppl (A1) and crossed nicolls (A2) showing the absence of quartz overgrowths due to the high primary matrix content of the rock. In these photos bedding orientation is vertical and note the compaction of the organic matter around some grains (F4).

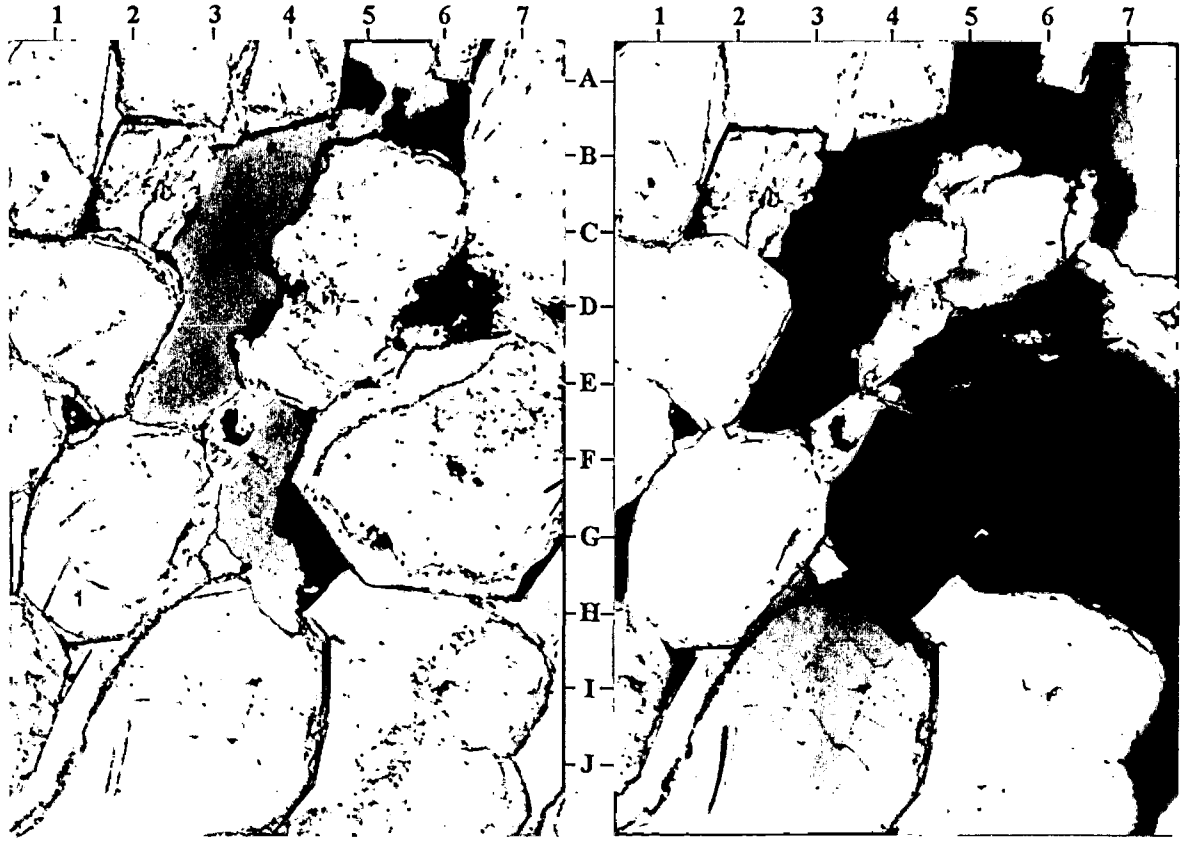

B1 Gidgealpa 32 6018'6" Field of view: 2mm **B2** Gidgealpa 32 6018'6" Field of view: 2mm

Quartz arenite under ppl (B1) and crossed nicolls (B2) showing the presence of secondary matrix (G4) from the dissolution of labile grains.

PLATE 11

absence of quartz overgrowths. 'Secondary matrix' (Lewis, 1984) may be present and is interpreted to consist of interstitial mineral matter that deposited within porosity during diagenesis from the breakdown of lithic, feldspar and mica grains. This type of matrix can be identified since its later formation does not inhibit the formation of quartz overgrowths, thus secondary matrix may be found lining the overgrowths of quartz grains. Plate **11** (B1 and B2) shows an example with the matrix lining quartz overgrowths; note adjacent porosity to the matrix is secondary dissolution of lithics, feldspars or micas and the matrix itself lacks the sericitic / illitic hash seen in the primary matrix.

6.2.7 Clays

Kaolinite and dickite are the main authigenic clays present within the Birkhead Formation, and kaolinite occurs in all of the samples while dickite occurs within most but not all. Only kaolinite is present within the Hutton Sandstone (table **6**, page 227). The amount of kaolin varies within samples from 0.5% to 30.5%. Using XRD analysis (table **9**) the authigenic minerals lizardite and clinochlore were also found to be present in minor amounts within the Birkhead Formation but were absent within the Hutton Sandstone.

Clinochlore is suggestive of a volcanic origin since it is generally formed as the alteration product of ferromagnesian minerals and volcanic glass. While kaolin is present within all samples, those that have elevated percentages (greater than 10%) seem to be isolated to the main delta and distributary sands. SEM analysis shows rare smectite and illite (plate **12** A, B and C) were found to be present. Due to their concentrations being so low within the samples they were not detected with XRD.

Thin section analysis indicates that kaolinite and dickite occur as subhedral to euhedral booklets that regularly replace dissolved or altered lithic and feldspar grains and line (plate **8**, page 246, B1 and B2) or even completely fills pore

Well	Depth	Facies	Quartz	Kaolinite	Dickite	Lizardite	Clinochlore	Muscovite	Siderite	Ankerite	Dolomite	Albite	Anorthite
Gidgealpa 26	5950'6"	Sh	**D**	M	tr	tr	tr	?	?	-	-	-	-
Gidgealpa 26	5956'4"	Sp	**D**	M	tr	?	-	-	?	-	-	-	-
Gidgealpa 26	5957'7"	Sh	**D**	M	-	tr	-	?	?	-	-	-	-
Gidgealpa 29	6025'4"	Sr	**D**	tr	-	tr	-	?	?	-	-	-	-
Gidgealpa 29	6038'1"	Sr	**D**	tr	?	?	-	-	?	-	-	-	-
Gidgealpa 29	6045'9"	Sd	**D**	?	tr	tr	?	tr	-	-	-	-	-
Gidgealpa 29	6047'2"	Sm	**D**	?	-	-	-	?	?	-	-	-	-
Gidgealpa 29	6055'4"	Sd	**D**	M	tr	M	tr	tr	?	-	-	-	-
Gidgealpa 29	6064'2"	St	**D**	M	-	-	-	-	-	-	-	-	-
Gidgealpa 30	6029'9"	St	**D**	tr	-	-	?	-	-	-	-	-	-
Gidgealpa 30	6032'6"	Sr	**D**	**S**	tr	tr	-	?	?	-	-	-	-
Gidgealpa 30	6037'6"	Sh	**D**	**S**	tr	-	-	?	?	-	-	-	-
Gidgealpa 30	6042'5"	Sd	**D**	M	-	tr	-	tr	?	-	-	-	-
Gidgealpa 31	5974'7"	Sr	**D**	M	tr	-	-	-	-	-	-	-	-
Gidgealpa 31	5981'10"	Sm	**D**	M	tr	-	-	?	?	**CD**	**S**	-	-
Gidgealpa 31	5985'10"	Sp	**D**	**S**	tr	?	-	tr	?	-	-	tr	-
Gidgealpa 31	5993'4"	Sr	**D**	M	-	-	-	?	M	**CD**	-	-	-
Gidgealpa 31	5997'3"	Sr	**D**	M	tr	tr	tr	?	M	-	-	M	tr
Gidgealpa 32	5989'9"	Sr	**D**	**S**	M	-	-	?	?	-	-	-	-
Gidgealpa 32	5992'2"	Sd	**D**	tr	-	tr	tr	?	?	-	-	-	-
Gidgealpa 32	6007'4"	Sm	**D**	tr	-	-	-	?	**S**	-	-	-	-
Gidgealpa 32	6015'9"	Sp	**D**	M	-	-	-	-	-	-	-	-	-
Gidgealpa 32	6018'6"	St	**D**	?	-	-	-	-	-	-	-	-	-

Table 9: XRD analysis of samples from the Gidgealpa south dome. **D**=Dominant, **CD**=Co-dominant, **S**=Subsidiary, M=minor, tr=Trace ?=Indication, -=Absent.

A

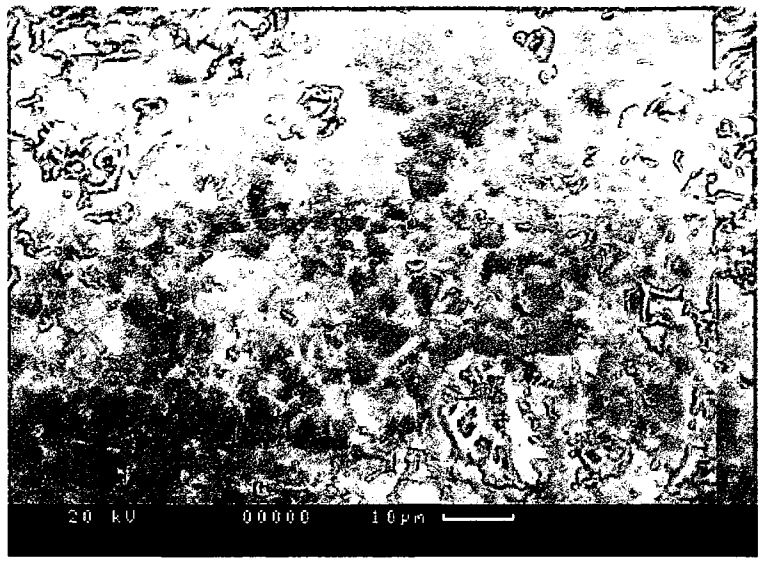

Abundant leafy, randomly orientated crystals of smectite.

Gidgealpa 32 6018'6"

B

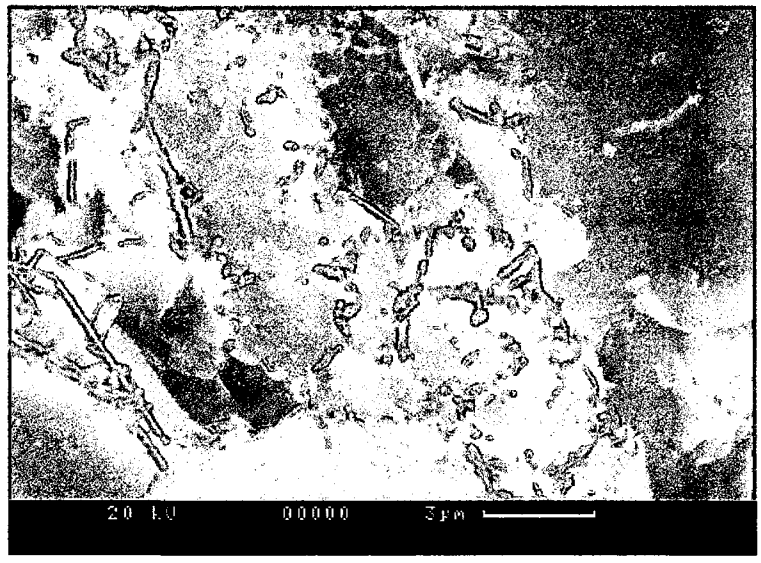

Authigenic illite forming noodle like crystals on the edge of mica plates.

Gidgealpa 32 5992'2"

C

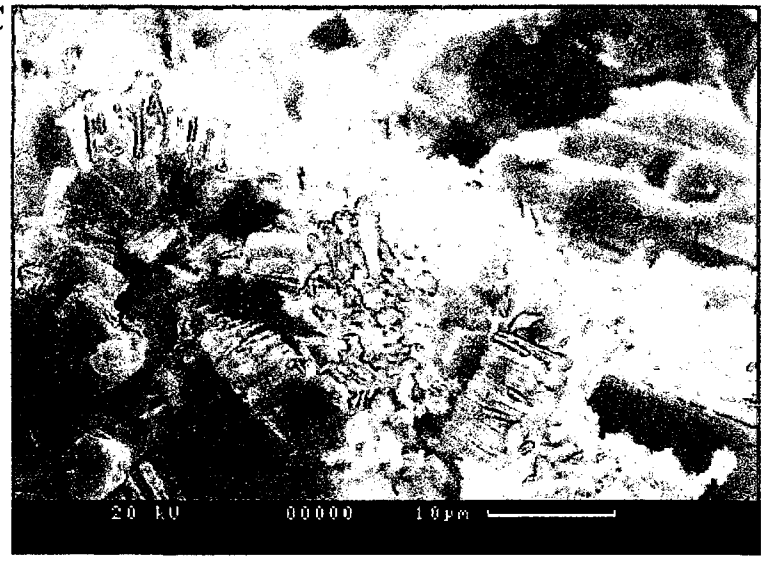

Authigenic illite forming noodle like crystals on vermiform kaolin.

Gidgealpa 32 5992'2"

PLATE 12

space (plate **8**, page 246, A1 and A2). Plate **13**A shows kaolin growing into secondary porosity developing after the dissolution of a lithic of feldspar grain while plate **13**B and C shows kaolin completely filling porosity. Under CL kaolin is easily identified by its brilliant royal blue luminescence, plate **14**A, B and C2 show kaolin lining and filling porosity as well as replacing lithic fragments.

Kaolin may form sharp or jagged contacts with quartz overgrowths, where the contact is sharp, kaolin has precipitated after the silica. However the rarer case where the contact is jagged is due to the concomitant precipitation of kaolin and silica. Plate **13**C shows the early precipitation of kaolin where it has been partially or entirely enclosed by quartz overgrowths. Similarly to Schulz-Rojahn and Philips (1989), kaolin has been seen in thin sections and SEM to occur in three different sizes ranging from 1-2μm to 10-15μm and 20-30μm within the Nappamerri Trough of the Cooper Basin. Schulz-Rojahn and Philips (1989) go on to determine that the larger occurrences of kaolin that form pseudohexagonal plates with ragged edges are in fact dickite. The presence of dickite in the Birkhead Formation samples is re-enforced by my findings that show the presence of dickite in XRD corresponds to the occurrences of larger kaolin booklets occurring in thin section.

The smaller crystals of kaolin have been determined to be kaolinite from microprobe analysis and ranges in shape from rounded blocky subhedral (plate **15**A) to sharp edged euhedral booklets (plate **15**B). The smaller booklets tend to form a honeycomb texture (Schulz-Rojahn and Philips,1989) and have also been seen to form between the bow-tie ends mica flakes (plate **15**C).

Kaolinite is likely to have formed from the alteration of K feldspars and micas in open diagenetic systems during periods of freshwater flushing. The formation of kaolin occurs at a similar pH as authigenic quartz and thus explains the similar times of formation (Schulz-Rojahn and Philips,1989). The later stage dickite consisting of larger crystals is thought to form from heated

A

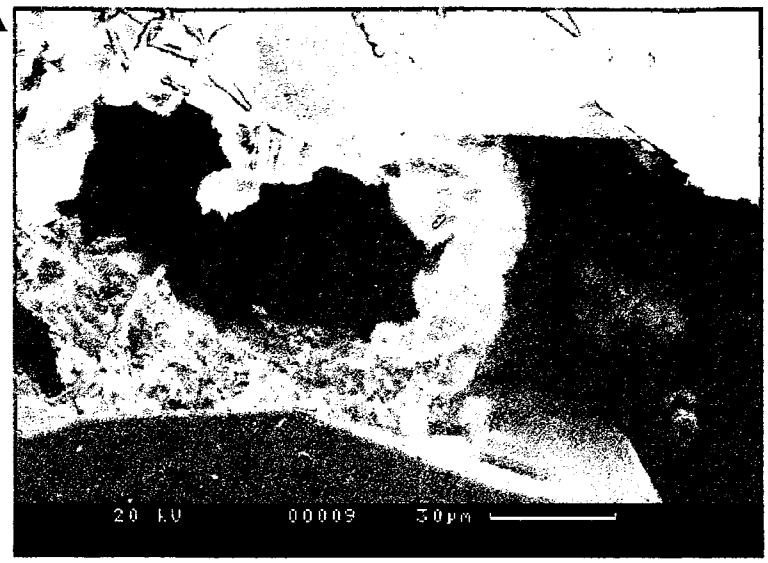

Authigenic kaolin booklets growing into secondary porosity after the dissolution of a labile grain.

Gidgealpa 30 6037'6"

B

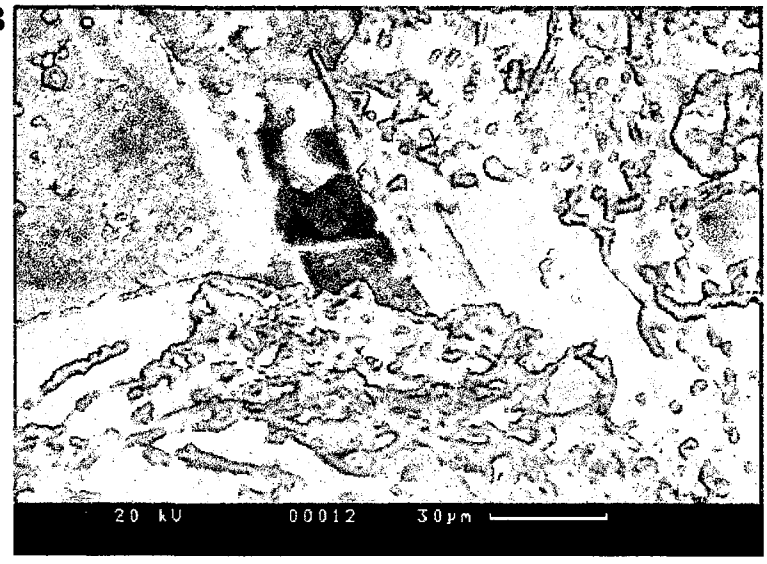

Kaolin with booklets approximately 10 micro metres in size blocking primary porosity. Note the microporosity associated with the kaolin.

Gidgealpa 30 6029'9"

C

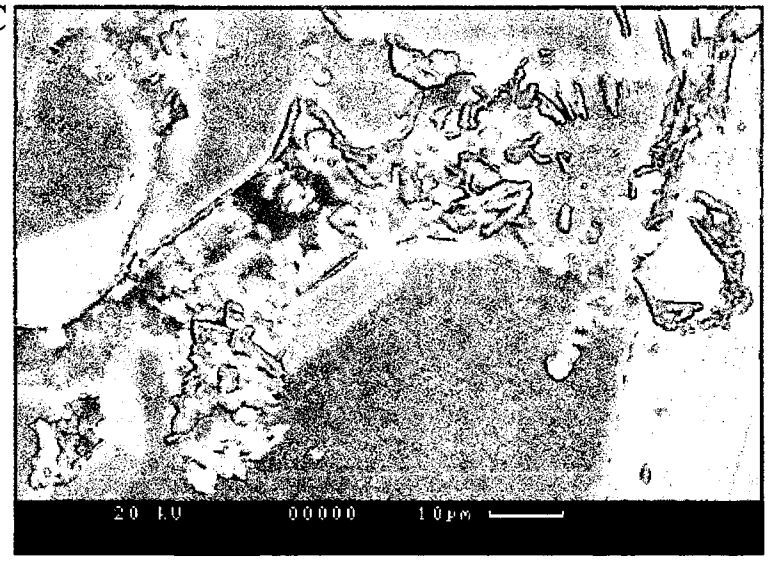

Another example of authigenic kaolin growing on quartz overgrowths and into primary porosity. From this micrograph it can also be seen how the quartz overgrowths partially grow around or engulf kaolin grains which suggests that precipitation is occurring at similar times.

Gidgealpa 32 6007'4"

PLATE 13

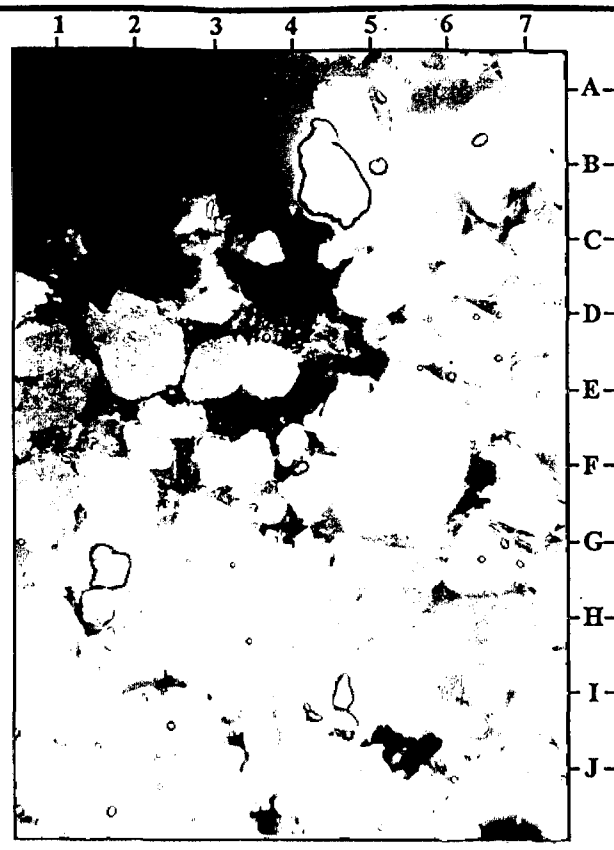

A Gidgealpa 32 6007'4" Field of view: 4mm
CL micrograph showing the presence of feldspars (B4.5) which luminesces a brilliant blue while pore filling kaolin (I5) luminesces royal blue.

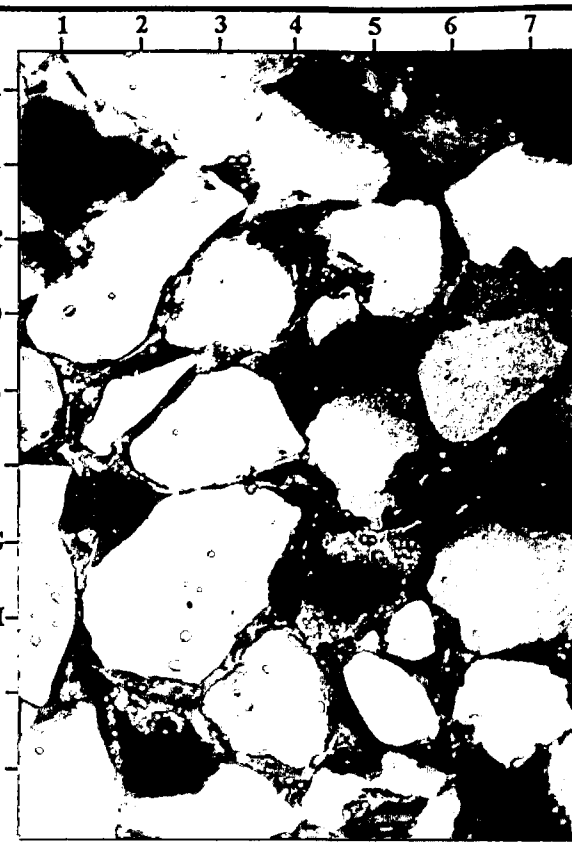

B Gidgealpa 30 6029'9" Field of view: 4mm
CL micrograph showing kaolin lining pores (A1) and replacing lithics (G5). Quartz overgrowths can be easily seen due to their poor luminescence.

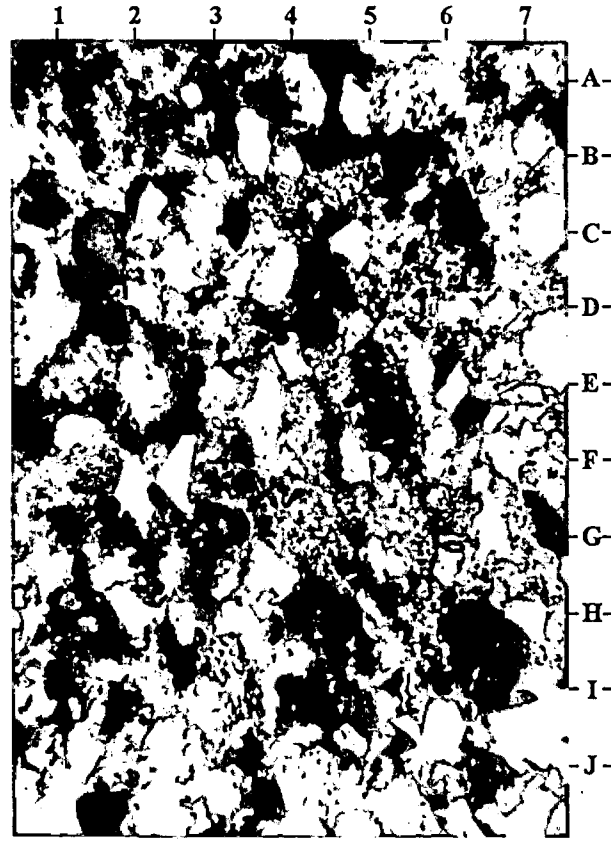

C1 Gidgealpa 31 5985'10" Field of view: 2mm

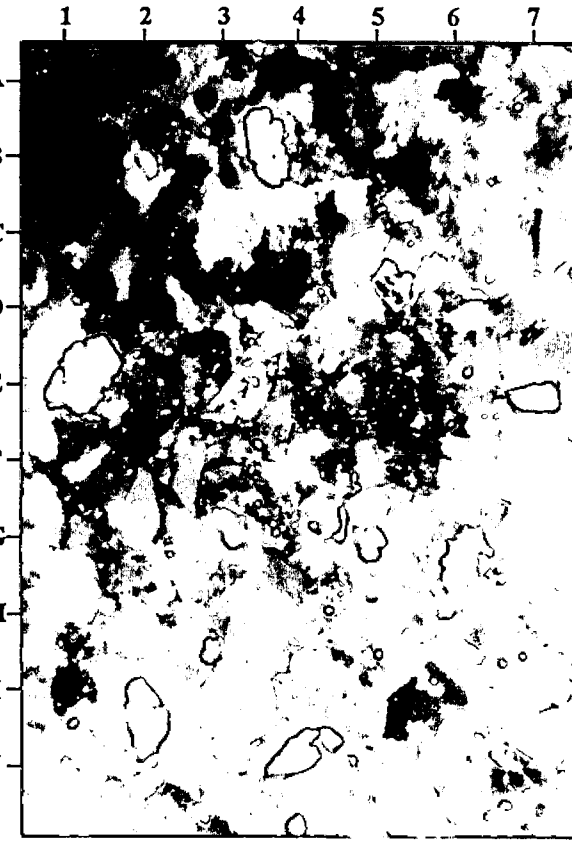

C2 Gidgealpa 31 5985'10" Field of view: 2mm

Litharenite under ppl (C1) and cathodoluminescence (C2) showing the high lithic content under plain light and feldspars (brilliant blue) (E1 and B3.5), pore filling kaolin (royal blue)(C3 and J4).

PLATE 14

A



Subhedral blocky, randomly orientated kaolin booklets filling primary porosity and replacing it with microporosity between books.

Gidgealpa 32 5992'2"

B



Early stage vermiform, blocky, sharp edged kaolin filling porosity.

Gidgealpa 32 6007'4"

C

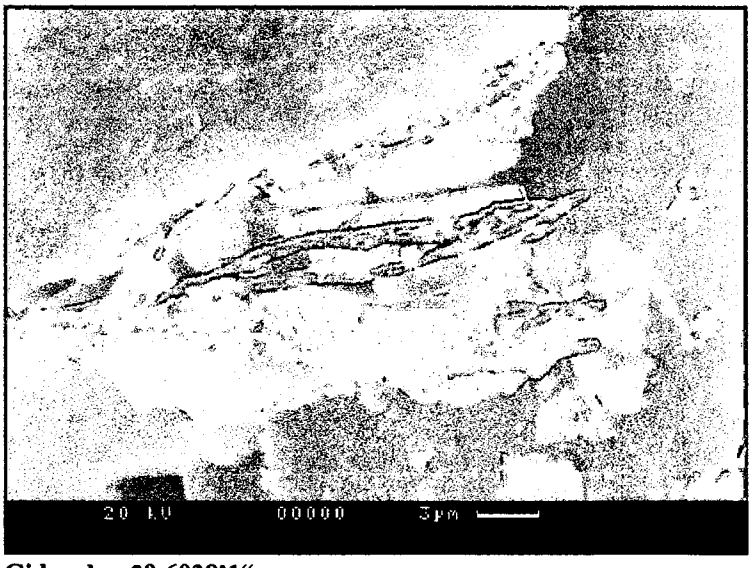

Growth of authigenic kaolin booklets on mica cleavage surfaces forcing the plates apart.

Gidgealpa 29 6038'1"

PLATE 15

ground waters flowing through sediments with high permeability and porosity (Kisch, 1983). This seems to be the case at the Gidgealpa south dome since transmitted light microscopy and XRD analysis show that dickite is late stage and fills most of any remaining porosity within samples. The large crystal size of the dickite is testimony to its slow precipitation under ideal conditions (Schulz-Rojahn and Philips, 1989).

6.2.8 Cements

6.2.8.1 Quartz

Silica cement occurs as quartz grain overgrowths within the Gidgealpa south dome samples and quantity varies from nil to 18.5% with values between 5% and 8% being common. Samples containing less than 1% quartz grain overgrowths are restricted to the slightly muddy litharenites due to the elevated levels of matrix lining quartz grain boundaries (table **6**, page 227). The percentage of rock fragments also affects authigenic quartz content. The elevated presence (43.5%) of lithic grains in Gidgealpa 31 (5985'10") (plate **14**, page 258, C1 and C2) has inhibited most growth due to the ductile grains bending and deforming around quartz grains before the commencement of silica growth. Abundant authigenic quartz is found in samples where matrix and lithic content are in less than trace amounts (plate **14**, page 258, B).

Silica cement occurs as syntaxial overgrowths on most sub-angular to rounded quartz grains. The presence of the overgrowths can usually be easily identified by the observation of a dust rim between the original grain and the overgrowth in plain polarised light. However, on occasion where the dust rim is not present it is difficult to determine whether grains contain overgrowths. This problem can be easily overcome by the use of CL. Detrital quartz can luminesce either dull blue / violet to dull red while in contrast the overgrowths can be seen by its non-luminescent properties(plate **14**, page 258B, plate **16**,

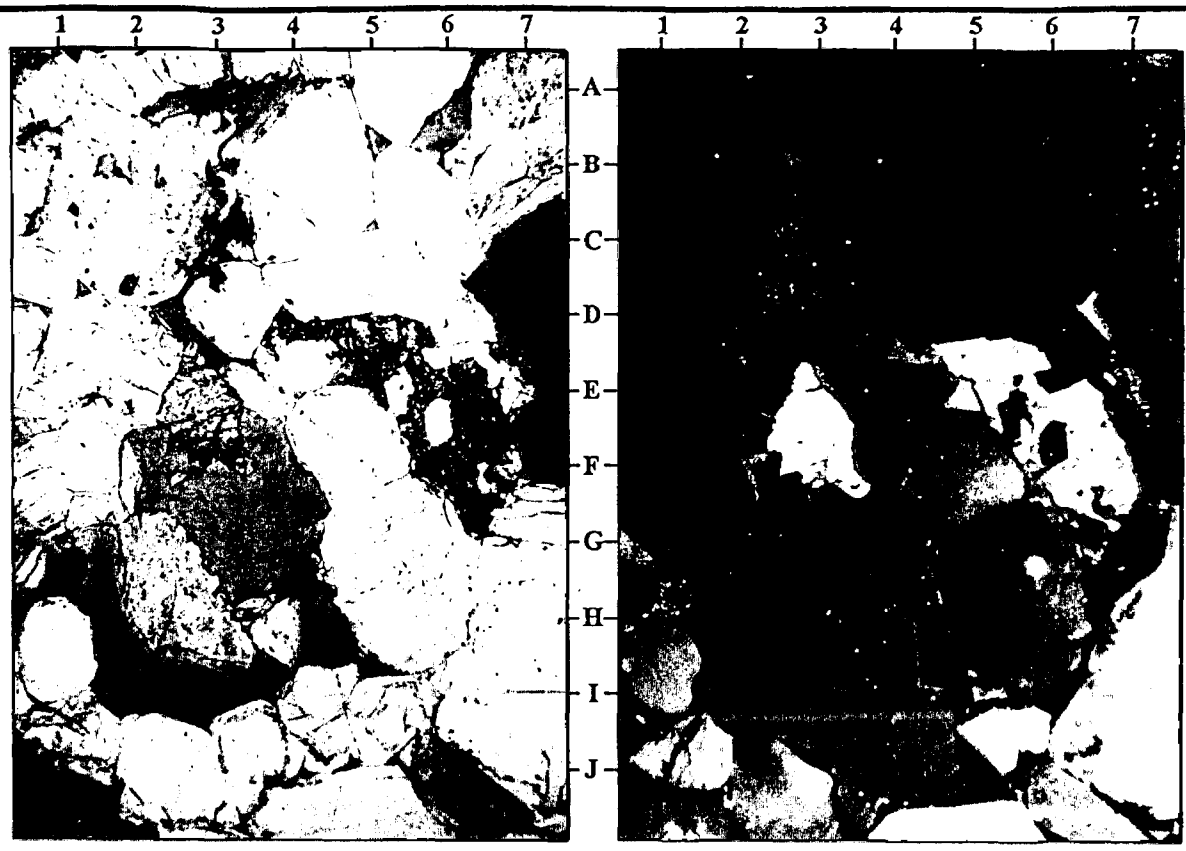

A1 Gidgealpa 30 6029'9" Field of view: 4mm **A2** Gidgealpa 30 6029'9" Field of view: 4mm

Quartz arenite under ppl (A1) and cathodoluminescence (A2) showing oversized porosity (G3) The CL micrograph also shows the tangential contacts of the quartz grains (G5) which are being held by the quartz overgrowths that do not luminesce (B5, F1). Overgrowths in A2 also show the grain ghosts which have etched the overgrowths and then subsequently dissolved (H3).

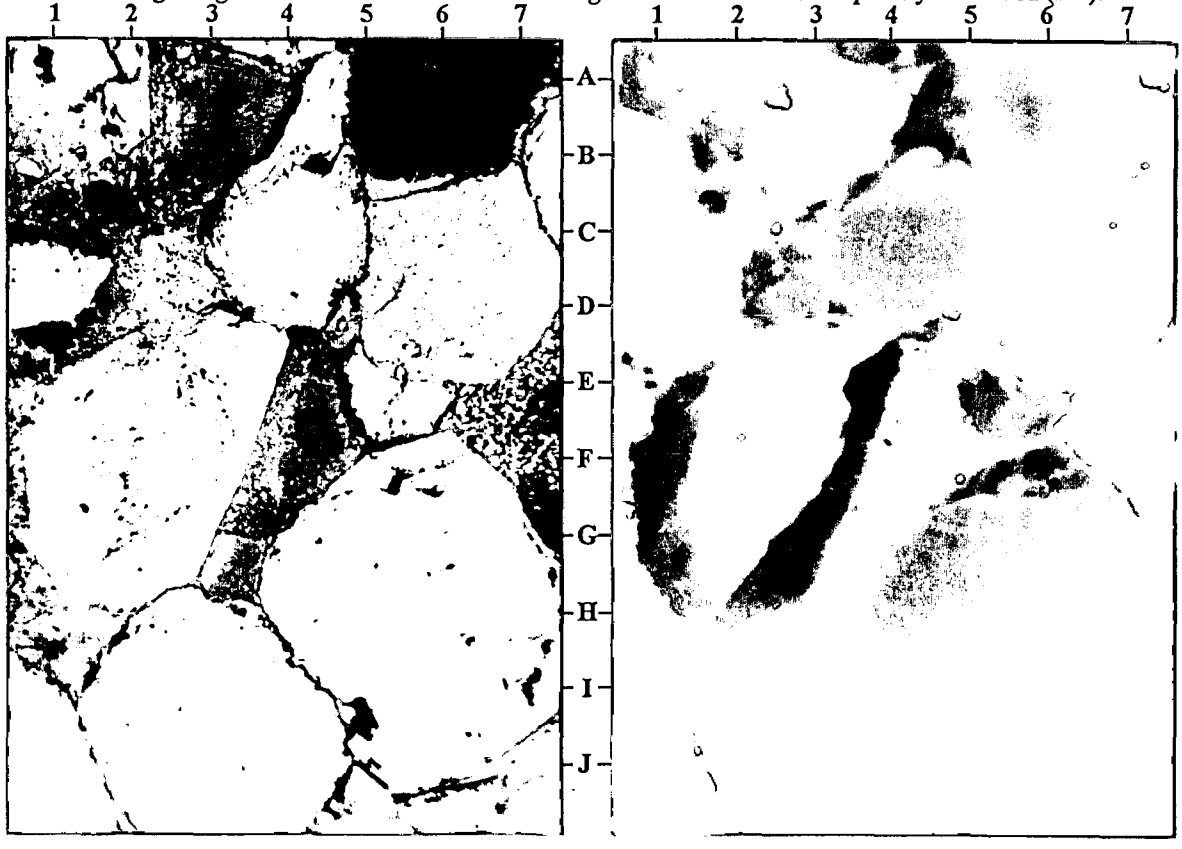

B1 Gidgealpa 32 6015'9" Field of view: 2mm **B2** Gidgealpa 32 6015'9" Field of view: 2mm

Quartz arenite under ppl (B1) and cathodoluminescence (B2) showing the presence of quartz overgrowths in photo B2 which are difficult to see in photo B1. In photo B2 kaolin (royal blue) is lining grains and filling porosity. In photo B2, as in other luminesced images the porosity appears a dull green colour due to the burning of the blue dye in the araldite.

PLATE 16

A1,A2 and B1,B2). From SEM studies authigenic quartz exhibits rhombohedral and prismatic terminations into porosity (plate **17** A and B) but may also reveal a drusey texture on detrital grains that protrude into porosity (plate **17** C). While this texture is visible under SEM it is too small to resolve under the transmitted light microscope.

CL shows that samples from both the Hutton Sandstone and the Birkhead Formation are relatively loosely packed with the initiation of quartz overgrowths very soon after the commencement of compaction. Detrital quartz grains commonly float in authigenic quartz or have tangential contacts with other grains (plate **16** A1). Evidence of some compaction is seen by the presence of some concavo-convex contacts which may also be sutured. Within the finer grained samples where matrix and / or lithic fragments are abundant quartz has limited overgrowths and quartz grains rarely come into contact. The lithic grains in these samples seem to be slightly compressed and deformed around the more rigid quartz and feldspar grains.

The occasional presence of carbonate incorporated within some quartz dust rims suggests that early precipitation of a minor phase occurred before the precipitation of authigenic quartz. Analysis of plate **13**C (page 257) shows that the growth of authigenic quartz continued until just after the initial precipitation of kaolin. A similar time of formation is inferred since no kaolin has been seen to be engulfed by quartz which would be the case if the kaolin had precipitated first. This similar relationship between authigenic quartz and early kaolin has also been noted by Bjorlykke (1988) in the North Sea Basin, Green et. al (1989) in the Eromanga Basin and Thomas (1990) in the Cooper Basin.

The origins of silica for the precipitation of authigenic quartz can come from many avenues. Silica can originate from the alteration of volcanic glass in lithics (Bjorlykke 1988), dissolution or kaolinisation of feldspars (Hawkins, 1978), the alteration of smectite to illite in shales (Towe, 1962), stylolitisation

A

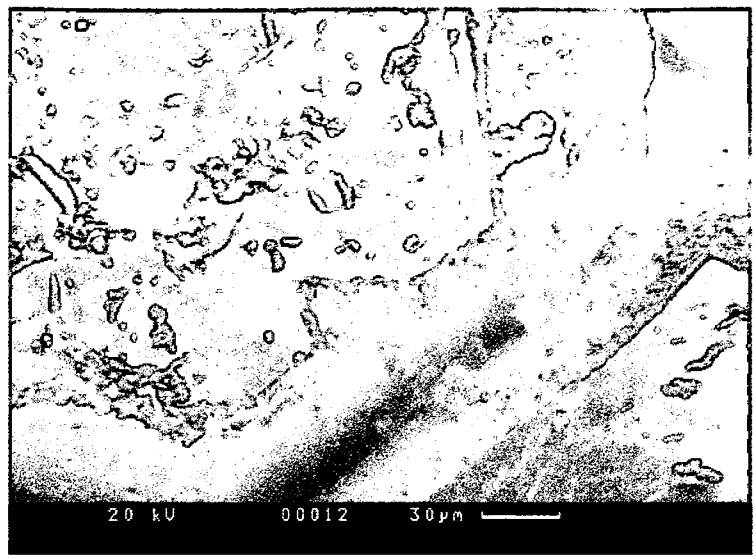

Rhombohedral overgrowths of authigenic quartz showing zoning due to different stages of growth.

Gidgealpa 30 6029'9"

B

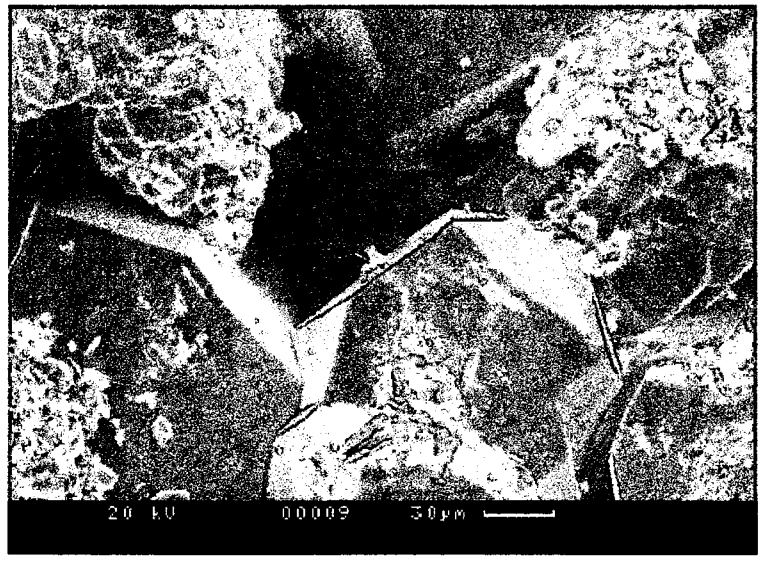

Prismatic terminations of authigenic quartz growing into primary porosity. In the top left carbonate is also filling porosity and possibly etching the quartz.

Gidgealpa 30 6037'6"

C

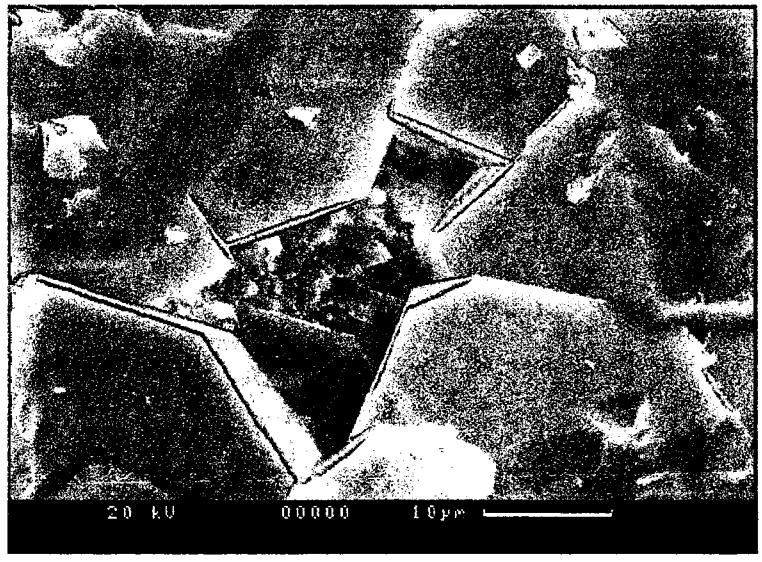

Drusey authigenic quartz texture in the centre of the pore throat reducing primary prosity and obstructing the pore. Also note kaolin casts to the bottom right which have been removed during sample preparation.

Gidgealpa 32 5992'2"

PLATE 17

(pressure dissolution) of quartz grains (Schulz-Rojahn and Philips, 1989) or the influence of meteoric waters after shallow burial (Bjorlykke 1988).

The most likely source of authigenic quartz at the Gidgealpa south dome would have to be from the influence of meteoric waters. The early precipitation of quartz can occur through the sub-surface movement of atmospheric waters that are rich in silica (Bjorlykke 1988, Schulz-Rojahn and Philips, 1989). If adequate porosity and permeability exists within the sediments mass fluid flow of mineral saturated waters will occur at a stage where the clastic sequence has been buried from shallow to intermediate depths (Schulz-Rojahn and Philips, 1989). This process is likely to occur in association with fresh water aquifers where sub-surface groundwater flow rates are high (Giles, 1987, Bjorlykke, 1988).

If the alteration of volcanic glass and the dissolution or kaolinisation of feldspars contributed silica it would have been in much lower quantities since the presence of these framework grains is likely to be very low. These processes are likely to have occurred later in the diagenetic history, allowing for subsequent silica precipitation to occur after the initial phase, producing zoned quartz overgrowths. Stylolitisation is not likely to be a source of vast amounts of silica since the amount of grain-grain suturing and concavo-convex contacts is limited. The relatively early initial phase of precipitation of the silica locked the grains in place inhibited any further compaction of the sediments. Smectite to illite alteration is not considered to be a source of silica since these clays were not found in large amounts.

6.2.8.2 Carbonate

All of the samples studied in both the Hutton Sandstone and the Birkhead Formation contain carbonate cement. Carbonate ranges from trace amounts to a maximum of 40.5% with most samples having amounts between 2% and

10% (table **6**, page 227). XRD analysis (table **9**, page 254) shows that siderite, ankerite and dolomite were present. Siderite is the dominant carbonate in all slides but does not show up on all XRD traces due to low concentrations within some samples.

Similarly to Thomas (1990) for the Permian Moomba Gas Field, the authigenic carbonate occurs as three different crystal habits. The variations seen within thin section and SEM are anhedral micrite (plate **18** A), an intermediate sized crystal carbonate described as rhombohedral or scalenohedral spar (plate **18** B) by Schulz-Rojahn and Philips (1989) and highly crystalline, poikilotopic spar (plate **18** C1 and C2). By correlation of XRD analyses with carbonates identified from thin sections the microspar and intermediate spar consist of siderite while the poikilotopic spar was determined to be either ankerite or dolomite. The siderite composition was re-enforced by the fact that the carbonate cements did not luminesce under CL due to quenching by the presence of Fe^{2+} (Miller, 1988). Micrite is commonly found to be dispersed within the matrix of the finer grained samples. Larger groupings of anhedral micrite is found to be associated with organic matter such as coal stringers (plate **18** A). Nodules of micrite approximately 1mm in width may also grow within the matrix incorporating silt and mud giving a dirty yellow-brown appearance. The timing of this carbonate is deemed to be very early (syndepositional) since micrite has been observed in between detrital quartz grains and the overgrowths.

The intermediate spar mainly occurs within medium to coarse grained samples. Where present this siderite can grow from existing micrite spar and displace the surrounding matrix or may grow into porosity (plate **19** A1,A2 and B1,B2 and plate **20** A). Carbonates have been seen to partially replace rock fragments, heavily etch feldspars and have commonly nucleated between cleavage of mica grains. From thin section analysis it appears that this intermediate stage of formation occurred before the major episode of kaolin precipitation since most siderite growths originate from quartz overgrowths

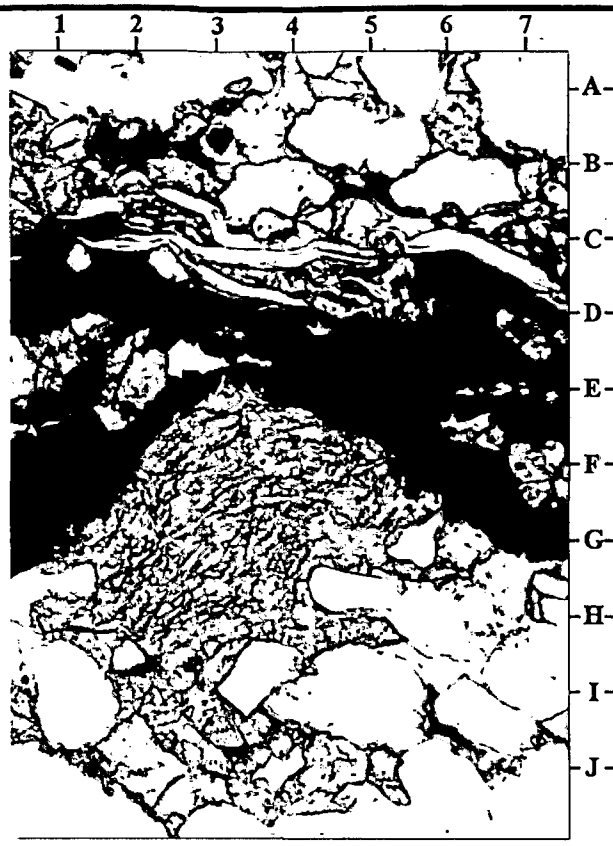

A Gidgealpa 32 6007'4" Field of view: 4mm
Quartz arenite under ppl showing early anhedral micrite (F3) associated with organic matter.

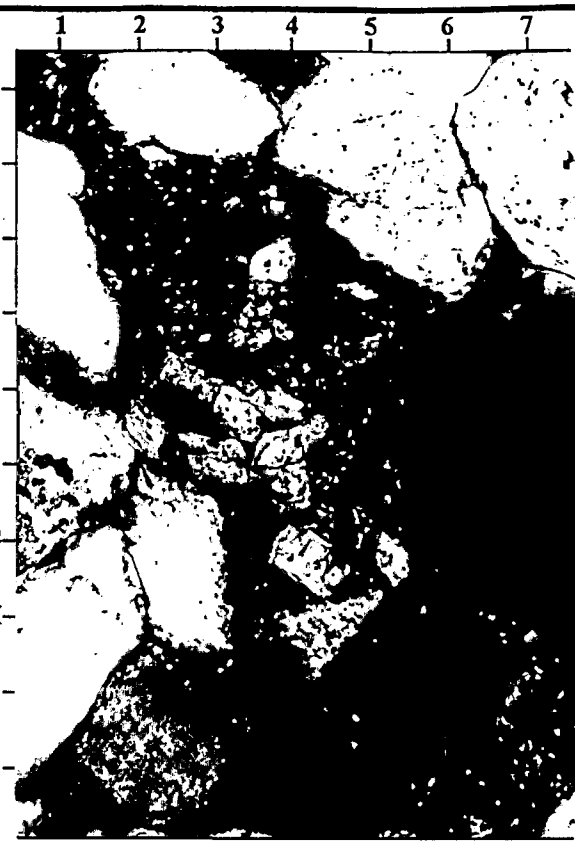

B Gidgealpa 32 6007'4" Field of view: 2mm
Quartz arenite under crossed nicolls showing the presence of rhombohedral carbonate spar (E3) surrounded by kaolin.

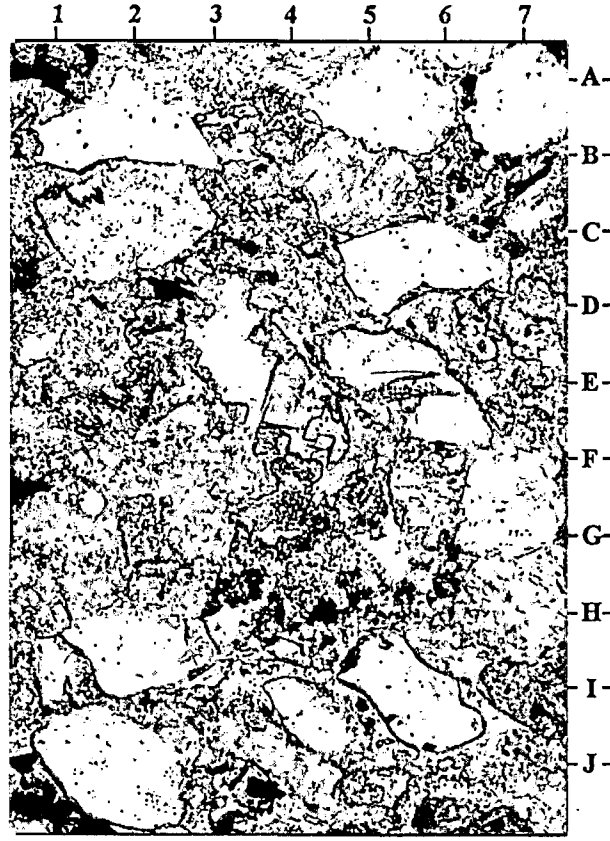

C1 Gidgealpa 31 5981'10" Field of view: 2mm

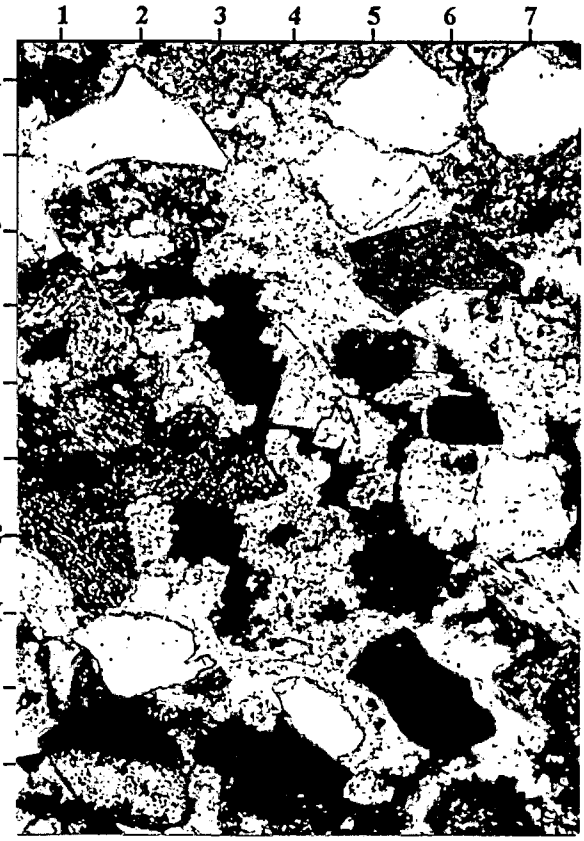

C2 Gidgealpa 31 5981'10" Field of view: 2mm

Volcanic Litharenite under ppl (C1) and crossed nicolls (C2) showing the late stage carbonate poikilotopic cement (D4) which fills porosity (G5), and replaces and etches grains (E5).

PLATE 18

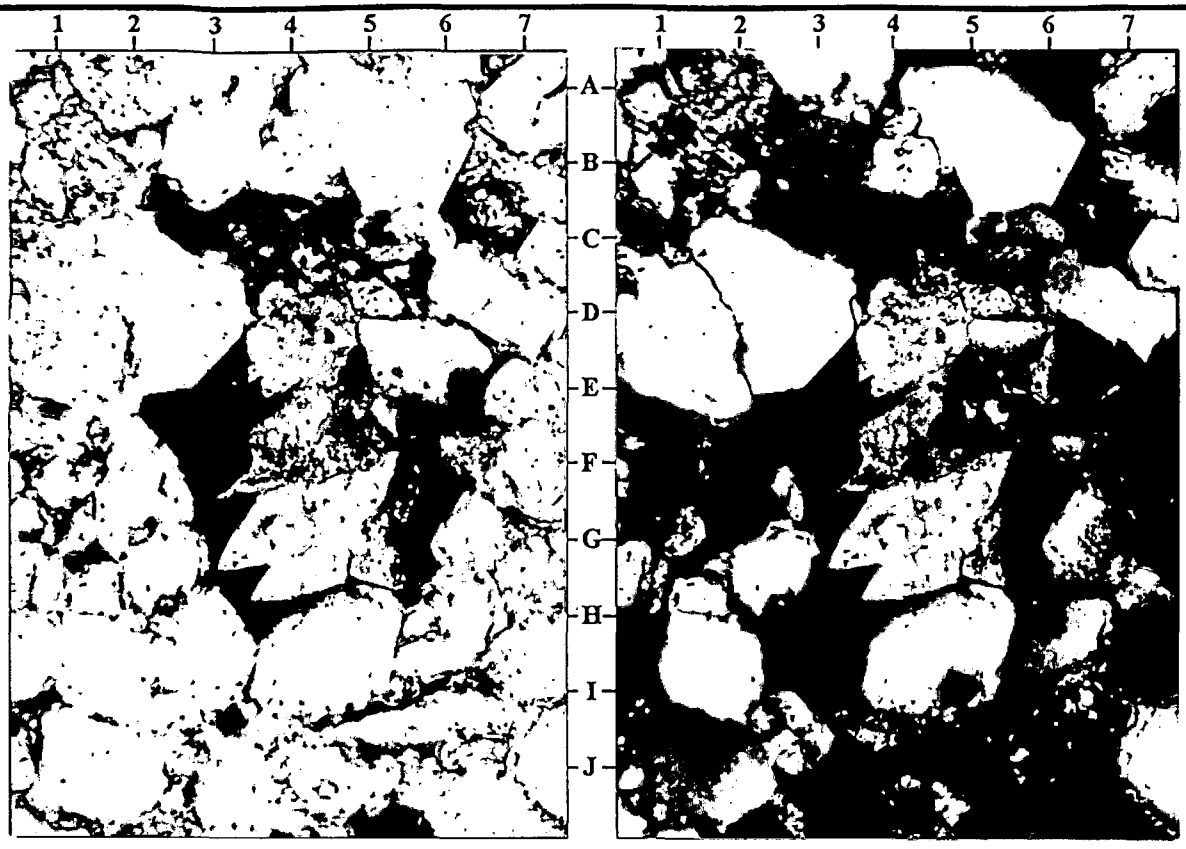

A1 Gidgealpa 29 6055'4" Field of view: 2mm **A2** Gidgealpa 29 6055'4" Field of view: 2mm

Muddy sub-litharenite under ppl (A1) and crossed nicolls (A2) showing intermediate carbonate spar rhombs (G4) nucleating from early micrite (C4) and growing into primary porosity (C4).

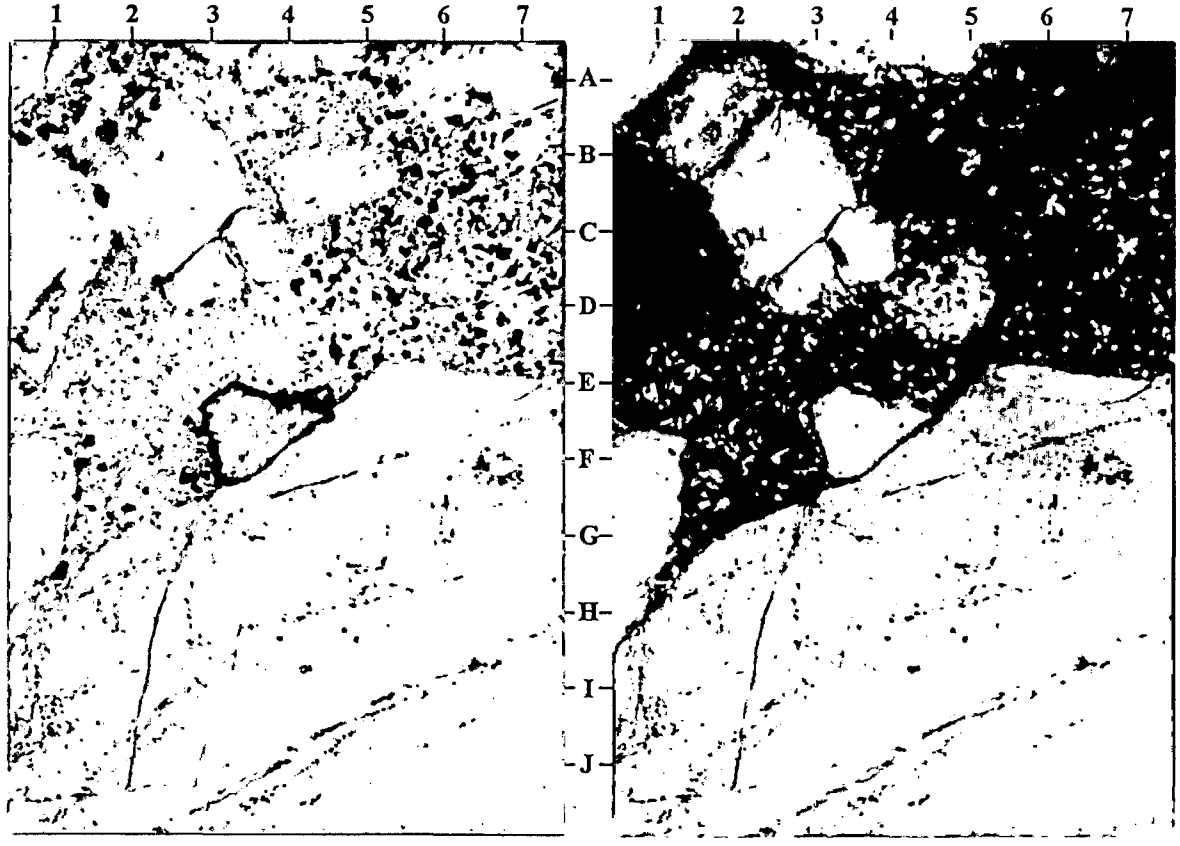

B1 Gidgealpa 32 6007'4" Field of view: 2mm **B2** Gidgealpa 32 6007'4" Field of view: 2mm

Quartz arenite under ppl (B1) and crossed nicolls (B2) showing the growth of intermediate carbonate spar into porosity (F4) which has subsequently been filled by kaolin (E2)

PLATE 19

A

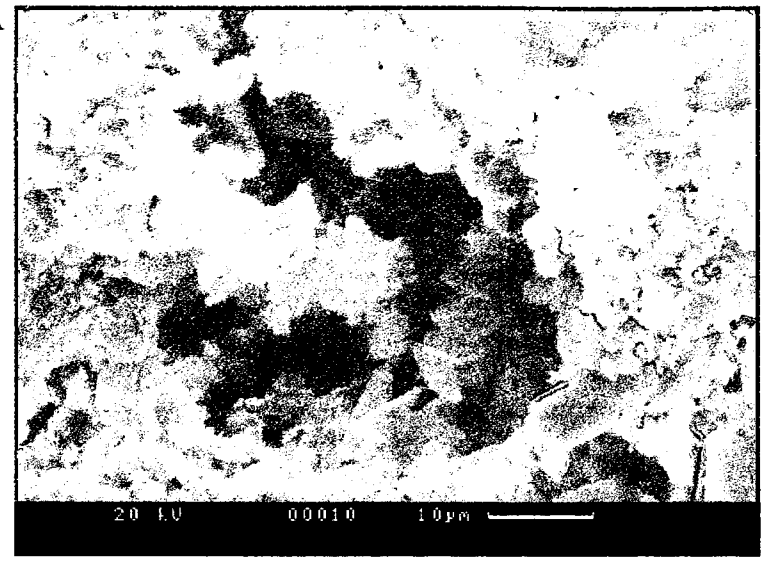

Early micritic and intermediate carbonate spar rhombs growing into secondary porosity created from the dissolution of a labile grain.

Gidgealpa 26 5956'6"

B

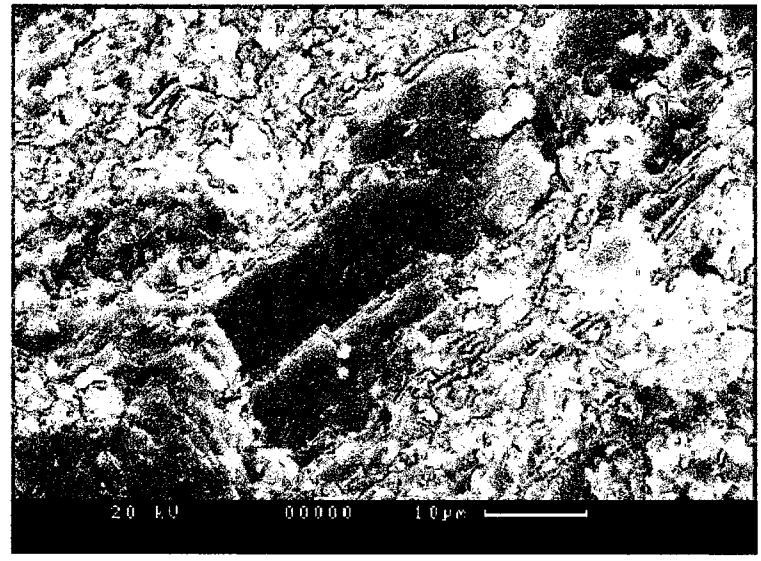

Late stage poikilotopic carbonate filling porosity and displacing matrix and cements.

Gidgealpa 31 5981'10"

C

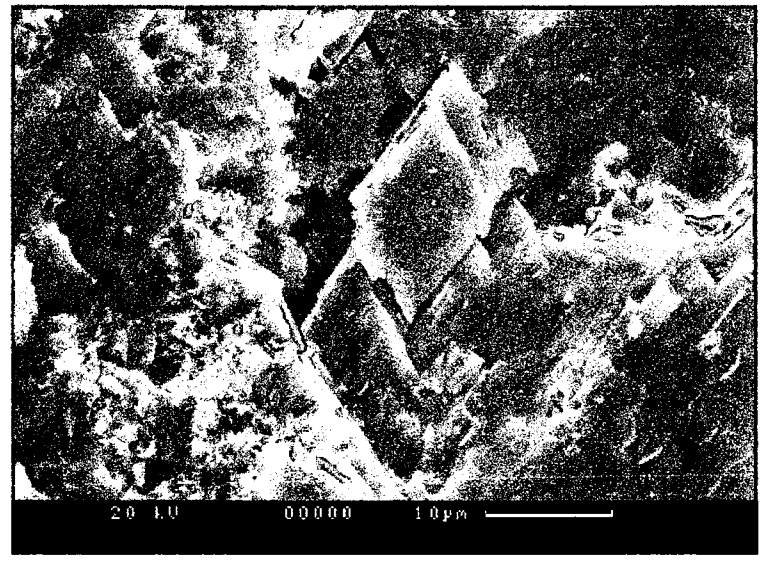

Late stage poikilotopic carbonate showing the interlocking of carbonate rhombs.

Gidgealpa 31 5981'10"

PLATE 20

which are subsequently surrounded by kaolin (Plate **19** B1 and B2). This phase of growth occurs after the initial micrite precipitation since at no stage is the intermediate spar surrounded by micrite. From CL analysis rare dolomite rhombs have been seen scattered throughout samples, because of their trace concentrations their presence is not recognised in XRD analysis.

The final stage of carbonate precipitation occurs late in the diagenetic sequence filling any remaining porosity, displacing or replacing kaolin, rock fragments or feldspars and etching quartz producing a poikilotopic texture (plate **18** C1 and C2, plate **20** B and C) throughout most of the samples. Interestingly this late stage cementation is isolated to samples within Gidgealpa 31 which has been interpreted not to be connected to the same deltaic system as the rest of the Gidgealpa south dome area and has thus undergone a slightly different diagenetic history.

Late stage cementation has also been observed by Boult (1996) in limited samples from Gidgealpa 32. From XRD and microprobe analysis this late stage carbonate consists of either ankerite or dolomite. The only other occurrence of late stage carbonate that was seen was in Gidgealpa 30 (6029'9) (plate **16**, page 261, B) where the blue / brown luminescence from low concentrations of Fe^{2+} suggests that the carbonate is ankerite. While the presence of the ankerite is rare there is evidence within the sample that late stage carbonate had precipitated and then dissolved due to the presence of etching of quartz overgrowths in the shape of carbonate rhombs (plate **16**, page 261, B).

The micritic siderite has been interpreted to be formed within the vadose zone while the spar cements formed after deeper burial within the phreatic zone (James and Choquette, 1984). The formation of the late stage ankerite and dolomite may have been caused by the movement of formation fluids rich in carbonate from the alteration and dissolution of volcanic lithic grains, the

alteration of plagioclase to clays and the breakdown of organic matter within the Birkhead Formation.

6.3 Diagenetic Sequence

Listed within this section and diagrammatically represented in figure **104** is a summary of the diagenetic sequence of the basal Birkhead Formation and the top Hutton Sandstone at the Gidgealpa south dome. The sequence of events was derived from textural relationships, cement stratigraphy and geochemical data using thin section, SEM and XRD analysis. The information derived is of a relative nature due to the many parameters effecting the processes of diagenesis, thus I have in no way tried to place timing constraints on events. It should also be noted that local variations can, and do occur within facies, wells and formations and this summary is a generalisation of these events. If major differences do occur they have been noted. More detailed diagenetic information of each sample can be found from thin section descriptions in appendix **6**.

Diagenetic events are listed in order from early to late:

- Micritic siderite precipitation occurred during or immediately after the deposition of sediments within the vadose zone. This event was minor except where siderite accumulated as cemented bands within siltstones. Early precipitation of micrite was noted by its presence between the detrital quartz grains and the authigenic cement. Micrite was also found to be present between grains that have undergone pressure solution from compaction.

- Sediment compaction was both early and short due to the subsequent precipitation of authigenic quartz. Compaction was observed by the limited presence of bent micas and concavo-convex contacts of quartz grains; these grain contacts may sometimes have associated suturing.

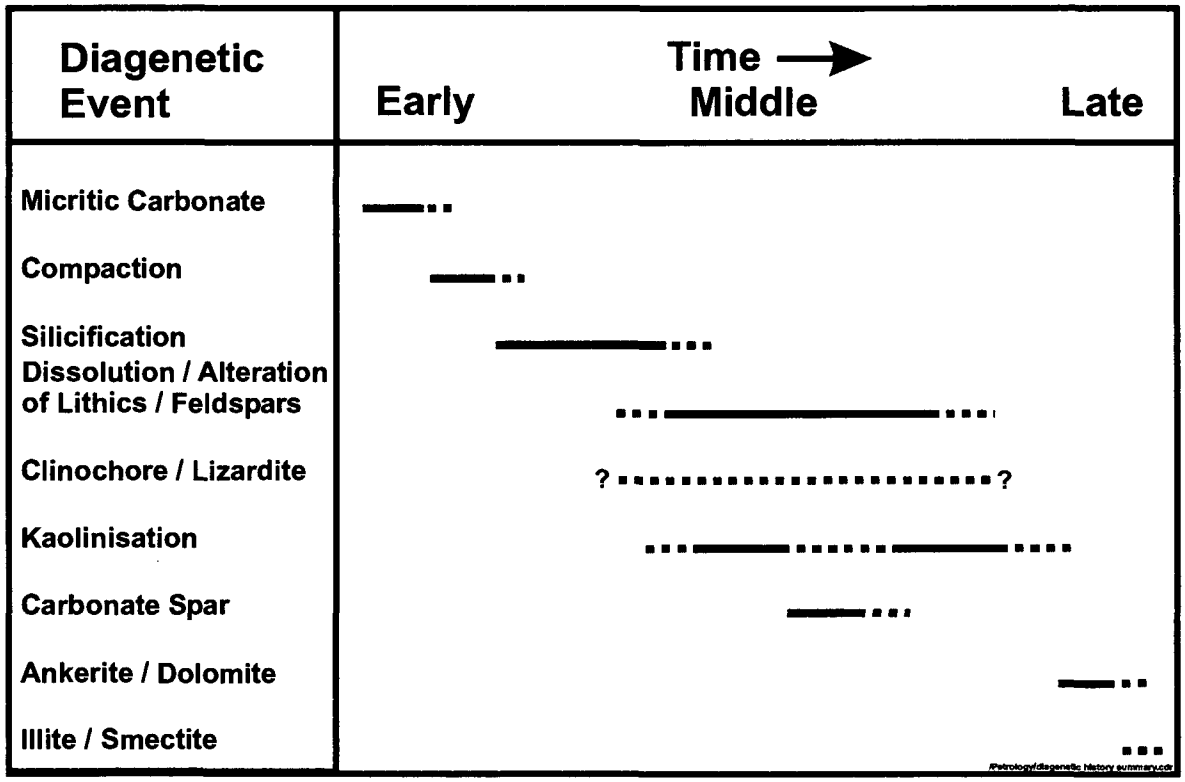

Figure 104: Diagenetic history summary of the basal Birkhead Formation and Top Hutton Sandstone at the Gidgealpa south dome.

• The onset of authigenic quartz was determined to be early due to the relative lack of significant compaction of the sediments. However where detrital quartz grains are rimmed by clays or matrix in the finer grained sediments limited compaction continued due to the absence of the overgrowths acting as a framework support. Sediments with abundant rock fragments also caused the inhibition of overgrowths. These sediments are significantly more compacted than the cleaner sediments but primary grain structure is still present.

• At some stage during the formation of authigenic quartz the feldspars and lithics were undergoing dissolution or alteration to kaolinite and sericite. This provided the necessary elements for the precipitation of kaolinite within limited amounts of primary and secondary porosity. This alteration / dissolution process probably was occurring throughout the diagenetic history and allowed for the precipitation of clinochlore and lizardite from these products. The precipitation of authigenic feldspar may have been initiated at this stage or any later stage where dissolution of detrital feldspars or lithics has taken place. The precipitation from surrounding clays of the mineral does not allow a distinction of any certain event except that it occurred after the deposition of the clay matrix.

• The initiation of kaolinite precipitation commenced just before the termination of authigenic silica. Some of this minor, early stage kaolinite occurs on top of quartz overgrowths showing that it precipitated after the authigenic quartz. However, under SEM, the presence of authigenic silica partially enclosing kaolin suggests some growth prior to termination of overgrowths had occurred.

• The removal of silica and aluminium from pore fluids during the formation of quartz overgrowths and the initial phase of kaolinite precipitation allowed carbonate to become over-saturated. This over-saturation along with the

presence of iron from the dissolution of volcano-lithics caused the precipitation of the second stage, intermediate spar siderite. The siderite spar precipitated in available secondary and primary porosity not filled by the early kaolin, the spar also precipitated around early micrite displaying its later timing.

• With another change in pore fluid chemistry; the second stage kaolinite precipitated within primary porosity not filled previously and newly developed secondary porosity from ongoing dissolution of lithic grains. Evidence of this later event occurring after the siderite precipitation is the growth of the spar on quartz overgrowths and the absence of kaolin between these two mineral phases. Where porosity was not completely filled by carbonate kaolin filled in most of the remaining pore space.

• This stage of diagenesis is marked by a number of variations within different samples and wells. It is possible that late stage dissolution of kaolinite is occurring from porosity within the Hutton Sandstone. These pore spaces are identified by kaolin lining pore edges. Within most of the Birkhead Formation samples, except those in Gidgealpa 31, the influx of heated fluids could possibly be the cause of late stage dickite precipitation within remaining porosity not filled by the earlier carbonate spar and kaolinite. The supply of elements for this precipitation may have originated from major dissolution of lithics, and feldspars as well as carbonates from Gidgealpa 30 (6029'9"). In Gidgealpa 31 and limited areas of Gidgealpa 32 late stage diagenesis is represented by the precipitation of poikilotopic ankerite etching quartz, feldspars, displacing matrix and cements and filling available porosity. This differing event from the other wells within the Gidgealpa south dome reflects the different diagenetic conditions that may be a result of the isolated nature of sand bodies.

• The conclusion of diagenesis is marked by the minor precipitation of illite and smectite within pore spaces and is probably a result of increasing depths of burial and temperature.

6.4 Factors affecting Porosity and Permeability

An understanding of the effects of diagenesis on porosity and permeability is important from the point of view of reserves estimation and ultimate recovery of the reservoir. From thin section analysis, SEM and mercury injection data it has been determined that diagenesis and the original textural properties of sediments has had a marked effect on porosity and permeability. The precipitation of authigenic clays such as kaolin and carbonate spar has transformed the majority of primary intergranular porosity to secondary or micro porosity. The presence of authigenic clays and carbonate has also affected permeability with decreases related to the amount of primary intergranular porosity.

Primary intergranular, secondary dissolution and micro porosity have all been recognised in samples from the Gidgealpa south dome and variations in the proportions exist within the different samples. Within the cleaner, coarser samples such as the Hutton Sandstone porosity is predominantly intergranular, although most pores have been reduced in size by quartz overgrowths. While these overgrowths have partly filled porosity they have had the added benefit of holding pore spaces open by holding quartz grains in place. Minor amounts of secondary porosity related to dissolution of clays and microporosity related to kaolin are associated with the abundant primary porosity. In general, typical Birkhead Formation samples contain more abundant clays and lithics and thus have minor intergranular porosity and elevated levels of dissolution and microporosity. In some cases the presence of secondary porosity may be the major contributor to overall porosity of a sandstone. For example, where the dissolution of labile grains has produced abundant oversized pores within the Birkhead Formation (plate **16**, A1 and A2, page 261).

The presence of microporosity is important within the Birkhead Formation. This type of porosity is mostly associated with pores between booklets of kaolin and less commonly between spar crystals which have partly filled pores. The abundance of kaolin within most samples means that this type of porosity is also high. The abundance of microporosity causes discrepancies between point counted and core plug porosities within samples. Where abundant microporosity is present within kaolin, it is not accounted for by point counting and subsequently porosity readings are lower than the core determined porosity. Authors such as Schulz-Rojahn and Philips (1989) and Thomas (1990) have demonstrated this fact by plotting core determined Helium injection porosity with porosity determined by point counting. The two types of porosity determination are only similar when the percentage of kaolin containing the microporosity is added to the point counted porosity (figure **105**).

The presence of clays such as illite, smectite and chlorite may reduce primary and secondary porosity by lining grain walls but would have minimal effects on porosity due to their minor presence.

Thomas (1990) determined that porosity trends existed within the Permian stratigraphic sequence of the Moomba Field. They are summarised here:

- Porosity increases with increasing grain size. Further, the trend is only recognised when using core plug data. If point counted values are used no apparent trend can be determined. The cause of the discrepancy was determined to be linked to the presence of microporosity within kaolin.

- Porosity increases with the degree of sorting. This increase in porosity was found to be independent of grain size.

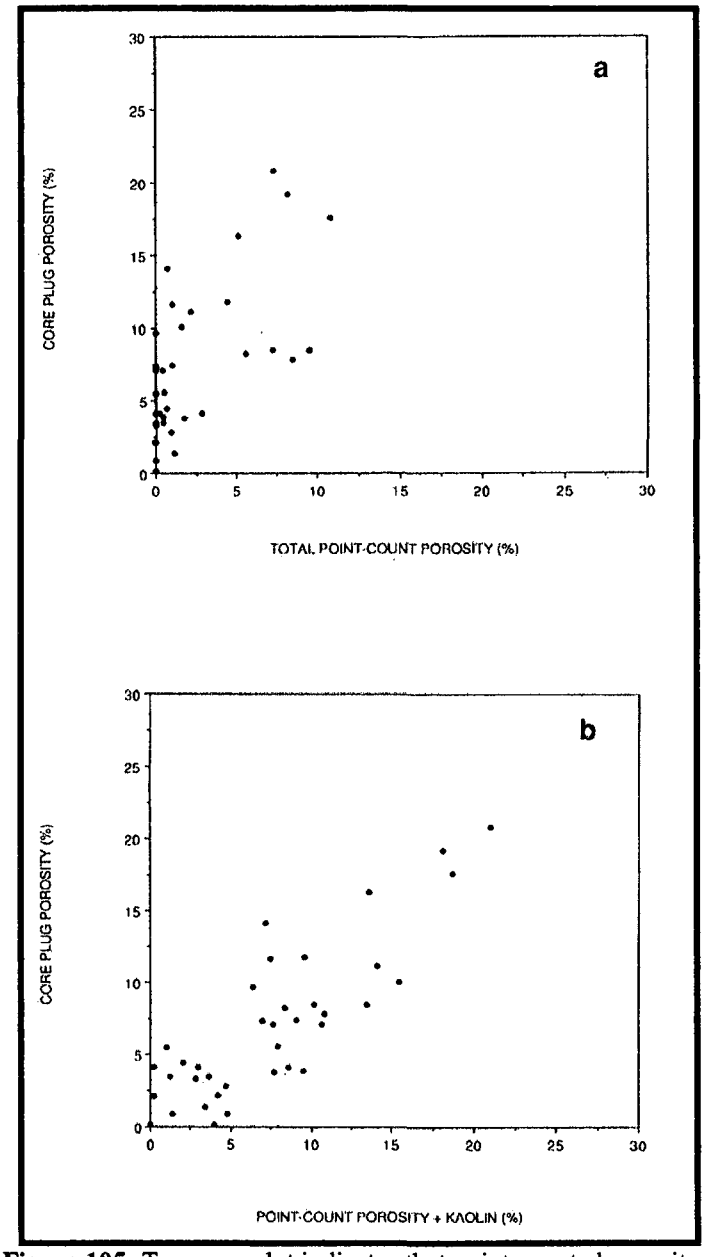

Figure 105: Top cross plot indicates that point counted porosity underestimates core plug porosity. The bottom cross plot shows a much better comparion between the data when the percentage of kaolin is added to the point counted porosity (From Schulz-Rojahn and Phillips, 1989).

• Porosity decreases with increasing depth. This trend was determined to be caused by increasing compaction and authigenic mineral growth with depth.

While grainsize and sorting have similar effects on porosity at the Gidgealpa south dome to those observed by Thomas (1990), it seems that the main controlling factor was sorting. This fact is re-enforced by figure **106** which shows the relationship between increasing porosity and increasing grain size and sorting. Table **6** (page 227) illustrates this point with generally low porosities associated with poorly sorted sandstones and higher porosities associated with well sorted sandstones. The effects of depth on porosity was not observed in the Birkhead Formation at Gidgealpa. Any trends, if present seemed to be related to original sandstone composition and diagenetic history. A good example of this fact is seen in Gidgealpa 30 (6029'9") which has a high porosity value when compared with samples of a similar nature. In this case a differing diagenetic history has caused abundant grain dissolution of labile grains, cements and clays whereas other samples have only undergone mild dissolution.

Permeabilities of sediments within the Birkhead Formation appear to be affected by the initial sediment grain size, sorting and diagenetic history. It is commonly accepted that permeability is party controlled by grain size with authors such as Steveson and Spry (1973), Martin and Hamilton (1981) and Little (1996) recognising this fact. Figure **106** demonstrates the relationship of grainsize and sorting to permeability. Theologou (1995) suggested that permeability is controlled by depositional environment and it seems likely that grain size and grain sorting are also related to the depositional environment. During deposition of sediments the varying depositional energy and processes occurring will cause grain size and grain packing to differ thus effecting the permeability of various sediments. The effects of sorting is also important within the Hutton Sandstone, the continuous deposition and reworking will produce well sorted sediments. This variation is reflected in the calculated

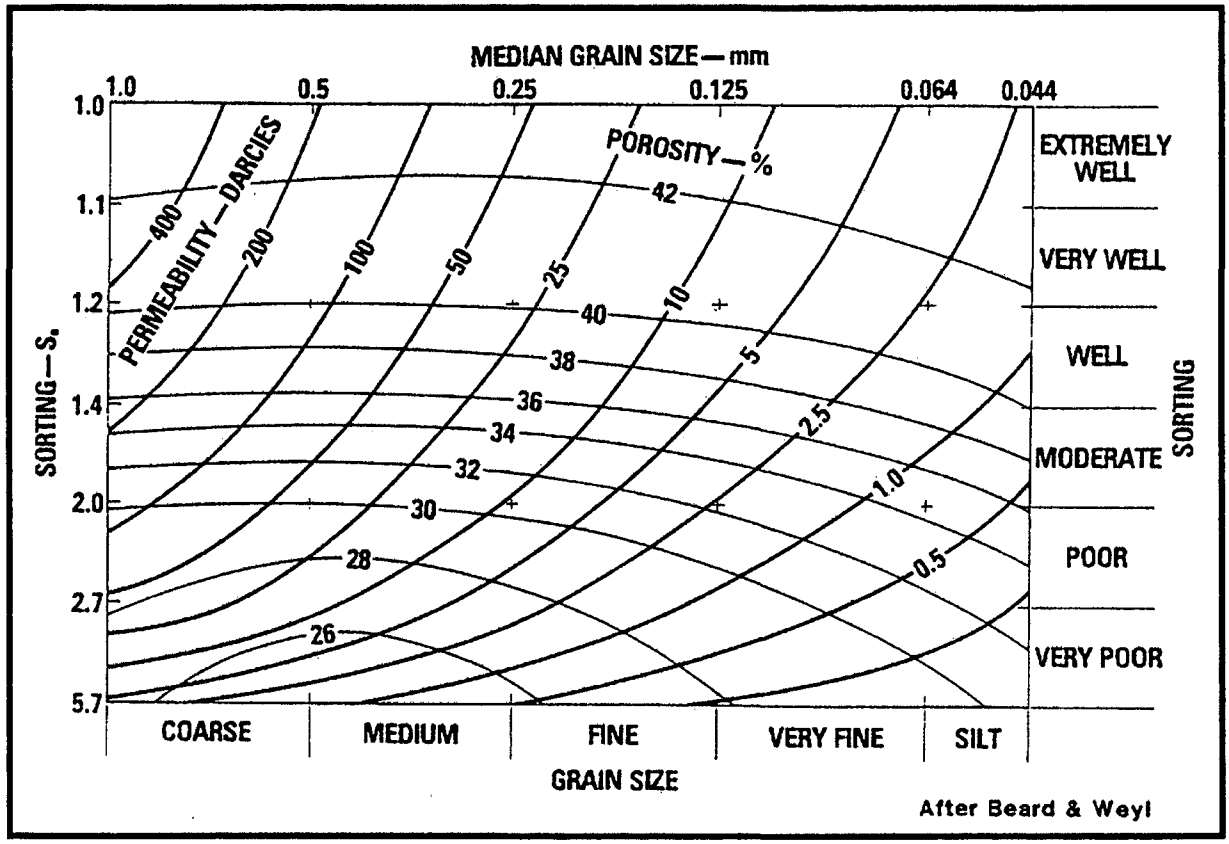

Figure 106: Porosity and permeability of artificially mixed and wet packed sand of different grain sizes and sortimg (From Sneider, 1992 after Beard and Weyl, 1973).

average permeabilities of facies (see section **7.3.2.2**). The Hutton Sandstone permeabilities are generally high owing to their deposition within a braided fluvial environment, while the Birkhead Formation has a greater permeability variation due to the differing depositional environments such as channel fill and delta fill sediments and the different provenance of sediments.

Little (1996) described how finer grained sandstones have pore throats that are less likely to be connected and the presence of silts and clays are more likely to block pores due to their smaller size. In contrast the medium to coarse grained sandstones have better pore connections due to their larger size with clay content having less of an effect and, in fact these sandstones generally contain less silt and clays than their finer counterparts. These observations were noted from thin sections and SEM analysis of the Birkhead Formation and Hutton Sandstone.

Permeability within the Gidgealpa south dome is a function of diagenesis with quartz overgrowths, authigenic and carbonate cements, compaction and clays all reducing values, however more rarely, permeability may be increased by secondary dissolution porosity. The presence of quartz overgrowths has been determined to be a benefit to permeability. Grains cemented by authigenic quartz hold the detrital grain framework in place resisting compaction effects. The loss of permeability by the presence is minor compared to the benefits since pore connections are preserved. The only case where overgrowths may be detrimental is within cleaner coarser sandstones that have abundant triple point junctions effectively closing pore throats. In the case of the Hutton Sandstone and the Birkhead Formation the formation of these triple junctions is not common. Schulz-Rojahn and Philips (1989) and Green et. al, (1989) describe similar effects of authigenic silica on permeability characteristics. Where overgrowths are not established within sediments permeability is heavily affected by compaction. This is especially the case where lithics are abundant, since the ductile grains are squeezed and bent around the more competent framework grains filling porosity and destroying pore throats.

The abundance of kaolin within the Birkhead Formation means that it is a major control on permeability. Where the clay is present pore throats are heavily restricted reducing permeability and the formation of microporosity increases pore tortuosity. Clays such as chlorite and minor amounts of illite and smectite line pore throats reducing their diameter thus reducing their permeability. These clays, that are more abundant within the finer grained sandstones, have a greater effect on permeability due to the initial smaller size of pore throats.

Carbonate cements, particularly the spar and poikilotopic cements, have reduced permeability by filling pores and blocking pore throats. The effect of carbonates are more evident within finer grained sediments where dissolution of carbonates is not as pronounced. Where poikilotopic carbonate exists, the sandstone has very low porosity and permeability values due to the carbonate totally filling porosity and pore throats and replacing or displacing kaolin. The nature of this particular cement means that pore fluids are unable to flow between grains to produce any potential secondary porosity.

Secondary dissolution of grains, in general, within the Birkhead Formation does not enhance permeability. Thomas (1990) found similar results within the Permian of the Moomba Field. Within most finer grained samples the dissolution of cements is rare and when present is only minor. While the dissolution of labile grains will increase porosity, their usually scattered and dispersed nature means that permeability is not elevated. Within coarser grained sandstones where porosity and permeability are still present late in the diagenetic history pore fluids can readily dissolve labile grains.
Extreme cases can occur within the Birkhead Formation where most labile grains including lithics, feldspars and micas as well as cements are highly dissolved producing oversized porosity. The nature of the pore spaces means that pore throat connections are large and abundant elevating permeability values. This high level of dissolution has also occurred within the Hutton

Sandstone where abundant dissolution of kaolin can be observed from remnant clay rimming porosity.

6.5 Discussion

The results of this diagenetic study have been invaluable in determining the reservoir characteristics and the identification of the provenance change at the Gidgealpa south dome. The associated use of SEM and XRD data has greatly aided the analysis of thin sections by enhancing the understanding of porosity and permeability trends and relationships. This study has allowed for an understanding on the controls of diagenesis and the reasons for variations from well to well and sample to sample of diagenetic events, the enhancement or inhibition of porosity and permeability and the identification and composition of the provenance change. The data, when associated with neodymium model age dating, core plug analysis, dipmeter data and sand correlations allow for a greater understanding of the processes that have produced the Birkhead Formation reservoir.

Three compositional variations exist; the top Hutton Sandstone consists of locally reworked braided fluvial sediments consisting of medium to coarse grained quartz arenites containing low amounts of lithics, feldspars and micas. Between the top Hutton Sandstone and the provenance change (Birkhead Formation pre-provenance change sediments) grain size is finer owing to its reworked nature and lower depositional energy from the top of the Hutton Sandstone. Thus this pre-provenance change section has undergone two stages of reworking which is reflected by the presence of some quartz grains containing two stages of overgrowths. The lower depositional energy of the reworked Hutton Sandstone sediments within the basal Birkhead Formation means that lithic grains are more abundant and are classified as sub-litharenites. These sediments also have similar framework grain compositions with variations occurring in matrix content. The significant change in framework content occurs after the provenance change within the Birkhead

Formation and is identified by a large increase in lithic content. These sandstones are generally classed as litharenites with varying grain sizes and amounts of matrix depending on the highly variable environments of deposition.

While grain size and matrix content may vary with depositional environment, there appears to be compositional trend of feldspars, quartz or lithic grains when related to lithofacies types and depositional environment. Figure **107**A shows that lithofacies St is restricted to the braided fluvial sediments of the Hutton Sandstone, probably due to the high energy conditions needed to form this type of cross-bedding. Other sandstone lithofacies present do not appear to have any compositional trends. Figure **107**B shows that braided fluvial deposits are restricted to the top 75% section of the plot while a large variation of channel deposits exists, this variation is probably due to the type of depositional environment occurring both before and after the provenance change boundary. The grouping of crevasse splay / prodelta sands is due to their having been sampled from within the pre-provenance basal Birkhead Formation section (compare with figure **102**, page 231). Had these samples been obtained above the provenance change boundary they would have been classed as litharenites due to the higher percentage of lithic grains present within the sandstones.

6.5.1 Provenance Change

The provenance change occurred in two stages and was identified in a number of ways. The change was noted by a change in sediment type from craton derived quartz arenite sandstones displaying a mature texture to reworked craton derived sediments and then finally to lithic arenite sediments of a volcanic origin. The two stages were identified by the changing percentages of rock fragments within each section and is illustrated in figure **102** (page 231). The craton derived quartzarenites occur within the top section of figure **102** at the Gidgealpa south dome and have a very low lithic content commonly

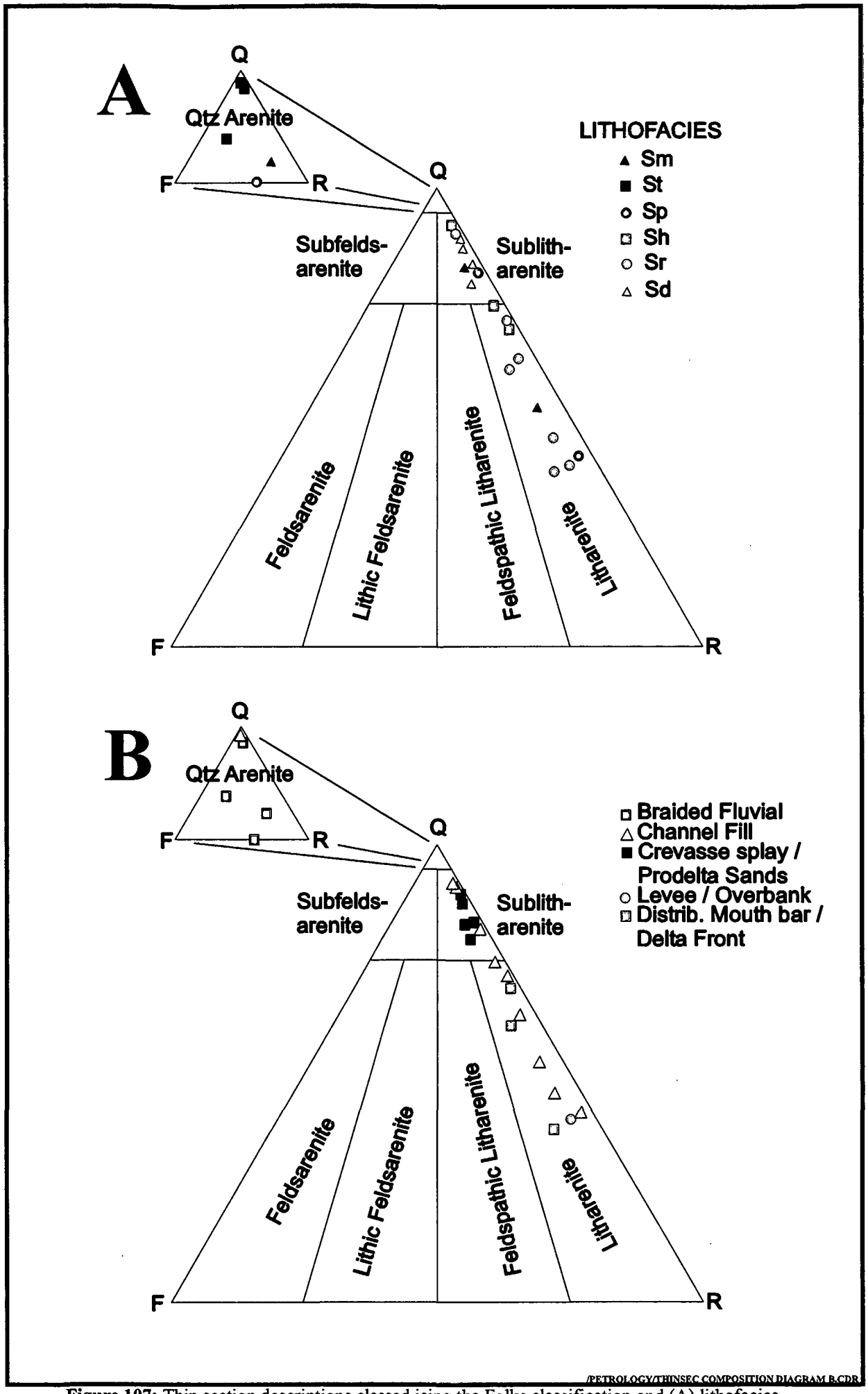

Figure 107: Thin section descriptions classed ising the Folks classification and (A) lithofacies or (B) depositional environment.

no greater than 2%. The lithics that are present consist of only sedimentary or metamorphic rock fragments. The transitional phase occurs within the basal section of the Birkhead Formation and also consists of craton derived sandstones but contains a higher proportion of rock fragments (no greater than 10.5%) due to the lower depositional energy of sediments. As in the Hutton Sandstone quartz arenites, the lithics present consist of sedimentary and metamorphic grains, however the proportion of sedimentary rock fragments is much higher.

It is not until after the provenance change within the upper portion of the basal Birkhead Formation that the presence of rock fragments of a volcanic origin are detected. Post-provenance change sediments contain the highest proportion of lithics and consequently are classed as litharenites, with percentages as high as 43.5% reflecting the added presence of volcanic grains with the sedimentary and metamorphic rock fragments. Harris (1989) determined that sandstones with a detrital quartz content of less than 35% are likely to undergo localised framework collapse due to ductile deformation of lithics. Boult (1996) also observed this phenomenon within the Birkhead Formation at Bodalla South, Jackson and the Gidgealpa south dome noting the abundance of collapsed lithic sandstones. From my own investigation elevated levels of lithic grains within samples of less than 35% quartz have indeed undergone some deformation but not to the degree where framework collapse has occurred. Thus it seems that the 35% value cut-off assigned by Harris (1989) for framework collapse does not necessarily mean that framework collapse has or will occur and suggests that other local factors may be important.

Complementary to the changes in lithic quantity and content, detrital quartz can indicate evidence of the provenance change. Within all samples the dominant quartz type is plutonic. This fact is expected as this quartz is also commonly referred to as 'common quartz' (Folk 1980) due to its presence from a number of sources. Varying amounts of metamorphic quartz are also

present throughout samples. Thus the use of these quartz types are limited. The important quartz type that can aid in the identification of the provenance change is volcanic quartz. This quartz is absent below where the first influx of volcanic arc derived sediments occurs. Above it is readily and easily observed by its fragmental bi-pyramidal or hexagonal crystal occurrence. Other common features of the quartz are straight extinction, large corrosion embayments and the common presence on inclusions such as volcanic glass or negative hexagonal crystals (plate **3**, page 236). One feature of volcanic quartz is its instability compared with other forms of quartz. During erosion and transportation these grains are easily broken down meaning that sediments of moderate to high maturities may be devoid of volcanic quartz.

Feldspars can be used as provenance indicators due to the varying types of feldspars displaying different optical properties. Their relative instability means that the maturity of sediments also affects feldspar content. Like volcanic quartz, the pre-provenance change mature quartz arenite sediments only contain the more stable orthoclase and microcline feldspars. The appearance of plagioclase, sanidine and anorthoclase within the more lithic rich sandstones indicate the sediments that occur above the provenance change within the volcanic-arc derived sediments. As well as being a provenance indicator, feldspars can give some insight into the length of time and climate during erosion and transportation. Feldspars from the Hutton Sandstone tend to be all moderately weathered, well rounded and have a smaller diameter than quartz while within the Birkhead Formation post-provenance change sediments, the feldspars range from heavily weathered to fresh, are angular to sub-rounded and are similar in grain size to quartz. Applying this information to figure **108**, the environment of deposition and the climate at that time may be inferred. Plotting the characteristics onto figure **108** indicates that the Hutton Sandstone was deposited during arid or cold conditions over a long period of time and low tectonic activity while the Birkhead Formation was deposited during a more temperate wet period within increased tectonic

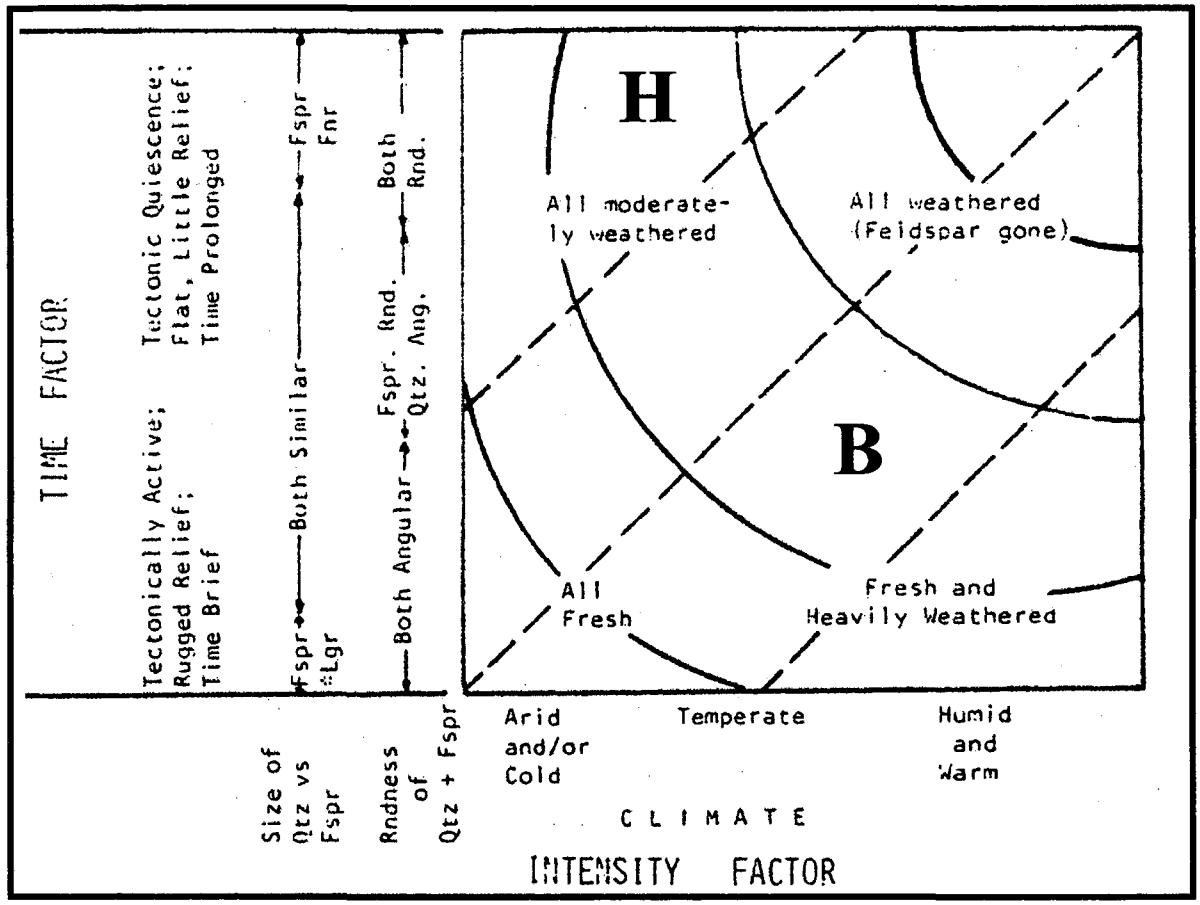

Figure 108: Determination of climate and tectonic activity from the analysis of feldspars. B represents feldspars within the Birkhead Formation. H represents feldspars within the Hutton Sandstone (After Folks, 1980).

activity. Climate at these times correspond well to those suggested by Frakes et. al (1992).

From the analysis of thin sections the compositional variations in lithic, quartz and feldspar grains individually may indicate the presence of a provenance change but combined these parameters very strongly support the fact. The presence of the provenance change is further re-enforced by work conducted by Boult (1996) and myself using dipmeter data (see section **4.7**) and neodymium model age dating (section **4.8**) which I performed over the Gidgealpa south dome.

6.5.2 Diagenesis

In the study area sandstones generally, with some exceptions, have similar diagenetic histories. The Hutton Sandstone is by far the cleanest and coarsest sandstone present at the Gidgealpa south dome. The only major diagenetic event that is evident in this section is the precipitation of quartz overgrowths. This initial event means that the Hutton Sandstone never became heavily compacted or cemented; the lack of silts and matrix also means that porosity and permeability are preserved. Evidence of authigenic clays and carbonate cements are present but the presence of kaolin rims around porosity and the rare occurrence of carbonate cements suggests that they have been subsequently dissolved.

The apparent increase in the authigenic kaolin and carbonate cement in sediments as they approach the top of the Hutton Sandstone boundary may be explained by two possibilities. Firstly, that pore fluids rich in minerals originating from dissolved lithics in the above Birkhead Formation have percolated down and passed through into the underlying Hutton Sandstone precipitating out the authigenic clays and cements. As precipitation occurs the pore fluids become less saturated in these minerals and its capacity to

precipitate out minerals subsequently decreases as a function of the distance away from the formation boundary. Secondly, the effects of the aquifer system present within the Hutton Sandstone increase with the distance away from the formation boundary. The increasing effects of the aquifer means that authigenic minerals and cements are more likely to be dissolved, or not form in the first place.

The precipitation of authigenic carbonate as carbonate cement occurred in three stages within the Birkhead Formation sediments. The initial siderite was the first diagenetic event and occurred within all samples, precipitating as a dispersed micrite that was concentrated around organic matter and commonly occurred within matrix rich sandstones. The micrite precipitated just after deposition while sediments were still within the vadose zone. Between the first and second event of deposition, probably after some depth of burial of the stratigraphic sequence, authigenic quartz was precipitated as quartz overgrowths. The second stage of carbonate was also determined to be crystalline siderite from XRD analysis. This spar commonly fills vacant porosity either partially or completely filling it or grows from the earlier micrite within the matrix displacing the matrix as it grows. This spar has also been found to nucleate within cleavage of micas splitting the detrital grains apart.

The final stage of carbonate occurs as a poikilotopic cement that displaced matrix, authigenic cements and replaced quartz and feldspar. This late stage carbonate seems to be extensive in Gidgealpa 31 but is rare within the other cored wells; XRD analysis identified the cement as ankerite or dolomite. This carbonate cement was not seen in other cores, except in Gidgealpa 32 by Boult (1996) who described the presence of a poikilotopic carbonate cement. The formation of the late stage carbonate is similar to that described by Green et. al (1989) who noted the existence of sideroplesite (magnesium rich carbonate) within the Queensland portion of the Hutton Sandstone and determined it as a late stage product. Both my findings and those of Green et. al (1989) differ

from those of Gravestock et. al (1983) who interpreted the carbonates to be formed early in the diagenetic history by pedogenic processes.

The silica cement formed syntaxial quartz overgrowths predominantly on grains that had straight to undulose extinction. Where porosity was abundant the overgrowths formed euhedral terminations into porosity and uncommonly formed triple point junctions where precipitation occurred for long enough periods. Overgrowths are most abundant in medium to coarse grained sediments that have low matrix and lithic contents and least abundant in fine to very fine grained sandstones that have abundant matrix and lithic content. Overgrowths are also absent on highly strained or polycrystalline quartz grains and where detrital clays are rimming detrital grains.

As in the Hutton Sandstone, the early precipitation of silica within the Birkhead Formation halted the compaction of sediments by forming a rigid framework of quartz grains cemented together by silica. Early signs of minor compaction are evident by the presence of tangential contacts and the rare presence of concavo-convex or sutured contacts. In sediments that have higher matrix or lithic contents, the precipitation of quartz was restricted or inhibited causing common grain contacts to have a concavo-convex or sutured character. In sediments where lithic content is very high, quartz grains float within the rock fragments and occasionally form tangential grain contacts with other quartz grains. Where this occurs, the sediments are more highly compacted, this higher degree of compaction and the ductile nature of the lithics means that porosity is very low or non-existent within these samples.

Just prior to the end of deposition of the authigenic silica, the first stage of kaolin occurred within most samples. The kaolin is characterised by its small crystal size lining porosity and has been seen to be partly devoured by quartz overgrowths or rarely lie between grains and overgrowths. The precipitation of kaolin was probably a result of changing pore water chemistry from the removal of silica to form authigenic quartz and from the dissolution of lithics

and feldspars. This diagenetic event was short lived with its termination probably due to another change in pore water chemistry.

The dissolution of lithics and feldspar probably initiated the formation of clinochlore and lizardite, but this point is uncertain since these clays are only detected from XRD analysis and are not visible under the transmitted light microscope. The initial kaolin along with the second stage kaolin was interpreted to be kaolinite from XRD. This second stage has larger crystals and commonly fills porosity that was either primary or partially filled by early kaolin and / or carbonate. From XRD analysis the third stage kaolin is dickite. The dickite consists of large crystals (larger than the second stage kaolin) and occurs within most Birkhead Formation samples but is absent from the Hutton Sandstone. This late stage kaolin occurs where earlier kaolin and carbonate have not completely filled porosity.

The absence of any hydrocarbons within the thin section samples except within primary intergranular and secondary dissolution porosity suggests that the initial charge did not occur until the late stages of diagenesis or after the main diagenetic events had taken place.

6.5.3 Porosity and Permeability

The main controls on permeability and porosity are the initial sorting, and to a lesser extent grain size and diagenetic history. Sorting and grain size of sediments are the main parameters that determine the size of pore throats, larger grained and better sorted sandstones tend to have higher porosity and permeability. The precipitation of the authigenic quartz in the Hutton Sandstone and the coarser and cleaner sandstones of the Birkhead Formation has partially reduced intergranular porosity by holding quartz grains in place. While the porosity is reduced the permeability remains relatively high due the preservation of pore throats between porosity (Green et. al, 1989).

The presence of silts and clays affect permeability and porosity by inhibiting the growth of authigenic quartz allowing for compaction to occur. This tends to occur in the finer grained sediments that also tend to have more diagenetic clays lining pores further reducing porosity and permeability. The finer grained and poorly sorted sediments tend to be isolated to the Birkhead Formation; this is reflected in the generally poor porosity and permeability values. Porosity and permeability may be further affected in sediments that have abundant lithics restricting the formation of overgrowths.

Sediments within the Birkhead Formation, that have a high initial lithic content and low permeability and porosity, tend to form scattered secondary porosity by the dissolution of lithic grains or feldspars. Sandstones with a higher quartz content as well as a higher clays content tend to have limited dissolution of framework grains and dissolution of authigenic cements. Sediments within the Hutton Sandstone form secondary porosity from the dissolution of authigenic clays and cements as well as lithics and feldspars. Giles (1987) suggests that the formation of secondary porosity may occur in a closed system where labile grains become unstable or in an open system where mass transport of minerals occurs. Within the sandstones where individual grains are dissolved and the passage of fluids is inhibited a closed system prevails. Where the initial porosity and permeability is high, fluids are free to flow through the sediments causing high levels of dissolution. Where open systems prevail intense leaching of sediments may occur within the Birkhead Formation and particularly within the Hutton Sandstone. The prediction of the locality of these zones is difficult due to the high number of parameters that may effect secondary porosity (Schulz-Rojahn and Philips, 1989).

Sandstones with high percentages of kaolin are characterised by low overall porosity and permeability due to the filling of most primary and some secondary porosity. These sediments also have high microporosity from pore spaces produced between kaolin booklets. While this type of porosity may be

abundant, the permeability is low due to the poor alignment of pore spaces. The microporosity within kaolin is classed as non-productive since the pore spaces are too small for the passage of liquid hydrocarbons. Thus core plug porosity tends to over-estimate porosity in relation to hydrocarbon volume. Kaolin may have other negative effects when considered in the production of the reservoir. Various authors have noted that kaolin booklets may dislodge during compaction, blocking pore spaces and impeding the flow of hydrocarbons (Thomas, 1990, Sneider, 1992, Little, 1996).

From the observed relationship between mineralogy and diagenesis and between permeability and porosity it would appear that the depositional environment is the major controlling factor. The depositional environment effects most of the properties of sediments including grain size, sorting and silt or matrix content. All these factors have affected both the permeability and porosity in some way. Thus areas of higher permeability and porosity at the Gidgealpa south dome are likely to correspond to channel fill and distributary mouth bar sediments that are medium to coarse grained, well sorted and contain low amounts of silts and clays. Composition of the sediments may also effect permeability and porosity in the volcano-lithic sandstones with high levels of lithics. Most studies on diagenesis of these sediments of volcanic origins suggest that reservoir quality is poor due to the relatively rapid formation of pore filling cements (Mathisen, 1984).

High secondary dissolution streaks may also occur where mass dissolution of lithic and feldspar grains as well as cements has occurred. These streaks have high proportions of oversized porosity and thus have elevated values of permeability and porosity. These high secondary dissolution zones are easily recognised in wireline logs as a low API value spike on the gamma ray due to the dissolution of lithics and feldspars which contain potassium.

7 Core Analysis

7.1 Capillary Pressure

7.1.1 Background

The evaluation of capillary pressure of potential reservoir and seal rocks is important since capillarity controls the static distribution of fluids through the interaction of capillary pressures, buoyancy and hydrodynamic forces between hydrocarbons and water (Vavra et. al, 1993, Boult, 1996). The capillary pressure of a rock containing porosity can be determined by driving a non-wetting phase fluid through its pore throats under pressure until the pore wetting fluid is displaced (Jennings, 1987). A non-wetting phase fluid is where the cohesive forces (such as surface and interfacial tension) are greater than adhesive (liquid-solid) forces between the liquid and surrounding solid. For a wetting liquid the opposite occurs where adhesive forces are greater than the cohesive forces.

Capillary pressure can be calculated using the equation (from Boult, 1996):

$$P_c = \frac{2.IFT.Cos\theta}{r} \qquad \text{Equation 4}$$

Where P_c = capillary pressure (dynes/cm^2)
IFT = interfacial tension (dynes/cm)
θ = contact angle
r = radius of the capillary tube (cm)

To calculate capillary pressure for samples from the Hutton Sandstone and Birkhead Formation the mercury injection method was used. This method was

used since it is simple to perform and samples can be run over short periods of time at little expense. Mercury injection data can also be readily converted to the reservoir fluid system although some assumptions on parameters such as wettability must be made (Vavra et. al, 1993).

Rock samples were obtained from cores using the diamond blade saw. These samples where then divided into four sections for analysis including mercury injection, thin section, SEM and XRD analysis. Sections obtained for mercury injection were dried at 60°C with humidity at 40% to release free water without damaging clay structure. The samples were then run on a semiautomatic Micromeritics Autopore 9200 which can operate up to a pressure of 60 000 psia and measures mercury intrusions as small as 0.0001 cc/gram of sample (Boult, 1996). Mercury injection data is acquired by injecting mercury into the cleaned core plug within a mercury / vacuum system so air compressibility can be excluded from pressure measurements (Theologou, 1995). The injection pressure is then increased in a stepwise manner with increasing amounts of rock pore volume saturated by mercury, when equilibrium is reached at each pressure increment the amount of saturation is recorded as a percentage (Vavra et. al, 1993). The amount of mercury saturation within the sample divided by the total pore volume is equal to the mercury saturation, these values are then plotted against the injection pressure (appendix 7). Relative pore volume plotted against pore throat size, determined by estimation from injection pressure, may also be displayed (appendix 7).

The description of reservoir properties from mercury injection samples can be determined from the capillary pressure curve (figure **109**). From this curve various reservoir parameters may be obtained. The parameters include entry pressure (P_e) where the sample first begins to accept mercury into the pore system, displacement pressure (P_d), when the mercury first imbibes into the sample and can be estimated by extending the slope of the plateau to the right side of the graph (figure **109**) and finally the irreducible water saturation (S_{wi})

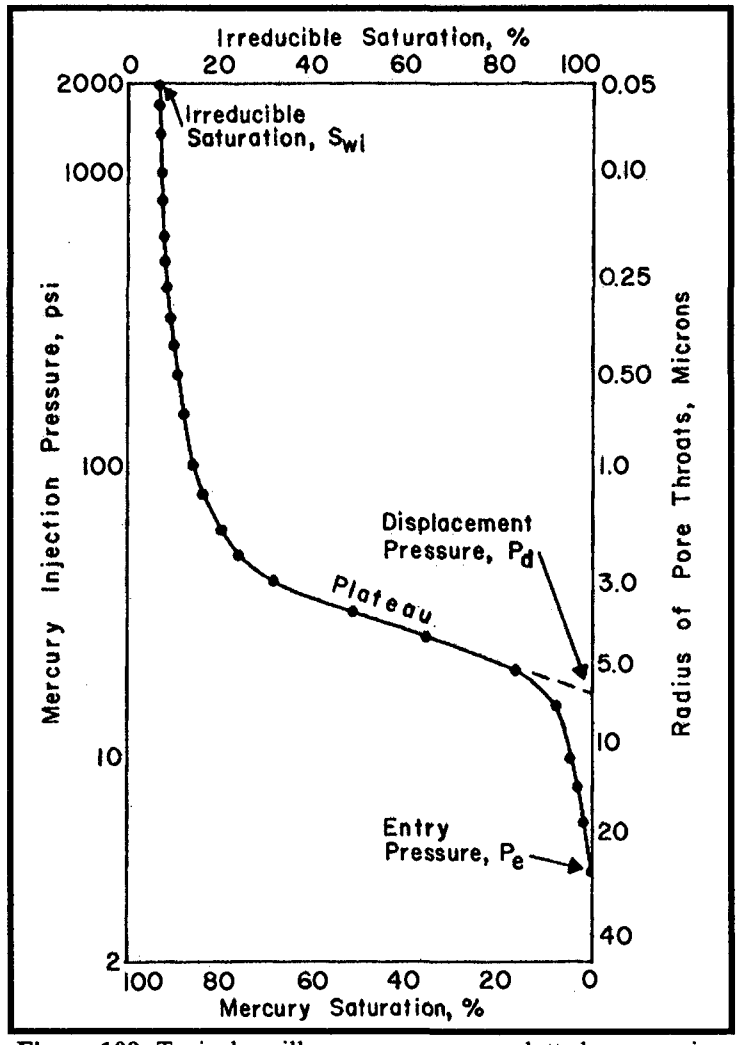

Figure 109: Typical capillary pressure curve plotted on a semi-log graph (From Jennings, 1987).

is the percentage of pore space that the mercury can not occupy (Jennings, 1987). Inspection of the plateau from the capillary curve can give an indication of pore throat sorting of any particular sample (Jennings, 1987, Vavra et. al, 1993) and from the re-arrangement of the capillary pressure equation (equation **4**) the effective pore throat radii can be calculated for any given capillary pressure. From visual inspection of the capillary pressure curves, samples that have well sorted pore throats, or pore throats of a similar size will have a broad flat plateau. As the variation in pore throat size increases the plateau steepens and then disappears all together when the pore throats are completely unsorted. Figure **110** consists of idealised capillary entry curves demonstrating the various shapes of the plateau with differing pore throat sorting. Jennings (1987) discusses the use of a pore throat sorting (PTS) value that measures the sorting of the pore throats within a rock sample. The PTS value is calculated by:

$$PTS = \left[\frac{3rdQuartile\,\mathrm{Pr}essure}{1stQuartile\,\mathrm{Pr}essure} \right]^{1/2} \qquad \text{Equation } \mathbf{5}$$

where the 3rd and 1st Quartile Pressures can be directly obtained from the capillary pressure curve and reflect the 75% and 25% mercury saturation pressures respectively which have been adjusted for irreducible water saturation. The PTS value gives a number between 1.0 (perfect sorting) and 8.0 (no sorting) allowing for quantitative measurements of pore throat sorting and effective comparisons between samples. Figure **111** is an example of how pore throat sorting is calculated from the capillary pressure curve.

The amount of recovery of oil from a reservoir in an oil-water system is dependent directly on pore geometry and can be calculated in relative terms by the determination of the withdrawal efficiency (W_e) within the mercury-air system. Factors effecting the pore geometry include effective pore throat heterogeneity, the ratio of pore body to pore throat size and the number of throats connecting each pore (Vavra et. al, 1993). From the data of a mercury

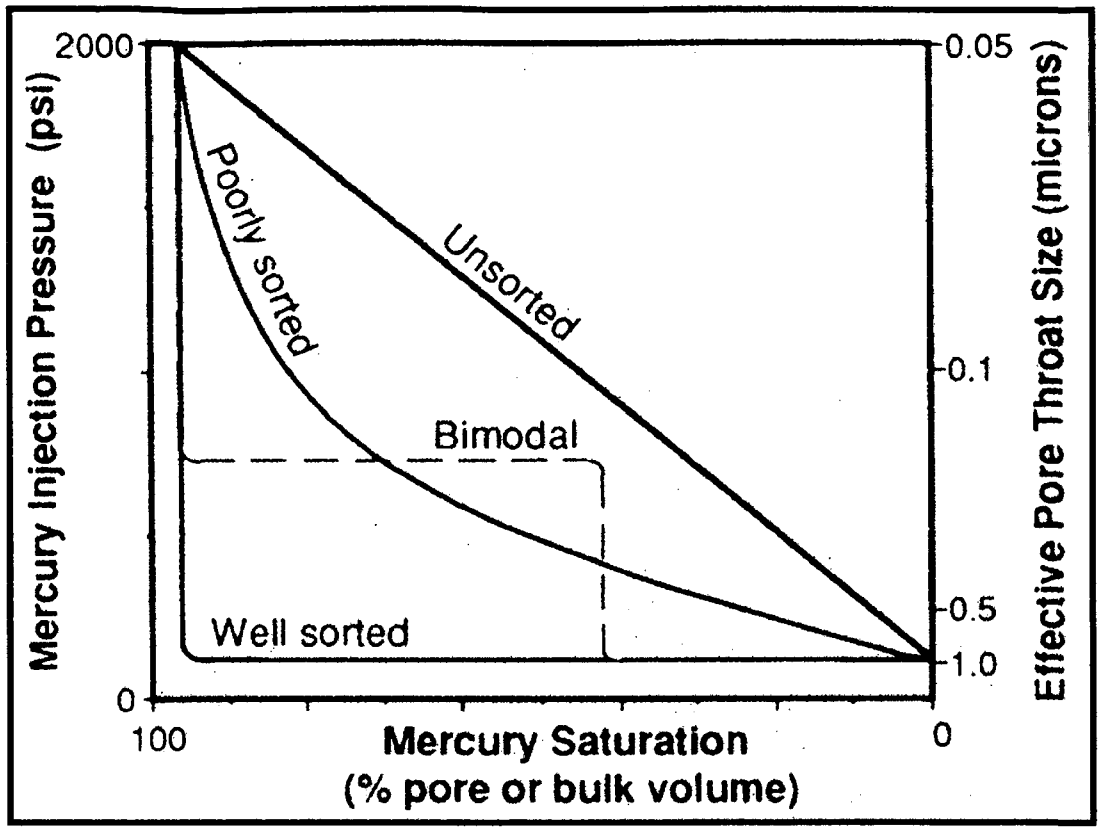

Figure 110: Idealized mercury injection capillary pressure curve shapes. Different shapes of the curves represent differnt sorting within the samples (From Vavra et. al, 1992).

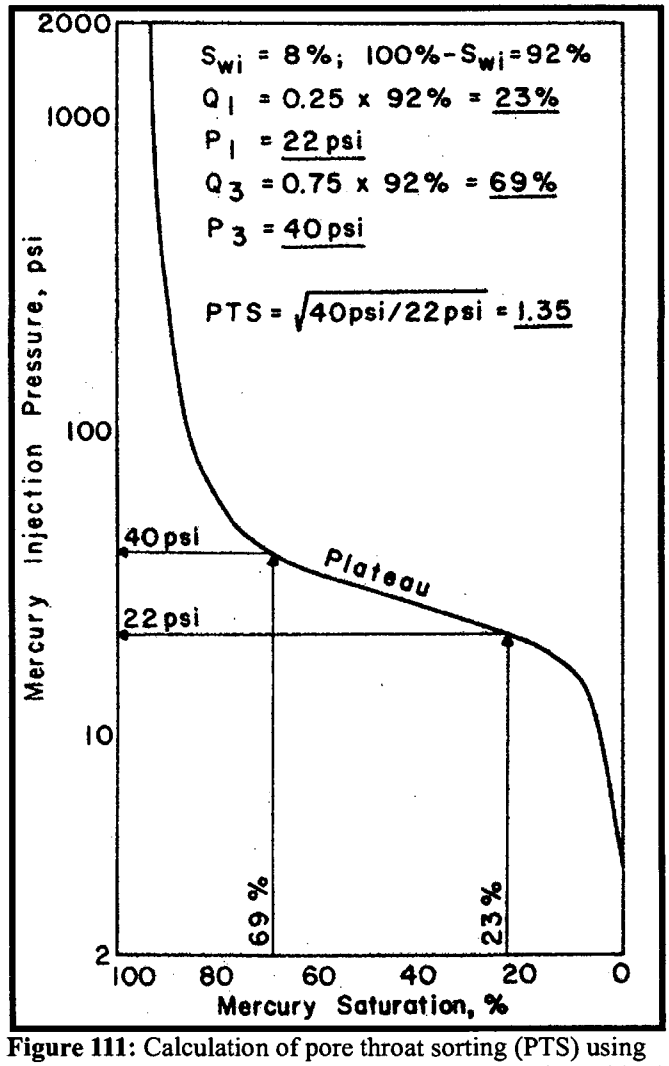

Figure 111: Calculation of pore throat sorting (PTS) using injection pressure values (From Jennings, 1987).

withdrawal curve (or air imbibition curve) the withdrawal efficiency of a rock sample can be calculated. The withdrawal efficiency is defined as the ratio of the mercury saturation in the sample at minimum pressure after the pressure has been reduced from the maximum pressure saturation (figure **112**) (Wardlaw and Taylor, 1976). The withdrawal efficiency is calculated by the equation (from Vavra et. al, 1993):

$$W_e = \frac{S_{max} - S_r}{S_{max}} \times 100 \qquad \text{Equation } \mathbf{6}$$

where S_{max} = saturation at maximum pressure
Sr = sample saturation at minimum pressure after reduction

The value is normalised since samples seldom reach 100% mercury saturation. A limitation in withdrawal efficiency is present since the mercury injection apparatus in this case could only obtain a minimum pressure of approximately 10 psia after the mercury injection run up to the maximum pressure.

To determine the hydrocarbon saturation of different rock types at various heights in a reservoir and the evaluation of seal capacity, mercury-air data must be converted to the oil-water system. The conversion of the data can be obtained by the relationship:

$$Pc_{b/hc} = Pc_{a/m} \times \frac{\sigma_{b/hc} Cos\theta_{b/hc}}{\sigma_{a/m} Cos\theta_{a/m}} \qquad \text{Equation } \mathbf{7}$$

where $Pc_{b/hc}$ = capillary pressure in the brine-hydrocarbon system of the reservoir
$Pc_{a/m}$ = capillary pressure in the air-mercury system
$\sigma_{b/hc}$ = interfacial tension of the brine-hydrocarbon system
$\sigma_{a/m}$ = interfacial tension of the air-mercury system
$\theta_{b/hc}$ = contact angle of the brine-hydrocarbon-solid system
$\theta_{a/m}$ = contact angle of the air-mercury-solid system

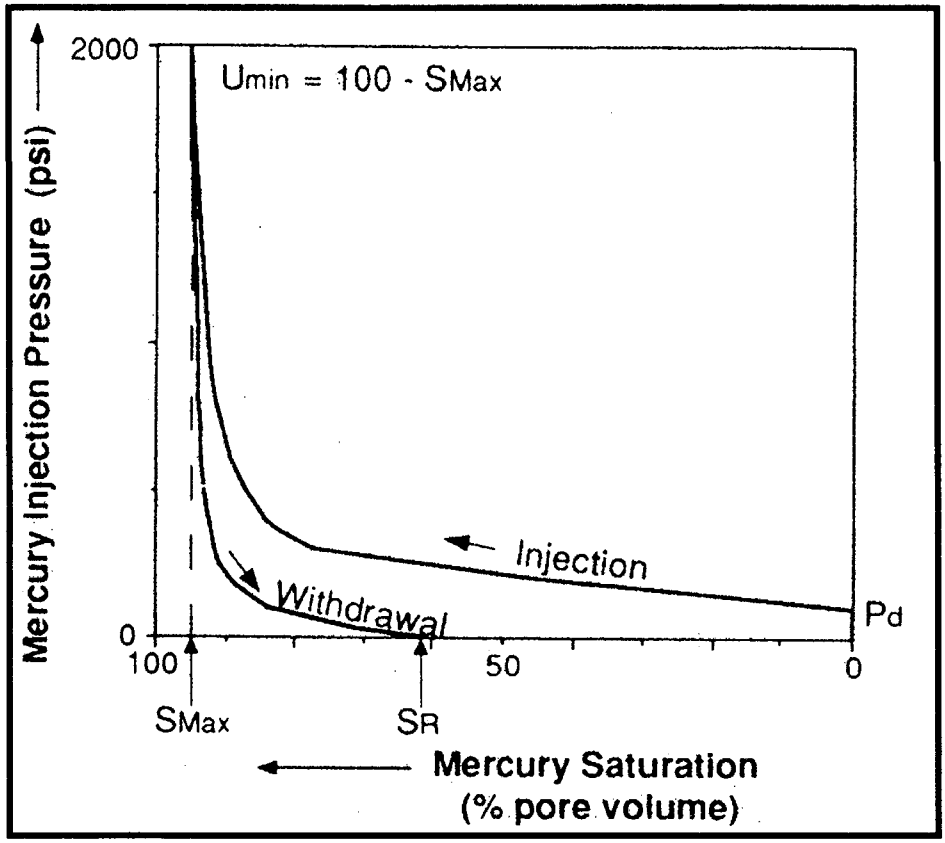

Figure 112: Mercury injection and withdrawal curves (From Vavra et. al, 1993).

Once the air-mercury data has been converted the height above free water level, saturation and seal capacity of cap-rocks can be calculated from equations **8** and **9** respectively (Vavra et. al, 1993). Thus, the amount of hydrocarbon column required from the free water level to attain the pressure of interest is calculated by:

$$h = \frac{P_c}{0.433(\rho_b - \rho_{hc})} \qquad \text{Equation } \mathbf{8}$$

where h = height above free water level (in feet)
P_c = hydrocarbon-brine capillary pressure (in psi)
ρ_b = specific density of brine at ambient conditions (in gm/cm3)
ρ_{hc} = specific density of hydrocarbons at ambient conditions (in gm/cm3)
0.433 = the gradient of pure water at ambient conditions

and the calculation of seal capacity is determined by the equation:

$$h_{max} = \frac{P_{ds} - P_{dr}}{0.433(\rho_w - \rho_{hc})} \qquad \text{Equation } \mathbf{9}$$

where h_{max} = height of the hydrocarbon column (in feet)
P_{ds} = brine-hydrocarbon displacement pressure of the seal (in psi)
P_{dr} = brine-hydrocarbon displacement pressure of the reservoir rock (in psi)

7.1.2 Results and Discussion

A number of samples were selected from each lithofacies for mercury injection. The samples selected were restricted to those that had been used for thin section analysis including SEM and XRD to compare petrological analysis to mercury injection data. Probe permeability values were used to help select a range of samples from porosity vs permeability crossplots derived

from core plugs (a detailed description of the probe permeameter is discussed in section **7.3**, page 319. Applying the probe permeability value straight onto the graph (see figure **118**B, page 318 (lithofacies Sr) in section **7.2.4**), the corresponding porosity was read off using the line of best fit for each of the lithofacies. This selection criterion was used to obtain a wide range of varying porosities and permeabilities of each lithofacies. Table **10** shows a summary of mercury injection data performed for this thesis.

Results of the mercury injection data have been grouped with regards to lithofacies and displayed on a number of graphs (figure **113**). In the figure the samples that are distinguished by a sample number were analysed for this thesis while the samples that are distinguished by a depth where analysed by Boult, 1996. The graphs show that decreasing mercury injection pressures are needed to inject mercury into the rocks for lithofacies that are coarser grained and better sorted. This relationship is reflected in the previous mercury injection data run by Boult (1996) in the Gidgealpa south dome. From the petrological study, the lower injection pressures are attributed to the larger interconnected pore throats present within the coarser, better sorted samples. These samples also contain less detrital and authigenic clays and matrix which would otherwise reduce the diameter of pore throats. Figure **114** compares capillary pressure curves with pore throat distribution graphs where samples have been separated into four different groups consisting of Hutton Sandstone, pre-provenance change Birkhead Formation, post-provenance Birkhead Formation and carbonate cemented rocks. Figure **114** shows that increasing pore throat size decreases the overall entry pressure in the capillary pressure curve of the rocks and also indicates a progressive decrease in pore throat size from the Hutton Sandstone to the Birkhead Formation after the provenance change. The increases in pressure are partly attributed to diagenetic effects. This point is strongly highlighted when the curves of the carbonate cemented rocks are observed. These rocks have very high capillary displacement pressures and a corresponding very small average pore throat size.

Sample Number	Well	Formation	Depth	Litho-Facies	Porosity (%)	Permeability (md)	PTS Value	W_e (%)
Gidg26-1	Gidgealpa 26	Birkhead	5956'4"	Sp	19.47	14.71	7.69	49.8
Gidg26-2	Gidgealpa 26	Birkhead	5957'7"	Sh	12.4	2.1	4.22	42.2
Gidg29-1	Gidgealpa 29	Birkhead	6025'4"	Sr	13.66	3.3	6.09	47.6
Gidg29-2	Gidgealpa 29	Birkhead	6047'2"	Sm	14.7	2.75	5.07	26.1
Gidg29-3	Gidgealpa 29	Hutton	6064'2"	St	14.12	289	5.75	18.9
Gidg30-1	Gidgealpa 30	Birkhead	6029'9"	St	11.34	40.67	7.08	39.4
Gidg31-1	Gidgealpa 31	Birkhead	5974'7"	Sr	13.45	0.011	5.96	45.0
Gidg31-2	Gidgealpa 31	Birkhead	5981'10"	Sm	6.02	0.021	1.43	25.0
Gidg31-3	Gidgealpa 31	Birkhead	5985'10"	Sp	9.28	0.02	1.18	28.2
Gidg32-1	Gidgealpa 32	Birkhead	5992'2"	Sd	19.33	2.6	4.73	31.7
Gidg32-2	Gidgealpa 32	Hutton	6007'4"	Sm	14.42	130	5.83	19.9
Gidg32-3	Gidgealpa 32	Hutton	6015'9"	Sp	17.46	1335	2.89	14.1
Gidg32-4	Gidgealpa 32	Hutton	6018'6"	St	16.19	473	2.02	9.7

Table 10: Samples used from mercury injection including lithofacies type, porosity, permeability, pore throat sorting value and withdrawal efficiency.

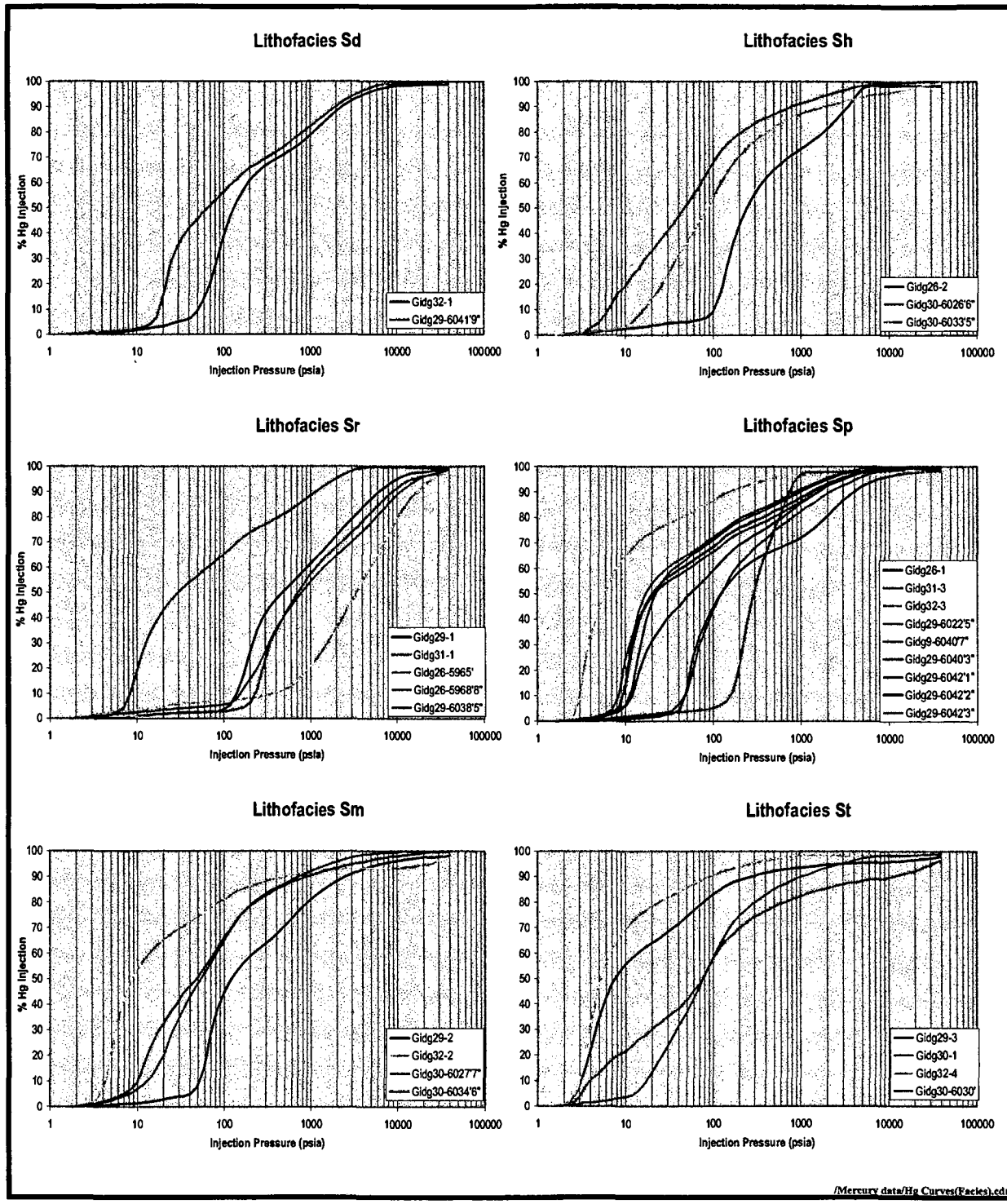

Figure 113: Capillary pressure curves grouped in terms of lithofacies. (Sd = soft sediment deformed sand/mud, Sh = horizontal bedded sand, Sr = ripple cross-laminated sand, Sp = planar cross-bedded sandstone, Sm = massive sandstone, St = trough cross-bedded sandstone).

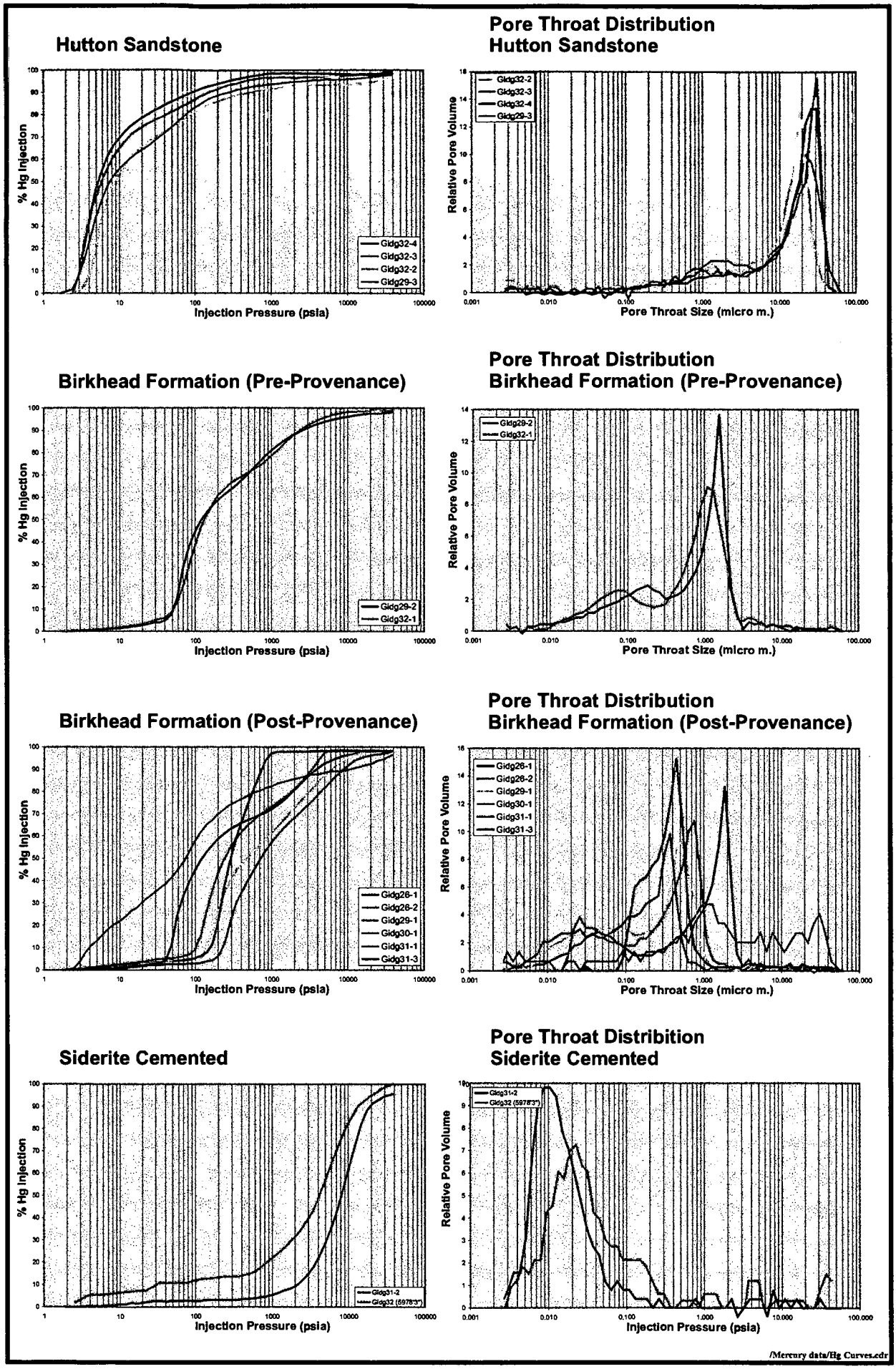

Figure 114: Comparison of injection curves and pore throat distributions for different parts of the top Hutton Sandstone and basal Birkhead Formation.

The pore throat distribution graphs for the Birkhead Formation show a bimodal distribution. This character is caused by the filling of primary and secondary porosity which ranges in size from 0.15 to 3 μm by kaolin which contains microporosity ranging in size from 0.01 to 0.1 μm. The variation in pore throat size is reflected in the capillary pressure curves and samples that have a bimodal grain distribution tend to have less steep curves than those that are uniform in size. This fact is reflected in the samples from the Hutton Sandstone and the cemented samples containing relatively uniform grain sizes as compared to the Birkhead Formation which have a range of pore throat sizes.

An extreme case of a large variation in pore throat sizes is reflected in the Gidg30-1 sample. Before the dissolution phase the rock would have had a similar distribution curve to the other Birkhead Formation samples with the most abundant pore throat size at 1 μm (figure **114**). The dissolution has caused the formation of oversized pore throats with abundant pores above the original 1 μm size. The larger pore throats have greatly reduced the capillary entry pressure of Gidg30-1 as compared with the other samples within the formation by the use of the PTS value. The high PTS value of Gidg30-1 reflects the poorly sorted nature of pore throats within the sample.

The withdrawal efficiency of the samples have been calculated with results displayed in table **10**. A graph showing drainage and imbibition curves of samples Gidg32-4, Gidg31-1 and Gidg30-1 are also displayed in figure **115**. Pore geometry affects the withdrawal efficiency of the rocks with the critical factors displayed in table **11**. In the table the coordination number is the ratio of pore throats to framework grains.

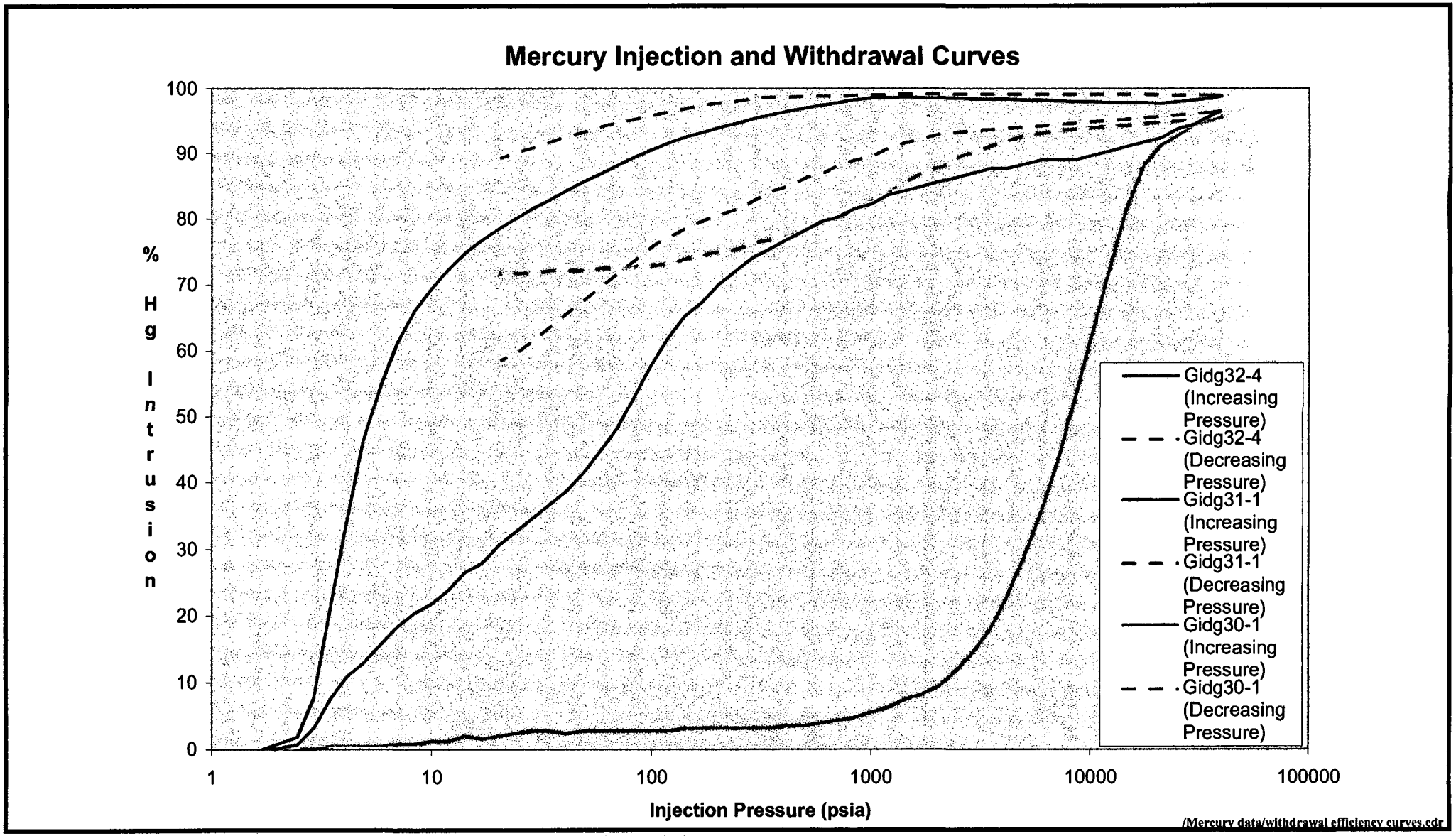

Figure 115: Withdrawal efficiency curves of various samples from the Gidgealpa south dome.

Factor	High W_e	Low W_e
Pore throat heterogeneity	Low	High
Pore body to pore throat size ratio	Low	High
Coordination number	High	Low

Table 11: Pore Geometry factors affecting withdrawal efficiency (W_e) (from Vavra et. al, 1993)

While the direct use of mercury injection data is useful to achieve relative comparisons between samples and rocks it is not as useful when considering the petrophysical behaviour of samples within the subsurface reservoir. For this reason the mercury injection capillary pressure data has been converted to brine / hydrocarbon reservoir equivalent values. For the various lithofacies the conversion of mercury injection data to the oil-brine reservoir system allows the determination of the expected oil saturation of the reservoir rocks in the subsurface by the calculation of the height above free water level. For the conversion of the data a number of parameters are required including water and oil densities, contact angles and interfacial tensions. Values used for the calculation of oil saturation above free water level are displayed in table **12**.

Parameter	Value	Units	Source
Interfacial tension (brine-hydrocarbon)	25	dynes/cm	Boult (1996)
Interfacial tension (mercury-air)	480	dynes/cm	Vavra et. al (1993)
Contact angle (brine-hydrocarbon)	20	degrees	Boult (1996)
Contact angle (mercury-air)	140	degrees	Vavra et. al (1993)
Specific density of Hydrocarbon	0.79	gm/cm^3	Gidgealpa 29 WCR
Specific density of brine	1.1	gm/cm^3	Vavra et. al (1993)

Table 12: Values used for the calculation of height above free water level.

Results from the calculations of samples for a number of different lithofacies are graphically represented in figure **116** by plotting wetting phase saturation

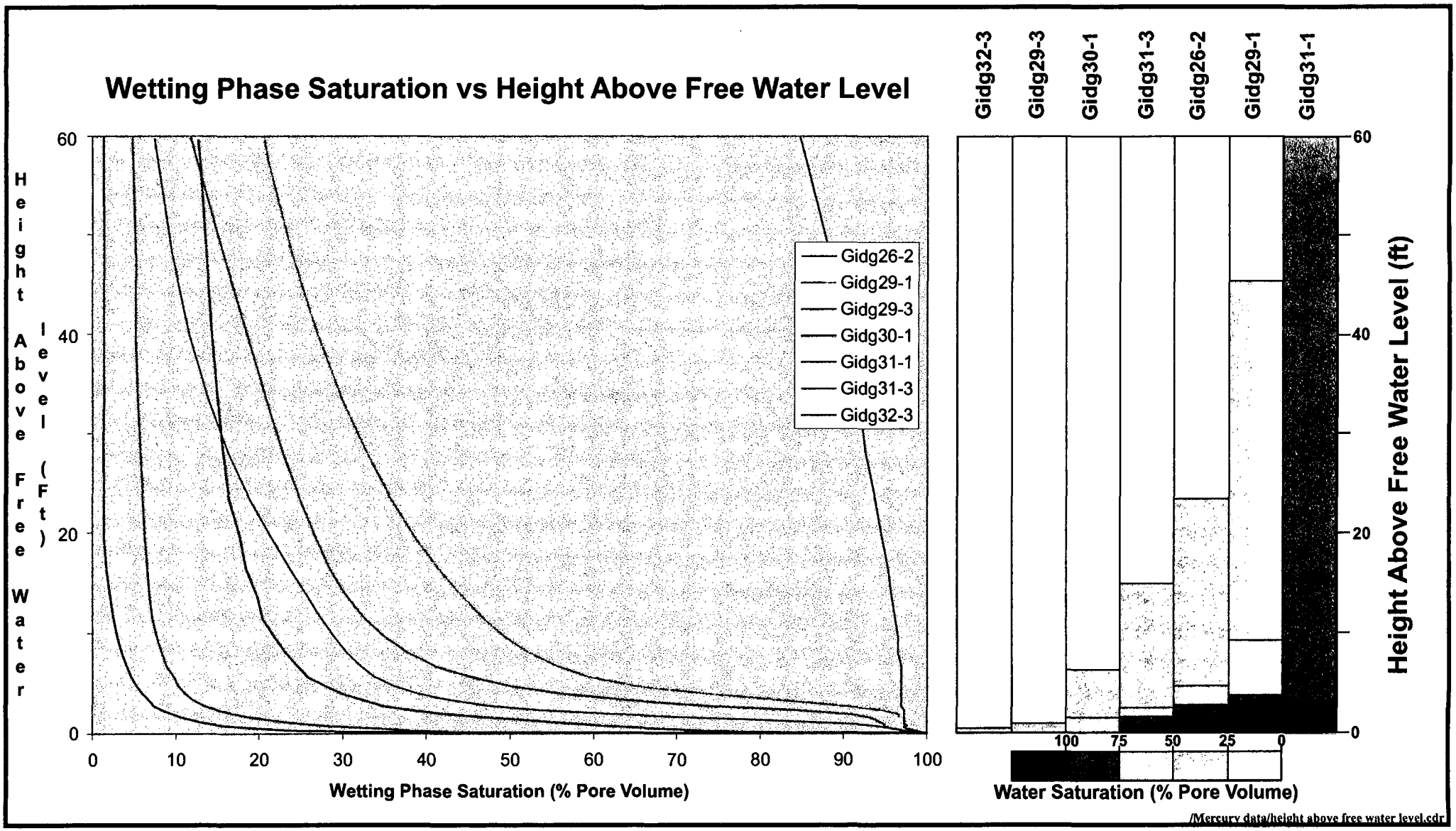

Figure 116: Height above free water level and oil saturation columns for samples from the Gidgealpa south dome (for sample details refer to Table 10).

against height above free water level and a display of the corresponding water saturation columns for each of the samples. The figure shows the variation in saturation values at various heights above the free water level with lithofacies Sr generally having the lowest oil saturations and St and Sp lithofacies having the highest. Figure **116** also shows the effects of carbonate cements with sample Gidg31-1 never producing an oil saturation of higher than 20 percent up to a height of 60 feet above the free water level. The determination of the curves in figure **116** are invaluable when looking at the reservoir rock saturations during reservoir characterisation. For sample details used in the figure refer to table **10**, page 302.

7.2 Determination of Permeability and Porosity From Core plugs

Permeability and porosity determination from core plugs is a regular and well exercised method of determining reservoir characteristics of sediments. Within a reservoir the porosity determines fluid storage capacity and permeability characterises the ease with which the stored fluids can flow through the sediments under a pressure gradient. Permeability and porosity readings have been previously taken from a number of positions within the Gidgealpa south dome cores during routine core analysis. This routine analysis tends to be biased towards the higher quality reservoir sands which give elevated overall reservoir quality. In this thesis I have conducted further analysis of core plugs to address the problem of biased sample collection. The collection of extra data has also been conducted to further characterise the Gidgealpa south dome lithofacies and for calibration with probe permeability data.

7.2.1 Sample Preparation

Quality and reliability of data obtained from core plugs can be highly dependent on the sample preparation and samples that are taken should be representative of the rock of interest. The plugs that I selected were cut from

pre-slabbed cores parallel to bedding using a 1.5 inch diametre diamond drill bit. The bit was mounted in a drill, which was connected to a drill press unit, and a water supply was added as a lubricant. The samples were drilled at 1.5" diameter with the intention to be used in the porosimeter matrix cup and the permeameter Hassler holder. When drilling the maximum length of the core plug was obtained since a longer sample will attain more reliable results when carrying out analysis. Samples were then trimmed at both ends with a diamond blade saw to produce a flat surfaces at both ends.

Once core plugs are trimmed to suitable dimensions they require cleaning and drying, since porosity analysis requires the removal of soluble hydrocarbons. For the removal of hydrocarbons in this case I used the soxhlet extraction method. This procedure involves the cleaning of plugs using an azeotrope of chloroform:methanol at a ratio of 3:1. For details of the setup and use of the soxhlet extractor refer to appendix **8**. Once the samples were cleaned they were dried in a humidity oven at 45% relative humidity and 60°C so that the destruction of clays did not occur from the removal of bound water. After drying, the samples were placed in a silica gel vacuum desiccater to stop the absorption of water from the atmosphere.

7.2.2 Definition and Determination of Porosity

While porosity can be quantified by core plug analysis, pore types within a sandstone can be visualised by using thin section descriptions, SEM and capillary pressure tests. These methods can reveal the types of porosity present including primary (intergranular), secondary (dissolution), microporosity and fracture porosity. Mechanical compaction of sediments, pressure solution and cementation may all occur to reduce porosity in sandstones while dissolution may enhance it (Pettijohn et. al, 1987). Work from Beard and Weyl (1973) indicate that porosity generally increases with grain sorting.

Porosity can be calculated as either total or effective porosity where the total volume determines all pore space within a sediment including those pores that are connected and those that are not. The effective porosity is a determination of the interconnected pore volume and excludes isolated pores. Because the calculation of porosity from core plugs can not measure isolated pores, it is a measure of effective porosity and is represented by the equation:

$$P_e = \frac{InterconnectedPoreVolume}{BulkVolume} \times 100 \qquad \text{Equation } \mathbf{10}$$

To determine the porosity from core plugs I used the Petrophysical Instruments Porosimeter. The porosimeter is capable of accurately measuring the porosity of samples via the calculation of grain density. For a detailed description of the procedure I used, see appendix **8**. The first step for the calculation of porosity is the calibration of the porosimeter reference volume. This involves the use a reference cell and a matrix cup that contains a number of billets (solid disks) of a known volume. After calibration of the equipment to determine the reference volume of the matrix cup, the grain volume of samples is calculated. Calculation of grain volume is determined by the equation (from Boult 1996):

$$G_v = V_b + \left(\frac{P_{of}}{P_f} \times R_v\right) - \left(\frac{P_{os}}{P_s} \times R_v\right) \qquad \text{Equation } \mathbf{11}$$

where G_v = grain volume (cc)
V_b = volume of removed billet (cc)
P_{of} = Pressure in reference cell during calibration (cc)
P_f = Pressure in reference cell plus
matrix cup with all billets in place during calibration (psi)
R_v = Reference volume
P_{os} = Pressure in reference cell during sample run
P_s = Pressure in reference cell plus
matrix cup with all billets in place during sample run (psi)

Once grain volume is obtained from the porosimeter the true bulk volume of samples is required to calculate the pore volume. The pore volume is calculated by subtracting the grain volume from the true bulk volume. Therefore:

Pore volume = True bulk volume - Grain volume Equation **12**

When all of the other analysis have been performed the bulk volume can be determined and is required in both the calculation of grain density and porosity. Bulk volume is determined by pressing a sample down into a volume of mercury of known weight and measuring the increase in weight due to volume repression. This method is a measure of the buoyancy of the plug where the change in weight corresponds to the repressed volume of mercury. The bulk density is calculated by dividing the density of mercury by the change in weight. This procedure is performed last since the mercury may be absorbed by samples thus effecting the core plugs weight, permeability and porosity. Once the bulk volume of the samples has been determined the porosity (as a percentage) can be calculated by the equation:

$$\text{Porosity} = \frac{PoreVolume}{TrueBulkVolume} \times 100 \qquad \text{Equation } \mathbf{13}$$

Results from porosity determination are shown in appendix **8**.

7.2.3 Definition and Determination of Permeability

Although abundant study of the effects of grainsize, sorting, orientation and packing of framework grains, cementation and bedding on permeability have been carried out, the relationships are still poorly understood. It has been found however, that finer grain size and poorer sorting of loose sand causes permeability values to decrease (Pettijohn et. al, 1987). Directional controls on the magnitude of permeability also exist with large variations that occur

perpendicular to bedding. At the time of deposition sediments will tend to align the long axis of grains parallel to depositional fluid flow thus causing anisotropy within the pore system. The waxing and waning of depositional energy may cause variations in vertical permeability since during periods of low depositional energy finer grained sediments are deposited and subsequently act as permeability barriers (Pettijohn et. al, 1987).

Permeability can be determined by the rate at which a fluid of known viscosity moves a given distance over a given time period. The calculation of permeability can be achieved by the fundamental relationship determined by Henry Darcy in 1856 (Ohen and Kersey, 1993); thus the subsequent units of permeability is the darcy. A permeability of one darcy allows the flow of one 1 mL of fluid with a viscosity of 1 cP (centipoise) to flow for 1 second under a pressure differential of 1 atmosphere through a porous material of cross sectional area of $1 cm^3$ and length 1 cm. Due to the normally low permeability values of rocks, the millidarcy (one-thousandth of a darcy) is used in core analysis. The equation for the calculation of apparent permeability is (Ohen and Kersey, 1993):

$$k_a = \frac{Q}{\mu} . \frac{\Delta P}{L} . A \qquad \text{Equation } \mathbf{14}$$

where K_a = apparent permeability (md)
Q = flow rate (cm^3/sec)
μ = fluid viscosity (cP)
ΔP = pressure differential (atm)
L = length (cm)
A = cross sectional area (cm^3)

Darcy's law assumes constant fluid properties. When a gas is used at low pressure the resistance to flow from drag is very low causing gas slippage in pores and an elevated permeability reading. At high flow rates of gas flow however, the changing sizes of pore and pore throats causes the gas to become turbulent causing lower than expected permeability readings (Ohen and

Kersey, 1993). These effects that may be present when determining permeability within core plugs are only minor and thus have not usually been corrected for in the past. In consistency with permeability values determined from previous studies, the non-linear flow effects are not corrected for in this thesis.

In this study I used the steady-state method to determine the permeability of the core plugs due to the low cost, the convenience of the technique, the ease at which the equipment can be operated and the speed at which analysis can be carried out. To determine permeability the Jones Permeameter was used. Briefly, this instrument is designed to measure permeabilities of core plugs over a range of 0.00001md to 2500 md. The equipment consists of a core holding section, a section for regulating and measuring the gas introduced to the sample and a section for measuring the flow rate of gas emitted downstream from the sample. Figure **117** is a schematic flow diagram illustrating the components of the Jones permeameter. For more detailed information on the description and operation of the permeameter see appendix **8**. The calculation of permeability using the steady state equipment is an integrated form of Darcy's law for a compressible fluid (Ohen and Kersey, 1993), thus:

$$k_a = \frac{2000 p_a \mu q_a L}{(p_1^2 - p_2^2) A} \qquad \text{Equation } \mathbf{15}$$

where k_a = air permeability (md)
p_a = atmospheric pressure (atm)
p_1 = upstream pressure (atm)
p_2 = outlet pressure (atm)
L = length (cm)
μ = air viscosity (cP)
q_a = gas flow rate at atmospheric pressure (cm^3/sec)
A = cross sectional area (cm^2)

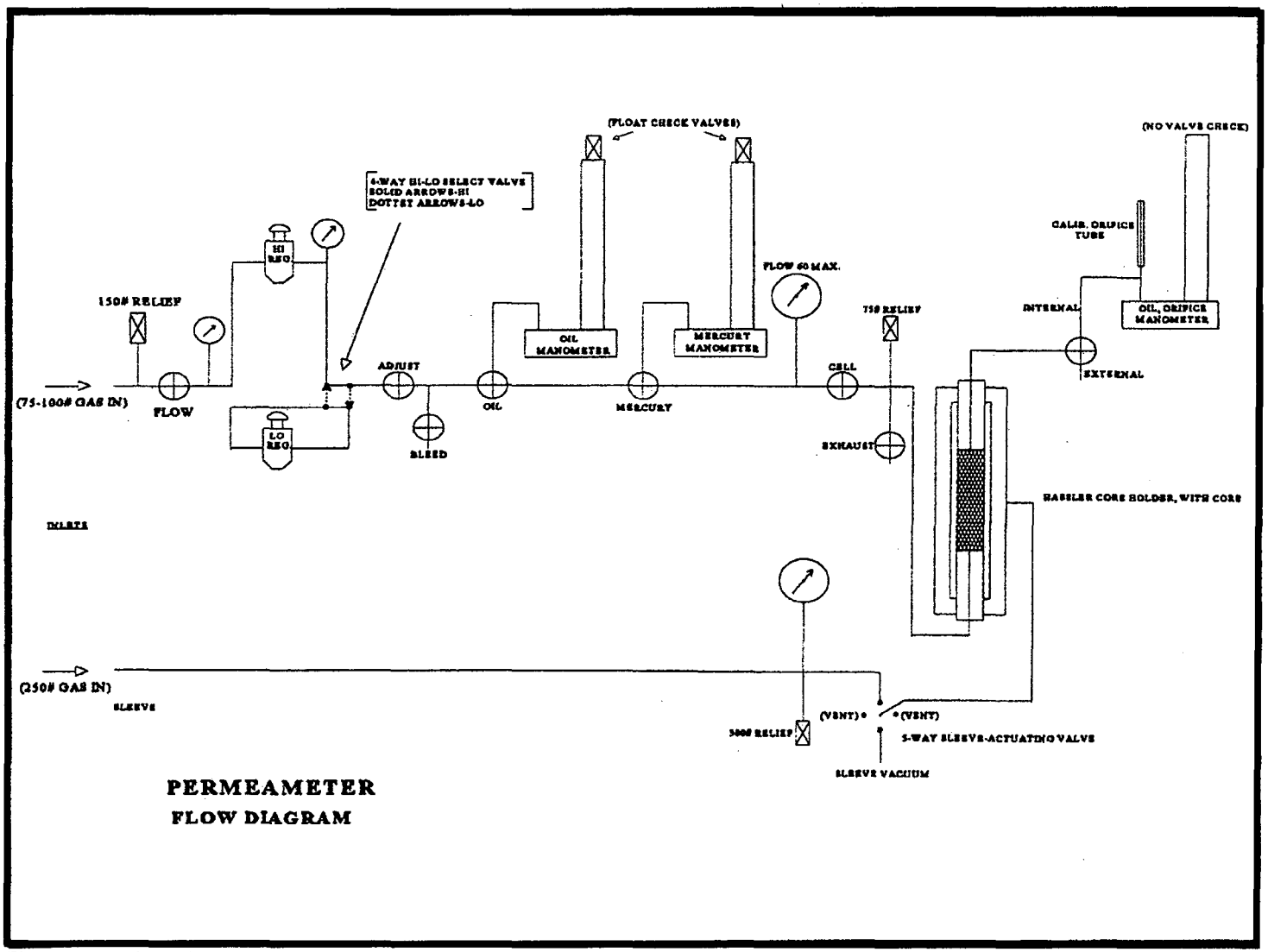

Figure 117: Flow diagram of the Jones Permeameter.

A spreadsheet showing the calculations of permeability for the selected core plugs can be found in appendix **8**. Table **13** is a summary of the results from this study of permeability and porosity.

Well	Depth (ft)	Facies	Porosity (%)	Permeability (md)
Gidgealpa 26	5950'8"	Sh	17.07	3.36
Gidgealpa 26	5955'9"	Sp	20.74	24.16
Gidgealpa 26	5956'9"	Sr	17.37	11.15
Gidgealpa 26	5958'6"	Sh	15.70	1.19
Gidgealpa 26	5969'6"	Sr	15.84	1.14
Gidgealpa 26	5971'7"	Sb/Fb	9.88	0.27
Gidgealpa 26	5973'1"	Sb/Fb	9.66	0.01
Gidgealpa 29	6015'5"	St	13.44	3.41
Gidgealpa 29	6041'8"	Sr	15.91	-
Gidgealpa 29	6046'8"	Fl	6.35	0.15
Gidgealpa 29	6047'4"	Sp	21.77	1437.98
Gidgealpa 29	6063'2"	St	12.50	679.31
Gidgealpa 30	6023'10"	Sr	19.19	8.39
Gidgealpa 30	6029'9"	Sp	19.09	510.55
Gidgealpa 30	6037'3"	Sh	22.73	577.08

Table 13: Summary of permeability and porosity results from core plugs.

7.2.4 Relationship between permeability and porosity

The relationship between porosity to permeability was studied by Beard and Weyl (1973), who found that permeability and porosity are related to grain size and sorting (see figure **106**, page 278). While this may generally be the case, Pryor (1973) determined that the relationship between permeability and porosity varies according to the depositional environment. Pryor showed that different depositional environments plot as different sub-fields (permeability-porosity trends) when applied to a permeability versus porosity graph. This evidence would suggest that depositional processes affect pore characteristics of sediments. Permeability and porosity in sediments that have undergone burial and diagenesis show good correlation and are best studied jointly because they are both related to pore space and distribution (Pettijohn et. al, 1987).

The identification of lithofacies with respect to reservoir description from core of the Birkhead Formation has been further characterised by petrophysical analysis of permeability and porosity. Using the results from table **13** (page 316) and data from routine core analysis conducted by SANTOS Ltd., gross porosity-permeability trends can be established. Figure **118**a is a summary of porosity-permeability crossplots with each facies illustrating different trends reflecting the different conditions of deposition. Figure **118**b represents the data from figure **118**a showing the trends of individual facies and the correlation coefficients (R^2 values) of the best fit lines. Table **14** is a summary of average porosity and permeability derived from core plug data. From this table it is evident that the lithofacies with higher permeability and porosity values corresponds to the coarser grained, better sorted sediments.

Lithofacies	Number of data points	Ave Permeability (Md)	Ave Porosity (%)
Fl	17	0.06	5.97
Fos	5	0.01	5.64
Sb/Fb	5	0.08	9.26
Sd	10	0.08	9.49
Sr	58	0.05	9.45
Sm	23	6.90	15.27
Sh	4	107.65	14.42
Sp	13	102.78	18.02
St	10	141.96	15.84

Table 14 Core plug averages of permeability and porosity.

The various points marked as 'extra samples' on the graphs of figure **118**b indicate the results determined in this study. Some of the lithofacies are not represented in figure **118**a and b due to time constraints and the low abundance of the facies in the core. From the plots of lithofacies Sr and Sm, it is evident that diagenesis and sediment composition can overprint the original depositional petrophysical characteristics of the samples, affecting porosity

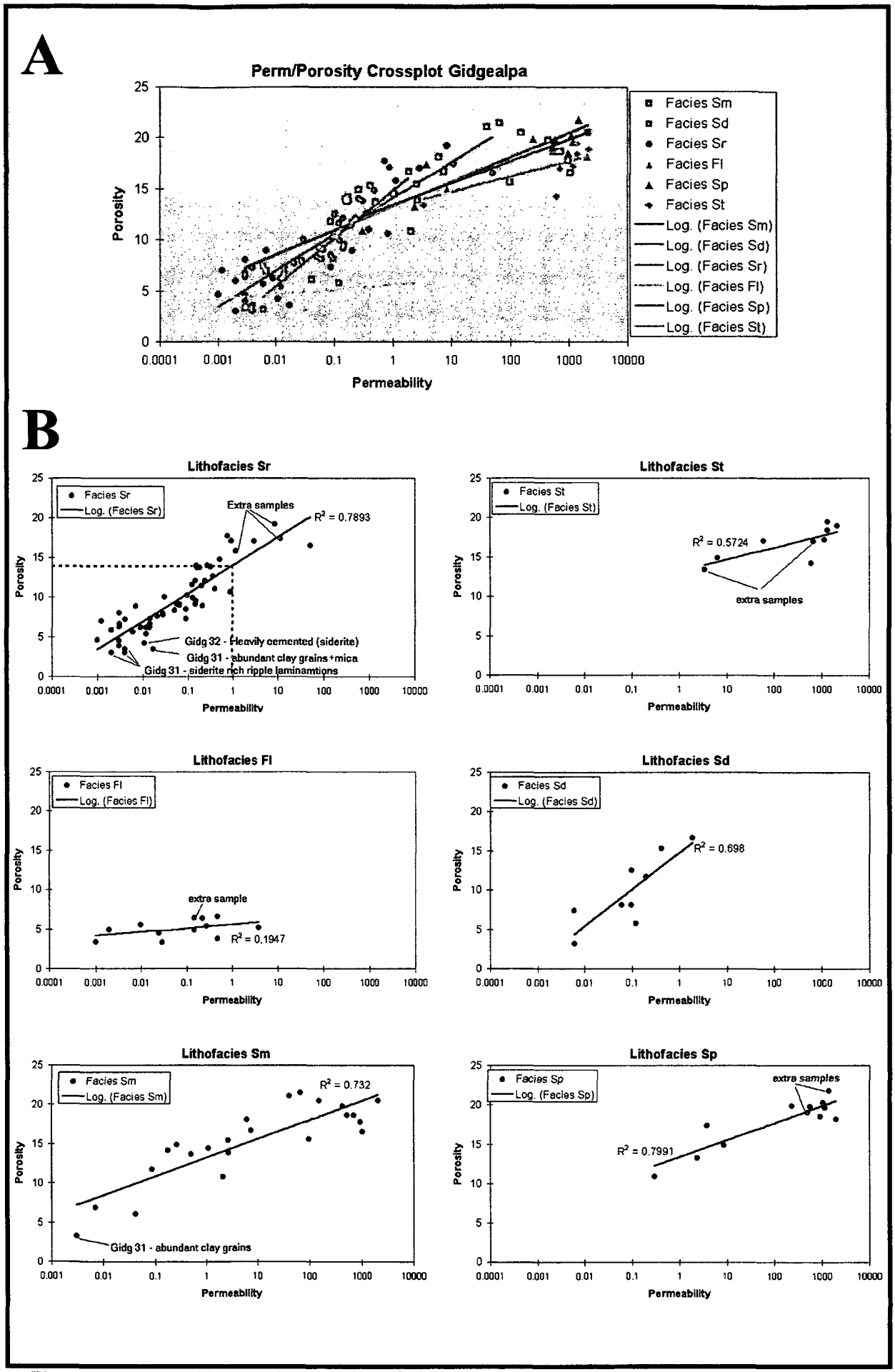

Figure 118: Permeability-porosity crossplots of Birkhead Formation, Gidgealpa south dome Lithofacies. (A) Crossplot of total lithofacies (B) Crossplots of individual lithofacies with best fit line and correlation coefficient. Points marked "extra samples" were determoned from this study.

and permeability values. The R^2 values were calculated using porosity and log(permeability) since permeability has a log-normal distribution.

The production of permeability versus porosity crossplots for each lithofacies can greatly aid in the characterisation of the reservoir when used in conjunction with probe permeability data. Core plug data is generally sparse from drill core with sample spacing usually no smaller than one foot (24 cm); in this study the probe permeability data was conducted at a one inch spacing (2.5 cm). Using the probe permeability data, the best fit lines of the permeability-porosity crossplots can be used to estimate porosity by simply applying the permeability value and reading off the corresponding porosity value. As an example: if we obtain a probe permeability value of 1 md for lithofacies Sr we can apply this value to the appropriate permeability-porosity crossplot graph (figure **118**b) and directly read off a value of 14% porosity. The probe permeability and cross-plot data were used to select a representative subset of samples from each lithofacies with varying porosities and permeabilities for mercury injection and petrological data from the cores.

7.3 Probe Permeametry

One of the most challenging problems for the petroleum geologist or engineer is the accurate description and quantification of the distribution of permeability within a hydrocarbon reservoir. To quantify the permeability variations within a reservoir the conventional acquisition of core plug data is performed. When the subsequent core plug derived permeability distributions in heterogeneous reservoirs are applied the data is often found to be unrepresentative of the small scale permeability variations that exist within the sediments (Robertson and McPhee, 1990). The fine scale permeability variations can be analysed in detail by the use of the probe permeameter on core. The probe permeameter can produce rapid, non-destructive and precisely located measurements of fluid flow in outcrop or drill core (Sutherland et. al, 1992). This, along with the fact that in recent years there has been

development of unsteady state and automated probe permeameters, has made the permeameter an increasingly attractive tool to use.

The probe permeameter is a simple instrument capable of measuring gas flow into porous media via a probe that is sealed against the rock surface by an 'O' ring. The flow response of the permeameter consists of steady state measurements of the gas rate and injection pressure at the probe tip. The primary factors affecting response are the gas permeability and stress state of the sample, gas viscosity under flowing conditions of temperature and pressure, tip seal quality and the gas flow geometry with respect to pore geometry (Goggin, 1992). The permeameter used in this study was the "Edinburgh Petroleum Services" (EPS) probe permeameter and is based on the instrument described by Eijpe and Weber (1971). Figure **119** is a schematic representation of the EPS probe permeameter.

7.3.1 Theory and Calibration of the Probe Permeameter

The theoretical analysis and determination of permeability using the probe permeameter was calculated by Goggin et. al (1988). The relationship between injection pressure, flow rate and gas flow geometry are affected by the tip and tip seal where gas flow is radial instead of linear (Goggin, 1992). Assuming that non-darcy flow effects such as gas slippage or turbulence are absent, a modified form of Darcy's Law was derived for probe permeameter measurements (Goggin, 1992):

$$k_a = \frac{2q_1 p_1 \mu}{aG_o\left(p_1^2 - p_0^2\right)} \qquad \text{Equation } \mathbf{16}$$

where k_a = apparent permeability
q_1 = volumetric injection rate at p_1
p_0 = atmospheric pressure
μ = viscosity of air
p_1 = injection pressure
a = internal radius of tip seal
G_0 = dimensionless factor representing the gas flow geometry

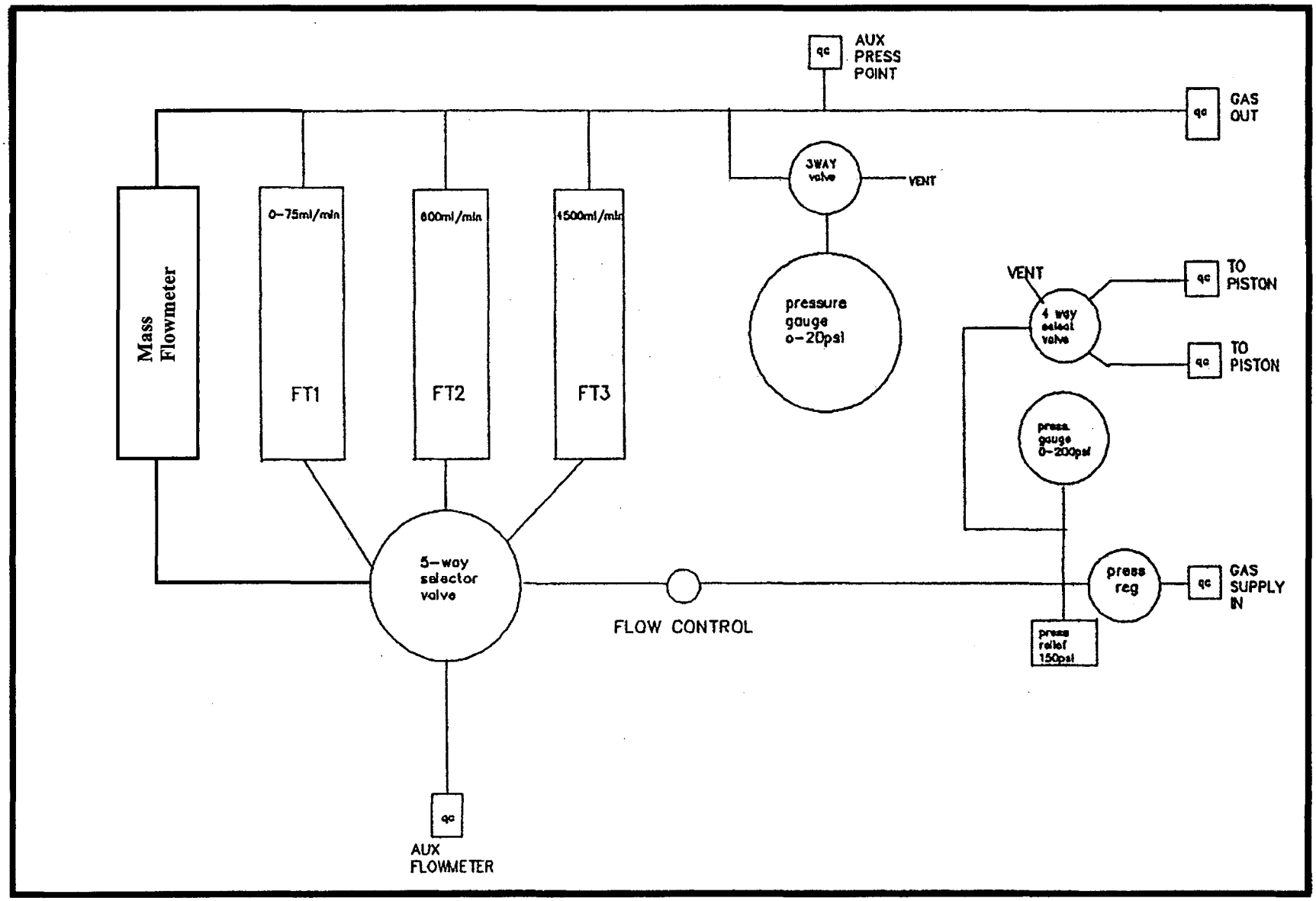

Figure 119: Flow diagram of probe permeameter used on the Gidgealpa south dome cores. In this study a mass flowmeter was incorporated into the apparatus.

Before any work commenced using the probe permeameter the equipment was inspected to assure that it would not be the cause of any erroneous measurements when determining permeability. The flow tubes (or rotameters) generally have the potential to be inaccurate, thus calibration should be carried out. Calibration of the tubes at various pressures (5, 20 and 70 psi) was conducted by Carbone (1993) on the same equipment used in this study and was therefore adopted for this thesis. For consistency with the calibration data readings were taken at 5 or 70 psi depending on permeability characteristics of the Birkhead Formation and Hutton Sandstone cores.

The EPS probe permeameter also had another problem with the minimum flow tube readings limited to 0.25cc/sec. The flow rate corresponds to an apparent permeability value of 0.35 md which is not low enough to measure a majority of the Gidgealpa south dome permeabilities. This fact has been noted (Boult et. al, 1995) to cause problems in distribution of probe permeability frequencies when looking at other tight, low permeability rocks. The log-normal distribution graph of probe permeameter permeabilities in figure **120** illustrates the limitation of the equipment. The inaccurate distribution of probe permeability frequencies may affect lithological permeability statistics by causing unrepresentative average permeability values and decreasing standard deviations (Boult et. al, 1995).

To overcome the limitations of the equipment I attached a mass flow meter to the auxiliary flow meter port of the probe permeameter, bypassing the three flow tubes that would otherwise determine gas flow rates (see figure **119**, page 321). The mass flowmeter is a Brooks Instrument Model 5860i that can accurately determine gas flow rates between 0 to 0.05 cc/sec. Unfortunately a gap occurs between the lowest reading of the mass flowmeter and the minimum value on the probe permeameter flow tubes of approximately 0.2cc/sec causing permeabilities between with corresponding flow rates of 0.05cc/sec and 0.25cc/sec to be plotted as 0.25cc/sec. Nevertheless, this result

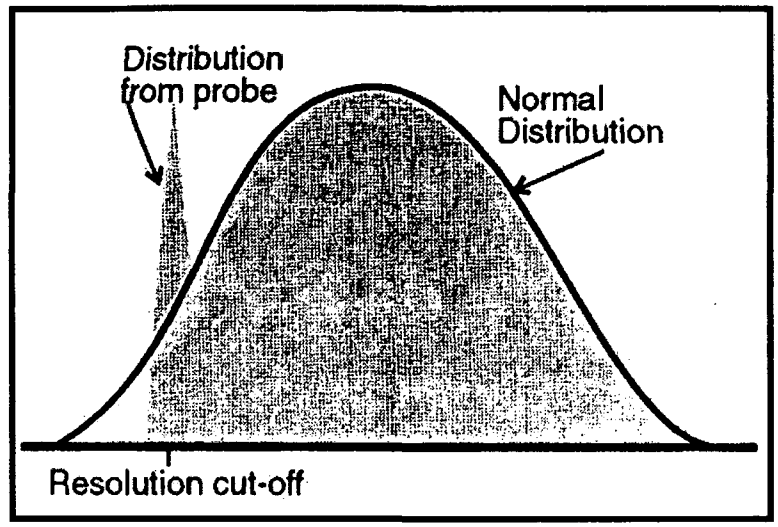

Figure 120: Hypothetical probe permeameter histogram showing the spike at the lower end of permeability data due to limitations of the probe permeameter (From Boult et. al, 1995).

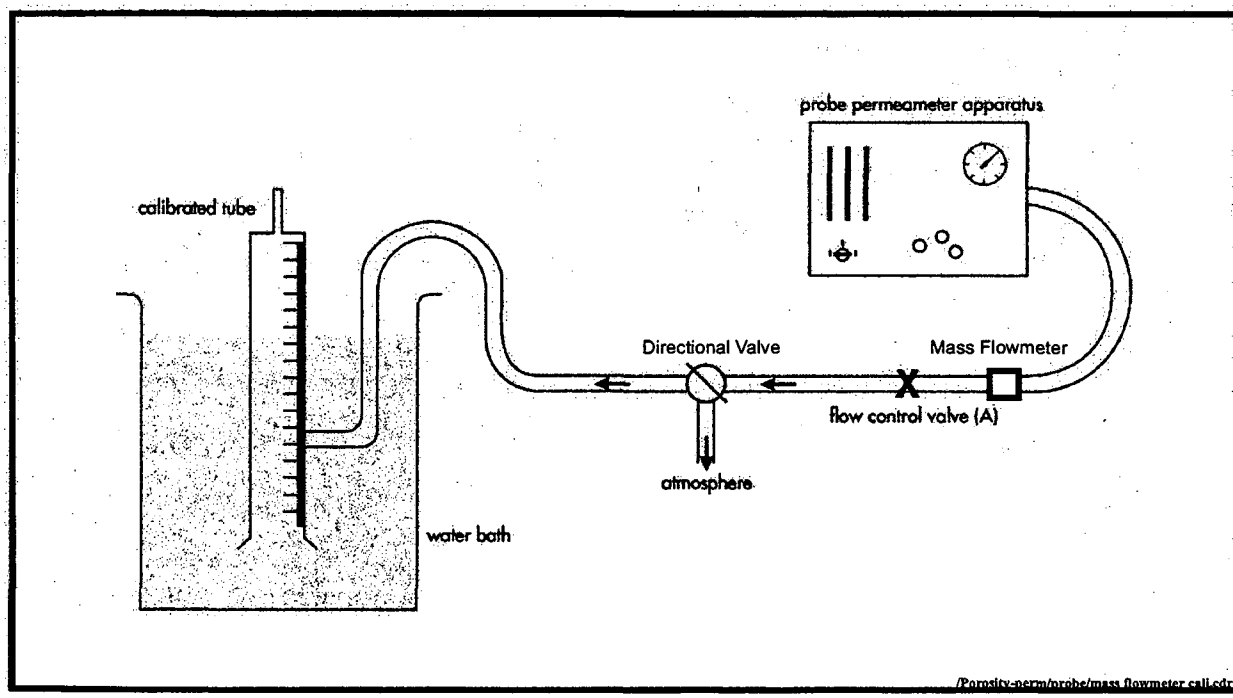

Figure 121: Equipment setup for calibration of the mass flowmeter.

is a great improvement on the basic equipment alone. Further work is required to correct the flow rate gap between the mass flowmeter and the flowtubes. The Brooks Instruments mass flowmeter was calibrated to gas flow rates using a similar technique adopted by Carbone (1993) when calibrating the flow tubes. Figure **121**, on the previous page, shows the set up of the equipment that I used during the calibration.

The apparatus was set up by partially immersing an inverted, graduated measuring cylinder within a water bath. Water was drawn up into to the cylinder by creating a vacuum and then the water height was recorded. The end of the gas line from the probe permeameter was positioned within the cylinder so any gas from the probe permeameter would be trapped within the cylinder. A variable flow control valve controlled gas flow and proir to the commencement of each reading the control valve was set while the gas flowed out to the atmosphere via the directional valve and the voltage was determined on the mass flowmeter. To start the reading the directional valve was opened so the gas flowed into the immersed cylinder over a set period of time so the flow rate could be determined. Each flow rate was tested 3 times for accuracy while making sure the mass flowmeter voltage stayed constant. The resultant flow rates and corresponding voltages were then compared and a linear relationship was derived. Figure **122** shows the excellent relationship between the data with an $R^2 = 0.998$, this graph can then be used to directly read of flow rates for any given voltage.

The calibration of the probe permeameter to determine apparent permeabilities in rocks can be performed a number of ways. Halvorsen and Hurst (1990) listed the techniques as:

- Measurement using the probe permeameter on standard "homogeneous" core plugs which have known Hassler-Sleeve permeabilities to derive a relationship between probe permeameter flowrates and permeability.

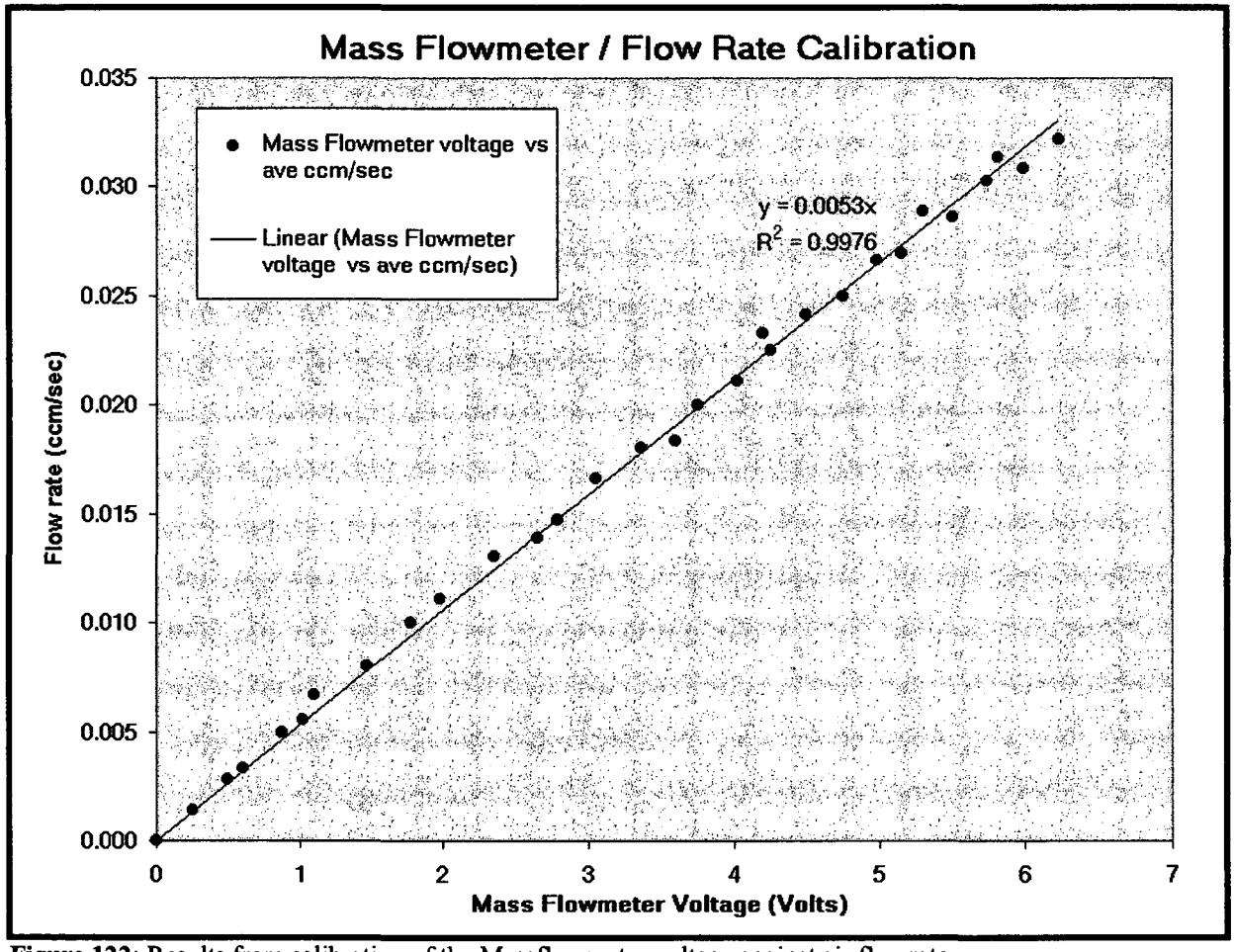

Figure 122: Results from calibration of the Massflowmeter voltage against air flowrate.

• Use of a modified form of Darcy's equation for an analytical solution.

• Comparison with core plug permeabilities measured over the same interval as the probe permeability readings.

From the literature the first method for calibration seems to be the most popular with authors such as Dreyer et. al (1990), Gibbons et. al (1993), Halvorsen (1993) and Boult et. al (1995) using this technique. While the selection of homogeneous core plugs may be trivial for mostly homogeneous reservoirs, problems may exist in heterogeneous reservoirs were core plugs fail to reflect the complex permeability distribution of the reservoir. Robertson and McPhee (1990) go further by highlighting the fact that even the core plugs that may appear homogeneous may in fact have complex permeability structuring. By using CT-scanning (3D Xray-imaging) they could identify the permeability variations due to the differing densities of a particular sample. This could pose problems for the geologist who is considering monetary or time constraints with the determination of core plug permeability from the probe permeameter already affecting these parameters.

The analytical determination of permeability using the modified Darcy's equation (equation **16**, page 320) developed by Goggin et. al (1988) contains a dimensionless factor (G_o) representing gas flow geometry from the probe tip. The G_o value can be determined in equation **16** from the ratio between the inside diameter and the outside of the probe tip. Again, this method of determination produces good results when compared with homogeneous core plugs but results are not as comparable when heterogeneous samples are used since the flow path of the gas becomes more complex and difficult to quantify (Goggin 1993).

Finally, the comparison of probe permeabilities to core plug permeabilities over an interval also has some problems. Generally, probe permeability is

conducted on core after the core plug samples have been removed meaning that direct comparisons of probe permeability to core plug determined permeability can not occur. In this situation probe determined values must be taken as close as practical to where the plug had previously been removed. The problem may become more prevalent if the rock of interest is heterogeneous in nature. This problem can be overcome as it was in this thesis by conducting probe permeability measurements before the removal of core plugs. Conducting the probe run first may have other advantages since the data can be used as a guide for the selection of core plugs which are representative of the reservoir rocks.

In this study the calibration of probe permeability data was conducted by the comparison of the probe permeability data to the Hassler-Sleeve permeabilities over the given intervals. Values were compared and matched in each core by altering the G_o value until a best fit of the data was obtained. Initially, probe permeability was conducted over the cores and the permeability was calculated using the modified form of Darcy's law. From the correction of the probe permeability data the G_o value varied from 3.5 to 6.5 for different cores suggesting that other factors are affecting the flow geometry of gas from the probe tip. The fact that the G_o value varies between wells means that other factors may be affecting radial gas flow. The causes in variations could be from a number of different possibilities including varying handling conditions at the well site or at the storage location, the types of drilling mud used while drilling of the cores or the relative exposure time

Plotting the probe permeabilities against Hassler-Sleeve values where they occurred at the same depths in the core tested the validity of the method I used for correlation. Figure **123** shows a relatively good relationship between the values with an R^2 value of 0.835. From the above discussion the direct comparison of probe permeability values calculated from the modified form of Darcy's equation and Hassler-Sleeve core plug permeabilities has its advantages. The calculation of permeabilities from the equation allows fast

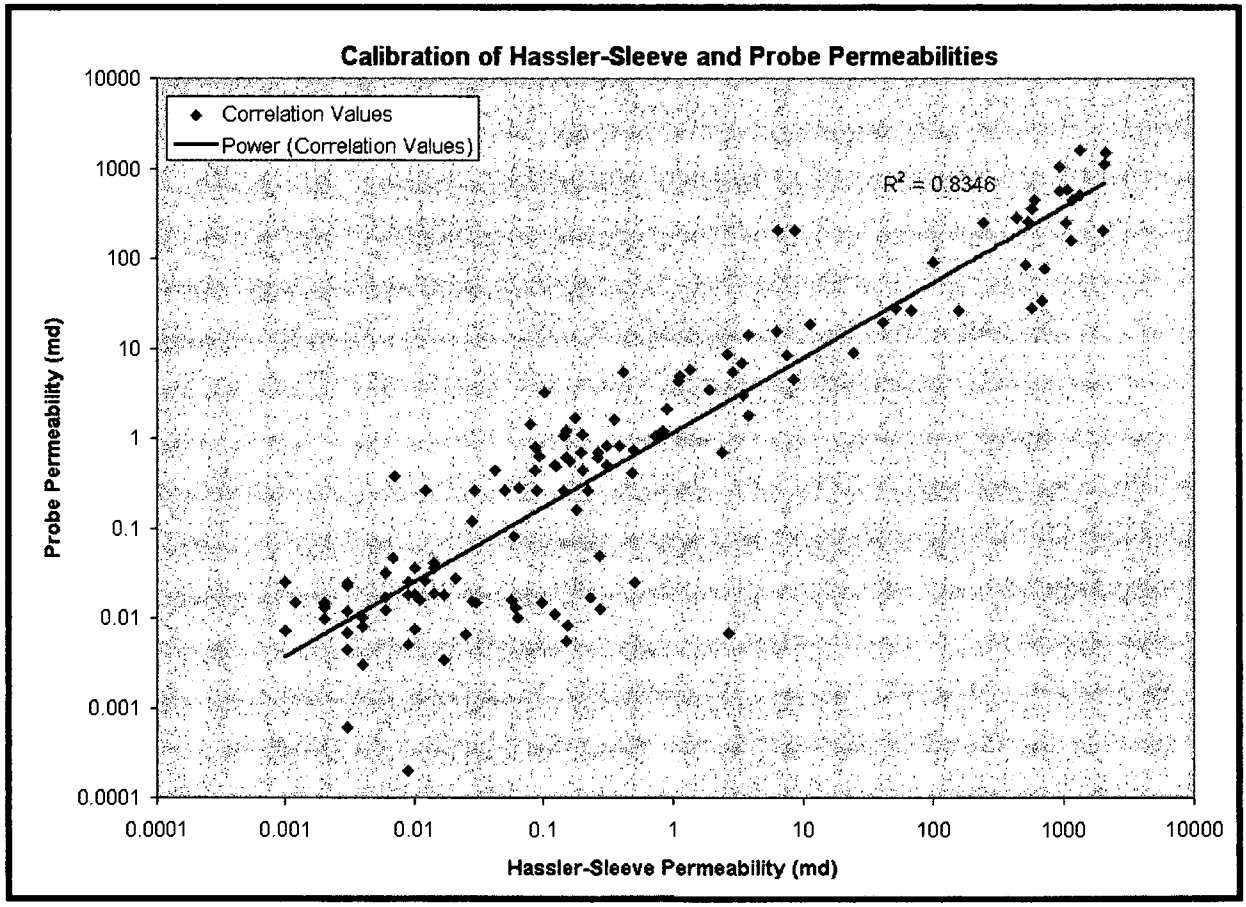

Figure 123: Crossplot of coreplug permeability versus probe permeability showing the good data fit with a correlation coefficient of 0.83 for the line of best fit.

determination of permeability values with no added costs. The comparison of probe data (gathered by my method) to core plugs that have not been corrected for non-linear flow conditions means that the effects of gas slippage and turbulence as well as the difference in conditions of the uncleaned cores and cleaned core plugs can be directly compared and therefore ignored in correlation. From comparison of data the direct value of G_o may be calculated even though the cause of variations may not be fully understood.

7.3.2 Probe Permeability Method and Results

Where core was present, I took over 2000 permeability readings using the probe permeameter from the lower part of the Birkhead Formation and top section of the Hutton Sandstone in the Gidgealpa south dome. To maximise permeability characterisation of lithofacies the probe readings were taken at a 1 inch (2.5 cm) spacing except where the core is fractured or near the core ends.

Where micro-fracturing was believed to be occurring probe values were omitted. The probe was positioned on the centre of the slabbed cores to minimise edge effects; where core plugs were previously taken the probe was placed as close as possible to the centre of the slab. During each reading the injection pressure was kept constant while the flow rate and lithofacies type for each reading was noted. Permeability calculations at each depth was conducted in EXEL by converting flow tube readings to flow rates by the use of the calibration equations and displayed in appendix **9**.

7.3.2.1 Probe Permeability Profiles

The effectiveness of the probe permeability data is illustrated in figure **124** that shows good correlation with core plug data and core lithofacies. The figure also demonstrates the true heterogeneity of the core with core plug sampling resolution to large to detect the small scale variations. Therefore, the low

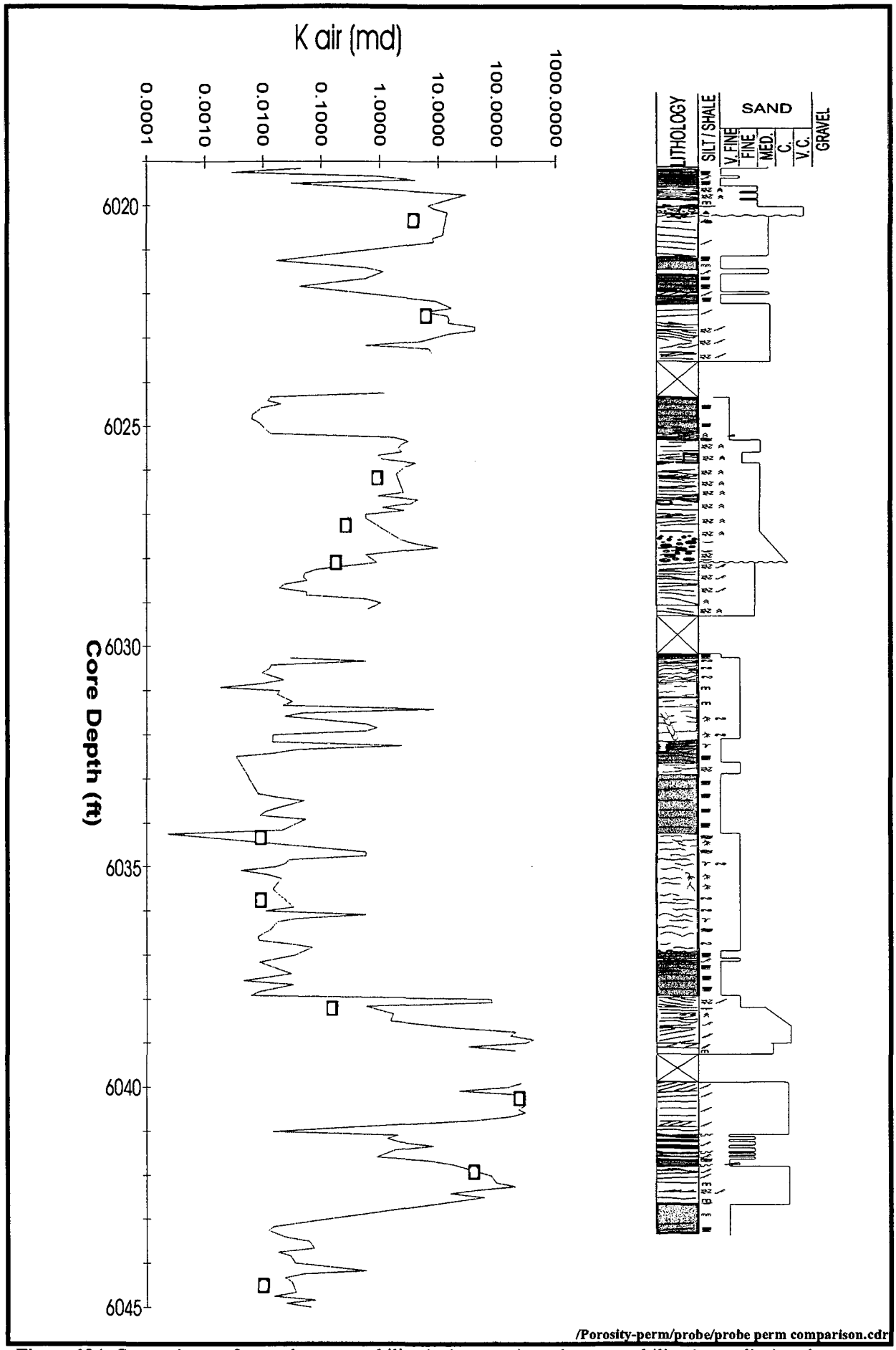

Figure 124: Comparisons of core plug permeability (red squares), probe permeability (green line) and core interpretation data. (Core interpretation legend can be found in appendix 2).

resolution of core plug data will affect permeability determination and characteristics within reservoir zones.

The inability to resolve fine scale low permeability zones will cause an over estimation of permeability averages for the pay intervals and secondly, these low permeability zones or streaks will greatly affect fluid flow characteristics during production. An example of the variations of average permeabilities is shown in table **15** and represent the interval from 6038' to 6042' in Gidgealpa 29. Figure **124** is a comparison of core plug permeability, probe permeability and core log interpretation showing the good fit of the data. Note from this figure the higher permeability detail that can be obtained from using the probe permeameter and the good match of probe permeability to the core log interpretation.

	Arithmetic Mean (md)	Geometric Mean (md)
Core Plug Data	133.93	69.28
Probe Data	107.57	26.06

Table 15: Comparison of core plug and probe permeability averages in Gidgealpa 29 (6038'-6042').

Since the probe permeability data has a log-normal distribution the data was converted using a logarithmic (base 10) transformation (figure **125**a). While the data in figure **125**a appears to be skewed, on separation of the Birkhead Formation and Hutton Sandstone data, these two formations show log-normal distributions with different geometric mean permeability values of 0.068md and 101.8md respectively (figure **125**b). The differences in the permeability distributions are attributed to the different environments of deposition where the Hutton Sandstone consists predominantly of high energy intra-channel sediments whereas the Birkhead Formation is dominated by low energy over bank, floodplain and lacustrine facies.

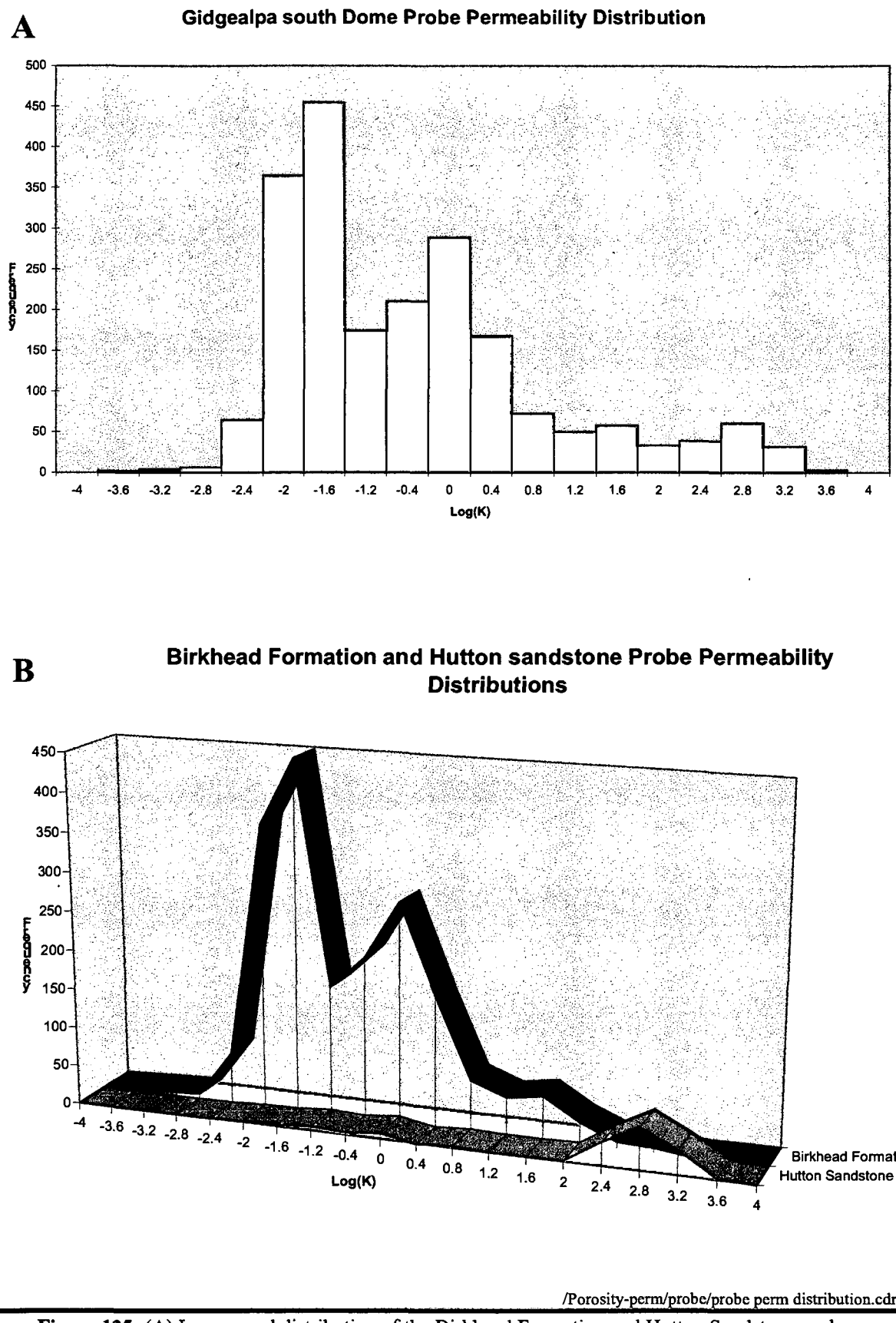

Figure 125: (A) Log normal distribution of the Birkhead Formation and Hutton Sandstone probe permeability data. (B) Log normal distributions of the separated Birkhead Formation (blue) and Hutton Sandstone (purple).

7.3.2.2 *Averaging Permeability*

Probe permeability data taken at such a fine scale on the Gidgealpa south dome cores is useful for determining the small scale heterogeneity within sediments but is too fine when comparing the data to wireline logs. To rectify this problem the probe data can be filtered using a box-car or rolling average, geometric mean estimator. The geometric mean is used due to the internal random nature of permeability within sediments away from the well bore (Goggin, 1992, Boult et. al, 1995). Box-car averaged permeability data can be used to calibrate permeability values from wireline logs to determine pay zones were core is unavailable.

7.3.2.3 *Permeability Histograms*

The allocation of lithofacies to sediments within the Birkhead Formation was determined by the interpreted environment of deposition and physical properties of the rocks (section **4.2**). For further analysis of the permeability distribution and characteristics within the reservoir the high resolution probe permeability data has allowed the correlation of the permeability data to lithofacies by use of histograms. The log-normal permeability distribution of each lithofacies in figure **126** indicates that increasing grain size and depositional energy correlates to higher permeability values. A summary of the number of values, standard deviation and the average permeability is summarised in table **16**.

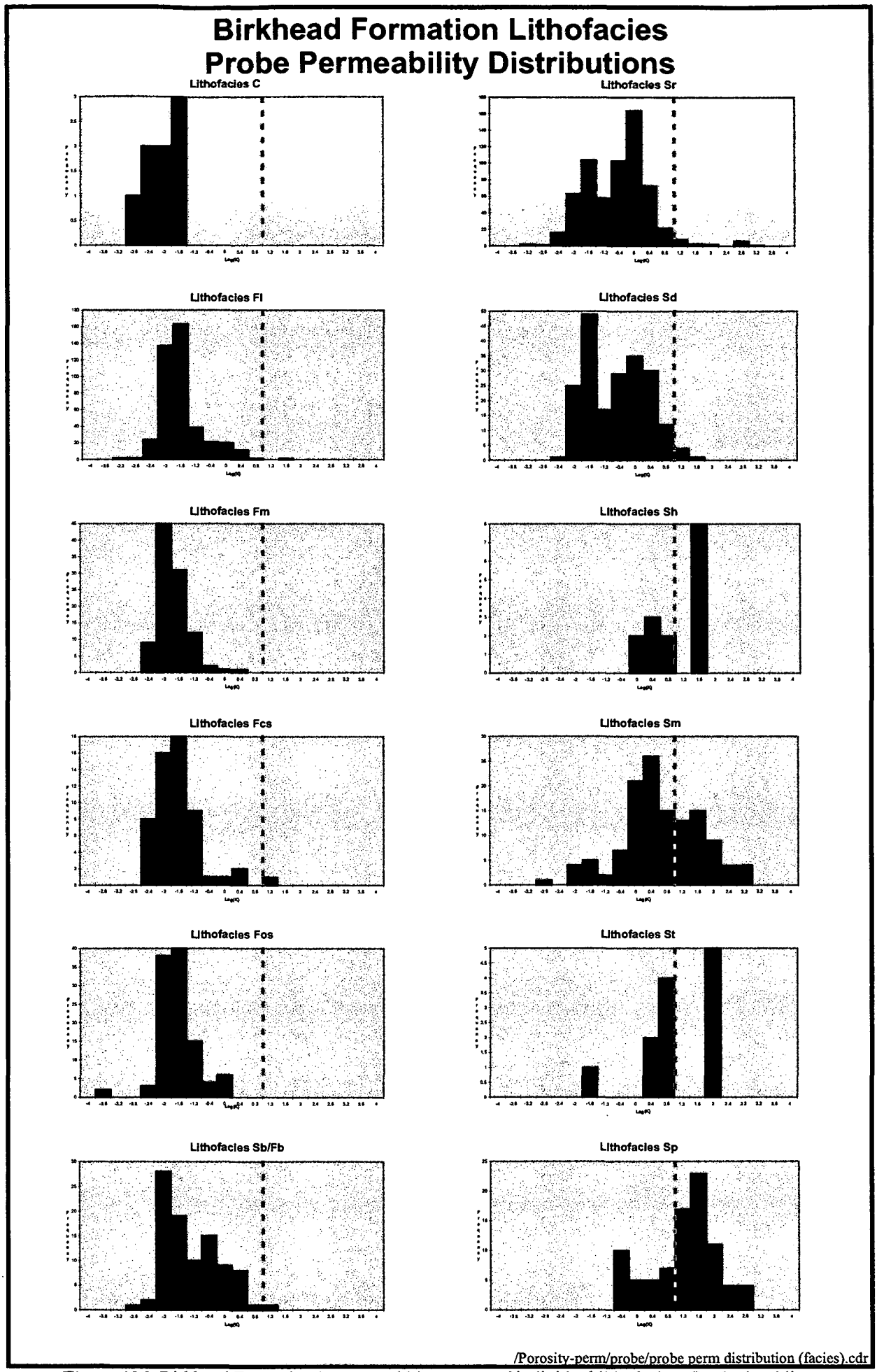

Figure 126: Birkhead Formation log-normal histograms of individual lithofacies. Dashed red line indicates 10md cutoff value for reservoir quality flowunit allocaton.

Facies	No. of Values	Standard Deviation	Ave. Perm. (md)
Sp	86	74.47	20.935
Sh	15	12.29	7.824
St	12	27.59	6.439
Sm	126	78.99	3.809
Sr	626	55.06	0.261
Sd	203	1.94	0.165
Sb/Fb	94	0.97	0.053
Fl	420	1.48	0.019
Fm	101	0.16	0.013
Fos	108	0.13	0.015
Fcs	56	1.44	0.017
C	8	0.01	0.005

Table 16: Permeability characteristics for lithofacies within the Birkhead Formation of the Gidgealpa south dome.

Figure **126** also shows that the lithofacies can be separated into three permeability classes. In this case the definition of a permeability class is a group of permeability measurements that give similar permeability distribution characteristics and are separate from the other permeability distributions (Dreyer et. al, 1990). Not surprising is the fact that the lithofacies that occur within the same permeability classes are deposited in similar depositional environments. From here on the permeability classes have been named as poor quality, intermediate quality and high quality permeability classes. The poor quality permeability class consists of sediments that have been deposited in a low energy lacustrine or floodplain environment and contain lithofacies Fl, Fm, Fos, Fcs, Sb/Fb and C. The intermediate quality permeability class consists of over-bank sediments within crevasse splays and channel levees as well as delta lobes where depositional energy is intermediate between the low and high quality permeability classes. Lithofacies Sd and Sr occur within this class. The high quality permeability class contains the lithofacies Sh, Sm, St and Sp which occur as high energy channel deposits. A summary of the permeability class characteristics is displayed in table **17**.

Permeability Class	Associated Facies	Depositional Environment.	Average Perm. (md)
Poor Quality	Fm, Fl, Fos, Fcs, Sb/Fb, C	Lacustrine to low energy floodplain	0.02md
Intermediate Quality	Sr, Sd	Crevasse splay, levee, delta lobe	0.21md
High Quality	Sm, Sh, Sp, St	High energy channel deposits	9.75 md

Table 17: Summary of permeability class characteristics.

The different permeability classes can be used to characterise the quality of the Birkhead Formation reservoir. Sediments affiliated with the poor quality permeability class have no reservoir potential while the intermediate class has limited potential to flow hydrocarbons while the high quality class has the highest potential to flow hydrocarbons and should be used as a guide when considering perforation intervals within the reservoir. The application of these permeability classes is demonstrated in section **8.2.2.4**, where the cut-off value of the high quality permeability class (10 md) has been used to determine reservoir flow units from log interpreted data. The cut-off values for the intermediate and poor quality permeability classes are 0.01 and 0.001 md respectively.

The permeability values that have been used in this section have been determined in the horizontal plane or along bedding. While these values may be accurate in a horizontal sence in the vertical direction some variations may occur. Variations may occur in those facies such as St, Sh and Sp that have an ordered flow path where unidirectional flow will preferentially align grains and cause higher permeability values in the direction of the flow. The ilignment of the grains is also likely to reduce the vertical permeability to a degree. The reduction in the vertical permeability is likely to be affected by the types of grains present in terms of their size and shape. The exception to this is facies Sm where the random deposition of the sediment may make the permeability distribution uniform in all directions.

The higher proportion of platy minerals such as mica within the siltier facies means that the horizontal to vertical permeabilities are likely to show a larger contrast than in the more sandy facies where the higher permeability values are in a horizontal direction.

7.3.2.4 *Semi-variograms*

Semi-variogram analysis expresses the average 'size' of similarity (or variability) between any pairs of data separated by some distance (Dreyer et. al, 1990). The use of the semi-variogram analysis on probe permeability data is useful in the determination of the degree of vertical permeability variation where core data is not available. The semi-variance of a data set is calculated from the equation described by Clark (1979) where:

$$2\gamma_z(l) = E\{[(x+1) - Z(x)]^2\} \qquad \text{Equation } \mathbf{17}$$

where Z(x) = value of property at point x
l = separation distance between values
E{} = mean value of x
$\gamma_z(l)$ = semi-variance of population z at spacing l

Equally spaced data from probe permeability analysis was input into the GEO-EAS geo-statistical program to determine the semi-variance of the data. Due to limitations on the software, a maximum of 1000 data values can be used or 16384 pairs created when using the program. For this reason the probe permeability data was separated into sections related to depositional environment. From figure **127** the measure of local scale variance (nugget effect) is determined where the curve intercepts with the semi-variance axis. The height of the plateau (sill) is a measure of the overall variance of the data while the distance required to reach the sill (range) is the correlation distance of the data. The semi-variogram data can be useful in reservoir simulation models where the range can be used to determine the size of grid cells (Boult et. al, 1995).

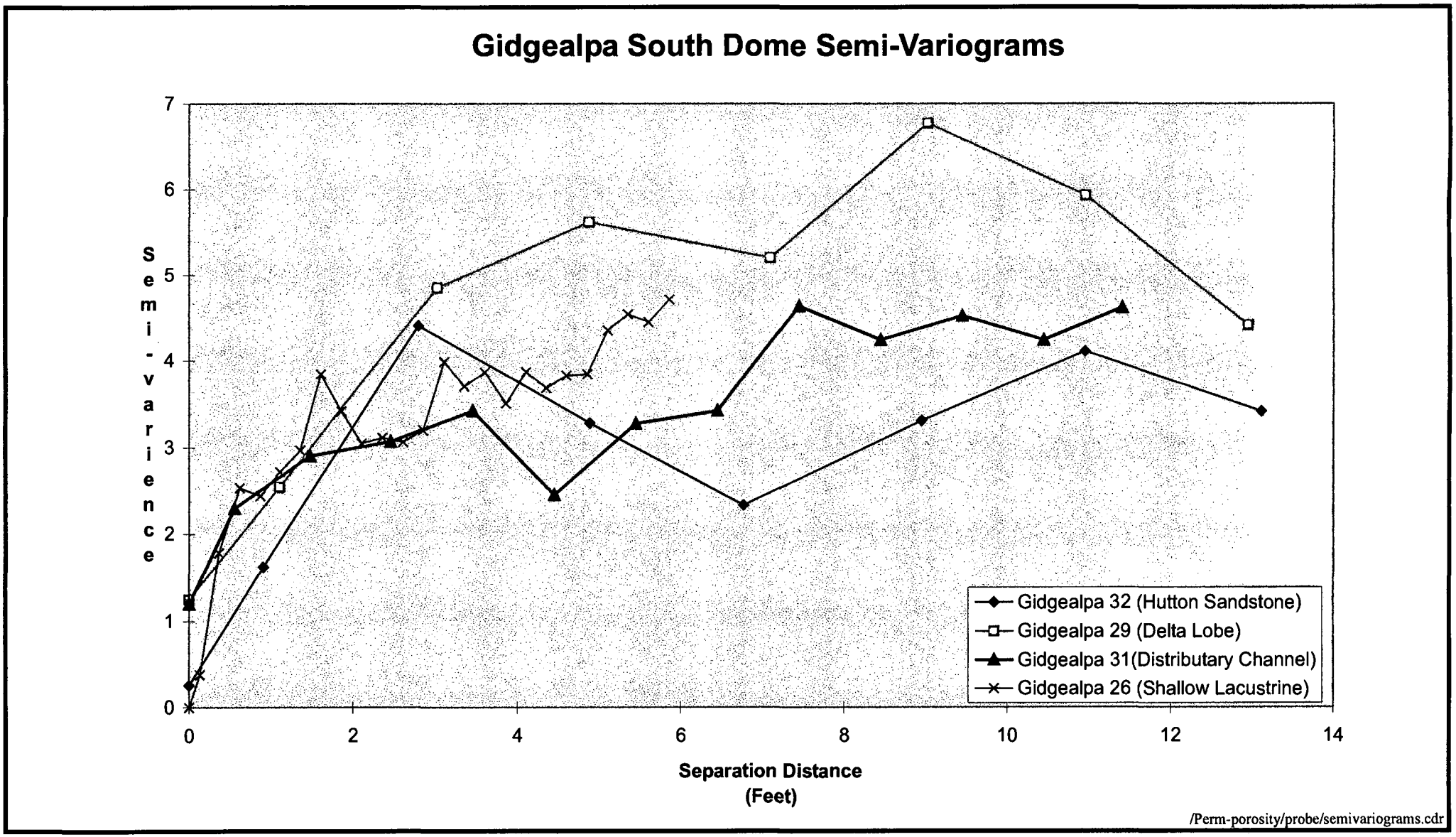

Figure 127: Semi-variograms of various depositional environments in the Birkhead Formation and Hutton Sandstone.

The low nugget effect values for the Hutton Sandstone and Gidgealpa 26, shallow lacustrine facies reflects the relatively low local variance of the data even though on a slightly larger scale (bed scale) the Gidgealpa 26 data is more variable between siltstones and sandstones. The higher local variance of the distributary channel and delta lobe facies is probably a reflection of the high number of variables controlling the depositional environment. The ranges of the Hutton Sandstone and the delta lobe facies of Gidgealpa 29 display a similar value of 3 ft (75 cm) reflecting the internal bed thicknesses while the distributary channel to delta lobe facies of Gidgealpa 31 has a slightly lower range of just under 2 feet (50 cm) also reflecting bed thickness. The range of the shallow lacustrine, Gidgealpa 26 sediments is approximately 6 inches (15 cm) which reflects the thinly bedded nature of the interbedded sands and silts.

It is hard to determine the overall variance of the data since only short intervals were used. However, it appears that Birkhead Formation data is more variable than the Hutton Sandstone data which is reflection the different environments of deposition between the two formations.

8 Reservoir Characteristics of the Gidgealpa south dome

8.1 Gross Sand Trends

Maps of gross sand between the transgressive surface and the maximum flooding surface of the lower Birkhead Formation were produced over the Gidgealpa south dome. For the determination of reservoir quality sands a gamma ray API value cut-off of 70 or less was used from wireline logs. This cut-off was determined by the correlation of wireline logs with cores (see Section **4.4**). Gross sand values were calculated using the LOGLAN module within GEOLOG for the appropriate intervals (Theologou, P., pers.comm.).

The gross sand values were calculated for each well and then applied to a base map of the area. To determine whether sand trends were related or influenced by topography an isopach map of thickness between the maximum flooding surface and the transgressive surface was produced (figure **128**). Because the maximum flooding surface is horizontal, any thickness variations are a reflection of topography of the transgressive surface or top of the Hutton Sandstone. The isopach map shows that early sands were concentrated in the thicker parts or depressed areas of the Gidgealpa south dome. Preceding sand packages also filled these depressions and are probably a result of dewatering of the underlying shales which filled these areas. The deposition of the higher density, older sands would have aided in the compaction of the shales. Gross sand trends were contoured by hand using all geological data available including production data.

The total gross sand map of the basal Birkhead Formation (figure **129**) shows an east-west trend with thinner packages of sands almost perpendicular to the

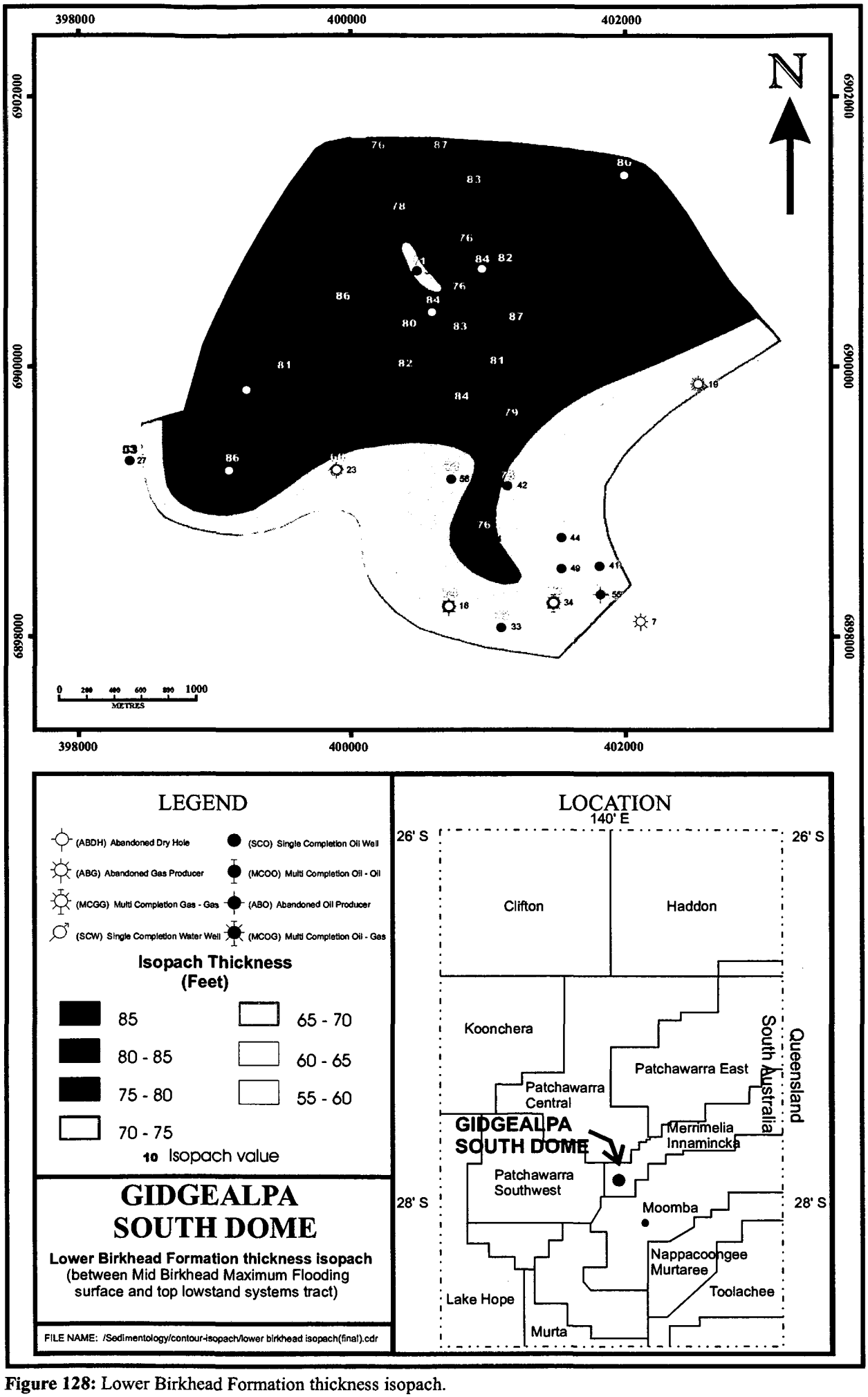

Figure 128: Lower Birkhead Formation thickness isopach.

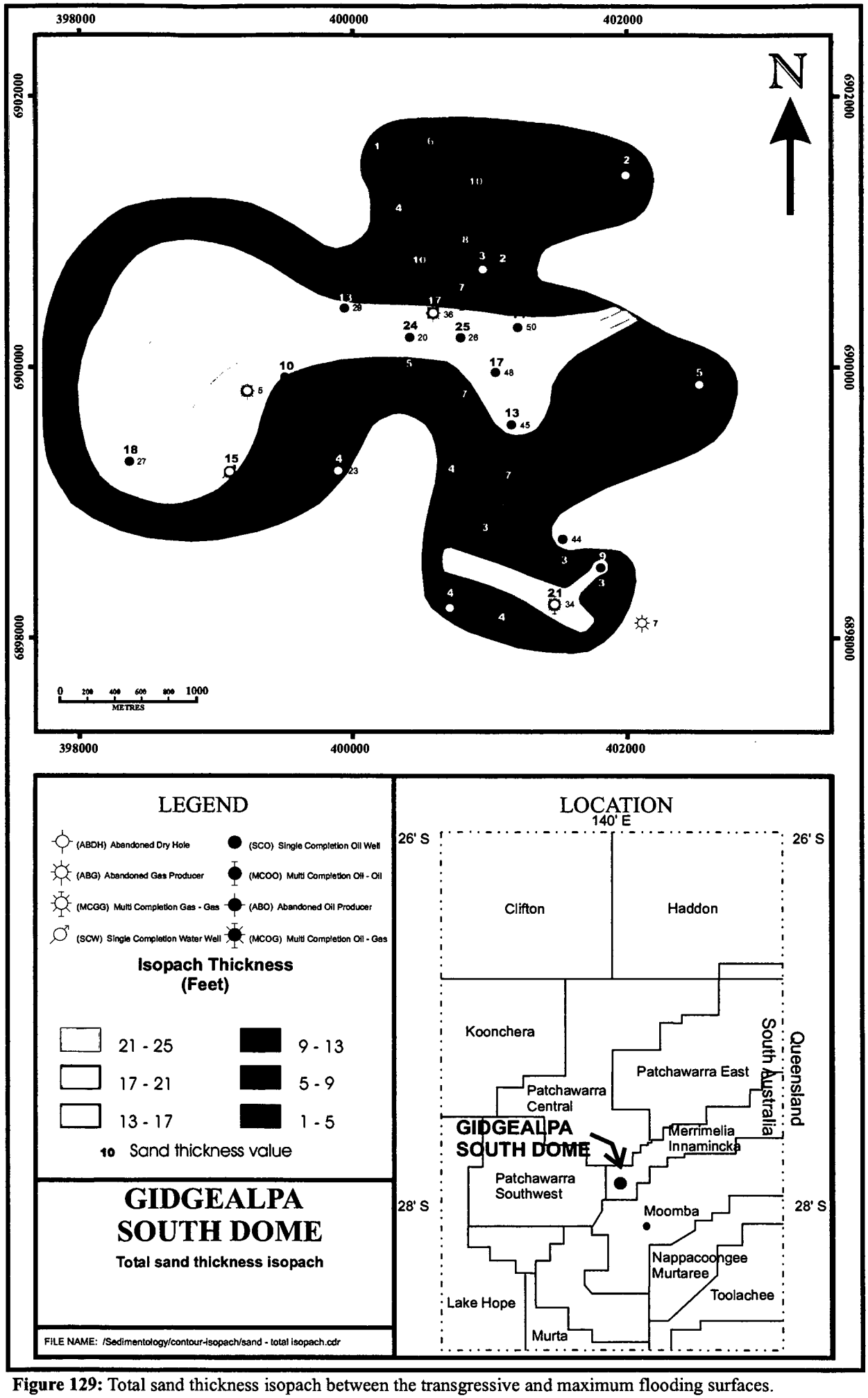

Figure 129: Total sand thickness isopach between the transgressive and maximum flooding surfaces.

main axis. The thicker and larger sand accumulations, or area of best sand development occurs on the western flank of the field. This sand trend is characteristic of a deltaic deposit and shows the shoestring nature of the distributary channel to the east feeding the delta lobe.

While the overall gross sand trend is summarised in figure **129**, from production data, reservoir compartmentalisation is known to occur. Thus to further characterise the sands at the Gidgealpa south dome they were divided into packages. From production data (see section **8.2.6.2**) four pressure regimes are identified and using accompanying wireline logs, five gross sand maps were produced and were labelled Sand A to E respectively (figures **130** to **134**).

Figure **135** shows the spatial distribution of the delta sands in the form of a fence diagram. The colour of each sand package corresponds to the sands displayed in figures **130** to **134**. Note in figure **135** how Sand B fills the topographic depression created at the top of the Hutton Sandstone and the delta lobe stacking pattern of the other sand packages.

8.2 Log Evaluation

8.2.1 Introduction

The determination of porosity and permeability is a straight forward task when analysis is carried out on drill core. Samples may be obtained at a chosen interval that best characterises the rock property distribution where resolution is controlled by the spacing from which samples have been taken. In the case of permeability determination, the sample spacing can be within the centimetre range when using the probe permeameter. However, due to the cost and time consuming practice of core analysis, the taking of core is not commonly carried out. This is indeed the case in the Gidgealpa south dome where 5 cores

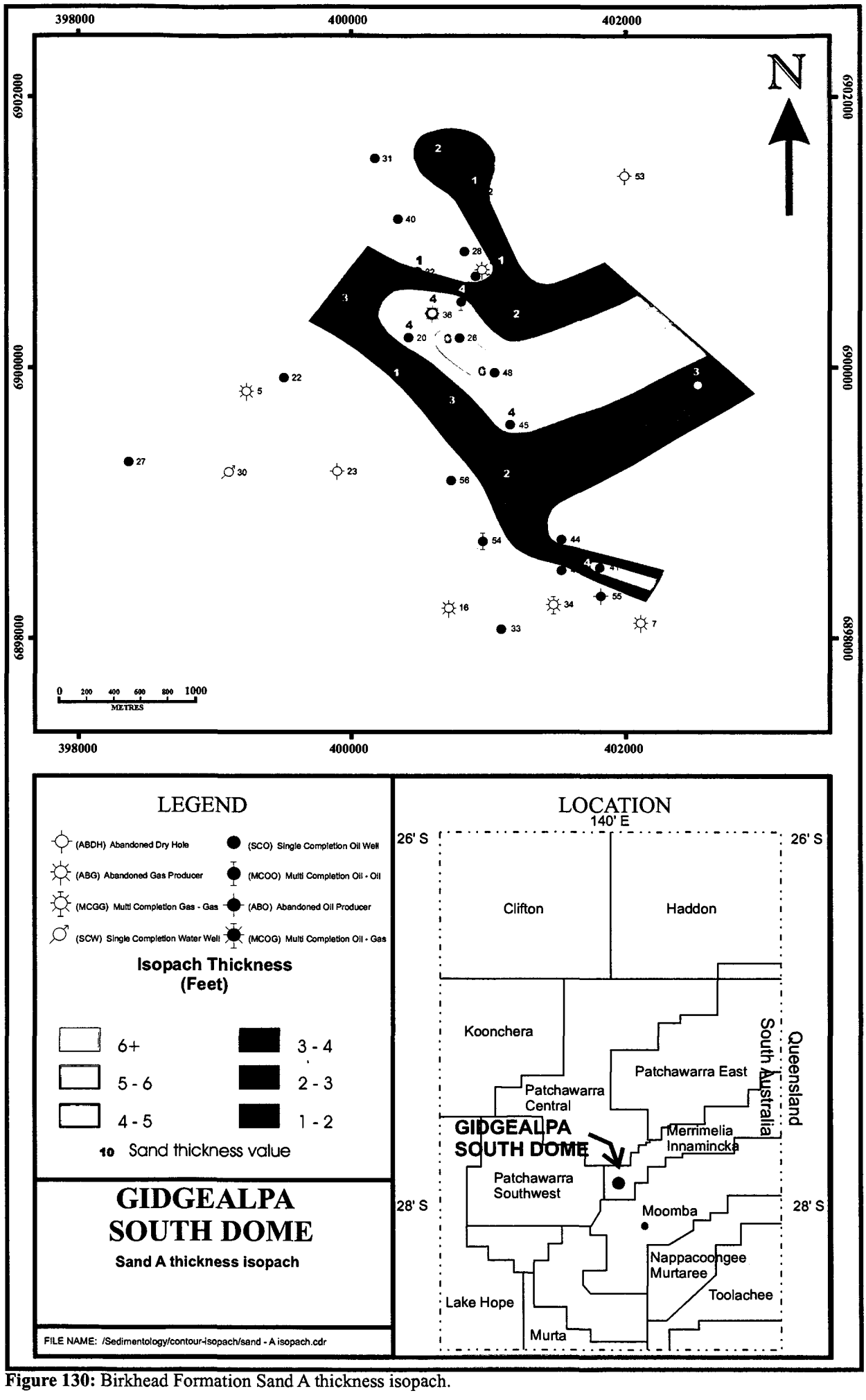

Figure 130: Birkhead Formation Sand A thickness isopach.

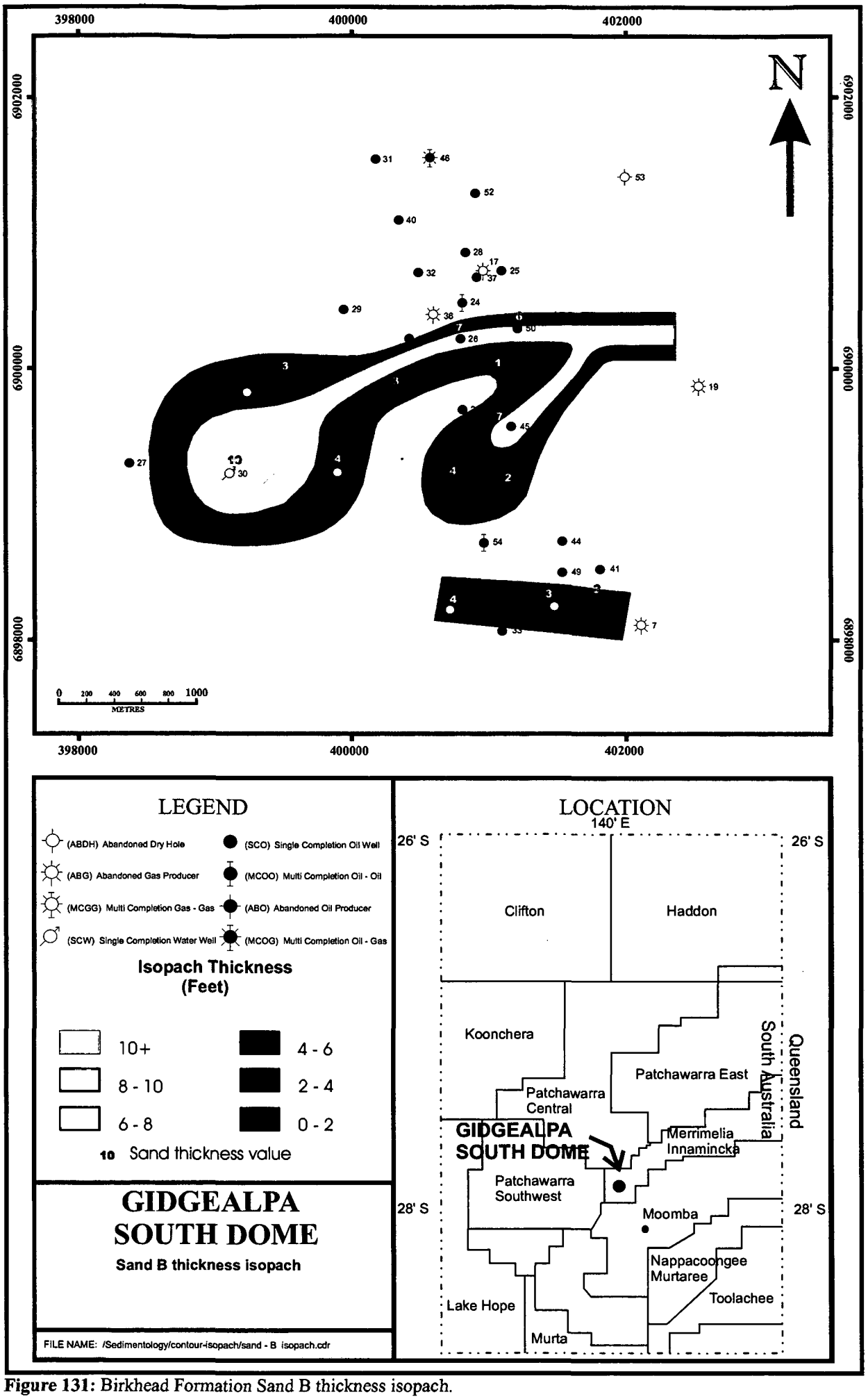

Figure 131: Birkhead Formation Sand B thickness isopach.

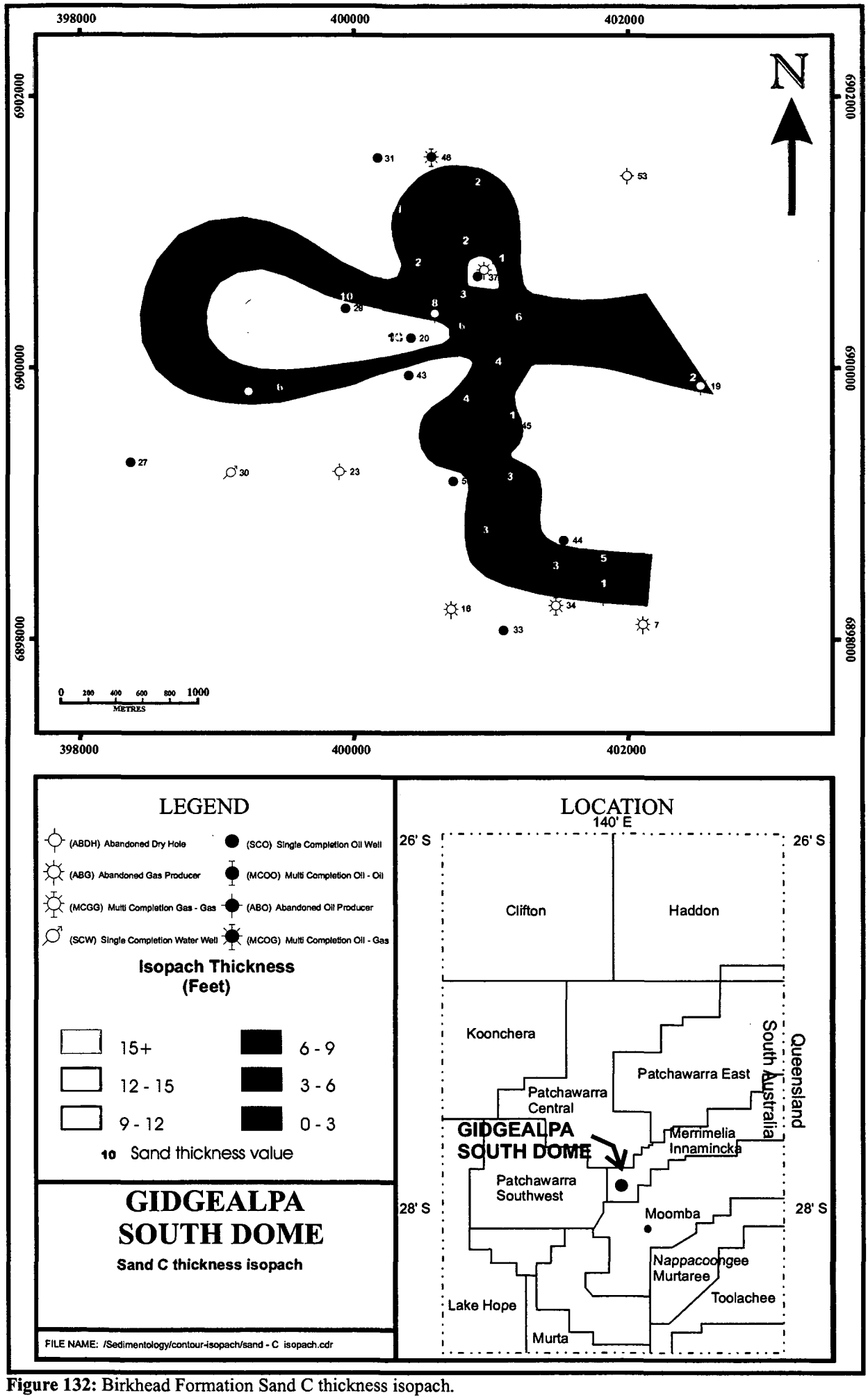

Figure 132: Birkhead Formation Sand C thickness isopach.

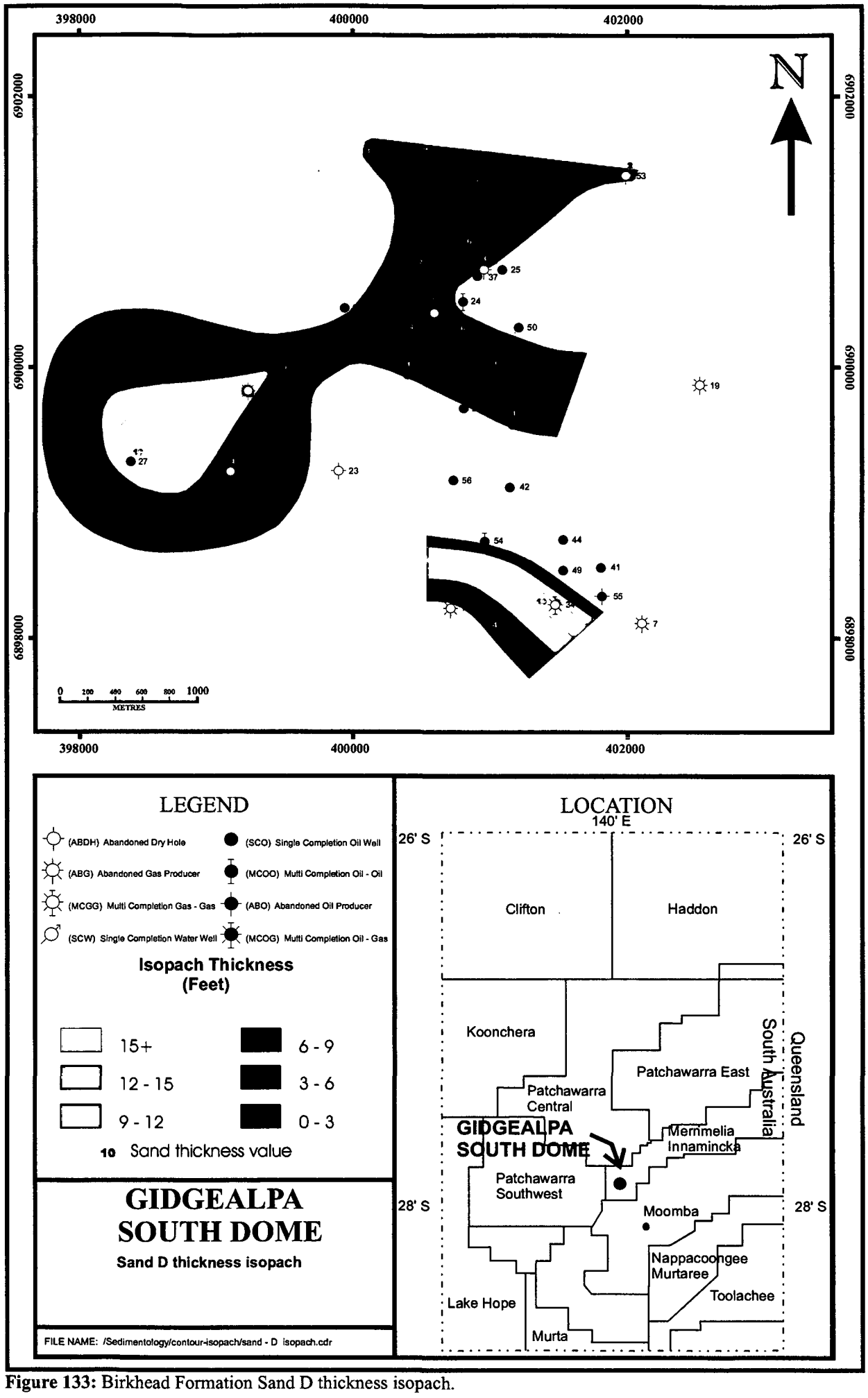

Figure 133: Birkhead Formation Sand D thickness isopach.

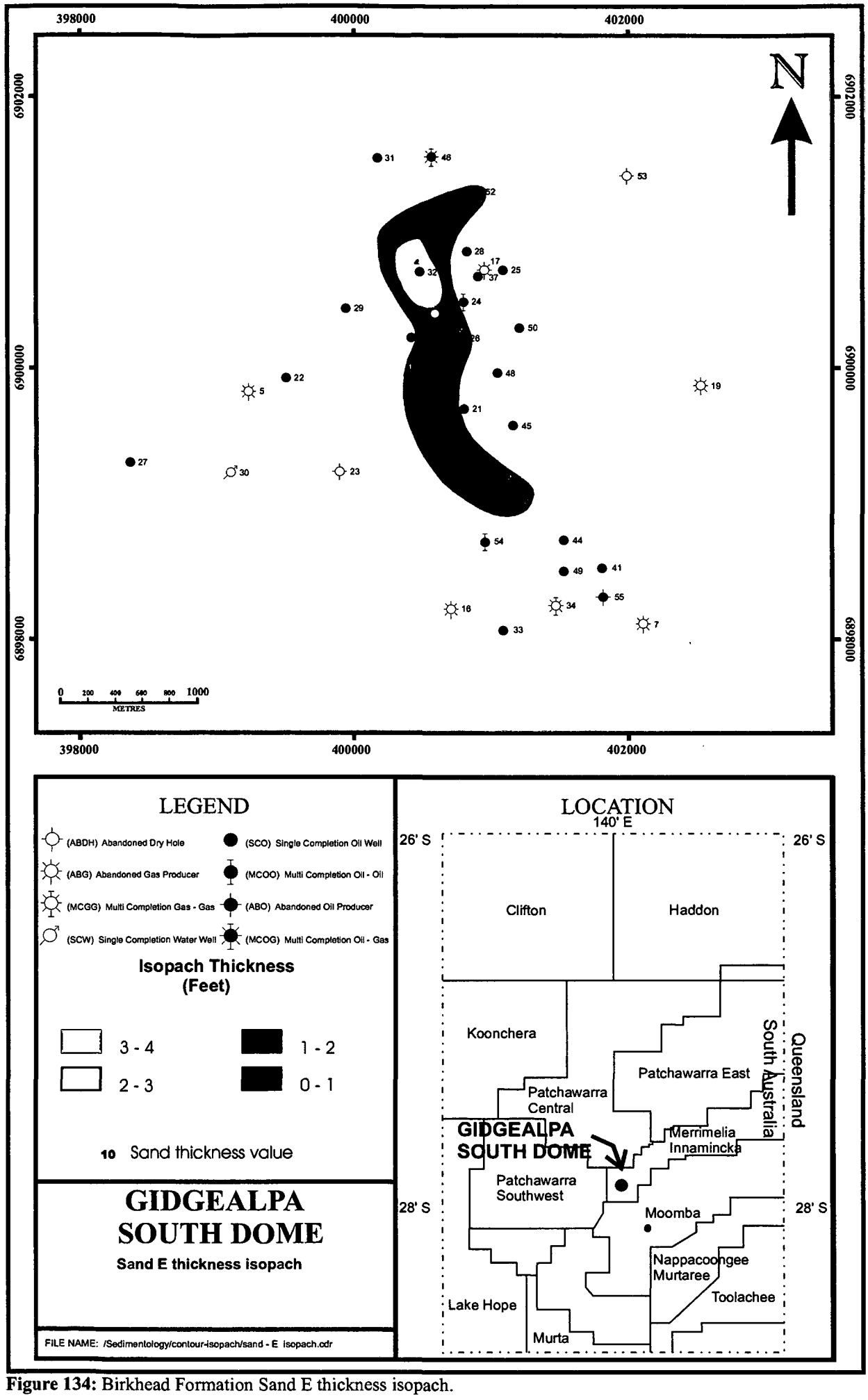

Figure 134: Birkhead Formation Sand E thickness isopach.

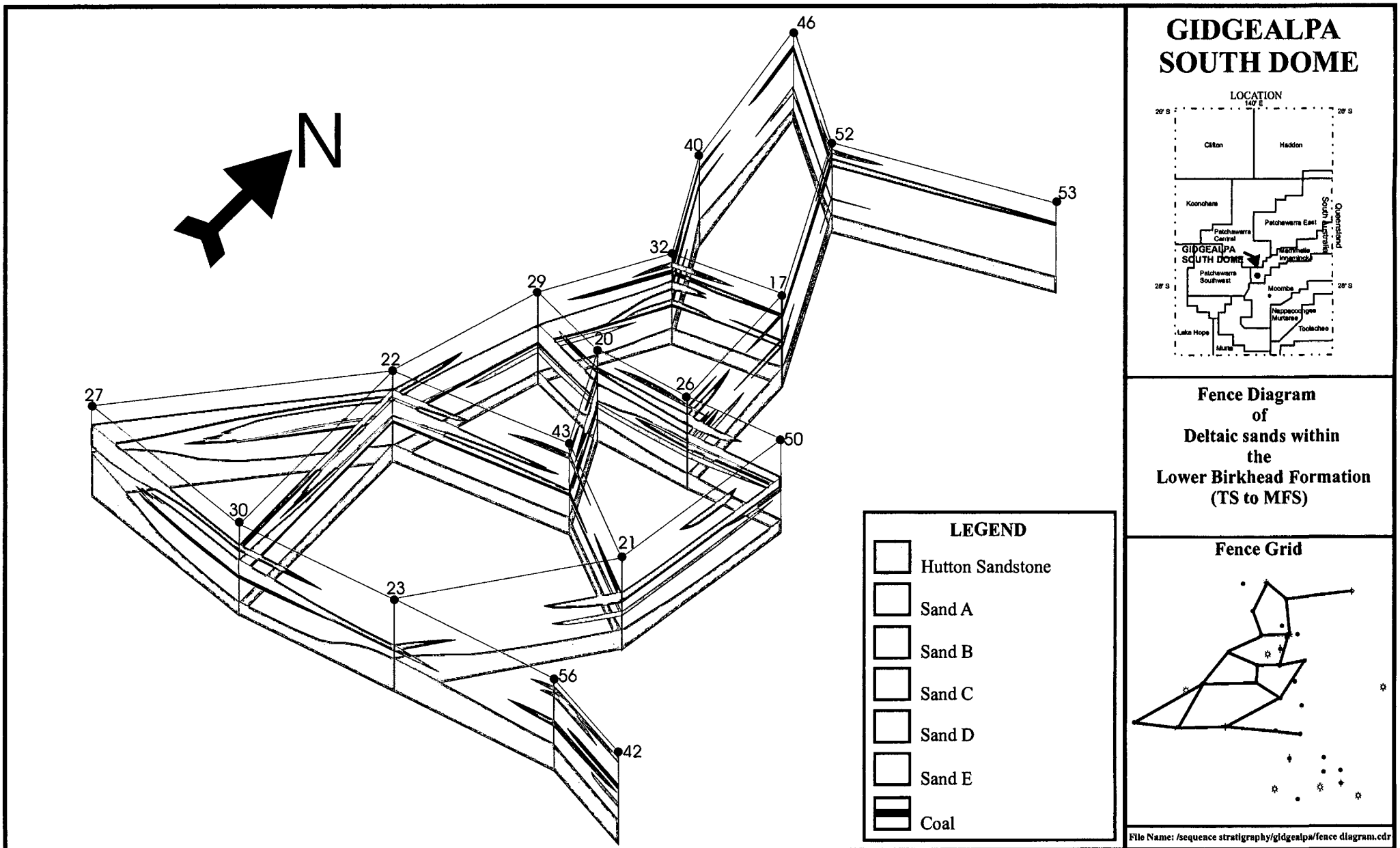

Figure 135: Fence diagram of sand distribution at the Gidgealpa south dome, basal Birkhead Formation. (Sands correspond the isopach maps shown in figures 130-134)

have been cut from 38 wells. To determine reservoir quality and distribution an alternative must be used to determine these important rock properties.

The alternative to core analysis is the use of electric logs for the determination of porosity and permeability as well as hydrocarbon saturation. Electric logs can not measure porosity and permeability directly but can be used to determine varying rock properties which are, in turn are related to porosity and permeability. The determination of the rock properties is based on a 'response relation' where assumptions must usually be made and therefore the determination of permeability and porosity from logs is only an estimation. The accuracy of the estimated values can only be as accurate as the assumptions made (Etnyre, 1989). Also limiting the accuracy of estimation is the resolution of the down-hole tools. Logging tools with the highest resolution of data is restricted to 6 inches (15 cm) which, in the case of the Birkhead Formation sediments, can cause the averaging of bed values when bed thickness is within or below the resolution of tool.

Archie's equation was initially used to determine water saturation of sandstones from resistivity logs. For the top of the Hutton Sandstone the equation worked well since it is modelled on clean porous sandstones. However, difficulty was experienced in the determination of water saturation when the equation was applied within the Birkhead Formation due to the high shaly content of the sands. The presence of the shaly sediments affect the conductivity properties of rocks and in turn affect resistivity logs producing non-Archie type characteristics. To overcome this problem for the Birkhead Formation I used a modified form of Archie's equation called the 'Indonesia equation' that takes into account the presence of shale within the sediments.

8.2.2 Log Interpretation: Background, Theory and Method

The petrophysical properties of the lower Birkhead Formation sediments were determined using the petrophysics module of the GEOLOG program by Mincom. The main parameters including porosity, water saturation and permeability were determined using a step-by-step procedure as well as other, more minor, parameters that are essential for accurate evaluation of the logs. Figure **136** is a summary of the procedures used. The following section is a discussion on the theory and determination of the more important parameters (ie porosity, water saturation and permeability).

8.2.2.1 Porosity

The density log is the most effective and sensitive tool for the determination of porosity due to the large density contrasts between the rock and surrounding fluids. The tool also has an added advantage in that it is not effected by lithological variation (Northcott, 1994). For these reasons I used the density log to calculate porosity within the Birkhead Formation sediments.

Also of note is the fact that it is the **effective porosity** that is of interest to the geologist since the obtainable hydrocarbons are contained within these void spaces. The effective porosity is the interconnected pore space within a rock which contains a fluid that has the potential to flow whereas the **total porosity** includes all void space regardless of whether the pores are interconnected or isolated. Total Porosity includes clay bound water associated with shales and irreducible capillary water.

The calculation of effective porosity from the density log involves the calculation of the total porosity and then the removal of the apparent shale and bound water porosities. Initially, I calculated the total porosity using the equation:

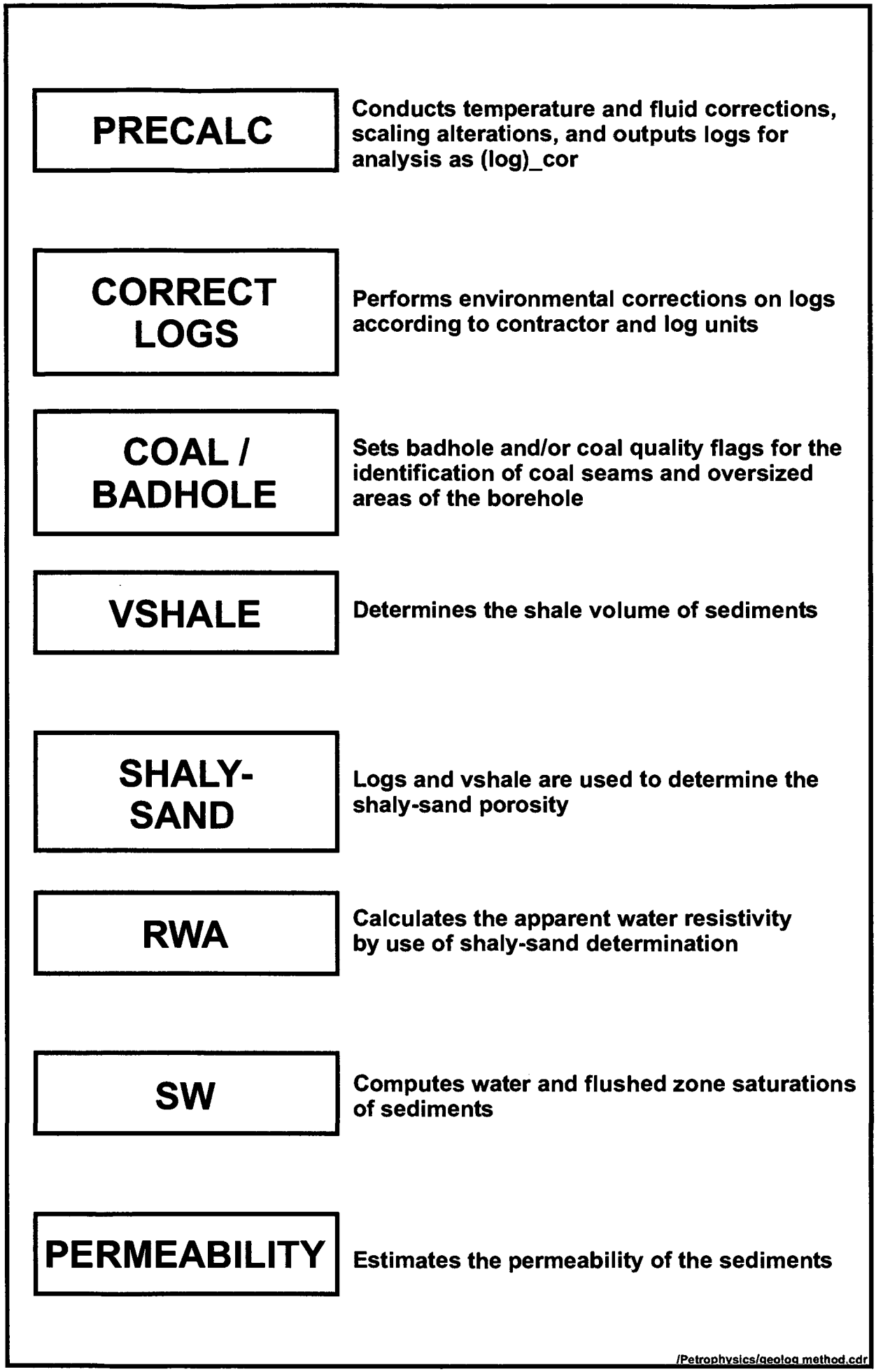

Figure 136: Procedure used for log interpretation in GEOLOG.

$$\phi_t = \frac{(\rho_{Ma} - \rho_b)}{(\rho_{Ma} - \rho_F)}$$ Equation **18**

Where ϕ_t = Total Porosity
ρ_{Ma} = Density of clay-free clean sandstone (2.65g/cc)
ρ_B = Log density
ρ_F = Density of fluid (1 g/cc for fresh drilling mud)

Alternatively, where the density log is unavailable in some wells, I used the sonic log to calculate ϕ_t by the basic Wyllie equation:

$$\phi_t = \frac{(DT - DT_{Ma})}{(DT_F - DT_{Ma})}$$ Equation **19**

where DT = Sonic log
DT_{Ma} = Interval transit time of a clay-free quartz sandstone with 0% porosity (55.5 msec/ft)
DT_F = Interval transit time of the fluid (189 msec/ft for fresh drilling mud)

Once total porosity is calculated the effective porosity was computed by use of the shale content within the rock which in turn was predetermined from Vshale using the gamma ray log (fig **136**, page 352). Therefore:

$$\phi_e = \phi_t - (Vsh.\phi_{Bw})$$ Equation **20**

where ϕ_e = Effective Porosity
ϕ_t = Total Porosity
Vsh = Shale volume
ϕ_{Bw} = Bound water porosity (constant)

8.2.2.2 *Water Saturation*

In 1942 Archie studied the resistivities of a large number of brine saturated sandstones and determined that for a clean, porous, water saturated sandstone the formation factor is represented by the equation:

$$F = \frac{R_o}{R_w} \qquad \text{Equation } \mathbf{21}$$

where F = Formation factor
R_O = resistivity of a clean, porous, water saturated formation
R_W = resistivity of the formation water

Archie also noticed that the formation factor was related to the porosity and the permeability of the reservoir rock. After further work was conducted in the 1950s he went on to determine the modified Archie equation where:

$$F = \frac{a}{\phi^m} \qquad \text{Equation } \mathbf{22}$$

where a = Archie constant
ϕ = porosity
m = cementation exponent (1.3 for unconsolidated sands and 1.8-2.0 for consolidated sands)

Further research on m determined that the value is a function of the electrical tortuosity of the granular matrix and can be calculated by:

$$m = \frac{Log(ThroatArea)}{Log(PoreArea)} \qquad \text{Equation } \mathbf{23}$$

Finally Archie developed the Archie equation for water saturation in clean formations by the relationship between the formation water saturation and rock resistivity such that:

$$S_w = \left(\frac{R_o}{R_t}\right)^{1/n}$$

$$= \left(\frac{F.R_w}{R_t}\right)^{1/n}$$

and therefore:

$$S_w = \left(\frac{a.R_w}{\phi^m.R_t}\right)^{1/n} \qquad \text{Equation } \mathbf{24}$$

where S_W =water saturation
a = Archie exponent
n = saturation exponent
R_W = formation water resistivity
R_t = rock resistivity

For clean, sandy, Archie type formations the values are a=1, m=2 and n=2. For shaly formations the values are a<1, m<2 and n<2. These lower values of the Archie constant, cementation exponent and saturation exponent respectively are an attempt to reflect the non-Archie behaviour of the sediments. The modified Archie equation is a 'quick fix' solution that increases the formation factor which counteracts the decreasing value of R_t due to the conductivity of shale. The use of the equation does not address the real problem of how to increase R_t to compensate for the conductivity of shale.

Briefly, the increase in shaly sand conductivity is attributed to the ionic substitution of divalent ions for trivalent ions, for example Al^{3+} replacing Mg^{2+} in the clay mineral lattice. The substitutions causes an excess of anions such as Cl^- within the dry clay which is balanced by the attraction of cations such as Na^+ which reside within the bound water on the clay surface. The Na^+ cations within the bound water provide an avenue for cation exchange and consequently, electrical conductivity (Northcott, 1994).

For shaly sands a conductive model can be used where the conductivity of the rock can be characterised by a non-conductive matrix with a conductive formation water electrolyte within the pore space and a clay matrix that provides the 'excess conductivity' via cation exchange. The concept of the model involves the relationship between the Archie term and the value of the excess conductivity due to the shale content, thus:

$$C_o = \frac{C_w}{F} + X \qquad \text{Equation } \mathbf{25}$$

= Archie Equation + Excess conductivity

where C_O = the conductivity of the rock at 100% water saturation
C_W = the conductivity of the formation water
F = formation factor (conducting path through electrolyte)
X = conductive path through clay

Poupon and Leveaux (1971) used the conductive model to develop the 'Indonesia equation' where:

$$C_t = \frac{C_w}{F}.S_w^n + 2\sqrt{\frac{C_w.Vsh^{2-Vsh}.Csh}{F}}.S_w^2 \qquad \text{Equation } \mathbf{26}$$

=Archie Equation + Excess Conductivity

where C_t = Rock conductivity
C_W = Formation water conductivity
Vsh =percent Vsh (decimal)
Csh =shale conductivity

The calculation of water saturations for the interval between the basal section of the Birkhead Formation and the top part of Hutton Sandstone required the use of both the modified Archie equation and the Indonesia equation. Because of the high clay content of the Birkhead Formation the Indonesia equation was used while the clean clay-absent nature of the Hutton Sandstone means that the modified Archie equation was used.

Before water saturations were calculated for each well the values of a, m, n and R_W had to be determined for use in the modified Archie equation and the Indonesia equation. For the calculation of n I used the value that was determined from core analysis; this value may also be obtained by local knowledge where as the determination of the other variables were calculated using the 'Pickett Plot'. The Pickett plot is based on the relationship of the modified Archie equation and the analysis of resistivity and porosity which are plotted on a log-log grid. From re-arrangement of the Archie equation (equation **24**):

$$R_t = F.a.R_w.I$$

where $F = R_O/R_W = \phi^{-m}$
I = saturation or
resistivity index= $R_t/R_O = R_t/FR_W = S_W^{-n}$

and if the log(10) is performed on both sides:

$$\begin{aligned} Log(R_t) &= Log(F) + Log(a.R_W) + Log(I) \\ &= Log(\phi^{-m}) + Log(a.R_W) + Log(I) \\ &= -mLog(\phi) + Log(a.R_W) + Log(I) \end{aligned}$$ Equation **27**

Thus from this equation a linear trend will be observed with a constant R_W (or more accurately aR_W) and constant I when the deep resistivity log is plotted versus a porosity log on a log-log scale. Figure **137** illustrates the linear nature of the slope m and that the value of aR_W can be determined where the 100% S_W line passes through the wet rock data points and intercepts the x axis.

8.2.2.3 *Permeability*

From section **6.5.3** it was determined that a relationship between porosity and permeability existed for the Birkhead Formation. This relationship can be applied to determine permeability from logs. To relate the density (RHOB) log to probe permeability data the probe data was placed next to the

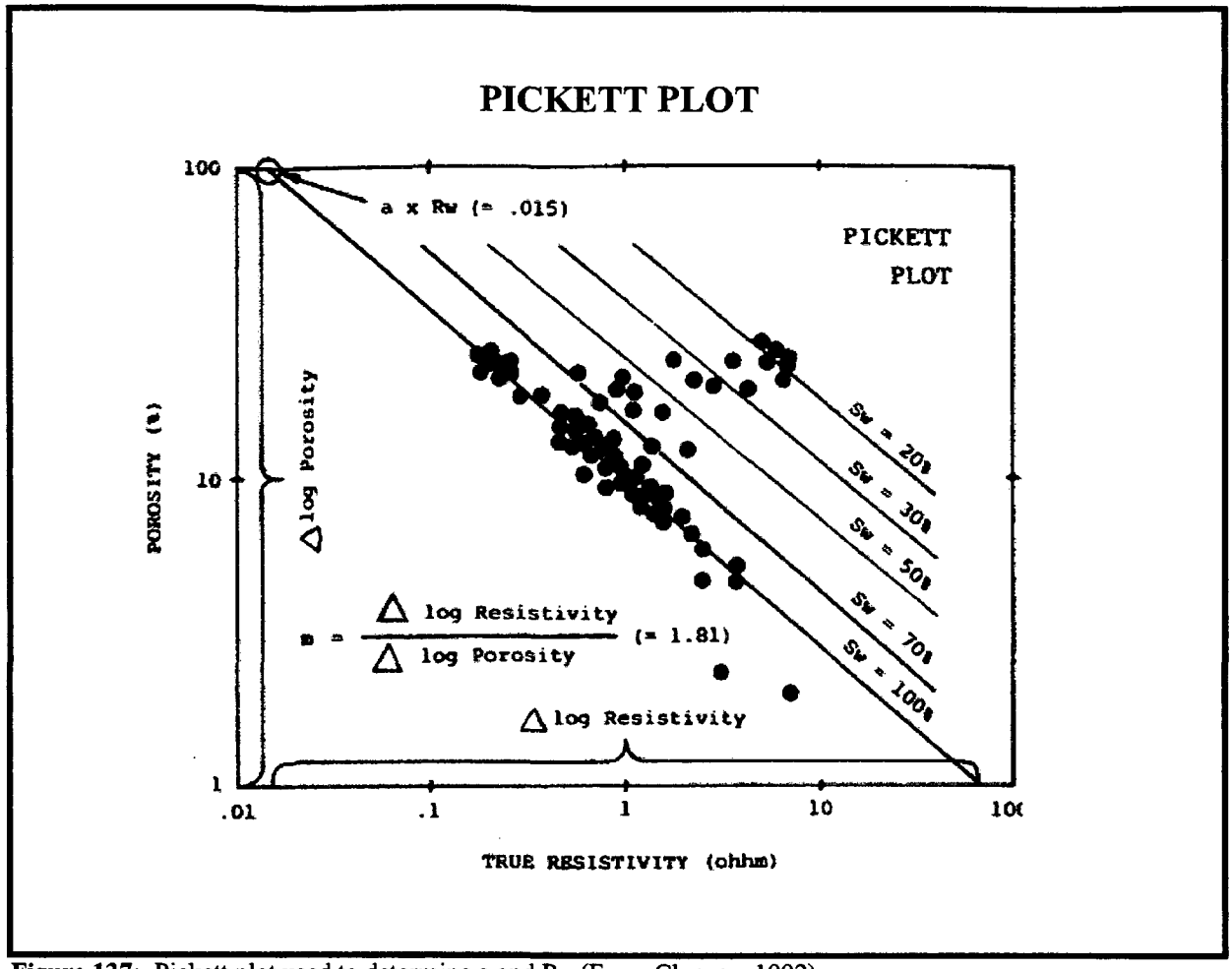

Figure 137: Pickett plot used to determine a and R_w (From Cleneay, 1992).

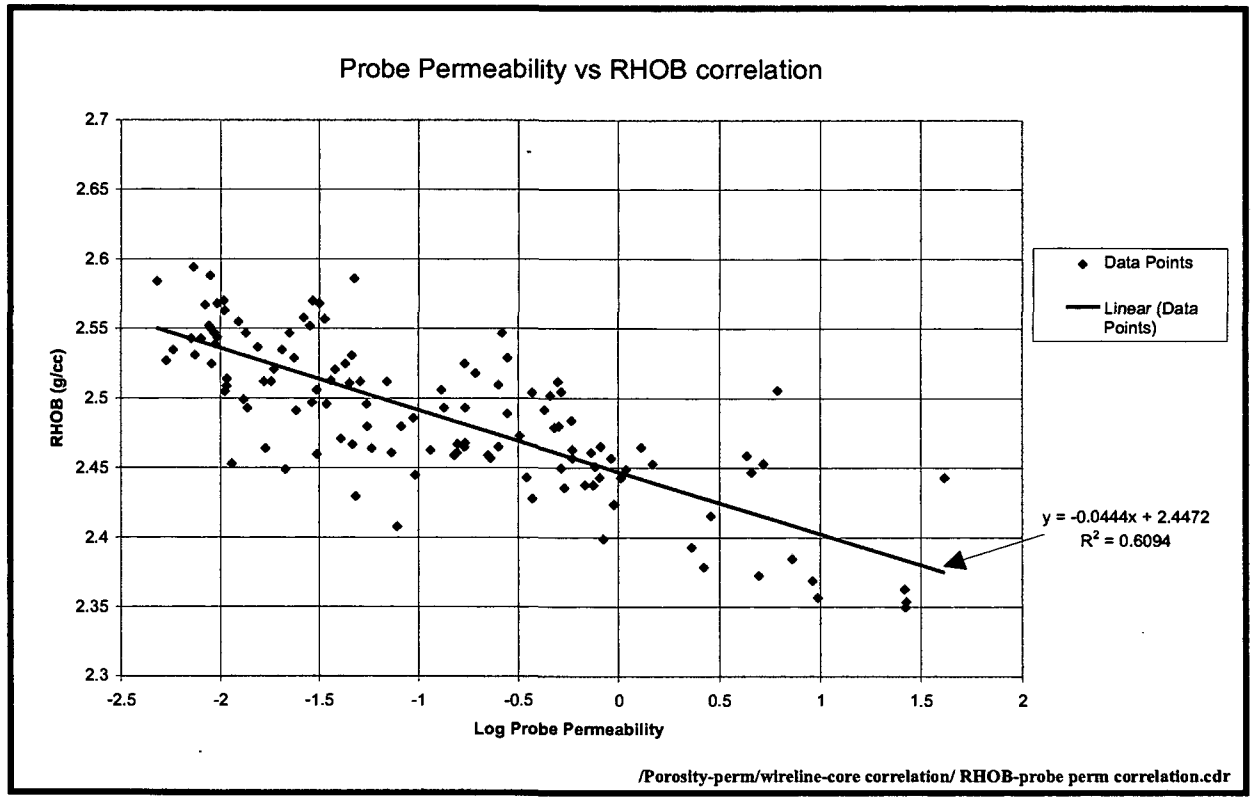

Figure 138: Correlation of probe permeability and the density log.

corresponding log value for each depth. Probe permeability data was used since a more accurate comparison can be obtained than by the use of core plug permeability, which is taken at large intervals and only represents point source permeability values. The probe permeability data which is separated by a one inch spacing can be averaged over an interval of 6 inches (15 cm) which corresponds to the resolution of the RHOB tool. Figure **138** (see previous page) shows the linear relationship between the RHOB logs and the Log (Probe permeability) data for the wells that contain cores in the basal section of the Birkhead Formation. The equation of the line of bet fit has a reasonably good correlation coefficient of 0.61 showing that the relationship exists statistically. The equation was then applied to each well where the RHOB log was present to produce the Permeability curve.

8.2.2.4 Log Interpretation Results

From log analysis of the Gidgealpa south dome wells, effective porosity, water saturation and permeability have been calculated in the absence of core. Where the core is present, it has been used to calibrate the log data. Figures **139** and **140** are examples of the log interpreted data. Log interpretation of the other wells can be found in appendix **11**. Starting from the left and working right: the first column contains the Vshale, caliper and gamma ray logs which indicate shale content, bore hole size and lithology respectively. The next two columns are indicators of core positions and formation limits which is then followed by the next column that contains the resistivity logs.

The resistivity logs are used in the determination of water and oil saturations and are also visual indicators of hydrocarbons where the resistivity of the shallow and deep resistivity logs are greatly increased with respect to the micro spherical focused log. The next column contains the porosity and sonic logs. The porosity logs indicate where porous sands are present by the crossover of the neutron porosity log with the density log (shaded areas) while

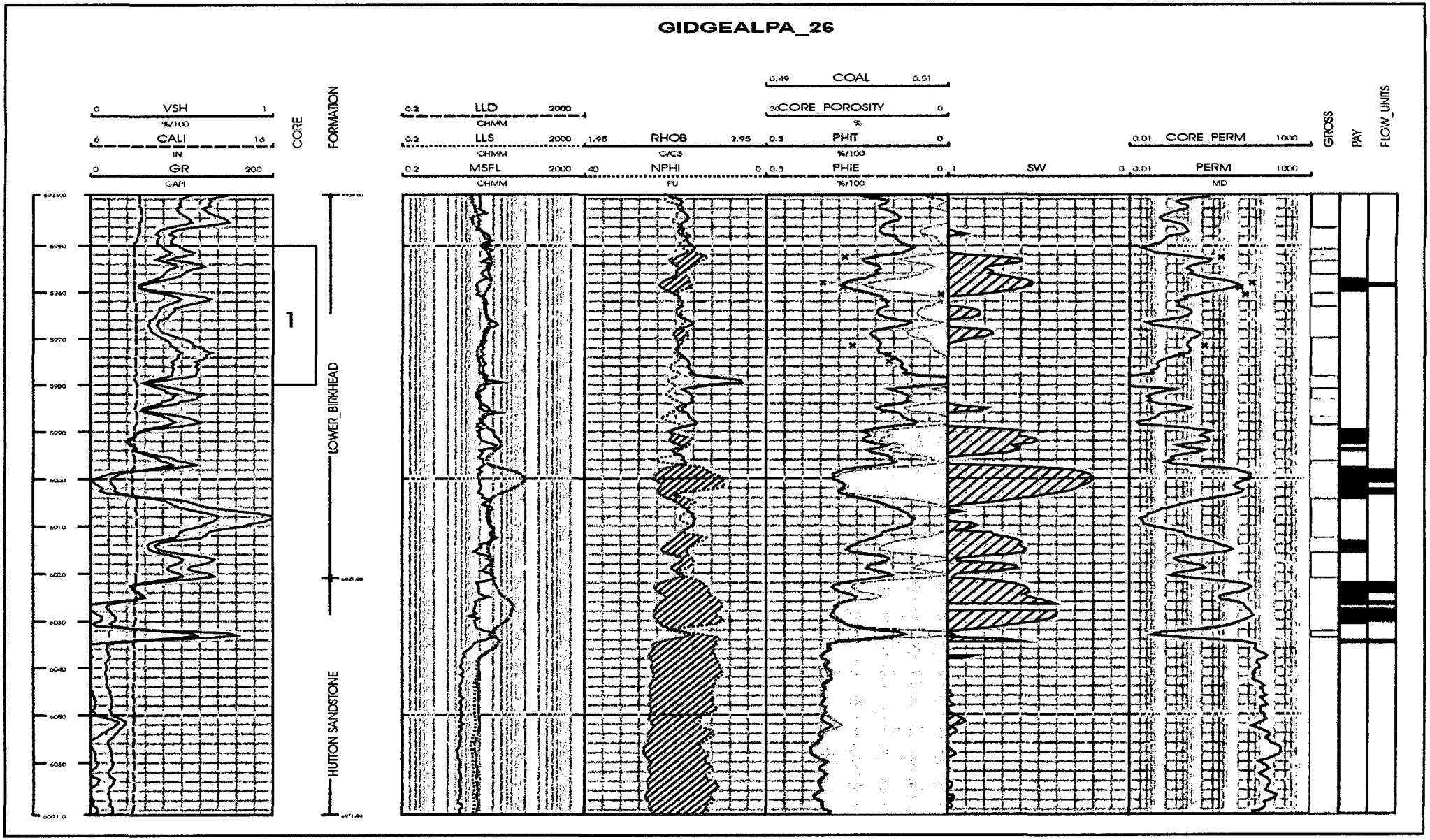

Figure 139: Log interpretation results of Gidgealpa 26.

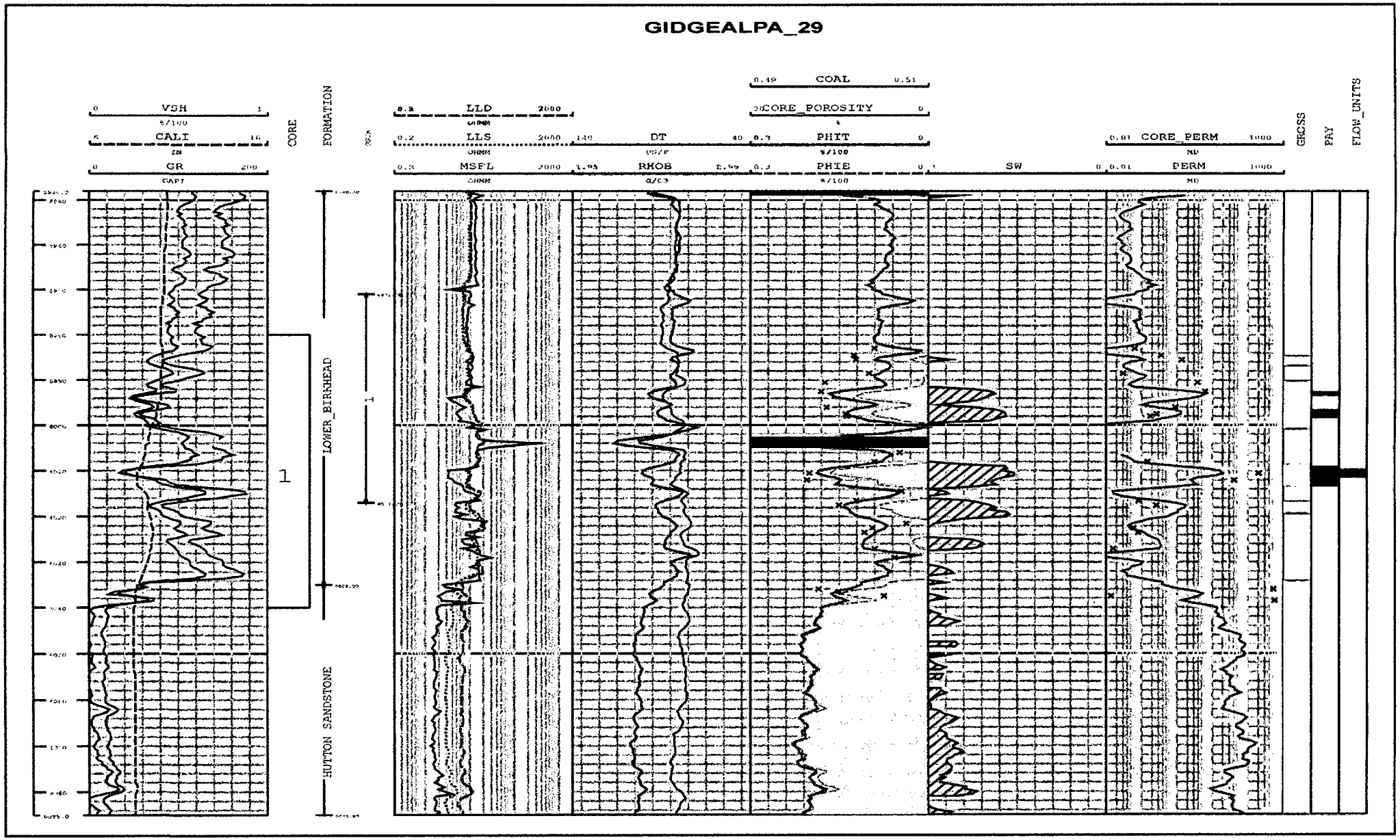

Figure 140: Log interpretation results of Gidgealpa 29.

the sonic log is used to identify coal within the formations. The cutoff value for coal using the sonic log is determined by calibration with the cores. Where the sonic log is absent the porosity logs can be used to determine coal.

The density and sonic logs are used to determine the total and effective porosities which are displayed next to the porosity and sonic logs column. The comparison of total and effective porosity aids in the visual comparison between the two logs with the difference mainly due to shale content. For calibration purposes Hassler-Sleeve core plug porosity has also been displayed. The effective porosity is used along with the resistivity logs to determine water saturations that are displayed in the next column. The final log curve displayed is the permeability log that has been determined from the density log. Core permeability data has been included in this column for visual comparison.

The final three columns in figures **139** and **140** are an evaluation of the log results of interest to determine reservoir distribution and properties. The 'Gross' column indicates the presence of sand within the formations where the Vshale content is less than 50%. The 'Pay' column is an indicator of pay zones, where the column is shaded green the formation rocks have met the criteria of less than 50% Vshale, less than 65% water saturation and greater than 8% effective porosity. The 65% water saturation cut-off value is used despite the fact that oil does not flow until oil occupies 45% or water saturation is 65% and 1:1 production of oil to water does not occur until oil saturation is at 50% (figure **141**). The elevated values of water saturation are due to the interbedded nature of the Birkhead Formation sandstones and siltstones where the siltstones reduce the resistivity of the adjacent oil saturated rocks. The final column is 'Flow units' which has the same criteria as the pay column but also considers permeability. Where permeability is greater than 10md the column is shaded blue. The 10md cut-off value corresponds to the high quality permeability zones that were determined from section **7.3.2.3**.

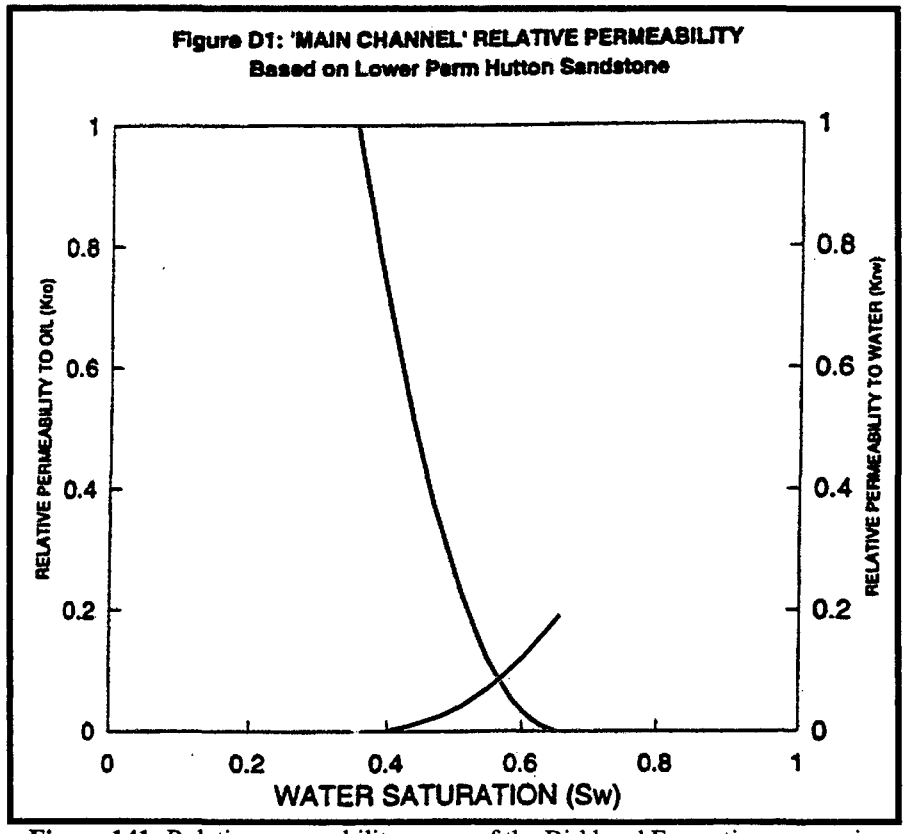

Figure 141: Relative permeability curve of the Birkhead Formation reservoir fluids (oil = red, water = blue) at the Gidgealpa south dome (From Wu, 1995).

8.2.3 Reservoir Mapping

The determination of effective porosity and water saturation for the basal Birkhead Formation and top Hutton Sandstone within the Gidgealpa south dome wells have been determined from calculations by log evaluation. Table **18** is a summary of the log evaluation data which has been applied to field maps to delineate reservoir size, shape and quality.

For the basal Birkhead Formation a number of porosity and hydrocarbon pore volume (HPV) maps were produced. The criteria used for the determination of reservoir quality sands from porosity was set at 8 percent with a vshale value of less than 50%, the total thickness of sediments greater than the cutoff values are then plotted onto a field base map.

The determination of the HPV was calculated to give a 'reservoir quality indicator' of the oil sands present. The HPV was determined by:

HPV = effective porosity x oil saturation x interval thickness Equation **28**

In normal circumstances the HPV can determine the volume of hydrocarbons within a sand by considering only rock porosity and the volume of oil within that porosity for a given sand volume. But because the interval thickness is used instead of the reservoir volume in this case, the HPV can only be used as a comparative ratio between wells and sands since the interval thickness is only one dimensional.

Figure **142** is a comparison between the porosity and HPV maps for sands A to D. What can instantly be noted is that the HPV of the sands in most cases corresponds very closely to porosity thickness which in turn to the distribution of the prograding delta sand lobes. This type of relationship between porosity

Gidg. Well Number	Birkhead Formation				Hutton Sandstone			
	Pay (ft)	Ave Porosity (%)	Ave Sw (%)	HPV	Pay (ft)	Ave Porosity (%)	Ave Sw (%)	HPV
17	-	-	-	-	21	18.4	36.5	2.46
20	19	15.5	42.2	1.24	-	-	-	-
21	3	15.3	40.1	0.18	12.5	21.5	35.6	1.73
22	5	13.6	48.5	0.33	-	-	-	-
24	5.5	11.8	48.7	0.32	19.5	18.7	35.1	2.51
25	0.5	9.9	61.5	0.03	18.5	17.4	37.5	2.06
26	17	11.9	50.8	1.03	4	16.7	43.2	0.39
27	16	14.6	43.6	1.32	-	-	-	-
28	1	8.7	64.3	0.06	13	20.6	30	1.92
29	4	11.4	62.1	0.28	-	-	-	-
30	-	-	-	-	-	-	-	-
31	-	-	-	-	3	17.6	45.4	0.29
32	0.5	9.8	63.7	0.03	8.5	22	33.7	1.24
33	-	-	-	-	-	-	-	-
34	-	-	-	-	-	-	-	-
36	1.5	19.2	62.9	0.18	-	-	-	-
37	-	-	-	-	3	13.8	41.8	0.24
40	-	-	-	-	9	19.1	32.2	1.17
41	-	-	-	-	10	19.8	40.6	1.18
42	0.5	14.8	63.9	0.05	-	-	-	-
43	-	-	-	-	-	-	-	-
44	-	-	-	-	16	19.9	40.4	1.84
45	2.5	11.1	62	0.17	11	19	35.9	1.34
46	1.5	9	55	0.07	-	-	-	-
48	4.5	15.7	58.6	0.41	7	22.2	37.7	0.97
49	-	-	-	-	5.5	10	43.3	0.33
50	7	11.7	58.4	0.48	-	-	-	-
53	0.5	11.5	64.4	0.04	-	-	-	-
55	1	8.7	52.7	0.05	-	-	-	-

Table 18: Log evaluation reservoir summary data for the Hutton Sandstone and Birkhead Formation, Gidgealpa south dome.

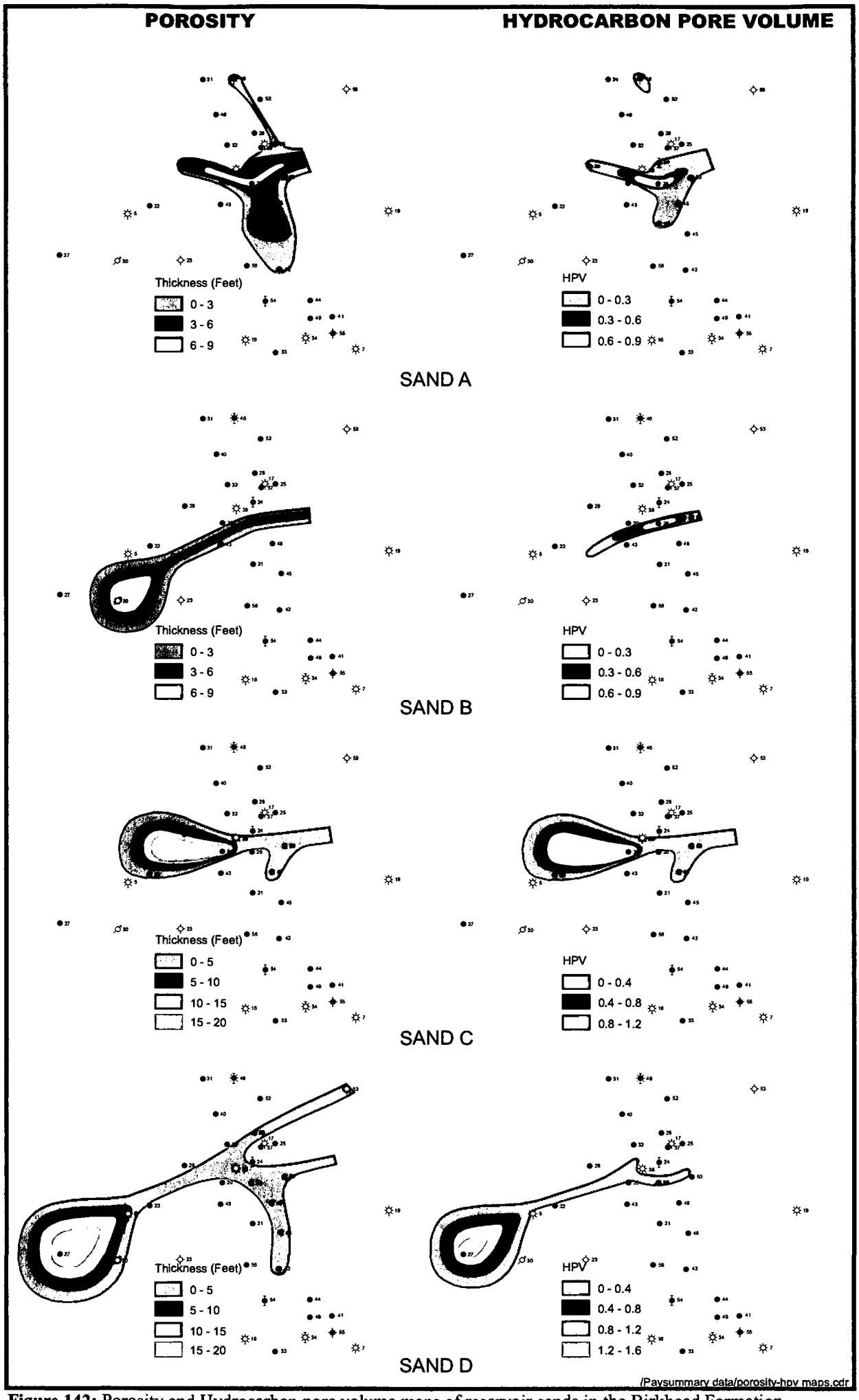

Figure 142: Porosity and Hydrocarbon pore volume maps of reservoir sands in the Birkhead Formation, Gidgealpa south dome.

and the HPV is expected due to the stratigraphic nature of the reservoir. An exception to this relationship occurs in Sand B where pay is absent but reservoir quality sands are present within the delta lobe region in the Gidgealpa 30 region. The absence of pay in this area is due to its low structural position (see section section **8.2.9**).

Figures **143** and **144** are comparisons of porosity and HPV for the entire basal Birkhead Formation interval. The figures also show the structural overlay of the 'top sand A porosity' of the area determined from 3D seismic. The two figures show that the hydrocarbon fairway is stratigraphically controlled and is related to the field areas where porosity is greater than or equal to 8%.

A different trapping style to the Birkhead Formation stratigraphic reservoir is present within the top Hutton Sandstone reservoir. Figure **145** represents a structure map of the 'top Hutton Sandstone' superimposed on a HPV map of the Hutton Sandstone reservoir. From this figure it can be clearly seen that the reservoir is structurally controlled with the oil water contact occurring at approximately 6925ft. The small variations in the reservoir shape and structural contours in figure **145** most likely represent minor variations in the reservoir quality of the sands. Therefore, sands of a higher reservoir quality will tend to correspond to higher HPV values.

8.2.4 Reservoir Engineering Characteristics

For further understanding of the Gidgealpa south dome Birkhead Formation reservoir the following section is a summary of the reservoir engineering characteristics. Some of the physical properties that are relevant to this section are summarised in table **19**.

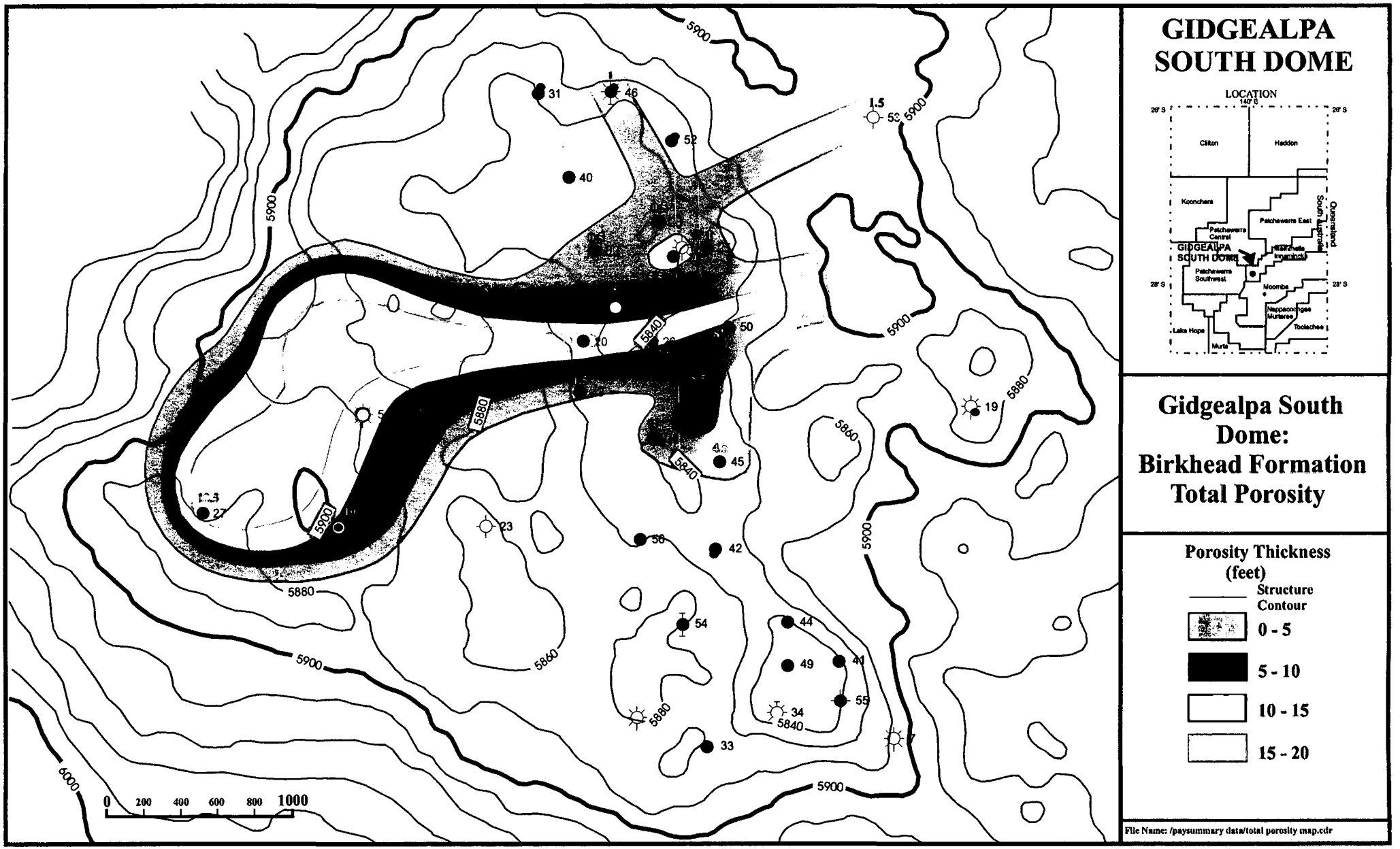

Figure 143: Total porosity thickness and structure map(feet below sea level) of the basal Birkhead Formation reservoir sands, Gidgealpa south dome.

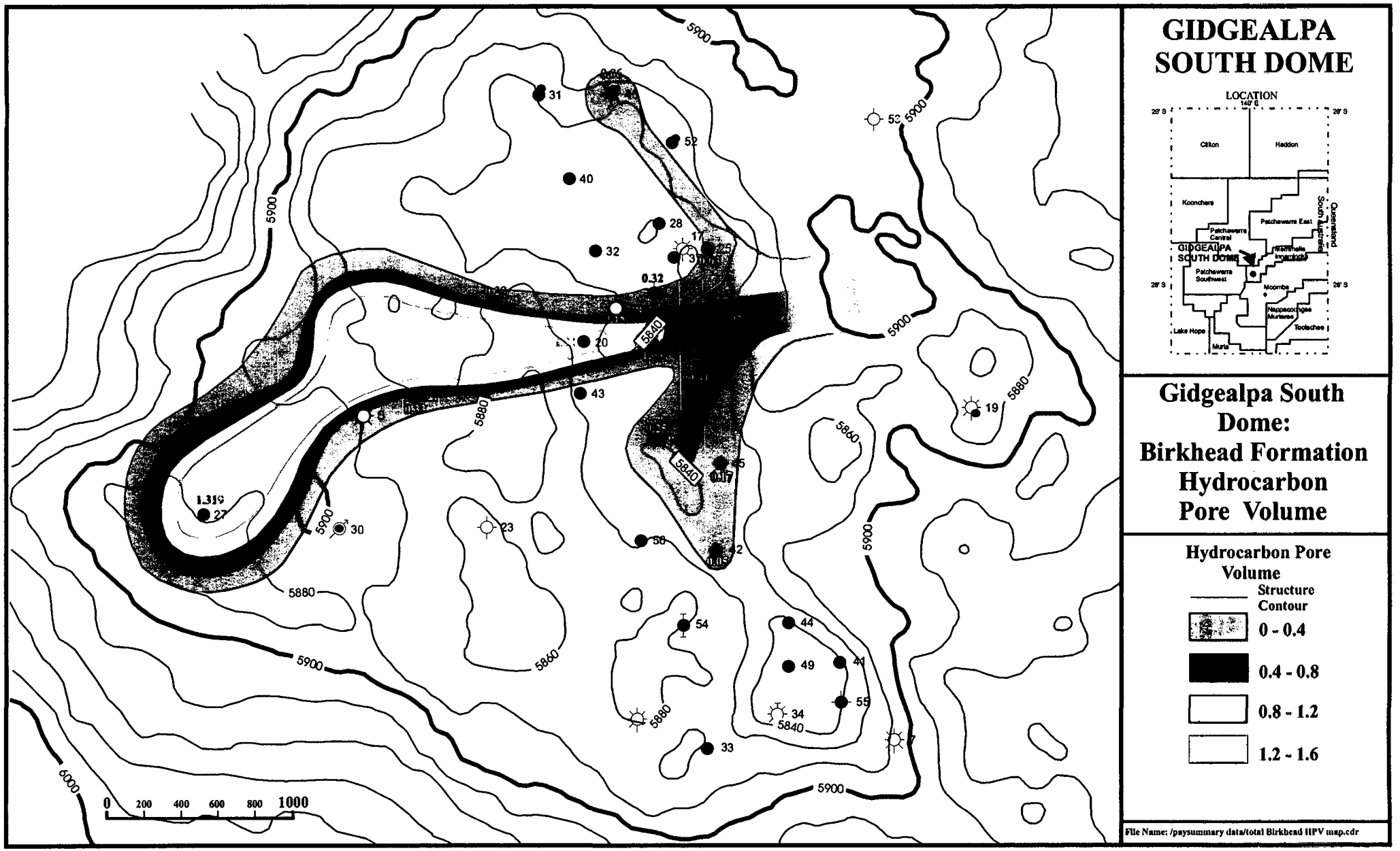

Figure 144: Total hydrocarbon pore volume and structure map (feet below sea level) of the basal Birkhead Formation reservoir sands, Gidgealpa south dome.

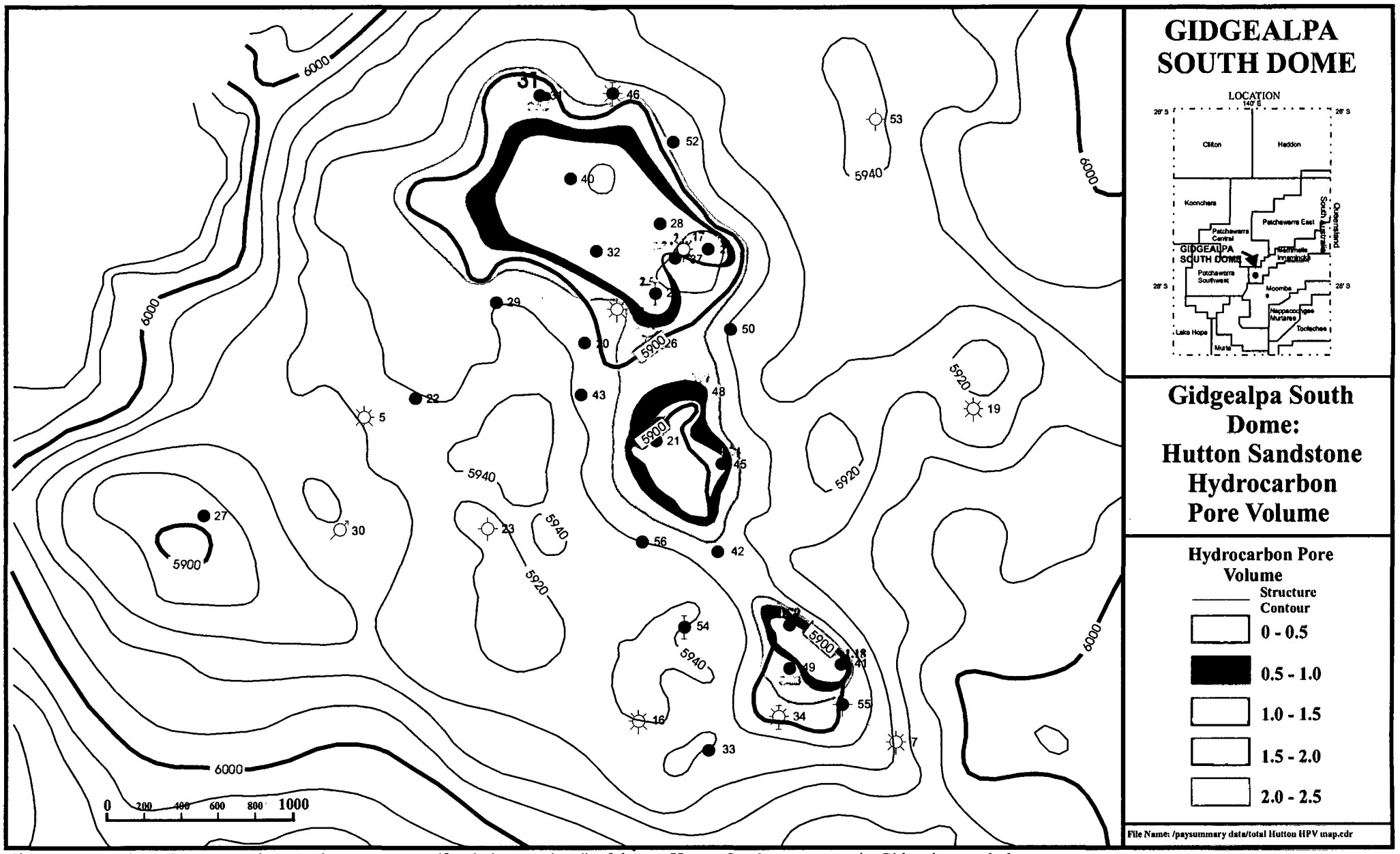

Figure 145: Hydrocarbon pore volume and structure map (feet below sea level) of the top Hutton Sandstone reservoir, Gidgealpa south dome.

Reservoir Properties	Value
Depth	5950ft - 6020ft
Ave. Reservoir Temp.	205°F
Initial Reservoir Pressure	2660psi
Bubble Point Pressure	438psi
Stock Tank Oil Gravity	47API@70°F
Gas / Oil Ratio	73 SCF/STB @ 50psi
Oil Viscosity	47.8cp@60°F
Average Well Spacing	125 Acres
Estimated Reserves	4.4 MMSTB
Drive Mechanism	Depletion Drive

Table 19: Summary of the Gidgealpa south dome reservoir properties.

8.2.5 Drill Stem Test Review

A number of drill stem tests (DST)s were run over the Birkhead Formation interval to test potential reservoir zones. Table **20** is a summary of the DST results showing depths at which the tests were run and the sands that were tested.

Well	DST	DEPTH (ft)	SAND TESTED	RECOVERY
Gidgealpa 17	3	5916 - 5950	D	273' oil, 393' mud
Gidgealpa 20	3	5977 - 6014	A,C	2800 bopd
Gidgealpa 22	1	5980 - 6015	B,C,D	1411 bopd
Gidgealpa 27	1	6016 - 6079	D	720 bwpd +trace oil
Gidgealpa 29	1	5971 - 6017	A,C	1780' oil
Gidgealpa 30	1	5984 - 6044	B,D	2409' mw
Gidgealpa 43	3	5982 - 6012	B,C	70'mw
Gidgealpa 46	6	5987 - 6014	A	922' oil, 432' ocmw
Gidgealpa 48	1	5987 - 6014	A	13.6 bbls oil
Gidgealpa 50	1	5964 - 6024	A,B,C	950' oil

Table 20: DST summary results from the Birkhead Formation.

From the DST's the wells can be separated into two different groups based on the fact that one group produced oil and / or drill stem mud and the second produced formation water. The first group of wells (Gidgealpa 17, 20, 22, 30, 29, 43, 48, 50) has sourced fluids from the Birkhead Formation reservoir and well bore. The absence of oil from Gidgealpa 30 is due to the reservoir quality sands occurring below the oil-water contact. The absence of oil from

Gidgealpa 43 is due to the water saturation falling below the cut-off for oil flow in the poor quality sands. The second group of wells (Gidgealpa 27, 46) are those that have produced significant amounts of water which have most likely been sourced from the underlying Hutton Sandstone.

Comparisons of results from the DST's show a good correlation with the cut-off values for pay from log interpreted data (appendix **11**), this fact holds true for all wells except Gidgealpa 27 which produced 100% water (Wu, 1995) (table **20**). The production of water can only be attributed to the fluids being sourced from the Hutton Sandstone where the bottom of the DST interval accessed the Hutton Sandstone.

8.2.6 Production History

8.2.6.1 Introduction

The Birkhead Formation reservoir to date (March 1998) has produced 1,491,360 barrels of oil in the near-absence of water. However some wells have shown uncharacteristically large quantities of water production which is likely to have been caused by well bore cross-flow between the Hutton Sandstone and the Birkhead Formation (Wu, 1995). Closer analysis of the production history in the area also reveals that the fluvial lacustrine sequence of the basal Birkhead section has caused relatively complex reservoir compartmentalisation which is reflected in reservoir pressure data (figure **146**a).

At the start of production the Birkhead Formation produced oil at an average rate of 400 barrels of oil per day (bopd) for a period of approximately 7 years after which production steadily decreased to a present day production rate of approximately 150 bopd. This production trend is represented by the blue curve shown in figure **147**; the figure also shows the corresponding water

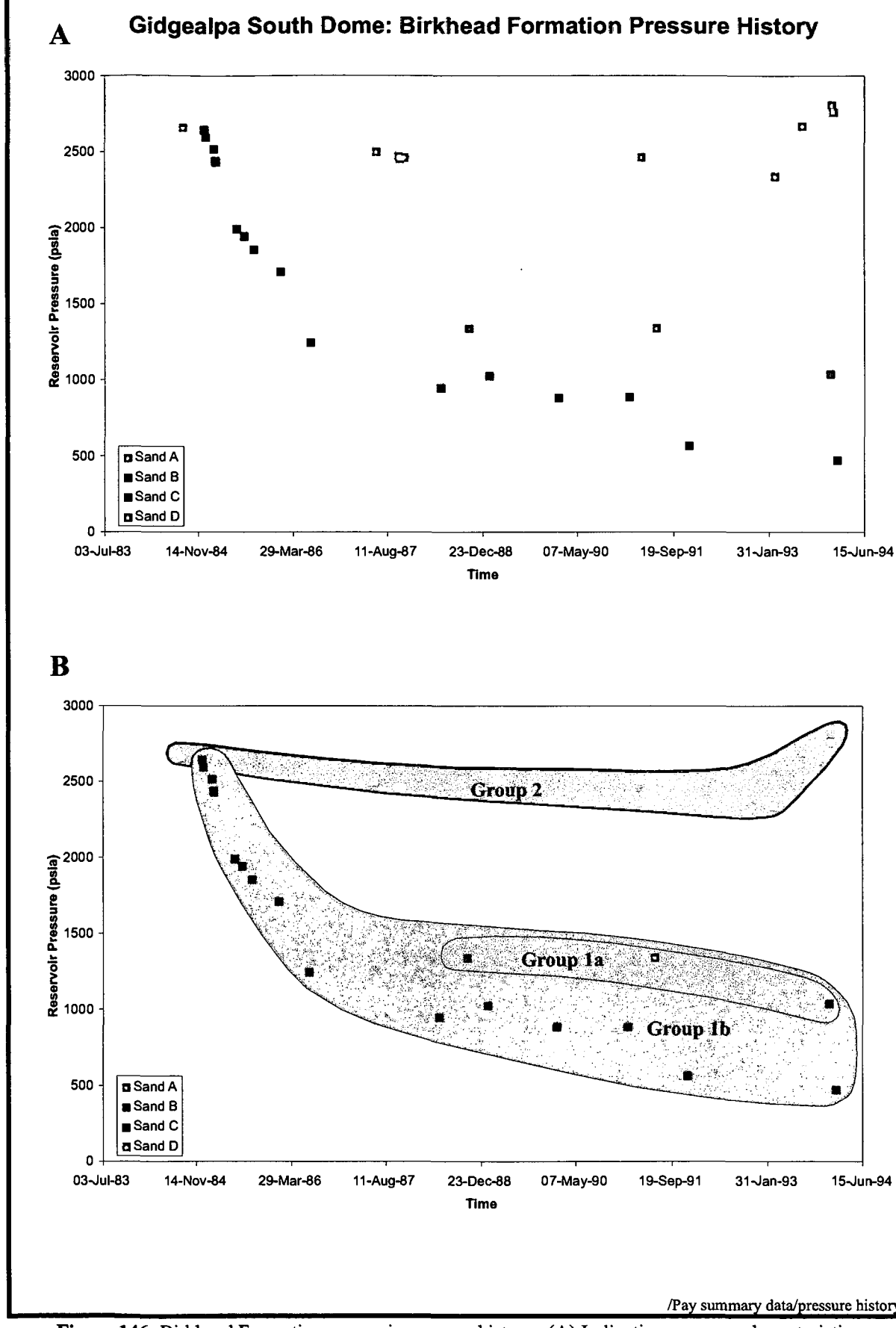

Figure 146: Birkhead Formation reservoir pressure history. (A) Indicating pressure characteristics of reservoir sands. (B) Pressure values grouped in terms of similar histories.

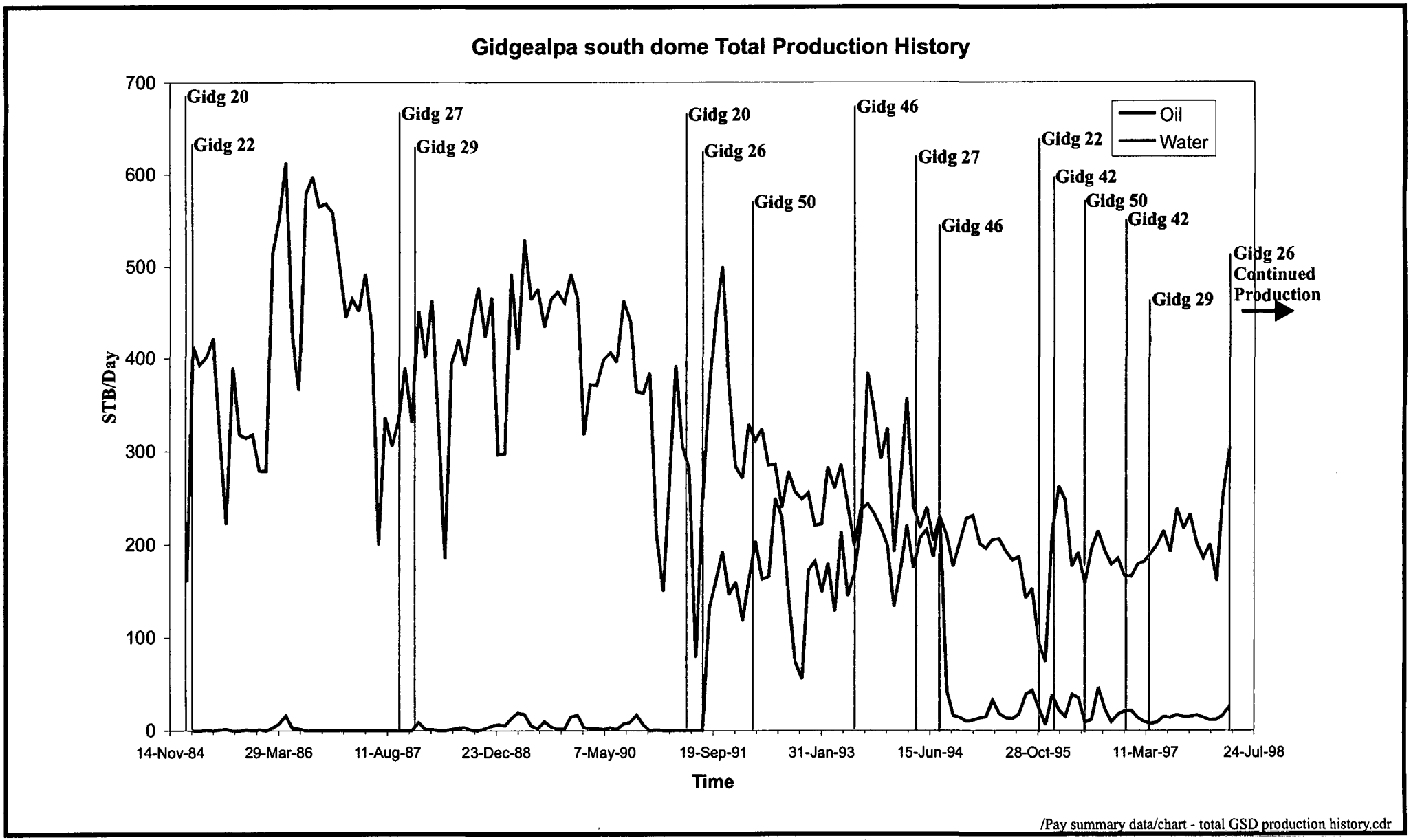

Figure 147: Production history chart of the Birkhead Formation reservoir showing time versus barrels of water or oil per day. Black lines indicate start of production and red lines represents termination of production for each well.

production rates (green line). The decrease in the production rate of oil from the Birkhead reservoir is a result of a poor drive system and relates to a declining reservoir pressure. The fact that a low reservoir pressure exists means that oil has to be produced by beam pumps. Figure **147** also indicates the period of time from start to finish of production for each individual well. The start of well production is indicated as a black line with the accompanying well name and the termination of production indicated by the red lines. The individual production histories for each producing well are discussed in section **8.2.6.3** and can be related to figure **147**.

8.2.6.2 Reservoir Pressure Analysis

The pressure history of the Birkhead Formation reservoir can be separated into two groups due to the isolation of, or very weak connection with different pressure compartments. The two groups are represented in figure **146**b (page 373) as the dark and medium grey shaded areas. Group 1 consists of those wells that occur within the main channel and delta lobe regions of sands A, B and C. This group can be further subdivided into two subgroups where partial or poor reservoir communication occurs. The first subgroup (subgroup 1a) consists of Sands A and B and is represented by the light grey shade area within the medium grey. The second subgroup (subgroup 1b) consists of Sand C. Group 2 is almost completely isolated from Group 1, this fact is reflected in the fact that the two groups have very different pressure histories. The Group 2 pressure compartments consist of Sand D and the crevasse splay sands corresponding to Sand A.

Group 1 pressure compartments are completely isolated from the underlying Hutton Sandstone, hence with ongoing production the compartment pressures have decreased significantly. Group 2 pressure compartments, however, have been re-pressurised and in fact have higher pressures (approximately 2740 psi) than was originally present within the Birkhead Formation reservoir (2661 psi)

suggesting that well bore cross-flow between the reservoir and the Hutton Sandstone has occurred. From figure **146**b (page 373) it can be seen that pressure readings taken from Sand A (green squares) occur in both Group 1b and Group 2. This discrepancy can be explained by the fact that the Group 1b readings occur within Gidgealpa 48 which occurs within the main delta lobe region while the Group 2 readings are from Gidgealpa 46 which consists of poor quality crevasse splay sands that are weakly connected to the main reservoir (see figure **130**, page 344).

8.2.6.3 Well Production Summary

Well production information in this section has been arranged in order of the 'start of production' from each well. Figure **147** (page 374) indicates the production time from the Birkhead Formation reservoir for each well.

The first well to produce oil from the Birkhead Formation in the Gidgealpa south dome was Gidgealpa 20. In December 1984 the well started to produce oil at an initial rate of approximately 200 bopd from the 59-3 sand (Sand C equivalent, this study). The initial reservoir pressure at this location was 2661 psia. Oil to surface continued until January 1986 when the well was put on pump due to the declining reservoir pressure in the Birkhead Formation (1712 psia). At this stage oil production was still steady on about 200 bopd. From February 1987 onwards the recovery rate had dropped to approximately 100 bopd with the reservoir pressure at 1200 psia. In May 1989 the Birkhead pump failed with subsequent production at below 10 bopd. In July of the same year the pump was repaired and recovery was increased to between 50-100 bopd.

Further production problems occurred with the Birkhead reservoir in February 1991. The Namur and Birkhead reservoirs were in communication causing a loss in production from the Birkhead reservoir. At this time the Birkhead

reservoir registered a pressure of 2682 psia which was 1792 psia higher than the pressure of 890 psia determined in February 1988. Due to the communication problems encountered, Birkhead production was suspended and the well was re-completed as a Namur producer. Total production from the Birkhead reservoir in Gidgealpa 20 was 207,249 bbls of oil and 5,934 bbls of water.

Two months after Gidgealpa 20 (February 1985) was completed Gidgealpa 22 was put on line as an oil producer in the 59-3 sand (Sand C, this study). Production from the same sand as Gidgealpa 20 caused accelerated pressure decline within 59-3 sand (figure **146**, page 373). At the start of production the reservoir pressure was 2519 psia in this well. Initial production was at an average of 350 bopd with a decline in production occurring around June 1987 of approximately 100 bopd. At this time a pump was installed to produce from the Birkhead. Since then Gidgealpa 22 production has steadily decreased along with pressure and was producing 24 bopd and 4 barrels of water per day (bwpd) at a pressure of 473 psia in August 1995. At this point the well had produced 542,400 bbls of oil and 2,164 bbls of water and was suspended to allow the well to be converted to a water injection well for a waterflood project in the 59-3 sand.

In September 1987, Gidgealpa 27 was completed in the Birkhead 59-2 sand (Sand D, this study) with an initial flow rate of 150 bopd and no water. The flowrate then increased to a maximum of approximately 250 bopd with no water for a period of 23 months after which the production steadily declined. At this stage the well was put on pump. An initial pressure survey taken the following month indicated a pressure of 2469 psia which was over 1000 psia higher than the pressure within the 59-3 sand (Sand C). In May 1991 the well was re-completed as a dual string Birkhead / Hutton oil producer, before re-completion well pressure for the Birkhead was at 2462 psia (taken in November 1987) . After a short period of 2 months the Birkhead started to produce significant amounts of water which coincided with the watering out of

the Hutton. This first occurrence of a high water cut is observed in figure **147** (page 374).

In September 1992 the well was re-entered to isolate the Hutton and Birkhead reservoirs to arrest water production in the Birkhead. The isolation of the 2 reservoirs was unsuccessful with continued high water production from the Birkhead reservoir. A pressure test in March and December 1993 showed an increase in pressure to 2340 and 2762 psia respectively suggesting communication with the Hutton had continued to occur. The continued poor recovery of oil and high water saw the shut-in of the Birkhead Formation in March 1994. Gidgealpa 27 had produced 286,813 bbls of oil and 138,059 bbls of water.

Gidgealpa 29 went on production in February 1988 to drain the Birkhead 59-3 sand (Sand A and Sand C, this study) using a beam pump. An initial pressure survey indicated a pressure of 2270 psia in October 1988. The initial production rate was at approximately 100 bopd with no water cut which very rapidly declined to a rate of below 20 bopd in the space of 12 months. The decrease in production rates coincided with a large drop in pressure to 541 psi (recorded in April 1994). Gidgealpa 29 produced oil sporadically from December 1990 onwards until March 1997 where the Birkhead was shut in. Gidgealpa 29 produced a total of 29,570 bbls of oil and 536 bbls of water.

Gidgealpa 26 was put on line in August 1991 and produced an initial flow of just under 250 bopd on pump with minimal water from the 59-3 sand (Sand A and B, this study). Pressure analysis at this time revealed a depleted reservoir pressure of 871 psia. With time the production rate steadily decreased until August 1993 when production steadied out at just over 150 bopd with minimal water. A repair program was conducted on the Birkhead pump in October 1995 and subsequently the well increased to produce just over 200 bopd. Gidgealpa 26 continued to produce at a steady rate until the effects of the water flood filtered through the reservoir from Gidgealpa 22, when production

increased to 300 bopd in March 1998. To date (end March 1998) Gidgealpa 26 is the only well producing from the Birkhead reservoir and has produced 402,092 bbls of oil and 27,565 bbls of water.

Gidgealpa 50 started production by beam pump from the Birkhead reservoir in May 1992 at an initial rate of 30 bopd with minimal water which then increased to an average of 50 bopd production rate. A pressure test in the 59-3 sand (Sand B and C, this study) showed that the reservoir was depleted to 552 psia in this well. In September 1992 the well was re-entered for repairs on the Birkhead pump after which the well produced at an increased rate of 70 bopd initially but quickly dropped off after only 2 months of renewed production. The Birkhead reservoir at Gidgealpa 50 was shut-in in September 1996. Total production from this well was 16,108 bbls of oil and 4,680 bbls of water.

Following the completion of Gidgealpa 50 as a producer, Gidgealpa 46 was re-completed as a producer in the Birkhead reservoir 59-3 sand (Sand A, this study) in July 1993. At this time a pressure test was conducted and the reservoir was depleted by 196 psia. The well initially produced at 10 bopd and 200 bwpd, the production rate continued until the well was shut in 13 months later. The high percentage of water is likely to be from well-bore communication with the Hutton Sandstone since the Birkhead reservoir at this point had re-pressured to that of the Hutton. At the time of closure Gidgealpa 46 had produced 5,214 bbls oil and 71,378 bbls of water.

The final well to be brought on line in the Gidgealpa south dome for the Birkhead reservoir 59-3 sand (Sand A, this study) is Gidgealpa 42 in February 1996. The well was re-completed in the Birkhead reservoir after the Hutton reservoir watered out in May 1994. Gidgealpa 42 had a short life with 1913 bbls of oil and 1633 bbls of water produced by beam pump over a period of 5 months.

8.2.7 Drive Mechanism

Early identification of the type of drive mechanism present within a petroleum reservoir is important, as the type will affect production efficiencies, strategies and characteristics. The Gidgealpa south dome, Birkhead Formation reservoir is no exception with production strategies and secondary oil recovery highly dependent on the drive mechanism. Through understanding of the drive mechanism the reservoir can be exploited to its full potential by the implementation of production and enhanced oil recovery (EOR) strategies.

From figure **147** (page 374) it is evident that the bulk of the Birkhead reservoir production is oil. However, a period of significant water production has occurred between September 1991 and June 1994. The pressure in the wells where water production was high, specifically Gidgealpa 27 and 46, increased to that of the Hutton Sandstone which is above the original Birkhead reservoir pressure. This fact suggests that communication has occurred between the two formations through well-bore cross flow. The lack of Birkhead water production would suggest that the reservoir is a closed system and that there is no aquifer or water leg acting as a drive mechanism on the accumulation. This fact is supported by the pressure data which shows a rapidly decreasing trend with production (figure **146**, page 373). The falling pressure during production is due to the fact that a displacement fluid is not present to replace the oil that is being removed from the reservoir, instead the decreasing amount of oil occupies the same volume and thus the pressure within the reservoir decreases.

The low water content and rapid decrease in reservoir pressure is characteristic of a 'solution-gas drive reservoir'. Helander (1988) describes this type of drive mechanism in terms of an enclosed volumetric tank. Within the tank is an under-saturated oil and small volume of associated water that does not have any influence on the drive mechanism. If wells are drilled and completed within the tank and oil is removed, then for each barrel of oil removed

something must replace the void space that has been created. Since the tank is a closed system the only possible source to replace the removed oil is for the existing oil in the tank to fill the space. To do this the oil must expand an amount that is equal to the volume removed. The result of this expansion is a proportionate drop in the reservoir pressure.

The typical daily production characteristics of a solution-gas drive reservoir are a high initial oil production rate that will tend to decline with increased exploitation and a subsequent decreasing reservoir pressure. The gas-oil ratio will also remain constant in the early stages of production since the gas that is produced is that gas which is initially dissolved in the oil and is liberated as free gas with the pressure drop at the surface. The gas that is liberated early will essentially be trapped within pore spaces due to the low reservoir permeability to the gas. As production continues and a critical pressure is reached the bulk of the dissolved gas will be liberated from the oil in the form of free gas. At this point there will be a dramatic increase in the gas-oil ratio as free gas will flow to the well bore and be produced. The instant at which the bulk of the gas is liberated is termed the 'bubble point' pressure and has a dramatic effect on the daily production rate of the reservoir.

The bubble point has a three-fold effect that is detrimental to daily production. Firstly the liberation of the gas from the oil will cause the oil to shrink thereby further decreasing reservoir pressure, secondly, the gas will fill the bulk of the pore spaces reducing the relative permeability of oil and thirdly, the loss of gas will cause an increase in viscosity in the reservoir oil making flow to the well bore more difficult. Some time after the bubble point is reached a stabilised but significantly lower production rate is obtained. If this rate is economic the reservoir may continue to be produced for a extended period of time (Skinner 1981, Helander 1988).

The Gidgealpa south dome Birkhead reservoir displays a similar daily production history to that of the description above. Production and pressure

data of the Birkhead reservoir have been combined and displayed in figure **148** and consists of the data from figure **146** (page 373) and figure **147** (page 374) respectively. The figure shows the characteristic high rate of daily oil production and rapid decrease in reservoir pressure. As time increases the gas that has been liberated and the lowering of the pressure will cause a reduction in the production rate. Figure **148** also indicates that at June 1994 reservoir pressure was very close to the bubble pressure of 438 psi. If the field had continued to be produced at a high rate the pressure would have fallen below the bubble point greatly decreasing production rates and ultimate recovery. At this point however another factor came into play affecting the rate of pressure decline.

At some stage during the production history, external forces started to act on the Birkhead reservoir. Wu (1995) noted that the pressure decline in the late stage of the history was being supported by oil and water entering the high permeability regions (or clean channel sands) from the low permeability / low porosity floodplain sands that surrounded the main reservoir. The influx of oil and water from the periphery is likely to be a caused by the large pressure differential that would exist between the two regions. Another source of pressure support was obtained from water entering the Birkhead reservoir from Gidgealpa 46. This support is likely to be weak since the connection of the sand at this well to the main reservoir is highly restricted causing a low rate of water flow. Figure **149** (previous page) is a plot of cumulative oil production and reservoir pressure showing the pressure maintenance at a pressure below approximately 600 psia and 600,000 bbls which is represented by a change in slope of the trend line.

This scenario of a solution-gas drive mechanism followed by pressure maintenance of the reservoir by the influx of fluids from surrounding sands is similar to that observed in the Cretaceous Denkman Sand of the Little Creek Field in south-western Mississippi (Cronquist, 1973). The Denkman Sand is a stratigraphically controlled series of sand bars deposited as part of an ancient

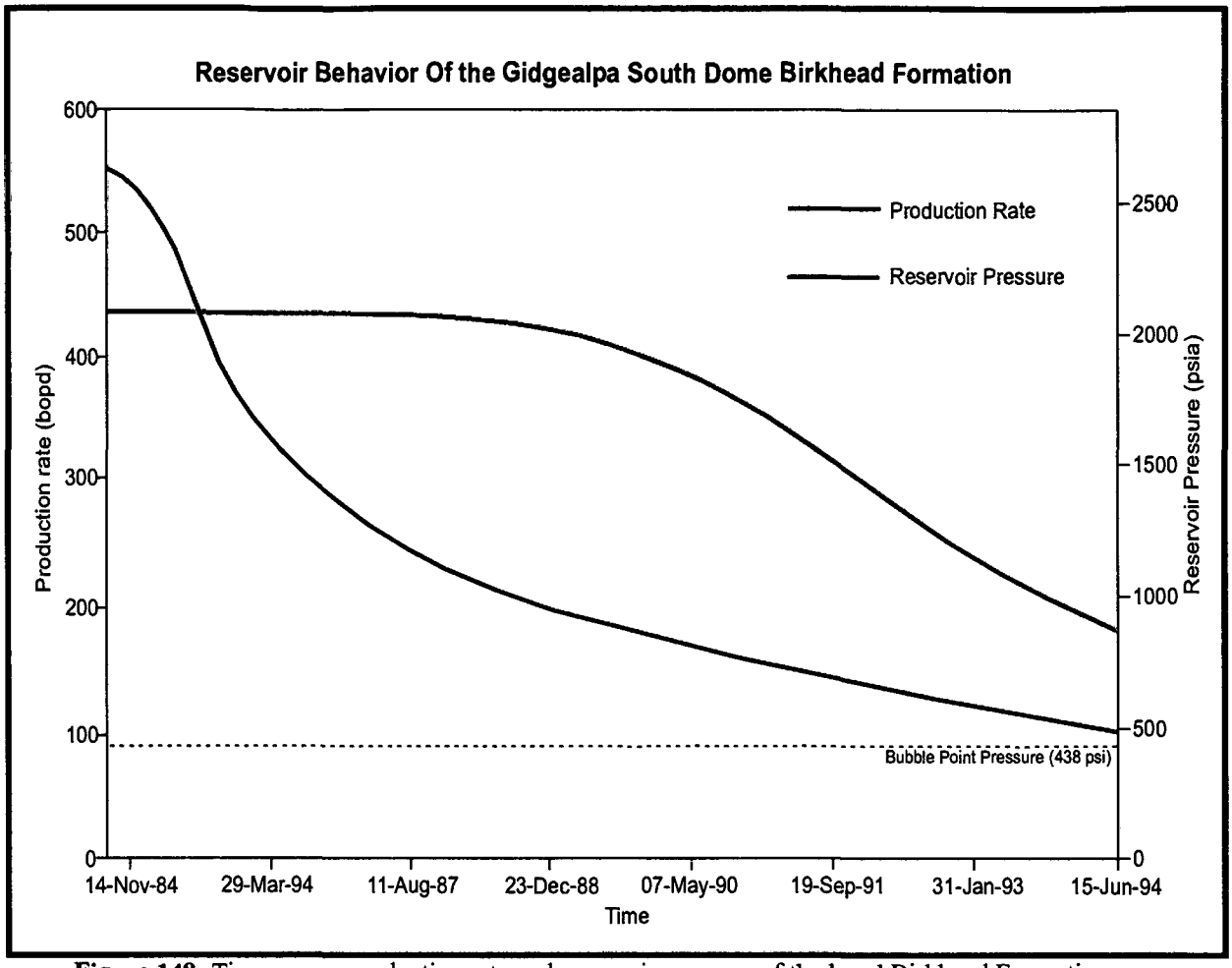

Figure 148: Time versus production rate and reservoir pressure of the basal Birkhead Formation, Gidgealpa south dome.

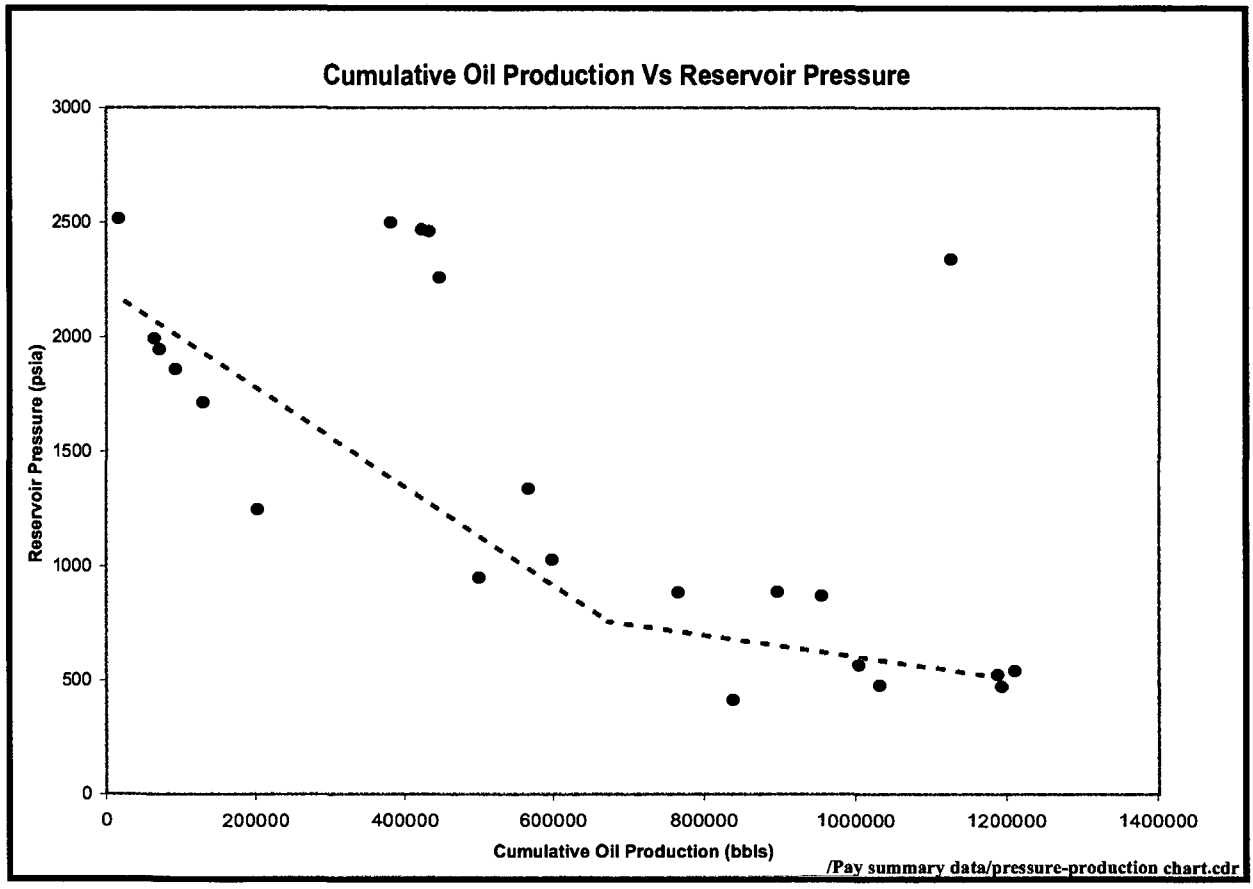

Figure 149: Cumulative oil production versus reservoir pressure of the basal Birkhead Formation reservoir, Gidgealpa south dome.

river. The liquid hydrocarbons were initially produced under solution-gas drive. Similar to the Birkhead Formation at the Gidgealpa south dome, the bottom-hole pressure of the sand declined rapidly. As production continued, increasing amounts of water were also produced which was unexpected from material balance calculations slowing the rate of pressure decline. The possibility of an aquifer drive was ruled out in this case since surrounding fields of a similar nature did not show this characteristic. More likely the increased influx of water was from poorer quality reservoirs sands which occupied the periphery of the main reservoir.

Production performance of a solution-gas drive mechanism is generally poor when compared with other drive mechanisms such as gas-cap drive or water drive. These alternative reservoir types are able to maintain high reservoir pressures since the removal of the oil during production is replaced by other fluids such as gas or water. The efficiency of solution gas-drive reservoir is poor causing oil recovery to range between 5-20% as compared to 20-30% for a gas-cap drive and 40-60% for and water drive systems (Helander, 1988). Because recovery is so low within a solution-gas drive reservoir it is a prime candidate for secondary recovery operations.

8.2.8 Reserves Estimation

With an improved understanding of reservoir distribution within the Birkhead Formation a more accurate determination of hydrocarbon reserves can be calculated within the Gidgealpa south dome. For the determination of reserves I have calculated volumetrically the original oil in place (OOIP) from the equation:

$$OOIP = V_b.\phi.S_h.B_o.7{,}758 \qquad \text{Equation } \mathbf{29}$$

where OOIP = original oil in place
V_b = bulk reservoir volume
ϕ = average field porosity
S_h = average hydrocarbon saturation
B_o = oil expansion factor

To calculate OOIP of the Birkhead Formation I used a planimeter to determine the area of pay in acres for each sand package displayed in figures **150** and **151** which were produced from log interpretation data, then I calculated bulk reservoir volume from the equation:

$$V_b = h\left(\frac{A_o}{2} + A_2 + ... + \frac{A_n}{2}\right) \qquad \text{Equation } \mathbf{30}$$

where V_b = bulk reservoir volume
h = contour interval
A_0 = zero contour
A_2 = second contour
A_n = n^{th} contour

The determination of the area of pay in acres and pay volume in acre-feet are displayed in appendix **12** and the results are summarised in table **21**. Once the bulk reservoir volume was calculated I used equation **29** to determine OOIP, the results have also been summarised in table **21**.

Sand	Net Acre-Feet	OOIP (MMSTB)
Sand A (Pay zone)	1409.2	0.812
Sand A (Tight zone)	89.1	0.025
Sand B (Pay zone)	344.8	0.199
Sand B (Tight zone)	280.6	0.086
Sand C (Pay zone)	5502.8	3.170
Sand C (Tight zone)	271	0.083
Sand D (Pay zone)	3621.5	2.086
Sand D (Tight zone)	2047.8	0.572
Total	13566.8	7.032

Table 21 Summary of OOIP volumetrics calculations for the Gidgealpa south dome, Birkhead Formation.

SAND A

Plan surface area= 449.4 Acres
Reservoir Volume= 1409.2 Acre Feet
Average porosity= 15%
Average HC saturation= 55%
Oil Expansion Factor (1/BO): 0.9
OIP=(Vb.Por.Sat.1/BO.7758)

Oil in place (MSTB)=811.7

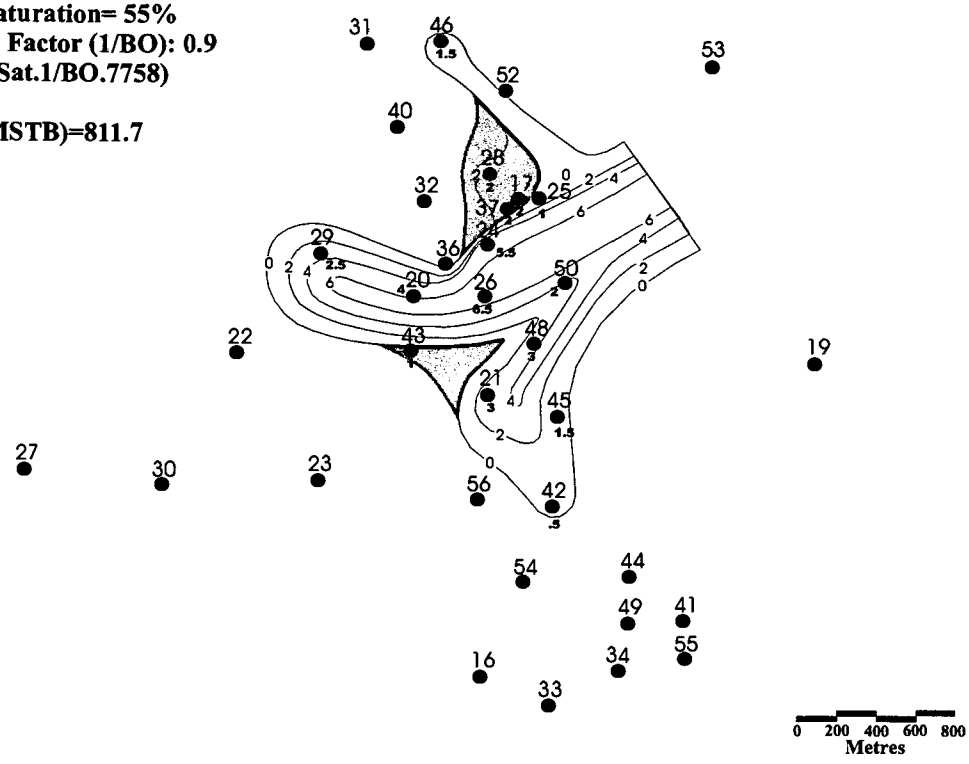

SAND B

Plan surface area= 104.1 Acres
Reservoir Volume= 344.8 Acre Feet
Average porosity= 15%
Average HC saturation= 55%
Oil Expansion Factor (1/BO): 0.9
OIP=(Vb.Por.Sat.1/BO.7758)

Oil in place (MSTB)= 198.6

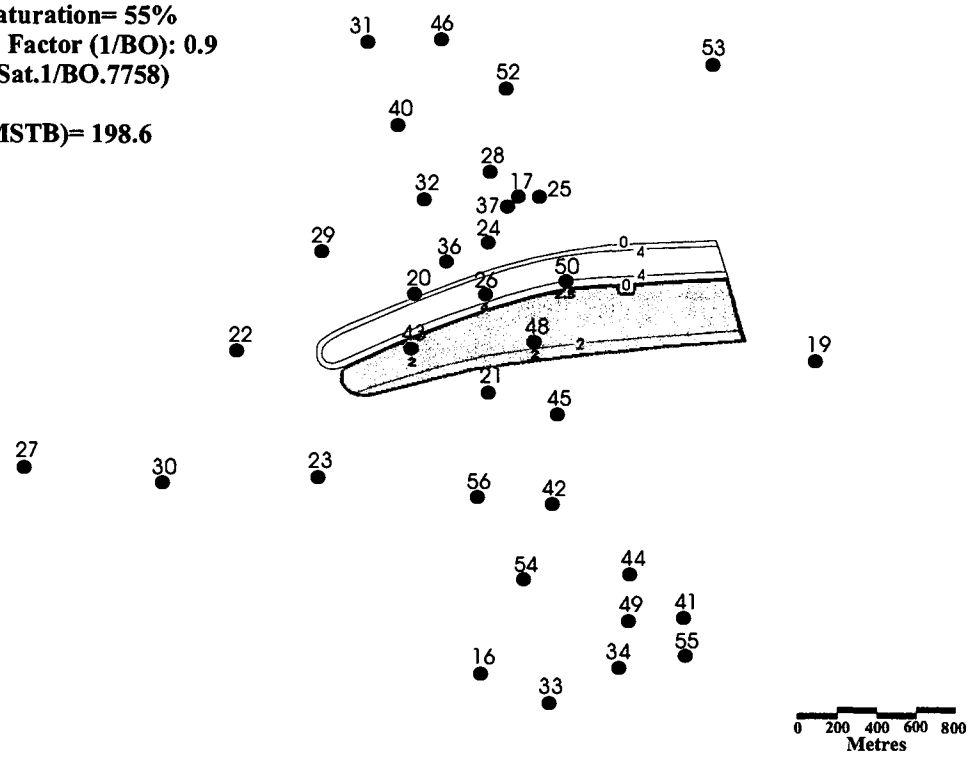

/Paysummary data/reserves calc.cdr

Figure 150: Pay thickness maps of Sands A and B.

SAND C

Plan surface area= 636 Acres
Reservoir Volume= 5502.8 Acre Feet
Average porosity= 15%
Average HC saturation= 55%
Oil Expansion Factor (1/BO): 0.9
OIP=(Vb.Por.Sat.1/BO.7758)

Oil in place (MSTB)= 3169.8

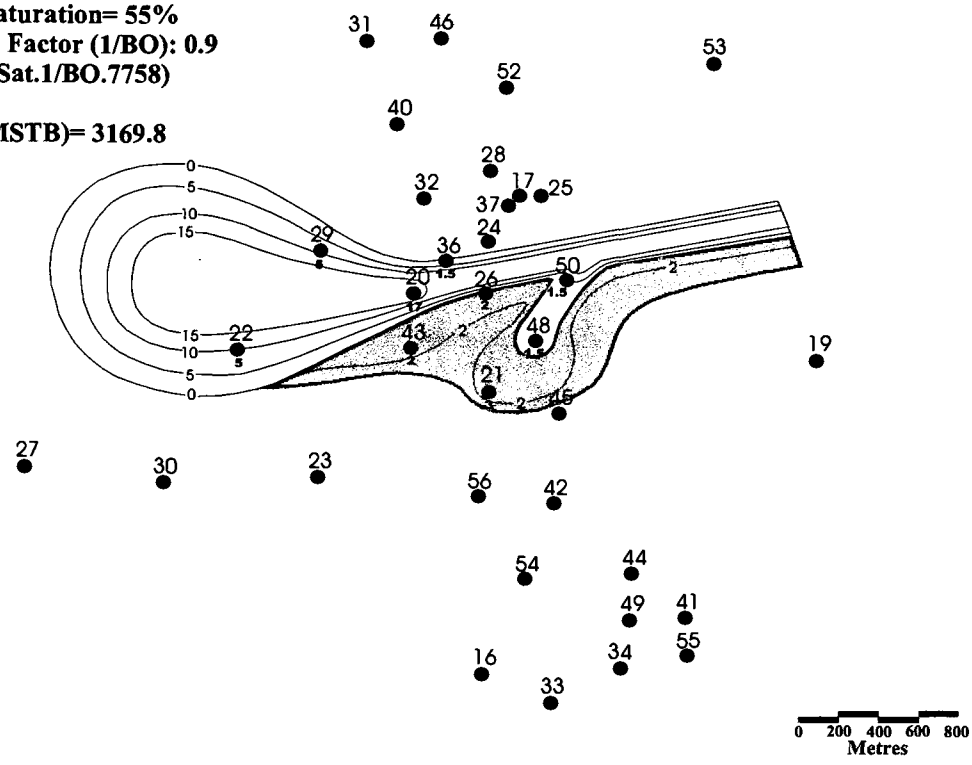

SAND D

Plan surface area= 491.6 Acres
Reservoir Volume= 3621.5 Acre Feet
Average porosity= 15%
Average HC saturation= 55%
Oil Expansion Factor (1/BO): 0.9
OIP=(Vb.Por.Sat.1/BO.7758)

Oil in place (MSTB)= 2086.1

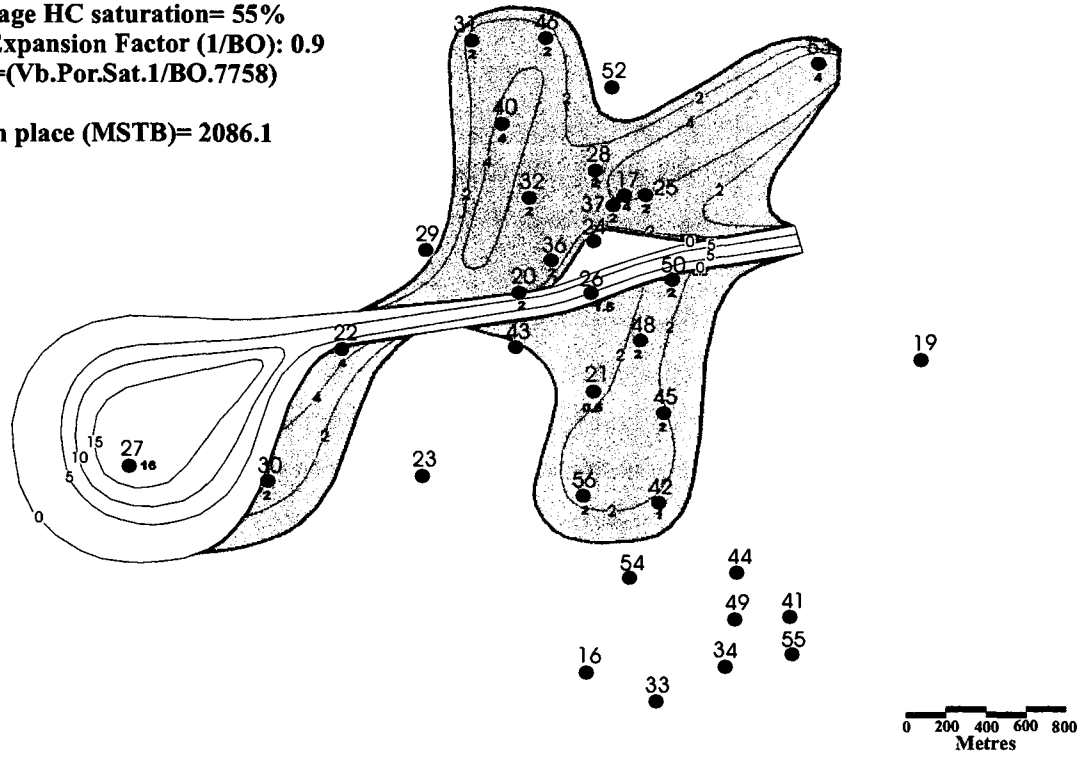

/Paysummary data/reserves calc2.cdr

Figure 151: Pay thickness maps of Sands C and D.

For the calculation of OOIP, 15% porosity, 55% hydrocarbon saturation and an oil expansion factor of 0.9 were used. The porosity value was determined by averaging porosity values over the pay intervals while the hydrocarbon saturation was selected to try to best represent the true hydrocarbon saturation for the reservoir sands (white shaded areas within contours of figures **150** and **151**) since values from log analysis are generally depressed (see section **8.2.2.4**, page 359). The oil expansion factor was obtained from Santos (Zwigulis, M., pers. comm.). For the calculation of reserves in the tight zones (grey shaded areas in figures **150** and **151**) a more qualitative approach was used, an average porosity of 8% and hydrocarbon saturation of 50% were determined from analysis of the processed log data (appendix **11**).

From table **21** a total of 7.032 MMSTB has been calculated from the summation of values from each sand package. This value of OOIP agrees well with the material balance evaluation, which has determined an OOIP value of-6.7 - 7.7 MMSTB (Zwigulis, M., pers. comm.). Primary recovery of 2 MMSTB from a total of 7.032 MMSTB has a corresponding recovery efficiency of 28% which is in the realms of the expected recovery for a solution-gas drive reservoir. This value is at the higher end of the efficiency range due to the influx of fluids from the tight zones elevating primary recovery oil volume. The Hutton Sandstone has also produced a significant amount of oil with 5.7 MMSTB of oil produced to date. With 12 MMSTB of OOIP at 55% recovery this pool has been significantly depleted (Zwigulis, M., pers. comm.). Thus a combined total of approximately 7.7 MMSTB of oil has been produced to date within the Hutton and Birkhead reservoirs.

8.2.9 Reservoir Characteristics: Summary

Deltaic sands within the basal section of the Birkhead Formation are initially controlled by topography of the top Hutton Sandstone or transgressive surface. Positioning of the sands also controlled by sands of previous delta lobes and the compaction of shales. The orientations of these sands are east-west with sand movement from east to west through distributary channels depositing as delta lobe sediments to the west. From production data it is evident that reservoir compartmentalisation occurs and a more detailed knowledge of sand distribution is required. From pressure data these sand packages could be identified.

From five sand packages four pressure compartments were produced with Sand E lacking any reservoir properties. The individual sands show a similar relationship to the overall distribution of sands. They represent distributary channels to the east and delta lobe facies to the west. Pressure analysis reveals that the Birkhead reservoir can be separated into two groups that display similar pressure characteristics internally. Group 1 consists of Sands A, B and C that occur within the main distributary channel and delta lobe. This group can be further sub-divided into subgroups 1a and 1b representing partial or poor reservoir communication respectively. Group 2 consists of Sand D and is completely isolated from Group 1 and has a very different pressure history. The Group 2 compartment is in contact with the Hutton Sandstone through well-bore cross-flow and thus has a similar pressure to the Hutton Sandstone whereas Group 1 sands have a highly depleted reservoir pressure.

From log evaluation the Birkhead reservoir has been mapped in terms of effective porosity, hydrocarbon saturation and HPV while the Hutton reservoir has been mapped using HPV. Log evaluation data of the Hutton Sandstone sediments was carried out using the Archie equation, which is effective when applied to clean porous sandstones. However, the shaly nature of the Birkhead Formation means that the Indonesia equation can be used to account for the

lower resistivity values that are recorded by the logging tool. Permeability estimation was also carried out by using the RHOB log and the relationship between porosity to permeability. Reservoir quality sands are defined by a porosity of greater than 8% and Vshale value of less than 50%. Because the use of the Indonesia equation did not completely characterise water saturation a cut-off value of 65% water saturation was used.

The porosity and HPV maps produced of the Birkhead Formation reservoir show the clear relationship between the delta sands and reservoir distribution indicating the stratigraphic nature of the accumulation. The only exception to this fact is the delta lobe sands of Sand B. Although Sand B has high quality reservoir sands its low structural position within the reservoir means oil will not flow since the hydrocarbon saturation is below 45%. From the relative permeability curve (figure **141** page 363) and using equation **9** (page 300) it was determined that to flow oil (at 45% water saturation) 24 feet of oil column is needed if a displacement pressure of 2 psi (from table 15 (page 199) of Boult, 1996) is assumed for the reservoir rock. When noting the position of Sand B in Gidgealpa 30 it is clear that the oil height required is not present in this part of the field.

In contrast to the Birkhead reservoir, which is stratigraphically controlled, the Hutton reservoir is controlled by structure. HPV calculation reveals how the extent of the reservoir conforms to the structure contours. Variations in HPV values occur due to the various thickness of the reservoir at each well location and the slight variations in reservoir quality of the sands.

Using all the available information from this section including gross sand maps, log evaluation and reservoir values a series of reservoir cross-sections have been created and are displayed as figures **152**, **153** and **154**. Figures **152** and **153** represent dip sections across the Gidgealpa south dome while figure **154** is a strike section on the eastern side of the structure. Reservoir quality in the figures is represented by different shades of green. Dark green areas

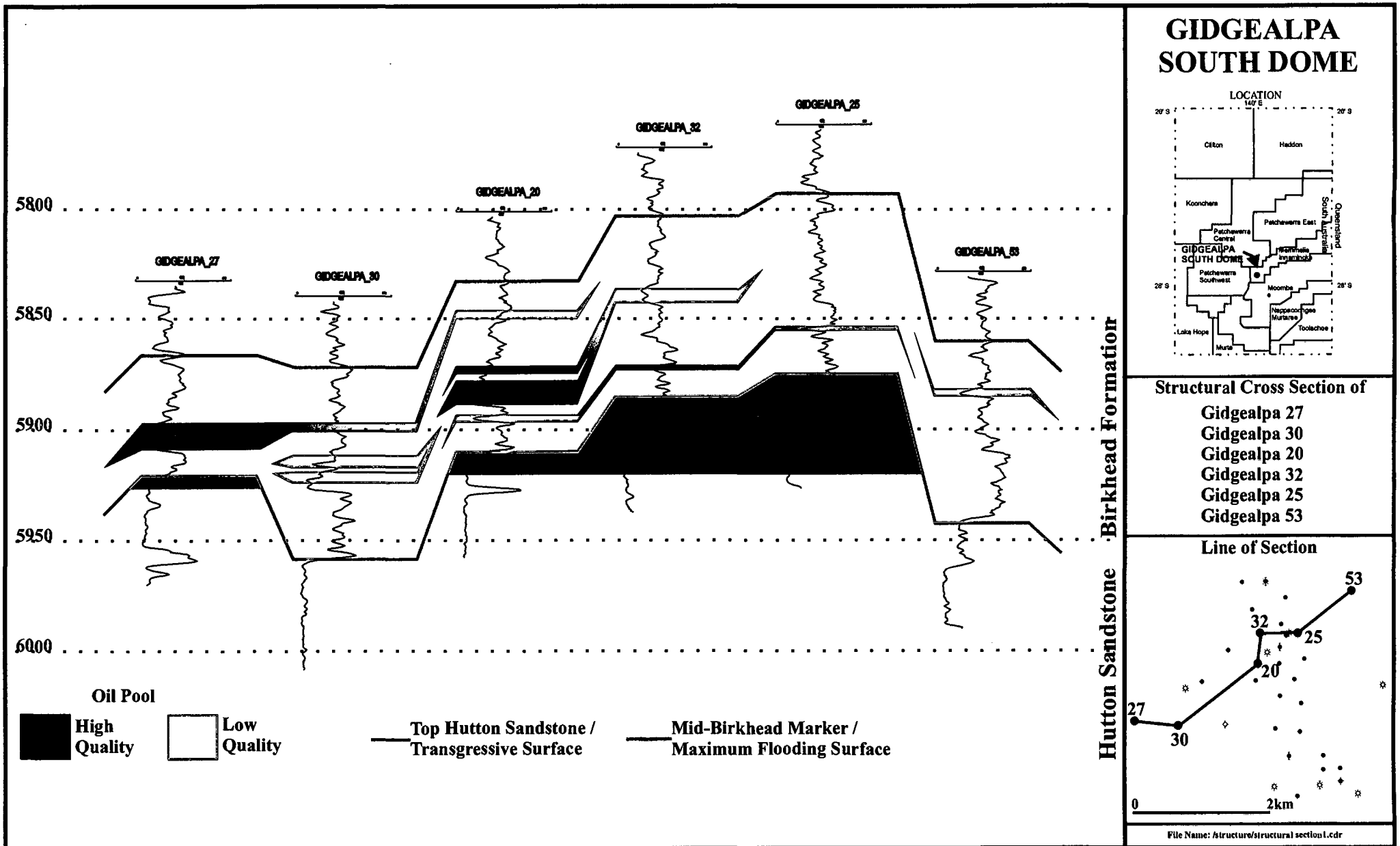

Figure 152: Structural cross sections of the Birkhead Formation and Hutton Sandstone reservoirs at the Gidgealpa south dome.

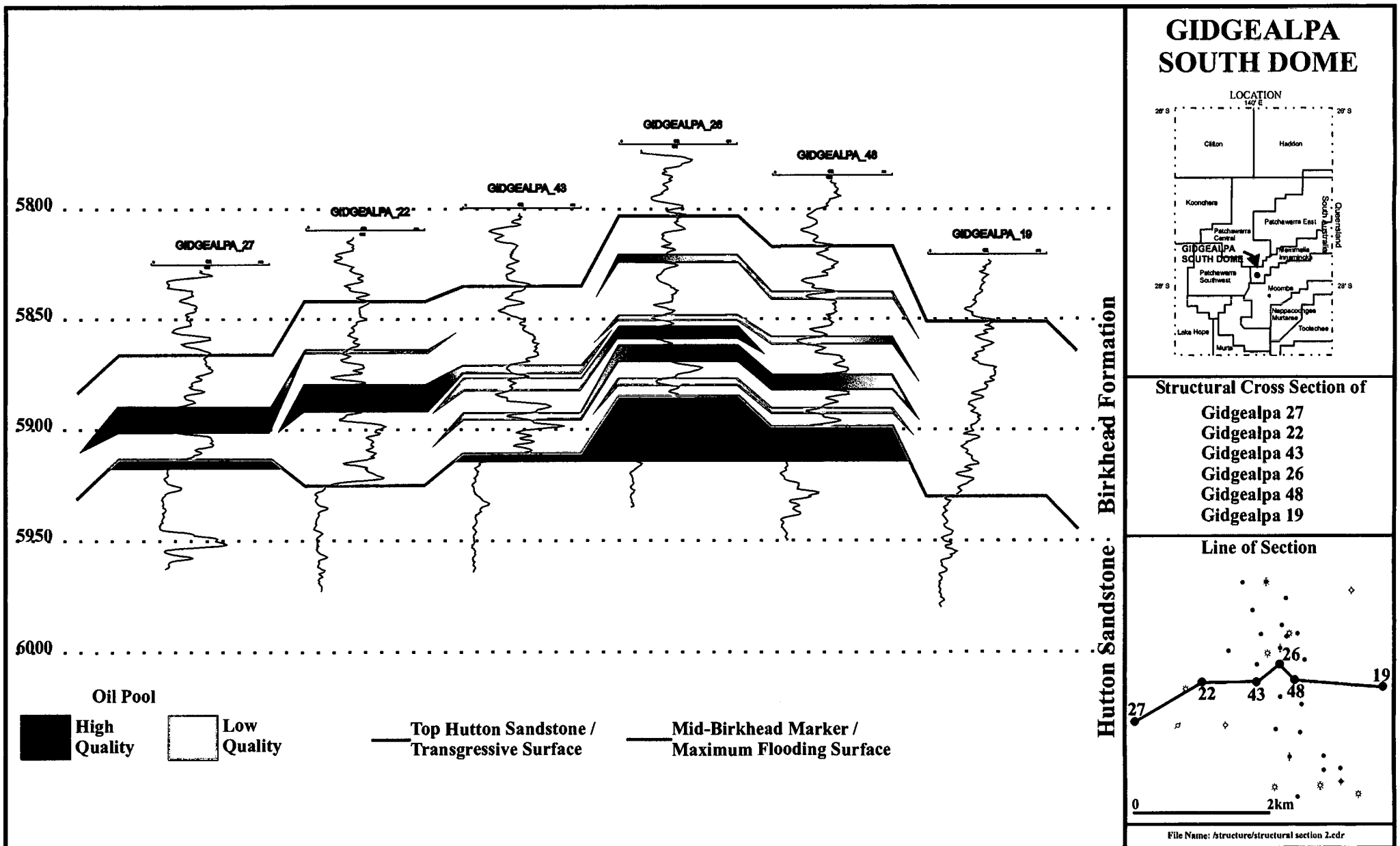

Figure 153: Structural cross sections of the Birkhead Formation and Hutton Sandstone reservoirs at the Gidgealpa south dome.

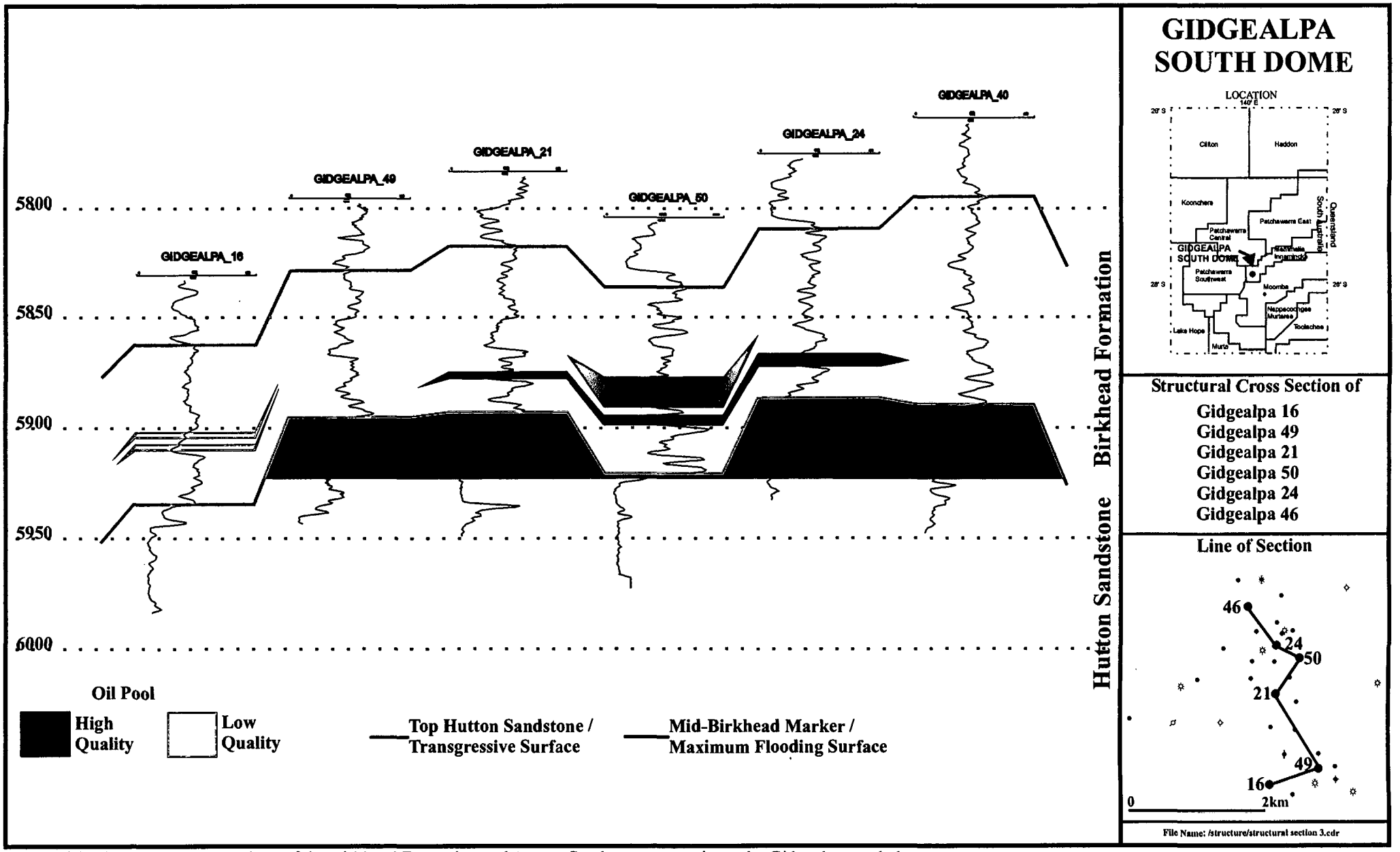

Figure 154: Structural cross sections of the Birkhead Formation and Hutton Sandstone reservoirs at the Gidgealpa south dome.

represent high quality reservoir sands while the light green areas represent sands of poorer quality. What can be noted from the dip sections (figures **152** and **153**) is the higher number and wider distribution of reservoir sands that occur on the western side of the field. These high quality reservoir sands represent the series of stacked delta lobes. A comparison between the dip sections and figure **154** also show the restricted distribution of the reservoir sands on the eastern side of the field representing the distributary channels.

The rapid decrease in pressure of the Birkhead reservoir during the history of its production indicates that a poor drive mechanism is acting on the system, more specifically the pressure decline and the lack of water production indicates that a solution-gas drive mechanism is acting on the reservoir. The declining pressure within the Birkhead means that most wells are producing oil by beam pump and the reservoir is close to bubble point.

The decreasing pressure has also caused the surrounding tighter sandstones to bleed oil into the main reservoir sands due to the large pressure differential between the two regions. Along with the well bore cross-flow from Gidgealpa 27 and 46, this bleeding has helped to maintain pressure within the reservoir and delayed the onset of the bubble point which would dramatically reduce production rates from the reservoir. The poor production performance of a solution-gas drive system means that 5-20% of the OOIP is normally recovered, however the influx of oil from the tight sands has increased the ultimate recovery to 28% currently.

Using pay thickness maps, an average porosity value of 15% and an average hydrocarbon saturation of 55% from log evaluation, the total reserves (OOIP) of the Birkhead reservoir have been calculated to be 7.032 MMSTB of oil from volumetrics. This value agrees well with material balance calculations, which have determined an OOIP value between-6.7 - 7.7 MMSTB. Material balance calculations have also determined that a potential value of 2 MMSTB of oil may be extracted from the Birkhead reservoir by primary production.

This value agrees well with the present day total production of the near depleted reservoir of 1.49 MMSTB. From OOIP calculations and the total production figures, a primary recovery ratio of 28% has been calculated. The percentage recovery is at an acceptable level considering the fact that the gas-solution drive has been affected by bleeding into the main reservoir increasing overall recovery values. From the Birkhead and Hutton reservoirs a combined total of 7.7 MMSTB of oil have been produced.

9 Waterflooding

9.1 Introduction

Waterflooding is the most common of all enhanced recovery operations due to its high success rate of secondary oil recovery at a low cost. As mentioned in section **8.2.7**, the Birkhead Formation at the Gidgealpa south dome is a prime candidate for waterflooding with an ultimate recovery rate as high as 50% (Skinner, 1981) which is 22% greater than primary flooding alone. Wu (1995) determined an ultimate recovery after waterflooding of 44%. Within the Birkhead Formation waterflooding has a three-fold function: firstly to recover reserves that have been missed from primary recovery operations, secondly to increase reservoir pressure to ensure that the bubble point is not reached and thirdly, to increase sweep efficiencies.

Figure **155** is an illustration of a production history profile showing primary production and then the implementation of a waterflood operation. From figure **155** the operation can be described by four different points labelled 'A,B,C and D' on the production history curve (Helander, 1988). The corresponding reservoir conditions are displayed in the same figure and are labelled appropriately. Point 'A' represents the reservoir conditions at the start of the waterflood. In this example the solution-gas drive reservoir contains 25% gas, 50% oil and 25% connate water saturation. At this point it is important to note that the three fluids are dispersed throughout the whole pore system and has only been displayed as layers for ease of description.

A short time after the operation has been running (point 'B') a water bank forms and moves radially from the well bore displacing most of the residual oil within the pore spaces producing a preceding oil bank. At point C water has continued to be injected into the well causing the water and oil banks to expand to a point where fill up is reached. Helander (1988) describes the fill

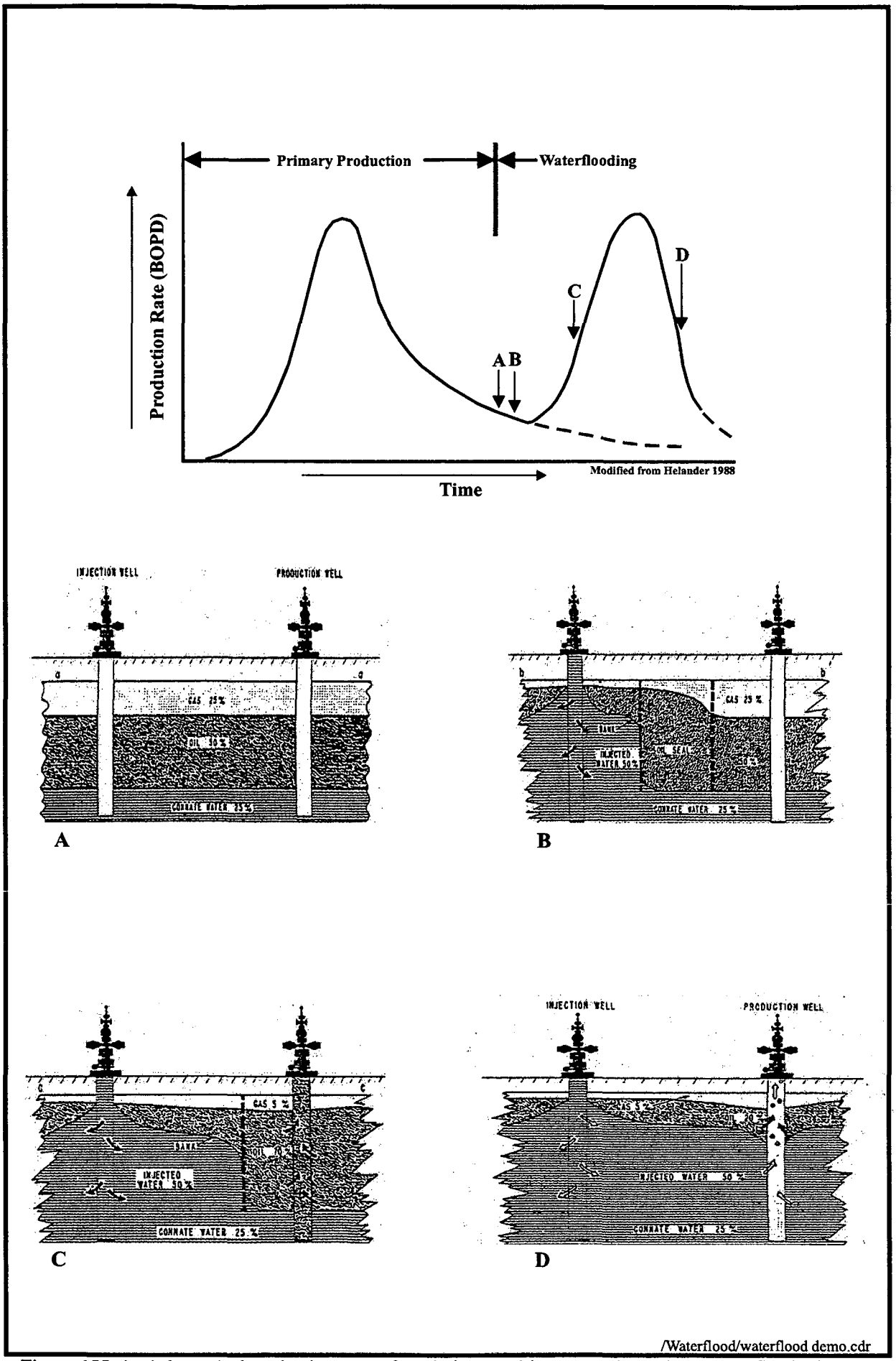

Figure 155: (top) theoretical production rates of a solution gas drive reservoir that has a waterflood scheme implemented to increase reserves and production rates. Points A,B,C and D correspond to the drawings which illustrate waterflooding at different times during the operation (After Helander, 1988).

up condition where the fluid within the reservoir, which includes water and oil, fills the area previously occupied by the free gas. At this stage a significant increase in reservoir pressure occurs. Point 'C' will see the rapid increase of oil recovery since the oil bank has reached the production well.

Point D represents the final stages of the waterflood. At this point the water bank has reached the production well causing the increase of water and decrease in oil recovery. When the water to oil recovery ratio reaches a certain limit the waterflood operation is terminated. The amount of oil recovered from waterflooding depends on the sweep efficiency, conformance efficiency and the displacement efficiency and demonstrates the importance of understanding the fluid and rock system before carrying out secondary recovery operations.

9.2 Waterflooding operations at the Gidgealpa south dome

Waterflooding, and more recently dump-flooding has been carried out within the Birkhead Formation with mixed results. The first attempt at a secondary recovery operation from the Birkhead Formation was conducted in October 1988 with a pilot waterflood study where 309 bbls of water was injected into the formation (Wu, 1995). However, injectivity problems caused the project to be suspended. A pressure test after the injection of the water revealed that the reservoir pressure at Gidgealpa 30 had increased by 143 psia. The well was shut in until another pressure test was conducted in December 1993 which indicated that the Birkhead Formation reservoir at Gidgealpa 30 had further decreased by 155 psia which was 541 psia higher than the main reservoir pressure in Sand C. Prior inadequate mapping of this region, I believe, caused the unforeseen problems with reservoir communication between Gidgealpa 30 and the main reservoir. Problems, which arose from the pilot study and communication characteristics between the two regions, are discussed in section **8.2.9**.

In November / December 1995 a dump-flood was conducted in Gidgealpa 22. Basically, the operation involved accessing the Hutton Sandstone aquifer system and allowing water flow from the aquifer system into Sand C of the Birkhead reservoir. Initially 50 bwpd flowed into the Birkhead Formation. At the same time as the initiation of this dump-flood, Gidgealpa 26 was the only well producing from the Birkhead reservoir at a rate of 150 bopd (figure **156**, point A). A short time after the dump-flood Gidgealpa 26 increased production to 200 bopd (figure **156**, point B). The injection of 50 bwpd into the Birkhead reservoir was deemed to be inadequate and the flow of at least 200 bwpd was required for an effective recovery from Gidgealpa 26 (Zwigulis, M., pers. comm.). Thus, to increase the flow rate of water into the Birkhead reservoir a frac was conducted in mid 1997 (figure **156**, point C).

The successful completion of the frac in Gidgealpa 22 saw the flow of 200 bwpd into the Birkhead reservoir. Approximately six months after the frac Gidgealpa 26 increased production to a rate of 300 bopd (figure **156**, point D). The use of radioactive tracers indicated that the increased production was a direct result of the dump-flood conducted in Gidgealpa 22. From the dump-flooding in Gidgealpa 22 alone, potential production in Gidgealpa 26 has risen from 350,000 bbls to 500,000 bbls of produceable oil (Zwigulis, M., pers. comm.).

The success of the dump-flood operation at the Gidgealpa south dome should be applied to the entire Birkhead reservoir to exploit the maximum amount of hydrocarbons present. From the detailed reservoir analysis in this thesis, the risk of reservoir damage and / or the loss of profits by conducting a field wide waterflood program has been lessened to a point where the operation is favourable to recover the residual reserves missed by primary production.

Due to the stratigraphic nature and limited extent of the Birkhead reservoir sands a peripheral waterflood pattern would be most effective. This fact has already been demonstrated from the Gidgealpa 22-26 dump-flood operation.

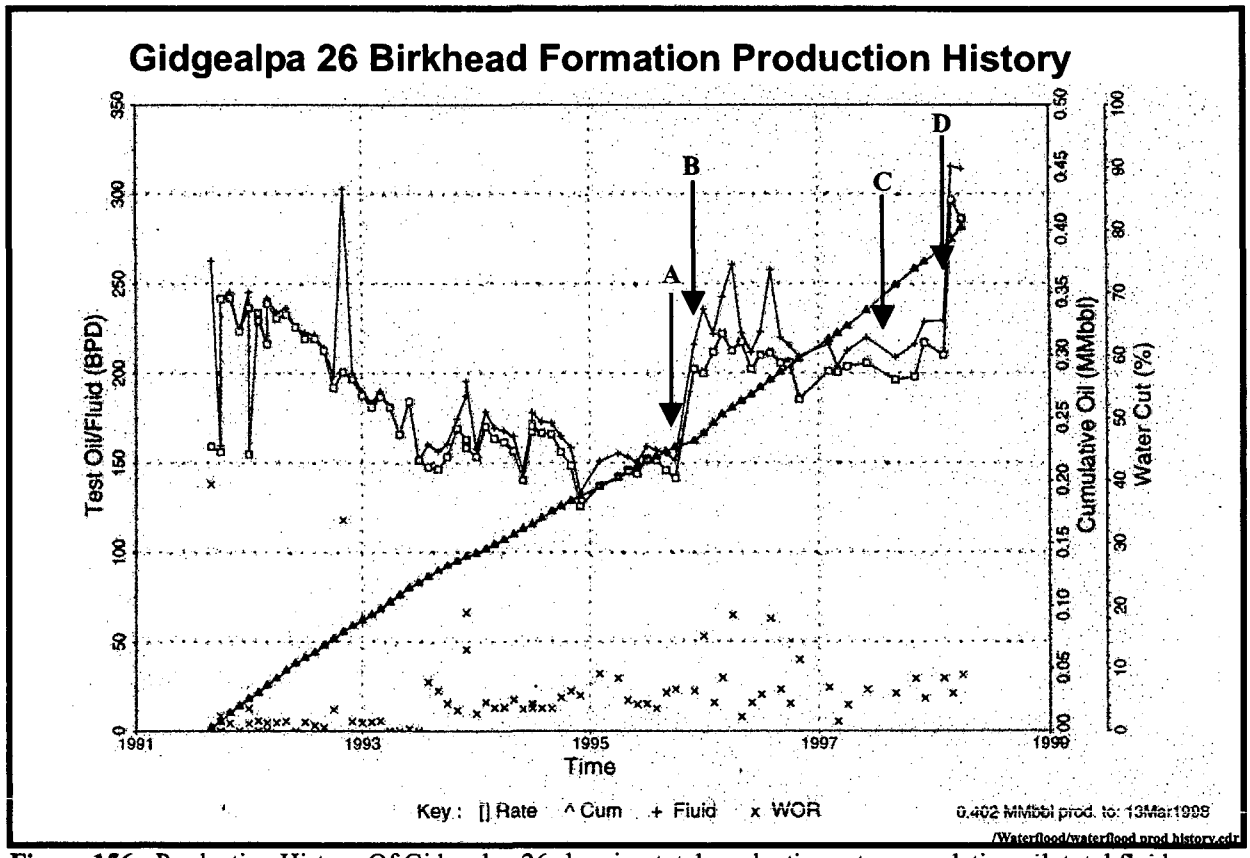

Figure 156: Production History Of Gidgealpa 26 showing total production rate, cumulative oil, total fluid and the water oil ratio. The points represented by the letters A and B represent the initiation of dumpflooding into the Birkhead at Gidgealpa 22 and the subsequent increase in production at Gidgealpa 26 respectively. Points C and D represent the points at which a frac job was done on the Birkhead reservoir and the subsequent production increase that occurred at Gidgealpa 26 respectively.

From the pay thickness maps (figures **150** and **151**, page 386 and 387 respectively) the wells chosen for injection or dump-flooding can be selected to access all of the compartments within the reservoir. As an initial consideration Gidgealpa 29, 22, 50 and 48 could be used as injector wells with Gidgealpa 26 acting as the producer. If the pressure increase from the injection wells was elevated substantially, Gidgealpa 20 could also be used as a producer to increase the oil recovery rate. In both cases well-bore cross-flow from Gidgealpa 46 would be allowed to continue the influx of Hutton water into the main channel region. Table **22** indicates the wells that have the potential to act as injectors or producers and the reservoir sands that have the potential to be accessed by the dump-flooding.

Well	Injector (I) / Producer (P)	Sands accessed
Gidgealpa 20	I or P	A,C,
Gidgealpa 22	I	C
Gidgealpa 26	P	A,B,C,D
Gidgealpa 29	I	A,C,
Gidgealpa 48	I	A,C,
Gidgealpa 50	I	A,B,C

Table 22: Wells where reservoir sands have the potential to be accessed during dump-flooding.

In the case where water flow into the Birkhead reservoir is inadequate a frac job may be performed on the reservoir of the particular well as conducted on Gidgealpa 22. One potential problem of waterflooding is the pressure build up of the main reservoir sands that may stop the influx of oil from the low permeability regions. For this reason a low pressure waterflood of below 1000 psia would be appropriate with the monitoring of the reservoir pressure to promote the influx of oil from the tighter regions (Wu, 1995).

The potential recovery from waterflooding alone has been determined between 660 - 1460 MSTB and if 100% influx is assumed from the low permeability regions recoverable reserves could be as high as 1732 MSTB (Wu, 1995).

Tertiary recovery of reserves by CO_2 flooding may also be a possibility but should be carried out after the waterflood since the reservoir pressure should not be more than 200 psia below the minimum miscibility pressure between the CO_2 and oil. The cost of the CO_2 flooding and the need for data from the waterflood operation means that it should be considered at a later stage. Incremental recovery of reserves from CO_2 flooding has been estimated at 17.5% (Wu, 1995). Figure **157** shows the inferred theoretical production history from the presence of a waterflood and a CO_2 flood demonstrating that these secondary recovery techniques both increase field life and increase the rate of recovery of reserves.

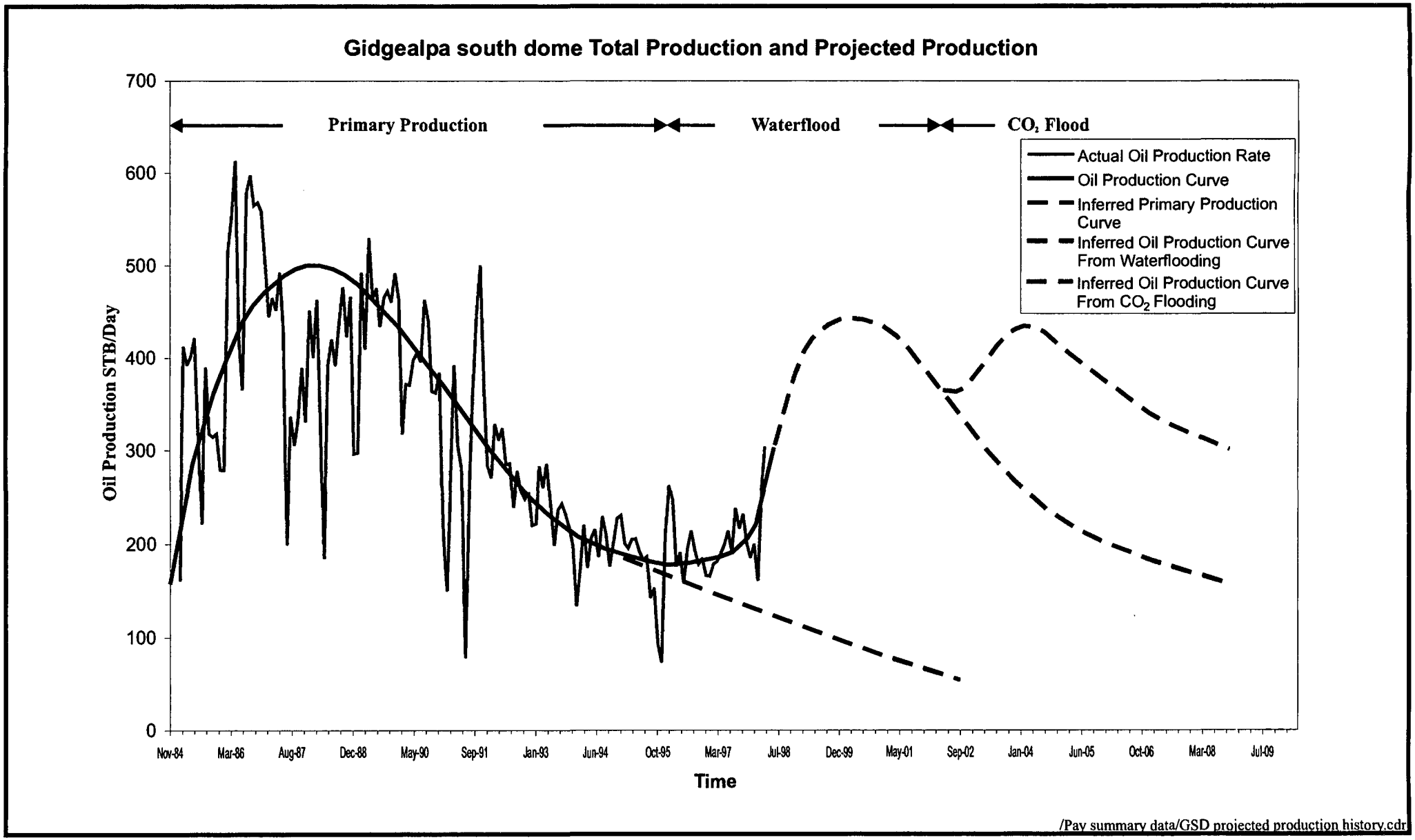

Figure 157: Gidgealpa south dome, Birkhead Formation reservoir production history (time versus oil production rate/day) showing inferred theoretical curves for waterflooding and CO_2 flooding.

10 Conclusions

From a large scale observation of the cores present over the top Hutton Sandstone / basal Birkhead Formation section at the Gidgealpa south dome, the sequence was interpreted to consist of a braided fluvial and then fluvial deltaic depositional succession. These depositional environments were further characterised by dividing the core into a number of lithofacies. Within the Hutton Sandstone section gravel lithofacies such as Gm and Gt, and sandy lithofacies such as St, Sp, Sm, Sh dominate with the sediments deposited as channel fill lithofacies. The channel fill lithofacies are minor, consisting of Sr, Sd, Fm and Fl and are deposited due to channel abandonment. In contrast, the Birkhead Formation contains a lower occurrence of channel fill lithofacies and instead is dominated by lithofacies such as Sr, Sd, Sb/Fb, Fl, Fm, Fcs, Fos and C that were deposited as lower energy, over bank, crevasse spaly, distributary mouth bar and interdistibutary bay sediments.

Common sequences of the lithofacies, or facies associations, were determined using embedded Markov chain analysis for the Birkhead Formation section. From the analysis four successions were determined and grouped into two classes. The classes consisted of the 'Birkhead Formation Group 1' sequences that are characterised by the classical point bar, fining upward channel sediments and the 'Birkhead Formation Group 2' sequences that represent low energy deposited, abandoned channel fill sediments overlying active channel fill deposits.

The identification of the sediment types and associations within the Birkhead Formation allowed for classification of the sequence as a mixed load, fluvial dominated delta system. The system was characterised by the presence of meandering channels in the upper delta plain that alter to shoe string, or linear channels, on the lower delta plain. The linear channels are dominated by gravel lags and cross-bedded sandstones. Associated with the lower delta

plain channels are levees, crevasse splays distributary mouth bars and swamps that dominate the sequence. From the analysis of wireline logs and sand correlations the delta complex evolved and changed shape from a fluvially dominated, elongate bird foot structure to a fluvially dominated lobate structure and finally, to a wave influenced fluvially dominated structure.

To determine the orientation of the delta complex dipmeter data was processed and then interpreted to obtain the palaeo-drainage direction at the Gidgealpa south dome. The data indicated that drainage occurred in a west to south-west orientation with the delta lobes located on the western side of the area. The orientation agreed well with an analysis of regional dipmeter data that also indicated a west to south-west drainage orientation during Birkhead Formation deposition. In contrast, palaeo-drainage within the Hutton Sandstone was orientated in an east to north-east direction. The change of palaeo-flow was located at the Hutton Sandstone / Birkhead Formation boundary.

As indicated from neodymium model age dating, the change in palaeo-drainage was also associated with a change in sediment provenance. Sediment derived from the south-west during Hutton Sandstone deposition had an average model age of 1700 Ma which corresponds to the age of rocks within the Gawler Craton area to the south-west of Gidgealpa. Sediment derived from the north-east had a very different model age of approximately 900 Ma reflecting the younger age of the rocks at the sediment origin. The younger age corresponds to the formation of a volcanic-arc complex that existed at the time off the present day coast of Queensland. While the change in neodymium model ages are associated with the change in palaeo-drainage they do not occur at the same stratigraphic level in the Gidgealpa area. The mismatch is due to the more distal position of the volcanic-arc complex than the Gawler craton. The longer distance that the sediments travelled from the north-east meant that initial deposition over the Gidgealpa south dome consisted of craton derived sediments that were reworked from the top Hutton Sandstone

section. These sediments consequently have older model ages than the volcanic-arc derived sediments that followed soon after.

The relatively simple structuring of the Eromanga Basin allowed the implementation of sequence stratigraphy in an intra-cratonic, fluvial-deltaic to lacustrine depositional environment. The interrelationship of tectonics and the supply of sediment controlled the formation of systems tracts within the basin. Regional tilting of the Eromanga Basin on the eastern edge caused the change in provenance at the Gidgealpa south dome. Associated with this event was the formation of a volcanic-arc complex off the present day coast of Queensland and a relative fall in base-level. The fall in base-level caused the formation of a sequence boundary that consisted of incised fluvial channels that eroded into the top Hutton Sandstone section. Above the boundary lowstand systems tract sediments were deposited. Associated with the base-level fall was an increase in silts and shales within the top Hutton Sandstone section and a decrease in depositional energy of the sediments derived from the cratonic area to the south-west of the basin. These lowstand systems tract sediments in the south-western section of the Eromanga Basin formed due to the slow rise in base-level.

Fluvial incision also occurred in the eastern Eromanga Basin with subsequent sediment supply increasingly occurring from the east during lowstand deposition. Initially, the sediment from the east consisted of reworked Hutton Sandstone that was then replaced by volcanic arc derived sediment. The increase in sediment content from the east caused the basin depocentre, located in the north-east, to fill with sediment. The filling process caused the rise in base-level and the formation of a transgressive surface that marked the change from a lowstand systems tract to a transgressive systems tract and the transition of the Hutton Sandstone to the Birkhead Formation.

The Birkhead Formation transgressive systems tract sediments consisted of retrogradational and backstepping fluvial-deltaic parasequences where

sediment became more distal in nature up-section. Sediments within this tract were dominated by volcanic-arc derived sediments. As the supply of volcanic-arc derived sediment waned, the base-level continued to rise flooding almost the entire Eromanga Basin. The rise in base-level continued until the maximum flooding surface was obtained. This surface represented the uppermost limit of the transgression and the maximum land-ward extent of lacustrine conditions. Associated with the waning volcanic-arc derived sediment was the slight uplift of the south-western margin of the basin causing the initiation of sediments once again from that area.

The highstand systems tract occurs directly above the maximum flooding surface and is characterised by an increase in depositional energy caused by the active uplift and erosion from the south-west of the basin. The tilting allowed for the re-opening of the drainage outlet to the north-east and the associated increase in sediment supply causing a relative base-level fall. Initially sediments consisted of vertically isolated sand bodies that became more amalgamated with the continued progradation of sediments. The filling of accommodation space continued within the Eromanga Basin until deposition was replaced by erosion due to the formation of negative accommodation space. The erosion marks the formation of a sequence boundary and end of the Birkhead Formation and start of the Namur and Adori Sandstones.

From regional sequence stratigraphic analysis the top Hutton Sandstone and Birkhead Formation can be separated into three units. 'Unit 1' is highly variable in thickness and consists of the top Hutton Sandstone section between the sequence boundary and the transgressive surface. 'Unit 2' is relatively uniform in thickness and consists of the transgressive systems tract section between the transgressive surface. 'Unit 3' consists of the transgressive systems tract section between the maximum flooding surface and the sequence boundary marking the end of the Birkhead Formation and start of the Namur

or Adori Sandstones. Unit 3 is variable in thickness due to erosion from the sequence boundary above.

While sequence stratigraphy has been applied regionally its application was used on the field scale at the Gidgealpa south dome. The identification of the delta progradation surface, emergence surface and flooding surface within the delta complex allowed for the determination of the start and end points of each parasequence that aided in reservoir distribution.

The basal section of the Birkhead Formation within a transgressive systems tract setting consists of a number of parasequences forming a delta complex. Initially, prograding deltaic sands had a sheet morphology, with continued deposition distributary channels formed that were restricted by levees. The stabilisation of channels by the levees mean that lagoons, swamps and marshes became established in the area and distributary mouth bars had a lobate morphology. Due to the build up of sediments in the distributary system the formation of isolated delta lobe parasequences was caused by the avulsion of channels that followed steeper hydraulic gradients. In the final stages of development, before the area became lacustrine, the delta complex retrograded due to a decrease in sediment supply and was dominated by lake processes.

The application of petrology with the aid of XRD, SEM and CL on samples taken from the Gidgealpa south dome cores allowed for the identification of critical factors that affected reservoir quality and also helped to identify the provenance change boundary within the area. Cratonic-arc derived sediments derived from the south-west of the basin during deposition of the Hutton Sandstone were dominated by plutonic quartz, low feldspar and rock fragment content and were usually medium to course grained. Framework grains were usually well rounded and multiple stages of overgrowths had been identified in reworked sediments of the basal Birkhead Formation section. The volcanic arc derived sediments generally were finer grained and had lower concentrations of quartz, were dominated by rock fragments, matrix and detrital clays and had

a higher proportion of feldspars. The higher proportion of the ductile lithic rock fragments and higher presence of authigenic cements meant that the reservoir quality of these sub-litharenites and litharenites were poor when compared with the quartz arenitic, craton derived sediments that had good to excellent reservoir qualities.

From the petrological study the main controls on permeability and porosity was the initial sorting of the sediment, grainsize, grain composition and diagenetic history. Within the cratonic-arc derived sediments the abundance of quartz and lack of lithics and detrital clays allowed for the cementation of framework gains. The cementation stopped compaction and held the pore throats open, allowing for easy storage and flow-though of reservoir fluids. Porosity and permeability within the volcanic-arc derived sediments were poor due to compaction and deformation of lithics. Included with the collapse of pore throats was the precipitation of authigenic clays and cements such as kaolin and calcite that further reduced porosity and permeability.

To further characterise the Hutton Sandstone / Birkhead Formation reservoir mercury injection was conducted to determine capillary entry pressure of rocks. Results indicated that decreasing mercury injection pressures were needed to inject mercury into the rocks for lithofacies that were coarser grained and better-sorted while diagenetic clays and cements had a counteracting effect that increased entry pressures. The Birkhead Formation capillary entry curves demonstrated a bimodal pore throat distribution. The relatively sharp peak located between 0.01 to 0.1 μm corresponds to micro porosity of kaolin while the greater diameter peak(s) correspond to primary and secondary porosity. The bimodal distribution of the Birkhead Formation sediments is in contrast to the Hutton Sandstone that is dominated by a unimodal distribution and reflects the low abundances kaolin. Mercury-air capillary entry pressure data was converted to an oil-brine system to determine the height above fee water level of hydrocarbons. This data indicated that the Hutton Sandstone required only a few feet of hydrocarbon column to have an

oil saturation of greater than 50 percent while the Birkhead Formation sediments required an average of 20 feet.

From the results of the capillary entry pressure curves it was not surprising that high porosity and permeability readings were from core plugs corresponding to rocks that were coarser grained and better sorted. The plotting of porosity versus permeability also revealed that each lithofacies had a unique straight line relationship. The relationship between porosity and permeability could be used for each lithofacies to characterise the reservoir where only probe permeability data may be available. Over 2000 probe permeameter readings were taken from the Hutton Sandstone / Birkhead Formation cores and by using core data the readings were calibrated to produce more accurate results. The probe permeability values were then used to profile the reservoir by producing histograms of permeability versus frequency for each lithofacies. The histograms indicated that the lithofacies could be separated into three permeability classes. They consisted of a poor quality class that had an average permeability of 0.02 md and consisted of lithofacies Fm, Fl, Fos, Fcs, Sb/Fb and C. The second class was of an intermediate quality, having an average permeability of 0.21 md and consisting of lithofacies Sr and Sd while the third class was high quality and had a corresponding average permeability reading of 9.75 md and consisted of lithofacies Sm, Sh, Sp and St. The high quality permeability class is the only class that was considered to be of reservoir quality.

The Birkhead Formation reservoir at the Gidgealpa south dome consisted of five sand packages that contained 4 pressure compartments. From the compartments; two separate groups existed where the sands were in pressure communication with each other. Further characterisation was conducted from petrophysical analysis where the reservoir was mapped in terms of effective porosity and hydrocarbon pore volume. To determine effective porosity the modified Archie equation was used for the Hutton Sandstone while the Indonesia equation was used for the Birkhead Formation due to the shaly

nature of the sands. The effective porosity and hydrocarbon pore volume maps clearly indicated the relationship between the areas of reservoir quality associated with distributary mouth bar and channel sands. The only exception to this trend was at Gidgealpa 30 where oil saturation is low due the low stratigraphic position of the Birkhead Formation sand.

The rapid decrease in pressure of the Birkhead Formation reservoir is due to the presence of a solution gas drive mechanism. This type of drive mechanism means that most oil from the reservoir has been produced by beam pump. From volumetric analysis the decreasing pressure of the reservoir has caused the bleeding of oil from the surrounding rocks that have poor reservoir properties. The poor production performance of a solution gas-drive system means that 5-20% of OOIP was recovered and the influx of oil from the surrounding tight sands has increased ultimate recovery to 28%. Using volumetrics the total reserves have been calculated at 7.032 MMSTB. To date (1998) 1.49 MMSTB had been produced from the reservoir and combining production from the Hutton Sandstone; 7.7 MMSTB has been produced. A waterflooding strategy has been initiated within the Birkhead Formation and from reservoir analysis a forward strategy has been determined with a number of wells that may either be used as injectors or producers. The use of waterflooding in the Birkhead Formation reservoir should increase ultimate production by as much as 1732 MSTB.

11 Recommendations and Further Research

- The application of a fluvial-deltaic model to the Birkhead Formation is in contrast to a fluvial model that has been applied to similar producing fields in the past within the Eromanga basin. The incorrect application of a depositional model means that hydrocarbons may remain untapped. Therefore, a review of the depositional and sedimentological characteristics of the Birkhead Formation producing fields should be conducted. The application of the correct model will also aid in secondary oil recovery strategies.

- The majority of oil accumulations near the top Hutton Sandstone / basal Birkhead Formation interval have been discovered within the Hutton Sandstone and Unit 1 (this study) as structural traps. Further exploration effort should be applied to stratigraphic plays within the Birkhead Formation Unit 2 to recover hydrocarbons from untapped reservoirs.

- To aid in the identification of the possible stratigraphic traps within the basal Birkhead section a more detailed sequence stratigraphic study should be undertaken and then tied in with regional interpretations.

- The identification of a fluvial-deltaic depositional environment in the Birkhead Formation of the Gidgealpa south dome has allowed for the determination of sand distribution. From the distribution; a major distributary mouth bar sand to the north of Gidgealpa 27 has not been penetrated. This fact along with the structurally high position of the area indicates that it is a good candidate for the drilling of another development well. The well would increase ultimate production of the Birkhead Formation reservoir. Once the area has been drained, the well may then be used as an injector in a water flood strategy.

- The characterisation of the Birkhead Formation reservoir involved the integration of multiple data sets. One such example was the use of core plug and the probe permeameter data that provided detailed reservoir properties and distribution. The use of the probe permeameter is non-destructive and has allowed for the detailed distribution permeability of lithofacies. Thus the probe permeameter should be applied to other fields to aid in reservoir characterisation.

- To obtain maximum returns on investment a CO_2 flood of the Birkhead Formation should be applied after the water flood. The data obtained from the water flood should be applied to the CO_2 flood to minimise risk.

- Reservoir simulation models should be implemented to determine the maximum reserves in both the water flood and CO_2 flood strategies. The simulations would allow for the determination of the most favourable waterflood strategy.

- In the case of the Gidgealpa south dome, the Birkhead Formation reservoir would have benefited from the early implementation of enhanced oil recovery strategy that would have maintained reservoir pressure levels. The maintenance of pressure within the reservoir would have delayed the need for manual lifting of the hydrocarbons and would have increased ultimate reserves recovery. Thus, in future developments, enhanced oil recovery methods should be employed as early as possible in life of a producing field.

12 References Cited

The following abbreviations have been used:

APEA	: Australian Petroleum Exploration Association
APPEA	: Australian Petroleum Production and Exploration Association (formerly APEA)
AAPG	: American Association of Petroleum Geologists
MESA	: Department of Mines and Energy South Australia
NCPGG	: National Centre for Petroleum Geology and Geophysics (Adelaide)
PESA	: Petroleum Exploration Society of Australia

Aitken, J.F. and Flint, S.S., 1995, **The Application of High-resolution Sequence Stratigraphy to Fluvial Systems: A Case Study From The Upper Carboniferous Breathitt Group, Eastern Kentucky, USA,** Sedimentology, Vol 42 p 3 - 30.

Alexander, E.M., 1996, **Reservoirs and Seals,** in Alexander, E.M. and Hibburt, J., (Eds), Petroleum Geology of South Australia, Volume 2: Eromanga Basin, p 141 - 147.

Alexander, E.M., Pegum, D., Tingate, P., Staples, C.J., Michaelsen, B.H., and McKirdy, D.M., 1996, **Petroleum Potential of the Eringa Trough in SA and the NT,** The APEA Journal, Vol 36, Part1, p 322 - 349.

Alexander, E.M. and Sansome, A., 1996, **Lithstratigraphy and Environments of Deposition,** in Alexander, E.M. and Hibburt, J., (Eds), Petroleum Geology of South Australia, Volume 2: Eromanga Basin, p 49 - 86.

Alexander, R. and Kagi, R.I., 1988, **Identification of Source Rocks of Eromanga/Cooper Basin Crude oils,** Internal SANTOS report.

Alexander, R., Larcher, A.V. and Kagi, R.I., 1988, **The Use of Plant-Derived Biomarkers for Correlation of Oils with Source Rocks in The Cooper/Eromanga Basin System, Australia,** The APEA Journal, Vol 28, p 310 - 324.

Allen, G.P., 1994, **Concepts and Applications of Sequence Stratigraphy to Siliciclastic Fluvial and Shelf Deposits,** Short course notes.

Allen G., Lang, S., Musakti, O. and Chirinos, A., 1996, **Application of Sequence Stratigraphy to Continental Successions: Implications for Mesozoic Cratonic Interior Basins of Eastern Australia,** in Mesozoic Geology of the Eastern Australia Plate Conference, Geological Society of Australia Inc. Extended Abstracts Number 43, p 22 - 26.

Allen, G. and Mercier, F., 1988, **Subsurface Sedimentology of Deltaic Systems,** PESA Journal, p 30 - 44.

Allen, G.P. and Posamentier, H.W., 1993, **Sequence Stratigraphy and Facies Model of an Incised Valley Fill: The Gironde Estuary, France,** Journal of Sedimentary Petrology, Vol 63 Number 3, p 378 - 391.

Allen, J.R.L, 1965, **Late Quaternary Niger Delta and Adjacent Areas: Sedimentary Environments and Lithofacies,** AAPG Bulletin, Vol 45, Number. 5, p 547 - 600.

Allen, J.R.L, 1970, **Studies in Fluviatile Sedimentation: A Comparison of Fining-Upwards Cyclotherms, With Special Reference To Course-Member Composition and Interpretation,** Journal of Sedimentary Petrology, Vol 40, No 1, p 298 - 323.

Allen, P.A. and Allen, J.R., 1990, **Depositional Systems and Facies Models.** Basin Analysis: Principles and Applications, Blackwell Scientific Publications, p 191.

Ambrose, G., 1990, **A Review of the Birkhead Formation Oil Fields In PEL's 5 & 6 and ATP 259P,** Unpublished SANTOS Ltd. Report.

Apak, S.N., Stuart, W.J. and Lemon N.M., 1995, **Compressional Control on Sediment and Facies Distribution SW Nappamerri Syncline and Adjacent Murteree High, Cooper Basin,** The APEA Journal, Vol 35, p 190 - 202.

Ayers, W.B., 1986, **Lacustrine and Fluvial-Deltaic Depositional Systems, Fort Union Formation (Paleocene), Powder River Basin, Wyoming and Montana,** AAPG Bulletin, Vol 70, Number 11, p 1651 - 1673.

Baillie, P.W., Powell, C. McA., Li, Z. X. and Ryall, A.M., 1994, **The tectonic Framework of Western Australia's Neoproterozoic to Recent Sedimentary Basins,** in Purcell, P.G. and Percell, R.R. (eds),Sedimentary Basins of Western Australia; Proceedings of PESA symposium, Perth 1994, p 45 - 62.

Baker, J.C., Kassan, J. and Hamilton, J., 1995, **Early Diagenetic Siderite as an indicator of Depositional Environment in the Triassic Rewan Group, Southern Bowen Basin, Eastern Australia,** Sedimentology, Number 43, p 77 - 88.

Bates, C.C., 1953, **Rational Theory of Delta Formation,** AAPG Bulletin, Volume 37, Number 9, p 2119 - 2162.

Bates, R.L. and Jackson, J.A., 1984, **Dictionary of Geological Terms (Third Edition),** The American Geological Institute, Anchor Books.

Beaumont, E.A., 1979, **Depositional Environments of Fort Union Sediments (Tertiary, Northwest Colorado) and their Relation to Coal,** AAPG Bulletin, V 63, Number 2 p 194 - 217.

Beard, D.C. and Weyl, P.K., 1973, **Influence of Texture on Porosity and Permeability of Unconsolidated Sand,** AAPG Bulletin, Volume 57, p 349 - 369.

Berner, R.A., 1971, **Principles of Chemical Sedimentology,** McGraw-Hill, Inc, p 199 - 200.

Bhattacharya, J.P. and Walker, R.G., 1992, **Deltas,** in Walker, R.G. and James, N.P. (Eds), 1992, Facies Models: Response to Sea Level Change, Geological Association of Canada, p 157 - 177.

Bjorlykke, K., 1988, **Sandstone Diagenesis in Relation to Preservation, Destruction and creation of porosity,** In Chilingarian, G.V. and Wolf, K.H. (eds), Developments in Sedimentology, Volume 41, p 55 - 70.

Borichansky, L.S. and Mikhailov, V.N., 1966, **Interaction of River and Sea Water in the Absence of Tides,** in Scientific Problems of the Humid Tropical Deltas and their Implications: UNESCO, p 175 - 180.

Boucher, R.K., 1991, **The Tectonic Framework of the Murteree Ridge, Warburton Basin: Structural Implications for the Cooper Basin.** Unpublished honours thesis, University of South Australia.

Boult, P.J., 1993, **Membrane Seal and The Tertiary Migration Pathways in the Bodalla South Oilfield**, Eromanga Basin, Australia, Marine and Petroleum Geology, Vol 10, p 3 - 13.

Boult, P.J., 1996, **An Investigation of reservoir/Seal Couplets in the Eromanga Basin: Implications for Petroleum Entrapment and Production. Development of Secondary Migration and Seal Potential Theory and Investigation Techniques,** University of South Australia, Ph.D Thesis (Unpublished).

Boult, P.J., LANZILLI, E., Michaelsen, B.H., McKirdy, 1998, **A New Model for the Hutton/Birkhead Reservoir/seal couplet and the Associated Birkhead-Hutton Petroleum System(!),** APPEA Journal, Number 37, Part 1.

Boult, P.J., Ryan, M.J., Michaelsen, B.H., McKirdy, P.R., LANZILLI, E. and Kagya, M.L.N., 1997, **The Birkhead-Hutton(!) Petroleum System of the Gidgealpa Area, Eromanga Basin, Australia,** Proceedings of the Petroleum Systems of SE Asia and Australasia Conference, May 1997, Indonesian Petroleum Association, p 213 - 235.

Boult, P.J., Theologou, P.N., Johnson, G.A. and Carbone, M., 1995, **Probe Permeability Studies for Better Reservoir Unit Evaluation with Examples From the Tirrawarra Sandstone, Cooper Basin and The Murta and McKinlay Members, Eromanga Basin,** The APEA Journal, Volume 35, Part 1, p 132 - 142.

Bowering, O.J.W., 1982, **Hydrodynamics and Hydrocarbon Migration - A Model For the Eromanga Basin,** The APEA Journal, Vol 22, Pt 1, p 227 - 236.

Bridge, J.S., 1993, **Description and Interpretation of Fluvial Deposits: A Critical Perspective,** Sedimentology, Vol 40, p 801 - 810.

Bridge, J.S. and Leeder, M.R., 1979, **A Simulation Model of Alluvial Stratigraphy,** Sedimentology, Vol 26, p 617 - 644.

Brierley, G.J., 1991, **Bar Sedimentology of the Squamish River, British Columbia: Definition and Application of Morphostratigraphic Units,** Journal of Sedimentary Petrology, Vol 61, Number 2, p 211 - 225.

Burger, D., 1986, **Palynology, cyclic sedimentation, and palaeoenvironments in the Late Mesozoic of the Eromanga Basin,** in Gravestock, D.I., Moore, P.S., and Pitt, G.M. (Eds) 1986, Contributions to the Geology and Hydrocarbon Potential of the Eromanga Basin, Geological Society of Australia Special Publication No 12, p 53 - 70

Campbell, R.L., 1968, **Stratigraphic Applications of Dipmeter Data in Mid-Continent.** AAPG Bulletin, Volume 52, p 1700 - 1719.

Cant, D.J. and Walker, R.G., 1976, **Development of a Braided-fluvial Model for the Devonian Battery Point Sandstone, Quebec,** Canadian Journal of Earth Sciences, Vol 13 p 102 - 119.

Carbone, M., 1993, **Permeability Controls Within the Tirrawarra Sandstone, Gidgealpa Field, Southern Dome, Cooper Basin,** University of Adelaide Honours Thesis: (Unpublished).

Carr, T.R., 1982, **Log-linear Models, Markov Chains and Cyclic Sedimentation,** Journal of Sedimentary Petrology, Volume 52, p 905 - 912.

Clark, I., 1979, **Practical Geostatistics,** Applied Science Publishers Ltd., London.

Cleneay, C.A, 1992, **Log Analysis Applications,** in Morton-Thompson, D., and Woods, A.M., 1992; Development Geology Reference Manual, AAPG Methods in Exploration Series, No 10, p 441 - 446.

Cohen, A.S., 1982, **Paleoenvironments of Root Casts From the Koobi Fora Formation, Kenya,** Journal of Sedimentry Petrology, Vol 52 Number 2 p 401 - 414.

Coleman, J.M., 1981, **Deltas: Processes of Deposition and Models for Exploration (2nd Ed),** Burgess Publishing Company, p 28 - 56.

Coleman, J.M. and Wright, L.D., 1975, **Modern River Deltas: Variability of Processes and Sand Bodies,** in Broussard, M. L. (Ed), 1975,Deltas: Models for Exploration, Houston Geological Society, p 99 - 149.

Collinson J.D. and Thompson D.B., 1989, **Sedimentary Structures,** The University Printing House, Oxford, (2nd Ed).

Conaghan, P.J. and Jones, J.G., 1975, **The Hawkesbury Sandstone and the Brahmaputra: A Depositional Model For Continental Sheet Sandstones,** Journal of the Geological Society of Australia, Vol 22, Pt. 3, p 275 - 283.

Cronquist, C., 1973, **Waterflooding by Linear Displacement in Little Creek Field, Mississippi,** in: Waterflooding, SPE Reprint Series Number 2a, p 24 - 32.

Davles, D.K., Williams, B.P.J. and Vessell, R.K., 1993, **Reservoir Geometry and Internal Permeability Distribution in Fluvial, Tight, Gas Sandstones, Travis Peak Formation, Texas,** SPE Reservoir Engineering, Februrary, 1993 p 7 - 12.

Davies, H.G., 1965, **Convolute Lamination and other structures from the Lower Coal Measures of Yorkshire,** Sedimentology, Number 5, p 305 - 325.

Doeglas, D.J., 1962, **The Structure of Sedimentary Deposits of Braided Rivers,** Sedimentology, Vol 1, p 167 - 190.

Donaldson, A.C., 1967, **Deltaic Sands and Sandstones,** in Symposium on Recently Developed Geologic Principles and Sedimentation of the Permo-Pennsylvanian of the Rocky Mountains, Wyoming Geological Association, 20th Ann. Field Conference, Casper, Wyoming 1966, p 31 - 62.

Doveton, J.H., 1994, **Theory and Applications of Vertical Variability Measures from Markov Chain Analysis,** in Yarus, M. and Chambers, R.L. (eds), Stochastic Modeling and Geostatistics: Principles, Methods and Case Studies, AAPG Computer Applications in Geology No.3, p 55 - 64.

Dreyer, T., Scheie, A. and Walderhaug, O., 1990, **Minipermeameter-Based Study of Permeability Trends in Channel Sand Bodies,** AAPG Bulletin, Volume 74, Number 4, p 359 - 374.

Eijpe, R. and Weber, K.J., 1971, **Mini-Permeameters for Consolidated Rock and Unconsolidated Sand,** AAPG Bulletin, Volume 55, Number 5, p 307 - 321.

Einsele, G., 1992, **Sedimentary Basins,** Springer-Verlag, p 29 - 53.

Elliott, L.G., 1993, **Post-Carboniferous Tectonic Evolution of Eastern Australia,** The APEA Journal, Vol 33, p 215 - 237.

Elliott, T., 1974, **Interdistrutary Bay Sequences and Their Genesis,** Sedimentology, Number 21, p 611 - 622.

Ellwood, B.B., Chrzanowski, T.H., Hrouda, F., Long, G.J. and Buhl, M.L., 1988, **Siderite Formation in Anoxic Deep-sea Sediments: A Synergetic Bacterially Controlled Process with Important Implications in Paleomagnetism,** Geology, Vol 16, p 980 - 982.

Emery, D. and Myers, K.J., 1996, **Sequence Stratigraphy,** Blackwell Science Publishers.

Ethridge, F.G., Jackson, T.J. and Youngberg, A.V., 1981, **Floodbasin Sequence of a Fine-Grained Meander Belt Subsystem: The Coal-Bearing Lower Wasatch and Upper Fort Union Formations. Southern Powder River Basin, Wyoming,** From Ethridge, F.G. and Flores, R.M. (Eds), 1981, Recent and Ancient Nonmarine Depositional Environments: Models For Exploration, Society of Economic Paleontologists and Mineralogists, Special Publication No. 31, p 191 - 209

Etnyre, L.M., 1989, **Finding Oil and Gas From Well Logs,** Van Nostrand Reinhold.

Faridi, H., 1985, **Palaeogeography and Hydrocarbon Potential of the Murta Member and Birkhead Formation in the Central Part of the Northern Eromanga Basin,** Unpublished Delhi Petroleum Ltd Report.

Finlayson, D.M., Leven, J.H. and Etheridge, M.A., 1988, **Structural Styles and Basin Evolution in Eromanga Region, Eastern Australia,** American Association of Petroleum Geologists Bulletin, Vol 72, Num. 1, p 33 - 48.

Fletcher, I.R., Williams, S.J., Gee, R.D. and Rosman, K.J.R., 1983, **Sm-Nd Model Ages Across the Margins of the Archaean Yilgarn Block, Western Australia: Northwest Transect into the Proterozoic Gascoyne Province,** Journal of the Geological Society of Australia, Number 30, 167 - 174.

Foden, J., Mawby, J., Kelley, S., Turner, S. and Bruce, D., 1995, **Metamorphic Events in the Eastern Arunta Inlier, Part 2. Nd-Sr-Ar Isotopic Constraints,** Precambrian Research, Number 71, p 207 - 227.

Folk, R.L., 1980, **Petrology of Sedimentary Rocks,** Hemphill Publishing Company.

Frakes, L.A., Francis, J.E. and Syktus, J.I., 1992, **Climate Modes of the Phanerozic,** Cambridge University Press (Pubs).

Galloway, W.E., 1975, **Process Framework for Describing the Morphologic and Stratigraphic Evolution of Deltaic Depositional Systems** in Broussard, M. L. (Ed), 1975, Deltas: Models for Exploration, Houston Geological Society, p 88 - 98.

Galloway, W. E., 1989, **Genetic Stratigraphic Sequences in Basin Analysis I: Architecture and Genesis of Flooding-Surface Bounded Depositional Units,** AAPG Bulletin, Volume 73, Number 2, p 125 - 142.

Galloway, W.E., 1994, **Siliciclastic Depositional Systems and Sequences,** Short course notes, Department of Geological Sciences, The University of Texas at Austin.

Garrels, R.M. and Christ, C., 1965, **Solutions, Minerals and Equilibria,** Harper & Row, Publishers, Incorporated, New York.

Garzanti, E. 1991, **Non-Carbonate intrabasinal Graines in arenites: Their Recognition, Significance and Relationship to Eustatic Cycles and Tectonic Setting,** Journal of Sedimentry Petrology, Vol 61, Number 6, p 959 - 975.

Gatehouse, C.G., 1986, **The Geology of the Warburton Basin in South Australia,** Australian Journal of Earth Sciences, Vol 33, p 161 - 180.

Gautier, D.L., 1982, **Siderite Concretions: Indicators of Early Diagenesis in the Gammon Shale (Cretaceous),** Journal of Sedimentary Petrology, Vol 52, Number 3, p 859 - 871.

Gibbons, K., Halvorsen, C. and Siring, E., 1993, **Vertical and Horizontal Permeability Variation Within a Sandstone Reservoir Based on Minipermeameter Measurements,** Marine and Petroleum Geology, Volume 10, p 325 - 334.

Gibson, H.J., Mooney, R.A. and Watson P.G., 1995, Apatite fission track, **Analysis of samples from the western Eromanga Basin and Eringa Trough, Australia,** Unpublished Geotrack report #582, prepared by MESA.

Giles, M.R.' 1987, **Mass Transfer and Problems of Secondary Porosity Creation in Deeply Buried Hydrocarbon Reservoirs,** Marine and Petroleum Geology, Volume 4, p 188 - 204.

Goggin, D.J., 1992, **Probe Permeametry: Is it Worth the Effort?,** Marine and Petroleum Geology, Volume 10, p 299 - 307.

Goggin, D.J., Thrasher, R.L. and Lake, L.W., 1988, **A theoretical and Experimental Analysis of Minipermeameter Responce Including Gas Slippage and High Velocity flow effects,** In Situ, Number 12, p 79 - 116.

Gravestock, D.I., Callen, R.A., Alexander, E.M. and Hill, A.J., 1995, **Strezelecki, South Australia,** 1:250,000 Geological Series - Explanatory Notes, MESA, 409p.

Gravestock, D., Griffiths, M. and Hill, A., 1983, **The Hutton Sandstone - Two Separate Reservoirs in the Eromanga Basin, South Australia,** The APEA Journal, Vol 23 Pt 1, p 109 - 119.

Gravestock, D.I., and Morton, J.G.G, 1984, **Geology of the Della Field, A Perspective on the History of the Cooper Basin,** The APEA Journal, Vol 24, p 266 - 277.

Green, P.M., Eadington, P.J., Hamilton, P.J. and Carmichael, D.C., 1989, **Regional Diagenesis - an Important Influence in Porosity Development and Hydrocarbon Accumulations Within the Hutton Sandstone, Eromanga Basin,** in O'Neil, B.J. (Ed) 1989, The Cooper and Eromanga Basins Australia, Proceedings of the Cooper and Eromanga Basins Conference, Adelaide (SPE), p 620 - 627

Greer, W.J., 1965, **The Gidgealpa Gas Field,** The APEA Journal, p 114 - 129.

Habermehl, M.A., 1980, **The Great Artesian Basin, Australia,** BMR Journal of Australian Geology and Geophysics, Number 5, p 9 - 38.

Halvorsen, C., 1993, **Probe Permeability in Laminated Sandstones,** Marine and Petroleum Geology, Volume 10, p 347 - 351.

Halvorsen, C. and Hurst, A., 1990, **Principles, Practice and Applications of Laboratory Minipermeametry,** In: Worthington, F.P. (Ed) 1990;Advances in Core Evaluation: Accuracy and Precision in Reserves Estimation: Reviewed Proceedings of the First Society of Core Analysts, European Core Analysis Symposium, London 1990, p 521 - 548.

Hamilton, D.S. and Tadros, N.Z., 1994, **Utility of Coal Seams as Genetic Stratigraphic Sequence Boundaries in Nonmarine Basins: An example from the Gunnedah Basin, Australia,** AAPG Bulletin, Volume 78, Number 2, p 267 - 286

Hamlin, H.S., Dutton, S.P., Seggie, R.J. and Tyler, N., 1996, **Depositional Controls on Reservoir Properties in a Braid-Delta Sandstone, Tirrawarra Oil Field, South Australia,** AAPG Bulletin, Vol 80, Number 2, p 139 - 156.

Harris, 1989, **Diagenetic Quartz Arenite and Destruction of Secondary Porosity: An Example From the Middle Jurassic Brent Sandstone of NW Europe,** Geology, Volume 17, p 361 - 364.

Hawkins, P.J., 1978, **Relationship Between Diagenesis, Porosity Reduction and Oil Emplacement in the Late Carboniferous Sandstone Reservoirs, Bothamsall Oilfield, E Midlands,** Journal of the Geological Society of London, Volume 135, p 7 - 24.

Heath, R., McIntyre, S. and Gibbons, N., 1989, **A Permian Origin for Jurassic Reservoired oil in the Eromanga Basin,** in O'Neil, B.J. (Ed) 1989, The Cooper and Eromanga Basins Australia, Proceedings of the Cooper and Eromanga Basins Conference, Adelaide (SPE), p 405 - 416

Helander. D, 1988, **Basic Reservoir Engineering,** Short course notes, Oil and Gas Consultants.

Herbert, C, 1995, **Sequence Stratigraphy of the Late Permain Coal Measures in the Sydney Basin,** Australian Journal of Earth Sciences, Number 42, p 391 - 405.

Hill, L.V., 1985, **Environmental Analysis of the Hutton Sandstone to Birkhead Formation Transition Within the South-Western Eromanga Basin, Queensland,** University of Adelaide Honours Thesis (Unpublished).

Horton, B.K. and Schmitt, J.G., 1996, **Sedimentology of a Lacustrine Fan-delta System, Miocene Horse Camp Formation, Nevada, USA,** Sedimentology, Number 43, p 133 - 155.

James, N.P. and Choquette, P.W., 1984, **Diagenesis 9. Limestones - the meteoric diagenetic environment,** Geoscience Canada, Number 11, p 161 - 194.

Jennings, J.B., 1987, **Capillary Pressure Techniques: Application to Exploration and Development Geology,** AAPG Bulletin, Volume 71, Number 10, p 1196 - 1209.

John, B.H., 1990, **Recent Exploratory Stratigraphic Drilling and Petroleum Investigations in South-West Queensland,** Queensland Government Mining Journal, Vol 91, Num 1064, p 307 - 316.

John, B.H. and Almond, C.S., 1987, **Lithostratigraphy of the Lower Eromanga Basin Sequence in South-West Queensland,** The APEA Journal, Vol 27, Pt 1, p 196 - 247.

Jordan, D.W., and Pryor, W.A., 1992, **Hierarchical Levels of Heterogeneity in a Mississippi River Meander Belt and Application to Reservoir Systems,** AAPG Bulletin, Vol 76, Number 10, p 1601 - 1624.

Kantsler, A.J., Prudence, T.J.C., Cook, A.C. and Zwigulis, 1983, **Hydrocarbon Habitat or the Cooper/Eromanga Basin, Australia,** The APEA Journal, Volume 23, Partl, p 75 - 92.

Kisch, H.J., 1983, **Mineralogy and Petrology of Burial Diagenesis and Incipient Metamorphism in clastic rocks,** in: Larsen, G., and Chilingar, G.V. (eds), Diagenesis in Sediments and Sedimentary Rocks 2, Developments in Sedimentology 25B, Elsevier, Amsterdam, p 289 - 493.

Krauskopf, 1967, **Introduction to Geochemistry,** McGraw-Hill Book Company, p 83 - 85 and 253 - 255.

Krzyszkowski, D, 1993, **Neogene Fluvial Sedimentation in the Kleszow Graben, Central Poland,** Journal of Sedimentary Petrology, Vol 63, Number 2, p 204 - 217.

Lanzilli, E., 1993, **Reservoir Characterization of the Birdrong Formation, Griffin 2 Well, Northwest Shelf Western Australia,** University of Adelaide Honours Thesis: (Unpublished).

LANZILLI, E. and Boult, P.J., 1996, **The Hutton Sandstone to Birkhead Formation Transition, Gidgealpa south dome: showing an associated unconformity and provenance change from craton-derived to volcanic-arc-derived sediments,** in: Mesozoic Geology of the Eastern Australia Plate Conference, Geological Society of Australia Inc. Extended Abstracts Number 43, p 337 - 342.

Le Blanc, R.J., 1975, **Significant Studies of Modern and Ancient Deltaic Sediments,** in Broussard, M. L. (Ed), 1975, Deltas: Models for Exploration, Houston Geological Society, p 13 - 85.

Lemon, N.M., 1993, **Sandstone Reservoirs: The Influence of Diagenesis on Reservoir Quality,** NCPGG Short Course Notes.

Lewis, D.W., 1984, **Practical Sedimentology,** Hutchinson Ross Publishing Company, p 225.

Lindholm, R., 1987, **A Practical Approach to Sedimentology,** Allen and Unwin (Pub), p 240 - 250.

Little, B., 1996, **The Petrology and Petrophysics of the Pretty Hill Formation in the Penola Trough, Otway Basin,** University of South Australia Masters Thesis (unpublished).

Lowe-Young, B.S., Mackie, S.I. and Heath, R.S., 1997, **The Cooper-Eromanga Petroleum System, Australia: Investigation of Essential Elements and Processes,** Proceedings of the Petroleum Systems of SE Asia and Australasia Conference, May 1997, Indonesian Petroleum Association, p 213 - 235.

MacKenzie, W.S. and Guilford, 1982, **Atlas of Rock-forming Minerals in Thin Section,** Longman Group Ltd., p 97.

Mackie, S.I. and Gumley, C.M., 1995, **The Dirkala South Oil Discovery: Focussing on cost-Efficient Reservoir Delineation,** The APEA Journal, Vol 35 Pt 1, p 65 - 78.

Marcus, G., 1983, **The Stratigraphy, Palaeogeography and Hydrocarbon Potential of the Birkhead Formation in South Australia,** SANTOS Ltd Report (Unpublished).

Martin, K.R. and Hamilton, N.J., 1981, **Diagenesis and Reservoir Quality, Toolachee Formation, Cooper Basin,** The APEA Journal, Volume 21 Number 1, p 143 - 154.

Mathisen, M.E., 1984, **Diagenesis of Plio-Pleistocene Nonmarine Sandstones, Cagayan Basin, Philippines: Early Development of Secondary Porosity in Volcanic Sandstones** in McDonald, D.A. and Surdam, R.C. (Eds) 1984. Clastic Diagenesis, AAPG Memoir 37, p 177 - 195.

McCulloch, M.T. and Wasserburg, G.J., 1978, **Sm-Nd and Rb-Sr Chronology of Continental Crust Formation,** Science, Volume 200, Number 4345, p 1003 - 1011.

McIntyre, S.M., Jamal, F.G., Pidcock, C.L. and Kabir, M.I., 1989, **The Gidgealpa Oil and Gas Field: a case history,** in O'Neil, B.J. (Ed) 1989, The Cooper and Eromanga Basins Australia, Proceedings of the Cooper and Eromanga Basins Conference, Adelaide (SPE), p 91 - 101.

Miall, A.D., 1973, **Markov Chain Analysis Applied to an Ancient Alluvial Plain Succession,** Sedimentology, Volume 20, p 347 - 365.

Miall, A.D., 1977, **A Review of the Braided-River Depositional Environment,** Earth-Science Reviews, Vol 13 p 1 -62.

Miall, A.D., 1992, **Alluvial Deposits,** in Walker, R.G. and James, N.P. (Eds), 1992, Facies Models: Response to Sea Level Change, Geological Association of Canada, p 119 - 142.

Michaelsen, B.H. and McKirdy, 1996, **Source Rock Distribution and Hydrocarbon Geochemistry,** in Alexander, E.M. and Hibburt, J., (Eds), Petroleum Geology of South Australia, Volume 2: Eromanga Basin, p 101 - 110

Miller, J.,1988, **Cathodoluminescence Microscopy,** in Maurice Tucker (Ed), Techniques in Sedimentology, Blackwell Scientific Publication, p 174 - 190

Moore, P.S., 1986, **Jurassic and Triassic Stratigraphy and Hydrocarbon Potential of the Poolowanna Trough (Simson Desert Rigion Northern South Australia,** in Gravestock, D.I., Moore, P.S., and Pitt, G.M. (Eds) 1986, Contributions to the Geology and Hydrocarbon Potential of the Eromanga Basin, Geological Society of Australia Special Publication No 12, p 195 - 201.

Moore, P.S., Hobday, D.K., Mai, H. and Sun, Z.C., 1986, **Comparison of Selected Non-Marine Petroleum- Bearing Basins in Australia and China,** The APEA Journal, Vol 26, p 285 - 308.

Moore, P.S. and Pitt, G.M., 1984, **Cretaceous of the Eromanga Basin - Implications for Hydrocarbon Exploration,** The APEA Journal, Vol 24, Pt 1, p 358 - 376.

Moore, S.E., Ferrell, R.E. and Aharon, P, 1992, **Diagenetic Siderite and Other Ferroan Carbonates in a Modern Subsiding Marsh Sequence,** Journal of Sedimentary Petrology, Vol 62, Number 3, p 357 - 366.

Mudge, W.J.,1980, **Hydrocarbon Potential and Environmental Interpretations of the Jurassic-Lower Cretaceous Section in Five Wells in the Eromanga Basin,** University of Adelaide Honours Thesis (Unpublished).

Nelson, A.W., 1985, **Tectonics of the Jackson-Naccowlah Area, Cooper-Eromanga Basins, Southwest Queensland, and Their Implications for Hydrocarbon Accumulation,** The APEA Journal, Vol 25, Part1, p 85 - 94.

Newton, C.B., 1986, **The Tintaburra oilfield,** The APEA Journal, Vol 26, Pt 1, p 334 - 352.

North, C.P. and Taylor, K.S., 1996, **Ephemeral-Fluvial Deposits: Integrated Outcrop and Simulation Studies Reveal Complexity,** AAPG Bulletin, Vol 80, Num. 6, p 811 - 830.

Northcott, I., 1994, **Practical Log Analysis,** Short course notes.

O'Brien, P.E. and Wells, A.T., 1986, **A Small, Alluvial Crevasse Splay,** Journal of Sedimentary Petrology, Vol 56, Number 6, p 876 - 879.

Ohen, H.A. and Kersey, D.G., 1993, **Permeability,** in: Morton-Thompson, D. and Woods, A.M., (Eds), Development Geology Reference Manual AAPG Methods in Exploration Series, No. 10, p 210 - 213.

Orton, G.J. and Reading, H.G., 1993, **Variability of Deltaic Processes in terms of Sediment Supply with Particular Emphasis on Grain Size,** Sedimentology, Number 40, 475 - 512.

Paton, I.M., 1986, **The Birkhead Formation-a Jurassic petroleum reservoir,** in Gravestock, D.I., Moore, P.S., and Pitt, G.M. (Eds) 1986, Contributions to the Geology and Hydrocarbon Potential of the Eromanga Basin, Geological Society of Australia Special Publication No 12, p 195 - 201.

Pettijohn, F.J., Potter, P.E. and Siever, R., 1987, **Sand and Sandstone: Second Edition,** Springer-Verlag, p 87 - 94.

Posamentier, H.W. and Allen, G.P., 1993, **Siliciclastic Sequence Stratigraphic Patterns in Foreland Ramp-Type Basins,** Geology
Volume 21, p 455 - 458.

Posamentier, H.W. and Weimer, P., 1993, **Siliciclastic Sequence Stratigraphy and Petroleum Geology - Where to From Here?,** AAPG Bulletin, Volume 77, p 731 - 742.

Postma, D., 1982, **Pyrite and Siderite Formation in Brackish and Freshwater Swamp Sediments,** American Journal of Science, Vol 282, Oct, p 1151 - 1183.

Poupon, A. and Leveaux, J., 1971, **Evaluation of Water Saturation in Shaly Formations,** The log Analyst, July-August, p 3 - 8.

Powell, T.G., Boreham, C.J., McKirdy, D.M., Michaelson, B.H. and Summons, R.E., 1989, **Petroleum Geochemistry of the Murta Member, Mooga Formation, and Associated Oils, Eromanga Basin,** The APEA Journal, Vol 29, Partl, p 114 - 129.

Powers, D.W. and Easterling, R.G., 1982, **Improved Methodology for Using Embedded Markov Chains to Describe Cyclical Sediments,** Journal of Sedimentary Petrology, Volume 56, p 913 - 923.

Reineck, H.E. and Singh, I.B., 1980, **Depositional Sedimentry Environments (2nd Ed),** Springer-Verlag Berlin Heidelberg New York (Publisher).

Reynolds, A.D., 1994, **Sequence Stratigraphy from Core and Wireline Log Data: The Viking Formation, Albian, South Central Alberta, Canada,** Marine and Petroleum Geology, Volume 11 Number 3, p 258 - 282.

Roberts, D.C. Carroll, P.G. and Sayers, J., 1990, **The Kalladeina Formation - A Warburton Basin Cambrian Carbonate Play,** The APEA Journal, Vol 30, p 166 - 183.

Robertson, G.M. and McPhee, C.A., 1990, **High Resolution Probe Permeability: An Aid to Reservoir Description,** in: Advances in Core Evaluation, Accuracy and Precision in Reserves Estimation (1990), Gordon and Breach Science Publishers, p 495 - 519.

Rust, B.R., 1971, **Structure and Process in a Braided River,** Sedimentology, Vol 18, p 221 - 245.

Rust, B.R., 1981, **Sedimentation in an Arid-Zone Anastomosing Fluvial System: Cooper's Creek, Central Australia,** Journal of Sedimentary Petrology, Vol 51, No. 3, p 745 - 755.

Ryan, M.J., 1996, **The use of Biomarkers and Molecular Maturity Indicators to Determine the Provenance of Residual and Produced oils in the Gidgealpa Field in the Cooper-Eromanga Basin, Australia,** University of Adelaide Honours Thesis (Unpublished).

Ryer, T.A., 1981, **Deltaic Coals of Ferron Sandstone Member of Mancos Shale: Predictive Model for Cretaceous Coal-Bearing Strata of Western Interior,** AAPG Bulletin, Volume 65, Number 11, p 2323 - 2340.

SANTOS Ltd, 1996, **Gidgealpa 57 - Well Proposal Report,** SANTOS Ltd Internal Report, Number PD.282/96.

Salomon, S.L., Keenihan, S.L. and Calcraft, A.P., 1990, **Bodalla South Field** in Beaumont, E.A. and Foster, N.H. (Eds), 1990, Treaties of Petroleum Geology - Atlas of Oil and Gas Traps Vol 1 The American Association of Petroleum Geologists (pub) p 129 - 155.

Schumm, S.A., 1993, **River Responce to Baselevel Change: Implications for Sequence Stratigraphy,** The Journal of Geology, Volume 101, p 279 - 294.

Schulz, J.P. and Philips, S.E., 1989, **Diagenetic Alteration of Permian Reservoir Sandstones in the Nappamerri Trough and Adjacent Areas, Southern Cooper basin,** in O'Neil, B.J. (Ed) 1989, The Cooper and Eromanga Basins Australia, Proceedings of the Cooper and Eromanga Basins Conference, Adelaide (SPE), p 91 - 101.

Selley, R.C., 1989, **Deltaic reservoir prediction from rotational dipmeter patterns,** in Whateley, M.K.G. and Pickering, K.T. (Eds), 1989, Deltas: Sites and Traps for Fossil Fuels, Geological Society Special Publication No 41, p 89 - 95.

Shanley, K.W. and McCabe, P.J., 1993, **Alluvial Architecture in a Sequence Stratigraphic Framework: A Case History From the Upper Cretaceous of Southern Utah, USA,** in Flint, S.S. and Bryant, I.D. (Eds), 1993, The Geological Modelling of Hydrocarbon Reservoirs and Outcrop Analogues International Association of Sedimentologists, Special Publication Number 15, p 21 - 56.

Shanmugam, G., 1985, **Significance of Secondary Porosity in Interpreting Sandstone Composition,** AAPG Bulletin, Vol 69, Num. 3, p 378 - 384.

Shanmugam, G., Lehtonen, Straume, T., Syvertsen, S.E., Hodgkinson, R.J. and Skibeli, M., **Slump and Debris-Flow Dominated Upper Slope Facies in the Cretaceous of the Norwegian and Northern North Seas (61-67°N):Implications for Sand Distribution,** AAPG Bulletin, Vol 78, Num. 6, p 910 - 937.

Shields, C. and Gahan, M.J., 1974, **The Dipmeter Used to Recognise Depositional Environment,** The APEA Journal, p 181 - 188.

Skinner, D.R., 1981, **Introduction to Petroleum Production: Volume 1,** Gulf Publishing Company, p 20 - 36.

Smith, D.G. and Putnam, P.E., 1980, **Anastomosed River Deposits: Modern and Ancient Examples in Alberta, Canada,** Canadian Journal of Earth Sciences, Vol 17, p 1396 - 1406.

Smith, D.G. and Smith, M.D., 1980, **Sedimentation in Anastomosed River systems: Examples from Alluvial Valleys Near Banff, Alberta,** Journal of Sedimentary Petrology, Vol 50, No. 1, p 157 - 164.

Smith, N.D., 1974, **Sedimentology and Bar Formation in the Upper Kicking Horse River, A Braided Outwash Stream,** Journal of Geology, Vol 82, p 205 - 223.

Smyth, M., Cook, A.C., Philp, R.P., 1984, **Birkhead Revisited: Petrological and Geochemical Studies of the Birkhead Formation, Eromanga Basin,** The APEA Journal, Vol 24, Pt 1, p 230 - 242.

Sneider, R.M., 1992, **Evaluation of Reservoirs and Seals,** Short course notes.

Soledad Garcia-Gil, 1993, **The Fluvial Architecture of the Upper Buntsandstein in the Iberian Basin, Central Spain,** Sedimentology, Vol 40, p 125 - 143.

Solomon, G. and Ormsby, W.R., 1984, **Birkhead Formation Regional Stratigraphic Study. Applications to Hydrocarbon Exploration, PEL's 5 & 6 and ATP-259P, South Australia & Queensland,** Internal SANTOS report (unpublished).

Steveson, B.G., and Spry, A.H., 1973, **Nature of Porosity in some Indurated Permian Sandstones from the Cooper Basin,** The APEA Journal, Volume 13 Number 1, p 86 - 90.

Sutherland, W.J., Halvorsen, C., Hurst, A., McPhee, C.A., Robertson, G., Whattler, P.R. and Worthington, P.F., 1992, **Recommended Practice for Probe Permeametry,** Marine and Petroleum Geology, Volume 10, p 309 - 317.

Theologou, P.,1995, **Murta Formation/McKinlay Member of the Murteree Ridge, Nappacoongee-Murteree Block - Improved Oil Recovery Project,** University of South Australia Ph.D Thesis (Unpublished).

Thomas, A, 1990, **The Diagenesis of Permian Arenaceous and Argillaceous Units in the Moomba Gas Field, Southern Cooper Basin, South Australia,** University of South Australia Masters Thesis (Unpublished)

Thornton, R.C.N., 1978, **Regional Lithofacies and Palaeogeography of the Gidgealpa Group,** APEA Journal, Vol 18, p.53-63.

Tingate, P., 1994, **Interpretation of Apatite Fission Track Data From the Officer Basin,** Unpublished Report for MESA.

Torkington, J. and Micenko, M.I., 1988, **A Stratigraphic Analysis of the Talgeberry Oilfield,** The APEA Journal, Vol 28, Pt 1, Num 1, p 113 - 121.

Towe, K.M., 1962, **Clay Mineral Diagenesis as a Possible Source of Silica Cement in Sedimentary Rocks,** Journal of Sedimentary Petrology, Volume 32, p 26 - 28.

Vail, P.R., 1988, **Part 1: Seismic Stratigraphy Interpretation Procedure** in Vail, P.R. and Sangree, J.B. (Eds), 1988, Sequence Stratigraphy Interpretation of Seismic, Well and Outcrop Data Work book

Van Wagoner, J.C., Mitchum, R.M., Campion, K.M., and Ramanian, V. D., 1990, **Siliciclastic Sequence Stratigraphy in Well Logs, Cores and Outcrops: Concepts for High-resolution Correlation of Time and Facies,** AAPG Methods in Exploration Series 7, p 55.

Vavra, C.L., Kaldi, J.G. and Sneider, R.M., 1993, **Capillary Pressure,** in: Morton-Thompson, D. and Woods, A.M., (Eds), Development Geology Reference Manual, AAPG Methods in Exploration Series, No. 10, p 221 - 228.

Veevers, J.J., 1984, **Phanerozoic Earth History of Australia,** Oxford University Press, New York.

Veevers, J.J., Jones, J.G. and Powell, C.McA.,1981, **Tectonic Framework of Australia's Sedimentary Basins,** The APEA Journal, Vol 22, Pt 1, p 283 - 300.

Veevers, J.J., Powell, C. McA. and Roots, S.R., 1991, **Review of Seafloor Spreading Around Australia. I. Synthesis of the Patterns of Spreading,** Australian Journal of Earth Sciences, Number 38, p 373 - 389.

Vincent, Ph., Gartner, J.E. and Attali, G., 1979, **An Approach to Detailed Dip Determination Using Correlation by Pattern Recognition,** Journal of Petroleum Technology, p 232 - 240.

Vincent, P.W., Mortimore, I.R. and McKirdy, D.M., 1985, **Hydrocarbon Generation, Migration and Entrapment in the Jackson-Naccowlah Area, ATP 259P, Southwestern Queensland,** The APEA Journal, Vol 25, Part1, p 62 - 84.

Walker, R.G., 1981, **Clastic Sedimentary Facies and Depositional Models,** The Australasian Sedimentologists Group of the Geological Society of Australia, course notes., The Department of Earth Sciences, Monash University.

Walker, R.G., 1984, **General Introduction: Facies, Facies Sequences and Facies Models,** in Walker, G. (Ed), 1984, Facies Models, Geoscience Canada, p 1 - 9.

Walker, R.G., 1990, **Facies Modelling and Sequence Stratigraphy,** Journal of Sedimentary Petrology, Volume 60, Number 5, p 777 - 786.

Walker, R.G. and Cant, D.J., 1984, **Sandy Fluvial Systems,** in Walker, G. (Ed), 1984,Facies Models, p 71 - 87.

Wardlaw, N.C. and Taylor, R.P., 1976, **Mercury Capillary Pressure Curves and the Interpretation of Pore Structure and Capillary Behaviour in Reservoir Rocks,** Bulletin of Canadian Petroleum Geology, Volume 24, p 225 - 262.

Watts, K.J., 1987, **The Hutton Sandstone-Birkhead Formation Transition, ATP 269P(1),** The APEA Journal, Volume 27 Number 1, p 215 - 228.

Wecker, H.R.B., 1989, **The Eromanga Basin,** The APEA Journal, Vol 29, Pt 1, p 379 - 397.

Whitford, D.J., Hamilton, P.J. and Scott, J, 1994, **Sedimentary Provenance Studies in Australian Basins Using Neodymium Model Ages,** The APEA Journal, Vol 34 Pt 1, p 320 - 329.

Williams, B.P.J., 1982, **Facies Analysis of Gidgealpa Group Reservoir Rocks, Southern Cooper Basin, South Australia,** Preliminary Report for South Australian Oil and Gas Corporation Pty Ltd, (Unpublished).

Williams, P.F. and Rust, B.R., 1969, **The sedimentology of a Braided River** Journal of Sedimentary Petrology, Vol 39, Number 2, p 649 - 679.

Wiltshire, M.J., 1989, **Mesozoic Stratigraphy and Palaeogeography, Eastern Australia,** in O'Neil, B.J. (Ed) 1989, The Cooper and Eromanga Basins Australia, Proceedings of the Cooper and Eromanga Basins Conference, Adelaide (SPE), p 279 - 291.

Wright, L.D., 1977, **Sediment Transport and Depostion at River Mouths: A synthesis,** Geological Society of America Bulletin, Volume 88, p 857 - 868.

Wright, L.D.,1985, **River Deltas,** in Davis Jr, R.A. (Ed), 1985, Coastal Sedimentary Environments, Springer-Verlag, p 1 - 76.

Wright, L.D. and Colemean, J.M., 1973, **Variations in Morphology of Major River Deltas as Functions of Ocean Wave and River Discharge Regimes,** AAPG Bulletin, Volume 57, Number 2, p 370 - 398.

Wu, C.R., 1995, **Gidgealpa Field Birkhead 'Main Channel' Reservoir Material Balance Analysis and IOR/EOR Potential,** SANTOS Ltd Internal Report (Unpublished), Number: PEDSA 021/94.